

Lecture Notes in Civil Engineering

Nikolai Vatin

Ekaterina Gennadyevna Pakhomova

Danijel Kukaras *Editors*

# Modern Problems in Construction

Selected Papers from MPC 2022

 Springer

# Lecture Notes in Civil Engineering

Volume 372

## Series Editors

Marco di Prisco, Politecnico di Milano, Milano, Italy

Sheng-Hong Chen, School of Water Resources and Hydropower Engineering,  
Wuhan University, Wuhan, China

Ioannis Vayas, Institute of Steel Structures, National Technical University of  
Athens, Athens, Greece

Sanjay Kumar Shukla, School of Engineering, Edith Cowan University, Joondalup,  
WA, Australia

Anuj Sharma, Iowa State University, Ames, IA, USA

Nagesh Kumar, Department of Civil Engineering, Indian Institute of Science  
Bangalore, Bengaluru, Karnataka, India

Chien Ming Wang, School of Civil Engineering, The University of Queensland,  
Brisbane, QLD, Australia

**Lecture Notes in Civil Engineering (LNCE)** publishes the latest developments in Civil Engineering—quickly, informally and in top quality. Though original research reported in proceedings and post-proceedings represents the core of LNCE, edited volumes of exceptionally high quality and interest may also be considered for publication. Volumes published in LNCE embrace all aspects and subfields of, as well as new challenges in, Civil Engineering. Topics in the series include:

- Construction and Structural Mechanics
- Building Materials
- Concrete, Steel and Timber Structures
- Geotechnical Engineering
- Earthquake Engineering
- Coastal Engineering
- Ocean and Offshore Engineering; Ships and Floating Structures
- Hydraulics, Hydrology and Water Resources Engineering
- Environmental Engineering and Sustainability
- Structural Health and Monitoring
- Surveying and Geographical Information Systems
- Indoor Environments
- Transportation and Traffic
- Risk Analysis
- Safety and Security

To submit a proposal or request further information, please contact the appropriate Springer Editor:

- Pierpaolo Riva at [pierpaolo.riva@springer.com](mailto:pierpaolo.riva@springer.com) (Europe and Americas);
- Swati Meherishi at [swati.meherishi@springer.com](mailto:swati.meherishi@springer.com) (Asia—except China, Australia, and New Zealand);
- Wayne Hu at [wayne.hu@springer.com](mailto:wayne.hu@springer.com) (China).

**All books in the series now indexed by Scopus and EI Compendex database!**

Nikolai Vatin ·  
Ekaterina Gennadyevna Pakhomova ·  
Danijel Kukaras  
Editors

# Modern Problems in Construction

Selected Papers from MPC 2022

 Springer



*Editors*

Nikolai Vatin  
Peter the Great St. Petersburg Polytechnic  
University  
Saint-Petersburg, Russia

Ekaterina Gennadyevna Pakhomova  
Faculty of Construction and Architecture  
Southwest State University  
Kursk, Russia

Danijel Kukaras  
Faculty of Civil Engineering  
University of Novi Sad  
Subotica, Serbia

ISSN 2366-2557                      ISSN 2366-2565 (electronic)  
Lecture Notes in Civil Engineering  
ISBN 978-3-031-36722-9              ISBN 978-3-031-36723-6 (eBook)  
<https://doi.org/10.1007/978-3-031-36723-6>

© The Editor(s) (if applicable) and The Author(s), under exclusive license to Springer Nature  
Switzerland AG 2024

This work is subject to copyright. All rights are solely and exclusively licensed by the Publisher, whether the whole or part of the material is concerned, specifically the rights of translation, reprinting, reuse of illustrations, recitation, broadcasting, reproduction on microfilms or in any other physical way, and transmission or information storage and retrieval, electronic adaptation, computer software, or by similar or dissimilar methodology now known or hereafter developed.

The use of general descriptive names, registered names, trademarks, service marks, etc. in this publication does not imply, even in the absence of a specific statement, that such names are exempt from the relevant protective laws and regulations and therefore free for general use.

The publisher, the authors, and the editors are safe to assume that the advice and information in this book are believed to be true and accurate at the date of publication. Neither the publisher nor the authors or the editors give a warranty, expressed or implied, with respect to the material contained herein or for any errors or omissions that may have been made. The publisher remains neutral with regard to jurisdictional claims in published maps and institutional affiliations.

This Springer imprint is published by the registered company Springer Nature Switzerland AG  
The registered company address is: Gewerbestrasse 11, 6330 Cham, Switzerland

Paper in this product is recyclable.

# Contents

<b>Integrated Heat Recovery of Waste Gases and Ventilation Emissions in a Multilayer Plate Heat Exchanger</b> .....	1
Aleksy Burtsev, Vladimir Yezhov, Natalia Semicheva, Nikita Perepelitsa, and Polina Akulshina	
<b>Calculation of the City Functions Realizability Indicator as a Tool for Deciding on the Rational Provision of a Land Plot for Construction</b> .....	9
Lilia Tchaikovskaya, Aleksei Shleenko, and Vladislav Pakhomov	
<b>Non-equilibrium and Nonlinear Processes in Robustness Potential Evaluation of Reinforced Concrete Structural Systems in Ultimate States</b> .....	19
Natalia Androsova, Vitaly Kolchunov, and Sergey Emelyanov	
<b>Reliability of Methods of Calculation of Heating Systems for Digital Model</b> .....	31
Yulia Elistratova, Artem Seminenko, Dmitry Elistratov, Roman Sheps, and Artem Umerenkov	
<b>Four-Wheel Drive Vehicle Optimum Control with a Partial Failure It's Drives</b> .....	41
Tatiana Kruglova, Michael Shoshiashvili, and Alexander Vlasov	
<b>Heat Pump Unit in Heating and Air Recuperation of Premises</b> .....	55
Pavel Orlov, Tat'yana Il'ina, Maksim Kolesnikov, Alina Echina, and Artem Umerenkov	
<b>Study of Composition and Characteristics of Wood-Gypsum Composite</b> .....	65
Timofey Gorokhov, Aleksander Erofeev, Nikita Kovalev, Sergey Gorokhov, and Sergey Emelyanov	

<b>Optimization of the Composition of Cement Composites</b> .....	73
Tatiana Elchishcheva, Ekaterina Abramova, Irina Erofeeva, Viktor Afonin, Vladislav Moiseev, and Alexei Atmanzin	
<b>Hydrodynamic Model of Stationary Drilling Fluid Flow in a Cylindrical Pipeline</b> .....	85
Boris Kumitskiy, Egor Aralov, Natalia Savrasova, Natalia Semicheva, and Victor Budnikov	
<b>Reference Beam Method for Determining Thermal Fluctuation Constants</b> .....	93
Aleksander Erofeev, Timofey Gorokhov, Sergey Emelyanov, and Ekaterina Pakhomova	
<b>Strength and Deformability of a Complex-Stressed Reinforced Concrete Element Based on the Plasticity Theory of G. A. Geniev</b> .....	103
Ngoc Tuyen Vu and Natalia Fedorova	
<b>Results of the Studies of Morphology and Granulometric Composition of Electro Erosive Tungsten-Free Hard-Alloy Powder Material</b> .....	115
Boris Sabelnikov, Alexey Simonov, and Ekaterina Ageeva	
<b>Results of X-Ray Studies of Electro Erosive Tungsten-Free Hard-Alloy Powder Material</b> .....	123
Boris Sabelnikov, Anton Alfimov, and Ekaterina Ageeva	
<b>Justification of Strengthening of Reinforced Concrete Structures of an Industrial Building with Composite Materials</b> .....	129
Vladimir Rimshin and Ekaterina Ketsko	
<b>Determination of the Volume of Air Entering Through Leaks into Aspiration Shelters</b> .....	139
Alexander Goltsov, Vitaly Kireev, and Ivan Pankov	
<b>Determination of Aerodynamic Coefficients in the Design of Buildings</b> .....	149
Vladimir Rimshin and Pavel Truntov	
<b>Effects of Glass and Plastic Additives on the Physical, Mechanical and Strength Characteristics of Concrete</b> .....	157
Alexey Bulgakov, Dmitrii Mishin, and Klaus Holschemacher	
<b>Reinforcement Methods for Timber Closed Lattice Vaults</b> .....	167
Nadezhda Tsaritova, Anastasia Shtankevich, Oksana Osipova, Igor Kosogov, and Alexey Bulgakov	
<b>Study of the Concrete Resistance to the Action of Anti-Icing Agents</b> .....	175
Alexey Bulgakov, Jens Otto, and Viacheslav Aseev	

<b>One of the Options for Using an Integrated Air Heater in Heat Supply Systems</b> .....	183
Aleksey Burtsev, Dmitry Tyutyunov, Alexander Burtsev, and Polina Akulshina	
<b>Development of an Electromagnetic Monitoring System for Urbanized Areas Near Power Lines</b> .....	193
Alexey Bulgakov, Jens Otto, and Pavel Maltsev	
<b>Deflections and Free Vibrations of Circular Isotropic Plates of Thickness Varying in Accordance with a Parabola</b> .....	203
Andrey Turkov, Kirill Marfin, Elena Finadeeva, and Sergey Poleshko	
<b>The Use of GIS Systems as a Decision-Making Tool for the Placement of Urban Development Objects</b> .....	213
Yana Zolotukhina, Ekaterina Prokshits, Olga Sotnikova, and Vladislav Pozdnyakov	
<b>Substantiation of Criteria for Supported Decision-Making in Urban Zoning on the Basis of the Concept of Sustainable Development</b> .....	223
Ekaterina Prokshits, Yana Zolotukhina, Olga Sotnikova, and Olga Mischenko	
<b>Truth May not Be Self-Evident but It is Demonstrable: The Case for the Construction of a Touristic Project at Ramla l-Hamra, Gozo</b> ....	237
Lino Bianco	
<b>Justification of the Heat Network Project Based on the Simulation of Hydraulic Models When Connecting Consumers</b> .....	259
Dmitry Kitaev, Svetlana Tulskaya, and Tatiana Polivanova	
<b>Control of Structure Formation of Reaction Powder Concretes by Triboelectrization</b> .....	269
Arsen Avakyan, Kirill Protsenko, Irina Erofeeva, Elita Balathanova, Alexey Bulgakov, and Wen-der Yu	
<b>Rational Design of Composite Strengthening of Reinforced Concrete Elements for Experimental Research</b> .....	281
Vladimir Rimshin and Pavel Amelin	
<b>Modeling of Reinforced Concrete in the “LIRA” Intelligence for the Problem of Crack Opening</b> .....	291
Vladimir Kolchunov	
<b>Experimental Investigation of RC Frame with Sway Columns Under Corner Column Removal Scenario</b> .....	313
Sergey Savin, Natalia Fedorova, and Pavel Korenkov	

<b>Energy Consumption Analysis During the Life Cycle of Buildings in Palestine</b> .....	321
Elena Gorbaneva, Elena Vinogradova, Mahmoud A. M. Hamdan, and Munther M. H. Abuasad	
<b>Failure Mechanism of Reinforced Concrete Frames Under Accidental Impacts</b> .....	333
Pavel Korenkov and Sergey Fedorov	
<b>Experimental Study of the Survivability of Monolithic Reinforced Concrete Frames</b> .....	343
Vitaly Kolchunov and Olesya Bushova	
<b>Analysis of Heat and Moisture Damage of Enclosing Structures Based on Contactless Diagnostics</b> .....	351
Margarita Tselyaritskaya, Yulia Pashchenko, Olga Sotnikova, and Vladislav Pakhomov	
<b>Investigation of Methods and Algorithms for Predicting Sound Insulation Characteristics of Prefabricated Enclosing Structures</b> .....	359
Yulia Pashchenko, Margarita Tselyaritskaya, Semyon Podvalny, and Daniil Fedyanin	
<b>Design and Calculation of Multifunctional Canopies in the Form of Shallow Shells</b> .....	373
Alexander Kolesnykov, Tatyana Tsurik, Sofya Kurakina, and Ksenia Litvinova	
<b>The Influence of Operational Factors on the Thermal Conductivity of Polystyrene Foam Boards</b> .....	385
Pavel Monastyrsev, Oleg Evdokimtsev, and Mikhail Loktionov	
<b>Comparative Analysis of Enclosing Facade Structures in Terms of Energy Efficiency</b> .....	395
Anastasiia Grokhovskaia and Daria Nemova	
<b>Changes in the Heating Period Parameters for the Belgorod Region in the Context of Global Warming</b> .....	409
E. O. Sheremet and A. S. Seminenko	
<b>Structural Construction Optimization of Fire Protection Systems</b> .....	417
Oleg Kochnov, Svetlana Sazonova, Alexey Kochegarov, Pavel Korkunov, and Roman Yemelyanov	
<b>Application of the White Noise Generator to Evaluate the System for Modeling the Impact of Soil on the Working Body of the Bulldozer</b> .....	429
Alexey Bulgakov, Georgii Tokmakov, and Wen-der Yu	

<b>The Study of the Suction Activated by the End Supply Jet from Plasma Cutting Area</b> .....	437
Oleg Zaitsev, Natalia Semicheva, Andrey Ishutin, Yuri Sivachenko, and Sergey Egorov	
<b>A Technique for Determining a Polymer Product Temperature Time Dependence Under Process Air Cooling</b> .....	447
Evgeny Umerenkov, Elina Umerenkova, Ekaterina Savelyeva, and Victor Budnikov	
<b>Some Aspects of Heat Accumulators Application in Thermal Power Engineering</b> .....	457
Evgeny Umerenkov, Elina Umerenkova, Ekaterina Savelyeva, and Rostislav Markov	
<b>Device for Extracting Water from Atmospheric Air</b> .....	465
Adylbek Akmatov and Olga Volichenko	
<b>Optimization of the Technological Process of Polymer Concrete Processing with a Change in the Magnetic Field</b> .....	473
Andrey Matrosov, Viktor Afonin, Ekaterina Matrosova, and Ekaterina Pakhomova	

# Integrated Heat Recovery of Waste Gases and Ventilation Emissions in a Multilayer Plate Heat Exchanger



Aleksey Burtsev , Vladimir Yezhov , Natalia Semicheva ,  
Nikita Perepelitsa , and Polina Akulshina 

**Abstract** One of the main problems in the operation of ventilation and air conditioning systems is the low efficiency of using low-potential heat emitted together with the fluxes of exhaust gases and ventilation emissions from the premises of industrial enterprises, public, administrative, residential buildings and structures. To solve the above problem in modern ventilation and air conditioning systems, heat recuperators and heat exchangers of various designs are used, while plate recuperators are the most effective and widespread. The main characteristic of a plate heat exchanger is the amount of heat transferred through a unit of heat exchange surface area at a temperature difference—the heat transfer coefficient. In order to increase the efficiency of heat exchange of plate heat exchangers, various methods of intensifying the heat transfer process are used, one of which is the installation of turbulators of various shapes and types of their location. This article presents the results of experiments conducted on a complex multilayer plate heat exchanger with integrated Peltier elements and cylindrical turbulators installed in a staggered and corridor arrangement, which allows to utilize low-potential heat while simultaneously obtaining thermoelectricity. The aim of the work is an experimental study of the temperature regime in the intersectional space of a complex multilayer plate heat exchanger during the utilization of waste gas heat and ventilation emissions for heating supply air and associated production of thermoelectricity. An original design of a complex multilayer plate heat exchanger is proposed. Experimental studies have been carried out at a fixed coolant velocity and air flow temperature, graphs of the dependences of thermoelectricity generation on the operating time of the experimental installation have been constructed. Due to the use of cylindrical turbulators, turbulence of flows increases, as a result of this, the heat transfer process is intensified with the associated production of thermoelectricity. The high efficiency of using a complex multilayer plate heat exchanger, turbulators with a staggered arrangement in comparison with a corridor and without their installation in the design of the cooling system has been established. The resulting electricity can be used for additional heating of the supply air or to ensure the autonomous operation of the automation and control system of the ventilation unit.

---

A. Burtsev (✉) · V. Yezhov · N. Semicheva · N. Perepelitsa · P. Akulshina  
Southwest State University, 94, 50 Let Oktyabrya Ul., Kursk 305040, Russia

**Keywords** Recuperator · Utilization · Heat transfer · Thermoelectricity · Intensification

## 1 Introduction

One of the main problems in the operation of ventilation and air conditioning systems is the low efficiency of using low-potential heat emitted together with the fluxes of exhaust gases and ventilation emissions from the premises of industrial enterprises, public, administrative, residential buildings and structures. To solve the above problem, modern ventilation and air conditioning systems use heat recuperators and heat exchangers of various designs, while plate recuperators are the most effective and widespread. The main characteristic of a plate heat exchanger is the amount of heat transferred through a unit of heat exchange surface area at a temperature difference—the heat transfer coefficient, the increase of which makes it possible to increase the efficiency of heat exchange, as a consequence, to reduce the temperature of exhaust gases and ventilation emissions, therefore, the task of intensifying heat transfer is relevant.

Modern plate heat recuperators, although they have a sufficiently high heat transfer coefficient of the heat exchange wall, do not allow deep utilization of low-potential heat simultaneously generating thermoelectricity to ensure autonomous operation of the ventilation unit.

There are various methods of intensifying the heat transfer process:

- intensification due to the use of finning of the walls of the recuperator;
- intensification by changing the design and shape of the surface of the heat exchange walls;
- intensification through the use of various forms of swirlers.

These methods are widely presented in the studies of A.S. Gorshenin, A.A. Zhukauskas, A.S. Sukomel and others [1–3].

The disadvantage of such methods is the lack of the possibility of complex utilization of low-potential heat of waste gases and ventilation emissions with the associated production of thermoelectricity.

## 2 Materials and Methods

Based on the conducted literature and patent search, an original experimental installation was developed—a complex multilayer plate heat exchanger [4, 5], consisting of two blocks: a plate heat exchanger and an adsorber filter block [6]. The plate heat exchanger is made of multilayer sections consisting of aluminum walls with Peltier semiconductor thermoelectric elements embedded in them [7]. To intensify the reception and removal of heat, T-shaped aluminum radiators are installed on top

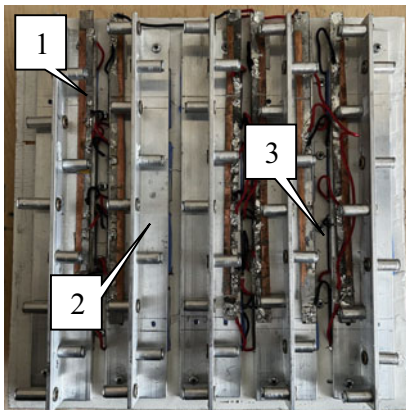
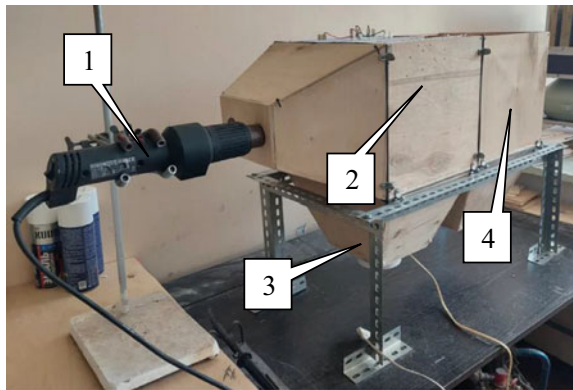


of the Peltier elements, on which cylindrical turbulators are installed in a staggered arrangement [8]. At the temperature difference created on the hot and cold sides, an electric current is generated, which is collected, converted, accumulated and can be used for autonomous power supply of fans or automation and control systems of the ventilation system [9, 10].

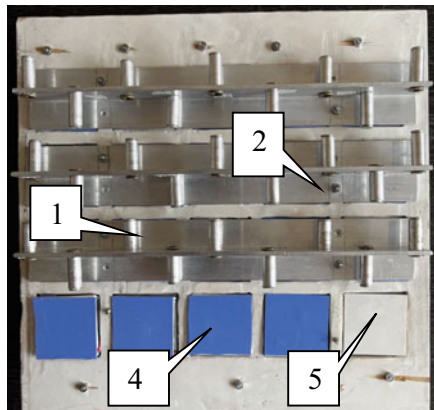
A general view of the experimental setup is shown in Fig. 1a. The type of thermoelectric sections is shown in Fig. 1b. Figure 2 shows a thermoelectric section with a staggered arrangement of turbulators. Figure 3 shows a thermoelectric section with a corridor arrangement of turbulators [11–13].

Experimental studies were carried out at the maximum air flow velocity at the outlet of the heater—3.4 m/s. The maximum air flow velocity at the outlet of the supply fan is 2.0 m/s. Measurements were made through: 1, 2, 3,5, 5, 10, 15, 30,

**Fig. 1** Test unit: **a**—overall view; **b**—hot air flow channels: 1—heater; 2—multilayer plate heat exchanger; 3—supply valve; 4—cleaning unit filled with blast furnace slag



(a)



(b)

**Fig. 2** Thermoelectric section with staggered arrangement of turbulators: **a**—cold side view; **b**—hot side view: 1—radiator; 2—turbulators; 3—current leads; 4—thermal pad; 5—Peltier element

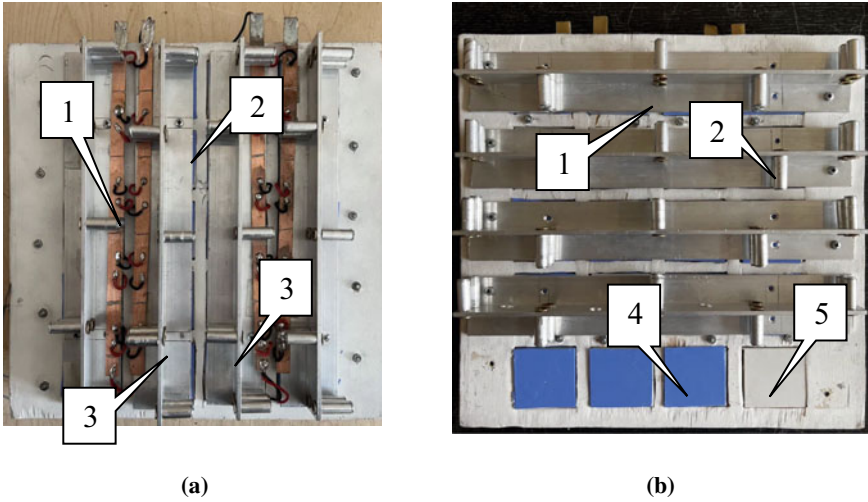


**Fig. 3** Thermoelectric section with corridor arrangement of turbulators: **a**—type of cold side; **b**—type of hot side: 1—radiator; 2—turbulators; 3—current outlets; 4—thermal pad; 5—Peltier element

60, 120 min. Dry air heated in the heater, with a temperature at the inlet to the CMPT of 45 °C, at the outlet of 25 °C, was used as the removed vent ventilation heat. As a heated medium, air was used, taken by a fan from a laboratory room with a temperature of 20 °C. Peltier TES1-12,712 semiconductor elements with the following technical characteristics are used in the installation: thermal EMF coefficient  $\alpha = 12.97 \cdot 10^{-3}$  V/K; Q factor  $Z = 2.8 \cdot 10^{-3}$  K<sup>-1</sup>; electrical conductivity coefficient  $\sigma = 8 \cdot 10^4$  Ohms<sup>-1</sup>·m<sup>-1</sup>; thermal conductivity coefficient of the element  $\lambda = 146$  W/m<sup>2</sup>·°C. The housing and walls of the CMPT are made of aluminum plates with a thermal conductivity coefficient  $\lambda = 221$  W/m<sup>2</sup> °C and a thickness of 4 mm. The Peltier thermoelectric element has dimensions of 40 × 40 mm.

The aluminum radiator of the Peltier element cooling system is made in the form of a T-shaped aluminum profile with a base length of 300 mm and a width of 40 mm. Radiator height is 25 mm, radiator thickness is 3.0 mm. Cylindrical turbulators are made in the form of aluminum rods with a length of 18 mm and a diameter of 8 mm.

### 3 Results

Figures 4 and 5 show the results of a thermal imaging study using a staggered arrangement of turbulators (Fig. 4a) and a corridor (Fig. 5a). Figures 4b, 5b show the temperatures of the points on the surface of the multilayer wall of the recuperator.

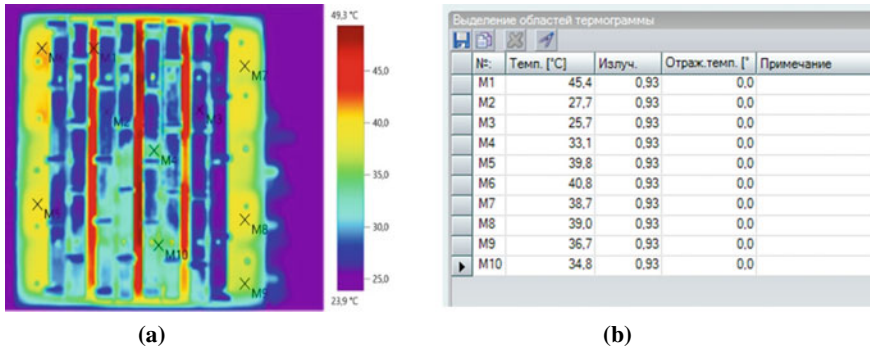


Fig. 4 Thermal diagram of the CMPT wall with a staggered arrangement of turbulators

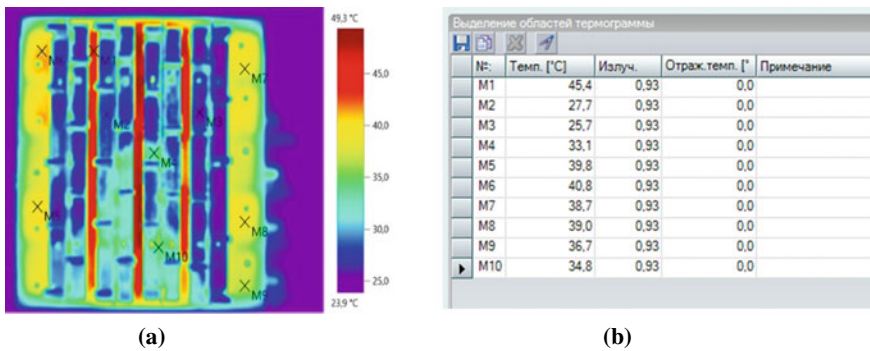


Fig. 5 Thermal diagram of the CMPR wall with a staggered arrangement of turbulators

### 4 Discussion

As can be seen from Fig. 6, in the first 5 min of the experiment, the strongest increase in voltage generation indicators is observed, which is caused by the "heating up" of the system. Starting from the 6th to the 30th minute, an increase of 11.2–11.9% is observed, but after, during 1.5 h of the experiment, due to the installation going into stationary mode and the establishment of thermal balance, the voltage indicators increase by only 0.5%.

Such indicators are caused by the installation of turbulators with a staggered arrangement on the walls of radiators. Vortices are formed in the plate heat exchanger, intensifying the heat transfer process, simultaneously obtaining thermoelectricity to ensure autonomous power supply of ventilation equipment.

When installing turbulators with a corridor arrangement, the voltage indicators after 30 min of operation decrease from 1.94 V to 1.46 V to 32.8% (Fig. 6), which is caused by the creation of additional aerodynamic drag, as a result, there is a decrease in the consumption of hot and cold air—there is overheating of the recuperator and,

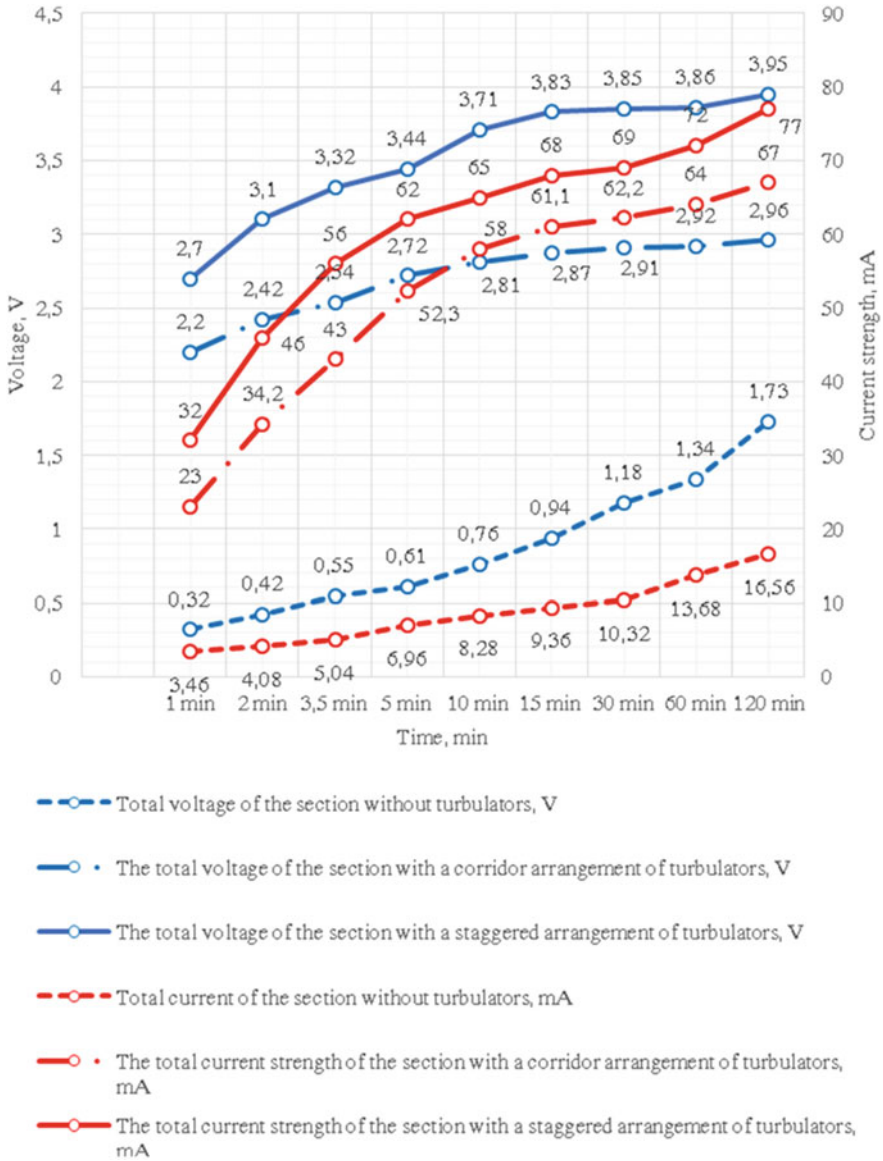


**Fig. 6** Experimental data on the generation of thermoelectricity in a recuperator with a different arrangement of turbulators

as a consequence, a decrease in the production of thermal EMF after 30 min of operation from 3.85 V to 2.91 V, and after 120 min of operation from 3.87 V to 2.3 V.

Thus, as a result of the experiment, the staggered arrangement of the turbulators is more efficient than the corridor one: the heat transfer coefficient of the multilayer wall of the recuperator increases from  $3.55 \text{ W/m}^2 \cdot ^\circ\text{C}$  to  $4.11 \text{ W/m}^2 \cdot ^\circ\text{C}$ —an increase of 15.7%; efficiency from 2.68 to 9.17% [9.10]; the indicator of the amount of heat by the amount of thermal EMF output has increased more than 3.4 times (from 72.06 W to 245.6 W). The same amount of heat is transferred to cold air through the multilayer wall of the recuperator. The total amount of heat utilized varies from 208.1 to 709 W. The efficiency of the recuperator when operating without turbulators is 20.8%, with a corridor arrangement of 43.4%, with a staggered arrangement of 71.0%.

Based on the conducted experimental studies, a high efficiency of using a multilayer plate heat exchanger with a staggered arrangement of cylindrical turbulators in the design of the cooling system has been established.

This arrangement makes it possible to ensure the efficiency of the installation more than 2 times higher than when installing a corridor type and more than 3.5 times more than without installing turbulators at all. Also, the amount of heat per the amount of thermoelectricity generation with a staggered arrangement is 245.6 W, which is more than 1.5 times higher than with a corridor arrangement and 3.5 times higher than without the installation of turbulators.

Based on experimental data, electricity generation at an experimental installation with a heat exchange area of  $1.3 \text{ m}^2$ , a cross-sectional area of  $0.048 \text{ m}^2$ , a hot flow rate of  $3.0 \text{ m/s}$ , an air flow through a heat exchanger of  $518.4 \text{ m}^3/\text{h}$ , electricity generation was 1.8 W.

For example, a typical plate heat exchanger with a capacity of  $5000 \text{ m}^3/\text{h}$  with a heat exchange area of  $25 \text{ m}^2$ , used in a ventilation system, when equipped with cylindrical turbulators and Peltier elements, provides a power output equal to 250 W. At the same time, the fan power for this standard size is 120 W.

Thus, the electricity generated is sufficient to ensure the autonomous operation of the ventilation system.

## 5 Conclusions

As a result of the conducted research, a design of a complex multilayer plate heat exchanger is proposed, the feature of which is the use of flat semiconductor thermoelectric converters (Peltier elements) embedded in the heat exchange walls with increased turbulence of air flows due to the installation of cylindrical turbulence.

Experimental studies of temperature and air conditions in the intersectional space of the CMPR have been carried out.

Due to the installation of cylindrical turbulators on radiators, the heat exchange area and turbulence of flows increases, as a result of which the heat transfer process is intensified with the associated production of thermal EMF.

The high efficiency of using cylindrical turbulators with a staggered arrangement in the design of the KMPT cooling system in comparison with the corridor and without their installation has been established.

The received electricity can be used to ensure the autonomous operation of the ventilation unit.

## References

1. Metallidou CK, Psannis KE, Egyptiadou EA (2020) Energy efficiency in smart buildings. *IoT approaches*. IEEE Access 8:63679–63699. <https://doi.org/10.1109/ACCESS.2020.2984461>
2. Sadeghi HM, Babayan M, Chamkha A (2020) Investigation of using multi-layer PCMs in the tubular heat exchanger with periodic heat transfer boundary condition. *Int J Heat Mass Transf* 147. <https://doi.org/10.1016/J.IJHEATMASSTRANSFER.2019.118970>
3. Arasteh H, Mashayekhi R, Ghaneifar M, Toghraie D, Afrand M (2020) Heat transfer enhancement in a counter-flow sinusoidal parallel-plate heat exchanger partially filled with porous media using metal foam in the channels' divergent sections. *J Therm Anal Calorim* 141(5):1669–1685. <https://doi.org/10.1007/S10973-019-08870-W>
4. Fu Z, Liang X, Li Y, Li L, Zhu Q (2021) Performance improvement of a PVT system using a multilayer structural heat exchanger with PCMs. *Renew Energy* 169:308–317. <https://doi.org/10.1016/J.RENENE.2020.12.108>
5. Zhu X, Haglind F (2020) Relationship between inclination angle and friction factor of chevron-type plate heat exchangers. *Int J Heat Mass Transf* 162. <https://doi.org/10.1016/J.IJHEATMASSTRANSFER.2020.120370>
6. Gusew S, Stuke R (2019) Pressure drop in plate heat exchangers for single-phase convection in turbulent flow regime: experiment and theory. *Int J Chem Eng* 2019:1–11. <https://doi.org/10.1155/2019/3693657>
7. Kapustenko P, Klemeš JJ, Arsenyeva O, Fedorenko O, Kusakov S, Bukhhalo S (2020) The utilisation of waste heat from exhaust gases after drying process in plate heat exchanger. *Chem Eng Trans* 81:589–594. <https://doi.org/10.3303/CET2081099>
8. Tyutyunov D, Burtsev A, Perepelitsa N, Burtsev A (2023) The mathematical model of automated control of heat flows in the supply and exhaust ventilation system. In: Vatin N, Pakhomova EG, Kukaras D (eds) *Modern problems in construction*. Lecture notes in civil engineering, vol 287. Springer, Cham, pp 177–187. [https://doi.org/10.1007/978-3-031-12703-8\\_18](https://doi.org/10.1007/978-3-031-12703-8_18)
9. Yezhov V, Semicheva N, Burtsev A, Perepelitsa N (2023) The mathematical model of a multi-layer wall of a plate heat exchanger. In: Vatin N, Pakhomova EG, Kukaras D (eds) *Modern problems in construction*. Lecture notes in civil engineering, vol 287. Springer, Cham, pp 1–11. [https://doi.org/10.1007/978-3-031-12703-8\\_1](https://doi.org/10.1007/978-3-031-12703-8_1)
10. Yezhov VS, Semicheva NE, Burtsev AP, Brezhnev AV, Perepelitsa NS (2022) Experimental research of main characteristics in a complex multi-layer plate heat exchanger. *IOP Conf Ser: Mater Sci Eng* 1242(1):012042. <https://doi.org/10.1088/1757-899X/1242/1/012042>
11. Ezhov V, Semicheva N, Tyutyunov D, Burtsev A, Perepelitsa N (2021) Version of a mathematical model of purge ventilation system with a complex recuperative heat exchanger. *J Appl Eng Sci* 19(1):246–251. <https://doi.org/10.5937/JAES0-30068>
12. Yezhov VS, Semicheva NE, Tyutyunov DN, Burtsev AP, Perepelitsa NS, Burtsev AP (2021) Mathematical model for automated heat flow control of an energy efficient ventilation system. *Proc Southwest State Univ* 25(1):38–52. <https://doi.org/10.21869/2223-1560-2021-25-1-38-52>
13. Yezhov V, Semicheva N, Burtsev A, Perepelitsa N (2021) Experimental calculation of the main characteristics of thermoelectric EMF source for the cathodic protection station of heat supply system pipelines. In: *Advances in intelligent systems and computing*, vol 1259. AISC, pp 225–237. [https://doi.org/10.1007/978-3-030-57453-6\\_19](https://doi.org/10.1007/978-3-030-57453-6_19)

# Calculation of the City Functions Realizability Indicator as a Tool for Deciding on the Rational Provision of a Land Plot for Construction



Lilia Tchaikovskaya , Aleksei Shleenko , and Vladislav Pakhomov 

**Abstract** The problem of providing land plots for the construction of specific real estate objects existing in the modern world without taking into account the potential impact of these objects existence on the state of the urban environment and, as a result, on the possibility of satisfying the rational needs of city residents has led to the unjustified placement of some shopping centers on the modern cities territory. As a solution to the problem, this article proposes to provide land plots for construction based on calculating the realizability of the functions of a biosphere-compatible city in the territory after the construction of a specific real estate object on the requested land plot.

**Keywords** Selection of a site for the real estate object construction · Meeting rational needs · Life quality of the urban population · A criterion of the urban environment state

## 1 Introduction

Each real estate property goes through some life cycle stages during the period of its existence, the initial of which is pre-project preparation [1]. As part of the pre-project preparation, the choice of a land plot for construction can be considered as a key point, because of not only its investment attractiveness but also the further state of the urban environment, as well as the existence possibility of such an object, depends on the location of the real estate object, the construction of which is supposed to be

---

L. Tchaikovskaya (✉) · A. Shleenko · V. Pakhomov  
Southwest State University, 94, 50 Let Oktyabrya Ul., Kursk 305040, Russia  
e-mail: [lili-zubkova@mail.ru](mailto:lili-zubkova@mail.ru)

A. Shleenko  
e-mail: [shleenko77@mail.ru](mailto:shleenko77@mail.ru)

V. Pakhomov  
e-mail: [vlad-pakhomov-03@mail.ru](mailto:vlad-pakhomov-03@mail.ru)



carried out, since the options for using land plots within the boundaries of settlements are strictly established by urban planning regulations of territorial zones, fixed by the rules of land use and development [2]. The key factor for a real estate developer when choosing a land plot for construction is the potential benefit that the constructed property will bring. At the same time, in most cases, neither the developer nor the authorities responsible for the formation and provision of land plots for construction do not assess how environmentally safe [3] favorable and useful the construction of a particular property is for residents of a quarter, a micro district and even an entire city.

## 2 Materials and Methods

The problem of providing land plots for the object construction without taking into account its potential impact on the state of the urban environment and, as a consequence, on the possibility of satisfying the rational needs of city residents is relevant for most urbanized areas. However, the human environment must be biosphere-compatible, safe and favorable [4], cities must fully satisfy the rational needs of their inhabitants [5, 12] since if any of the person needs are not satisfied, then harmonious existence and development is impossible. All human needs are reflected in Maslow's pyramid [6], and the relationship between human needs and city functions through which they can be satisfied is described in [7, 16]. One of the options for solving this problem is the introduction for the authorities authorized to dispose of land plots in state or municipal ownership of a mandatory preventive assessment of the impact of the projected object on the state of the urban environment after its commissioning. In this case, the methodology for determining the indicator of the biosphere-compatible city functions implementation [8] can be used as a tool, while the micro district in which the projected object will exist, and the same micro district, but in the case of the other objects construction, should be taken as the area under study. For example, if a real estate developer applies for obtaining a land plot for the construction of a shopping centre, the authorized body must determine the city's functions realizability indicator in the case of the construction of this real estate object, as well as in the case of the social sphere object construction on the requested land plot (for example, a hospital, a palace of creativity, etc.) or residential real estate. The excess of the city functions realizability indicator when providing a site for the construction of a specific real estate object over the city functions realizability indicator with other options for using the land plot indicates the need to construct an object of this group (residential, industrial building, trade object, social infrastructure object, etc.), and should be the basis for refusal to provide a land plot for the construction of a property that is not included in this group. The excess of the values must be small because, within such an assessment framework, the contribution of just one real estate object to the city functions realizability indicator in the territory of an entire micro district will be reflected. However, when applying such an assessment, the possibility of providing adjacent or located near land plots for similar objects construction will be





**Fig. 1** Panoramas of Kursk' streets

excluded, as was done, for example, on the st. Studencheskaya or st. Kryukova in Kursk (Fig. 1), where two similar shopping centers were built close to each other. The indicator of the implementation level of biosphere-compatible city functions must be a criterion of the urban environment state based on the adopted biosphere compatibility paradigm [8, 19–21], therefore, the calculation of this indicator on an ongoing basis, among other things, will provide systematic monitoring of urban environment state.

### 3 Results and Discussion

Using the methodology for determining the biosphere-compatible city functions realizability indicator, described in [8, 10, 17], we calculate the city functions realizability indicator within the Волокно micro district in Kursk, assuming that the land plot with cadastral number 46:29:103,126:5, on which the Пятёрочка shopping center is located (Fig. 1), is just requested for the construction of the said shopping centre.

For comparison, let us assume that this land plot can be provided for the construction of a children's sports school or for the placement of an apartment building, which is possible, since, by [9], this land plot is located in the zone "Ж-4"—for residential development high number of stories (9 floors or more). The methodological basis for a quantitative assessment of city functions realizability level on the territory of the micro district under study will be an expert opinion on the state of its infrastructure.

The systematization of micro district infrastructure components in the implementation of the functions of a biosphere-compatible city, as well as the values of the coefficients from the contribution of the component C1—Dwelling houses, will be taken by the works [11, 17] (Tables 1, 2).

Similarly, we will calculate for other city functions.

#### Function F 2—Entertainment and Recreation

Component C1—cafes and restaurants, C2—Fitness centers and sports clubs, C3—Leisure and recreation centers, cinemas.

The micro district has a cafe, a sports centre, children's art schools, the city cultural center Лира, but there is no children's sports centre where you can practice various sports, including figure skating. There is a cinema, libraries, therefore, we will take the following values of the realizability and availability coefficients of the function  $\Phi_2$ :

- (a) During the construction of a shopping centre:  
 $\beta_{2,1} = 0,283; \alpha_{2,1} = 0,378.$
- (b) During the construction of a children's sports school:  
 $\beta_{2,1} = 0,315; \alpha_{2,1} = 0,378.$
- (c) During the construction of an apartment building:  
 $\beta_{2,1} = 0,283, \alpha_{2,1} = 0,378.$

**For Functions F3—Power, F4—Mercy, F5—Knowledge, F6—Creativity, F7—Connection with nature** the construction of any real estate object on the considered land plot will not lead to a significant change in the values of the realizability factors and the availability of the function, and therefore we take them equal for each object planned for construction.

On the micro district territory, there are post offices and police departments. The micro district is fully provided with schools, kindergartens, and a college. On the Волокно territory there is an exhibition centre, music and art schools, parks, squares, massive green spaces, alleys and other interspersed natural landscapes. In the immediate vicinity, there is a river and a lake. At the same time, unfortunately, most of the apartment buildings located on the Волокно territory do not meet the requirements for ensuring the availability of facilities for the low-mobility group of the population (LGP): the modern period is characterized by increased consumer requirements for product quality, including the design of dwellings [15], and some houses were built before the introduction of accessibility requirements for LGP. At the same time, shopping centers and other public buildings meet the specified requirements, therefore we will assume that:

$\beta_{3,1} = \beta_{5,1} = \beta_{6,1} = \beta_{7,1} = 0,378; \alpha_{3,1} = \alpha_{4,1} = \alpha_{5,1} = \alpha_{6,1} = \alpha_{7,1} = 0,378,$   
and  $\beta_{4,1} = 0,189.$

Taking into account the accepted values and based on the formula obtained in [7], we calculate the integral of city functions realizability indicators on the Волокно micro district territory:

**Table 1** To the assessment of city function realizability parameter F1—Life support within the micro district Волокно in the Kursk city

Function	Component	Implementation coefficient in case of construction on a land plot 46:29:103,126:5			Notice
	Indicators	Shopping center	Children's sports school	Apartment building	
F1—Life support	Component C1—residential buildings				
	Housing provision level	0,283	0,283	0,378	The micro district has been built up for a long ago, the sale of apartments is carried out inactive, but there is a demand for housing, new houses construction is not underway
	Technical condition level	0,038	0,038	0,038	The construction of a new house will not have a significant impact on houses technical condition levels within the entire micro district, the level will remain average [12, 13]
	Houses service life	0,076	0,076	0,076	The construction of a new house will not have a significant impact on the useful life of a houses within the entire micro district
	House duplication level	0,113	0,113	0,113	Buildings are not duplicated
	Complex indicator of the component in the implementation of city investigated function	0,128	0,128	0,151	
	Component C2—Infrastructure				
Infrastructure provision level	0,378	0,378	0,378	The level of infrastructure provision is high, there is a powerful transport link with all city areas	

(continued)

**Table 1** (continued)

Function	Component	Implementation coefficient in case of construction on a land plot 46:29:103,126:5			Notice
	Indicators	Shopping center	Children's sports school	Apartment building	
	Technical condition level	0,038	0,038	0,038	Infrastructure technical condition level is average [14]
	Lifetime	0,076	0,076	0,076	Lifetime is average
	Complex indicator of the component in the implementation of the investigated function of the city	0,164	0,164	0,164	
Component C3—Health service					
	Availability of health care institutions, diagnostic clinics (a comprehensive indicator of the component in the implementation of city investigated function)	0,378	0,378	0,378	The micro district is fully provided with health care services
Component C4—Grocery and non-grocery stores					
	Availability of trade objects (a complex indicator of the component in the implementation of the investigated function of the city)	0,378	0,378	0,378	On the territory of the micro district, there are a large number of small supermarkets, as well as the shopping center Европа-9, therefore the area is fully provided with trade objects, therefore, the construction of a new shopping center will not affect the value of the indicator of the component
Component C5—communication services					

(continued)

**Table 1** (continued)

Function	Component	Implementation coefficient in case of construction on a land plot 46:29:103,126:5			Notice
	Indicators	Shopping center	Children’s sports school	Apartment building	
	Availability of communication infrastructure (a complex indicator of the component in the implementation of the investigated function of the city)	0,378	0,378	0,378	Internet is in every house, cellular communication works without interference
Component C6—vehicles location					
	Availability to open and closed parking lots, garages (a complex indicator of the component in the implementation of the city investigated function)	0,283	0,283	0,283	Provision is at a high level, but in some parts of the micro district there are not enough places to accommodate transport
	City function performance indicator $\Phi 1$	0,285	0,285	0,287	

(a) During the construction of a shopping centre:

$$\xi = \sum_{n=1}^{n=n} \sum_{i=1}^{i=i} \alpha_{in} \beta_{in} / \sum_{n=1}^{n=n} \sum_{i=1}^{i=i} \alpha_{in}^* \beta_{in}^* = 0, 856;$$

(b) During the construction of a children’s sports school:

$$\xi = \sum_{n=1}^{n=n} \sum_{i=1}^{i=i} \alpha_{in} \beta_{in} / \sum_{n=1}^{n=n} \sum_{i=1}^{i=i} \alpha_{in}^* \beta_{in}^* = 0, 866;$$

(c) During the construction of an apartment building:

$$\xi = \sum_{n=1}^{n=n} \sum_{i=1}^{i=i} \alpha_{in} \beta_{in} / \sum_{n=1}^{n=n} \sum_{i=1}^{i=i} \alpha_{in}^* \beta_{in}^* = 0, 855.$$

**Table 2** To the assessment of city function accessibility parameter F1—Life support within the microdistrict Волокно» in the Kursk city

Function	Component	Availability coefficient in case of construction on land plot 46:29:103,126:5			Notice
		Shopping center	Children's sports school	Apartment building	
F1: Life support	C1—Residential buildings	0,378	0,378	0,378	Access is fully provided
	C2—Infrastructure	0,378	0,378	0,378	Access is fully provided
	C3—Health service	0,378	0,378	0,378	On the district territory, there is Kursk city hospital № 4
	C4—Grocery and non-grocery stores	0,378	0,340	0,340	Access to some branded stores is limited. access will be provided if the shopping centre is built and these objects are placed in it
	C5—Communication services	0,378	0,378	0,378	Access is fully provided
	C6—Vehicles location	0,340	0,340	0,340	Access is not fully provided
	City function availability coefficient $\Phi_1$	0,371	0,365	0,365	

From the above assessment, it follows that the most rational is the construction of a children's sports school on this land plot, which will create conditions for the residents of the Волокно micro district and the entire Kursk city to meet the needs for physical activity, belonging, achievements and recognition [7, 16]. In addition, an object of spiritual and moral education and development of youth will appear in the city, and additional jobs for highly qualified personnel will be created.

## 4 Conclusion

To substantiate the correct choice of a land plot for building a real estate object, as well as for its competent and expedient provision by state and local authorities, it is possible to calculate the indicator of a biosphere-compatible city function

realizability on the territory of the micro district where the object construction is planned, while several land using options should be considered. The land plot must be provided for the real estate object construction, the existence of which will have a positive impact on the ability to meet the rational needs of the city's residents.

## References

1. GOST R 10.0.03-2019/ISO 29481-1:2016 System of standards for information modeling of buildings and structures. Information modeling in construction. Directory of information exchange. Part 1. Methodology and format [Electronic resource]. Access mode: <https://base.garant.ru/73828150/3e22e51c74db8e0b182fad67b502e640/>
2. Federal Law No. 190-FZ of 29.12.2004 Urban planning code of the Russian Federation [Electronic resource]. Access mode: [http://www.consultant.ru/document/cons\\_doc\\_LAW\\_51040/](http://www.consultant.ru/document/cons_doc_LAW_51040/)
3. Emelyanov SG, Pakhomova EG, Dubrakova RO (2019) Reliability of RC frame-braced systems in dangerous geological conditions. *J Appl Eng Sci* 17(2):245–250. <https://doi.org/10.5937/jaes17-21685>
4. Burenin VS, Ezersky VA, Monastyrev PV (2017) Investigation of modern trends in the design of residential buildings in Russia and abroad. *Arch Time* 5:2
5. Ilyichev VA (2009) Can a city be biospheric compatible and develop a person? *Arch Constr Mosc*, 2(544), 8–13
6. Maslow AH (1999) *Motivation personality*. SPb.: Eurasia
7. Bakaeva NV, Chernyaeva IV, Chaykovskaya LV (2017) Numerical analysis and method of the assessment of the realization of the city functions (by the example of the Russian biggest cities. *Proc Southwest State Univ* 4(73):88–100
8. Il'ichev VA, Emelyanov SG, Kolchunov VI, Gordon VA, Bakaeva NV (2010) Principles of transformation of a city in biosphere compatible and developing the person. *Ind Civ Eng*, 6 (June)
9. The decision of the Kursk City Assembly of October 23, N 388–3-RS On the Rules of land use and development of the municipal formation “The City of Kursk [Electronic resource]. Access mode: [https://kurskadmin.ru/node/1102\\_](https://kurskadmin.ru/node/1102_) (2007)
10. Bakaeva NV, Shishkina IV (2011) Technique of definition of the generalized criteria of the estimation of the condition of the territorial motor transportation system from the position concepts of biospheric compatibility. *Academia Arch Constr* 4:112–117
11. Tchaikovskaya LV, Bakaeva NV (2016) Satisfaction of rational needs through the functions of the city. In: *Sat. mat. II Bryansk International Innovation Forum “Construction-2016”*. Bryansk, pp 146–154
12. Bakaeva NV, Tchaikovskaya LV, Zuleta DP (2020) Toward the construction of a comfort model for urban environment. In: *IOP Conference Series: Materials Science and Engineering. International Conference on Civil, Architectural and Environmental Sciences and Technologies. CAEST 2019. Samara 2019*. Samara: Institute of Physics Publishing
13. Dubrakov SV, Kutsenko OI, Dubrakova KO (2019) The main problems revealed during the inspection of apartment buildings in Kursk after total renovation. *Proc Southwest State Univ* 23:94–102
14. Dubrakov SV, Kutsenko OI, Andrienko VV et al. (2016) Theoretical study of thermal engineering properties of enclosing structures of buildings after reconstruction. In: *Science today: problems and prospects of development: materials of the international scientific and practical conference: in 2 parts, Vologda. Scientific Center “Disput”*. Vologda: LLC “Marker”, pp 36–38
15. Chernyshov EM, Potamoshneva ND, Monastyrev PV, Yartsev VP (2016) Industrial waste recycling for construction purposes as a complex systemic problem. *Issues Mod Sci Pract Voronezh State Univ Arch Civ Eng* 4(62):67–86

16. Bakaeva NV, Chernyaeva IV, Chaykovskaya LV (2017) Numerical analysis and method of the assessment of the realization of the city functions (by the example of the russian biggest cities). In: *Safe and Comfortable city: Collection of Scientific Papers Based on the Materials of the I International Scientific And Practical Conference Of Young Scientists*, Orel, September 29. Orel State University named after I.S. Turgenev, pp 186–191
17. Bakaeva NV, Shishkina IV (2015) Assessment of feasibility of the biosferosovmestimy functions of the city in modern inhabited residential districts. *Proc Southwest State Univ Ser: Eng Technol* 1(14):43–54
18. Bakaeva NV, Chernyaeva IV (2016) Function biosphericcompatibility city and their availability to person. *Biosph Compat: Hum, RegN, Technol* 3(15):63–72
19. Ilyichyov VA (2010) Principles of transformation of a city in biosphere compatible and developing the person. *Ind Civ Eng* 6:3–13
20. Ilyichev VA, Kolchunov VI, Bersenev AV, Pozdnyakov AL (2009) Some points of designing of settlements from the point of biospheric compatibility concept. *Academia Arch Constr* 1:74–80
21. Ilyichyov VA (2014) Biospherical compatibility of nature and human being—the way to systematic solution of global problems. *Strat Priorities* 1(1):42–58



# Non-equilibrium and Nonlinear Processes in Robustness Potential Evaluation of Reinforced Concrete Structural Systems in Ultimate States



Natalia Androsova , Vitaly Kolchunov , and Sergey Emelyanov 

**Abstract** The problems of non-equilibrium and nonlinear processes in the evaluation of reinforced concrete structural systems robustness potential in ultimate states are considered. The definition of concept of “robustness exposition” is given for a quantitative assessment of the robustness potential. A calculation model based on the generalization of the well-known classical relationship between the current relative deficit change rate of the reinforced concrete stress–strain state with respect to each fixed time value is proposed to describe in time non-equilibrium processes of structural materials force resistance depending on the mode and level of loading. On the basis of the linear creep theory, aging materials, an algorithm was developed to determine the measure of creep, corrosion-damaged concrete and reinforced concrete and to determine the parameter “robustness exposition” of a reinforced concrete statically indeterminate structural system, taking into account non-equilibrium and nonlinear processes of its deformation in time. An example of a single-span rigidly clamped reinforced concrete beam calculating the robustness potential from the position of a special limiting state criterion is considered.

**Keywords** Progressive collapse · Robustness potential · Reinforced concrete structures · Creep · Accidental actions

---

N. Androsova (✉) · V. Kolchunov · S. Emelyanov  
Southwest State University, 50 Let Oktyabrya Street, 94, Kursk 305040, Russia  
e-mail: [ramia84@rambler.ru](mailto:ramia84@rambler.ru)

S. Emelyanov  
e-mail: [yz\\_swsu@mail.ru](mailto:yz_swsu@mail.ru)

N. Androsova · V. Kolchunov  
Scientific and Research Institute of Construction Physics of RAASN, Lokomotivny Proezd, 21.,  
Moscow 127238, Russia

N. Androsova  
Orel State University after I.S. Turgenev, Komsomolskaya Street, 95, Orel 302026, Russia

## 1 Introduction

The problem of buildings and structures constructive robustness under accidental actions is currently one of the new directions in the research of building structures. Over the past two decades, some results of theoretical research have been accumulated in the country and abroad to study the reinforced concrete structures resistance during a sudden structural restructuring of a structural system caused by the removal of a bearing element or connection and the establishment of possible patterns of destruction under such an action. However, to date, very few experimental and theoretical researchers have been carried out to solve the problems of maintaining the robustness potential of exploited reinforced concrete structural systems over time, taking into account the accumulation of a non-equilibrium nature damage. Bondarenko [1], Kolchunov [2], Fedorova [3], Savin [4], Tamrazyan [5], Kabantsev [6], Trekin [7], Li [8], Vasanelli [9] and etc. were engaged in separate problems of reinforced concrete structures power resistance under the influence of regime long-term non-equilibrium processes.

Under the term “robustness” of a constructive system in scientific publications, there is no established definition and somewhat different definitions and concepts are used. So, Professor Reiser [10] defines robustness as a property of structures to retain the ability to perform basic functions during emergency actions, preventing an avalanche-like (cascade) development of disturbances and failures.

Nazarov [11] proposes to define robustness as the property of maintaining the overall bearing capacity during local destruction caused by natural and technogenic actions, at least for some time.

In the works of Bondarenko, Kolchunov [2, 12], robustness is understood as the ability of the system to distribute the load between the remaining elements in the damage or weakening event of one of the elements (sudden shutdown of “extra” elements of statically indeterminate systems).

However, all these definitions imply an estimate of robustness under unchanged initial conditions, i.e. for newly designed structures, the robustness of which is calculated without taking into account the operational accumulation of damage and, accordingly, changes in the bearing capacity of the sections of structural elements over time at different values of the operational load and modes of its application. To take into account structures these features in operation when calculating reconstructed objects, in [2] it was proposed, along with the concept of “robustness”, to introduce additionally the concept of “robustness exposition”, which means the duration of the preservation of the building system robustness potential in time with a problem non-equilibrium formulation (overlay in time creep deformations and corrosion damage) to the destructive effects of an aggressive environment with the exclusion from the system of structural elements responsible for the geometric invariability of the structure.

The solution of these problems is associated with the involvement of deformation models based on estimates of concrete creep. Analysis of the concrete creep theories currently existing in Russia and abroad (Arutyunyan [13], Aleksandrovsky [14],

Bondarenko [15], Vasiliev [16], Gvozdev [17], Geniev [18], Kabantsev [6], Maslov [19], Prokopovich [20], Rabotnov [21], Rzhantsyn [22], Sanzharovsky [23], Ulitsky [24], Kharlab [25], Bažant [26], Gilbert [27], Hamed [28] and others) showed that all existing creep theories are phenomenological in nature. Many of them, due to the lack of normalized parameters, cannot currently be brought to a number.

In this regard, to solve the problems under consideration on the robustness potential quantitative assessment of reinforced concrete structural systems in transcendental states, it is advisable to involve the simplest creep rheological models. This approach makes it possible to obtain fairly simple analytical expressions for the robustness exposition criteria and robustness criteria that are convenient for practical use, and most importantly, bring the proposed solutions to a number.

## 2 Materials and Methods

In the theory of structures force resistance, professors Bondarenko V. and Karpenko N. proposed development out-of-stage description in time of force resistance non-equilibrium processes of solid bodies made of structural materials, depending on the mode and level of loading [15]. This model is a non-linear generalization of the well-known classical relationship between the change rate of the current relative deficit of the studied factor value of the solid stress–strain state  $a$  with respect to its each time-fixed value:

$$\frac{d(\Delta C)}{dt} = -\alpha \cdot [\Delta C]^m \quad (1)$$

where  $\Delta C = (C_f - C)/C_f$ —current and limit (fixed) values of concrete creep measure;  
 $t$ —observation time;

$\alpha$ ,  $m$ —empirical parameters of speed and load level.

Non-equilibrium processes of concrete force resistance in time of force and environmental origin are described by a single mathematical model proposed by Bondarenko [29] and based on dependence (1). This model is a specific premise of the kinetics phenomenological uniformity of damage promotion and development non-equilibrium processes of creep concrete deformations:

$$\frac{\Delta[\Delta L(t, t_0)]}{dt} = \alpha \cdot [\Delta L(t, t_0)]^m \quad (2)$$

where  $\Delta L$ —relative deficit of the studied factor current value of non-equilibrium force resistance  $L(t, t_0)$  in relation to the limit value  $L_{ult}$ ;

$t, t_0$ —observation time;

$\alpha$ —empirical parameter of speed change  $\Delta L$ ;

$m$ —empirical parameter of the non-linear relationship between the deficit value  $\Delta L$  and the speed of its change in time.

It is important to note that relation (2) determines the constancy of regime, thermodynamic and physicochemical factors of force resistance. We will assume that this ratio is applicable for taking into account non-equilibrium processes and for analyzing the survivability potential of building frames reinforced concrete structural systems at accidental impact. With such an impact in the elements of a reinforced concrete structural system, in addition to additional loading caused by the static redistribution of power flows along alternative ways of transferring the load, additional dynamic loading will occur [30]. To determine the forces in the frame elements, taking into account their dynamic additional loading, the following approach was used in this work: the quasi-static method in the formulation proposed by Geniev [18, 31].

On the basis of the linear creep theory of an aging material (Maslov-Arutyunyan model) [32] and the Recommendations for taking into account creep [33], a calculation was made and a plot of the dependence of the concrete creep  $C(t)$  measure on loading time  $t$  was plotted (Fig. 1). The concrete creep measure at the time  $t$  under concrete loading at the age  $t_0$  is determined by the formula [33]:

$$C(t, t_0) = \left[ \frac{1}{E_b(t_0)} \right] - \left[ \frac{1}{E_b(t)} \right] + C_{28,besk} \cdot \Omega(t_0) \cdot f(t, t_0), \quad (3)$$

where  $C_{28,besk}$  is the limiting value of the creep measure [33];

$\Omega(t_0)$  is a function that takes into account the concrete aging effect on the creep measure ( $t_0$  is the loading time of the structure);

$f(t, t_0)$  is a function that takes into account the increase in time of the creep measure ( $t$  is the total test time of the sample, the observation time).

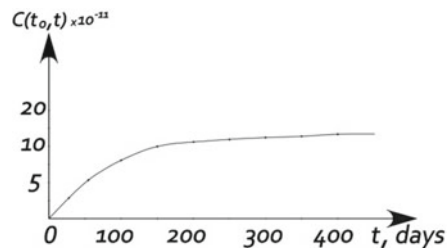
The function  $\Omega(t_0)$  is determined by the following formula:

$$\Omega(t_0) = c + d \cdot e^{-\gamma \cdot t_0}, \quad (4)$$

The function  $f(t, t_0)$  is determined by the formula [33]:

$$f(t, t_0) = 1 - k \cdot e^{-\gamma_1 \cdot (t-t_0)} \quad (5)$$

**Fig. 1** Dependence graph of the creep measure on time  $t$  at the loading beginning at the age of  $t_0 = 28$  days for concrete B20



The limiting value of the creep measure  $C_{28,besk}$  is calculated by the formula:

$$C_{28,besk} = C_{28,besk}^N \cdot \xi_{2c} \cdot \xi_{3c}, \quad (6)$$

where  $\xi_{2c}$ ,  $\xi_{3c}$ —coefficients depending on the modulus of the open surface of the element  $M_0$  and the relative humidity of the environment;

$C_{28,besk}^N$ —the limiting value of the concrete creep measure loaded at the age of  $t_0 \leq 28$  days.

A similar dependence graph of the concrete creep measure function on time  $t$  was constructed by Travush and Marashkin [34].

The concrete deformations long-term modulus corresponding to the linear relationship between stresses and deformations at time  $t$  at the beginning of loading  $t_0$  is found by the formula [33]:

$$E_b(t, t_0) = \left[ \frac{1}{E_b} + C(t, t_0) \right]^{-1}, \quad (7)$$

where  $E_b$  is the modulus of initial elasticity.

To solve the problem of assessing the robustness potential, the following hypotheses and assumptions are introduced. It is assumed that the limiting deformations of concrete at static and dynamic loading modes are equal to each other; also, the function of damage to concrete by corrosion  $k(z)$  remains the same for all physical and mechanical characteristics of the concrete force resistance (the sign of equivalence is the constancy of regime and physical and mechanical factors) [29, 35, 36].

Following [31, 33, 37], if the generalized load parameter  $\lambda_n$  is taken to assess the robustness exposition, then the robustness exposition of the structural system at its loading can be described by the dependence “ $\lambda_n(t)$ — $M^*(t)$ ”. Let us determine the robustness exposition parameter of a statically indeterminate reinforced concrete beam clamped on supports loaded with a distributed load (Fig. 2a).

Figure 2b shows a dependence graph «robustness parameter—moment (“ $\lambda_n(t)$ — $M^*(t)$ ”) for an arbitrary section  $k$  of the considered beam structure, reflecting the development of non-equilibrium nonlinear creep processes in time when analyzing the robustness potential of the pinched beam bent reinforced concrete element at accidental impact. Section “0–1” of the graph characterizes the loading ( $n$ )-times of a statically indeterminate system by the operational load.

Section “1–2” of the graph characterizes the accepted state in the beam most stressed section the non-equilibrium processes during long-term action of a power nature in the concrete creep form. At the action of a constant long-term load  $P_\tau$  at the moment of load application  $t = 0$ , the compressed zone in the section of the reinforced concrete bending element will be shortened by the value  $\Delta_{el}$ , and the relative deformations will be equal in compressed concrete and compressed reinforcement  $\varepsilon'_b(\tau)$  and  $\varepsilon'_s(\tau)$ , respectively. The stresses in the concrete of the compressed zone will be equal to  $\sigma_b$ , in the compressed reinforcement— $\sigma'_s$  (Fig. 2c).

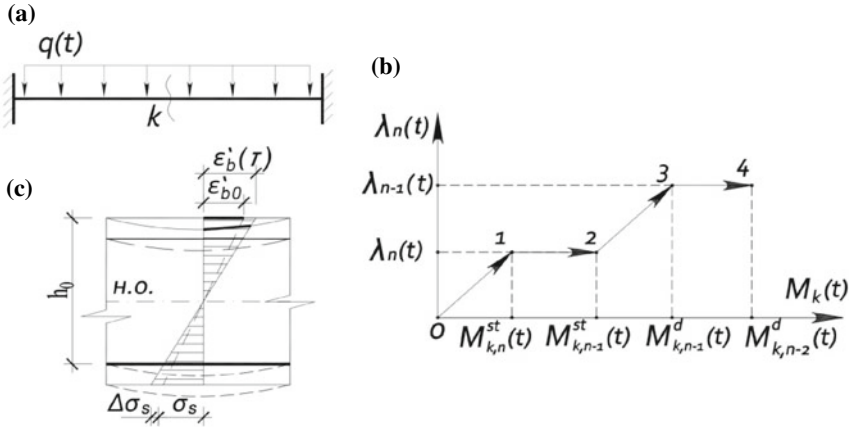


**Fig. 2** To assess the robustness of a rigidly pinched reinforced concrete beam: design scheme of a pinched beam bent reinforced concrete element (a); graph of the dependence «robustness parameter—moment» (“ $\lambda_n - M^b(t)$ ”) for an arbitrary section  $k$  of the considered beam structure (b); to determine the change in the section deformations of a bent reinforced concrete element in the creep’s process (c)

After a certain period of time  $t = \tau$ , under the creep influence, the fiber layer of the concrete compressed zone will still be shortened by the value  $\Delta\tau$ . But due to the concrete adhesion and reinforcement during their joint work, the deformations are the same. Compressed reinforcement shortens by the same amount as the fiber layer of the compressed concrete zone in the beam section due to the deformations continuity of the longitudinal reinforcement and the surrounding concrete:

$$\varepsilon'_s(\tau) = \varepsilon'_b(\tau) = \sigma_b / E'_b. \tag{8}$$

As a result, after a certain period of time  $t = \tau$  in the considered most loaded section of the beam, the moment reaches the limit value and a plastic hinge is formed. The beam static indeterminacy is reduced by one.

The algorithm for determining the robustness exposition parameter of a reinforced concrete statically indeterminate structural system includes the following steps:

1. Determination of forces in the structural system elements at a given level of operational load over time.
2. Determination of the system elements deformation moduli at a given level of loading and criteria-based verification of the limiting forces achievement depending on the loading time. In an accidental limit state, it is possible to allow greater opening of cracks and the development of deflections, as well as partial destruction of some sections, which contradicts the current criteria for limit states that ensure the operational suitability of structures and buildings, but excludes the onset of geometric variability of the structural system in the zone of possible local destruction.

3. Determination of the most stressed section  $k$  in the structural system elements, in which, when a given load of duration  $t = \tau$  is applied, the limit force (moment) is reached and the first plastic hinge is formed in the original  $n$ -fold statically indeterminate structural system ( $\lambda_n(t)$  in Fig. 2b).
4. Criteria verification of the limit forces achievement in the other elements sections of the structural system.
5. If at least one  $k$  section of other elements reaches the limit force, respectively, the static indeterminacy of the system decreases  $(n - 2)$  times, then with the calculated level of robustness exposition  $\lambda_n(t)$  determined the robustness parameter  $\lambda_{n-1}(t)$ ,  $\lambda_{n-2}(t)$ , etc.

### 3 Results and Discussion

Calculating example of the robustness potential assessment of the of a rigidly clamped reinforced concrete beam at accidental action.

1. The geometric dimensions and reinforcement scheme of a reinforced concrete beam with  $120 \times 70$  mm section and 1000 mm length are shown in Fig. 3a. The beam is designed from heavy concrete class B20. Armature A500C, diameter of longitudinal upper and lower armature 8 mm. Value  $\xi = 0.493$ . The limiting design value of the moment in the beam section will be:  $M_{ult} = 3.7$  kN m. The value of the creep measure calculated by formula (3) will be  $C(t, t_0) = 0.898 \times 10^{-10} \text{ m}^2/\text{N}$ .
2. Forces in a rigidly clamped reinforced concrete beam from an operational uniformly distributed load  $q(t) = 31.2$  kN/m in the form of a moment diagram  $M_{k,n}^{st}(t)$  (where  $k = 1, 2, 3, \dots$ , section number in element) are shown in Fig. 3b. In the middle of the span (Sect. 1,  $k = 1$ ) the moment will be  $M_{1,n}^{st} = ql^2/24 = 1.3$  kN m. In the supporting zone of the beam (Sect. 2,  $k = 2$ ), the moment will be  $M_{2,n}^{st} = ql^2/12 = 2.6$  kN m.
3. The deformation modulus from a short operating load will be: deformation modulus of concrete at the initial moment of time  $E_b(t_0) = 27.5 \times 10^3$  MPa (according to SP 63.13330 [38]); the reduced deformation modulus of a reinforced concrete beam in a loaded state in a section with cracks in the tension zone  $E_{b,red} = 5.36 \times 10^3$  MPa.

The deformation modulus from a long-term operational load, taking into account non-equilibrium processes (creep) will be the following value. For the practical (quantitative) determination of the concrete deformation modulus  $E_b(t)$  were used the Recommendations, NIIZhB [33]. The long-term concrete deformation modulus, corresponding to a linear relationship between stresses and deformations at the time  $t = \tau$  at the beginning of loading  $t_0$ , is found by the formula (7):

$$E_b(t, t_0) = \left[ \frac{1}{27.5 \times 10^9} + 0.898 \times 10^{-10} \right]^{-1} = 7.93 \times 10^3 \text{ MPa}.$$

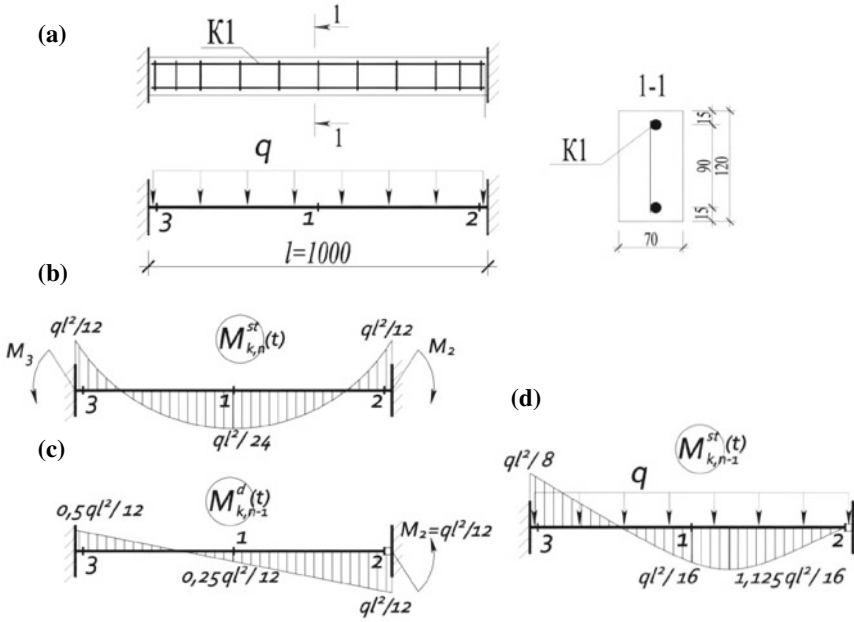


**Fig. 3** To assess the robustness potential of a rigidly clamped reinforced concrete beam: design scheme (a); diagram of moments in a reinforced concrete beam  $n$ -times statically indeterminate at a given level of operational load in time (b); diagram of moments from dynamic additional loading (c); diagram of moments in the beam  $(n - 1)$ -times statically indeterminate after the redistribution of forces from dynamic additional loading (d)

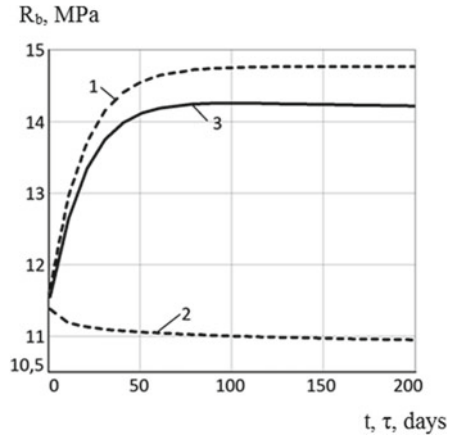
4. Determination of the most stressed section  $k$  in the structural system elements and the parameter  $\lambda_n(t)$ . The first plastic hinge in the most stressed section  $k$  of the structural system element is formed when the limiting force (moment) is reached. Such a deformation of the reinforced concrete element cross section is explained by the fact that non-equilibrium processes of force resistance and processes of reinforced concrete degradation from corrosion appear in the structure. Such multidirectional non-equilibrium processes of increasing the concrete strength over time, neutralizing concrete by an aggressive environment, the process of «aging» and corrosion of concrete simultaneously, following [39], can be represented by diagrams in Fig. 4.

In the first approximation, changes in the strength of loaded and corrosion-damaged concrete over time, taking into account the process of increasing the healthy concrete strength (concrete aging theory), and the process of the aggressive environment impact on concrete, can be described using the deformation model of Geniev [31, 38] in the following form:

$$R_b(t, \tau) = R_b^*(\tau) + R_b(t) - R_b(t_0). \quad (9)$$



**Fig. 4** Diagram of the change of a concrete limit strength  $R_b$  at time: 1—the process of increasing the concrete strength at time  $t$  (aging of concrete); 2—the process of neutralizing concrete with a corrosive medium at time  $\tau$  (concrete corrosion); 3—at the same time the process of “aging” and concrete corrosion



where  $R_b^*(\tau)$ —compressive strength dependence of corrosion-damaged concrete in time  $\tau$ ;  $R_b(t)$ —compressive strength dependence of sound concrete in time  $t$ ;  $R_b(t_0)$ —concrete compressive strength up to the moment of exposure to an aggressive environment.

With regard to the considered reinforced concrete beam, the concrete compressive strength until the moment of exposure to an aggressive environment will be:  $R_b(t_0) = 11.5$  MPa.

The strength of loaded and corrosion-damaged concrete in time will be at  $t = 40$  years and the time of exposure to an aggressive environment  $\tau = 40$  years will be  $R_b(t, \tau) = 3.75$  MPa.

A plastic hinge is formed in Sect. 2 (figure c) and the limit value of the moment in the loaded beam section at the action of an aggressive environment in 40 years will be  $M = M_{ult}^* = 2.6$  kN m. In this case, the system becomes  $(n - 1)$ -times statically indeterminate, the robustness parameter is equal to  $\lambda_{n-1}(t)$ .

- Criteria verification of the limit forces achievement in sections other elements of structural system. At a special limit state in the most loaded section (Sect. 1 of the beam), the strength test is performed, and then the deformation criterion of the special limit state is checked. After the formation of a plastic hinge (Sect. 2 of the beam) in the most loaded section (Sect. 1 of the beam), the moment due to dynamic additional loading will reach the value:  $M_{1,n-1}^{st} = M_{1,n}^{st}(t) + M_{1,n}^d = ql^2 / 16$ , where  $M_{1,n}^d$ —moment in Sect. 1  $n$ -times of a statically indeterminate system from an instantaneous load  $M_2 = ql^2 / 12$ .

With regard to the considered beam design at  $q = 31.2$  kN/m,  $l = 1.0$  m, beam deflection  $f = 1.9 \times 10^3$  m = 1.9 mm <  $1/30 L = 0.033$  m = 33 mm, i.e. for a given operating time  $t = 40$  years after an accidental action, the beam survivability will be exhausted.

## 4 Conclusions

1. The quantitative assessment of the building system robustness potential in time to the destructive effects of an aggressive environment is given with the exclusion from the system of structural elements responsible for the geometric immutability of the structure.
2. When calculating the structures of buildings and structures reinforced concrete frames, taking into account non-equilibrium processes of long-term exposure to force and environmental factors, when assessing the its robustness exposition, the duration of building structures operation and the degree of its corrosion damage over time should be taken into account.

## References

1. Bondarenko VM, Migal RE, Ygupov BA (2014) Reserves and exposition of constructive safety of buildings operated in an aggressive environment. *Build Reconstr* 1:3–10
2. Bondarenko VM, Kolchunov VI (2018) The concept and directions of theory development of buildings and structures constructive safety under force and environmental influences. *Ind Civ Eng* 2:28–31
3. Fedorova NV, Gubanova MS (2018) Crack-resistance and strength of a contact joint of a reinforced concrete composite wall beam with corrosion damages under loading. *Russ J Build Constr Archit* 2:6–18
4. Kolchunov VI, Savin SY (2018) Survivability criteria for reinforced concrete flame at loss of stability. *Mag Civ Eng* 80:73–80. <https://doi.org/10.18720/MCE.80.7>
5. Tamrazyan AG, Mineev TK, Zhukova LI (2019) Influence of chloride corrosion on probabilistic assessment of bearing capacity of beamless slabs overlap. In: IOP conference series: materials science and engineering, vol 012117. <https://doi.org/10.1088/1757-899X/661/1/012052>
6. Kabantsev O, Mitrovic B (2017) Modeling post-critical deformation processes of flat reinforced concrete elements under biaxial stresses. In: MATEC web of conference, vol 117, p 00071. <https://doi.org/10.1051/mateconf/201711700071>
7. Kodysh EN, Trekin NN (2018) Special limiting state of reinforced concrete structures under emergency impacts. Concrete and reinforced concrete—problems and prospects. *Bull Sci Res Center Constr* 1:120–125
8. Li J, Yao Y (2001) A study on creep and drying shrinkage of high performance concrete. *Cem Concr Res* 31:1203–1206. [https://doi.org/10.1016/S0008-8846\(01\)00539-7](https://doi.org/10.1016/S0008-8846(01)00539-7)
9. Vasanelli E, Micelli F, Aiello MA, Plizzari G (2013) Long term behavior of FRC flexural beams under sustained load. *Eng Struct* 56:1858–1867. <https://doi.org/10.1016/j.engstruct.2013.07.035>
10. Räiser VD (2012) Problem of buildings and structures survivability. *Struct Mech Anal Constr* 5:77–78
11. Nazarov YP, Gorodetsky AS, Simbirkin VN (2009) On the problem of ensuring the survivability of building structures under emergency impacts. *Struct Mech Anal Constr* 4:5–9
12. Kolchunov VI, Tamrazyan AG (2014) The main directions of development of constructive safety theory and reinforced concrete structures synthesis of buildings and structures. In: Concrete and reinforced concrete—a look into the future: scientific works of the III All-Russian (II International) conference on concrete and reinforced concrete, vol 7, pp 176–191
13. Arutyunyan NKh, Kolmanovsky VB (1983) Theory of creep of inhomogeneous bodies. Publisher Nauka Moscow

14. Aleksandrovsky SV, Vasiliev PI (1976) Experimental studies of concrete creep. Creep and shrinkage of concrete and reinforced concrete structures. Publisher Stroyizdat, Moscow
15. Bondarenko VM, Karpenko NI (2007) Stress state level as a factor of structural changes and rheological power resistance. ACADEMIA. Archit Constr 4:56–59
16. Vasiliev PI, Livshits YD (1976) Application of concrete creep theory to the calculations of structures and bridges. Creep and shrinkage of concrete and reinforced concrete structures. Publisher Stroyizdat, Moscow
17. Gvozdev AA, Yashin AV, Petrova KV (1978) Strength, structural changes and concrete deformations. Publisher Stroyizdat, Moscow
18. Geniev GA (1992) On the evaluation of dynamic effects in beam systems made of brittle materials. *Concr Reinf Concr* 9:25–27
19. Maslov GN (1941) Thermal stress state of concrete masses when taking into account the concrete creep. Publisher Izvestiya VNIIG, Moscow
20. Prokopovich IE, Zedgenidze VA (1980) Applied theory of creep. Publisher Stroyizdat, Moscow
21. Rabotnov YN (1966) Creep of structural elements. Publisher Nauka, Moscow
22. Rzhantsyn AR (1968) Creep theory. Publisher Nauka, Moscow
23. Sanzharovsky RS (2014) Nonlinear hereditary theory of creep. *Struct Mech Eng Constr Build* 1:63–68
24. Ulitsky II (1963) Determination of creep deformations values and concrete shrinkage. Publisher Gosstroyzdat USSR, Kyiv
25. Kharlab VD (2014) Fundamental questions of the linear theory of creep (with reference to concrete): monograph. Publisher St. Petersburg State University of Architecture and Civil Engineering, ASV, St. Petersburg
26. Bažant ZP, Prasanna S (1989) Solidification theory for concrete creep, I: formulation. *Eng Mech ASCE* 115(8):1691–1703
27. Gilbert RI (2002) Creep and shrinkage models for high strength concrete—proposals for inclusion in AS3600. *Aust J Struct Eng* 4(2):95–106
28. Hamed E (2012) Nonlinear creep response of reinforced beams. *J Mech Mater Struct* 5:435–460
29. Bondarenko VM, Kolchunov VI (2007) Exposition of robustness. *News of Higher Educational Institutions. Construction* 5:4–8
30. Kolchunov VI, Fedorova NV, Savin SY (2022) Dynamic effects in statically indeterminate physically and structurally nonlinear systems. *Ind Civ Eng* 9:42–50
31. Geniev GA, Kolchunov VI, Klyueva NV (2004) Strength and deformability of reinforced concrete structures under accidental actions. ASV Publishing House, Moscow
32. Arutyunyan NK (1952) Some questions of the theory of creep. Publisher Gostekhizdat Moscow
33. NIIZHB Gosstroy USSR (1988) Recommendations for taking into account creep and shrinkage of concrete in the calculation of concrete and reinforced concrete structures. Publisher Stroyizdat, Moscow
34. Travush VI, Murashkin VG (2017) Influence of creep to deformation and stress distributions of bending element. *Build Reconstr* 2:57–70
35. Bondarenko VM (1968) Some questions of the nonlinear reinforced concrete theory. Publisher Kharkov University Press, Kharkov
36. Fedorova NV, Medyanin MD, Bushova OB (2020) Determination of static-dynamic deformation parameters of concrete. *Ind Civ Constr* 1:4–11
37. Kolchunov VI, Klyueva NV, Androsova NB, Bukhtiyarova AS (2016) Robustness of buildings and structures under accidental actions. ASV Publishing House, Moscow
38. SP 63.13330.2018 Concrete and reinforced concrete structures. Basic Provisions
39. Fedorova NV, Kolchunov VI, Gubanova MS (2022) Deformation of composite plane-stressed reinforced concrete structures: monograph. Publishing House MISI-MGSU, Moscow

# Reliability of Methods of Calculation of Heating Systems for Digital Model



Yulia Elistratova , Artem Seminenko , Dmitry Elistratov ,  
Roman Sheps , and Artem Umerenkov 

**Abstract** The paper focuses on the fact that today's modern digital technologies are a productive tool in the field of energy efficiency and energy conservation of thermal energy complex of the Russian Federation. The paper analyses different methods of hydrodynamic calculation of heating systems. The main task includes the analysis of existing hydraulic regime models to determine the prospects of the need to refine the techniques to build digital twin systems. The results of the calculations of the hydraulic regime of the heating systems are presented by summarising the existing mathematical description approaches, the convergence of which was assessed by comparing the values obtained as a percentage of the adopted basic calculation method. The authors note significant discrepancies in the results obtained, which are explained by the assumptions adopted in a particular method in order to simplify calculations and save time in the course of their implementation. It is suggested to use in calculations the values of local resistance coefficients according to the known dependences presented in scientific literature, where the influence of liquid movement mode on the value of local resistance coefficient is taken into account. It is pointed out that the concept of digital twin construction requires development and validation of mathematical models with high level of adequacy. In this connection it is concluded that the mathematical description of thermal and hydraulic regimes of heating systems requires clarification and additional theoretical and experimental research.

**Keywords** Digital twin · Energy savings · Hydraulic calculation · Heating system · Dispatching · Monitoring

---

Y. Elistratova (✉) · A. Seminenko · D. Elistratov  
Belgorod State Technological University named after Shukhov V.G., 46, Kostyukova Str.,  
Belgorod 308012, Russia  
e-mail: [tg.v.info@mail.ru](mailto:tg.v.info@mail.ru)

R. Sheps  
Voronezh State Technical University, 84, 20-Letiya Oktyabrya ul., Voronezh 394006, Russia  
e-mail: [romansheps@yandex.ru](mailto:romansheps@yandex.ru)

A. Umerenkov  
Southwest State University, 94, 50 Let Oktyabrya ul., Kursk 305040, Russia

## 1 Introduction

Today's measures for principles of energy efficiency and energy saving implementation within the framework of the RF energy policy [1–3] are actively integrated through the introduction of digital technologies in almost all spheres of human life. Reducing energy intensity as well as improving the functioning of residential heating systems are not exception [4–6]. The aim of improving such systems and finding efficient solutions is explained by the existing problem of providing a flexible and favorable thermal regime in the premises for all users (occupants) at the same time [7–9].

To date, most of the solutions to this problem have focused on the heat point [5, 8], namely the introduction of advanced control and regulation methods for the flow and temperature of the heating medium [9, 10]. However, this approach assumes a whole building heating system as a single end consumer. Such an assumption reduces the effect of optimizing the heat consumption systems, as external factors have a point impact on the thermal comfort level in each room [11, 12]. Consequently, there is a need to diagnose and implement mental control methods for heating systems as a single unit and its individual components (radiators, standpipes, distribution mains).

The progressive growth in the application of information technology in both the construction and housing sectors [13–16] is generating resources that can be used to create digital models of buildings and structures, and engineering systems are no exception [17]. The idea of creating a digital duplicate of an object implies its integration with dispatching systems as a way to manage [18].

Creating a digital twin of the heating system requires not only the verification of the design parameters of each system element, but also the adequacy of the intelligent link, namely the description of the heat and hydrodynamic processes that take place in the system.

## 2 Materials and Methods

There are several methods in the scientific literature for describing the hydraulic behaviour of heating systems, the classification of which is shown in Fig. 1 [19].

Let us calculate a single pipe heating system, with one of the branches shown in Fig. 2. Calculation of heating pipes will be carried out by the method of dynamic pressures. As the most unfavorable ring, we take the circulation ring including standpipe 10 (St10).

The input data and the diameters obtained are entered in Table 1. It should be noted that column 5 shows adopted diameters, and column 6 shows diameters, which initially must be specified, starting calculation of risers and main sections of the system depending on the flow rate of the heat carrier, see [(Table 58, Table 60) [20]]. For selecting the pre-diameter for the riser pipes, we use [(Table 58) [20]], and for the main pipes we use [(Table 60) [20]].

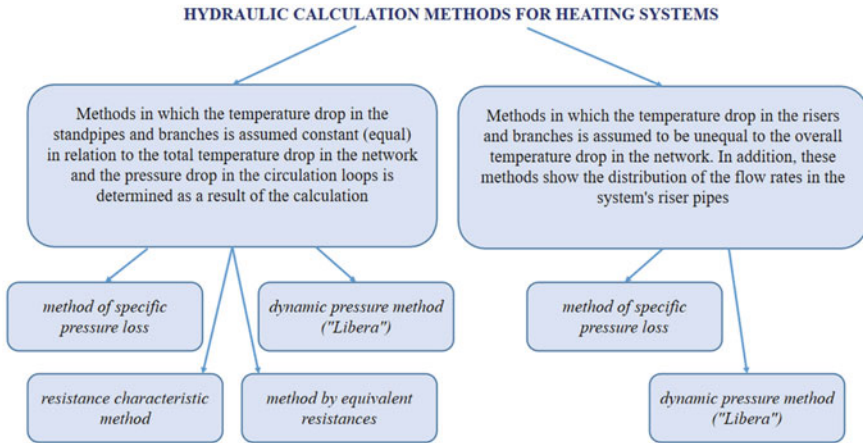


**Fig. 1** The main groups of hydraulic calculation methods for heating systems

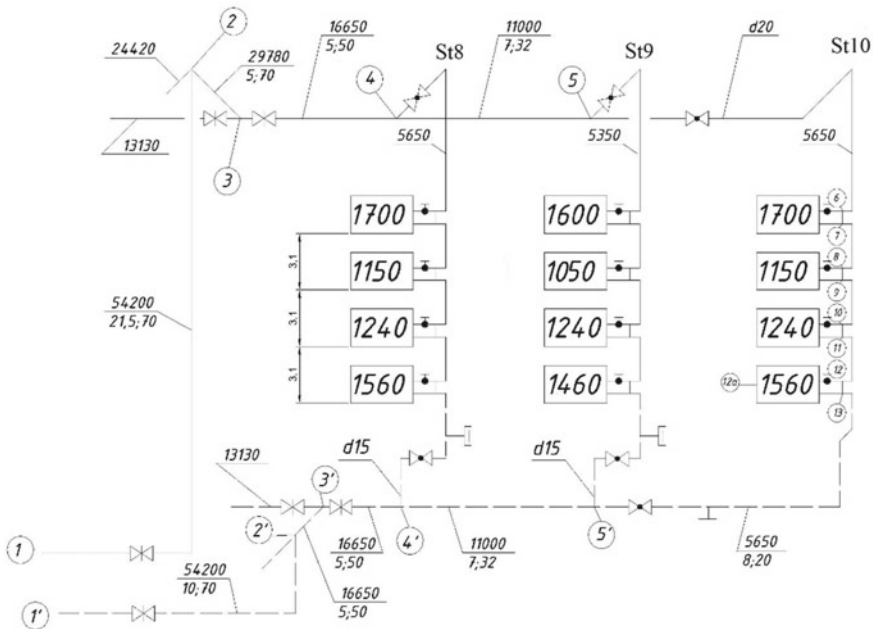


**Fig. 2** Schematic diagram of the calculated heating system. *Note* above the extension line, the heat load  $Q, W$  is shown; below the extension line, the first number indicates the section length  $m$  and the second number the pipe diameter  $mm$ ; each radiator has its heat output shown,  $W$ ; the sections are numbered from the supply main through the main ring to the return main

**Table 1** Values for input data and accepted pipeline diameters

Section	Raw data			Calculation results	
	Q, W	L, m	G, kg/h	d <sub>adopted</sub> , mm	d <sub>provisional</sub> , MM
1	2	3	4	5	6
St10	5650	–	194.4	20	20
St 9	5350	–	184	20/15	20
4–5	11,000	7	378.4	32	20
4'–5'	11,000	7	378.4	32	20
St 8	5650	–	194.4	20/15	20
3'4	16,650	5	572.8	32	25
3'–4'	16,650	5	572.8	32	25
2–3	29,780	5	1024.4	40	32
2'–3'	29,780	7	1024.4	40	32
1–2	54,200	10	1864.5	50	40
1'–2'	54,200	10	1864.5	50	40

*Note* For St9 and St8 the numerator in column 5 is the riser diameter and the denominator is the pipe diameter of the return connection

Local resistance coefficients  $\xi$  are taken according to Table 2 [20]. Values of local resistance coefficients for T-pieces on trunkings are accepted depending on the distribution of flow rates by branches [(Table 53) [20]].

Let us calculate the same branch of the heating system using several existing hydraulic calculation methods, in order to compare the final results. Accordingly, the input data for the following methods will be the same as for the dynamic pressure method.

### 3 Results and Discussion

According to the results of the “forward” and “reverse” hydraulic calculation methods [19] of one branch of the heating system (Fig. 2), we have obtained the pressure losses in the main and secondary rings, as well as the distribution of flow rates across the risers. Let us present the results of the calculations in the form of diagrams Figs. 3, 4 and 5. The main circulation ring Ck1 and the two secondary rings Ck2 and Ck3 pass through St10, St9, St8 respectively.

Let us take the “direct” method of resistance characteristics as the basic method and in relation to it express the deviation of the obtained pressure losses by other methods in St10 in %.

**Table 2** Local resistance coefficient values  $\xi$

Resistance	Nominal diameter, $d_y$ , mm	$\xi$
Double sided radiators with connection diameter	15	1.6
Same	20	1.2
Plug valves	15	3.5
Same	20 and more	1.5
Parallel gate valves	–	0.5
Double adjustment faucet with cylindrical plug	15	4
Same	20	2
Indentation	–	0.5
Straight tees	–	1
Tee-joints on the passage with a swivel	–	1.5
Tees on the countercurrent	–	3
Bends, bent under $90^\circ$	15	1.5
Same	20	1
Same	25	0.5
Same	32 and more	0.3
Bent bends	15	0,8
Same	20	0.7
Same	25 and more	0.6

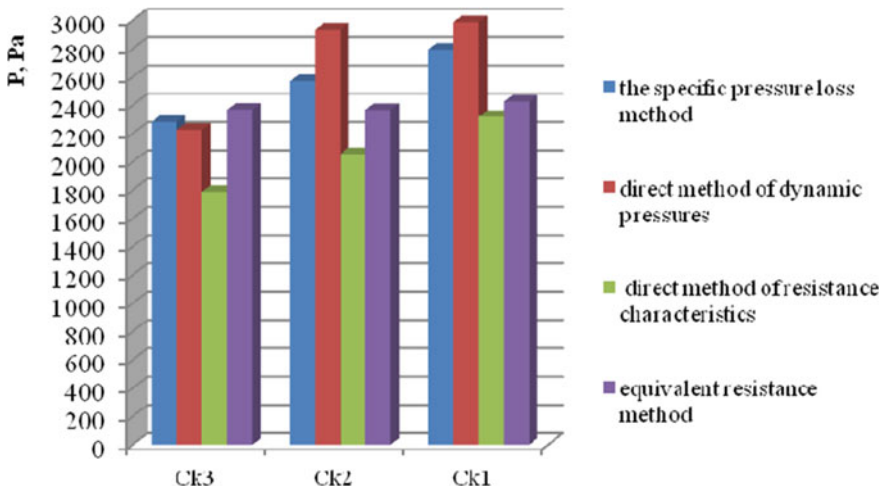


**Fig. 3** Circulation ring pressure loss distribution diagram



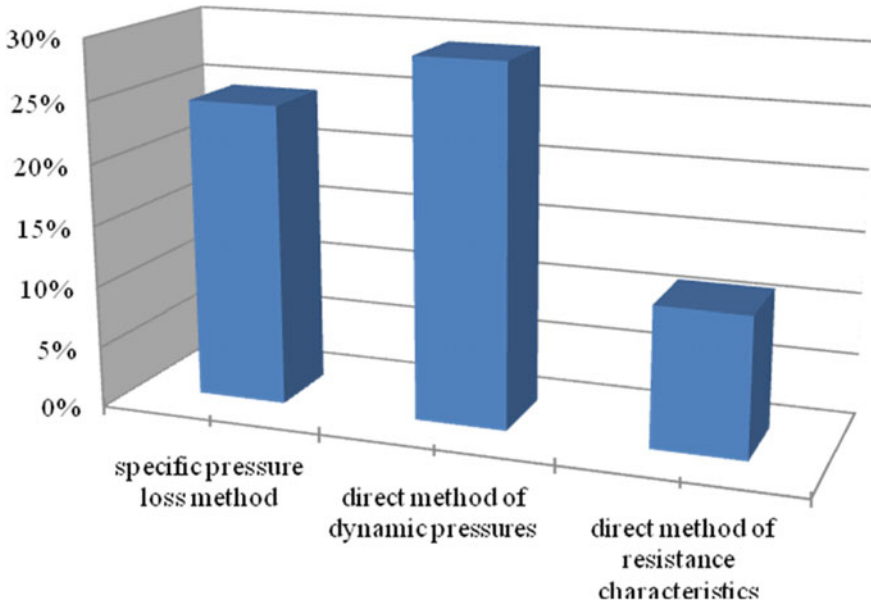


Fig. 4 Diagram of the percentage of pressure loss obtained in St10 by the different methods, in relation to the drag characteristic method

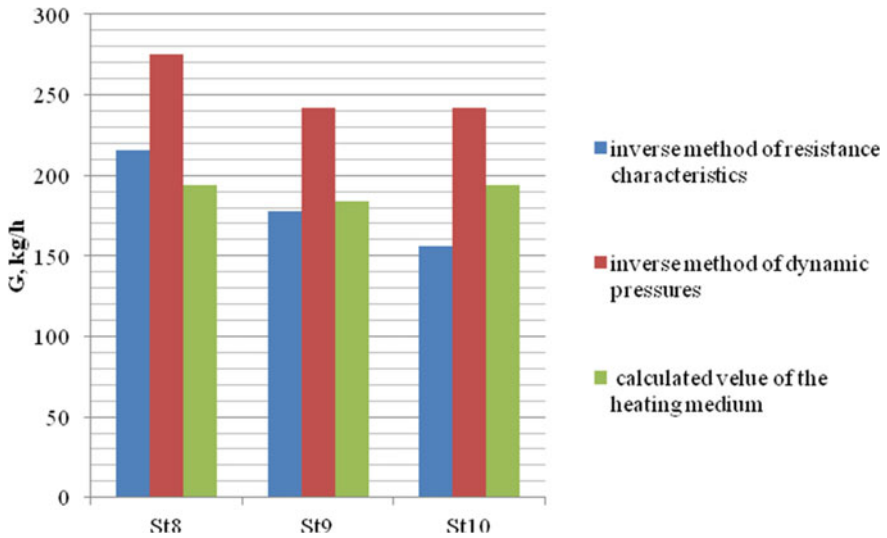


Fig. 5 Flow rate distribution diagram for the system risers

As shown in the diagram (Fig. 5), the distribution of flow rates in the riser pipes takes on different values, depending on the calculation method. Moreover, these values are not equal to the flow rates used to calculate the system by “direct” calculation methods.

Differences in the results obtained may be based on certain uncertainties of each of the methods considered, due to their peculiarities. Methods such as the resistance characteristic method, the equivalent resistance method and the dynamic pressure method have been developed by the authors to simplify and save time during the calculations. Therefore, appropriate multiplying indicators (drag characteristic  $S$ , hydraulic criterion  $\mu$ , reduced local drag coefficient  $\xi_p$ ) were applied. The application of such aggregated indicators can affect the accuracy of the calculation result and subsequently the performance of the heating system, which is determined by a correct hydraulic calculation.

## 4 Conclusion

Nowadays, such calculations can be carried out using computer programs, so it is necessary not to use simplified methods, but on the contrary, to complicate them and to identify new dependencies. For example, to use not tabulated averaged values of local resistance coefficients (hereinafter l.r.c) of elements of heating systems, but to calculate them using appropriate formulas from the reference book [21], in which dependence of l.r.c. on the fluid flow mode is taken into account, which is not reflected in any of the calculation methods. Consider changes in l.r.c. values under condition of overgrowing of pipes and additional increase of hydraulic friction coefficient due to considerable cooling of water in pipelines. The hydraulic calculation must also reflect changes in the temperature of the heat transfer medium, in particular under conditions of regulating the heat output of the radiators.

Therefore, mathematical description of thermal and hydraulic regimes of heating systems requires clarification and additional theoretical and experimental research. Since the concept of building digital analogues of considered objects and systems is based on development and validation of mathematical models with high level of adequacy.

The research was carried out within the framework of the Grant of the President of the Russian Federation for the Leading Scientific School No. NSH-25.2022.4 using the equipment of the High Technology Center of the Belgorod State Technological University named after V.G. Shukhov.

## References

1. Federal Law of the Russian Federation (2009) On energy saving and on improving energy efficiency and on amendments to certain legislative acts of the Russian federation. Dated November 23, No 261-FZ
2. Decree of the President of the Russian Federation dated 09.05.2017 No. 203 On the strategy for the development of the information society in the Russian Federation for 2017–2030 [Electronic resource]. <http://www.garant.ru/products/ipo/prime/doc/71570570/>
3. Decree of the Government of the Russian Federation No. 1632-r dated 28.07.2017 (2017) On the approval of the program. Digital Economy of the Russian Federation [Decree of the Government of the Russian Federation dated July 28, 2017 No. 1632-R. On the approval of the program Digital Economy of the Russian Federation. <http://base.garant.ru/71734878/>
4. Gribkov IN, Lykov AN (2012) Analysis of heating systems and prospects of automation. Bulletin of PNRPU. Electr Eng, Inf Technol Control Syst 6:192–202
5. Lupey AG (2004) On diagnostics of the state of heating systems of consumers of thermal energy [Electronic resource]. JUICE, 8. Access mode: <https://www.c-o-k.ru/articles/o-diagno-stike-sostoyaniya-sistem-otopleniya-potrebitelnykh-teplovoy-energii>
6. Safullin RN, Afanasyev AS, Reznichenko VV (2019) The concept of development of monitoring systems and management of intelligent technical complexes. J Min Inst 237:322–330 [In Russ]. <https://doi.org/10.31897/pmi.2019.3.22>
7. Paramonova Eyu, Elistratova YuV, Seminenko AS (2013) The problem of overflows and underdots in the heating period. Mod High-Tech Technol 8–1:48–50
8. Trukhny AD, Zroychikov NA, Lomakin BV, Sedov IV (1998) Information and diagnostic control system for mains water heaters of the turbine unit T-250/300-240. Heat Power Eng 1:30–34
9. Tol H, Desmedt J, Salenbien R (2020) A novel demand-responsive control strategy for district heating systems, featuring return temperature reduction. Energy Built Environ 2(1):105–125
10. Yumin L, Yiqun P, Xiaolei Y, Wenqi J, Zhizhong H (2022) Surrogate modeling for long-term and high-resolution prediction of building thermal load with a metric-optimized KNN algorithm. Energy Built Environ. ISSN 2666-1233. <https://doi.org/10.1016/j.enbenv.2022.06.008>
11. Drozd DV, Elistratova YuV, Seminenko AS (2013) Influence of wind on indoor microclimate. Mod Sci Intensive Technol 8–1:37–39
12. Ling J, Dai N, Xing J, Tong H (2021) An improved input variable selection method of the data-driven model for building heating load prediction. J Build Eng 44(10):103255. <https://doi.org/10.1016/j.jobte.2021.103255>
13. Yakimchuk YaYu, Martemyanov VS, Averyaskin SG, Soloviev VI (2014) Electronic government and the state information system of housing and communal services of the region. Innov Life Innov Life 1(8):56–67
14. Lund H, Stergaard PA, Chang M, Werner S, Svendsen S et al (2018) The status of 4th generation district heating: research and results. Energy 164:147–154
15. Krasilnikova KV, Soloviev VI (2016) Models of integration of information resources of the regional system of housing and communal services. Innovations in life 1(16):69–80
16. Housing and communal services on the threshold of digital transformation. Access mode: <https://www.eprussia.ru/teploenergetika/35/3829884.htm>. Accessed 25 Oct 2022. in Russian
17. Soloviev VI (2022) Digital transformation of municipal heat supply systems [Electronic resource]. Information and mathematical technologies in science and management, 2 (2019). Access mode: <https://cyberleninka.ru/article/n/tsifrovaya-transformatsiya-sistem-teplosnabzheniya-munitsipalnogo-obrazovaniya>. Date of request: 15 Oct 2022
18. Vasiliev AN, Tarkhov DA, Malykhina GF (2022) Methods of creating digital doubles based on neural network modeling. Modern information technologies and IT education, 3 (2018). <https://cyberleninka.ru/article/n/metody-sozdaniya-tsifrovyyh-dvoynikov-na-osnoveneyrosetevogo-modelirovaniya>. Accessed 25 Oct 2022

19. Minko VA, Seminenko AS, Alifanova AI, Elistratova JuV, Tkach LV (2015) Assumptions and premises of heating systems hydraulic calculation methods: part 1. *Ecol, Environ Conserv Pap* 21(1):55–60
20. Shchekin RV, Berezovsky VA, Potapov VA (1975) Calculation of central heating systems. Publishing Association Vyshcha Shkola
21. Bogoslovsky VN, Skanavi AN (1991) Heating: Uch. For Universities. M, Stroyizdatr

# Four-Wheel Drive Vehicle Optimum Control with a Partial Failure It's Drives



Tatiana Kruglova , Michael Shoshiashvili , and Alexander Vlasov 

**Abstract** The article is devoted to the development of a system for optimal planning of the trajectory of the movement of construction machines, taking into account the deterioration of the technical condition of their drives. A fuzzy model for optimizing the movement of a vehicle takes into account the technical condition and the load on the driving wheels. The model allows, based on the results of the assessment of the technical condition and load, to select the required operating mode for each drive: four-wheel drive; front-wheel drive; rear-wheel drive; termination of operation. To continue operation in the selected mode, the criteria for the optimal trajectory of the vehicle are formulated, taking into account the length of the trajectory, the number of right and left turns and the technical condition of the drives. Three analytical solutions of the optimization problem are given. Possible trajectories of movement are built and the number of turns of the car is calculated. The same problem was solved using genetic and ant colony algorithms for the same input data. A comparative analysis of the obtained results was carried out.

**Keywords** Four-wheel drive vehicle · Motion optimization · Trajectory planning · Partial drive failure

---

T. Kruglova (✉) · M. Shoshiashvili · A. Vlasov  
Platov South-Russian State Polytechnic University (NPI), 132, Prosveshcheniya, Rostov Region,  
Novocherkassk 346428, Russia  
e-mail: [tatyana.kruglova.02@mail.ru](mailto:tatyana.kruglova.02@mail.ru)

M. Shoshiashvili  
e-mail: [shosh61@yandex.ru](mailto:shosh61@yandex.ru)

© The Author(s), under exclusive license to Springer Nature Switzerland AG 2024  
N. Vatin et al. (eds.), *Modern Problems in Construction*,  
Lecture Notes in Civil Engineering 372,  
[https://doi.org/10.1007/978-3-031-36723-6\\_5](https://doi.org/10.1007/978-3-031-36723-6_5)

## 1 Introduction

Wheeled vehicles are very popular during the constructions. There are graders, excavators, bulldozers, scrapers, trenchers, soil compactors (Fig. 1) and many other types of earthmoving equipment. Construction equipment works in a complex dynamic environment under various weather conditions, high humidity and dustiness of the workspace. This may lead to its partial failure. The most vulnerable elements of any type of mobile equipment are wheel drives. Therefore, it is important to ensure their high reliability during operation. The most widely used machines with four wheels. In general, three control options can be used: Four-wheel drive, front-wheel drive and rear-wheel drive.

The option of all-wheel drive is preferred, since this option allows you to evenly load all four-wheel drive and provide better handling. Also, this option allows you to independently change the speed of rotation of the wheels, which can be very useful, for example, when one of the wheels gets stuck.

Front-wheel drive is often used. Vehicle with such control has residual maneuverability, it is cheaper option compared to all-wheel drive due to the presence of only two wheels. However, drive deterioration is faster than with all-wheel drive. Also, this configuration is less effective when the wheels get stuck.

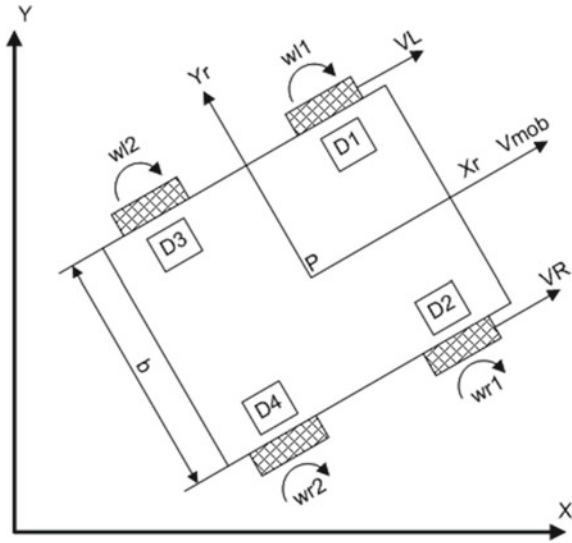
As for control, rear-wheel drive is the most inconvenient. This vehicle's type of robot is the least maneuverable, so this configuration is applied only if it is impossible to use a full or front drive.

During the vehicle's operation, the most actual problem is to ensure the reliability of their drives operation and coordinated interaction with others equipment inside



**Fig. 1** Wheeled vehicles in construction

**Fig. 2** Kinematic scheme of a four-wheel drive vehicle



the technological process. The solution of this problem can be achieved by using diagnostics system of drives technical condition integrated into the casing of each vehicle, which performs continuous measurement of their working parameters with subsequent analysis of the received information. Further, on the basis of the technical conditions of all vehicles, the technological process optimization should be carried out in such a way to extend the equipment life without compromising the quality of the operations performed.

Consider a vehicle model with four-wheel drive (Fig. 2). In general, it can be driven in one of three ways:

- (1) using wheels D1 and D2 (front-wheel drive);
- (2) using wheels D3 and D4 (rear-wheel drive);
- (3) the use of all four wheels at the same time (all-wheel drive).

All-wheel vehicle drive is the preferred control option, since the wheel drive resource is used evenly.

However, in the event of failure of one of the engines, the control system can be returned to the front or rear-wheel drive. To implement this approach, it is necessary that all the drives of the car work at a reduced load.

A method for technical condition and on each drive loads determine has been developed [1–11].

According to this method, the current state of each drive can be attributed to one of the following diagnosis classes:

- “11”—healthy without load;
- “12”—healthy with load;
- “21”—fault without load;
- “22”—fault with load.

Once the technical condition of each motor is determined, it becomes necessary to select the mode of operation of the technical equipment in which the motors operate.

## 2 Materials and Methods

As an example, consider a vehicle with four independent electric drives “motor-wheel” [12]. In general, a four-wheel drive vehicle (Fig. 2) can move in space in one of three ways: using wheels D1 and D2 (front-wheel drive); using wheels D3 and D4 (rear-wheel drive); using all four wheels at the same time (four-wheel drive).

The preferred mode of operation of the vehicle is four-wheel drive, therefore, in the case of a serviceable unloaded state of all drives,  $D1 = D2 = D3 = D4 = “11”$  it is advisable to choose this mode.

In the case of a healthy loaded “12” operating mode for all wheels, it’s also advisable to use all-wheel drive without operating mode changing. If the front drives D1, D2 are loaded (when the vehicle is traveling on a down slope movement), it is necessary to increase load for vehicle D3, D4. If the rear-wheel D3, D4 are loaded (when the vehicle up slope movement), it is necessary to increase the rotation speed of the front drives D1, D2. When one of the front drives D1 or D2 is loaded properly (when the wheel is stuck), it is necessary to increase the rotation speed of the rear-wheel of the same nomination D3 or D4 respectively. If the rear-wheel D3 or D4 is stuck, it is necessary to increase the rotation speed for the both front wheels (D1, D2).

Changing the control mode occurs when the “21” or “22” condition of one of the drives is faulty. So if one or two rear-wheel drives are in failure, it is necessary to switch to front-wheel drive. If there is failure of one or both of the front drive, it is necessary to switch to rear-wheel drive, or turn to 180° thereby moving to front-wheel drive (if the process permits). In case of failure of one front and one rear drive, it is necessary to stop the operation of the vehicle.

The above control logic can be implemented using *Mamdani* fuzzy logic model [13], which four inputs and outputs (Fig. 3).

The four possible conditions for each motor are set as inputs (Fig. 4a), and outputs—the current each drives operation mode (Fig. 4b). The range of output variables is set in the range  $[-1, 1]$ . At the same time, the value “-1” corresponds to the drive shutdown; “0”—use the current mode; “1”—increase the drive speed. The output control solution for each of the four wheels can be obtained using the algorithm [14], which has the following form:



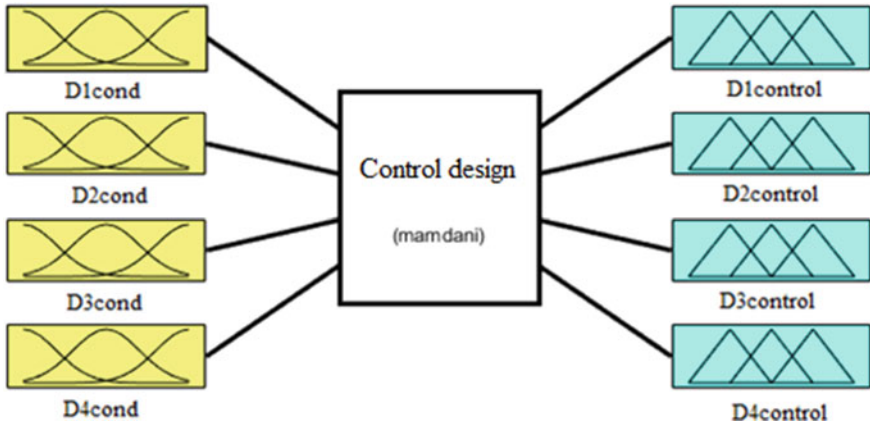


Fig. 3 The structure of the vehicle movement optimizing fuzzy model

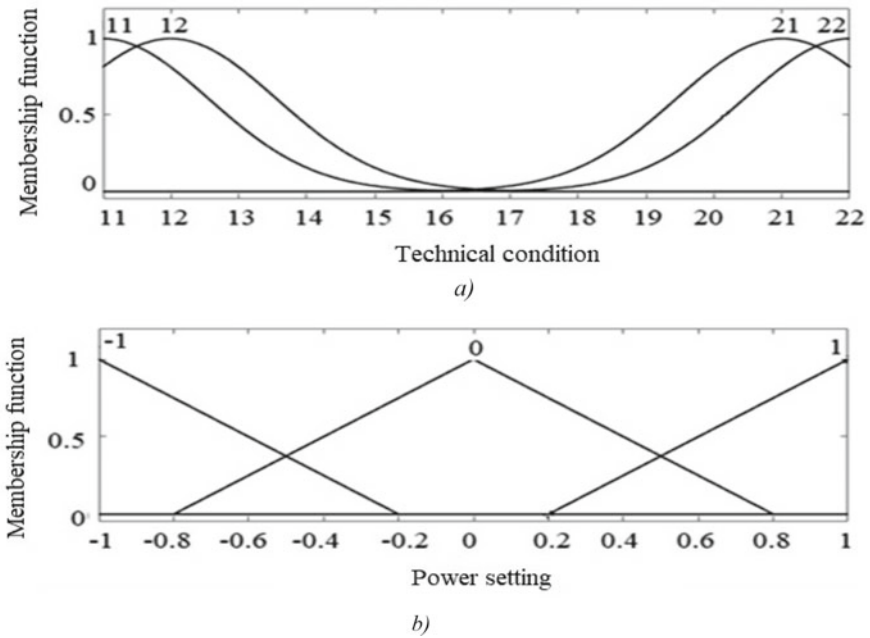


Fig. 4 Membership functions for vehicle movement optimizing fuzzy model: a—input functions; b—output functions

1. The input variables have acquired some concrete values  $x_1^0, x_2^0, x_3^0, x_4^0$ , and there are levels of “clipping” for the prerequisites of each rules:

$$\begin{aligned}
 \alpha_1 &= \min[A_1(x_1^0), A_1(x_2^0), A_1(x_3^0), A_1(x_4^0)]; \\
 \alpha_2 &= \min[A_2(x_1^0), A_2(x_2^0), A_2(x_3^0), A_2(x_4^0)]; \\
 \alpha_3 &= \min[A_3(x_1^0), A_3(x_2^0), A_3(x_3^0), A_3(x_4^0)]; \\
 \alpha_4 &= \min[A_4(x_1^0), A_4(x_2^0), A_4(x_3^0), A_4(x_4^0)].
 \end{aligned}
 \tag{1}$$

2. Outputs for each rule are calculated

$$y_1^* = f_1; \dots; y_n^* = f_n. \tag{2}$$

3. The aggregate output of fuzzy logic system is calculated

$$y_i^* = \sum_{i=1}^n \alpha_i \cdot y_i^* / (\sum_{i=1}^n \alpha_i) \tag{3}$$

The example of fuzzy inference graphic interpretation is the response surface (Fig. 5).

The result of the model can be interpreted as follows. After substitution of the coefficients showing the current state of each drive, for each of the four drives the

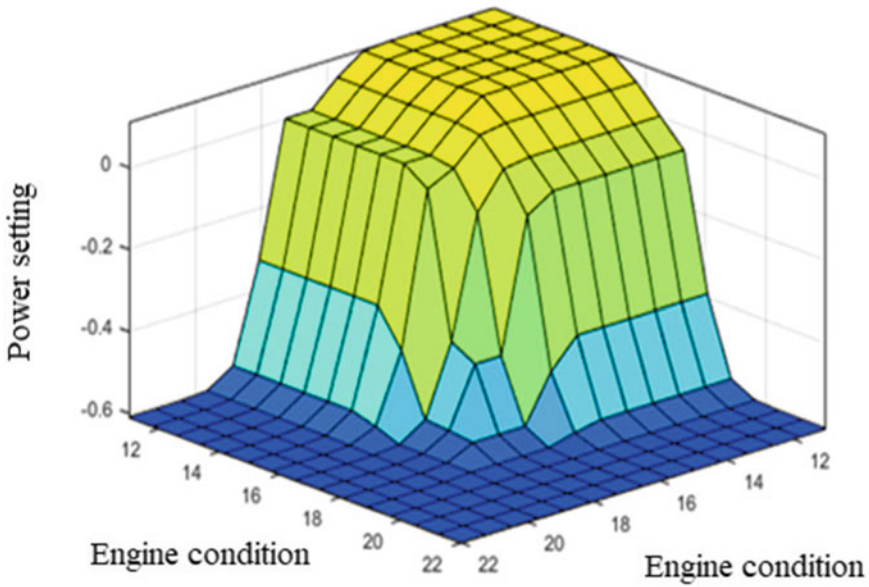


Fig. 5 The response surface of the vehicle movement optimizing fuzzy model

coefficient defining the required operating mode will be defined. A negative value indicates that the motor must be switched off. A value close to zero indicates that the operating mode should be left unchanged. The number close to 1 indicates the need to increase the engine speed.

The purpose of optimization is to ensure maximum speed and increase equipment life. As an example, a four-wheel drive vehicle (Fig. 2) [15] is considered. The degree of wear of the four-wheel drive vehicle is the sum of the degrees of wear of the drives of each wheel when performing a single technological operation  $t_i$  (4).

$$P(t_i) = p^1 + p^2 + p^3 + p^4, \tag{4}$$

where  $p^1, p^2, p^3, p^4$  is the degree of wear when performing a single technological operation of the drives  $D1, D2, D3$  and  $D4$  respectively.

At the same time, the wear of the drive for each wheel for a separate technological operation is defined as a function of three arguments:  $L$ —the length of the path traveled by the vehicle;  $M_{turn}$ —a variable that determines the additional load on the motor when performing rotation (for each drive, turns are taken into account as follows: for drives  $D1$  and  $D3$ —right, for  $D2$  and  $D4$ —left);  $S_{turn}$ —the total number of turns made by robots during the technological operation:

$$\begin{cases} p^1 = f(L, M_{turn}^1, S_{turn}) \\ p^2 = f(L, M_{turn}^2, S_{turn}) \\ p^3 = f(L, M_{turn}^3, S_{turn}) \\ p^4 = f(L, M_{turn}^4, S_{turn}) \end{cases} \tag{5}$$

To set the vehicle's trajectory, a specific configuration of the working space is selected, which is divided into  $n$  segments of equal area so that each of them uniquely determines the limits of one technological operation  $t_i$  ( $i = 1 \dots n$ ) for the vehicle (Fig. 6a). The task for vehicle movement is the set of all segments of the field so that the overall wear  $P_o$  of the drives was minimal:

$$P_o = \sum_{i=1}^n P(t_i) \rightarrow \min \tag{6}$$

Optional set is the condition that the wear  $P_o$  received minimal by its even distribution between the drives  $D1, D2, D3$  and  $D4$ .

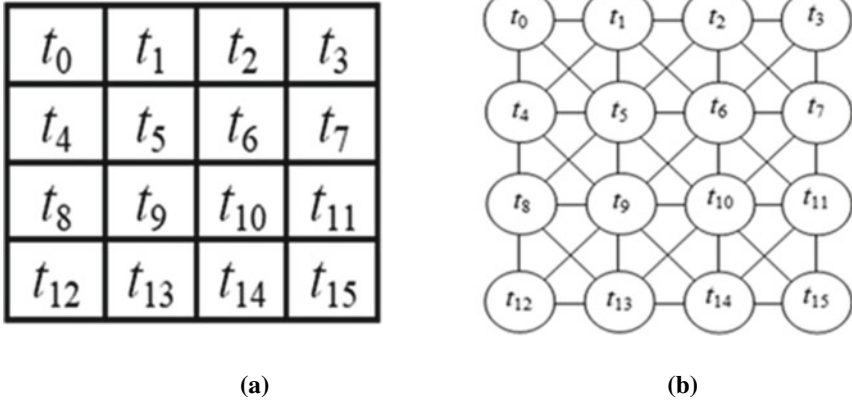


**Fig. 6** Working configuration (a) and graph representation (b) of a rectangular working space

The latter can be achieved with a minimum difference between the robot's right  $M_{turn(R)}$  and left turns  $M_{turn(L)}$

$$\sum M_{turn(R)} - \sum M_{turn(L)} \rightarrow \min \tag{7}$$

If for a specific configuration of the working area all  $n$  segments are presented in the form of a corresponding graph (Fig. 6b)  $T(V, E)$ , whose vertex set ( $V$ ) uniquely corresponds to the working area segments, and the edge set ( $E$ ) logically specifies the possible transitions between adjacent segments (technological operations), then the optimization objective function will have the following form:

$$G(P_0) = \left\{ t_i | f(t) = \sum_{i=1}^n P(t_i) \rightarrow \min \right\} \tag{8}$$

where

$$f(t) = k_1 \cdot L + k_2 \cdot M_{turn(R)} + k_3 \cdot M_{turn(L)} + k_4 \cdot S_{turn} \tag{9}$$

where  $i = 1 \dots n$ —the number of segments of the vehicle's working space;  
 $k_1, k_2, k_3, k_4$ —the weight of the control parameters of the optimization parameters.



$$\text{Fig. 7a } G(P_0) = \{t_0, t_1, t_2, t_3, t_7, t_6, t_5, t_4, t_8, t_9, t_{10}, t_{11}, t_{15}, t_{14}, t_{13}, t_{12}\}, \quad (10)$$

$$\text{Fig. 7b } G(P_0) = \{t_0, t_1, t_5, t_4, t_8, t_9, t_{10}, t_6, t_2, t_3, t_7, t_{11}, t_{15}, t_{14}, t_{13}, t_{12}\} \quad (11)$$

$$\text{Fig. 7c } G(P_0) = \{t_0, t_1, t_8, t_7, t_7, t_6, t_{11}, t_{15}, t_{14}, t_{13}, t_{12}, t_8, t_4, t_5, t_6, t_{10}, t_9, t_8, t_{12}\} \quad (12)$$

For the demonstration of turns within the chosen trajectories, the matrix of turns is introduced  $G(M_{turn})$ , the following notation is used: 0—no turn, 1—turn to the right, 2—turn to the left.

Then the matrix  $G(M_{turn})$ :

$$\text{Fig. 7a } M_{turn} = \{0, 0, 0, 1, 1, 0, 0, 2, 2, 0, 0, 1, 1, 0, 0, 0\} \quad (13)$$

$$\text{Fig. 7b } M_{turn} = \{0, 1, 1, 2, 1, 0, 2, 0, 1, 1, 0, 0, 2, 0, 0, 0\} \quad (14)$$

$$\text{Fig. 7c } M_{turn} = \{0, 0, 0, 1, 0, 0, 0, 2, 0, 0, 1, 0, 1, 1, 0, 2, 0\} \quad (15)$$

The results of the analysis of the given trajectories of movement are given in Table 1.

From this table it is clear that the trajectory 1 is optimal, since it is performed in the minimum number of operations and has 6 turns. The difference between the number of right and left turns is 2. Therefore, when working out a rectangular working space, the “snake” trajectory is optimal in terms of speed and deterioration parameters.

This task was solved using the genetic and ant colony algorithms. Figure 8 shows the results of these optimization algorithms when moving on a rectangular working area (Fig. 7).

From these graphs, it can be seen that both algorithms with the same source data have produced different trajectories of the same length with an equal number of right and left turns. However, the number of iterations of the ant algorithm is smaller, hence the speed is higher. Therefore, this algorithm can better solve the problem of multidimensional optimization of the movement distance by work in the workspace configuration, consider the wear of vehicle drives.

**Table 1** Results of the analysis of the specified trajectories of the robot

Trajectory number	Number of operations	Right turns	Left turns
1	16	4	2
2	16	5	3
3	19	5	2

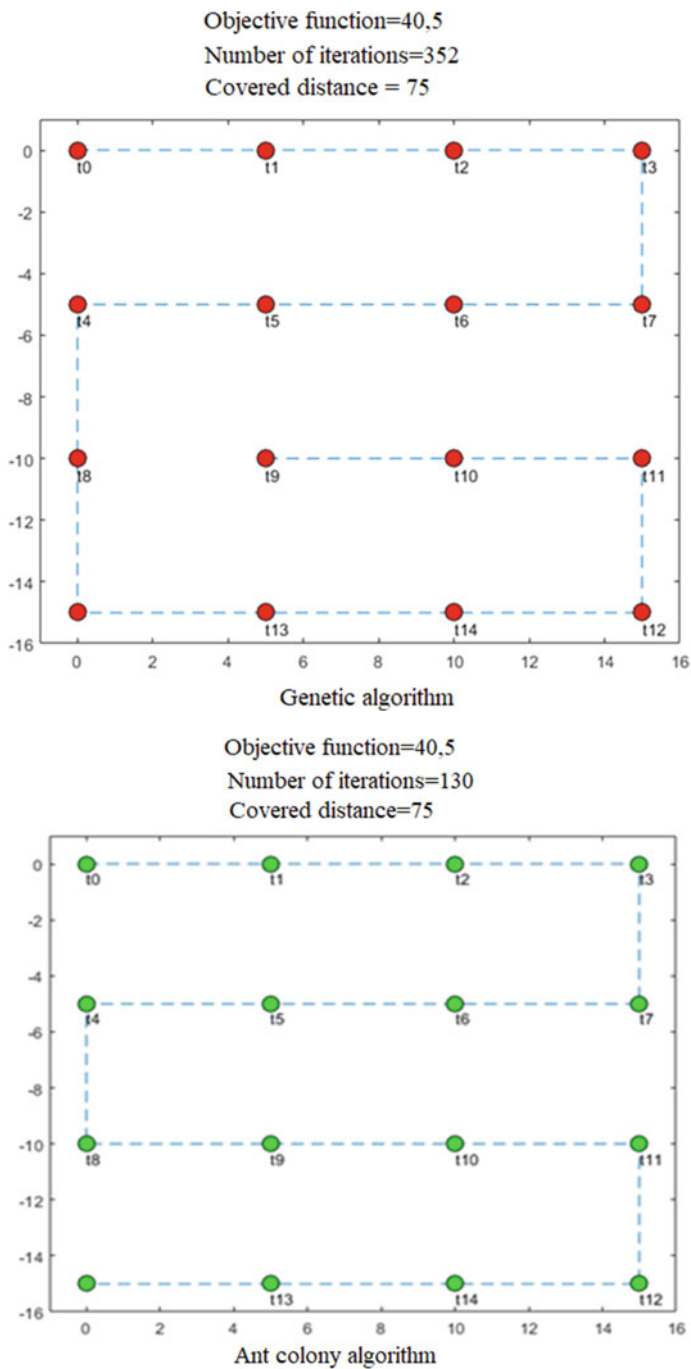


Fig. 8 Results of multivariate optimization of vehicle motion on a rectangular area

## 4 Conclusion

As a result of the work carried out, a vehicle movement optimizing fuzzy model, consider the technical condition and loads to the wheel drives. The criteria for vehicle optimal trajectory are formulated, taking into account the length of the trajectory, the number of right and left turns and the technical condition of the drives. For a specific configuration of the workspace consisting of  $n$  segments, a graph has been developed whose set of vertices uniquely corresponds to the segments of the workspace, and the set of edges logically defines possible transitions between adjacent segments (technological operations). The goal of optimization is to pass all segments of the working area along the shortest path with a minimum number of turns. In this case, the number of right and left turns should be approximately the same. Three analytical solutions of the optimization problem are given. Possible trajectories of movement are constructed and the number of turns of the vehicle is calculated. The same problem was solved using the genetic and ant colony algorithm. Both algorithms with the same source data have produced different trajectories of the same length with an equal number of right and left turns. The number of iterations of the ant algorithm is smaller, hence the speed is higher. Therefore, this algorithm can better solve the problem of multidimensional optimization of the vehicle movement.

**Acknowledgements** The researchers were carried out on the basis of Platov South-Russian State Polytechnic University (NPI) within the framework of the initiative research project P3-955 “Mechatronic and robotic systems for special purposes”.

## References

1. Bulgakov A, Kruglova T, Bock T (2018) A cyber-physical system of diagnosing electric drives of building robots. In: Digests 35th international symposium on automation and robotics in construction (ISARC 2018), pp 8–15
2. Bulgakov A, Kruglova T (2017) Intelligent method of electric drive diagnostic with due account for its operation mode. *J Appl Eng Sci* 15.4(465), 426–432
3. Bulgakov A, Kruglova T, Bock T (2018) Synthesis of the AC and DC drives fault diagnosis method for the cyber-physical systems of building robots. In: MATEC web of conferences, vol 251, p 03060
4. Kruglova T, Shaykhutdinov D, Shurygin D, Yanvarev S, Litvin D, Tarkovalin S, Zinin A (2016) Intelligent Sensorless fault diagnosis of mechatronics module wavelet transformation. *Asian J Inf Technol* 15(22):4694–4697
5. Kruglova TN (2017) Wavelet analysis for fault diagnosis of electrical machines using current signals. In: 2nd international conference on industrial engineering, applications and manufacturing (ICIEAM). IEEE Xplore, p 16838753
6. Kruglova TN (2015) Intelligent diagnosis of the electrical equipment technical condition. *Procedia Eng* 129:219–224
7. Peter WT, Yangb WX, Tama HY (2004) Machine fault diagnosis through an effective exact wavelet analysis. *J Sound Vib* 277:1005–1024



8. Nandi S, Toliyat HA, Li X (2005) Condition monitoring and fault diagnosis of electrical motors. In: IEEE conference transactions on energy conversion, vol 20, no 4, pp 719–729. Vancouver, Canada; J Mag
9. Shakouhi M, Mohamadian M, Afjei E (2015) Fault-tolerant control of brushless DC motors under static rotor eccentricity. *IEEE Trans Ind Electron* 62(3):1400–1409
10. Awadallah MA, Morcos MM (2005) Diagnosis of stator short circuits in brushless DC motors by monitoring phase voltages. *IEEE Trans Energy Convers* 20(1):2460–2470
11. Blum C, Roli A (2003) Metaheuristics in combinatorial optimization: overview and conceptual comparison. *ACM Comput Surv* 35(3):268–308
12. Dorigo M (1992) Optimization, learning and natural algorithms. PhD thesis, Dipartimento di Elettronica, Politecnico di Milano
13. Dorigo M, Stützle T (2010) Ant colony optimization: overview and recent advances. *Handbook Metaheuristics* 146(8):227–263
14. Mokhov VA, Kruglova TN, Shaikhutdinov DV, Vlasov AS (2019) Optimal technological process planning approach based on the state of mechatronic systems. In: IOP conference series: materials science and engineering, vol 483:012103, p 6
15. Kruglova TN, Shmelev IA, Sushkov I, Filatov RS (2019) Cyber-physical system of the mobile robot's optimal trajectory planning with taking into account electric motors deterioration. In: 2019 international multi-conference on industrial engineering and modern technologies (FarEastCon). IEEE

# Heat Pump Unit in Heating and Air Recuperation of Premises



Pavel Orlov , Tat'yana Il'ina , Maksim Kolesnikov , Alina Echina ,  
and Artem Umerenkov 

**Abstract** Energy-efficient methods of creating a microclimate of premises using renewable energy sources are considered. The feasibility of using heat recuperators of exhaust air is shown. Various types of recuperators are considered, their comparative characteristics are given. It has shown that the proposed calculations of their effectiveness give overestimated results, that does not correspond to reality. This work has developed a system for creating a microclimate of premises using an air heat pump of the Air–Water type. The use of such installations in areas with a cold climate is possible only with the use of the MOVEBIT de-icing system developed by us in the form of magneto-constrictive transducers installed on the surface of the heat exchanger of the evaporation unit. The microclimate system includes two evaporation circuits. The primary circuit works for heating using outdoor heat. The second evaporator connected in series to the first one is located in the exhaust air heat recovery circuit of the ventilation system. Heat exchanger of evaporation unit is made of aluminium and has certain shape, which is most favorable for de-icing. The tests showed an increase in the overall coefficient of performance (COP) of the complex heat pump installation by 20%.

**Keywords** Heat pump · Recuperator (heat exchanger) · Evaporation unit · De-icing system · Coefficient of performance of a heat pump

---

P. Orlov (✉) · T. Il'ina · M. Kolesnikov · A. Echina  
Belgorod State Technological University Named After Shukhov V.G, 46, Kostyukova Str.,  
Belgorod 308012, Russia  
e-mail: [orlovpavel67@gmail.com](mailto:orlovpavel67@gmail.com)

T. Il'ina  
e-mail: [ilina50@rambler.ru](mailto:ilina50@rambler.ru)

M. Kolesnikov  
e-mail: [makskol97@mail.ru](mailto:makskol97@mail.ru)

A. Umerenkov  
Southwest State University, 94, 50 Let Oktyabrya Ul., Kursk 305040, Russia

## 1 Introduction

The Russian government pays great attention to the conservation of the environment, as well as the development of energy-saving technologies, supporting Russian producers at all stages of production [1]. Domestic manufacturers of ventilation equipment, in cooperation with technical universities, conducting large research work, have achieved high indicators in scientific research and increasing the technical level of energy-saving equipment. Taking into account that heat loss through ventilation systems accounts for an average of 25% of the energy spent on heating of the building, the relevance of the introduction of heat energy utilization systems from the exhaust air becomes the most urgent task in the field of energy saving [2].

For forced ventilation systems of residential and public buildings, various types of recuperators have recently been used. The most common are plate heat exchangers, rotary heat exchangers and recuperators with intermediate coolant. Simplicity of design, low power consumption and long service period made this equipment the most in-demand in private households. For example, in Finland, at the legislative level, a mandatory installation of plenum and exhaust ventilation with heat recovery from the exhaust air was adopted. In Russia, the regulation SP 55.13330.2016 for private houses does not yet provide for the arrangement of forced ventilation, subject to air exchange, guided to a greater extent by the norms of SanPiN 2.1.2.2645 and GOST 30494–2011, nevertheless, interest in various energy-saving ventilation systems is constantly growing.

Despite the favorable conditions created by the government for domestic manufacturers of heat recovery units, the Russian consumer prefers European, Japanese, Korean and Chinese manufacturers, guided by high energy-saving indicators declared by foreign manufacturers and confirmed by graphs, diagrams, as well as the presence of a heat recovery energy efficiency class. According to Regulation (EU) No 1253/2014 of the European Parliament, a system of classes from A to G is introduced for heat recovery units, special attention is paid to the class table indicating energy efficiency (SEC)—the specific energy consumption per  $1\text{m}^2$  of heated building area. The calculation is made according to the equation [3], which takes into account a large set of parameters.

Obtaining the entire data set is a very problematic task, and the energy conversion efficiency of recuperation unit is the most important indicator of the efficiency of the equipment offered. The average temperature of the heating season does not correspond to the Russian average working hours per year. The use of inverter electric fans increases energy efficiency twice, which is impossible to implement in practice, since the cost of starting currents in start-stop and stepper fans does not exceed 25%.

Considering that the buildings put into operation are obliged to test the tightness of the enclosing structures, air inflow is carried out only through ventilation systems.

It is not always possible to calculate the standard heat losses of a residential building through enclosing structures with sufficient accuracy, therefore there are empirical calculation methods for selecting the necessary parameters of recovery

equipment, which allow assessing the main consumer qualities of ventilation equipment, their energy-saving capabilities.

According to the law of transitivity of thermodynamic equilibrium (the zeroth law of thermodynamics) and design features, the rotary recuperator is unable to overcome the 50% barrier of heat extraction from the exhaust air. If we still take into account the flow of air through the brush seals and seals along the perimeter of the case, where the air masses of the supply and exhaust air are mixed, we can conclude that the rotary recuperator is even less effective than conventional plate recuperators, since it requires additional costs of electricity driving the rotor using a stepper or inverter motor. Its real figure corresponds to 40–50%. As an advantage in favor of rotary recuperation units, there is no frostbite on the heat transfer plates of the rotor, however, the installation instructions and settings of this equipment give clear instructions for activating the defrosting function.

In practice, this problem is solved by increasing the speed of the fan installed on the exhaust duct after the rotor. This is a very effective method of heating the rotor, but heat losses during this period increase in proportion to the difference in the supply and removed air flows, since warm air does not have time to transfer half of its heat to the heat-removing elements [5]. Another method of increasing the temperature of the supply air is the installation of an electric heating element.

Taking into account the fact that from 1 kW of electricity, one kilowatt of thermal energy can be obtained, and from 1 m<sup>3</sup> of gas about 7 kW of heat, with their small difference in the cost of electric heating reduces the economic feasibility of installing expensive supply and exhaust systems [5, 6]. As a rule, the power of electric heating elements ranges from 3 to 7 kW, the reduction in gas consumption for heating the room does not cover the cost of electricity consumed by the recuperator, which makes the recuperators even less efficient.

There are also design solutions used in recuperation units, such as cascade recuperators. This is a unit with 3–6 plate heat exchangers with a declared efficiency up to 90%. In practice, in such recuperators, the flow of supply and exhaust air is mixed between the channels due to the lack of density at the connection points of the modules. The actual recovery efficiency of the plate recuperator cannot exceed 50% of the heat extraction mark, does not depend on its shape, the same applies to countercurrent heat exchangers [6]. The main problem of the existing assessment of the efficiency of the recuperation units is the fact that the exhaust air has arithmetic mean values of the exhaust and supplied air, according to it heat is not fully extracted. One solution to this technical problem is to install a heat pump evaporator in the path of the air to be exhaust. Without the establishment of high temperature pressure (the difference between the boiling point of the refrigerant and the temperature of the exhaust air), 100% heat extraction cannot be carried out.

## 2 Materials and Methods

Heat pump units are increasingly used in microclimate systems of buildings and structures [7, 8]. This is explained by environmental compatibility, the possibility of using renewable energy sources, requirements for reducing harmful emissions into the atmosphere when burning fuel, both gaseous and solid [9]. Taking into account the current political situation, the use of heat pumps is especially important for the countries of Europe and Scandinavia. It is known that the source of thermal energy can be earth, water, air, thermal emissions of various technological processes [9, 10]. Considering the cost of laying and operating heat pump units, air heat pumps are preferred. However, their use is limited in countries with cold climates as a result of frost and ice on the surface of the heat exchanger of the evaporator unit. To prevent and remove ice, various methods (bypass, heaters, special compositions, etc.) are invented, which suspend the operation of the unit for a while, which reduces the efficiency of the cycle [11]. We have proposed and developed a method for de-icing with the help of mechanical vibrations created using magnetostrictive radiators [12]. The material, the shape of the radiator, the method of attachment on the surface of the heat exchanger of the evaporating unit are selected, the shape of the heat exchanger is developed, which contributes to the best defrosting [13]. Testing of the pilot unit in a wide temperature range showed satisfactory results, the coefficient of performance of a heat pump is 4.5–5.6 [14]. Significant interest should be noted in studies of various types of heat pumps, their design, methods of use in heat supply systems of both private houses and industrial premises, as well as methods of ice control [15–21].

This work uses the air heat pump system with the MOVEBIT anti-icing system of the Air–Water type for the heating and air recovery system of the premises. To increase the energy efficiency of the microclimate system, a sequential installation of evaporating units is proposed. The primary circuit evaporator is used to take outside air heat and transfer it to the heating circuit condenser. The second circuit evaporator is located in the exhaust air recuperator.

The work uses a steam compression refrigeration unit operating according to the reverse reversible Carnot cycle. A coolant circulates along the closed circuit, changing its aggregate state and the heat of phase transitions is used to remove and release heat. Proposed unit comprises evaporator, condenser, compressor to control valve to reduce pressure downstream of condenser. The installation diagram is shown in Fig. 1.

An example of implementation of the integrated air ventilation and recovery system is presented in Fig. 2, designations to Fig. 1.

The installation works in the following way: Refrigerant evaporates in the primary circuit evaporator (1). Gaseous refrigerant flows into compressor 12 to compress refrigerant in gaseous state to increase its temperature and pressure. Gas at temperature  $\approx 65$  °C is supplied to heat exchanger (refrigerant–water) of condenser (11). The removed heat is supplied via the water supply to the heating radiators (10) and the warm floor (9), as well as to the fan oil (5) for heating the supply air (winter operating mode) or cooling (summer operating mode).

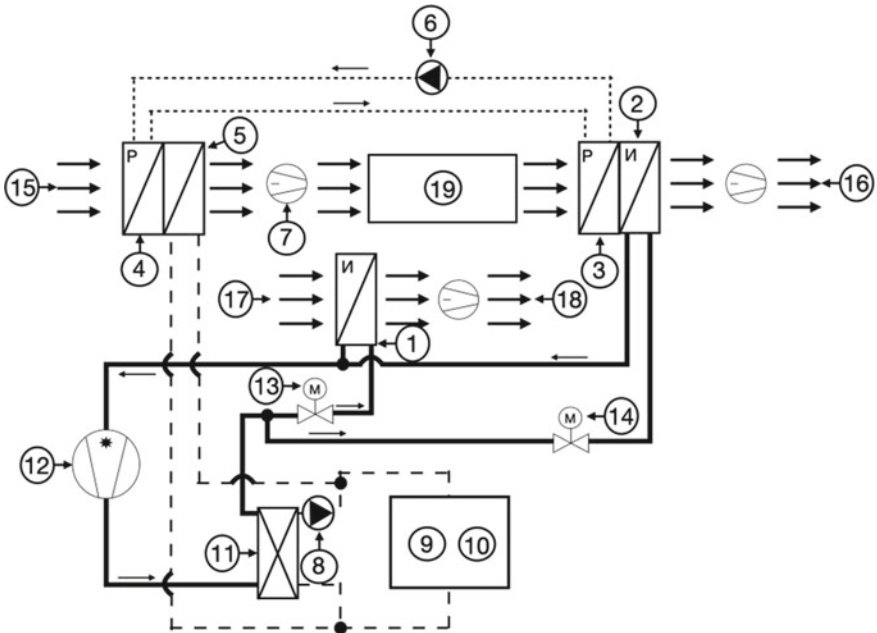


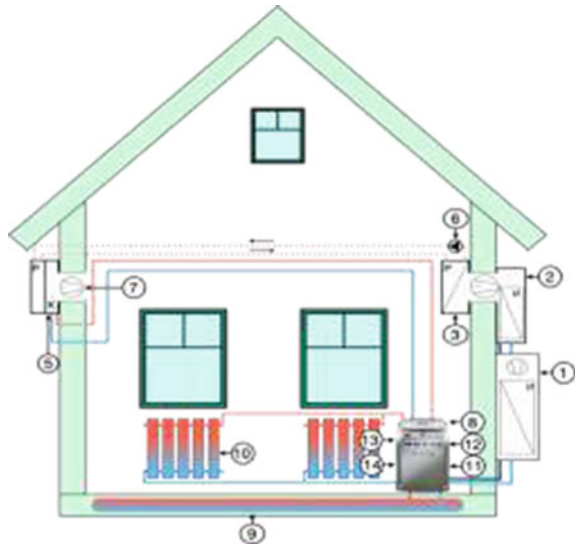
**Fig. 1** Diagram of the air heating and recovery system using the Air–Water air heat pump: 1—primary circuit evaporator; 2—evaporator of the secondary circuit; 3—heat exchanger of air recuperator; 4—heat exchanger in the supply channel; 5—fancoil; 6—circulation pump; 7—supply fan; 8—circulation pump on heating line; 9, 10—heating devices (radiators, heat-insulated floor); 11—heat exchanger of condenser; 12—compressor of the heat pump unit; 13—throttling device of the primary circuit evaporator; 14—throttling device of the secondary circuit evaporator; 15—flow of external air of the recuperation circuit; 16—flow of recuperation circuit air to be removed; 17—plenum external air of the primary heat removal circuit; 18—exhaust air after the primary heat removal circuit evaporator; 19—premise

Coolant circulation is performed by means of pump (8). Supercooled refrigerant is supplied through throttling device (13) to external unit of primary circuit evaporator (1). Second pipeline with coolant is fed to second circuit evaporator 2 via throttling device 14.

The evaporator (2) of the secondary circuit is located in the exhaust air channel, in which additional heat extraction takes place after the heat exchanger (3), which is part of the Water–Air recuperation system. Heated water containing 25% glycol is supplied by means of pump (6) to heat exchanger (4), which is located in supply channel before fan coil (5). Air flow is produced by using axial fans—supply fan (7) and exhaust fan (16). The prepared air enters the premise (19).

To cool the air in the warm period, the heat pump is operated in the refrigeration cycle with the reverse of the coolant movement in the opposite direction.

**Fig. 2** An embodiment of an integrated heating and air recirculation system



### 3 Results and Discussion

An experimental installation was used to determine the efficiency of the heat pump in the complex heating and ventilation system.

The heat exchanger designed for the external AHP unit was used as a heat exchanger in the air recuperator. The installation diagram is shown in Fig. 3.

The experiments were carried out in two stages. The first stage is the operation of the heat pump without a recuperator. At the second stage evaporator is connected in heat recovery system of exhaust air. The same conditions are established for the operation of the pressure block of both circuits. For this purpose, the external unit was placed in a refrigeration chamber with an air temperature of  $-4.3\text{ }^{\circ}\text{C}$ . The temperature of the exhaust air from the premise was  $25\text{ }^{\circ}\text{C}$ , the air temperature after the recuperator was within  $0\text{ }^{\circ}\text{C}$ . The test results are shown in Table 1.

By using a traditional rotary or plate recuperator, its efficiency was no more than 50%. In this embodiment, the heat recovery percentage is 85%.

I.e. we get the efficiency of the developed recuperator 1.8 times higher than existing on the market air recuperators without using a scheme in which the evaporator is installed in the stream of removed air after a conventional recuperator.

Analysis of the results of the operation of the recuperator integrated into the heat pump heating system showed that:

- power consumption decreased from 601 to 532 W, which amounted to 11.3%;
- heat pump COP increased from 3.16 to 3.95 by 20%;
- the heating capacity of the unit increased from 1900 to 2100 W.

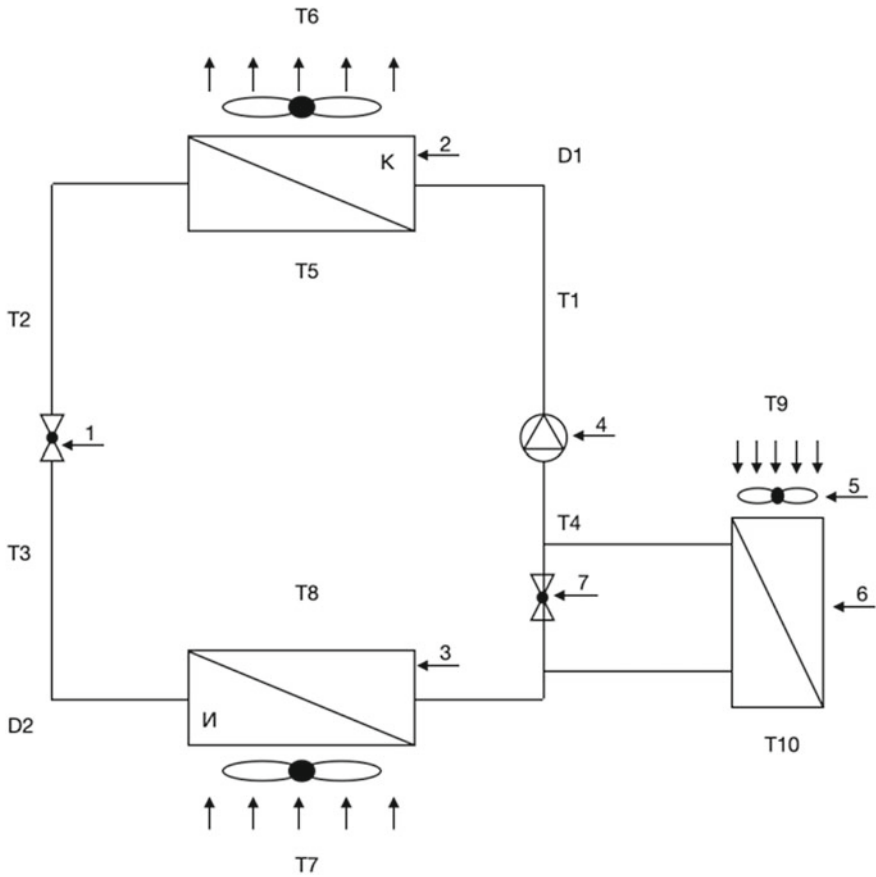


**Fig. 3** Diagram of the laboratory installation of the integrated heating and recovery system using the heat pump installation: 1—TEV—thermal expansion valve; 2—capacitor; 3—evaporator of the external AHP unit; 4—compressor; 5—exhaust fan; 6—heat exchanger of the recuperator of exhaust from the premise; 7—adjustment valve

## 4 Conclusion

Analysis of existing types of recovery units showed that their actual efficiency does not exceed 50%. Heat losses through exhaust ventilation can be significantly reduced by using the evaporator in the heat recovery system. Experimentally, it was found that the temperature of the exhaust air was approximate to the temperature of the outside. A promising method of ensuring the microclimate parameters of the premise is a complex system for using an air heat pump with an additional evaporating unit built into the air recovery system. This will lead to an increase in the heat transformation of the heat pump unit, a decrease in electricity consumption and an increase in the heat capacity of the microclimate system.



**Table 1** Test results of the integrated heating and air recovery system

Test data					
Nº	Measurable values	Unit of measurement	With recuperator	Without recuperator	Symbols in the diagram
1	Ambient temperature	°C	−4.3	−4.7	T7
2	Air temperature downstream of evaporator	°C	−5.1	−8.0	T8
3	Refrigerant temperature downstream of TEV	°C	−11,2	−11.5	T3
4	Suction line pressure	Bar	4.51	3.37	D2
5	Compressor inlet temperature	°C	−11.2	−11.5	T4
6	Refrigerant temperature upstream of compressor outlet condenser	°C	67.3	69.7	T1
7	Refrigerant temperature downstream of condenser	°C	32.9	30.9	T2
8	Discharge pressure	Bar	21.42	21.26	D1
9	Air temperature upstream of condenser	°C	25.1	25.6	T5
10	Air temperature downstream the condenser	°C	35.7	35.1	T6
11	Heat performance of the heat pump	W	2100	1900	
12	Air temperature prior to recuperator	°C	25.0	–	T9
13	Air temperature at the recuperator outlet	°C	0.1	–	T10
14	Line voltage	°C	229	236	
15	Current consumption value	I	3.1	3.4	

(continued)

**Table 1** (continued)

Test data					
Nº	Measurable values	Unit of measurement	With recuperator	Without recuperator	Symbols in the diagram
16	COS F		0.75	0.75	
17	Active power	W	532	601	
18	COP		3.95	3.16	

This work was realized in the framework of the program «Priority 2030» on the base of the Belgorod State Technological University named after V G Shukhov, Using equipment of High Technology Center at BSTU named V. G. Shukhov.

Analytical research/research was done using equipment of NRC “Kurchatov Institute”—IREA Shared Knowledge Center.

## References

1. Federal Law of the Russian Federation dated November 23 (2009) No. 261-FZ. On energy saving and on improving energy efficiency and on amending certain legislative acts of the Russian Federation
2. Suszanowicz D (2018) Optimisation of heat loss through ventilation for residential buildings. Atmosphere. [mdi.com](https://mdpi.com/mdi.com)
3. CEN/TC 156—Ventilation for buildings EN 13141-7:2021 (2021)
4. De Antonellis S, Intini M, Joppolo CM, Leone C (2014) Design optimization of heat wheels for energy recovery in HVAC systems. *Energies* 7:7348–7367. <https://doi.org/10.3390/en7117348>
5. Kalabin SE (2005) Economic effect from the introduction of energy-saving equipment: plate heat exchangers, unit individual heating stations [Electronic resource]. J “S.O.K” 8. <https://www.c-o-k.ru/articles/ekonomicheskij-effekt-ot-vnedreniya-energoberegayuschego-oborudovaniya-plastinchatyh-teploobmennikov-blochnyh-individual-nyh-teplovyh-punktov>
6. Marketing research of the Russian plate heat exchanger market [Electronic resource]. Techart. <https://research.techart.ru/report/heat-exchange-equipment-market-research.htm>
7. Orlov PA, Uvarov VA, Il'ina TN, Orlova VA, Orlov KP, Orlov SP (2020) Environmental impact of installation and use of geothermal heat pumps. In: Intercollegiate international congress. Graduate School: Scientific Research, Moscow, December 10, 2020, vol 1 S. Infinity Publishing House, Moscow, pp 136–147. <https://doi.org/10.34660/INF.2020.35.61.024>
8. Serikov SV, Il'ina TN (2013) Heat utilization of the outgoing gases of the boiler plant in the air heating system. *Bull BSTU named after V.G. Shukhova* 4:53–55
9. Il'ina TN, Belmaz DN (2014) Analysis and methods of recycling secondary energy resources of oil refinery. *Bull BSTU named after V.G. Shukhova* 3:170–173
10. Il'ina TN, Mukhamedov RY, Verevkin OV (2009) Prospects for the use of heat pumps in heating systems for low-rise residential buildings in the Belgorod Region. *Bull BSTU named after V.G. Shukhova* 3:142–146
11. Orlov PA, Il'ina TN, Orlov KP (2021) Promising methods of ice control of air heat pump evaporators. In: Innovations and technologies in construction (BUILDINTECH BIT 2021). *J Phys: Conf Ser* 1926:012017. IOP Publishing. <https://doi.org/10.1088/1742-6596/1926/1/012017>
12. Orlov PA, Il'ina TN, Orlov KP (2021) Impact of mechanical vibrations on the icing of air heat pump evaporators. *Bull BSTU named after V.G. Shukhova* 6(6):36–44. <https://doi.org/10.34031/2071-7318-2021-6-6-36-44>

13. Il'ina TN, Orlov PA, Chizhov AV (2021) Influence of material structure on the magnetostrictive properties of a radiator for defrosting heat exchangers of ventilation equipment. *Construct Mater Prod* 4(4):5–10
14. Orlov PA, Il'ina TN, Orlov KP (2022) Test of heat pump unit with MOVEBIT anti-icing system. *Construct Mater Prod* 5(2):43–50
15. Sayegh MA et al (2018) Heat pump placement, connection and operational modes in European district heating. *Energy Build* 166:122–144
16. Jiang Y, Fu H, Yao Y, Yan L, Gao Q (2014) Experimental study on concentration change of spray solution used for a novel non -frosting air source heat pump system. *Energy Build* 68:707–712
17. Tressler JF (2008) Piezoelectric transducer designs for sonar applications. In: Safari A, Akdoğan EK (eds) *Piezoelectric and acoustic materials for transducer applications*. Springer, Boston, MA. [https://doi.org/10.1007/978-0-387-76540-2\\_11](https://doi.org/10.1007/978-0-387-76540-2_11)
18. Ewald F, Mohammad AS (2008) *Power quality in power systems and electrical machines*, 1st edn. Masoum Publisher and Academic Press
19. Jiankai D, Yigiang J, Yang Y, Xue-dan Z (2011) Operating performance of novel reverse-cycle defrosting method based on thermal energy storage for air sources heat pump. *J Cent South Univ Technol* 18:2163–2169
20. Giles DS, Atherton DL (1984) Theory of ferromagnetic hysteresis (invited). *J Appl Phys* 55(6):2115–2120
21. Pecherskaya RM, Chizhov AV (2014) Method of determination of maximum magnetic permeability of permalloys in constant magnetic field. *Sci Tech Bull Volga Region* 3:202–206

# Study of Composition and Characteristics of Wood-Gypsum Composite



Timofey Gorokhov , Aleksander Erofeev , Nikita Kovalev ,  
Sergey Gorokhov , and Sergey Emelyanov 

**Abstract** The composition and characteristics of the developed wood-gypsum composite material of the optimal composition were investigated. The wood-gypsum composite material can be used both as a finishing material for interior finishing and as a repair composition. Optimal is the following composition by weight: 45% gypsum grade G16, 16% second grade pine sawdust with a fraction of 5 mm, 39% water. The moisture content of the composite material was determined using a gravimetric measurement method based on the extraction of moisture from the material and the calculation of its mass fraction. The moisture content of the wood-gypsum composite material is  $26.3 \pm 1.2\%$ . The study was conducted on a moisture meter AND ML-50 instrument. The specific surface area was measured by the Brunauer–Emmett–Teller (BET) method using a highly efficient gas absorption analyzer with three micropore analysis stations and four specialized built-in ports for sample preparation (degassing). The specific surface area of the material was  $9.9 \text{ m}^2/\text{g}$ . Elemental analysis was also performed, which makes it possible to quantitatively and qualitatively establish the composition of the composite material. Elemental analysis showed that the developed wood-gypsum composite is more than 98% composed of Ca and Sx.

**Keywords** Gypsum · Gravimetric method · Elemental composition · Composite · Specific surface area · Wood

---

T. Gorokhov · A. Erofeev (✉) · N. Kovalev · S. Gorokhov  
Tambov State Technical University, 106, Sovetskaya Ul, Tambov 392024, Russia

S. Emelyanov  
South West State University, 50 Let Oktyabrya Street, 94, Kursk 305040, Russia

© The Author(s), under exclusive license to Springer Nature Switzerland AG 2024  
N. Vatin et al. (eds.), *Modern Problems in Construction*,  
Lecture Notes in Civil Engineering 372,  
[https://doi.org/10.1007/978-3-031-36723-6\\_7](https://doi.org/10.1007/978-3-031-36723-6_7)

## 1 Introduction

The modern market of building materials every year offers new types and varieties of materials, including finishing. One such material is a wood-gypsum composite. It uses gypsum binder of G16 grade as matrix. Second grade pine sawdust with a fraction of 5 mm acts as a filler and is designed to reduce the cost of making the product, as well as improve the thermophysical characteristics of the material. Also, the use of wood sawdust in the production of composite material partially solves the issue of their disposal. In the course of experimental studies, it was found that the optimal composition of the wood-gypsum composite is the following composition by weight: 45% gypsum grade G16, 16% second-grade pine sawdust with a fraction of 5 mm, 39% water.

Due to the fact that the developed wood-gypsum composite is a new material, it is necessary to study its characteristics, including composition.

## 2 Materials and Methods

To determine the moisture content of the wood-gypsum composite, a gravimetric method for measuring moisture was used, which is based on determining the mass fraction of moisture in the material. The method is versatile and highly accurate. The error of the method is due to the probability of incomplete removal of moisture from the sample, as well as the removal of volatile components or oxidation occurring during drying. The main drawback is the duration of the measurement (from 5 to 15 h, sometimes more).

To determine the moisture content of the wood-gypsum composite, an AND ML-50 device (moisture meter) was used (Fig. 1), the principle of which is based on the analysis of moisture that evaporates when the sample is heated (thermographic method). Thus, air-heat drying of weighed material weighing up to 50 g takes place to equilibrium with the environment (removal of moisture from the sample). The device consists of analytical scales and a drying cabinet.

The study was carried out according to the following program: 1) heating a sample of wood-gypsum composite to 250 °S; 2) holding until weight loss ceases for 15 min.

The specific surface area of the wood-gypsum composite was measured using the Brunauer–Emmett–Teller (BET) method using an Autosorb IQ station 1 high-performance gas sorption analyzer. The physisorption/chemisorption micropore analyzer (Fig. 2) with three micropore analysis stations and four specialized built-in ports for sample preparation (degassing). The BET (Brunauer–Emmett–Teller) specific surface is the most common method. It is worth noting that a number of assumptions are used when applying the method. The first assumption is that the adsorbent surface is uniform. By adsorbent is meant the phase on which adsorption takes place, i.e. the phase which will form the surface. A second assumption is

**Fig. 1** Moisture meter AND ML-50



that the reaction in the adsorbate–adsorbate system is weaker than in the adsorbant–adsorbate system. By adsorbate is meant a substance which is adsorbed. The third assumption is that the interaction of adsorbed molecules is only taken into account in the direction perpendicular to the surface and is considered as condensation.

In fact, any type of microporous solid is analyzed with the Autosorb IQ station 1 analyzer. The physics/chemisorption micropore analyzer is analyzed with equal ease thanks to powerful Windows-based software, the most extensive set of methods for calculating pore sizes from density functional theory (DFT) and a wide range of cell types for samples. Metal-to-metal (VCR) fittings used in the measuring manifold (s) to provide extremely low leakage rates allow high quality micropore size measurements using 0.1 torr or 1 torr sensors. Each physical absorption analysis station is served by its own specialized measuring collector and a set of sensors. A special  $P_0$  (saturation pressure) sensor and a dewar with a long life (more than 90 h even with three samples) are standard functions.

One port is available as a chemisorption station to fully characterize the catalyst complete with a high temperature oven combined with fan cooling. This

**Fig. 2** Autosorb IQ station 1



station retains its physical absorption capability. Chemisorption versions are also offered with additional flow-based measurement capabilities (TPR, TPO, TPD, pulse titration).

The steam dosing option is available for both physical and chemisorption versions and is equipped with a collector chamber with 50 °C thermostating.

To calculate the surface area of the adsorbent, the gas volume relative to the monomolecular layer and the cross-sectional area of the adsorbed gas molecule are determined. The accuracy of measuring the surface area with such a device is about 90%.

### 3 Results and Discussion

The moisture content of the material was determined by the gravimetric method on the moisture meter AND ML-50 (program: heating the material to 250 °S and holding until the weight loss ceases for 15 min):  $26.3 \pm 1.2\%$  [1–3].

The total pore volume of the wood-gypsum composite of the optimal composition is  $0.016 \text{ cm}^3/\text{g}$ . The DFT report is shown in Fig. 3. The histogram of the distribution of pores of the wood-gypsum composite of the optimal composition is shown in Fig. 4. According to the studies, the specific surface area of the wood-gypsum composite was  $9.9 \text{ m}^2/\text{g}$  [4, 5]. The results of the Brunauer–Emmett–Teller method are reported in Fig. 5.

Elemental analysis of the developed wood-gypsum composite was also carried out, which made it possible to carry out qualitative detection and quantitative determination of the elemental composition of the material [6, 7]. Studies were performed on two sample samples. The results are shown in Fig. 6.

Elemental analysis showed that the developed wood-gypsum composite is more than 98% composed of Ca and Sx in a ratio of 65.23 and 33.23%, respectively. In addition, minor amounts of Fe, Sr, Px (up to 0.1% each) and Si, Ti, Mn (up to 0.01% each) were found in the material [8].

**Fig. 3** Data processing results

<u>DFT method summary</u>	
Pore volume =	0.016 cc/g
Surface area =	6.348 m <sup>2</sup> /g
Lower confidence limit =	4.702 Å
Fitting error =	2.324 %
Half pore width (Mode) =	7.049 Å
Moving point average :	off

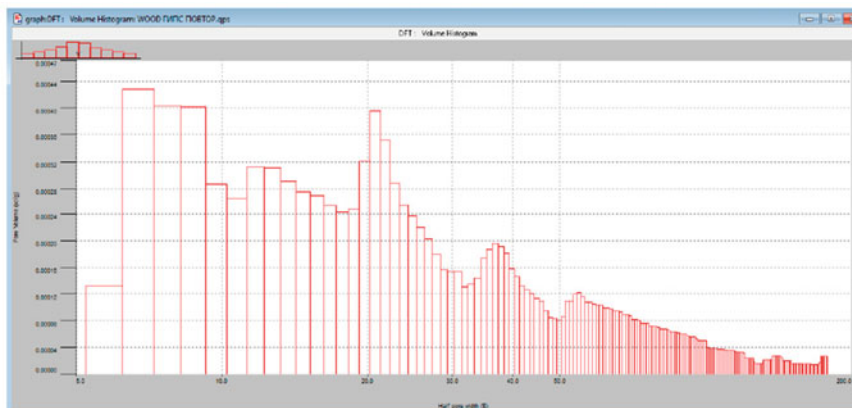


Fig. 4 Histogram of pore size distribution

Quantachrome® ASiQwin™ - Automated Gas Sorption Data			
Acquisition and Reduction			
© 1994-2016, Quantachrome Instruments			
version 5.0			
<b>Analysis</b>		<b>Report</b>	
Operator: TGTU	Date:2022/05/06	Operator: Öböyüä	Date:2022/06/01
Sample ID: WOOD ÄÄÑ ÄÄÖÖ	Filename: WOOD ÄÄÑ ÄÄÖÖ.qps	Comment: WOOD ÄÄÑ ÄÄÖÖ	
Sample Desc:	Instrument: Autosorb IQ Station 1		
Sample Weight: 1.2988 g	Final Outgas Temp.: 200 °C	Extended info: Available	
Approx. Outgas Time: 2.5 hrs	Non-ideality: 6.58e-05 1/Torr	CellType: 12mm	
Analysis gas: Nitrogen	Bath temp.: 77.35 K	VoidVol Remeasure: off	
Analysis Time: 10.43 hr:min	Cold Zone V: 13.1393 cc	Warm Zone V: 19.3931 cc	
Analysis Mode: Standard	<b>Data Reduction Parameters</b>		
VoidVol. Mode: He Measure	Eff. mol. diameter (D): 3.54 Å	Eff. cell stem diam. (d): 4.0000 mm	
Thermal Transpiration: on			
<b>Adsorbate mode</b>	<b>Nitrogen</b>	<b>Temperature</b> 77.350K	<b>Liquid Density:</b> 0.808 g/cc
	<b>Molec. Wt.:</b> 28.013	<b>Cross Section:</b> 16.200 Å²	
<b>Relative Pressure</b>	<b>Volume @ STP</b>	<b>1 / [ W(Po/P) - 1 ]</b>	
<b>P/Po</b>	<b>cc/g</b>	<b>1/g</b>	
5.06922e-02	1.9333	2.2099e+01	
7.39650e-02	2.1148	3.0220e+01	
9.92497e-02	2.2751	3.8751e+01	
1.24855e-01	2.4104	4.7271e+01	
1.49886e-01	2.5298	5.5764e+01	
1.75030e-01	2.6508	6.4040e+01	
2.00330e-01	2.7401	7.3150e+01	
2.25169e-01	2.8397	8.1881e+01	
2.50122e-01	2.9395	9.0791e+01	
2.75133e-01	3.0362	1.0002e+02	
3.00072e-01	3.1359	1.0938e+02	
	<b>BET summary</b>		
	Slope = 347.776 1/g		
	Intercept = 4.014e+00 1/g		
	Correlation coefficient, r = 0.999820		
	C constant = 87.651		
	Surface Area = 9.899 m²/g		

Fig. 5 Experimental report



## Проба №1

SAMPLE ANALYSIS REPORT  
 ARL QUANT'X EDXRF ANALYZER

THERMO FISHER SCIENTIFIC  
 UNIQUANT(TM) STANDARDLESS METHOD

---

C:\UQed\USER\RhKetV\Job\JOB.194 2022-04-25 13:17:37  
 Proba1

Quant'X No.2028 Rh-tube Ketec - CAL-Vac  
 C:\UQed\USER\RhKetV\Appl\AnySampleAir.kap 2017-11-22  
 Calculated as : Elements Matrix (Shape & ImpFc) : 4|Ca..  
 X-ray path = Air Film type = No supporting film  
 Case number = 0 All known  
 Eff.Diam. = 13.0 mm Eff.Area = 132.7 mm2  
 KnownConc = 0 %  
 Rest = 0 % Viewed Mass = 1901.250 mg  
 Dil/Sample = 0 Sample Height = 15.0 mm

El	m/m%	StdErr
Ca	65.24	0.24
Sx	33.22	0.24
Fe	0.648	0.032
Sr	0.539	0.027
Px	0.205	0.020
Si	0.095	0.015
Ti	0.0306	0.0017
Mn	0.0150	0.0028

KnownConc= 0 REST= 0 D/S= 0  
 Sum Conc's before normalisation to 100% : 42.1 %

## Проба №2

SAMPLE ANALYSIS REPORT  
 ARL QUANT'X EDXRF ANALYZER

THERMO FISHER SCIENTIFIC  
 UNIQUANT(TM) STANDARDLESS METHOD

---

C:\UQed\USER\RhKetV\Job\JOB.195 2022-04-25 13:17:37  
 Proba2

Quant'X No.2028 Rh-tube Ketec - CAL-Vac  
 C:\UQed\USER\RhKetV\Appl\AnySampleAir.kap 2017-11-22  
 Calculated as : Elements Matrix (Shape & ImpFc) : 4|Ca..  
 X-ray path = Air Film type = No supporting film  
 Case number = 0 All known  
 Eff.Diam. = 13.0 mm Eff.Area = 132.7 mm2  
 KnownConc = 0 %  
 Rest = 0 % Viewed Mass = 1901.250 mg  
 Dil/Sample = 0 Sample Height = 15.0 mm

El	m/m%	StdErr
Ca	65.23	0.24
Sx	33.24	0.24
Fe	0.642	0.032
Sr	0.524	0.026
Px	0.224	0.020
Si	0.091	0.015
Ti	0.0288	0.0017
Mn	0.0148	0.0028

KnownConc= 0 REST= 0 D/S= 0  
 Sum Conc's before normalisation to 100% : 40.9 %

Fig. 6 Report on the results of the performed element analysis

## 4 Conclusion

Thus, the moisture content of the wood-gypsum composite is  $26.3 \pm 1.2\%$ . Total volume— $0.016 \text{ cm}^3/\text{g}$ . The specific surface area of the wood-gypsum composite was  $9.9 \text{ m}^2/\text{g}$ . The wood-gypsum composite is more than 98% Ca and Sx.

## References

1. Kumaran MK, Mukhopashyaya P, Normandin N (2007) Determination of equilibrium moisture content of building materials: Some practical difficulties. ASTM Special Technical Publication 1495 STP, c. 71–79
2. Kumaran MK, Mitalas GP, Bomberg MT (1994) Fundamentals of transport and storage of moisture in building materials and components. ASTM Manual Seri MNL 18:c.3–17
3. Macher JM, Mendell MJ, Chen W, Kumagai K (2017) Development of a method to relate the moisture content of a building material to its water activity. *Indoor Air* 27(3):c.599–608
4. Yang W, Liu H (2015) Preparation of a pH-responsive porous materials functionalized by pyridine groups via the Hack reaction. *Acta Chimical Sinica* 73(6):c. 623–628
5. Wang D, Li W, Yang W, Zuo Y, Feng S, Liu H (2014) POSS-based luminescent porous polymers for carbon dioxide sorption and nitroaromatic explosives detection. *RSC Adv* 4(104):c. 59877–59884
6. Pijarn N, Intaraprasert J, Ophap S, Uma T, Deekarnkol S, Bowornkietkaew W (2021) Microstructural characterization of white charcoal for rapid reduction of chemical oxygen demand and automatically adjust pH to neutral in wastewater treatment. *J Mater Res Technol* 13:c.336–345
7. Colao F, Fantoni R, Ortiz P, Vazquez MA, Martin JM, Ortiz R, Idris N (2010) Quarry identification of historical building materials by means of laser induced breakdown spectroscopy, X-ray fluorescence and chemometric analysis. *Spectrochimica Acta—Part B Atomic Spectrosc* 65(8):c.688–694
8. Fellin M, Negri M, Zanuttini R (2014) multi-elemental analysis of wood using energy dispersive X-ray fluorescence (ED-XRF) analyzer. *Eur J Wood Wood Prod* 72(2):c.199–211

# Optimization of the Composition of Cement Composites



Tatiana Elchishcheva , Ekaterina Abramova , Irina Erofeeva , Viktor Afonin , Vladislav Moiseev , and Alexei Atmanzin 

**Abstract** The purpose of this work is to study the properties and optimize the composition of cement composite materials containing special modifying additives—sodium sulfate and Neolith P8800 redispersible powder. To achieve the goals set in the work, the following methods were used: the method of mathematical planning of the experiment, standard methods for testing materials for fungus resistance, strength; mixture composition optimization method. Modifying additives are introduced into cement composite materials to improve consumer properties. Samples of cement composites containing various amounts of additives were made. Tests were carried out for fungus resistance and strength of control samples and samples with additives. An increase in the fungus resistance of composites with the introduction of additives has been established, which allows the use of products and structures made of them in adverse operating conditions in the presence of a biologically active environment. A decrease in the strength properties of composites with additives was revealed. The problem of optimizing the composition of composites was solved with the identification of the concentration of additives at which the material has fungus resistance, and the strength properties decrease slightly, up to 15% of the level of compressive and bending strength of the material without additives. The results of the study serve to determine the composition and concentration of components in the manufacture of dry building mixes.

**Keywords** Composite materials · Cement binder · Biocidal additive · Compressive and bending strength · Cellulose fibers · Composition optimization

---

T. Elchishcheva (✉)

Tambov State Technical University, 106, Sovetskaya Ul, 392000 Tambov, Russia  
e-mail: [elschevat@mail.ru](mailto:elschevat@mail.ru)

E. Abramova · I. Erofeeva · V. Afonin · V. Moiseev · A. Atmanzin  
National Research Ogarev Mordovia State University, 68, Bolshevistskaya Ul, Saransk 430005,  
Republic of Mordovia, Russia

## 1 Introduction

A promising direction in the production of building materials is the introduction of dry building mixtures on a cement binder into the construction technology. They have a number of advantages over the use of ready-made mortars and concretes, as they allow improving the quality of construction, labor productivity, the shelf life of materials, refusing to use special equipment when delivering dry mixes to the construction site, and ensuring the organization of mixes for a long time. In Russia, dry building mixes have been introduced into construction practice since the second half of the 1990s. The market for dry building mixtures is continuously expanding [1]. To improve consumer properties and improve physical, mechanical and operational performance, modifying technological additives are introduced into dry building mixes [2–4]. The paper considers the introduction of two types of additives into composites, which, according to the classification, belong to additives for special purposes. This is an additive that increases the resistance to biological corrosion, and an additive that increases adhesion. It is known that the introduction of additives can not only improve, but also change and worsen some indicators of cement composite materials [5]. In this regard, it is necessary to solve the problem of optimizing the composition of mixtures [6–10].

Dry building mixtures of various compositions on a cement binder are delivered to the construction site in finished form. The composition of mixtures in the Russian Federation is determined by GOST 31,357–2007 “Dry building mixes based on cement binder. General technical conditions”, and test methods—GOST R 58277–2018 “Dry building mixes on a cement binder. Test Methods”. Immediately before use, the mixture is mixed with water.

The strength of composites from dry mixes depends on the brand of binder, filler, and additives that are introduced to give the material the required physicochemical and consumer properties [11–14]. In Russia, the properties of additives intended for the modification of dry mortars, concretes and mortars comply with GOST 24211–2008 “Additives for concrete and mortars. General technical conditions”. At the same time, it is very important to use additives for special purposes, which, under adverse operating conditions, increase the biological resistance of materials and structures [5, 15–21].

In addition to the use of biocidal additives, various fillers are often used in the production of cement composites to increase the adhesion strength to the base, improve water resistance in order to improve consumer characteristics [22, 23], which also belong to special purpose additives.

An important task is to create new formulations of mixtures with the required properties. This is ensured by the development and optimization of the composition of biocidal dry mortars based on a cement binder, modified with technological additives to improve the properties of the mixture, and having high physical, mechanical and operational performance.

The purpose of the work was to optimize the compositions of cement composites and to identify the optimal concentrations of sodium sulfate additives and Neolith

P8800 redispersible powder, which improve the consumer qualities of composites and only slightly reduce their strength properties.

To achieve the goal of the work, the following tasks were solved: (1) To produce cement composites: control samples and composites with modifying additives; (2) Determine experimentally the compressive and bending strength of cement composite samples; (3) Determine the biostability of composites in neutral and aggressive biological environments; (4) Propose an approach to optimize the composition of cement composites to identify the content of additives, which increases their consumer properties and reduces the compressive and bending strength insignificantly.

## 2 Materials and Methods

For the manufacture of a composite based on a cement binder, the following components were used:

Portland cement without mineral additives PC 400-D0, according to GOST 10178–85 “Portland cement and slag Portland cement. Specifications (With Amendments No. 1, 2)”. Producer—JSC “Mordovcement” (working settlement Komsomolsky, Chamzinsky district, Republic of Mordovia, Russia);

- quartz sand, according to GOST 8736–2014 “Sand for construction work. Specifications”. Belongs to the II class of sands in terms of grain composition and content of dust and clay particles (a group of very fine sands), fineness modulus 1.4;
- sodium sulfate ( $\text{Na}_2\text{SO}_4$ ), pure, for analysis (analytical grade) according to GOST 4166–77 “Sodium sulfate. Specifications”. It is used as an additive in concretes and mortars to increase frost resistance and biocidal properties, manufactured by Component-Reaktiv LLC, Moscow;
- Neolith P8800 redispersible organic terpolymer powder. Organic terpolymer powder (obtained by polymerization of 3 different monomers). Designed for highly hydrophobic systems containing hydraulic binders. Chemical composition—Vinyl Acetate Vinyl Ester of Versatic Acid, acrylic compound, pH = 7.0–7.5; sh content 10–14%; when mixed with water, it forms an aqueous dispersion. It is introduced into the composition of the dry mix in an amount of 1% or more by weight of cement, depending on the requirements for the composite. When binding water and setting the solution, the dispersed particles are combined and form a polymer film. Improves adhesion to the base, elasticity (resistance to deformation and dynamic loads); increases strength properties, water resistance, mechanical strength, hydrophobic properties, abrasion resistance, spreading, vapor permeability, frost resistance, water-holding capacity, durability; reduces water absorption. Producer—FAR SPA, Italy.

To plan experiments on testing cement composites with the introduction of  $\text{Na}_2\text{SO}_4$  and Neolith P8800, a D-optimal plan was adopted—ca two-factor Kono

plan with the arrangement of experimental points (in geometric interpretation) on a square. The experiments were carried out at 9 points: at the vertices (4 points), the midpoints of the sides (4 points) and the center of the square (1 point). The specific weights of the points are as follows: the vertices of the square—0.148, the midpoints of the edges—0.078, the center of the square—0.096. An experiment matrix with 9 experiments is presented in Table 1, where the variable factors are  $X_1$  factor (sodium sulfate  $\text{Na}_2\text{SO}_4$ ) and  $X_2$  factor (Neolith P8800).

The work used data from the results of experimental studies of cement composites, carried out by Abramova E. N. (Suraeva E. N.), and described in Loganina et al. [14].

The fungus resistance and fungicidal properties of the composites were evaluated in accordance with GOST 9.049.91 “Unified Corrosion and Aging Protection System (ESZKS). Polymeric materials and their components” according to method 1 and method 3. Method 1 allows you to identify whether there are food sources for micromycetes in the building material under study. In this case, in addition to the test material itself, when tested according to method 1, there should be no other power sources. Therefore, infected samples were placed in Petri dishes with distilled water. Mushroom resistance was assessed on a 6-point scale—from zero to 5 points. The material was considered to have passed the test if its fungus resistance is no more than 3 points. When tested according to method 3, infected material samples were placed in Petri dishes with Czapek’s nutrient medium, which feeds mold spores.

**Table 1** Strength and fungus resistance of composites with additions of  $\text{Na}_2\text{SO}_4$  and Neolith P8800

Composition number	The amount of additive part by weight of the mass of cement		Fungus resistance, points/ characteristics of the material		Sample strength	
	$X_1$ ( $\text{Na}_2\text{SO}_4$ )	$X_2$ (Neolith P8800)	According to method 1	According to method 3	$R_c$ , MPa	$R_b$ , MPa
1	0	0	3/PTT	5/NF	15	3.0
2	3	0	1/F-R	2/NF	19	2.3
3	6	0	0/F, F-R	0/SFE	12	1.9
4	0	6.5	0/F, F-R	3/NF	11	3.1
5	3	6.5	0/F, F-R	2/NF	15	3.4
6	6	6.5	0/F, F-R	2/NF	18	3.0
7	0	13	0/F, F-R	1/WF	9	2.1
8	3	13	0/F, F-R	3/NF	14	3.0
9	6	13	0/F, F-R	2/NF	12	2.8

*Legend* F—fungistatic; SFE—strong fungistatic effect; WF—weak fungicide; F-R—fungus-resistant; NF—not fungicidal; PTT—passed the test

Method 3 determined whether the building material had fungicidal properties, i.e. can completely inhibit the growth of fungi.

Chapek's medium is manufactured in accordance with TU 9229–014-00419789–95 "Chapek's dry nutrient medium", manufacturer HiMedia, India (distributor BIOLIGHT, Moscow). The composition of Chapek's medium: distilled water (1 l), sodium nitrate  $\text{NaNO}_3$  (2.0 g), potassium chloride  $\text{KCl}$  (0.5 g), magnesium sulfate  $\text{MgSO}_4$  (0.5 g), potassium dihydrogen phosphate  $\text{KH}_2\text{PO}_4$  (0.7 g), potassium hydrogen phosphate  $\text{K}_2\text{HPO}_4$  (0.3 g), iron sulfate  $\text{FeSO}_4$  (II) (0.01 g); sucrose (30 g), agar (20 g).

The strength of the composites was determined on prisms measuring  $10 \times 10 \times 30$  mm according to GOST 30744–2001 "Cements. Test methods using polyfractional sand" and GOST 10180–2012 "Concrete. Methods for determining the strength of control samples. The samples were tested for bending by the force applied in the middle of the span to the beam on 2 supports. The compressive strength was determined by transferring the load through the pressure plates to ensure uniform application.

The problem of optimizing the composition of composites was solved using the GlobalSearch MATLAB system [24].

### 3 Results and Discussion

The properties of cement composites were studied with the introduction of the  $\text{Na}_2\text{SO}_4$  biocide additive and the Neolith P8800 redispersible powder in accordance with the second-order Kono two-factor plan. Variable factors are the addition of sodium sulfate  $\text{Na}_2\text{SO}_4$  (factor  $X_1$ ) and the addition of Neolith P8800 (factor  $X_2$ ).

The properties of cement composites were studied with the introduction of the  $\text{Na}_2\text{SO}_4$  biocide additive and the Neolith P8800 redispersible powder in accordance with the second-order Kono two-factor plan. Variable factors are the addition of sodium sulfate  $\text{Na}_2\text{SO}_4$  (factor  $X_1$ ) and the addition of Neolith P8800 (factor  $X_2$ ).

Investigated: compressive strength  $R_c$  (MPa), bending  $R_b$  (MPa) and fungus resistance of the material (Table 1).

Five samples were tested at each of the nine points on the response surface, for a total of 45 samples. After statistical processing of the results of the experiment, the coefficients of the equations were calculated and regression Eqs. (1) and (2) were obtained for changing the optimization criterion from the factors  $X_1$  and  $X_2$ .

$$R_c^2 = 15.0 + 3.50X_1 - 2.50X_2 - 0.50X_1^2 + 1.50X_1X_2 + 1.50X_2^2 + 1.0X_1^2X_2 - 3.50X_1X_2^2 - 4.0X_1^2X_2^2 \quad (1)$$

$$R_b^2 = 3.40 - 0.050X_1 + 0.350X_2 - 0.350X_1^2 + 0.450X_1X_2 - 0.750X_2^2 - 0.350X_1^2X_2 - 0.050X_1X_2^2 + 0.150X_1^2X_2^2 \quad (2)$$

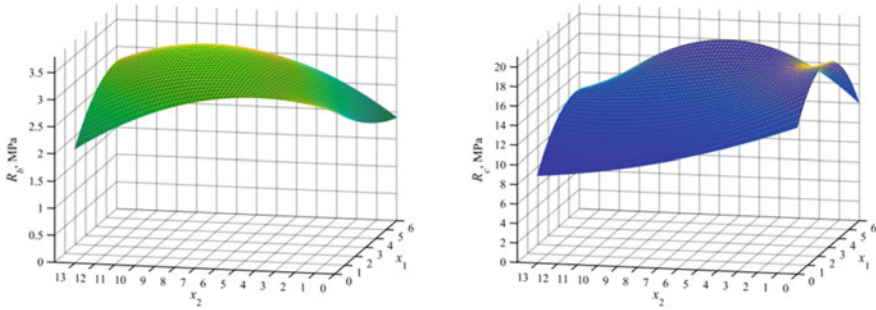


**Fig. 1** Additives  $\text{Na}_2\text{SO}_4$  and Neolith P8800. Surface of the calculated response function of compressive strength  $R_c$ , MPa (left), and bending  $R_b$ , MPa (right):  $X_1$ —content of sodium sulfate ( $\text{Na}_2\text{SO}_4$ ),  $X_2$ —content of Neolith P8800, parts by weight of cement mass

According to the equations, graphs of the dependence of the compressive and bending strength in the form of surfaces are constructed, which are points of the value of the response function for two variables—the amount of  $\text{Na}_2\text{SO}_4$  and Neolith P8800 additives introduced into the composite material (see Fig. 1). Graphic dependencies are used to select the compositions of modified mixtures that have the required physical and technical properties.

The addition of  $\text{Na}_2\text{SO}_4$  in the amount of 3 parts by weight and Neolith P8800 in the amount of 6.5 parts by weight of cement (composition No. 5) increases the bending strength of the samples by 11% relative to the strength of the base composition No. 1. In this case, the compressive strength of samples of composition No. 5 is equal to the strength of the base composition No. 1. The addition of  $\text{Na}_2\text{SO}_4$  in the amount of 6 parts by weight and Neolith P8800 in the amount of 6.5 parts by weight of cement (composition No. 6) increases the compressive strength of the samples by 17% relative to the strength of the base composition No. 1. In this case, the bending strength of samples of composition No. 6 is equal to the strength of the base composition No. 1. For formulation No. 8 (3 parts  $\text{Na}_2\text{SO}_4$  and 13 parts Neolith P8800 by weight based on the weight of cement),  $R_c$  is reduced by 6.7%, while  $R_b$  remains at the level of values for samples without additives.

For formulation No. 9 (6 parts  $\text{Na}_2\text{SO}_4$  and 13 parts Neolith P8800),  $R_c$  is reduced by 20% and  $R_b$  is reduced by 6.7%.

Method 1 determined the biological stability of the samples. It was found that the introduction of  $\text{Na}_2\text{SO}_4$  biocidal additive and Neolith P8800 redispersible polymer powder into the composition of the samples in the amount presented in Table 1 gives the material fungus-resistant properties. The introduction of the polymer into the samples (without the addition of  $\text{Na}_2\text{SO}_4$ ) increases the biological resistance of the samples. When tested according to method 1 from the PTT category (3 points, sample No. 1), the samples pass into the F, F-R category (0 points, samples Nos. 4, 7).

The addition of Neolith P8800 to the sample with the biocidal additive  $\text{Na}_2\text{SO}_4$  (composition No. 2, characteristic F-R) increases the fungi-resistant properties of



the material, it acquires the properties F, F-R (composition No. 5), the bioresistance is increased and the composites are fungi-resistant and fungistatic when tested according to method 1.

When tested according to method 3 in the Czapek-Dox nutrient medium, all samples compared to the control sample No. 1 (5 points, NF) show an increase in bioresistance (from 0 points, SFE, to 3 points, NF). The joint introduction of  $\text{Na}_2\text{SO}_4$  and Neolith P8800 additives into the composition showed the best values—at the level of 2–3 points—with a combination of strength properties and bioresistance of the material (samples Nos. 5, 6, 8 and 9) compared with sample No. 1 (5 points). Sample No. 3 (6 parts  $\text{Na}_2\text{SO}_4$  by weight of cement) has a strong fungistatic effect of SFE, sample No. 7 (13 parts of Neolith P8800 by weight of cement) has a weak fungicidal effect of WF—1 point, however, these samples show a strong decrease in strength indicators: for bending—up to 6.7–20%, for compression—up to 6–36.7%. Thus, experimental studies have shown the preference for using compositions that contain 3–6 parts by weight of  $\text{Na}_2\text{SO}_4$  and 6.5–13 parts by weight of Neolith P8800 cement (Fig. 1).

The solution of the problem of determining the optimal composition of composites was based on the regression Eqs. (1) and (2), which were used for calculations and diagramming. To translate real (real) factors to coded values, data from Table 1 was used. 1. Coded values are presented in Table 2.

The regression dependences of compressive strength ( $R_c$ ) and bending ( $R_b$ ) are non-linear and depend on two variable factors  $X_1$  and  $X_2$ , so their graphical representation, as a rule, is complex. At the same time, nonlinear regression functions are extremely rarely unimodal functions (with one extremum). Therefore, it is advisable to apply the methods of searching for a global extremum on the entire domain of definition of the considered regression equation, which in the optimization problem should be called the objective function.

First stage. Analysis of the ultimate strength using regression equations (objective functions  $R_c$  and  $R_b$ ) consisted in choosing a method/algorithm for searching for a global extremum. This problem was solved using the GlobalSearch toolkit of the MATLAB system [24], which is supported starting from version R2010a of the MATLAB system.

Second phase. Based on the solution of the problem of the first stage, the extreme values (maximum and minimum) of the strength  $R_c$  and  $R_b$  were determined with the corresponding values of the factors  $X_1$  (sodium sulfate) and  $X_2$  (Neolith P8800). Extreme values were used to construct lines of equal influence depending on a given percentage of the levels of the maximum values of  $R_c$  and  $R_b$ . For this, the “contour” and “clabel” functions presented in the MATLAB system were used.

**Table 2** Coded and actual factor values

Factor	Coded factor values/actual values of factors								
$X_1$	-1/0	0/3	1/6	-1/0	0/3	1/6	-1/0	0/3	1/6
$X_2$	-1/0	-1/0	-1/0	0/1	0/1	0/1	1/2	1/2	1/2

Third stage. The “meshgrid” and “mesh” functions were used to visualize the response surfaces  $R_c$  and  $R_b$ .

Fourth stage. Lines of equal influence (levels) were plotted separately using the “contour”, “clabel”, “line”, “patch”, “xlabel”, “ylabel”, “legend”, and “title” functions of the MATLAB system. The “patch” function was used to fill a closed figure on a plane. The resulting figure(s) is(are) lines of equal influence (level). The entire shaded area ensures that the specified condition is met so that the strength value  $R_c$  or  $R_b$  is the required percentage of the maximum values (or). The coordinates of the points of maximum values of the functions are included in these areas.

$$R_{c\max} = 19.1023. \text{ Factor values: } X_1 = 2.590909, X_2 = 0, 0.$$

$$R_{c\min} = 9.0. \text{ Factor values: } X_1 = 0.0, X_2 = 13.0.$$

$$R_{b\max} = 3.44269. \text{ Factor values: } X_1 = 3.211229, X_2 = 8.140373.$$

$$R_{b\min} = 1.9. \text{ Factor values: } X_1 = 6.0, X_2 = 0.0.$$

The difference in the extreme values calculated by the regression equations and the data in Table 1 is due to the difference in digits after the decimal separator (in the coefficients of the regression equations—3 digits, and for computer calculations in MATLAB for double types—up to 15 digits).

The relative errors in the calculation of the maxima  $R_c$  max and  $R_b$  max are:

$$\delta R_{c\max} = (19.1023 - 19.0) \cdot 100/19.0 = 0.5384(\%).$$

$$\delta R_{b\max} = (3.44269 - 3.4) \cdot 100/3.4 = 1.2556(\%).$$

The calculated response functions built according to the regression Eqs. (1) and (2) are shown in Fig. 1.

Figure 2 shows diagrams of lines of equal influence (level) of response functions, with strength (MPa) in compression ( $R_c$ ) and bending ( $R_b$ ) of at least 85, 90 and 95% of the maximum of the functions:  $R_{c, \max}$  and  $R_{b, \max}$ .

In Fig. 3, the shaded areas guarantee compressive and flexural strength values of at least 95% of the respective maximum  $R_{c, \max}$ , and  $R_{b, \max}$ .

Optimization of the composition of the cement composite according to two factors:  $X_1$  ( $\text{Na}_2\text{SO}_4$ ) and  $X_2$  (Neolith P8800) is shown in Fig. 3 by line diagrams of equal levels with highlighted (shaded) areas (optimal values), within which a level of compressive and bending strength of at least than 95% of the respective maximum compressive and flexural strengths. The choice of factor values from the optimal areas is carried out visually according to the diagrams and programmatically based on the properties of the “patch” function of the MATLAB system.

The results of calculations of intersection points (factors  $X_1$  and  $X_2$ ) with equal percentages of the maximum strength levels are given in Table 3. The boundary interpolation curve and the ranges of  $S_c$  and  $S_b$  values that guarantee the strength of  $R_c$  and  $R_b$  in the range from 85.0 to 91.5% are shown in Fig. 4.

The analysis of the obtained results showed that the optimal strength, which is from 85 to 91.5% of the maximum compressive strength ( $R_{c, \max}$ , MPa) and bending

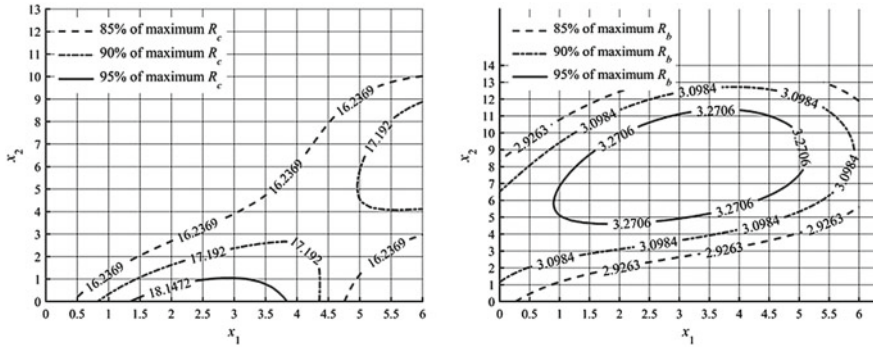


**Fig. 2** Additives Na<sub>2</sub>SO<sub>4</sub> and Neolith P8800. The maximum strength is: for compression  $R_{c, \max} = 19.1023$  MPa; bending  $R_{b, \max} = 3.44269$  MPa

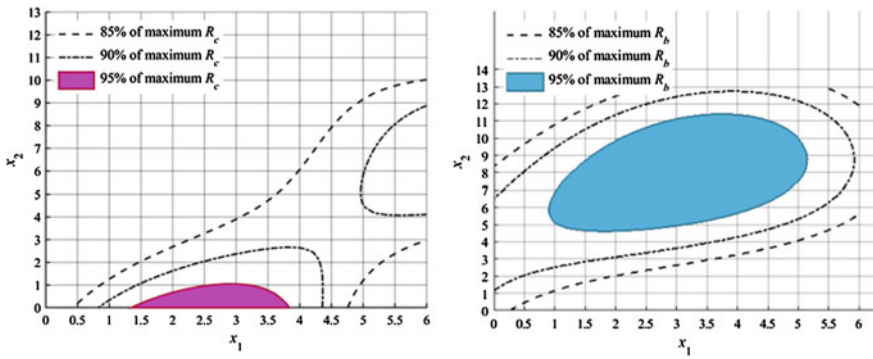
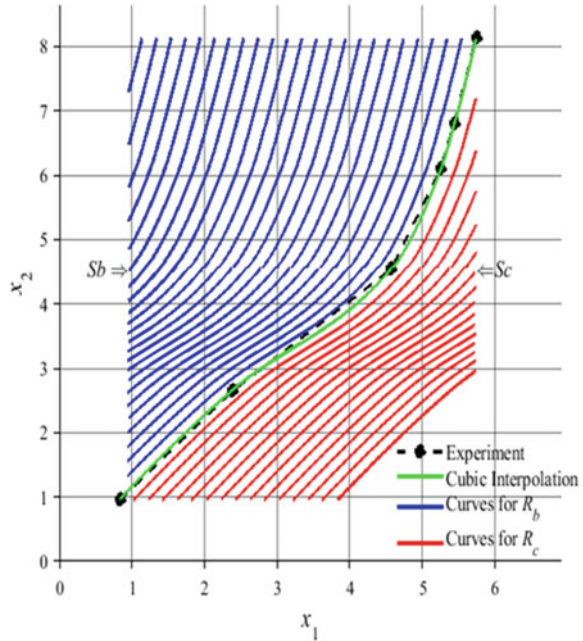


**Fig. 3** Additives Na<sub>2</sub>SO<sub>4</sub> and Neolith P8800. Contours of values of compressive strength  $R_c$ , MPa (left), and bending  $R_b$ , MPa (right), as a percentage of the maximum values of compressive strength  $R_{c, \max}$ , MPa, and bending  $R_{b, \max}$ , MPa

**Table 3** Intersection points ( $X_1$  and  $X_2$  factors) with equal values, %, of the maximum strength levels for  $X_1$  (Na<sub>2</sub>SO<sub>4</sub>) and  $X_2$  (Neolith P8800)

Strength, MPa	Calculated data, %, from the maximum values of $R_c$ and $R_b$						
	85%	87%	89%	91% (1)	91% (2)	91,5%	100%
$R_c$	16.2360	16.6180	17.0000	17.3821	17.3880	17.4776	19.1023
$R_b$	2.9253	2.9941	3.0630	3.1319	3.1378	3.1491	3.4427
$X_1$	0.8322	2.3818	4.5705	5.2507	5.7401	5.4391	2.5909/0.0000
$X_2$	0.9529	2.6474	4.5371	6.0912	8.1321	6.8028	6.0000/1.2600

**Fig. 4** Additives  $\text{Na}_2\text{SO}_4$  and Neolith P8800. Boundary curve and regions  $S_c$  and  $S_b$  interpolation curves providing compressive strength  $R_c$ , MPa, and bending  $R_b$ , MPa, from 85 to 91.5% of the maximum values, respectively,  $R_{c \max}$  and  $R_{b \max}$



strength ( $R_{b \max}$ , MPa) is represented by the area with the values of the amount of modifying additives:  $\text{Na}_2\text{SO}_4$  (factor  $X_1$ )—from 0.83 to 5.43 parts by weight by weight of cement and Neolith P8800 (factor  $X_2$ )—from 0.95 to 6.80 parts by weight by weight of cement, while ensuring the fungus resistance of composites.

## 4 Conclusion

As a result of the study, optimization criteria were established, the sequence and scheme for selecting the optimal composition of cement composite materials containing modifying additives were presented. The concentration of modifying additives has been revealed, which makes it possible to achieve the required properties of the composite, guaranteeing a decrease in strength by no more than 9.5–15% of the initial values. The indicated concentrations were:  $\text{Na}_2\text{SO}_4$ —from 0.83 to 5.43 parts by weight by weight of cement and Neolith P8800— from 0.95 to 6.80 parts by weight by weight of cement. The developed scheme allows you to determine the optimization criteria for any number of modifying additives and the level of required values of compressive and bending strength.

**Acknowledgements** The study was carried out within the framework of the project under grant 3.1.8.1 “Fundamental scientific research of high-strength lightweight concrete for 3D-printing technology on non-firing ash gravel with the provision of environmentally friendly and resource-saving

energy”, which is part of the plan of fundamental scientific research of the Ministry of Construction and Housing and Communal Services of the Russian Federation and the Russian Academy of Architecture and Building Sciences for the Research Institute of Building Physics of the Russian Academy of Architecture and Building Sciences.

## References

1. Dry building mixes market in Russia: research and forecast until 2025 Issue: April, 202. <https://roif-expert.ru/stroitelstvo/stroitel-nye-smesi/rynok-suhih-stroitel-nyh-smesej/rynok-suhih-stroitel-nyh-smesej-v-rossii-issledovanie-i-prognoz.html>. Accessed 30 Oct 2022
2. Tarakanov, O.V.: Chemical additives in mortars and concretes: monograph, Penza, PGUAS (2016). <https://topuch.com/1027752/index.html>
3. Kalashnikov VI, Tarakanov OV (2017) On the use of complex additives in new generation concretes. Construction materials. 1–2. <https://cyberleninka.ru/article/n/o-primenenii-kompleksnyh-dobavok-v-betonah-novogo-pokoleniya>
4. Satyukov AB, Dergunov SA, Orekhov SA (2019) Nanomodified composite binder: monograph. OSU, Orenburg
5. Elchishcheva T, Erofeev V (2020) The influence of salts’ presence in the materials on their moisture and thermal conductivity. materials science forum. Trans Tech Publications, Ltd., September 2020. <https://doi.org/10.4028/www.scientific.net/MSF.1011.179>
6. Smirnov DS, Garaev TR, Khamitov AR (2017) Methods for optimizing concrete compositions. Bull Kazan Technol Univ 2. <https://cyberleninka.ru/article/n/sposoby-optimizatsii-sostavov-betonov>
7. Avlakulov M, Khurramov, SK, Gaimnazarov I.KH (2015) Optimization of the composition of concrete mixtures used in water management construction. Young Sci 8(88):159–162. <https://moluch.ru/archive/88/17078/>
8. Rezaev RO, Dmitriev AA, Borodulya NA, Chernyavsky DV (2021) Application of an integrated approach to optimization of production compositions on the example of ready-mixed concrete. ALITinform: Cement. Concrete. Dry Mixes 2(63):42–55
9. Ivanov IM, Kramar LY (2020) Mathematical model for assigning a high-performance concrete composition using ground granulated blast-furnace slag. Bulletin of the South Ural State University. Ser: Constr Archit 20(4):28–41. <https://doi.org/10.14529/build200404>
10. Rezaev RO, Sebelev IM, Dmitriev AA, Dyatchina AA (2021) Technology for complex optimization of ready-mixed concrete compositions with chemical additives using an online service. News of higher educational institutions. Construction 6(750):52–60. <https://doi.org/10.32683/0536-1052-2021-750-6-52-60>
11. Kalashnikov VI, Tarakanov OV, Volodin VM, Erofeeva IV, Abramov DA (2015) Concretes of transitional and new generations. Status and prospects. Mod Prob Sci Educ 2–1. <https://science-education.ru/ru/article/view?id=20386>
12. Medvedeva IN, Zozulya PV, Korneev VI (2019) Dry mortar technology. Doe, Moscow
13. Kuzmina VP (2016) Modification of composite conglomerates based on binders. Dry Mixes 6:21–29. <http://izvuzstr.sibstrin.ru/uploads/publication/fulltext/2013-N10.pdf>
14. Loganina VI, Kislitsyna SN, Zhegera KV (2013) The use of synthesized aluminosilicates in the composition of cement-based tile adhesive. News High Educational institutions. Construction 10(658):23–27
15. Kuzmina VP (2018) Features of the use of dry building mixes during finishing work in various climatic conditions. Part 2. Dry building mixes 6:30–36. [https://elibrary.ru/download/elibrary\\_36403167\\_63641793.pdf](https://elibrary.ru/download/elibrary_36403167_63641793.pdf)

16. Belikov DA (2013) Dry building mixes for repair work on composite binders. PhD dissertations of Cand. Tec. Sci. Belgorod. <https://www.dissercat.com/content/sukhie-stroitelnye-smesi-dlya-remontnykh-rabot-na-kompozitsionnykh-vyazhushchikh/read>
17. Belyakov VA, Yarkov MY (2016): Modification of the composition of building mixtures for concrete repair in order to improve their performance. Basic Res 11-4:681–686. <https://fundamental-research.ru/ru/article/view?id=41238>
18. Erofeev VT, Smirnov VF, Myshkin AV (2019) The study of species composition of the mycoflora, selected surface samples polimerization composites in humid maritime climate. IOP Conf Ser: Mater Sci Eng 698(2):022082. <https://doi.org/10.1088/1757-899X/698/2/022082>
19. Erofeev VT, Smirnov VF, Myshkin AV (2019) The study of polyester-acrylate composite's stability in the humid maritime operating conditions. Mater Today: Proc 19:2255. <https://doi.org/10.1016/j.matpr.2019.07.547>
20. Suraeva E, Elchishcheva T, Svetlov D, Smirnov V, Afonin V, Erofeeva I (2021) Influence of granulometric composition and type of fillers and additives on the strength and biostability of cement composites based on dry building mixtures. Mater Sci Forum 1043:163–175. <https://doi.org/10.4028/www.scientific.net/msf.1043.163>
21. Elchishcheva T, Afonin V, Erofeeva I, Saltanova T, Atmanzin A, Matrosova C (2021) Biostability of plastering systems in buildings and structures. In: Vatin N, Borodinecs A, Teltayev B (eds) Proceedings of EECE 2020: EECE 2020. Lecture notes in civil engineering, vol 150. Springer, Cham, pp 379–390. [https://doi.org/10.1007/978-3-030-72404-7\\_37](https://doi.org/10.1007/978-3-030-72404-7_37)
22. Ilyinskaya GG, Kozlov VA (2014) On the choice of reinforcing additives for dry building mixtures. Modern problems of construction and life support: safety, quality, energy and resource saving: collection of materials of the III All-Russian scientific and practical conference, Yakutsk, March 3–4, 2014. North-Eastern Federal University named after M.K. Ammosov. Yakutsk: International Center for Research Projects, pp 257–261. <https://elibrary.ru/item.asp?id=22217845>
23. Suraeva EN (2015) Development of dry building mixtures with biocidal properties: diss. ... Cand Tech Sci. Penza
24. Zsolt U, Lasdon L, Plummer J, Glover F, Kelly J, Martí R (2007) Scatter search and local NLP solvers: a multistart framework for global optimization. INFORMS J Comput 19(3):328–340. <https://doi.org/10.1287/ijoc.1060.0175>

# Hydrodynamic Model of Stationary Drilling Fluid Flow in a Cylindrical Pipeline



Boris Kumitskiy , Egor Aralov , Natalia Savrasova ,  
Natalia Semicheva , and Victor Budnikov 

**Abstract** The stationary axisymmetric flow of drilling mud under the action of a constant pressure drop created by a drill pump in a horizontal pipeline is investigated. The relevance of the proposed work is determined by the fact that the quality of drilling mud is one of the most important components of the technological process of drilling oil wells. In this regard, there is a need to develop a formulation of a dispersed system, which is a drilling mud, which allows for effective cooling of the rock-destroying tool, high-quality removal of sludge to the surface in compliance with the requirements for solutions, with minimal material costs. The purpose of this work is: to establish a relationship between structural parameters and hydraulic resistance of the fluid flow within the framework of the Ostwald-de Waele rheological model; to study the stress–strain state of the model medium in a stationary, axisymmetric flow; to establish a relationship between the average flow hydrodynamic characteristics with its viscosity parameters. Analytical dependences of the distribution of effective viscosity and axial velocity of the medium flow are obtained. The dependence of the flow rate of the model medium on the magnitude of the pressure drop, as well as the distribution of the dynamic shear stress along the pipeline section, are determined.

**Keywords** Drilling mud · Viscosity · Hydrodynamic model · Suspension

---

B. Kumitskiy · E. Aralov (✉)  
Voronezh State Technical University, 84, 20-Letiya Oktyabrya Ul., Voronezh 394006, Russia

N. Savrasova  
Military Educational and Scientific Center of the Air Force, N.E. Zhukovsky and Y.A. Gagarin  
Air Force Academy, 153/4, Krasnoznamennaya Ul., Voronezh 394052, Russia  
e-mail: [teplosnab\\_kaf@vgasu.vrn.ru](mailto:teplosnab_kaf@vgasu.vrn.ru)

N. Semicheva · V. Budnikov  
Southwest State University, 94, 50 Let Oktyabrya Ul., Kursk 305040, Russia

## 1 Introduction

The most important national economic task of hydrocarbon production is to extract them as much as possible from oil reservoirs. In order to increase the recoverable product and shorten the time of field development, new methods of influencing oil formations are being sought while ensuring greater drainage of the reservoir and the formation of extended boreholes [1–4]. All this can be provided by the construction of directional horizontal wells.

In parallel with these structures, due to the development and complication of the technological process of oil drilling, the well flushing technique should be improved, the composition of drilling fluids should be improved in terms of developing their formulation, which contributed to a better removal of sludge from the wellbore [5, 6]. Modern studies of drilling fluids are mainly aimed at optimizing the composition, improving their properties, methods of preparation, chemical treatment and purification [7–9], as well as modeling their behavior [10].

Practice shows that their rheological properties have a predominant influence on the main indicators of drilling fluids when drilling wells. From the standpoint of rheology, the optimal drilling fluid in a fast-flowing stream should have an effective viscosity comparable to that of water, and when rising at a lower speed, its viscosity should meet the conditions for transporting sludge to the surface without accumulating it inside the well [3, 11–13]. The main problems in creating a unified rheological classification of drilling fluids are: the variety of their types, the need to regulate their properties during drilling, a large spread of deformation rates in different parts of the well, the presence of variable temperatures and pressures. This explains the inefficiency of the numerous rheological models known [14, 15], since for the removal of small particles it is necessary that the solution be low-viscosity, and for the removal of large ones—more viscous, however, the viscosity limits should not be violated. The analysis shows that drilling fluids with a low content of clays, foams treated with diluents, as well as emulsions and solutions with polymers have plastic properties.

## 2 Materials and Methods

The purpose of this work is to study the rheological properties of drilling mud during its stationary flow in a horizontal cylindrical pipe.

Solutions to this problem will be carried out within the framework of the Ostwald-de Weil hydrodynamic model. The choice of this model is due to the fact that drilling fluids, after being treated with polymers, acquire the properties of a plastic liquid, which increases the efficiency of removing particles of destroyed rock (sludge) from the face, as well as their transportation to the surface [1, 2].



Consider the stationary axisymmetric flow of drilling fluid in a straight horizontal pipe of radius  $R$  and length  $L$  when transporting it from the preparation point to the wellhead under the action of a constant pressure  $\Delta P$  drop created by a drilling pump.

In cylindrical coordinates  $(x, r)$ , the rheological equation of a plastic fluid is written as

$$\tau_{xr} = k \left( \frac{dv_x}{dr} \right)^n, \quad (1)$$

where  $x$  is the coordinate directed along the fluid flow along the pipe axis;  $n < 1$  is an indicator of the nonlinearity of the medium;  $k$ —the consistency index;  $\tau_{xr}$ —dynamic shear stress;  $\frac{dv_x}{dr}$ —axial velocity gradient.

In the case of steady flow, the pressure gradient  $\frac{dP}{dx}$  is constant

$$\frac{dP}{dx} = -\frac{\Delta P}{L} = \text{const}, \quad (2)$$

and the dynamics equation for a plastic fluid has the form:

$$\frac{1}{r} \frac{d}{dr} \left( kr \frac{du}{dr} \left| \frac{du}{dr} \right|^{n-1} \right) = - \left| \frac{dP}{dx} \right|. \quad (3)$$

Assuming the conditions of axisymmetry of the problem ( $\frac{dv_x}{dr} = 0$  at  $r = 0$ ) and ideal adhesion on the inner wall of the pipe ( $v_x = 0$  at  $r = R$ ), a single integration (3) leads to the result

$$\frac{dv_x}{dr} = - \left( \frac{r}{2k} \left| \frac{dP}{dx} \right| \right)^{1/n}. \quad (4)$$

### 3 Results and Discussion

Taking into account the rheological Eq. (1), expression (4) can be represented as

$$\tau_{xy} = -k \left| \frac{dv_x}{dr} \right|^n = -\frac{r}{2} \left| \frac{dP}{dx} \right|, \quad (5)$$

representing the distribution of shear stress over the cross-section of the pipe, from which it can be seen that the absolute value  $\tau_{xy}$  at  $\frac{dP}{dx} = \text{const}$  increases linearly from zero on the axis of the pipeline to a maximum on its wall:

$$\tau_{xr/r=R} = \frac{1}{2} \left| \frac{dP}{dx} \right| R = \frac{\Delta P}{L} \frac{R}{2} = \tau_{\max}. \quad (6)$$

Integrating (4), we obtain the radial distribution of the axial velocity

$$v_x(r) = \frac{n}{n+1} \frac{R^{\frac{n+1}{n}}}{(2x)^{\frac{1}{n}}} \left| \frac{dP}{dx} \right|^{1/n} \left[ 1 - \left( \frac{r}{R} \right)^{\frac{n+1}{n}} \right]. \quad (7)$$

It can be seen that with a nonlinear dependence  $v_x(r)$ , it turns to zero at  $r = R$  and reaches its maximum value at  $r = 0$ :

$$v_{x/r=0} = \frac{n}{n+1} \frac{R^{\frac{n+1}{n}}}{(2k)^{\frac{1}{n}}} \left| \frac{dP}{dx} \right|^{\frac{1}{n}} = v_{x \max}. \quad (8)$$

The obtained radial distribution of the axial velocity (7) makes it possible to determine the medium flow characteristics necessary for practical use: volumetric flow rate  $Q$  and the average flow velocity of the liquid along the pipe section  $\bar{v}_x$  according to well-known formulas:

$$Q = 2\pi \int_0^R v_x(r) r dr = \frac{n\pi R^3}{3n+1} \left( \frac{R}{2k} \left| \frac{dP}{dx} \right| \right)^{1/n}, \quad (9)$$

$$\bar{v}_x = \frac{Q}{\pi R^2} = \frac{nR}{3n+1} \left( \frac{R}{2k} \left| \frac{dP}{dx} \right| \right)^{1/n}. \quad (10)$$

To characterize the viscous properties of a moving medium, we introduce two rheological parameters using expressions (9) and (10): effective viscosity  $\mu_{ef}$  and  $\bar{\mu}$ , characterizing the local and integral properties of the fluid flow, respectively.

For stationary flow of plastic fluid in a cylindrical channel  $\mu_{ef}$  can be found by the formula:

$$\mu_{ef} = k \left| \frac{dv_x}{dr} \right|^{n-1}, \quad (11)$$

which, taking into account (4), will take the form

$$\mu_{ef} = k^{1/n} \left( \frac{r}{2} \left| \frac{dP}{dx} \right| \right)^{1-\frac{1}{n}}. \quad (12)$$

Medium viscosity  $\bar{\mu}$  we define as the dynamic viscosity of a Newtonian fluid that moves in a pipeline of radius  $R$  with an average velocity (10) under the action of a constant pressure gradient  $\left| \frac{dP}{dx} \right|$ . This makes it possible to use a Newtonian fluid with the parameter instead of a nonlinear viscous medium in the conditions of hydrodynamic studies and practical calculations  $\bar{\mu}$ , for which the volume flow is

equal to

$$Q = \frac{\pi R^4}{8\bar{\mu}} \left| \frac{dP}{dx} \right|. \quad (13)$$

Equating (13) and (9), we find the value of the average viscosity  $\bar{\mu}$ :

$$\bar{\mu} = \frac{3n+1}{8n} (2k)^{1/n} \left( R \left| \frac{dP}{dx} \right| \right)^{1-\frac{1}{n}}. \quad (14)$$

It is known that the pressure gradient with dynamic pressure is related in accordance with the well-known Darcy-Weisbach expression

$$\frac{dP}{dx} = \xi \frac{\rho v_x^2}{4R}, \quad (15)$$

where  $\rho$ —the density of the medium under study;  $\xi$ —the coefficient of hydraulic resistance, the value of which can be determined by a combination of expressions (15) and (10):

$$\varepsilon = \left( \frac{6n+2}{n} \right)^2 \frac{(2k)^{2n}}{\rho R^{1+\frac{2}{n}}} \left| \frac{dP}{dx} \right|^{1-\frac{2}{n}}. \quad (16)$$

If we construct the Reynolds criterion (Re) by the average values of viscosity  $\bar{\mu}$ , the speed of the current  $\bar{v}_x$  and the diameter of the pipe  $d = 2R$ , then taking into account the dependencies (10) and (14), it is possible to characterize the flow of plastic fluid:

$$\text{Re} = \frac{\rho \bar{v}_x d}{\bar{\mu}} = 16\rho \left( \frac{n}{3n+1} \right)^2 \frac{R^{1+\frac{2}{n}}}{(2k)^{2/n} \left| \frac{dP}{dx} \right|^{1-\frac{2}{n}}}, \quad (17)$$

since the comparison of expressions (16) and (17) relates the coefficient of hydraulic resistance to the flow regime of the medium (the number Re):

$$\xi = \frac{64}{\text{Re}}. \quad (18)$$

It can be shown that for a stationary flow of a power fluid in a cylindrical channel, the hydraulic resistance is due only to friction losses in the absence of mass forces.

## 4 Conclusion

The results of the work performed allow us to draw the following conclusions:

- (a) a hydrodynamic model describing the rheological properties of drilling mud within the framework of the Ostwald-de Waele plastic fluid flow law is proposed;
- (b) analytical expressions of the radial distribution of the axial velocity are obtained, which decreases non-linearly from a maximum in the center of the pipe to zero on its wall; the effective viscosity is also non-linearly distributed along the pipe section, taking zero values on the axis of the pipeline and a maximum on its wall;
- (c) the dependence of the volume flow rate of the liquid on the magnitude of the pressure gradient increases with increasing pressure drop is determined;
- (d) it is shown that the hydraulic resistance decreases with an increase in the pressure gradient, which is probably due to the destruction of the structural bonds of the medium under study;
- (e) the introduction of the concept of average viscosity, which characterizes the rheological properties of the flow of a model liquid, allows you to link the parameters of the resistance of the medium from the side of the pipeline wall with the viscous properties of the liquid itself.

## References

1. Ulyasheva NM, Leusheva EL, Galishin RN (2020) Development of the drilling mud composition for directional wellbore drilling considering rheological parameters of the fluid. *J Mining Inst* 244:454–461. <https://doi.org/10.31897/PMI.2020.4.8>
2. Saxena A et al (2016) Experimental and modeling hydraulic studies of foam drilling fluid flowing through vertical smooth pipes. *Egypt J Pet* 26(2):279–290. <https://doi.org/10.1016/j.ejpe.2016.04.006>
3. Lou S, Wang H, Liu H et al (2021) Laboratory study of the effects of flexible vegetation on solute diffusion in unidirectional flow. *Environ Sci Eur* 33:80. <https://doi.org/10.1186/s12302-021-00521-y>
4. Beloglazov I, Morenov V, Leusheva E (2021) Flow modeling of high-viscosity fluids in pipeline infrastructure of oil and gas enterprises. *Egypt J Pet* 30:43–51. <https://doi.org/10.1016/j.ejpe.2021.11.001>
5. Winiowski R, Skrzypaszek K, Maachowski T (2020) Selection of a suitable rheological model for drilling fluid using applied numerical methods. *Energies* 13(12):3192. <https://doi.org/10.3390/en13123192>
6. Flayh S, Sultan H, Alshara A (2019) Numerical study of drilling fluids pressure drop in wellbores with pipe rotation. In: *IOP conference series: materials science and engineering*, vol 518, p 032037. <https://doi.org/10.1088/1757-899X/518/3/032037>
7. Gao Z, Efthymiou M, Cheng L, Zhou T, Minguez M, Zhao W (2021) Towards a model of hydrodynamic damping for a circular cylinder with helical strakes at low KC. *Mar Struct* 78:103025. <https://doi.org/10.1016/j.marstruc.2021.103025>
8. Okorie E, Julius U, Moses E, Udoinyang G, Daniel E, Imoh J, Olufemi S (2021) A critical review of drilling mud rheological models. *J Petrol Sci Eng* 203:108659. <https://doi.org/10.1016/j.petrol.2021.108659>

9. Livescu S (2012) Mathematical modeling of thixotropic drilling mud and crude oil flow in wells and pipelines. *J Petrol Sci Eng* 98–99:174–184. <https://doi.org/10.1016/j.petrol.2012.04.026>
10. Kunshin A, Dvoynikov M (2018) Design and process engineering of slotted liner running in extended reach drilling wells. In: SPE Russian petroleum technology conference, 15–17 October 2018. Russian Federation, Moscow. <https://doi.org/10.2118/191520-18RPTC-RU>
11. Dvoynikov MV (2017) Research on technical and technological parameters of inclined drilling. *J Mining Inst* 223:86–92. <https://doi.org/10.18454/PMI.2017.1.86>
12. Litvinenko VS, Dvoynikov MV (2019) Justification of the technological parameters choice for well drilling by rotary steerable systems. *J Mining Inst* 235:24–29. <https://doi.org/10.31897/PMI.2019.1.24>
13. Grigorev BS, Eliseev AA, Pogarskaya TA, Toropov EE (2019) Mathematical modeling of rock crushing and multiphase flow of drilling fluid in well drilling. *J Mining Inst* 235:16–23. <https://doi.org/10.31897/PMI.2019.1.16>
14. Nutskova MV, Kupavykh KS, Sidorov DA, Lundaev VA (2019) Research of oil-based drilling fluids to improve the quality of wells completion. In: IOP conference series: materials science and engineering. Quality management and reliability of technical systems, vol 666, 20–21 June 2019. Russian Federation, St. Petersburg. <https://doi.org/10.1088/1757-899X/666/1/012065>
15. Morenov V, Leusheva E, Martel A (2018) Investigation of the fractional composition effect of the carbonate weighting agents on the rheology of the clayless drilling mud. *Int J Eng, IJE Trans A: Basics* 31(7):1517–1525. <https://doi.org/10.5829/ije.2018.31.07a.21>

# Reference Beam Method for Determining Thermal Fluctuation Constants



Aleksander Erofeev , Timofey Gorokhov , Sergey Emelyanov ,  
and Ekaterina Pakhomova 

**Abstract** A new method for determining the thermal fluctuation constants of the generalized Zhurkov equation is proposed. The method is based on the experimentally established dependences of the obtained thermal fluctuation constants on the coordinate of the pole point and the limiting temperature. The choice of the subject of the study is justified, methods of conducting experiments and processing experimental data are given. Solid polyvinyl chloride plates were selected as the sample material for the study, which were broken by transverse bending on a six-position bench. To increase the reliability of the obtained results, the static processing method was used according to GOST R 8.736-2011. According to the obtained experimental data, graphs were plotted in coordinates « $\lg \tau - \sigma$ ». A reference beam and the corresponding reference constants are proposed, as well as a system of coefficients necessary for finding the thermal fluctuation constants of a material on the basis of reference constants. To verify the adequacy of the developed technique, the thermofluctuation constants of the generalized Zhurkov equation for the decorative protective plate on the polyester resin binder were determined by the reference beam method, which were compared with values with constants for this material obtained by the graphical and graphoanalytic method.

**Keywords** Durability · Zhurkov equation · Forecasting · Performance · Coefficient system · Construction

---

A. Erofeev (✉) · T. Gorokhov  
Tambov State Technical University, 106, Sovetskaya Ul, Tambov 392024, Russia  
e-mail: [av.erofeev@yandex.ru](mailto:av.erofeev@yandex.ru)

T. Gorokhov  
e-mail: [gorohowt@yandex.ru](mailto:gorohowt@yandex.ru)

S. Emelyanov · E. Pakhomova  
South West State University, 50 Let Oktyabrya Street, 94, Kursk 305040, Russia  
e-mail: [yz\\_swsu@mail.ru](mailto:yz_swsu@mail.ru)

## 1 Introduction

Thermofluctuation constants of the generalized Zhurkov equation are currently determined on the basis of experimentally obtained data of the dependence of durability from stress and temperature by a graphical analytical method [1–5]. This method is based on rearranging the experimentally obtained graph into the graph with coordinates of the logarithm of durability versus stress ( $\log\tau-\sigma$ ) and into a graph of the dependence of the logarithm of durability versus inverse temperature ( $\log\tau-1000/T$ ). Two constants  $\lg\tau_0$  and  $T_m$  are found from the position of the pole, and the other two,  $U_0$  and  $\gamma$ , from the graph of the dependence of the activation energy on stress [1, 6]. This method of determining the thermal fluctuation constants is rather complicated, and the need to perform graphical rearrangements reduces the accuracy of the results [7, 8]. This is due to the fact that according to the existing method for determining the constants, it is required to determine the durability (logarithm of durability) for each of three temperatures at five voltages. This is also due to the need to work in semi-logarithmic coordinates, when even minor deviations of the logarithm of durability in the zone of low durability (the range of experiments) leads to significant errors in further calculations of the durability of the material.

The established linear dependence of the change in the constant  $\log\tau_0$  on the magnitude of the pole displacement along the ordinate (Fig. 1a); the change in the thermal fluctuation constant  $U_0$  also has a linear dependence on the magnitude of the displacement of the beam pole only along the abscissa axis (Fig. 1b). The obtained dependences, along with other regularities due to the thermal fluctuation nature of fracture and deformation of solids (Fig. 1c–e), make it possible to propose a reference beam method for determining the thermal fluctuation constants of the generalized Zhurkov equation [9–11]. The proposed method does not imply rearranging the experimentally obtained graph. Its principle is based on manipulation with a reference beam.

## 2 Materials and Methods

For experimental verification of the hypothesis, polyvinyl chloride plates were chosen as the object of the study. This choice is due to the fact that it has a homogeneous structure and the presence of temperature–time force equivalence of the destruction process is clearly traced for it.

To identify the temperature–time–force equivalence, beams samples were made of polyvinyl chloride. The total number of samples was 150 pieces. The length of the samples was 6 cm. The cross section is rectangular ( $b \times h = 1.5 \text{ cm} \times 0.3 \text{ cm}$ ).

For transverse bending and fracture tests, a six-position stand was used (Fig. 2). This stand consists of a frame 1 made of corners. On the support platform of the frame 2, support rods 3 are installed at a distance from each other equal to the span of the beam. Sample 4 is placed on support pedestals and loaded with a load device

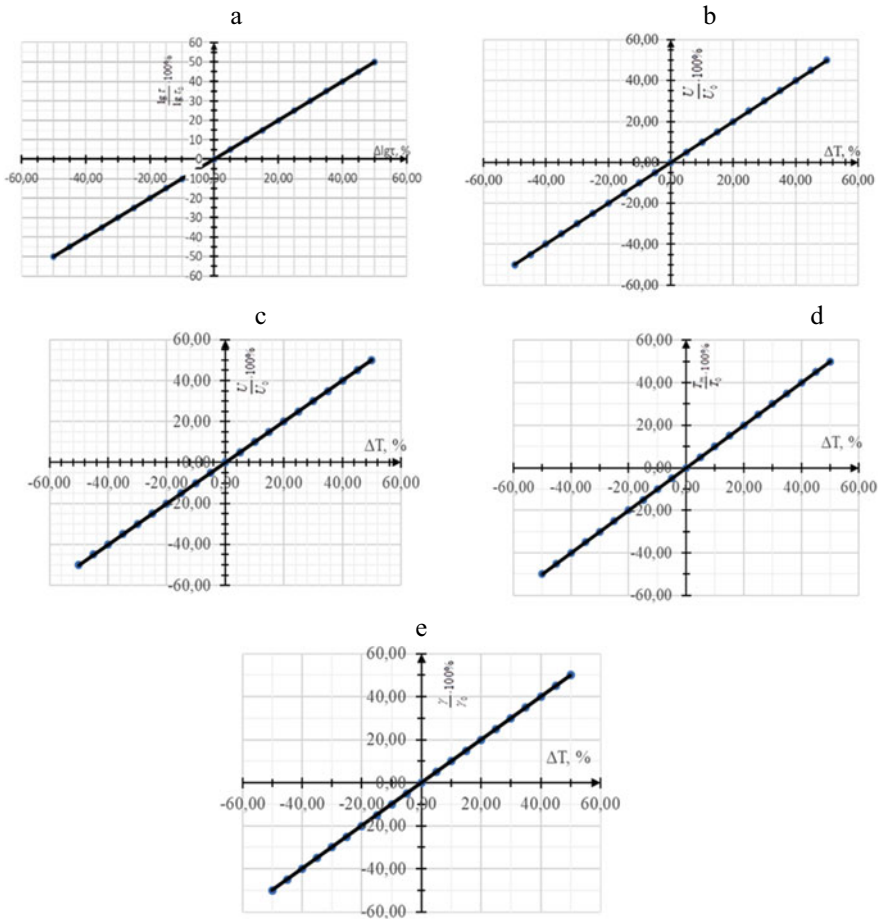


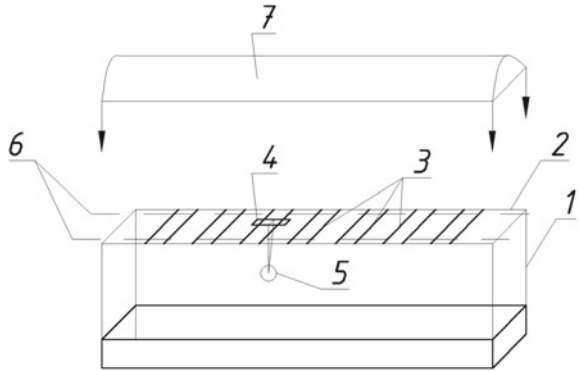
**Fig. 1** a dependence of the relative change in  $\log \tau_0$  on  $\Delta \lg \tau$ , b dependence of the relative change in  $U_0$  on  $\Delta \sigma$ ; c dependence of the relative change in  $U_0$  on  $\Delta T$ ; d dependence of the relative change in  $T_m$  on  $\Delta T$ ; e dependence of the relative change in  $\gamma$  on  $\Delta T$

5. Elevated temperature is created by rod electric heaters 6. To reduce heat loss and create a directed heat flow, a casing 7 is installed and fixed to the frame on the support platform. The temperature is set by LATR 1 M 220 V-9A and is regulated by a potentiometer EPV2-11A gr. HC 0300 °C.

For each temperature, five voltages are selected in the range from 0.75 to 0.95 of breaking. The temperatures at which the measurements were carried out were 15, 30, 45 °C. To obtain each point, at least 8 samples were tested under similar conditions. The results obtained were subjected to statistical processing according to the method according to GOST R 8.736–2011 to eliminate gross errors and establish the boundaries of the confidence interval [12, 13].



**Fig. 2** Experiment equipment



Thermofluctuation constants for the reference beam (Fig. 3a) were obtained on the basis of experimentally determined constants of PVC plates at transverse bending ( $\log\tau_0 = -2.34$ ;  $\gamma = 43.85$  kJ/(mol MPa);  $T_m = 437.95$  K,  $U_0 = 313.85$  kJ/mol) [14–16]. The beam with the coordinates of the pole point (10; 11) was taken as the reference beam, i.e.  $\log\tau = -1$ ,  $\sigma = 10$  MPa and the maximum temperature possible  $T_m = 500$  K (Fig. 3b).

The obtained thermal fluctuation constants of the reference beam are summarized in Table 1.

To determine the thermal fluctuation constants by the reference beam method, the reference constants of Table 1 must be multiplied by the conversion factors (system of coefficients):  $k_\sigma$ ,  $k_k$ . However, initially it is required to determine the

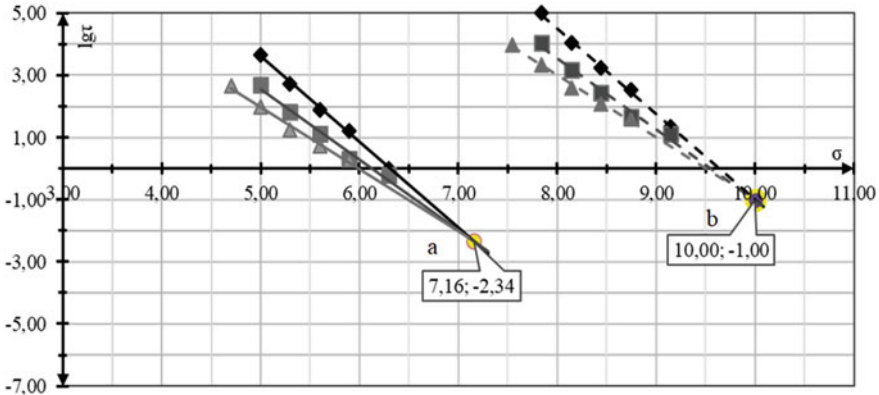


**Fig. 3** a base beam; b reference beam

**Table 1** Thermofluctuation constants of the reference beam

$\gamma$ , kJ/(mol $\times$ MPa)	$U_0$ , kJ/mol	$T_m$ , K	$\lg\tau_0$
50	500	500	-1

limiting temperature of material possible [6], which is determined based on the linear dependence of the change in the slope of the equation:

$$\lg \tau(\sigma) = a \cdot \sigma + b \quad (1)$$

where  $a$ —is the slope or the tangent of the angle of inclination of a straight line, the physical meaning of which is the rate of the process;

$b$ —the free term of the equation, which determines the logarithm of the life in the absence of stresses.

In fact, Eq. (1) is the equation of the direct temperature of the graph, experimentally constructed in the coordinate system of the dependence of the logarithm of durability on stresses.

The linearity of the dependence of the slope on temperature (inverse temperature) is verified in three ways: theoretical, proof against the contrary, and practical [17]. Let the dependence of the change in the coefficients of “Eq. 1” be linear and described by the equation:

$$a = k \cdot T + d, \quad (2)$$

Then, substituting them into “Eq. 1”, we obtain:

$$\lg \tau = (k \cdot \sigma + d) \cdot T + c \cdot T + \mu \quad (3)$$

solving which relative to the variable (temperature) or its reciprocal, taking into account that the stress is in this case a constant ( $\sigma = const$ ), it turns out:

$$\lg \tau = (k \cdot \sigma + c) \cdot T + (d \cdot \sigma + \mu) \quad (4)$$

thus we have a linear dependence.

In this case, it is assumed that the dependence of the change in the coefficient  $b$  on temperature or its inverse value is also linear:

$$b = c \cdot T + \mu \quad (5)$$

Thus, the resulting “Eq. 4” is the equation of forward stresses constructed in the coordinate system of the logarithm of durability versus temperature (reciprocal temperature), which are obtained by remaking the graph in the coordinate system.

« $\lg \tau - \sigma$ » into the coordinate system « $\lg \tau - T$ » (« $\lg \tau - \frac{1}{T}$ ») in practice. Consequently, the hypothesis put forward is confirmed.

In the case of proof from the opposite, let the dependences of the change in the coefficients of “Eq. 1” are not linear, but obey, say, parabolic dependences. Then, solving “Eq. 1” with respect to a variable  $T$  at a constant voltage, the dependence of the logarithm of durability on temperature (reciprocal temperature) will not have a linear form, which contradicts the experimental data.

Having established the values of the coefficients  $c$  and  $d$  of “Eq. 2” and equating  $a$  to zero, the limiting temperature of the existence of a solid is found.

The constant  $\lg\tau_0$  is determined by the ordinate of the pole point of the resulting beam [1].

To determine the thermal fluctuation constants by the reference beam method, a system of coefficients is used:  $k_\sigma, k_k$ . It seems possible to determine the structural-mechanical constant  $\gamma$  and the value of the activation energy of destruction  $U_0$  on the basis of the ratio of the angular coefficients of “Eq. 2” of the reference and the desired beam, expressed by the coefficient  $k_k$ .

The coefficient  $k_\sigma$  is determined as follows:

$$k_\sigma = \frac{\sigma}{\sigma_\sigma}, \quad (6)$$

where  $\sigma$ —the abscissa point of the pole of the obtained direct temperature graph;  
 $\sigma_\sigma$ —abscissa point of the pole of the reference direct temperature graph;

$$k_k = \frac{k}{k_\sigma}, \quad (7)$$

where  $k$ —slope of “Eq. 2” for experimental data;

$k_\sigma = -2,619$ —slope of “Eq. 2” of the reference graph.

The constant  $U_0$  is determined by multiplying the reference constant  $U_{0,\sigma}$  by the system of coefficients  $k_\sigma$  and  $k_k$ :

$$U_0 = k_\sigma \cdot k_k \cdot U_{0,\sigma}, \quad (8)$$

The constant  $\gamma$  is determined by multiplying the reference constant  $\gamma_\sigma$  by the coefficient  $k_\sigma$ :

$$\gamma = k_\sigma \cdot \gamma_\sigma. \quad (9)$$

### 3 Results and Discussion

To check the developed technique, let us determine the thermal fluctuation constants of the generalized Zhurkov equation for a decorative protective slab based on a polyester resin binder using the reference beam method and compare the obtained values with the constants for this material obtained by the graphic and graphic-analytical method [19, 20]. Experimental data are presented in Table 2 [21].

On the basis of the experimentally obtained data (Table 2), a graph of direct temperatures in the coordinates  $\lg\tau - \sigma$  for a decorative protective board on a binder made of polyester resin was built (Fig. 4).

**Table 2** Experimental data on the dependence of durability on voltage and temperature for a decorative protective board on a binder made of polyester resin

T = 20,00 °C		T = 40,00 °C		T = 60,00 °C	
$\sigma$	$\lg\tau$	$\sigma$	$\lg\tau$	$\sigma$	$\lg\tau$
42,60	0,540	41,99	0,950	41,37	0,600
40,40	2,740	41,10	1,700	40,50	1,150
38,20	5,500	39,78	2,220	39,20	3,260
41,70	3,200	38,90	2,460	38,20	2,170
39,50	2,830	37,57	4,200	37,02	3,120

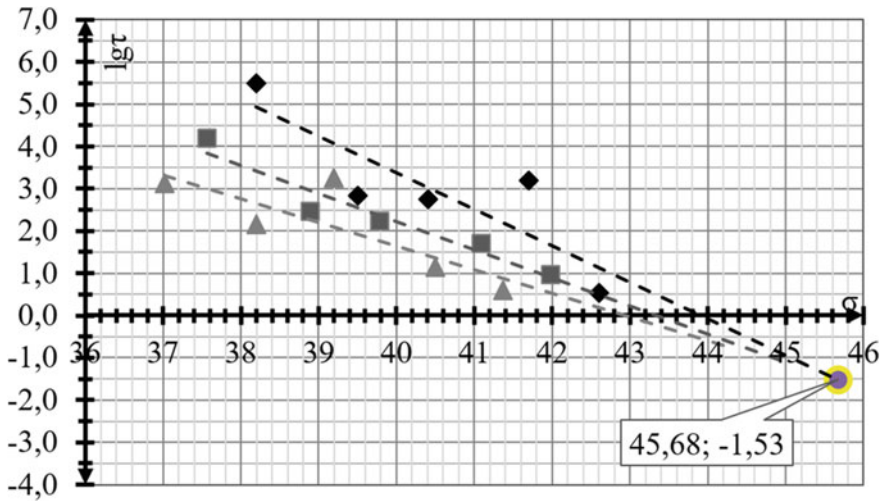


**Fig. 4** Graph of the dependence of the decimal logarithm of durability on voltage at a given temperature

According to the obtained graph (Fig. 4), the pole point has coordinates along the abscissa axis  $\sigma = 45.68$  MPa and along the ordinate axis  $\lg\tau = -1.53$ , and the resulting straight lines are expressed by the equations:

- at T = 20 °C  $y = -0,863x + 37,896$ ;
- at T = 40 °C  $y = -0,6629x + 28,734$ ;
- at T = 60 °C  $y = -0,5581x + 23,969$ .

The limiting temperature of the existence of the material is determined from the linear dependence of the change in the slope of the slope of direct temperatures, shown in Fig. 5.

The equation of direct change in the slope of the formula (1) for a decorative-protective plate on a binder made of polyester resin (Fig. 5) with  $R_2 = 0.98$  is expressed by the equation:

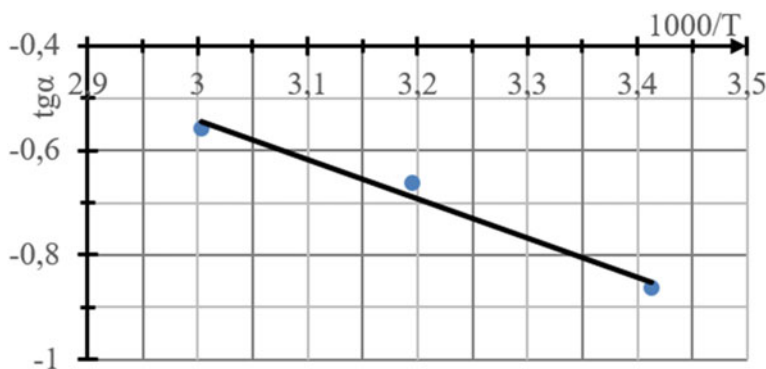


Fig. 5 Graph of the change in the slope of the «Eq. 1»

$$a = -0.7477(1000/T_m) + 1.7008,$$

hence at  $a = 0$   $T_m = 439.64$  [22, 23].

The values of the coefficients  $k_\sigma$  and  $k_k$  are determined by “Eqs. 5, 6”, respectively:

$$k_\sigma = \frac{45,68}{10} = 4,57,$$

$$k_k = \frac{-0,748}{-2,619} = 0,285$$

Let us determine the thermal fluctuation constants  $U_0$  and  $\gamma$  for a decorative protective board based on a polyester resin binder according to “Eqs. 5, 6”, respectively:

$$U_0 = 4,57 \cdot 0,285 \cdot 500 = 652,79 \text{ kJ/mol.}$$

$$\gamma = 0,29 \cdot 50 = 14,50 \text{ (mol MPa).}$$

The obtained values coincide with the results obtained by graphic and graphic-analytical methods and presented in Table 3.

Analysis of Table 3 shows a high convergence of the results of calculations performed by the graphical-analytical method and by the method of the reference

**Table 3** Thermofluctuation constants for a decorative protective board based on a polyester resin binder

Method of obtaining constants	Thermofluctuation constants			
	$\gamma$ , kJ/(mol MPa)	$U_0$ , kJ/mol	$T_m$ , K	$\lg \tau_m$
Graphic	15,85	701,00	454,50	-1,00
Graphoanalytical	14,29	652,79	439,64	-1,53
Reference beam method	15,50	652,79	439,64	-1,53

beam, which indicates the adequacy of the proposed method for determining the thermal fluctuation constants [24].

## 4 Conclusion

Thus, the technique of the reference beam makes it possible to determine the durability of the material according to the generalized Zhurkov formula without additional plotting in the coordinates  $tga - (1000/T)$  and  $U - \sigma$ , which reduces labor intensity, and also, more importantly, avoids errors and errors that arise in the process of graphic constructions.

The next stage of work is the need to test the proposed methodology on a wide range of building materials.

## References

1. Regel VR, Slutsker AI, Tomashevsky EE (1974) The kinetic nature of the strength of solids. Science, Moscow
2. Sokolova S, Smirnova N (2018) Innovative technological solutions to ensure the reliability of operated buildings. In: J MATEC Web Conf 251:06018. <https://doi.org/10.1051/mateconf/201825106018>
3. Pakhomov EI (2015) Indicator of operational reliability of construction materials working under difficult loading conditions. National priorities of Russia. Ser 1: Sci Milit Secur 3:120–124
4. Mishin VM, Shchitov DV, Volokonsky MV (2018) Appendix to the journal. Bull Tambov Univ 23(123):236
5. Loganina VI, Uchaeva TV, Monastirev PV (2016) The method to estimate the surface appearance quality of the paint applied to the cement. J Eng Appl Sci 11(11):2409–2410. <https://doi.org/10.36478/jeasci.2016.2409.2410>
6. Yartsev VP (1998) Physical and technical foundations of the performance of organic materials in parts and structures. Dissertation of doctor of technical sciences (Voronezh)
7. Drannikov RN, Erofeev AV, Gorokhov TI (2020) The influence of the data processing technique on the obtained values of thermofluctuation constants on the example of polyvinyl chloride plates. J Constr: New Technol—New Equip 7:40–45
8. Erofeev AV, Drannikov RN, Gorokhov TI (2020) The role of the human factor in determining the thermofluctual constants of the generalized Zhurkov equation in a graphical way. J Constr Mater, Equip, Technol Twenty-First Century 7–8(258–259):25–28
9. Potapova LB, Yartsev VP (2005) The mechanics of materials in a complex stress state. How is the ultimate stress predicted? Publishing House Mashinostroyeniye-1, Moscow
10. Sokova S, Smirnova N (2018) Innovative technological solutions to ensure the reliability of operated buildings. J MATEC Web Conf 251:06018. <https://doi.org/10.1051/mateconf/201825106018>.
11. Bogoslovsky VN, Rightman VM, Parfentjeva NA (1982) On the possibility of predicting the durability of building materials and structures based on the kinetic approach. Proceedings of universities. Building 9:62–68
12. Kiseleva OA (2003) Predicting the working capacity of wood-shaving and wood-fiber composites in building products: dissertation ... Candidate of technical sciences: 05.23.05. - Voronezh

13. Andrianov KA (2002) Forecasting the durability (working capacity) of expanded polystyrene in the enclosing structures of buildings: dissertation ... candidate of technical sciences: 05.23.05. - Tambov
14. Drannikov RN, Erofeev AV, Gorokhov TI (2020) Determination of the initial data for calculating the thermofluctuation constants of the generalized Zhurkov equation of polyvinyl chloride plates. In: The II-th All-Russian (national) scientific and practical Conference "Modern science: theory, methodology, practice" May 28–29, 2020, 116–119. Russia, Tambov
15. Miyase A, Wang SS (2018) Test method development and determination of three-dimensional stiffness properties of polyvinyl chloride structural foams. *J Compos Mater* 52(5):679–688
16. Tager AA (1968) *Physicochemistry of polymers*. Chemistry, Moscow
17. Zagorodnikova MA, Yartsev VP, Monastyrev PV (2016) Evaluation of durability and chemical resistance for pvc-membranes used in the construction of livestock complexes. *Bull Tambov State Tech Univ* 22(4):657–665. <https://doi.org/10.6060/ivkkt.20206305.6084>
18. Sokova S, Smirnova N (2019) The choice of durable blocking waterproofing mathematical method. *J Phys: Conf Ser* 1425
19. Yartsev VP, Podolskaya MA (2014) Composites based on polyester resins with polymer additives. *Bull Tambov State Tech Univ* 20(3):557–563
20. Mamontov SA, Yartsev VP, Monastyrev PV (2017) An artificial and natural aging of wood-fiber composite. *Izvestiya Vysshikh Uchebnykh Zavedenii, Seriya Tekhnologiya Tekstil'noi Promyshlennosti* 1:95–100
21. Erofeev AV (2014) Durable decorative and protective boards based on wood composites for facade finishing of buildings: dis. ... Cand. tehn sciences: 05.23.05—Building materials and products. Voronezh
22. Golovanchikov AB, Minh CD, Shubitova NV (2019) The approximation of experimental data using the least squares method and the least relative squares method. *Energy Resour Sav: Ind Transp* 1(26):42–44. <https://doi.org/10.26102/2310-6018/2020.28.1.042>
23. Musatov MV, L'vov AA (2009) Analyzing the models of the least squares method and derivation of estimates estimates methods. *Vestnik Saratovskogo gosudarstvennogo tekhnicheskogo universiteta. Sci J Saratov State Tech Univ* 4(2):137–140
24. Golovanchikov AB, Doan MK, Petrukhin AB, Merentsov NA (2020) Comparison of the accuracy of experimental data approximation using the least relative squares method with the least squares method. *Model, Optim Inf Technol* 81(28):38–39

# Strength and Deformability of a Complex-Stressed Reinforced Concrete Element Based on the Plasticity Theory of G. A. Geniev



Ngoc Tuyen Vu  and Natalia Fedorova 

**Abstract** In connection with ensuring the necessary reliability in the operation of both the building and the structure as a whole and its elements, as well as the need to prevent progressive collapse under special actions, it is important to develop effective calculation models for analyzing the strength and deformability of the most used structural material—concrete and reinforced concrete. The article summarizes the working prerequisites and hypotheses necessary for the construction of general physical relationships (relationships between stresses and deformations) of a complex-stressed reinforced concrete element. The criteria for assessing the strength and deformability of reinforced concrete under triaxial and biaxial stress are presented. When constructing the calculation model of the resistance of this composite material, the physical non-linear work of concrete was taken into account based on the theory of plasticity by G. A. Geniev, as well as its anisotropy in the form of reinforcement coefficients and other factors.

**Keywords** Deformability · Strength · Complex stress states · Reinforced concrete · Plasticity theory

## 1 Introduction

In modern construction, there is an increasing tendency to complicate the design solutions of buildings and structures, especially from monolithic reinforced concrete [1–3]. Among such solutions are spatial frames of buildings with an irregular grid of load-bearing columns and walls [4], monolithically connected with floor slabs, transition slabs; structurally heterogeneous foundation slabs [5], bearing systems of

---

N. T. Vu (✉) · N. Fedorova  
Moscow State University of Civil Engineering, 26, Yaroslavskoye Shosse, Moscow 129337,  
Russia  
e-mail: [ngoctuyennd91@gmail.com](mailto:ngoctuyennd91@gmail.com)

N. Fedorova  
e-mail: [klynavit@yandex.ru](mailto:klynavit@yandex.ru)

© The Author(s), under exclusive license to Springer Nature Switzerland AG 2024  
N. Vatin et al. (eds.), *Modern Problems in Construction*,  
Lecture Notes in Civil Engineering 372,  
[https://doi.org/10.1007/978-3-031-36723-6\\_11](https://doi.org/10.1007/978-3-031-36723-6_11)



high-rise buildings with heavily loaded massive columns, walls, stiffening cores [6], foundation slabs and their joints. All these structures, as well as the structures of conventional buildings, operate under conditions of complex inhomogeneous stress states, which significantly affects the nature of cracking, deformation, and destruction of a physical nonlinear material such as reinforced concrete, without taking into account which the necessary reliability and economic efficiency of modern design solutions are not provided [7–9].

However, at present, the main methods for calculating reinforced concrete structures laid down in the regulatory documents of many countries around the world, are based on the isotropic linear elastic behavior of materials whose physical characteristics are described by a minimum number of parameters [10]. Empirical coefficients derived from the results of limited experimental studies are often used to take into account the non-linear characteristics of the deformation property of reinforced concrete. This method was considered satisfactory if the behavior of “typical” structures (not special) was considered under short-term loads not exceeding the operational level.

In recent years, the problem of the progressive collapse of buildings and structures under special emergency actions has been given special attention by many domestic and foreign scientists [11–13]. Limited experiments have been carried out to study the behavior of reinforced concrete frame structures with a sudden shutdown of load-bearing columns or ties [14–16]. The results of these experiments show that under such an emergency action, the structure fully operates in the nonlinear stage, accompanied by large deformations before failure [17–19]. Therefore, it is not possible to apply traditional calculation methods based on the theory of elasticity and the system of empirical coefficients, which are set out in the current standards for the above task.

In this regard, the creation of methods for calculating the structures of buildings, taking into account various factors of physical nonlinearity in complex stress states, is an urgent problem of modern design. The purpose of this work is to build a computation model of the nonlinear deformation of reinforced concrete under complex stressed states based on the theory of plasticity by Geniev [20].

## 2 Materials and Methods

### 2.1 Deformation Theory of Plasticity of Concrete

The main physical dependencies of the deformation theory of plasticity of concrete Geniev [20] for a complex stress state can be represented as a system of equations relating normal stresses  $\sigma_{bi}$  with linear strains  $\varepsilon_{bi}$  ( $i = x, y, z$ ):

$$\begin{cases} \sigma_{bx} = \frac{E_b(\gamma_i)}{(1-\nu)(1-2\nu)} [(1-\nu)\varepsilon_{bx} + \nu(\varepsilon_{by} + \varepsilon_{bz})]; \\ \sigma_{by} = \frac{E_b(\gamma_i)}{(1-\nu)(1-2\nu)} [(1-\nu)\varepsilon_{by} + \nu(\varepsilon_{bx} + \varepsilon_{bz})]; \\ \sigma_{bz} = \frac{E_b(\gamma_i)}{(1-\nu)(1-2\nu)} [(1-\nu)\varepsilon_{bz} + \nu(\varepsilon_{bx} + \varepsilon_{by})]; \end{cases} \quad (1)$$

and in the form of a system of equations relating the tangential strains  $\tau_{bij}$  to the angular strains  $\gamma_{bij}$

$$\begin{cases} \gamma_{bxy} = \frac{\tau_{bxy}}{G(\gamma_i)} = \frac{\tau_{bxy}}{\frac{1}{2(1+\nu)}E(\gamma_i)} = \frac{2(1+\nu)}{E(\gamma_i)} \tau_{bxy}; \\ \gamma_{byz} = \frac{\tau_{byz}}{G(\gamma_i)} = \frac{\tau_{byz}}{\frac{1}{2(1+\nu)}E(\gamma_i)} = \frac{2(1+\nu)}{E(\gamma_i)} \tau_{byz}; \\ \gamma_{bzx} = \frac{\tau_{bzx}}{G(\gamma_i)} = \frac{\tau_{bzx}}{\frac{1}{2(1+\nu)}E(\gamma_i)} = \frac{2(1+\nu)}{E(\gamma_i)} \tau_{bzx}; \end{cases} \quad (2)$$

where  $G(\gamma_i)$  is the secant shear modulus of concrete for the considered type of stress state,  $\nu$  is the lateral expansion coefficient and  $E_b(\gamma_i)$  is the current modulus of concrete deformation is determined depending on the intensity of shear deformations  $\gamma_i$  by a linear function:

$$E_b(\gamma_i) = E_0 \left( 1 - \frac{\gamma_i}{2\gamma_{is}} \right), \quad (3)$$

$$\gamma_i = \sqrt{\frac{2}{3}} \sqrt{(\varepsilon_{bx} - \varepsilon_{by})^2 + (\varepsilon_{by} - \varepsilon_{bz})^2 + (\varepsilon_{bz} - \varepsilon_{bx})^2 + \frac{3}{2}(\gamma_{bxy}^2 + \gamma_{byz}^2 + \gamma_{bzx}^2)}. \quad (4)$$

In the above formulas, the limiting value of the intensity of shear strains for the considered type of stress state  $\gamma_{is}$  is determined by the product of the limiting intensity of shear stresses in pure shear  $\gamma_{ic}$  by the coefficient of change in the limiting value of the shear strain intensity  $k(\lambda, \delta)$ :

$$\gamma_{is} = \gamma_{ic} k(\lambda, \delta), \quad (5)$$

$$\gamma_{ic} = \frac{T_c}{G_s}, \quad (6)$$

where

$$T_c = \frac{1}{\sqrt{3}} \sqrt{R_c R_p} \quad (7)$$

- the ultimate intensity of shear stresses in pure shear;

$$G_s = \frac{1}{2} \cdot G_0 = \frac{1}{2} \cdot \frac{E_b}{2(1 + \nu)} \quad (8)$$

- limit secant shear modulus, which is equal to half of the initial shear modulus;  $R_c$ —ultimate strength in uniaxial compression, equal to the prism strength of concrete;  $R_p$ —uniaxial tensile strength, which is the uniaxial tear strength.

Putting (7) and (8) in (6) we get:

$$\gamma_i = \frac{4(1 + \nu)\sqrt{R_b R_{bt}}}{\sqrt{3}E_b}. \quad (9)$$

The quantity  $k(\lambda, \delta)$  represents the change in the limit value of the shear strain intensity  $\gamma_{is}$  for the considered stress state compared to the limit value for pure shear  $\gamma_{ic}$ :

$$k(\lambda, \delta) = \frac{\lambda(1 + \delta)}{2} + \sqrt{\frac{\lambda^2(1 + \delta)^2}{4} + (1 + \delta)}, \quad (10)$$

where

$$\lambda = f \frac{\sigma}{T}, \quad (11)$$

$$\delta = e \left( \frac{S}{T} \right)^3, \quad (12)$$

$\sigma$ —average stress coinciding up to a constant coefficient with the first invariant of the stress tensor  $I_{\sigma 1}$ ,

$$\sigma = I_{\sigma 1} = \frac{\sigma_{bx} + \sigma_{by} + \sigma_{bz}}{3}, \quad (13)$$

$T$ —shear stress intensity, the square of which is numerically equal to the second invariant of the stress deviator  $I_{D2}$ ,

$$T = \sqrt{I_{D2}} = \frac{1}{\sqrt{6}} \sqrt{(\sigma_{bx} - \sigma_{by})^2 + (\sigma_{by} - \sigma_{bz})^2 + (\sigma_{bz} - \sigma_{bx})^2 + 6(\tau_{bxy}^2 + \tau_{byz}^2 + \tau_{bzx}^2)}, \quad (14)$$

$f$ - dimensionless coefficient,

$$f = \frac{3T_c(R_c - R_p)}{R_c R_p} = 3 \frac{1}{\sqrt{3}} \sqrt{RR} \frac{(R_c - R_p)}{R_c R_p} = \sqrt{3} \frac{(R_c - R_p)}{\sqrt{RR}}, \quad (15)$$

$S$ - invariant quantity, the third power of which, with the accuracy of a constant coefficient, coincides with the third invariant of the stress deviator  $I_{D3}$ .

$$S = \sqrt{3} \left( \frac{1}{2} I_{D3} \right)^{\frac{1}{3}} = \sqrt{3} \left( \frac{1}{2} \begin{vmatrix} \sigma_{bx} - \sigma & \tau_{bxy} & \tau_{bxz} \\ \tau_{byx} & \sigma_{by} - \sigma & \tau_{byz} \\ \tau_{bzx} & \tau_{bzy} & \sigma_{bx} - \sigma \end{vmatrix} \right)^{\frac{1}{3}}, \quad (16)$$

$e$ - dimensionless coefficient,

$$e = \frac{R_c R_p}{3T_c^2} - 1 = \frac{R_c R_p}{3 \left( \frac{1}{\sqrt{3}} \sqrt{R_c R_p} \right)^2} - 1 = 0, \quad (17)$$

We put (14), (16), and (17) in (12) we get the value of the coefficient  $\delta$ ,

$$\delta = 0. \quad (18)$$

We put (13), (14), and (15) in (11) we get the value of the coefficient  $\lambda$ ,

$$\lambda = \sqrt{\frac{2}{R_c R_p}} (R_c - R_p) \frac{\sigma_{bx} + \sigma_{by} + \sigma_{bz}}{\sqrt{(\sigma_{bx} - \sigma_{by})^2 + (\sigma_{by} - \sigma_{bz})^2 + (\sigma_{bz} - \sigma_{bx})^2 + 6(\tau_{bxy}^2 + \tau_{byz}^2 + \tau_{bzx}^2)}}. \quad (19)$$

From (18) and (19), the coefficient of change of the limiting value of the shear strain intensity can be determined by the formula:

$$k(\lambda, \delta) = \frac{\lambda}{2} + \sqrt{\frac{\lambda^2}{4}} 1. \quad (20)$$

## 2.2 Deformation Theory of Plasticity of Reinforced Concrete

Using the deformation theory of concrete plasticity of G. A. Geniev presented above, we obtain the relationship between stresses and strains for reinforced concrete. Let's make the following additional assumptions:

1. The reinforcement is located in orthogonal directions coinciding with the coordinate axes, and the dimensions of the characteristic reinforced concrete element are large compared to the average distance between the rods. This makes it possible to neglect local stresses at the contact between reinforcement and concrete and spread the reinforcement by specifying its reinforcement coefficients as continuous functions of coordinates. Thus, the reinforcement, presented in the form

of continuously arranged dispersed fibers, is considered an elastic anisotropic medium.

2. Reinforcing framework (without concrete) is a geometrically variable system under the action of tangential stresses on areas perpendicular to the reinforcement. Therefore, it is assumed that on these sites the reinforcement perceives only normal stresses and its Poisson's ratios in the axes coinciding with the directions of reinforcement are equal to zero.
3. Total normal stresses are the sum of stresses in concrete and reinforcement.
4. The condition for the compatibility of two media (concrete and reinforcement) is the equality of deformations.

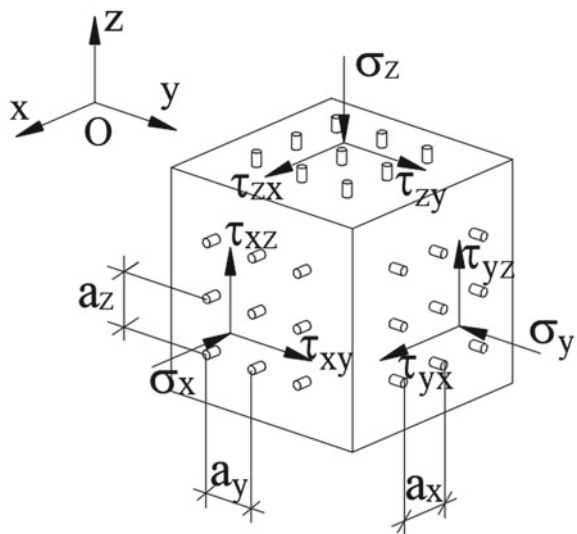
Consider a typical three-dimensional reinforced concrete element that models a complex stressed zone of a structure, the faces of which are parallel to the coordinate planes. Six components (components) of stress act on the edges of the sites: three normal  $\sigma_x, \sigma_y, \sigma_z$  and three tangential  $\tau_{xy}, \tau_{yz}, \tau_{zx}$ .

Normal stresses are considered positive if they are directed toward the internal normal to the site, and vice versa. According to this rule, positive normal stresses are considered to be compressive, while negative normal stresses are considered to be tensile. For shear stresses, the following rules of signs are accepted. On a site whose outward normal is directed in the positive (or negative) direction of the corresponding axis, the tangent direction is considered positive if it is also directed in the positive (or negative) direction of the axis. Figure 1 shows positive stresses.

The reinforced concrete element is reinforced with orthogonal reinforcing bar cages, coinciding with the directions of the coordinate axes of the Oxyz system.

In three-dimensional frames, the rods are located with certain steps  $a_x, a_y, a_z$ , respectively, along the coordinates  $x, y, z$  (this reinforcement is also called

**Fig. 1** Loading diagram of a typical reinforced concrete element



orthotropic). Each direction of the rods ( $i = x, y, z$ ) is characterized by the coefficient of reinforcement  $\mu_i$ , which is equal to the area of the rods per unit area of the site, drawn normally to the direction  $i$ . According to Fig. 1:

$$\mu_x = \frac{A_{sx}}{a_y a_z}; \mu_y = \frac{A_{sy}}{a_x a_z}; \mu_z = \frac{A_{sz}}{a_x a_y}, \tag{21}$$

where  $A_x, A_y, A_z$  is the area of individual reinforcing bars of the corresponding direction  $x, y, z$ .

In this paper, we use a linear relationship between stresses  $\sigma_s$  and strains  $\varepsilon_s$  of reinforcing bars.

$$\sigma_{sx} = E_s \cdot \varepsilon_{sx}; \sigma_{sy} = E_s \cdot \varepsilon_{sy}; \sigma_{sz} = E_s \cdot \varepsilon_{sz}, \tag{22}$$

where  $E_s$ - elastic modulus of reinforcement.

From the second assumption, it follows that the shear stresses on the areas of the reinforced concrete elements are perceived by concrete:

$$\tau_{bxy} = \tau_{xy}; \tau_{byz} = \tau_{yz}; \tau_{bzx} = \tau_{zx}. \tag{23}$$

From the fifth assumption, we obtain the equilibrium conditions: the total normal stresses in the characteristic elements are the sum of the stresses in concrete and reinforcement (Fig. 2).

$$\sigma_{bx} + \mu_x \cdot \sigma_{sx} = \sigma_x; \sigma_{by} + \mu_y \cdot \sigma_{sy} = \sigma_y; \sigma_{bz} + \mu_z \cdot \sigma_{sz} = \sigma_z. \tag{24}$$

In the fourth assumption, the condition of compatibility of axial deformations of reinforcement and the corresponding linear deformations of concrete is accepted:

$$\varepsilon_{bx} = \varepsilon_{sx} = \varepsilon_x, \varepsilon_{by} = \varepsilon_{sy} = \varepsilon_y, \varepsilon_{bz} = \varepsilon_{sz} = \varepsilon_z. \tag{25}$$

We put (1), (22), (25) in (24) we obtain a system of nonlinear equations for determining linear and angular deformations in a characteristic reinforced concrete element:

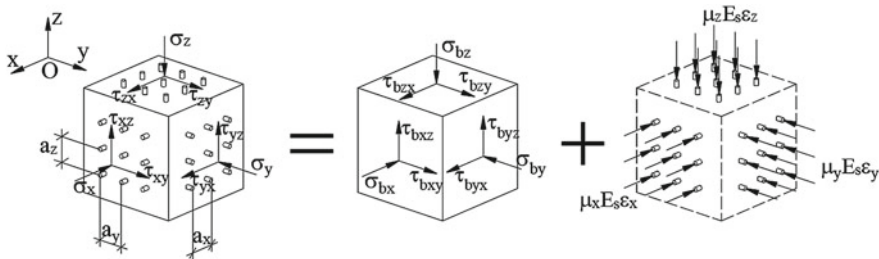


Fig. 2 Scheme for determining normal stresses in concrete and reinforcement

$$\begin{cases} \frac{E_b(\gamma_i)}{(1-\nu)(1-2\nu)} [(1-\nu)\varepsilon_x + \nu(\varepsilon_y + \varepsilon_z)] + \mu_x E_s \varepsilon_x = \sigma_x; \\ \frac{E_b(\gamma_i)}{(1-\nu)(1-2\nu)} [(1-\nu)\varepsilon_y + \nu(\varepsilon_x + \varepsilon_z)] + \mu_y E_s \varepsilon_y = \sigma_y; \\ \frac{E_b(\gamma_i)}{(1-\nu)(1-2\nu)} [(1-\nu)\varepsilon_z + \nu(\varepsilon_x + \varepsilon_y)] + \mu_z E_s \varepsilon_z = \sigma_z. \end{cases} \quad (26)$$

$$\gamma_{xy} = \frac{2(1+\nu)}{E(\gamma_i)} \tau_{xy}; \quad \gamma_{yz} = \frac{2(1+\nu)}{E(\gamma_i)} \tau_{yz}; \quad \gamma_{zx} = \frac{2(1+\nu)}{E(\gamma_i)} \tau_{zx}. \quad (27)$$

To simplify the solution of the system of Eqs. (26), we set:

$$A = \frac{E_b(\gamma_i)}{(1-\nu)(1-2\nu)}. \quad (28)$$

Then the linear deformations in this characteristic reinforced concrete element are determined by the formula:

$$\begin{cases} \varepsilon_x = \frac{(1-2\nu)[\sigma_x - \nu(\sigma_y + \sigma_z)]A^2 + E_s [(1-\nu)(\mu_z + \mu_y)\sigma_x - \nu(\mu_z\sigma_y + \mu_y\sigma_z)]A + E_s^2 \mu_y \mu_z \sigma_x}{(1+\nu)(1-2\nu)^2 A^3 + E_s(1-2\nu)(\mu_x + \mu_y + \mu_z)A^2 + E_s^2(1-\nu)(\mu_x\mu_y + \mu_y\mu_z + \mu_z\mu_x)A + E_s^3 \mu_x \mu_y \mu_z}; \\ \varepsilon_y = \frac{(1-2\nu)[\sigma_y - \nu(\sigma_x + \sigma_z)]A^2 + E_s [(1-\nu)(\mu_x + \mu_z)\sigma_y - \nu(\mu_z\sigma_x + \mu_x\sigma_z)]A + E_s^2 \mu_x \mu_z \sigma_y}{(1+\nu)(1-2\nu)^2 A^3 + E_s(1-2\nu)(\mu_x + \mu_y + \mu_z)A^2 + E_s^2(1-\nu)(\mu_x\mu_y + \mu_y\mu_z + \mu_z\mu_x)A + E_s^3 \mu_x \mu_y \mu_z}; \\ \varepsilon_z = \frac{(1-2\nu)[\sigma_z - \nu(\sigma_x + \sigma_y)]A^2 + E_s [(1-\nu)(\mu_x + \mu_y)\sigma_z - \nu(\mu_x\sigma_y + \mu_y\sigma_x)]A + E_s^2 \mu_x \mu_y \sigma_z}{(1+\nu)(1-2\nu)^2 A^3 + E_s(1-2\nu)(\mu_x + \mu_y + \mu_z)A^2 + E_s^2(1-\nu)(\mu_x\mu_y + \mu_y\mu_z + \mu_z\mu_x)A + E_s^3 \mu_x \mu_y \mu_z}. \end{cases} \quad (29)$$

After determining the linear and angular deformations in a characteristic reinforced concrete element, it is possible to determine the complex stress state of concrete (six derived concrete stress components  $\sigma_{bx}$ ,  $\sigma_{by}$ ,  $\sigma_{bz}$ ,  $\tau_{bxy}$ ,  $\tau_{byz}$ ,  $\tau_{bzx}$ ), and reinforcement ( $\sigma_{sx}$ ,  $\sigma_{sy}$ ,  $\sigma_{sz}$ ) separately by supplying (27) in (1) and (22).

### 2.3 Strength Criterion for Concrete and Reinforcement

Let's check the strength conditions of concrete. In the rectangular coordinate system Oxyz, which does not coincide with the principal stress axes of the concrete, the stress state does not cause failure when the following inequality is fulfilled:

$$\begin{aligned} & \sigma_{bx}^2 + \sigma_{by}^2 + \sigma_{bz}^2 - (\sigma_{bx}\sigma_{by} + \sigma_{by}\sigma_{bz} + \sigma_{bz}\sigma_{bx}) + 3(\tau_{bxy}^2 + \tau_{byz}^2 + \tau_{bzx}^2) - \\ & - (R_c - R_p)(\sigma_{bx} + \sigma_{by} + \sigma_{bz}) - R_c R_p \leq 0. \end{aligned} \quad (30)$$

The reinforcement strength conditions are reduced to the requirement that the stresses in absolute value do not exceed the magnitude of the design resistance of the reinforcement:

$$|\sigma_{sx}| \leq R_s; |\sigma_{sy}| \leq R_s; |\sigma_{sz}| \leq R_s. \quad (31)$$

### 3 Results and Discussion

We apply the developed calculation model for two particular types of stress states—plane and uniaxial stress states.

**Plane stress state.** For this case we have:

$$\mu_x \neq 0; \mu_y \neq 0; \mu_z = 0; \sigma_x \neq 0; \sigma_y \neq 0; \sigma_z = 0; \tau_{xy} \neq 0; \tau_{yz} = 0; \tau_{zx} = 0. \quad (32)$$

In this case, linear deformations in a characteristic reinforced concrete element are determined by the formula:

$$\begin{cases} \varepsilon_x = \frac{[(E_s \cdot \mu_y + E_b(T)) - E_s \cdot \mu_y \cdot \nu^2] \cdot \sigma_x - E_b(T) \cdot \nu \cdot \sigma_y}{E_s^2 \cdot \mu_x \cdot \mu_y \cdot (1 - \nu^2) + E_b(T) \cdot E_s \cdot (\mu_x + \mu_y) + E_b^2}, \\ \varepsilon_y = \frac{[(E_s \cdot \mu_x + E_b(T)) - E_s \cdot \mu_x \cdot \nu^2] \cdot \sigma_y - E_b(T) \cdot \nu \cdot \sigma_x}{E_s^2 \cdot \mu_x \cdot \mu_y \cdot (1 - \nu^2) + E_b(T) \cdot E_s \cdot (\mu_x + \mu_y) + E_b^2}. \end{cases} \quad (33)$$

The concrete strength condition is written in the following form:

$$\sigma_{bx}^2 + \sigma_{by}^2 - \sigma_{bx}\sigma_{by} + 3\tau_{bxy}^2 - (R_c - R_p)(\sigma_{bx} + \sigma_{by}) - R_c R_p \leq 0. \quad (34)$$

**Uniaxial stress state.** We have

$$\mu_x \neq 0; \mu_y = 0; \mu_z = 0; \sigma_x \neq 0; \sigma_y = 0; \sigma_z = 0; \tau_{xy} = 0; \tau_{yz} = 0; \tau_{zx} = 0; \quad (35)$$

Linear deformation in a characteristic reinforced concrete element is determined by the formula:

$$\varepsilon_x = \frac{-2\sqrt{R_c^2(E_s \cdot \mu_x + E_b)^2 - R_c \cdot \sigma_x \cdot E_b^2 + 2 \cdot R_c(E_s \cdot \mu_x + E_b)}}{E_b^2}. \quad (36)$$

The strength condition of the concrete in this case:



$$\sigma_{bx} = E_b \left( 1 - \frac{E_b}{4 \cdot R_c} \varepsilon_x \right) \varepsilon_x \leq R_c. \quad (37)$$

## 4 Conclusion

Using the theory of plasticity of concrete and reinforced concrete, G. A. Geniev, the following new results were obtained:

A model of the deformation of reinforced concrete under a complex stress state (in the form of physical relationships between stresses and strains) is proposed, taking into account the physical nonlinearity of reinforced concrete.

New dependencies of physical relations for plane and uniaxial stress states are obtained.

The developed deformation models of reinforced concrete can be used to analyze the limiting and transcendental states of reinforced concrete elements of structural systems of frames of buildings and structures.

## References

1. Travush VI, Shulyat'ev OA, Shulyat'ev SO, Shakhraman'yan AM, Kolotovichev YA (2019) Analysis of the results of geotechnical monitoring of 'Lakhta Center' tower. *Soil Mech Found Eng* 562, 56:98–106
2. Fu G, Quan Y, Gu M, Huang Z, Feng C (2022) Dynamic performance evaluation of a 492 m super high-rise building with active tuned mass dampers during four consecutive landfall typhoons within a month. *J Build Eng* 61:105259
3. Zhou K, Li QS, Zhi LH, Han XL, Xu K (2023) Investigation of modal parameters of a 600-m-tall skyscraper based on two-year-long structural health monitoring data and five typhoons measurements. *Eng Struct* 274:115162
4. Xu F et al (2022) Shaking table test on seismic response of a planar irregular structure with differential settlements of foundation. *Structures* 46:988–999
5. Travush VI, Gordon VA, Kolchunov VI, Leontiev EV (2019) Dynamic deformation of a beam at sudden structural transformation of foundation. *Mag Civ Eng* 91:129–144
6. Hu JW, Makarios TK, Athanatopoulou A (2022) Center of stiffness, principal axes and principal start point of thin-walled open-sections of cores: a new modified calculation technique based on Vlasov Torsion theory. *Build* 12:1804
7. Gvozdev AA, Karpenko NI (1965) Operation of reinforced concrete with cracks under plane stress. *Struct Mech Calc Struct.* (rus)
8. Karpenko NI, Karpenko SN, Petrov AN (2018) Improvement of calculation methods for planar reinforced concrete structures, taking into account the actual properties of high-strength concrete. *Int J Comput Civ Struct Eng* 14:78–89 (2018). (rus)
9. Bondarenko VM, Kolchunov VI (2004) Calculation models of force resistance of reinforced concrete. *ASV.* (rus)
10. Kolchunov VI, Klyueva NV, Androsova NB, Bukhtiyarova AS (2014) Survivability of buildings and structures under beyond-design impacts. *ASV.* (rus)
11. Kolchunov VI, Fedorova NV, Savin SY, Kovalev VV, Iliushchenko TA (2019) Failure simulation of a RC multi-storey building frame with prestressed girders. *Mag Civ Eng* 92:155–162

12. Tamrazyan AG, Fedorov VS, Kharun M (2019) The effect of increased deformability of columns on the resistance to progressive collapse of buildings. IOP Conf Ser Mater Sci Eng 675:012004
13. Kabantsev O, Mitrovic B (2018) Deformation and power characteristics monolithic reinforced concrete bearing systems in the mode of progressive collapse. MATEC Web Conf 251
14. Fedorova NV, Ngoc VT (2020) Deformation and failure of monolithic reinforced concrete frames under special actions. J Phys: Conf Ser 1425:12033 (Institute of Physics Publishing)
15. Pham AT, Tan KH (2017) Experimental study on dynamic responses of reinforced concrete frames under sudden column removal applying concentrated loading. Eng Struct 139:31–45
16. Lu X et al (2017) Experimental investigation of RC beam-slab substructures against progressive collapse subject to an edge-column-removal scenario. Eng Struct 149:91–103
17. Alshaikh IMH, Bakar BHA, Alwesabi EAH, Akil HM (2020) Experimental investigation of the progressive collapse of reinforced concrete structures: an overview. Structures 25
18. Qian K, Liang S-L, Feng D-C, Fu F, Wu G (2020) Experimental and numerical investigation on progressive collapse resistance of post-tensioned precast concrete beam-column subassemblages. J Struct Eng 146:04020170
19. Ren P, Li Y, Lu X, Guan H, Zhou Y (2016) Experimental investigation of progressive collapse resistance of one-way reinforced concrete beam–slab substructures under a middle-column-removal scenario. Eng Struct 118:28–40
20. Geniev GA (1969) Variant of the deformation theory of plasticity of concrete. Concr Reinf Concr 2:18–19 (1969). (rus)

# Results of the Studies of Morphology and Granulometric Composition of Electro Erosive Tungsten-Free Hard-Alloy Powder Material



Boris Sabelnikov , Alexey Simonov , and Ekaterina Ageeva 

**Abstract** The purpose of this work was to study the morphology and particle size distribution of new tungsten-free hard-alloy powder materials produced by electro erosive dispersion in an oxygen-containing medium (distilled water). To produce new tungsten-free hard-alloy powder materials, an experimental laboratory setup for electro erosive dispersion was used. The analysis of the grain size composition of electro erosive tungsten-free hard-alloy particles was carried out by means of an Analysette 22 Nano Tec laser particle size analyzer. The method of scanning electron microscopy using a QUANTA 600 FEG microscope was used to study the morphology of the experimental powder material. The results of the analysis of the particle size distribution of electro erosive tungsten-free hard-alloy particles showed that the particle size ranges from 0.372  $\mu\text{m}$  to 65.5  $\mu\text{m}$ . It is shown that the average size of the particles obtained in distilled water is 41.63  $\mu\text{m}$ . The study of morphology showed that in the process of electro dispersion of metal waste, the particles that ejected from the electric discharge channel in molten form crystallized very quickly. The process of rapid crystallization of the molten material in a liquid working medium contributes to the formation of particles of the correct spherical and elliptical shape.

**Keywords** Tungsten-free hard alloy · Electro erosive dispersion · Shape and morphology · Powder material · Oxygen-containing medium · Distilled water

## 1 Introduction

At present, sintered hard alloys are widely used in various industries, especially in the production of construction machines and equipment [1–3]. At the same time, there is an acute problem of saving expensive tungsten and titanium. An attempt to save them led to the development of tungsten-free hard alloys of the titanium carbonitride

---

B. Sabelnikov (✉) · A. Simonov · E. Ageeva  
Southwest State University, 94, 50 Let Oktyabrya Ul., Kursk 305040, Russia  
e-mail: [sabelnikovboris1@mail.ru](mailto:sabelnikovboris1@mail.ru)

© The Author(s), under exclusive license to Springer Nature Switzerland AG 2024  
N. Vatin et al. (eds.), *Modern Problems in Construction*,  
Lecture Notes in Civil Engineering 372,  
[https://doi.org/10.1007/978-3-031-36723-6\\_12](https://doi.org/10.1007/978-3-031-36723-6_12)

(TCN) type, but still requiring the use of rather expensive titanium, so this is a partial solution to the problem [4–6].

One of the most radical possible techniques for solving the problem is recycling of hard alloy waste. The currently existing techniques of processing hard alloy waste are large-tonnage, energy-intensive and environmentally harmful. Electro erosive dispersion is one of the promising techniques for grinding any electrically conductive material, including tungsten-free hard alloys but it is not industrially used [7–10].

At the moment, in modern scientific and technical papers, there are no complete and comprehensive information about the composition, structure and properties of the particles of tungsten-free hard alloys dispersed by electro erosion and alloys obtained on their basis. For these purposes, it is necessary to conduct complex theoretical and experimental studies.

The purpose of this work was to study phase and elemental compositions of new tungsten-free hard-alloy powder materials produced by electro erosive dispersion in an oxygen-containing medium.

## 2 Materials and Methods

A new experimental tungsten-free hard-alloy powder material was produced by electro erosive dispersion using the setup according to the diagram given in Fig. 1.

The process for producing powders from tungsten-free hard alloys (TFHA) waste includes the following main operations:

1. Collection and sorting of waste tungsten-free hard alloys according to grades (chemical composition).

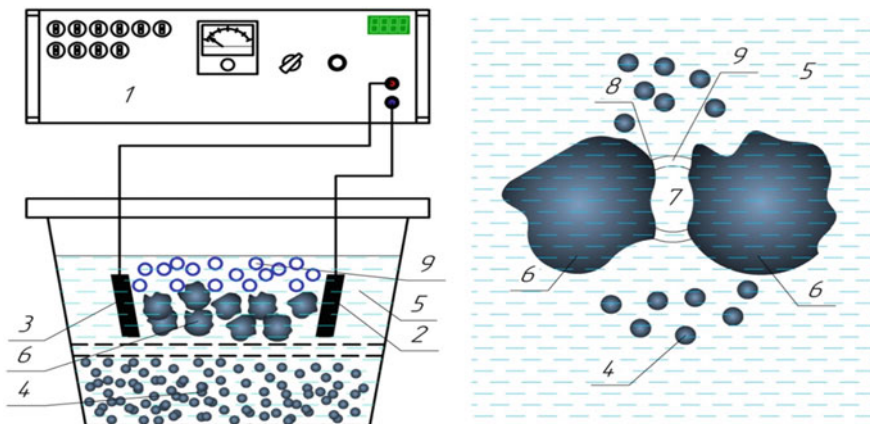


**Fig. 1** The diagram of the electro erosive dispersion process: 1—pulse generator; 2, 3—electrodes; 4—drops of molten material; 5—working fluid (distilled water); 6—waste of tungsten-free hard alloy; 7—discharge channel; 8—discharge point; 9—gas bubble

2. Impurities, swarf or shaving removals from waste.
3. Loading of tungsten-free hard alloy waste into the reactor and electrodes connecting.
4. Filling the working fluid (WF) (distilled water) into the reactor.
5. Selection of dispersion parameters (voltage, capacitor capacitance and pulse repetition rate).
6. Electro erosive dispersion.
7. Working fluid settling and draining.
8. Separation of the nanoscale fraction by centrifuging.
9. Chemical treatment of the powder (if necessary).
10. Calcination of the powder in an oven at a temperature of 150–200 °C for 20 - 30 min.
11. Quality inspection.

The process of electro erosive dispersion proceeds in the following way: the impulse voltage of the pulse generator 1 is applied to the electrodes 2 and 3 and then to the hard alloy plates 6 (hard alloy plates are also used as electrodes); when the voltage reaches a certain value, an electrical breakdown of the working fluid 5 in the interelectrode space occurs with the formation of a discharge channel 7 [11].

Due to the high concentration of thermal energy, the material melts and evaporates at the discharge point 8; the WF evaporates and surrounds the discharge channel with gaseous decomposition products 9 (gas bubble). As a result of significant dynamic forces developing in the discharge channel and gas bubble, drops of the molten material 4 eject outside the discharge zone into the WF surrounding the electrodes and solidify in it forming spherical or elliptical hard alloy powder particles [11].

The analysis of the particle size distribution of electro erosive tungsten-free hard alloy particles was carried out by means of an Analyst's 22 Nano Tec laser particle size analyzer shown in Fig. 2.

The method of scanning electron microscopy using a QUANTA 600 FEG microscope (Fig. 3) was used to study the morphology of the experimental powder material.

### 3 Results and Discussion

Figure 4 shows the results of the study of the granulometric composition of the experimental tungsten-free hard-alloy powder material produced by electro erosive dispersion of TCN grade alloy waste.

The results of the analysis of the granulometric composition of electro erosive tungsten-free hard-alloy particles showed that the particle size ranges from 0.372  $\mu\text{m}$  to 65.5  $\mu\text{m}$ . It is shown that the average particle size obtained in distilled water is 41.63  $\mu\text{m}$ .

Figure 5 shows the results of the study of the experimental powder material morphology.



**Fig. 2** Analysette 22 nanotec laser particle size analyzer

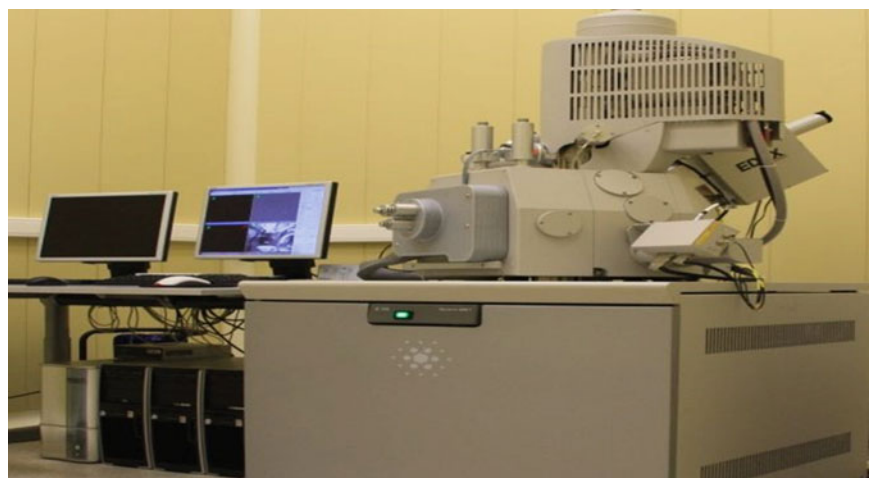


**Fig. 3** QUANTA 600 FEG scanning electron microscope

The study of morphology showed that in the process of electro dispersion of metal waste, the particles ejected from the electric discharge channel in molten form crystallize very quickly. The process of rapid crystallization of the molten material in a liquid working medium contributes to the formation of the particles of the correct spherical and elliptical shape.

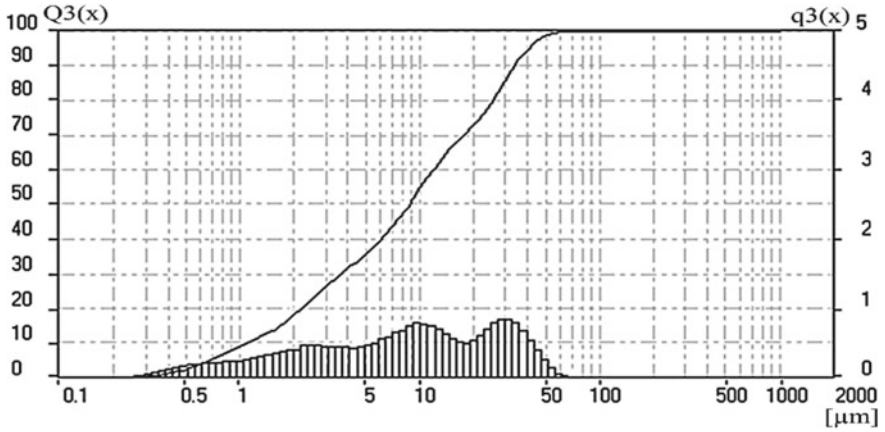


**Fig. 4** The results of the study of the particle size distribution of the experimental tungsten-free hard-alloy powder material: an integral curve and a histogram: the integral curve in the coordinates  $Q3(x) = f(\mu\text{m})$  (left scale)—each point on the curve, amount of sample % has a particle size less than or equal to the given; the histogram in the coordinates  $q3(x) = f(\mu\text{m})$  (right scale)—the amount of sample with a given particle size

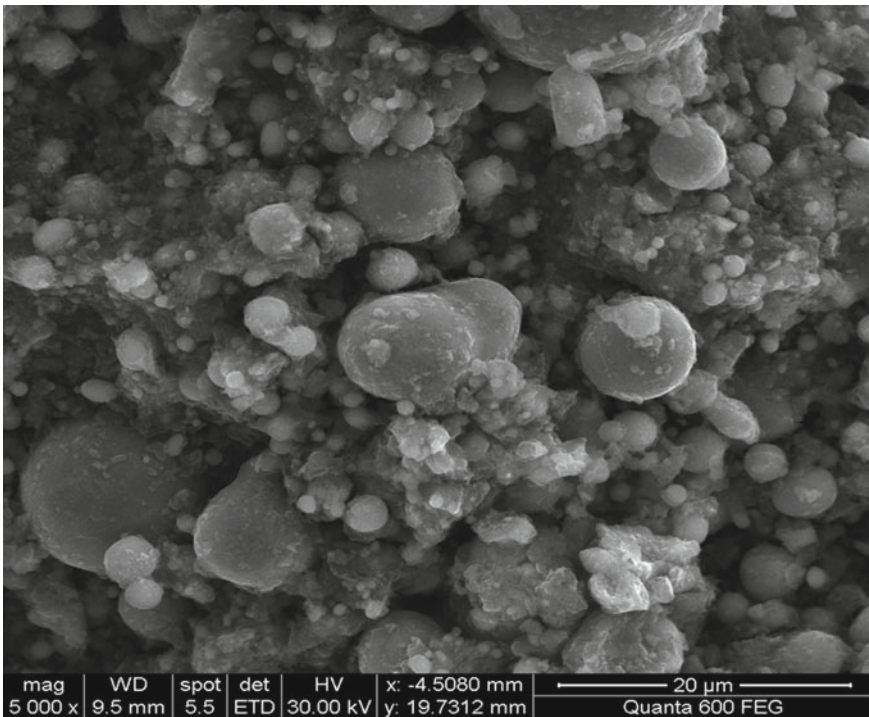


**Fig. 5** Results of the study of the experimental powder material morphology

## 4 Conclusion

Based on the experimental study on the production and inspection of tungsten-free hard-alloy powder by means of electro erosive dispersion in distilled water, it was found that the properties of the starting material and the technique of its processing affect the final properties of the product.

The presented results allow us to conclude that the production of new tungsten-free hard-alloy powder materials by means of electro erosive dispersion of wastes of similar alloys in an oxygen-containing liquid medium leads to the formation of the particles of regular spherical and elliptical shape with an average size of 41.63  $\mu\text{m}$ .

The particles of the obtained shape and size are the most suitable for the production of new tungsten-free hard-alloy products, since they can provide the highest compatibility of the material and the lowest porosity, which, in turn, will favorably affect the properties of the final product.

## References




1. Ageeva EV, Ageev EV, Horyakova NM, Sabelnikov BN (2021) Tungsten-free hard alloys based on electroerosive powders of titanium carbonitride. Closed Joint Stock Company, University Book. ISBN 978-5-907441-07-1. EDN BQVXJL
2. Ageeva EV, Sabelnikov BN (2021) Structure and properties of a tungsten-free hard alloy based on titanium carbonitride sintered from electroerosive powders obtained in a carbon-containing medium. *Hardening Technol Coat* 4(196):158161. EDN EKGUJX
3. Serebrovsky V, Sabel'nikov B (2020) X-ray diffraction analysis of electroerosive powder materials, obtained from waste of tungsten-free hard alloy grade KNT16. In: MATEC web of conferences, vol 315. p 01002. <https://doi.org/10.1051/mateconf/202031501002>
4. Ageev EV, Selyutin VL, Pikalov SV (2020) X-ray microanalysis of electro-erosive powder materials, obtained from tungsten-nickel-iron (TNI) alloy wastes in water. In: MATEC web of conferences, vol 315. p 01004. <https://doi.org/10.1051/mateconf/202031501004>
5. Latypov RA, Ageeva EV, Latypova GR (2019) X-ray microanalysis of powders, obtained by electroerosion dispersion of the alloy W-Ni-Fe. In: MATEC web of conferences, vol 298. p 00125. <https://doi.org/10.1051/mateconf/201929800125>
6. Sabel'nikov BN, Ageeva AE, Podanov VO, Korolev MS (2020) Investigation of the microstructure and X-ray spectral microanalysis of powder material obtained from waste of the KNT16 brand tungsten-free hard alloy. In: MATEC web of conferences, vol 329. p 02011. <https://doi.org/10.1051/mateconf/202032902011>
7. Ageev EV, Khardikov SV, Vorobyev EA, Sysoev AA (2019) Shape and morphology of the particles surface of electroerosive powders of micro- and nanometric fractions, obtained from H17MYuA steel in kerosene. In: MATEC web of conferences, vol 298. p 00127. <https://doi.org/10.1051/mateconf/201929800127>
8. Ageev EV (2012) Patent 2449859, Russian Federation, C2, B22F9/14. Installation for producing nanodispersed powders from conductive materials, applicant and patent holder Southwestern State University. No. 2010104316/02; application 2010/08/02, publ. 2012/10/05
9. Pereverzev A, Ageev E (2019) X-ray diffraction analysis of products sintered from isostatically pressed leaded bronze powders. In: MATEC web of conferences, vol 298. p 00037. <https://doi.org/10.1051/mateconf/201929800037>



10. Loktionova OG, Ageeva EV, Sabelnikov BN (2020) Results of X-ray studies of sintered samples obtained from the electroerosive powder material of the KNT16 alloy. Proc Southwest State University Ser: Eng Technol 10(4):22–34
11. Ageev EV, Ageeva EV, Sabelnikov BN (2021) Patent 2756465 C1, Russian Federation, IPC B22F 3/16, C22C 29/04, B22F 9/14. Method for producing tungsten-free hard alloy KNT from powder materials obtained in distilled water, applicant and patent holder Southwestern State University. No. 2020138425: application 2020/11/24, publ 2021/09/30

# Results of X-Ray Studies of Electro Erosive Tungsten-Free Hard-Alloy Powder Material



Boris Sabelnikov , Anton Alfimov , and Ekaterina Ageeva 

**Abstract** The purpose of the work was to study the phase and elemental compositions of new tungsten-free hard-alloy powder materials produced by electro erosive dispersion in an oxygen-containing medium. To produce new tungsten-free hard-alloy powder materials, an experimental laboratory setup for electro erosive dispersion was used. X-ray spectral microanalysis (elemental composition study) was carried out by means of a QUANTA 600 FEG scanning electron microscope with a built-in EDAX analyzer. X-ray diffraction analysis (the study of the phase composition) was carried out using a Rigaku Ultima IV X-ray diffractometer. The results of X-ray diffraction analysis and X-ray spectral microanalysis of the new electro erosive tungsten-free hard-alloy powder materials obtained in an oxygen-containing medium showed that the main elements are Ti, Ni, C, O, Mo, and the main phases are TiC, MoNi<sub>3</sub>, Ni<sub>2</sub>O<sub>3</sub>, Ni, and Mo.

**Keywords** Tungsten-free hard alloy · Electro erosive dispersion · X-ray diffraction analysis · X-ray spectral microanalysis · Powder material · Oxygen-containing liquid · Distilled water

## 1 Introduction

Currently, sintered hard alloys are widely used in various industries, especially in the production of construction machines and equipment [1–3]. However, there is an acute problem of saving expensive tungsten and titanium. An attempt to save tungsten and titanium led to the development of tungsten-free hard alloys of the titanium carbonitride (TCN) type, but still requiring the use of rather expensive titanium, so this study is a partial solution to the problem [4–6].

Recycling of hard-alloy waste is one of the most radical possible techniques for solving the problem. The currently existing techniques of processing hard alloy waste are large-tonnage, energy-intensive and environmentally harmful. Electro erosive

---

B. Sabelnikov (✉) · A. Alfimov · E. Ageeva  
Southwest State University, 94, 50 Let Oktyabrya Ul., Kursk 305040, Russia

© The Author(s), under exclusive license to Springer Nature Switzerland AG 2024  
N. Vatin et al. (eds.), *Modern Problems in Construction*,  
Lecture Notes in Civil Engineering 372,  
[https://doi.org/10.1007/978-3-031-36723-6\\_13](https://doi.org/10.1007/978-3-031-36723-6_13)

dispersion is one of the promising techniques for grinding any electrically conductive material, including tungsten-free hard alloys but it is not industrially used [7–10].

To date, in modern scientific and technical literature, there are no complete comprehensive information about the composition, structure and properties of the particles of tungsten-free hard alloys dispersed by electro erosion and alloys based on obtained on their basis. For these purposes, it is necessary to conduct complex theoretical and experimental studies.

The purpose of this work was to study the phase and elemental compositions of new tungsten-free hard-alloy powder materials obtained by electro erosive dispersion in an oxygen-containing medium.

## 2 Materials and Methods

A new experimental tungsten-free hard-alloy powder material was produced by electro erosive dispersion using the setup according the diagram given in Fig. 1.

The process for producing powders from tungsten-free hard alloys (TFHA) waste includes the following main operations:

1. Collection and sorting of tungsten-free hard alloys waste according to grades (chemical composition).
2. Impurities, swarf or shavings removal from waste.

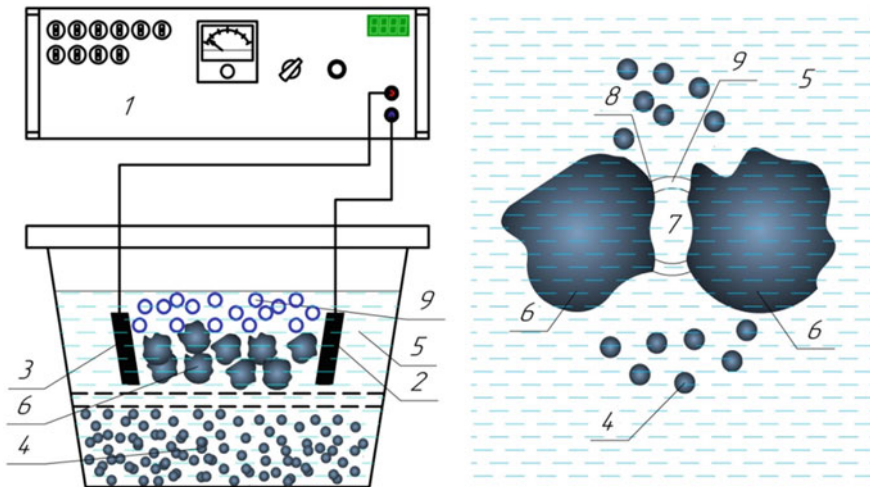


**Fig. 1** The diagram of the electro erosive dispersion process: 1—pulse generator; 2, 3—electrodes; 4—drops of molten material; 5—working fluid (distilled water); 6—waste of tungsten-free hard alloy; 7—discharge channel; 8—discharge point; 9—gas bubble

3. Loading of tungsten-free hard alloys waste into the reactor and electrodes connecting.
4. Filling the working fluid (WF) (distilled water) into the reactor.
5. Selection of dispersion parameters (voltage, capacitor capacitance and pulse repetition rate).
6. Electro erosive dispersion.
7. Working fluid settling and draining.
8. Separation of the nanoscale fraction by centrifuging.
9. Chemical treatment of the powder (if necessary).
10. Calcination of the powder in the oven at a temperature of 150–200 °C for 20–30 min.
11. Quality inspection.

The process of electro erosive dispersion proceeds in the following way: the impulse voltage of the pulse generator 1 is applied to the electrodes 2 and 3 and then to the hard alloy plates 6 (hard alloy plates are also used as electrodes); when the voltage reaches a certain value, an electrical breakdown of the working fluid 5 in the interelectrode space occurs with the formation of a discharge channel 7 [10].

Due to the high concentration of thermal energy, the material melts and evaporates at the discharge point 8; the WF evaporates and surrounds the discharge channel with gaseous decomposition products 9 (gas bubble). As a result of significant dynamic forces developing in the discharge channel and in the gas bubble, drops of the molten material 4 eject outside the discharge zone into the WF surrounding the electrodes and solidify in it forming spherical or elliptical hard-alloy powder particles [10].

X-ray spectral microanalysis (elemental composition study) was carried out by means of a QUANTA 600 FEG scanning electron microscope with a built-in EDAX analyzer, shown in Fig. 2.

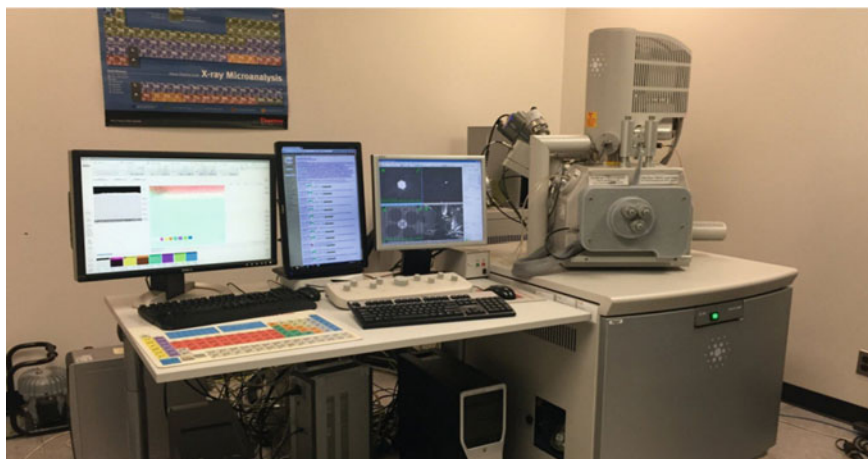


**Fig. 2** A scanning Quanta 600 FEG electron microscope with built-in EDAX analyzer

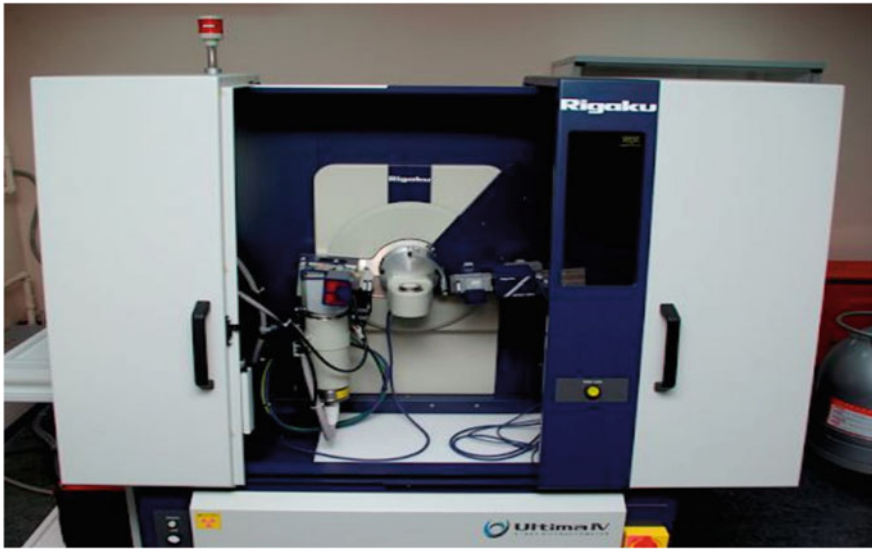


**Fig. 3** Rigaku Ultima IV diffractometer

X-ray diffraction analysis (phase composition study) was carried out using a Rigaku Ultima IV X-ray diffractometer, shown in Fig. 3.

### **3 Results and Discussion**

Figure 4 shows the results of the X-ray spectral microanalysis of the experimental tungsten-free hard-alloy powder material obtained by electro erosive dispersion of the waste of the TCN16 grade (titanium carbonitride) alloy.

X-ray spectral microanalysis showed that some oxygen was found on the surface of particles obtained in distilled water. It was also revealed that Ti, Ni, C, and Mo are the main elements in the TCN16 alloy particles dispersed by electro erosion in distilled water.

Figure 5 shows the results of studying the phase composition of the sample. It was found that the dispersion of TCN16 alloy by electro erosion in distilled water leads to the formation of TiC, MoNi<sub>3</sub>, Ni<sub>2</sub>O<sub>3</sub>, Ni, and Mo phases.

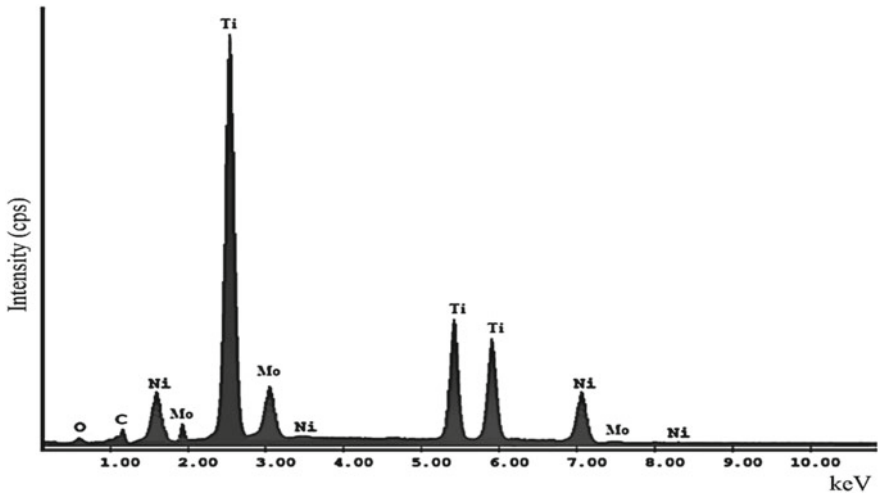


Fig. 4 Results of the X-ray spectral microanalysis of the experimental tungsten-free hard-alloy powder material

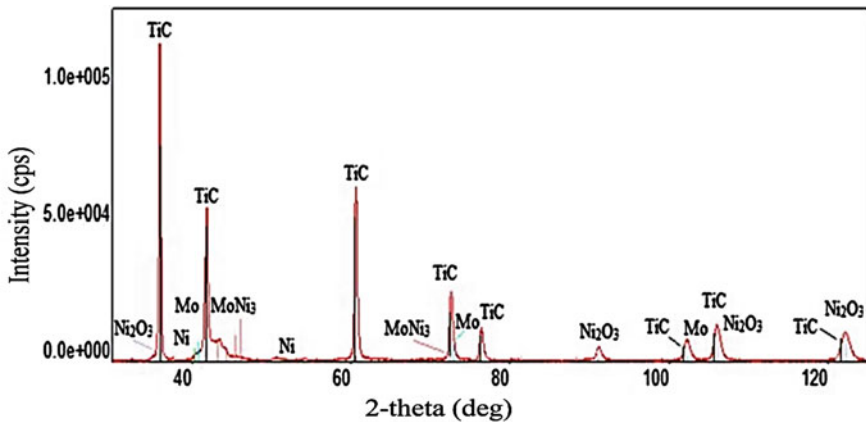


Fig. 5 The diffraction pattern of the sample

## 4 Conclusion

Based on the experimental studies of the production of tungsten-free hard-alloy powder by electro erosive dispersion in distilled water, it was found that the properties of the starting material (TCN16) affect the final properties of the product.

The presented results allow us to conclude that the production of new tungsten-free hard-alloy powder materials by electro erosive dispersion of similar alloys waste in an oxygen-containing medium leads to the formation of a product whose chemical

composition and structure differ from those of the starting material, which results in changes in the final product properties.

The properties of a tungsten-free hard-alloy electro erosive powder also largely depend on the properties of the working fluid (distilled water). The processes occurring during electro erosive dispersion proceed in the interelectrode space filled with the working fluid, which, being in the working area, make a physical, chemical, washing, and mechanical impact on the process, the electrodes, the pieces of the dispersed material and the erosion products. This influence affects all the stages of the EED process.

## References

1. Ageeva EV, Ageev EV, Horyakova NM, Sabelnikov BN (2021) Tungsten-free hard alloys based on electroerosive powders of titanium carbonitride. Closed Joint Stock Company “University Book”. ISBN 978-5-907441-07-1. EDN BQVXJL
2. Ageeva EV, Sabelnikov BN (2021) Structure and properties of a tungsten-free hard alloy based on titanium carbonitride sintered from electroerosive powders obtained in a carbon-containing medium. *Hardening Technol Coat* 4(196):158–161. EDN EKGUJX
3. Serebrovsky V, Sabel'nikov B (2020) X-ray diffraction analysis of electroerosive powder materials, obtained from waste of tungsten-free hard alloy grade KNT16. In: MATEC web of conferences, vol 315. p 01002. <https://doi.org/10.1051/mateconf/202031501002>
4. Ageev EV, Selyutin VL, Pikalov SV (2020) X-ray microanalysis of electro-erosive powder materials, obtained from tungsten-nickel-iron (TNI) alloy wastes in water. In: MATEC web of conferences, vol 315. p 01004. <https://doi.org/10.1051/mateconf/202031501004>
5. Latypov RA, Ageeva EV, Latypova GR (2019) X-ray microanalysis of powders, obtained by electroerosion dispersion of the alloy W-Ni-Fe. In: MATEC web of conferences, vol 298. p 00125. <https://doi.org/10.1051/mateconf/201929800125>
6. Sabel'nikov BN, Ageeva AE, Podanov VO, Korolev MS (2020) Investigation of the microstructure and X-ray spectral microanalysis of powder material obtained from waste of the KNT16 brand tungsten-free hard alloy. In: MATEC web of conferences, vol 329. p 02011. <https://doi.org/10.1051/mateconf/202032902011>
7. Ageev EV, Khardikov SV, Vorobyev EA, Sysoev AA (2019) Shape and morphology of the particles surface of electroerosive powders of micro- and nanometric fractions, obtained from H17MYuA steel in kerosene. In: MATEC web of conferences, vol 298. p 00127. <https://doi.org/10.1051/mateconf/201929800127>
8. Ageev EV (2012) Patent 2449859, Russian Federation, C2, B22F9/14. Installation for producing nanodispersed powders from conductive materials, applicant and patent holder Southwestern State University. No 2010104316/02; application 2010/08/02, publ 2012/10/05
9. Pereverzev A, Ageev E (2019) X-ray diffraction analysis of products sintered from isostatically pressed leaded bronze powders. In: MATEC web of conferences, vol 298. p 00037. <https://doi.org/10.1051/mateconf/201929800037>
10. Ageev EV, Ageeva EV, Sabelnikov BN (2020) Patent 2756465 C1, Russian Federation, IPC B22F 3/16, C22C 29/04, B22F 9/14. Method for producing tungsten-free hard alloy KNT from powder materials obtained in distilled water, applicant and patent holder Southwestern State University. No. 2020138425: application 2020/11/24, publ. 2021/09/30

# Justification of Strengthening of Reinforced Concrete Structures of an Industrial Building with Composite Materials



Vladimir Rimshin  and Ekaterina Ketsko 

**Abstract** The effectiveness of using composite materials as external reinforcement systems on full-scale structures of reinforced concrete beams of industrial buildings, aimed at increasing their bearing capacity are substantiated in the article. It has been established that the strengthening of non-prestressed bending reinforced concrete structures with composite materials based on carbon fibers leads to an increase in their bearing capacity, and the recommended technology for their reinforcement with composite materials is given. The object of study in this work is the reinforced concrete structures of the beams covering the sludge pool of the cement industry with non-stressed reinforcement before and after reinforcement with composite materials. The subject of the study is the bearing capacity of reinforced concrete structures reinforced with composite materials of the sludge pool cover beams. The purpose of the study is analyzing and evaluating the technical condition of the supporting structures in the sludge pool, determining the bearing capacity of reinforced concrete structures reinforced with composite materials, calculating and justifying the external reinforcement of carbon fiber reinforced concrete crossbars of the sludge pool cover.

**Keywords** Reinforcement with composite materials · Strength calculation of normal sections · Longitudinal external reinforcement · Industrial buildings and structures · Sludge pool

---

V. Rimshin (✉)

Moscow State University of Civil Engineering, Yaroslavskoe Shosse, 129337 Moscow, Russia  
e-mail: [v.rimshin@niisf.ru](mailto:v.rimshin@niisf.ru)

E. Ketsko

Research Institute for Building Physics of Russian Academy of the Architecture and Construction Sciences, Lokomotivny, 129238 Moscow, Russia  
e-mail: [kkuzzina@mail.ru](mailto:kkuzzina@mail.ru)



## 1 Introduction

Technological complex of the cement industry enterprise is a complex of structures and buildings on the enterprise territory, which ensures the operation of its economy, as well as warehousing, processing and shipment to consumers. The main stages of portland cement production are raw materials extraction, raw mixture preparation (crushing, grinding, homogenization), raw mixture roasting, calcined product (clinker) grinding with additives to obtain a fine powder (cement) [1–4].

There is a need to strengthen the structures due to the appearance of defects and damage over time or the need to increase the bearing capacity when the calculated permanent and temporary loads change in the process of industry buildings and structures operation in order to ensure their mechanical safety. At the same time, the main material of the supporting structures of such buildings and structures is monolithic or prefabricated reinforced concrete. It is necessary to replace or strengthen bending or compressible load-bearing reinforced concrete elements when performing major repairs or reconstruction of buildings and structures, to increase the bearing capacity. Currently, one of the effective ways to restore and increase the bearing capacity of both compressible and bendable reinforced concrete elements is their reinforcement with polymer composite materials. The use of composite materials in reinforcing reinforced concrete structures of industrial buildings and structures, in comparison with other existing reinforcement technologies, has a number of significant advantages, the main of which are the reduction of labor costs for reinforcement and the relatively low total cost of the materials used [5–8].

In the practice of buildings and structures reconstruction in cement industry enterprises, bending, compressible reinforced concrete elements that are in a complex stress state, for example: floor slabs, load-bearing structures of industrial buildings (intermediate supports, columns, crossbars, and so on) are reinforced with composite materials. Also, woven fabrics of various weaves and laminates are used for reinforcement.

Reinforced concrete buildings and structures are a significant part of the real estate infrastructure of cement industry enterprises. In this regard, the issues of operation and repair of these structures should be given considerable attention. During the operation of such buildings and structures, in order to ensure their mechanical safety, there is often a need to restore or increase the bearing capacity of individual structures due to the appearance of defects and damage over time, or an increase in the calculated permanent and temporary loads during their reconstruction [9, 10].

## 2 Materials and Methods

The object of study in this work is the reinforced concrete structures of the beams covering the sludge pool of the cement industry with non-stressed reinforcement before and after reinforcement with composite materials. The subject of the study

is the bearing capacity of reinforced concrete structures reinforced with composite materials of the sludge pool cover beams. The purpose of the study is analyzing and evaluating the technical condition of the supporting structures in the sludge pool, determining the bearing capacity of reinforced concrete structures reinforced with composite materials, calculating and justifying the external.

**Analysis and assessment of the structures technical condition.** The assessment was made of the cumulative impact of the identified defects and damage in order to determine the technical condition of the building structures of the horizontal sludge pool building located in the industrial area. It was concluded that the building structures of the horizontal sludge pool building are in a limited working condition, except for the roof structures (the roof slabs and secondary roof beams are in an unacceptable state) based on the results of the analysis of defects and damages that affect the bearing capacity and technical condition of the building to varying degrees. It is necessary to carry out repair and preventive measures and restoration work, due to the peculiarities of the technological process in the building, characterized by a large release of water vapor, it is recommended to impregnate the internal surfaces of the wall fencing with polymer-composite compounds, to strengthen reinforced concrete structures covering the structure with composite materials to maintain and bring the building structures into working condition. It is necessary to carry out safety measures to prevent the development of damage before performing work to strengthen the coating structures, exclude the impact of additional loads on the roof, including snow, loads from the storage of materials, restrict people's access to the premises until the damage is repaired [11–15].

### 3 Results and Discussion

**Calculation with justification of longitudinal external reinforcement.** The section area is:

$$3 \cdot 7.5 = 22.5 \text{ m}^2.$$

Loads:

Small-sized floor slabs: 190 kg weight of 1 piece  $\gamma_f = 1.1$ . Total: 3.135 t (15 pieces).

Roofing pie:

Vapor barrier is  $0.002 \text{ t/m}^2$   $\gamma_f = 1.2$

$$22.50 \cdot 0.002 \cdot 1.2 = 0.054 \cdot t$$

Thermal insulation is  $0.016 \text{ t/m}^2$   $\gamma_f = 1.2$

**Table 1** Reinforcement characteristics

Reinforcement	Class	Working conditions coefficient
Longitudinal	A500	1
Transverse	A240	1

$$22.5 \cdot 0.016 \cdot 1.2 = 0.432 \cdot t$$

Cement-sand screed 30 mm thick is  $0.054 \text{ t/m}^2$   $\gamma_f = 1.3$

$$22.5 \cdot 0.054 \cdot 1.3 = 1.58 \cdot t$$

Ruberoid is  $0.003 \text{ t/m}^2$   $\gamma_f = 1.2$

$$22.5 \cdot 0.003 \cdot 1.2 = 0.081 \cdot t$$

Total: 2.147 t.

The roof scheme is taken straight. Snow:  $0.168 \text{ t/m}^2$   $\gamma_f = 1.4$

$$22.5 \cdot 0.168 \cdot 1.4 = 5.29 \cdot t$$

Reinforcement is taken based on the calculation in the SCAD PC. Liability factor  $\gamma_n = 1$ . Element type is bending. Stress state is uniaxial bending. Maximum reinforcement percentage is 10. Distance to the gravity center of the reinforcement  $a_1 = 25 \text{ mm}$  and  $a_2 = 25 \text{ mm}$ . Reinforcement characteristics are presented in Table 1.

The type of concrete is heavy. Concrete class is B15. The coefficients of working conditions are presented in Table 2.

Humidity of environment air is more than 75%. Crack width is limited. The requirements for the width of the crack opening are selected from the condition of the reinforcement safety. Permissible crack opening width: short opening is 0.4 mm, continuous opening is 0.3 mm.

Structural element 1. Element No. 2. The element length is 0.85 m (support area). Reinforcement characteristics are presented in Table 3.


The calculation results are shown in Table 4.

Structural element 1. Element No. 7. The element length is 5.8 m (the center of the span). The characteristics of the given reinforcement are presented in Table 5.

**Table 2** Coefficients of concrete working conditions

Coefficient	Name	Value
$\gamma_{b1}$	Accounting long-term loads	0.9
$\gamma_{b2}$	Accounting the nature of destruction	1
$\gamma_{b3}$	Accounting the vertical position during concreting	1
$\gamma_{b5}$	Accounting freezing/thawing and negative temperatures	1


**Table 3** Given reinforcement

Plot	Reinforcement	Cross section
1	Transverse reinforcement along the Z-axis is 9Ø6, transverse reinforcement pitch is 100 mm. Transverse reinforcement along the Y-axis is 9Ø6, transverse reinforcement step is 100 mm	

**Table 4** Calculation results

Plot	Utilization factor	Verification	Checked according to SNiP
1	0.75	Strength at the ultimate moment of the section	pp. 8.1.8–8.1.14
	0.38	Deformations in compressed concrete	pp. 8.1.20–8.1.30
	0.07	Deformations in tension reinforcement	pp. 8.1.20–8.1.30
	0.52	Strength on a concrete strip between inclined sections	pp. 8.1.32, 8.1.34
	0.45	Inclined strength	pp. 8.1.33, 8.1.34

**Table 5** Given reinforcement

Plot	Reinforcement	Cross section
1	S <sub>1</sub> —3Ø16. S <sub>2</sub> —3Ø16 Transverse reinforcement along the Z axis is 9Ø10, transverse reinforcement pitch is 100 mm. Transverse reinforcement along the Y-axis is 9Ø10, transverse reinforcement step is 100 mm	

The calculation results are presented in Table 6.

**External reinforcement calculation «Composite».** The diagrams of moments and transverse forces are shown in Figs. 1 and 2, respectively.

Characteristics of FibArm Tape 230/15P. Tensile modulus is 245 GPa. Tensile strength is 4000 MPa (40,770 kg/cm<sup>2</sup>). The calculated thickness of the tape is 0.128 mm, the monolayer area is 0.192 cm<sup>2</sup>.

**Calculation of the normal sections strength.** The design value of tensile strength is determined according to Eq. 1.

$$R_f = \frac{\gamma_{f1} \cdot \gamma_{f2} \cdot R_{fn}}{\gamma_f} \quad (1)$$

**Table 6** Calculation results

Plot	Utilization factor	Verification	Checked according to SNiP
1	0.82	Strength at the ultimate moment of the section	pp. 8.1.8–8.1.14
	0.3	Deformations in compressed concrete	pp. 8.1.20–8.1.30
	0.07	Deformations in tension reinforcement	pp. 8.1.20–8.1.30
	0.06	Strength on a concrete strip between inclined sections	pp. 8.1.32, 8.1.34
	0.03	Inclined strength	pp. 8.1.33, 8.1.34

**Fig. 1** Diagram of moments**Fig. 2** Diagram of transverse forces

$$R_f = (0.9 \cdot 0.9 \cdot 4000) / 1.2 = 2700 \text{ MPa}$$

It should taking into account the existing steel reinforcement when calculating a reinforced structure, the condition according to Eq. 2 should be met:

$$R_f \leq (\varepsilon_{s2} - \varepsilon_s^0) \cdot E_f \quad (2)$$

$R_f = 2700 \leq 1225$  the condition is not met, it is accepted  $R_f = 1225 \text{ MPa}$ .

$$\varepsilon_s^0 = (12.09 / (0.209 \cdot 71,530)) \cdot 27 \text{ cm} = 0.02.$$

The strength calculation of bending elements sections reinforced with external reinforcement made of composite materials should be carried out from the condition:

$$M \leq M_{ult} \quad (3)$$

$$M_{ult} = R_b \cdot b \cdot x \cdot (h_0 - 0.5 \cdot x) + R_{sc} \cdot A_{s'} \cdot (h_0 - a') + R_f \cdot A_f \cdot a \quad (4)$$

$$x = \frac{R_s \cdot A_s - R_{sc} \cdot A_{s'} + R_f \cdot A_f}{R_b \cdot b} \quad (5)$$

$$M = 12.09 \cdot t \cdot m \leq M_{ult} = 13.11 \cdot t \cdot m$$

The lower reinforcement area is reduced by 20%. The condition is met; 1 layer of tape is accepted along the bottom edge of the beam.

**Bending elements calculation according to the strength of a concrete strip between inclined cracks.** The calculation should be carried out according to SP 63.13330 without taking into account the work of external reinforcement made of composite materials. The transverse reinforcement area is reduced by 20% and carried out the calculation in SCAD. The characteristics of the given reinforcement are shown in Table 7. The calculation results are presented in Table 8.

The calculation of bending elements along inclined sections for transverse forces action is performed according to Eq. 6.

$$Q \leq Q_b + Q_{sw} + Q_{fw} \quad (6)$$


$Q_b$ —transverse force perceived by concrete in an inclined section, determined according to SP 63.13330;

$Q_{sw}$ —transverse force perceived by steel transverse reinforcement installed in an inclined section with a step  $S_w$ , determined according to SP 63.13330;

$Q_{fw}$ —the shear force taken up by the transverse composite reinforcement in a sloped section, determined according to Eq. 7.

$$Q_{fw} = w_f \cdot \frac{A_{fw} \cdot R_{fw} \cdot \sin\alpha \cdot C_{fw}}{S_f} \quad (7)$$

**Table 7** Given reinforcement

Plot	Reinforcement	Cross section
1	S <sub>1</sub> —3∅16. S <sub>2</sub> —3∅16 Transverse reinforcement along the Z-axis is 7∅6, transverse reinforcement pitch is 120 mm. Transverse reinforcement along the Y-axis is 7∅6, transverse reinforcement step is 120 mm	

**Table 8** Calculation results

Plot	Utilization factor	Verification	Checked according to SNiP
1	0.75	Strength at the ultimate moment of the section	pp. 8.1.8–8.1.14
	0.38	Deformations in compressed concrete	pp. 8.1.20–8.1.30
	0.07	Deformations in tension reinforcement	pp. 8.1.20–8.1.30
	0.52	Strength on a concrete strip between inclined sections	pp. 8.1.32, 8.1.34
	0.58	Inclined strength	pp. 8.1.33, 8.1.34

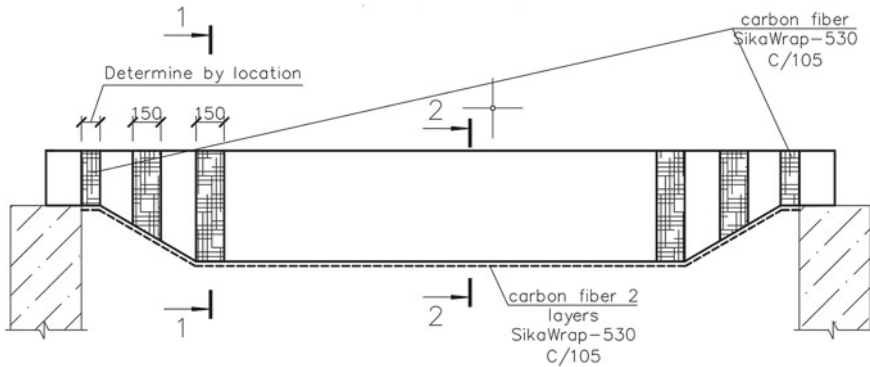


**Fig. 3** Crossbar reinforcement scheme

$$Q_b = 8721 \text{ kg. } Q_{sw} = 18635 \text{ kg. } Q_{fw} = 3897 \text{ kg.}$$

$$Q = 6450 \text{ kg} \leq 8721 + 18635 + 3897 = 31253 \text{ kg}$$

External transverse reinforcement is not required according to the calculation; 3 external clamps on three sides of a 7.5 cm wide at the beam support, at a distance of  $L/8$  and  $L/4$  to a height, without bringing 2 cm to the upper edge of the beam are structurally accepted. The crossbar reinforcement scheme is shown in Fig. 3.

The recommended amplification technology is as follows. It is recommended to dry the surface, remove oils, dust, grease, coating residues before applying the primer Sikadur-330 or equivalent. The surface to be glued is recommended to be leveled to a deviation of 2 mm per 0.3 m of length. Irregularities protruding more than 0.5 mm are recommended to be removed by sandblasting or grinding. The corners on which the fabric is applied must be rounded, with a minimum rounding radius of 20 mm. The preparation of concrete and masonry substrates must be carried out mechanically using sandblasting or grinding equipment to remove laitance, loose particles and obtain an open profile surface. Carbon fiber should be cut with special scissors or a sharp knife, and wrinkling and creases should not be allowed on the surface of the fabric. The minimum overlap must be 150 mm in the direction of the fibers. It is not necessary to overlap when joining the fabric in width. It is recommended to lay the impregnated fabric on a damp, primed surface in the desired direction and smooth by hand to remove wrinkles and folds. It is recommended to roll with a Sika plastic roller after laying and leveling. Rolling should be carried out along the fibers of the fabric until the glue is evenly distributed over the fabric and the entrained air is removed, without applying excessive force when rolling to avoid wrinkling of the fabric [16–18].

It is recommended to apply Sikadur-300 or equivalent on the previous layer using the wet-on-wet method within two hours (at + 23 °C) after laying the previous layer and repeat the rolling procedure when laying additional layers of SikaWrap fabric.

If it is not possible to apply a layer within 2 h, it is recommended to wait at least 12 h before applying the next layer. Works are recommended to be carried out at air and adhesive surface temperatures not lower than +15 °C and not higher than +40 °C. Structural strengthening operations are structural and should be performed by experienced specialists [19, 20].

## 4 Conclusion

The effectiveness of using composite materials as external reinforcement systems on full-scale structures of reinforced concrete beams of industrial buildings, aimed at increasing their bearing capacity are substantiated in the article. It has been established that the strengthening of non-prestressed bending reinforced concrete structures with composite materials based on carbon fibers leads to an increase in their bearing capacity, and the recommended technology for their reinforcement with composite materials is given.

## References

1. Donchenko OM, Suleymanova LA, Rimshin VI, Ryabchevskiy IS (2021) Tensile Deformations of “Mild” Reinforcing Steels for Reinforced Concrete Structures Lecture Notes in Civil Engineering, 147:302–308
2. Krishan AL, Rimshin VI, Shubin IL, Astafeva MA, Stupak AA (2022) Compressed reinforced concrete elements bearing capacity of various flexibility lecture notes in civil. Engineering 182:283–291
3. Kuzina E, Rimshin V, Neverov A (2019) Reserves and exposure assessment of reinforced concrete structures safety while reducing its power resistance E3S Web of Conferences 135:03010
4. Kuzina ES, Rimshin VI (2020) Calculation method analysis for structure strengthening with external reinforcement. IOP Conf Series: Mater Sci Eng 753(2):022004
5. Lisyatnikov MS, Roshchina SI, VYu, Chukhlanov, Ivaniuk AM (2020) Repair compositions based on methyl methacrylate modified with polyphenylsiloxane resin for concrete and reinforced concrete structures. IOP Conf Series: Mater Sci Eng 896(1):012113
6. Lukin M, Martynov V, Rimshin V, Aleksievets I (2022) Reinforced concrete vertical structures under a gently sloping shell of double curvature under the influence of progressive collapse lecture notes in civil. Engineering 182:577–587
7. Martinov V, Lukin M, Rimshin V, Rusak K, Ivaniuk A (2022) Influence of Different Types of Aggregates on the Structural Properties of Fiber-Reinforced Concrete Lecture Notes in Networks and Systems, 403 LNNS, pp. 1467–1476
8. Merkulov S, Rimshin V, Akimov E, Kurbatov V, Roschina S (2020) Regulatory support for the use of composite rod reinforcement in concrete structures. IOP Conf Series: Mater Sci Eng 896(1):012022
9. Mishchenko E, Monastirev P, Evdokimtsev O (2018) Quality improvement of specialists training for energy-efficient construction. IOP Conf Series: Mater Sci Eng 463(3):032046
10. Mishchenko ES, Monastirev PV, Evdokimtsev OV (2020) Improving the Quality of Training in Building Information Modeling Advances in Intelligent Systems and Computing 916:453–459



11. Neverov AN, Truntov PS, Ketsko ES, Rimshin VI (2022) Calculating the Strengthening of Construction Structures Before the Reconstruction of the Building Lecture Notes in Civil Engineering, 182:173–179
12. Rimshin V, Kuzina E, Neverov A (2019) Residual resource of force resistance to deformation E3S Web of Conferences, 135:01069
13. Rimshin VI, Kalaydo AV, Semenova MN, Bykov GS (2020) Regularities research of radon transfer to underground enclosing buildings structures. IOP Conference Series: Materials Science and Engineering 953(1):012088
14. Rimshin VI, Roshchina SI, Ketsko ES, Truntov PS, Kuzina IS (2022) Engineering Calculations of Acidifier Retaining Walls During Water Treatment Facilities Designing Lecture Notes in Civil Engineering, 182:55–73
15. Rimshin VI, Telichenko VI, Krishan AL, Truntov PS, Bykov GS (2021) Assessment of the impact of high temperature on the strength of reinforced concrete structures during operation. Key Eng Mater 887 KEM: 460–465
16. Roshchina SI, Lukin MV, Lukina AV, Sergeyev MS, Lisyatnikov MS (2015) Experimental research on pressed-bending reinforced timberwork. Int J Appl Eng Res 10(24):45307–45312
17. Tho VD, Korol EA, Rimshin VI, Anh PT (2022) Model of stress-strain state of three-layered reinforced concrete structure by the finite element methods. Int J Comput Civ Struct Eng 18(2):62–73
18. Erofeev VT, Bogatov AD, Smirnov VF, Rimshin VI, Kurbatov VL (2015) Bioresistant building composites on the basis of glass wastes. Biosci Biotechn Res Asia 12(1)
19. Bazhenov YM, Erofeev VT, Rimshin VI, Markov SV, Kurbatov VL (2016) Changes in the topology of a concrete porous space in interactions with the external medium. Eng Solid Mech 4(4)
20. Shubin IL, Zaitsev YV, Rimshin VI, Kurbatov VL, Sulygova PS (2017) Fracture of high performance materials under multiaxial compression and thermal effect. Eng Solid Mech 5(2)

# Determination of the Volume of Air Entering Through Leaks into Aspiration Shelters



Alexander Goltsov , Vitaly Kireev , and Ivan Pankov 

**Abstract** In various industries, technological processes often occur, characterized by the release of dust into the working area. To maintain the required air parameters in terms of dust content in industrial premises, it is necessary to use a set of systems, including an aspiration system, a centralized vacuum dust removal system and general ventilation. The efficiency and performance of the above systems are interrelated, but the aspiration system is decisive. The aspiration shelter, which is the most important element of the aspiration system, localizes the source of dust emission. Seals are used to prevent the entry of dust from the aspiration shelter into the area of the working area, as well as to minimize the volume of air removed. In this work, analytical studies of methods for determining the suction and the amount of air entering the aspiration shelters through leaks were carried out, 3 characteristic approaches were proposed to determine the magnitude of the suction, based on the degree of tightness of the aspiration systems.

**Keywords** Dedusting systems · Suction systems · Suction shelters · Leaks in suction shelters · Leaks in process equipment · Air flow coming through leaks

## 1 Introduction

As you know, in many industries, dust emissions are generated to varying degrees. The resulting dust in production is the cause of urban air pollution and the occurrence of various occupational diseases of workers. In addition, in some cases it creates explosive situations, worsens the production and technological environment, leading to premature failure of technological equipment, causing significant social

---

A. Goltsov (✉) · V. Kireev  
Belgorod State Technological University Named After V.G. Shukhov, 46, Kostyukov St,  
Belgorod 308012, Russia  
e-mail: [abgolcov@gmail.com](mailto:abgolcov@gmail.com)

I. Pankov  
Southwest State University, 94, 50 Let Oktyabrya Ul., Kursk 305040, Russia

© The Author(s), under exclusive license to Springer Nature Switzerland AG 2024  
N. Vatin et al. (eds.), *Modern Problems in Construction*,  
Lecture Notes in Civil Engineering 372,  
[https://doi.org/10.1007/978-3-031-36723-6\\_15](https://doi.org/10.1007/978-3-031-36723-6_15)

and economic damage in general. To prevent this, various dust removal and air purification systems are used, however, for many processes, the available solutions are inefficient, energy-intensive, or non-existent [1, 2]. For industrial enterprises, the cost of electricity for the operation of a complex of dust removal systems can be up to 20% of the total costs, which undoubtedly affects the competitiveness of the enterprise, and also causes environmental damage. As we enter the phase of the fourth industrial revolution, when advanced manufacturing technologies dominate, this problem is a deterrent. As previous studies have shown, aspiration systems play a decisive role in the complex of dust removal systems.

It is possible to solve the problem of dust removal only when using a set of measures, which include the following systems: aspiration systems (local exhaust ventilation), general ventilation systems and vacuum dust collection systems, they are also secondary dust control systems (CPU).

The main element that determines both the efficiency of the aspiration system and its required performance is the aspiration shelter, which is designed to prevent dust from entering the working area. The required flow rate of air removed from the aspiration shelter, and hence the energy consumption of the systems as a whole, depends on the degree of tightness of the shelter. Thus, the study of technical issues related to the compaction of aspiration shelters and technological equipment in general is an extremely urgent task.

## 2 Materials and Methods

As is known, in shelters of a closed type, in order to ensure the conditions for not knocking out dust into the air of the working area, it is necessary to create a stable rarefaction  $P_y$ , reduce the cross-sectional area of leaks  $F_n$  to the maximum, or complicate the nature of existing leaks. The task of ensuring tightness in shelters is very important: it provides a direct impact on the volume of aspiration air, and, accordingly, on the energy intensity of industrial ventilation systems. At the same time, an increase in tightness can significantly reduce air volumes and the required vacuum; solutions are known that provide significant tightness of shelters, but they are associated with increased capital costs and ease of operation of process equipment. In general, the source of dust emission localized by the aspiration shelter is shown in Fig. 1.

A reasonably efficient solution for conveyor belt loading areas is offered by Sandvik Mining and Sandvik Construction. The technical solution offered by this company consists in the effective compaction of the place where the conveyor belt is loaded (Fig. 2).

It is known that the flow rate of air entering through the leak can be determined by the formula:

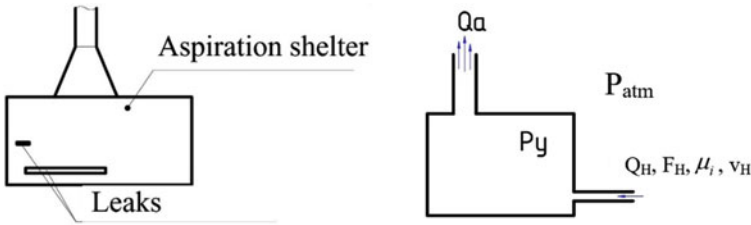


Fig. 1 Principal and design scheme of an aspiration shelter with leaks present in it

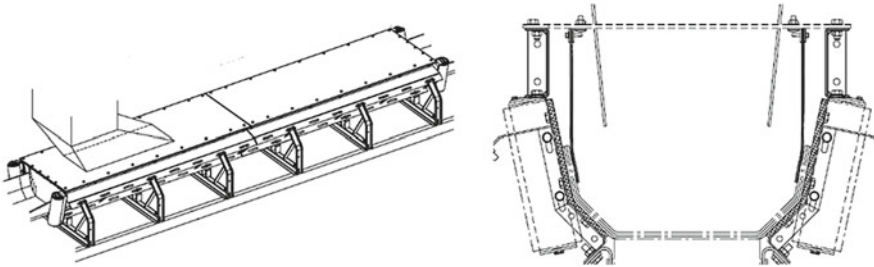


Fig. 2 Suction shelter for Sandvik conveyor belt loading

$$Q = \sum_{i=1}^N \mu_i \sqrt{\frac{2P_i}{\rho_i}} F_i \tag{1}$$

where  $\mu = \zeta^{-0.5}$ , flow coefficient of the  $i$ -th hole,  
 $P_i$ —rarefaction in the area of the  $i$ -th hole, Pa;  
 $\rho_i$ —air density,  $\text{kg/m}^3$ ;  
 $F_{Hi}$ —area of leaks of the  $i$ -th hole,  $\text{m}^2$ .

For the majority of aspiration shelters, leaks can be considered as equal in area with respect to hydraulic resistance and can be taken as holes in a thin wall, for which  $\zeta = 2.4$ . The equation for determining the flow rate of air entering through leaks will take the form [3]:

$$Q = \sqrt{\frac{2P_i}{\rho_i}} F_i \tag{2}$$

After analyzing the possible situations with aspiration shelters, a graph of the dependence of the volumes of air entering the shelter through leaks was obtained in the case of maintaining the required vacuum in the shelter (Fig. 3).

From this graph it can be seen that the lower the leakage and the higher the flow rate, the smaller the air volumes  $Q_{it}$ , and the vacuum affects to a lesser extent. Therefore, it is advisable to create a smaller vacuum in shelters with a large vacuum, i.e. choose more preferable shelters, for example, use shelters that work with the

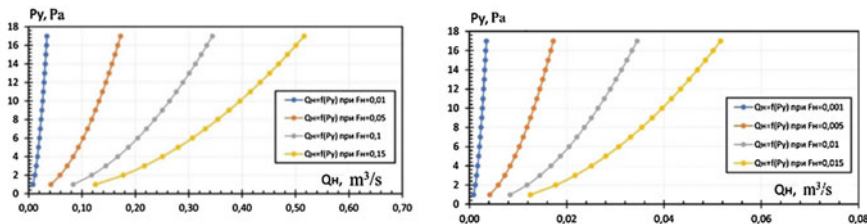


**Fig. 3** Dependence of the flow rate of air entering the shelter through leaks  $Q_n$ , on the rarefaction  $P_y$  (up to 18 Pa) and the area of existing leaks  $F_n$  with equal areas of the open section as holes in a thin wall

effect of double walls for loading the conveyor belt. Accordingly, when using shelters with a high degree of sealing, it is possible to create a higher vacuum or create the possibility of fluctuations in the vacuum in the shelter in a wider range when regulating technological processes.

Experience in the operation of aspiration systems shows the expediency in the design process to take leaks slightly higher than the actual ones, since over time, during the operation of the systems, the existing connections will lose their design tightness. In our opinion, a margin of 10–15% will avoid problems during further operation. If in the course of operation the leaks turn out to be higher, then it is imperative to restore the required tightness of the equipment and aspiration shelters.

For shelters with a low degree of relative tightness (the width of the gap along the perimeter of the shelter does not exceed 3 cm), the above calculation method has become famous and has shown its high efficiency. You can also use the basic formula to determine air flow through leaks using area and velocity parameters:

$$Q = v \cdot F, \tag{3}$$

This dependence is suitable for calculation with large areas of leaks, as well as cases when it is impossible to create a high vacuum in the shelter. This dependence can be used in determining the actual costs in the operation of shelters.

In cases of sealed construction of shelters, when the following types of connections are used (bolted, flanged, welded, nipple, rack, clamps, etc.), a different approach is required to calculate the air entering through leaks. Preliminary calculations in Figs. 3 and 4 show a significant reduction in air consumption with a small vacuum in the shelter, otherwise, with significant vacuums up to 50 Pa, the amount of suction increases significantly. Thus, it can be seen that a refinement of the calculation of the volume of air entering through leaks is required for the case of localization of technological equipment by hermetic shelters, in which a high vacuum is maintained.

To develop a methodology for calculating  $Q_n$  at high discharges in a shelter (more than 50 Pa), we turn to known developments, studies and reference materials [4].

A well-known classification is presented in [5], where four directions are distinguished according to the nature of analytical studies of hermetic joints:

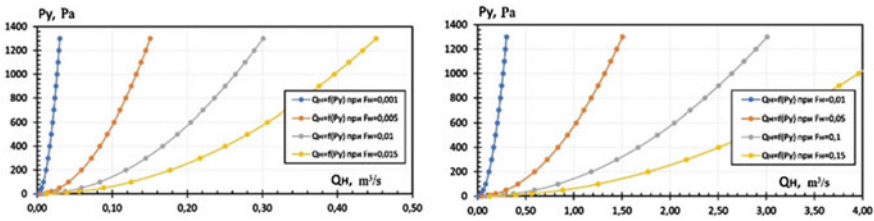


**Fig. 4** Dependence of the flow rate of air entering the shelter through leaks  $Q_n$ , on the rarefaction  $P_y$  (up to 1300 Pa) and the area of existing leaks  $F_n$  with equal areas of the open section as holes in a thin wall

- (1) representation of the contact zone of the sealing surfaces in the form of a narrow slot of constant or variable cross section [6–10];
- (2) representation of the contact zone in the form of a porous medium [11–15];
- (3) representation of the contact zone as a group of capillaries of a certain cross section [16–19];
- (4) representation of the contact zone in the form of a system of channels of a certain cross-sectional shape formed by microroughnesses; in this case, the dimensions of the channels are determined by the accepted statistical law of the distribution of microprotrusions in height [11, 20–24].

All proposed models assume the presence of empirical coefficients in them, which are determined in the course of experimental studies. In this regard, before using one or another mathematical expression for practical application, it is necessary to conduct an experimental study to determine the coefficients included in it (permeability coefficient, radius of curvature of microprotrusions, the nature of their distribution along the height or the reference curve, the hardness of the material of the mating surfaces, etc.).

For practical purposes, the amount of leakage is described by an equation like:

$$[q] = +B \cdot q \tag{4}$$

Coefficients A and B depend on various factors: the material of the sealing element, the state of its sealing surfaces, the type of medium being sealed, the lower sensitivity limit of the device that detects leakage [5]. The latter factor is essential both for assessing the accuracy of the obtained values and for practical applicability. In expression (4), the parameter A reflects the range of q values in the initial stage of formation of the actual contact area of the sealing surfaces, the coefficient B characterizes the intensity of the influence of the pressure of the medium being sealed on the specific load [q] required to exclude leakage with the method used to evaluate it, i.e.  $B = dq/dp$  [5].

Consider the tightness of the joints, based on the analytical model in the form of a narrow gap, it is important to take into account the air flow in small gaps, which has features in sealing.

It is known that the nature of gas motion in the gap is determined by the Knudsen number:

$$K_n = \frac{\lambda}{L} \quad (5)$$

where  $\lambda$ —is the mean free path of a gas molecule;

$L$ —is the characteristic gap size [5, 25, 26].

The Knudsen number for certain conditions of gas flow in the gap can be calculated from the expression [27]:

$$K_n = 10^5 \cdot \mu \cdot \frac{\left(\frac{2\pi RT}{M}\right)^{0.5}}{L(P_1 - P_2)} \quad (6)$$

where  $\mu$ —is the dynamic viscosity of the gas;

$R$ —is the gas constant;

$T$ —is the absolute temperature of the gas;

$M$ —is the molecular weight of the gas;

$P$ — is the gas pressure.

Normative conditions for testing equipment [15] for tightness depend on the operating conditions of the equipment (properties of the working medium, its operating pressure), type of equipment and environmental standards of operation. Thus, for the equipment of the chemical and petrochemical industries, in the currently existing regulatory documents, leak tests of equipment are recommended by measuring the pressure drop. This is the simplest and cheapest method for assessing tightness, which does not require special expensive equipment. However, the assessment of tightness by this method is quite approximate. The allowable leakage coefficient  $m$  is introduced, corresponding to the pressure drop per unit time when testing the object for tightness:

$$m = \frac{(PT_k - P_k T)}{PT_k \tau}$$

where  $R_n = P_{bn} + P_{mn}$ ;  $P_k = P_{bk} + P_{mk}$ —absolute pressures at the beginning and end of the test (Pa); indices “ $b$ ” and “ $m$ ”—barometric and pressure gauge readings;

$T$ —is the absolute temperature of the medium in the equipment under test.

If the temperature and barometric pressure remain constant during the test, then  $m = \Delta P/\tau P_n$ . If the tests are carried out at pressures lower than the operating pressure, then an amendment is introduced that takes into account the effect of pressure at  $P$  less than 0.2 MPa  $m = 0.04 \text{ h}^{-1}$ . Values of permissible leakage coefficients  $m$  for certain types of equipment:

mechanical dust collectors—pressure drop < 250 Pa/h for 1 h at  $P = 2.5 \text{ kPa}$ ;

electrostatic precipitator for soot—pressure drop < 50 Pa/h for 1 h at  $P = 2.5 \text{ kPa}$ .

The tightness test is carried out with air or nitrogen, and then, when estimating the amount of leakage, it is recalculated for the working gas according to the expression:

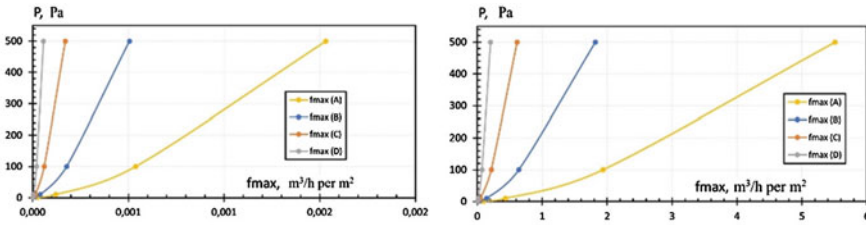


**Fig. 5** Leakage limit  $f_{max}$  ( $m^3/s$  and  $m^3/h$  per  $m^2$ ) in air ducts per sq.m at static pressure drop  $p$  for 4 tightness classes (A, B, C, D)

$$G = 1, 2 \cdot 10^{-4} \eta m V P \left( \frac{M_p}{T_p} \right),$$

where  $\eta$  is the safety factor that takes into account the deterioration of the tightness of the joints over the time of their operation,  $\eta = 1.5 \dots 2.0$ ;

$M_p$ —is the molar mass of the working gas;

$T_p$ —is its operating temperature;

$V$ —is the volume of the working cavity of the object.

Consider the issue of tightness of ventilation systems. In accordance with [28], “tightness (airtightness) of the air duct—the value of allowable leakage/suction of air through the material of the air duct, connection, device or equipment of the ventilation system.

In accordance with [28], there are 4 classes of air tightness of air ducts, which are characterized by the limiting value of air leakage  $f_{max}$  ( $m^3/h$  per  $m^2$ ) at the limiting static negative pressure  $P_s$ , and static pressure  $P$  (Fig. 5):

Class A,  $P_s = 500$  Pa,  $f_{max} = 0.097p^{0.65}$ ;

Class B,  $P_s = 750$  Pa,  $f_{max} = 0.032p^{0.65}$ ;

Class C,  $P_s = 750$  Pa,  $f_{max} = 0.0108p^{0.65}$ ;

Class D,  $P_s = 750$  Pa,  $f_{max} = 0.0036p^{0.65}$ .

As can be seen from the requirements for ventilation systems from [28], the criterion for choosing a tightness class is the allowable percentage of air leakage in the system under operating conditions (air infiltration into equipment operating at reduced pressure). At the same time, the standard regulates the amount of suction for ventilation equipment in accordance with class B.

When designing aspiration systems and, in particular, aspiration shelters, it is necessary to strive for a high degree of tightness, it is not always possible to achieve this and it is not always economically feasible, however, it is possible to design aspiration systems with a high degree of tightness. When calculating the tightness of flange connections in such systems, you can use the methods proposed in GOST 32,388 and GOST R 55,430–2013 for cases with a high degree of tightness, you can determine such a tightening torque for flange connections that will not leak at a given nominal pressure drop.



### 3 Results and Discussion

After reviewing the calculation of the amount of leakage and analytical studies, the following sequence of calculation of  $Q_{st}$  for aspiration shelters of process equipment is proposed for several cases:

Case A. “High degree of tightness of the equipment (discharge up to 50 Pa)”.

1. The required degree of tightness of aspiration shelters is determined, taking into account the requirements for energy saving, sanitary and hygienic, technological, explosion and fire protection and individual features of production.
2. The characteristic length of all connections of technological equipment is determined.
3. The amount of leakage through the connections used is calculated.
4. The actual value of leaks is compared with the required degree of tightness, if the actual values are equal or less than required, then this type of connection is accepted, otherwise a change in the density of connections and seals is required.

Case B. “Medium degree of tightness of equipment (discharge up to 50 Pa)”.

1. Depending on the type of aspiration shelter, we set the required vacuum in the shelter.
2. Determine the cross-sectional area of the existing leaks.
3. We calculate the volumes of air entering the shelter.

Case C. “Low degree of tightness of the equipment (half-open suction or the presence of openings in shelters that do not allow creating a stable vacuum.”

1. The optimal air velocity in leaks is determined based on the condition of non-knocking out of dust.
2. The area of existing leaks and open openings is determined.
3. We determine the volume of air entering the shelter through the existing leaks.

From the point of view of energy efficiency, it is preferable to use shelters with a high degree of containment (Case A).

### 4 Conclusion

Analytical studies of methods for determining the suction and the amount of air entering the aspiration shelters through leaks were carried out, during which 3 characteristic approaches were established to determine the magnitude of the suction, based on the degree of tightness of the aspiration systems at a pressure in the shelter equal to atmospheric (semi-open suction), as well as at discharge up to and above 50 Pa.

On the basis of the conducted analytical studies, nomograms and algorithms for calculating the volumes of air entering the shelter through leaks for 3 characteristic approaches are proposed.

**Acknowledgements** The article was supported by a grant President of the Russian Federation NSh-25.2022.4.

## References

1. Logachev IN, Logachev KI (2005) Aerodynamic basis of ventilation. St. Petersburg: Khimizdat
2. Logachev IN, Logachev KI (2014) Industrial air quality and ventilation: controlling dust emissions. CRC Press, Boca Raton
3. Minko VA, Kuleshov MI (1987) Dedging in foundries of machine-building enterprises. Mechanical Engineering, Moscow
4. Kopteva VB, Koptev AA (2011) Flange connections: designs, dimensions, strength calculation: guidelines. Tambov: Publishing House of FGBOU VPO "TSTU"
5. Sold VD (2012) Tightness of detachable connections of equipment operated under the pressure of the working environment: study guide. Tambov: Publishing House of FGBOU VPO "TSTU"
6. Bartosz ET (1961) Aerodynamic calculation of contact seals. Proc Res Inst Railway Trans 214:121–136
7. Gurevich DF (1964) Hydraulic density of cylindrical interfaces with small gaps. Vestnik Mashinostroeniya 10:31–37
8. Domashnev AD (1980) Stuffing box seals for NPP fittings. Atomizdat, Khmelniker. M.
9. Zikeev VA (1970) Investigation of flow features in deformed slots of mechanical seals. Engineering 3:83–91
10. Forest O (1985) Metal-to-Metal and Metal Gasketed seals. Machin Design
11. Babkin VT (1977) Tightness of immovable connections of hydraulic systems. M.: Mashinostroenie
12. Demkin NB, Lembersky VB, Sokolov VI (1976) Influence of microgeometry on the tightness of detachable joints with gaskets from low-modulus materials. Proc Univ Eng 7:26–30
13. Lembersky VB, Fishkin RV, Domashnev AD (1977) Calculation of leakage through fixed detachable connections. Chem Oil Eng 4:10–11
14. Tkach LI (1968) Investigation of the tightness of mechanical seals: dis. ...cand. tech. Sciences. MIHM
15. Seals and sealing technology: a handbook. M.: Mashinostroenie (1994)
16. Kiselev PI (1950) Fundamentals of seals in high pressure fittings. M.: Gosenergoizdat
17. Kondakov LA (1972) Sealing of hydraulic systems. M.: Mashinostroenie
18. Kondakov LA (1982) Working fluids and seals of hydraulic systems. M.: Mashinostroenie
19. Graham J (1964) Gas leakage in sealed systems. Chem Eng 71(10):169–174
20. Dobrushkin DB, Eckel ES, Orlov ZD (1963) Study of the conditions for extrusion of vulcanized rubber through a gap. Rubber and Rubber 9:19–24
21. Livshits VI (1982) Investigation of tightness at contact of steel rough surfaces. In: 7th International Meeting and 1st International Exhibition on Sealing Technology, vol 2, pp 563–577. Budapest
22. Feddman EB, Rumyantsev OV, Uyk GK (1968) Study of the mechanism of operation of a double conical seal of high-pressure vessels. Chem Oil Eng 7:26–30
23. Exler LI (1966) On the work of a contact metal seal. Chem Oil Eng 2:5–8
24. Fukizoc Fadasu (1964) On the mechanism of contact betwin metall surface—the penetrating daphth and the overage cltarance. Paper Amer Soc Mech
25. Sold VD, Baranova ML (2001) Errors in determining the minimum sealing load. Chem Oil Gas Eng 4:10–12
26. Radchenko IV (1965) Molecular physics. M.: Nauka
27. Cherginyants K (1973) Mathematical methods of the kinematic theory of gas. M.: Mir
28. SP 60.13330.2020. Set of rules. Heating, ventilation and air conditioning. SNiP 41-01-2003

# Determination of Aerodynamic Coefficients in the Design of Buildings



Vladimir Rimshin  and Pavel Truntov 

**Abstract** The article considers the variable definition of wind loads on a building. In order to determine the wind load on the building, various options for setting the wind load were considered, taking into account the standards of various countries. 4 schemes were considered. The first and second determination schemes are carried out taking into account the provisions of the Russian standard SP 20.13330.2016, the third and fourth schemes in accordance with the Load Code for The Design Of Building Structures, GBJ 9–87. As amended by GB 50,009–2001 from 2006. To select the load application scheme in the design model of the building, the total (for the entire length) aerodynamic coefficient in the direction of the vertical axis was determined. According to the results of the study, the scheme of action of the wind load corresponding to the highest load value was determined. It is also noted that more accurate aerodynamic coefficients can be obtained from the results of model aerodynamic tests conducted in a wind tunnel.

**Keywords** Aerodynamic coefficient · Wind load · Calculation model · Wind pressure

## 1 Introduction

In order to determine the wind load on the building, the paper considers various options for setting the wind load, taking into account the standards of various countries. To conduct the study, a building built according to the project of 1988 was considered. The building has 22 aboveground floors. The building has a complex shape, the main volume has the shape of a three-pointed star [1–4].

The overall stability of the building in the scheme of the connecting frame is ensured by the joint work of the frame structures, walls of rigidity, vertical ties and horizontal discs of floors. The spatial rigidity of the frame as a whole, as well as the

---

V. Rimshin · P. Truntov (✉)

National Research Moscow State University of Civil Engineering, Yaroslavskoe Shosse, 26, Moscow 129337, Russia

stability of individual elements, is ensured by the rigidity of transverse and longitudinal frames, prefabricated monolithic flooring and monolithic bottom, monolithic walls of rigidity. Prefabricated structures of reinforced concrete frame columns, beams, panels are accepted according to the TC-1 and CMS catalog. Reinforced concrete columns of the basement, basement and from the first floor to the sixth inclusive have steel cores, portal frames and metal floor beams are made of steel [5–9]. During installation, all steel elements in the attachment points were covered with tread soil and plaster on the frame and mesh or concreted. The walls of rigidity with half-timbered steel structures are made of reinforced concrete. The floors from 1 to 19 are prefabricated and monolithic. Enclosing structures made of expanded clay concrete wall panels [10–13].

Floor heights:

- basement—4.5 m;
- 1st-5th floors—4.8 m;
- 6th-22nd floors—3.3 m.

## 2 Materials and Methods

During the preparatory work for the simulation of the design model, the schemes of applying wind loads are considered, taking into account the aerodynamic coefficients determined in accordance with SP 20.13330.2016 Appendix V. P. V.1.2 (Scheme № 1), P. V.1.15 (scheme № 2), as well as in accordance with the Load Code For The Design Of Building Structures, GBJ 9–87. as amended by GB 50,009–2001 from 2006 (schemes № 3 and 4) [14, 15].

*Wind load application scheme № 1. (Fig. 2).*

The wind pressure is determined in accordance with Sect. 11.1 and taking into account P. V.1.2 Appendix B SP 20.13330.2016 (Fig. 1).

The conditional total aerodynamic coefficient for scheme 1 is equal to:

$$C_{yc\pi}^1 = 46.150 \times (0,8 + 0,5) = 60$$

*Wind load application scheme № 2 (Fig. 3).*

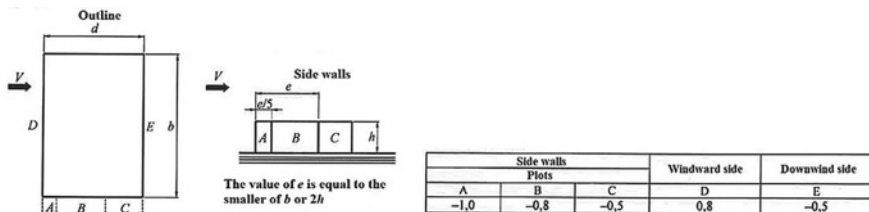


**Fig. 1** Normative aerodynamic coefficients (clause 1.2 of the appendix In SP 20.13330.2016)

**Fig. 2** Aerodynamic coefficients used in calculations according to the wind load application scheme № 1

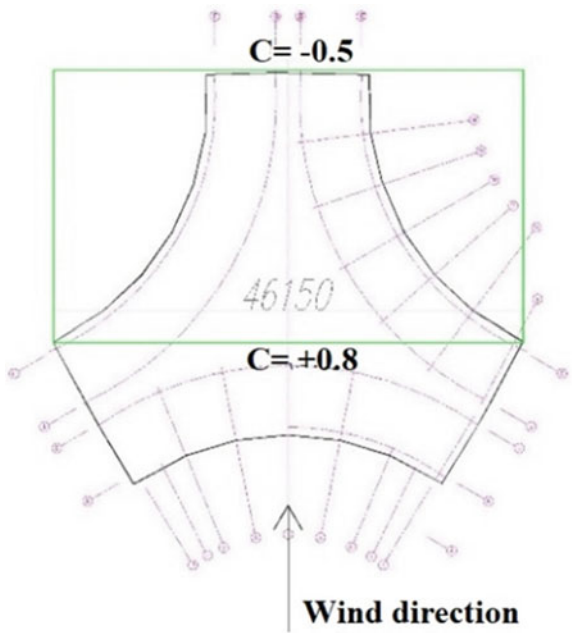
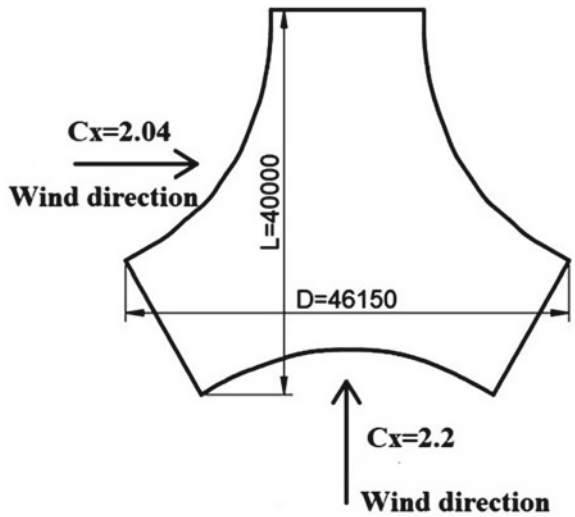


**Fig. 3** Aerodynamic coefficients used in calculations according to the wind load application scheme № 2



The wind pressure is determined in accordance with Sect. 11.1 and taking into account P. V.1.15 Appendix B SP 20.13330.2016.

When  $L/D = 40/46 = 0.87$  coefficient  $C_x = 2.2$ .

When  $L/D = 46/40 = 1.15$  coefficient  $C_x = 2.04$ .

The value of the drag is taken according to the formula (V.3) SP 20.13330.2016:

$$C_x = k_\lambda \cdot C_x = 1 \cdot 2.2 = 2.2 \text{ when the wind direction is on axis 4.}$$

$$C_x = k_\lambda \cdot C_x = 1 \cdot 2.04 = 2.04 \text{ with direction 3 perpendicular to axis 4.}$$

The conditional total aerodynamic coefficient for scheme 2 is equal to:

$$C_{yc\pi}^2 = 46.150 \times 2.2 = 101.53$$

*Wind load application scheme №3 (Fig. 4–6).*

The wind pressure was determined in accordance with Sect. 11.1 and at the same time the aerodynamic coefficients were taken into account the regulatory document Load code for the design of building structures, GBJ 9–87. as amended by GB 50,009–2001 from 2006 [16–18].

The conditional total aerodynamic coefficient for Scheme 3.1 is equal to (taking into account the symmetry of the building):

$$C_{yc\pi}^{3.1} = 2 \times (0.94 \times 16.2 - 0.36 \times 16.2 + 0.08 \times 16.2 + 0.5 \times 16) = 49.84.$$

The conditional total aerodynamic coefficient for Scheme 3.2 is equal to:

**Fig. 4** Standard aerodynamic coefficients (GB 50,009–2001 from 2006)

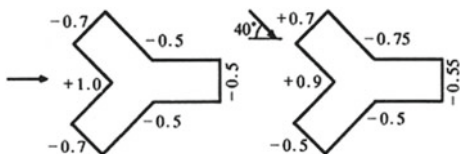


**Fig. 5** Aerodynamic coefficients used in calculations according to the wind load application scheme № 3.1

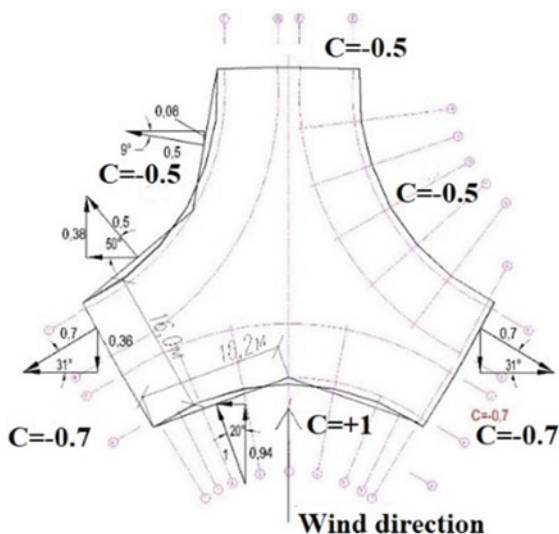


**Fig. 6** Aerodynamic coefficients used in calculations according to the wind load application scheme № 3.2

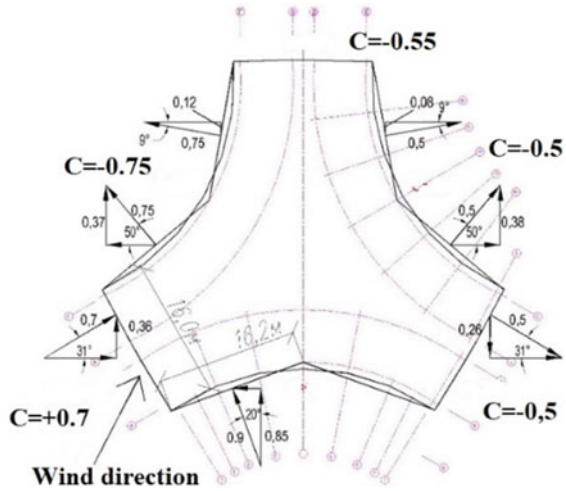
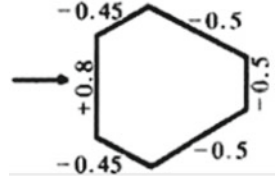


**Fig. 7** Standard aerodynamic coefficients (GB 50,009–2001 from 2006)



$$C_{yc\pi}^{3.2} = 2 \times 0.85 \times 16.2 + 0.36 \times 16 + 0.37 \times 16.2 + 0.12 \times 16.2 + 0.55 \times 16 + 0.08 \times 16.2 + 0.38 \times 16.2 - 0.26 \times 16 = 53.33$$

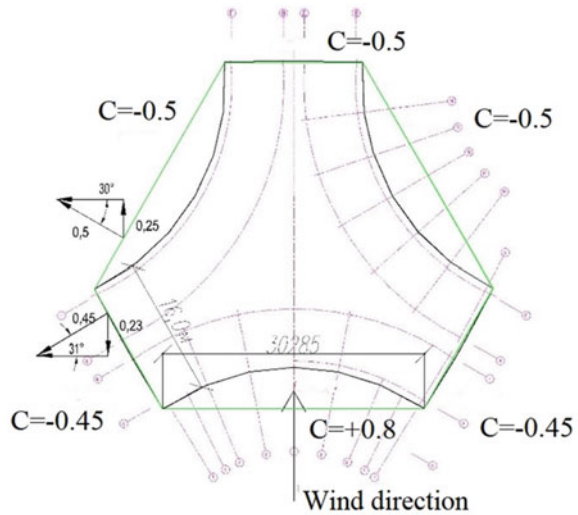
*Wind load application scheme № 4 (Fig. 7–8).*

The wind pressure was determined in accordance with Sect. 11.1 and the aerodynamic coefficients were taken into account in the regulatory document Load Code for the design of building structures, GBJ 9–87. as amended by GB 5009–2001 from 2006.

The conditional total aerodynamic coefficient for scheme 4 is equal to (taking into account the symmetry of the building):

$$C_{yc\pi}^4 = 30.285 \times 0.8 - 0.23 \times 16 + 30.285 \times 0.25 + 0.5 \times 16 + 30.285 \times 0.25 - 16 \times 0.23 = 40.01$$

**Fig. 8** Aerodynamic coefficients used in calculations according to the wind load application scheme № 4



### 3 Results and Discussion

To select the load application scheme in the design model of the building, the total (for the entire length) aerodynamic coefficient in the direction of the vertical axis was determined. The coefficient corresponding to the 1st scheme of wind action is taken as a unit [7, 8].

For scheme № 1, the total coefficient was:  $C = 1$ ;

For scheme № 2, the total coefficient was:  $C = 1.69$ ;

For scheme № 3 (3.1), the total coefficient was:  $C = 0.83$ ;

For scheme № 3 (3.2), the total coefficient was:  $C = 0.89$ ;

For scheme № 4, the total coefficient was:  $C = 0.67$ .

### 4 Conclusion

According to the calculation results, the largest total coefficient  $C = 1.69$  corresponds to scheme № 2. The resulting value is 69% higher than for scheme No. 1. In comparison with the regulatory document Load code for the design of building structures, GBJ 9–87. As amended by GB 50,009–2001 from 2006, the obtained values of the total aerodynamic coefficient according to scheme № 2 (SP 20.13330.2016) are 80–102% higher.

For further design, the scheme of Appendix № 2 was adopted as the scheme corresponding to the highest value of the wind load. More accurate aerodynamic coefficients can be obtained from the results of model aerodynamic tests conducted in a wind tunnel.



## References

1. Rimshin VI, Truntov PS, Ketsko ES, Kuzina IS (2020) Method of determining wind loads and impacts using the software. *Build Reconst* 6(92):43–50
2. Kuzina E, Rimshin V, Kurbatov V (2018) The reliability of building structures against power and environmental degradation effects. *IOP Conf Series: Mater Sci Eng* 463(4):042009
3. Rimshin V, Truntov P (2019) An integrated approach to the use of composite materials for the resto-ration of reinforced concrete structures. *E3S Web of Conferences*, vol 135. ITESE-2019
4. Kuzina E, Rimshin V, Neverov A (2019) Residual resource of power resistance during building structures deformation. *E3S Web of Conferences*, vol 135. ITESE-2019
5. Kuzina E, Cherkas A, Rimshin V (2018) Technical aspects of using composite materials for strengthening constructions. *IOP Conf Series: Mater Sci Eng* 365(3):032053
6. Karpenko NI, Eryshev VA, Rimshin VI (2018) The limiting values of moments and deformations ratio in strength calculations using specified material diagrams. *IOP Conf Series: Mater Sci Eng* 463(3):032024
7. Varlamov AA, Rimshin VI, Tverskoi SY (2018) The general theory of degradation. *IOP Conf Series: Mater Sci Eng* 022028. Vladivostok
8. Telichenko V, Rimshin V, Eremeev V, Kurbatov V (2018) Mathematical modeling of groundwaters pressure distribution in the underground structures by cylindrical form zone. *MATEC Web of Conf* 196:02025
9. Varlamov AA, Rimshin VI, Tverskoi SY (2018) The modulus of elasticity in the theory of degradation. *IOP Conf Series: Mater Sci Eng* 022029. Vladivostok
10. Karpenko NI, Eryshev VA, Rimshin VI (2018) The limiting values of moments and deformations ratio in strength calculations using specified material diagrams. *IOP Conf Series: Mater Sci Eng* 032024. Vladivostok
11. Churin P, Poddaeva O (2014) Aerodynamic testing of bridge structures. *Appl Mech Mater* 467:404–409
12. Krishan AL, Rimshin VI, Chernyshova EP, Astafeva MA, Chernyshov VE (2018) Calculation of strength resistance of load-bearing structures of architectural object of cultural heritage. *Heritage for planet Earth Proceedings of the international symposium heritage for planet Earth*, pp. 280–284
13. Kuzina E, Rimshin V, Kurbatov V (2018) The reliability of building structures against power and environmental degradation effects. *IOP Conf Series: Mater Sci Eng*. Electronic edition, 042009. Vladivostok
14. Merkulov S, Polyakova N, Rimshin V, Kuzina E, Neverov A (2019) Construction building systems protection under emergency exposure. *E3S Web of Conf* 135. ITESE-2019
15. Rimshin V, Kuzina E, Neverov A (2019) Residual resource of force resistance to deformation. *E3S Web of Conferences*, vol 135. ITESE-2019
16. Rimshin V, Aralov R (2019) Sustainable regeneration of urban areas (using the example of Moscow renovation program). *E3S Web of Conf* 110:01011
17. Rimshin V, Truntov P (2019) Determination of carbonation degree of existing reinforced concrete structures and their restoration. *E3S Web of Conf* 135. ITESE-2019
18. Kuzina E, Rimshin V, Neverov A (2019) Reserves and exposure assessment of reinforced concrete structures safety while reducing its power resistance. *E3S Web of Conf* 135. ITESE-2019

# Effects of Glass and Plastic Additives on the Physical, Mechanical and Strength Characteristics of Concrete



Alexey Bulgakov , Dmitrii Mishin , and Klaus Holschemacher 

**Abstract** The aim of the work is to study the possibility of the influence of fiber-glass additives on the physical, mechanical and strength characteristics of concrete. Concrete with the addition of cullet and plastic as a fine aggregate is considered as an object. In modern construction, research works aimed at studying high-tech concretes using recycled waste are of the greatest value. The practical significance of the study lies in obtaining concretes with improved characteristics using municipal waste, which will increase the efficiency of processing industrial waste and reduce their harmful impact on the environment. The analysis of the properties of concrete mixture and concrete using cullet and plastic as a filler is carried out. The analysis of the mechanism of influence of additives made of glass and plastic on the properties of concrete is carried out. Recommendations for the production of concrete using additives made of glass and PET-flex as a fine aggregate have been developed. An experimental plan was developed, the composition of the concrete mixture was selected and tested, natural sand was used as a fine aggregate for the manufacture of concrete, bituminous glass was crushed using a cylinder and a plunger on a hydraulic press to a fine fraction as a cullet. Based on the experimental data obtained, graphs of the dependence of the strength of concrete on the amount of PET-flex filler, the dependence of the strength of concrete on the amount of cullet were constructed. The analysis of experimental data with determination of the greatest ultimate strength of concrete is carried out. It was found that glass and plastic waste can be used as additives to concrete, since the strength of these concretes is comparable to the strength of conventional concrete.

**Keywords** Concrete · Additive · Glass · Plastic · PET flex · Tensile strength · Cement

---

A. Bulgakov (✉) · D. Mishin  
Southwest State University, 50 Let Oktyabrya St. 94, 305040 Kursk, Russia

K. Holschemacher  
Leipzig University of Applied Sciences, Karl-Liebknecht-St. 132, 04277 Leipzig, Germany  
e-mail: [klaus.holschemacher@htwk-leipzig.de](mailto:klaus.holschemacher@htwk-leipzig.de)

## 1 Introduction

In modern construction, the use of high-tech concretes of a new generation is becoming increasingly popular. Raw materials are characterized by high cost, therefore the most valuable research works aimed at studying the possibility of using recyclables in the production of building materials and structures. The deteriorating environmental situation in the world makes it necessary to pay more and more attention to the disposal of industrial and household waste. The use of man-made raw materials and waste in the production of concrete structures is not only innovative, but also the most important and necessary. In this regard, it is impossible not to mention such famous scientists as I. Asadi [1], M. Behera, [2], H. Binici [3], Y. D. Blanco [4], G. Giada [5], B. Liguori [6], A. A. Torres-Acosta [7], K. McNeil [8], I. Marie [9], B. H. Bharatkumar [10], E. F. Hernández [11], Y. Jianming [12], B. Liguori [13], L. W., Zhang [14], M. Ortega-Lera [15], C. L. Nogueira [16], F. M. León-Martínez [17], D. C. González-Sandoval [18].

The depletion of natural resources is one of the global environmental problems of mankind, and therefore resource-saving technology is becoming increasingly necessary. The concept of resource conservation implies not only the rational use and economy of natural resources, but also measures to minimize or eliminate the formation of waste and product residues during production, and also includes the reuse of raw materials. A distinctive feature of the resource-saving direction in the policy of foreign countries is the use of incentive measures for the use of resource-saving technologies. In a number of countries, tax incentives have been introduced for enterprises using resource-saving technologies in production, resource-saving financing systems have been adopted, and subsidies are allocated for the introduction of resource-saving technologies and necessary equipment. The main purpose of the work is to conduct a complex of experimental and theoretical studies to substantiate the possibility of using cullet and plastic as a filler for the production of concrete, to study the properties of the resulting concrete using cullet and plastic, to clarify the mechanism of the influence of waste on the properties of concrete. In connection with the above-mentioned studies, a promising direction is the study of concretes with improved characteristics using municipal waste, which will increase the efficiency of processing industrial waste and reduce their harmful effects on the environment. A large number of researchers have been and continue to be engaged in the study of concretes with improved characteristics.

## 2 Materials and Methods

To study the possibility of adding cullet and PET-flex to concrete, the concrete mixture was first kneaded without additives.

The loading of the sample during the compression test was carried out smoothly until its complete destruction, the maximum force determined the destructive load.

In order to study the effect of plastic additives on the strength characteristics of concrete, cube samples were made with the addition of plastic to the composition of the concrete mixture in the amount of 5, 10 and 15% of the mass of fine aggregate, replacing sand with a given amount of plastic. Also, cube samples were made with the addition of crushed glass to the composition of the concrete mixture in the amount of 30, 50, 70 and 100% of the mass of fine aggregate, replacing sand with a given amount of glass.

### 3 Results and Discussion

The content of pulverized and clay particles is determined by the change in the mass of sand after the grinding of particles with a size of up to 0.05 mm.

The content of pulverized and clay particles as a percentage by weight:

$$P_{otm} = \frac{m - m_1}{m} \cdot 100, \quad (1)$$

where,  $m$  is the mass of the dried sample before filtration;  $m_1$  is the mass of the dried sample after filtration.

True density is the mass of a unit volume of a material in an absolutely dense state without pores and voids.

True sand density:

$$\rho = \frac{(m - m_1)\rho_1}{m - m_1 + m_2 - m_3}, \quad (2)$$

where,  $m$  is the mass of the pycnometer with sand;  $m_1$  is the mass of an empty pycnometer;  $m_2$  is the mass of the pycnometer with distilled water;  $m_3$  is the mass of the pycnometer with sand and distilled water after removing air bubbles;  $\rho_1$  is the density of water.

The bulk density is determined:

$$\rho_b = \frac{m_1 - m}{v}, \quad (3)$$

where,  $m$  is mass of the measuring vessel;  $m_1$  is mass of the measuring vessel with sand;  $V$  is vessel capacity.

The voidness of sand is determined as a percentage by volume:

$$V_{m.p.} = \left(1 - \frac{\rho_p}{\rho \cdot 1000}\right) \cdot 100, \quad (4)$$

where,  $p$  is the true density of sand;  $p_n$  is the bulk density of sand.

The average density of the concrete mixture is the ratio of the mass of the compacted concrete mixture to its volume. A measuring vessel is used to determine the average density. It is weighed, then filled with a concrete mixture and compacted. The excess is cut level with the edges of the vessel, then weighed.

The average density is determined:

$$\rho_{ad} = \frac{m - m_1}{V} \cdot 1000, \quad (5)$$

$\rho_{ad}$ -is the mass of a measuring vessel with a concrete mixture;  $m_1$  is the mass of the measuring vessel without mixture;  $V$  is the capacity of the measuring vessel.

The loading of the sample during the compression test was carried out smoothly until its complete destruction; the maximum force determined the destructive load.

Compressive strength  $R_{sj}$  (MPa) of the test sample:

$$R_{sj} = \frac{10 F_{dp}}{A}, \quad (6)$$

where,  $A$  is the cross-sectional area of the sample;  $F_{dp}$ —destructive force.

In accordance with the requirements, there is a coefficient of recalculation of the strength of samples of this size for the strength of samples of standard size ( $150 \times 150 \times 150$  mm) for cube samples with a size of  $100 \times 100 \times 100$  mm.

The results of determining the ultimate strength of concrete with the addition of PET-flex are shown in the graph:

In the course of research, it was revealed that when sand is partially replaced with plastic in an amount of 5%, the strength of concrete decreases by 6%, in an amount of 10%—by 16%, in an amount of 15%—by 25%.

To determine the dependence of the influence of the size of plastic on the strength characteristics of concrete, a batch of concrete samples was made with a plastic content of 5% of the sand weight and fractions of 0–1, 1–2 and 2–4 mm.

The results of determining the tensile strength of concrete with the addition of PET-flex of various sizes in the amount of 5% are shown in the graph:

In the course of research, it was revealed that with the partial replacement of sand with plastic in the amount of 5% grain size 0–1 mm, there is an increase in the strength of concrete by 6%, grain size 1–2 mm—a decrease in strength by 10%, grain size 2–4 mm—a decrease in strength by 8%.

According to the test results, it is clear that the highest tensile strength was shown by concrete with the addition of PET-flex in an amount of 5% with a fraction size from 0 to 1 mm, the lowest strength limit was with a fraction size from 1 to 2 mm.

The plastic additive had a strong effect on the mobility of the concrete mix. When 5% PET-flex was added, the mobility of the mixture was 6 cm, 10% PET-flex—mobility was 3 cm, 15% PET-flex—mobility was 1 cm. The average density of the concrete mix with plastic additives decreased by an average of 6%.

In order to study the effect of plastic waste on the strength characteristics of concrete, cube samples were made with the addition of crushed glass to the composition of the concrete mixture in the amount of 30, 50, 70 and 100% of the mass of fine aggregate, replacing sand with a given amount of glass.

In the course of research, it was revealed that with the partial replacement of sand with cullet in the amount of 30%, there is a decrease in the strength of concrete by 0.06%, in the amount of 50%—an increase of 6%, in the amount of 70%—a decrease of 0.8%, in the amount of 100%—a decrease of 1.2%.

To determine the dependence of the influence of the grain size of glass on the strength characteristics of concrete, a batch of concrete samples with a glass content of 50% of the sand weight and fractions of 0–1, 1–2 and 2–4 mm was made.

In the course of research, it was revealed that with the partial replacement of sand with glass in the amount of 50% grain size 0–1 mm, there is an increase in the strength of concrete by 10%, grain size 1–2 mm—a decrease in strength by 12%, grain size 2–4 mm—a decrease in strength by 1%.

According to the test results, it can be seen that the highest tensile strength was shown by concrete with the addition of cullet in the amount of 50% with a fraction size from 0 to 1 mm, the lowest strength limit was with a fraction size from 1 to 2 mm.

The effect of the glass additive on the mobility of the concrete mixture. With the addition of 30% glass, the mobility of the mixture was 13.5 cm, 50% glass—mobility of 10 cm, 70% glass—mobility of 7 cm, 100% glass—mobility of 2 cm.

The average density of the concrete mix with glass additives decreased by an average of 4%.

## 4 Conclusion

In the course of scientific research, it was found that when plastic with a grain size of 0–4 mm is added to the concrete mixture in the amount of 5, 10 and 15% of the sand weight, the strength of concrete decreases. The smallest decrease in strength was observed with the addition of PET-flex in an amount of 5% by weight of sand.

The strength of concrete is strongly influenced by the grain size of the plastic additive. It has been experimentally established, but with the partial replacement of sand with plastic in the amount of 5% of the sand mass, the grain size from 1 to 2 mm and from 2 to 4 mm, there is a decrease in the strength of concrete by 10% and 8%, respectively. The highest index of ultimate strength was observed during the compression test of concrete B25 with the addition of PET-flex with grain size from 0 to 1 mm in the amount of 5% of the sand weight, the increase in ultimate strength was 6%.

It was found that when using an additive made of glass of a fraction of 0–4 mm as a partial replacement of a fine aggregate in the amount of 30, 70 and 100%, it slightly reduces the strength of concrete by 0.06, 0.8 and 1.2%, respectively. The highest strength was shown by concrete with the addition of glass in the amount of

50% of the mass of sand, the increase in strength compared to conventional concrete was 6%.

When determining the dependence of the influence of the grain size of cullet on the strength of concrete stone, it was found that the greatest reduction in strength is given by additives from crushed glass in the amount of 50% grain size from 1 to 2 mm and is 12%. The highest index of ultimate strength was recorded during the compression test of concrete B25 with the addition of glass grain size from 0 to 1 mm in the amount of 50% of the mass of sand, the increase in ultimate strength compared to concrete without additives was 10%.

When glass and plastic additives are introduced into concrete, a sharp decrease in the mobility of the concrete mixture is recorded, which reduces its workability. Also, the average density of concrete with additives is reduced by an average of 5%.

According to the test results, it was revealed that it is possible to use glass and plastic waste with grain size from 0–1 mm as additives for concrete, since the strength of these concretes is comparable to the strength of ordinary concretes.



**Fig. 1** Manufactured samples-concrete cubes

**Fig. 2** Sample-concrete cube after compression test

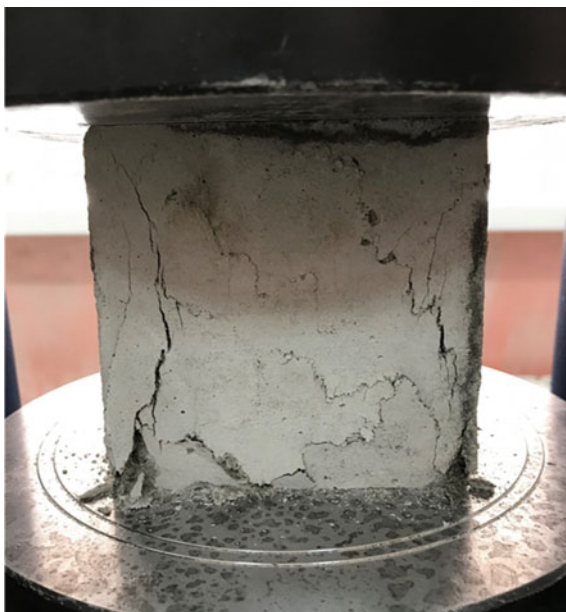


**Fig. 3** Holding concrete samples in a normal hardening chamber



**Fig. 4** Dependence of concrete strength on the amount of PET flex

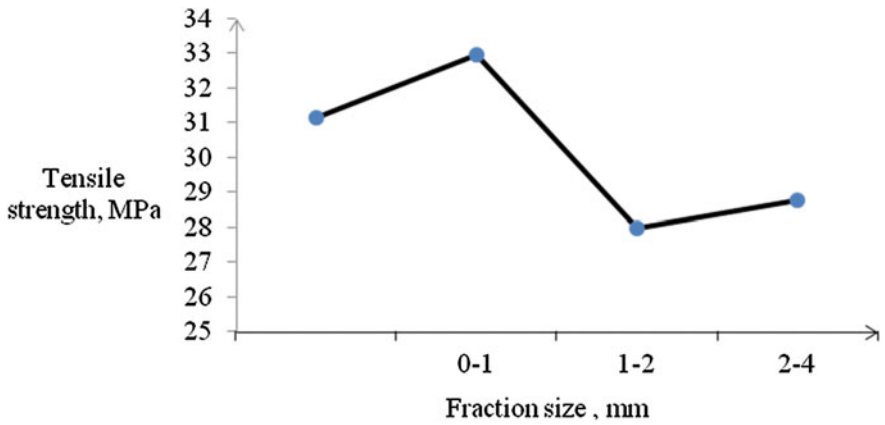
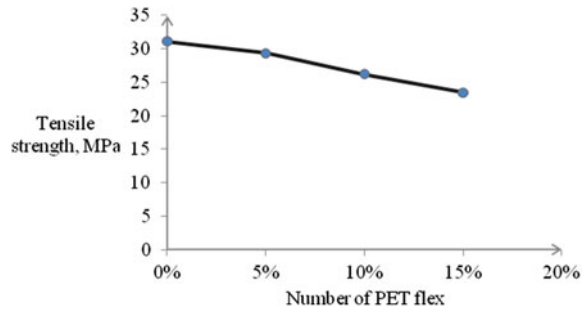


**Fig. 5** The dependence of the strength of concrete with PET-flex in the amount of 5% of the grain size of the fraction

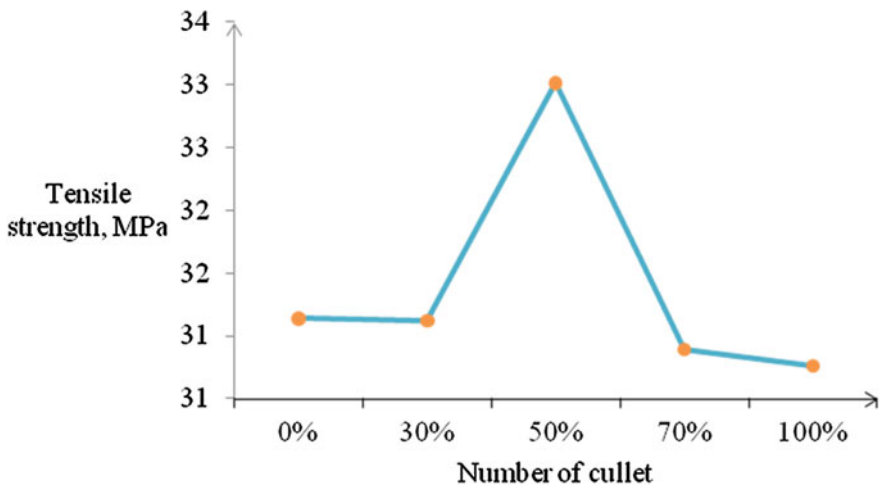


**Fig. 6** Dependence of concrete strength on the amount of glass

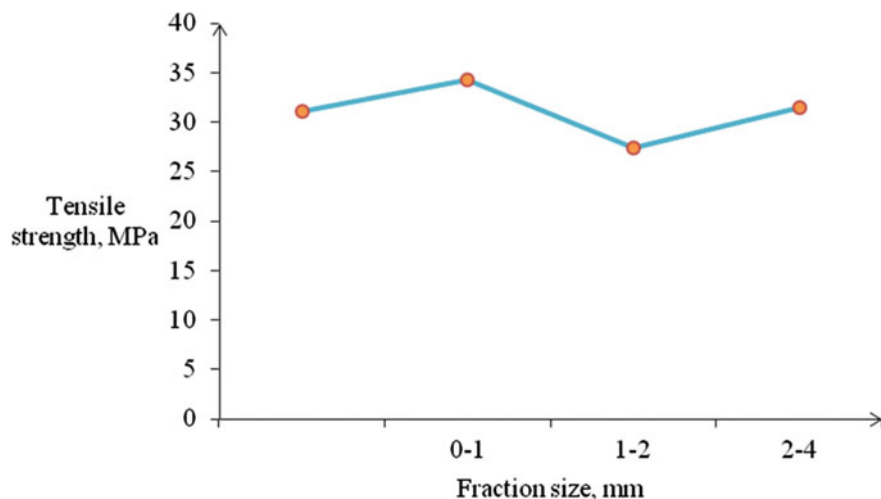


**Fig. 7** The dependence of the strength of concrete with glass in the amount of 50% on the grain size of the fraction






## References

1. Asadi I, Shafiqh P, Hassan ZFBA, Mahyuddin NB (2018) Thermal conductivity of concrete-a review. *J Buil Eng* 20:81–93. <https://doi.org/10.1016/j.jobe.2018.07.002>
2. Behera M, Bhattacharyya SK, Minocha AK, Deoliya R, Maiti S (2014) Recycled aggregate from C&D waste & its use in concrete—a breakthrough towards sustainability in construction sector: a review. *Constr Build Mater* 68:501–516. <https://doi.org/10.1016/j.conbuildmat.2014.07.003>
3. Binici H, Aksogan O (2018) Durability of concrete made with natural granular granite, silica sand and powders of waste marble and basalt as fine aggregate. *J Build Eng* 19:109–121. <https://doi.org/10.1016/j.jobe.2018.04.022>
4. Blanco YD, Campos ECM, Valdés CIR, Chavarín JU (2019) Natural additive (nopal mucilage) on the electrochemical properties of concrete reinforcing steel. *Revista ALCONPAT* 9(3):260–276. <https://doi.org/10.21041/ra.v9i3.429>
5. Giada G, Caponetto R, Nocera F (2019) Hygrothermal properties of raw earth materials: a literature review. *Sustainability* 11(19):5342. <https://doi.org/10.3390/su11195342>
6. Liguori B, Iucolano F, Capasso I, Lavorgna M, Verdolotti L (2014) The effect of recycled plastic aggregate on chemical-physical and functional properties of composite mortars. *Mater Des* 57:578–584. <https://doi.org/10.1016/j.matdes.2014.01.006>
7. Torres-Acosta AA, Díaz-Cruz LA (2020) Concrete durability enhancement from nopal (opuntia ficus-indica) additions. *Constr Build Mater* 243:118170. <https://doi.org/10.1016/j.conbuildmat.2020.118170>
8. McNeil K, Kang THK (2013) Recycled concrete aggregates: a review. *Intern J Conc Struct Mater* 7(1):61–69. <https://doi.org/10.1007/s40069-013-0032-5>
9. Marie I (2016) Zones of weakness of rubberized concrete behavior using the UPV. *J Clean Prod* 116:217–222. <https://doi.org/10.1016/j.jclepro.2015.12.096>
10. Bharatkumar BH, Raghuprasad BK, Ramachandra Murthy DS, Narayanan R, Gopalakrishnan S (2005) Effect of fly ash and slag on the fracture characteristics of high performance concrete. *Mater Struct* 38:63–72. <https://doi.org/10.1007/BF02480576>

11. Hernández EF, Cano-Barrita PDJ, Torres-Acosta AA (2016) Influence of cactus mucilage and marine brown algae extract on the compressive strength and durability of concrete. *Mater Constr* 66(321):074. <https://doi.org/10.3989/mc.2016.07514>
12. Jianming Y, Luming W, Jie Z (2019) Experimental study on the deformation characteristics of magnesium potassium phosphate cement paste at early hydration ages. *Cement Concr Compos* 103:175–182. <https://doi.org/10.1016/j.cemconcomp.2019.05.003>
13. Liguori B, Iucolano F, Capasso I, Lavorgna M, Verdolotti L (2014) The effect of recycled plastic aggregate on chemico-physical and functional properties of composite mortars. *Mater Des* 57:578–584. <https://doi.org/10.1016/j.matdes.2014.01.006>
14. Zhang LW, Sojobi AO, Kodur VKR, Liew KM (2019) Effective utilization and recycling of mixed recycled aggregates for a greener environment. *J Clean Prod* 236:117600. <https://doi.org/10.1016/j.jclepro.2019.07.075>
15. Ortega-Lera M, Arenda-Jiménez YG, Zuniga-Leal C, Sanchez-Medrano MT, Gallegos-Villa RR (2016) Mechanical analysis of an Ixtle based cable for its use in architecture. *IOSR J Mech Civil Eng (IOSRJMCE)* 14(1):36–38. <https://doi.org/10.9790/1684-1401053638>
16. Nogueira CL, Rens KL (2018) Ultrasonic wave propagation in EPS lightweight concrete and effective elastic properties. *Constr Build Mater* 184:634–642. <https://doi.org/10.1016/j.conbuildmat.2018.07.026>
17. León-Martínez FM, Cano-Barrita PDJ, Lagunez-Rivera L, Medina-Torres L (2014) Study of nopal mucilage and marine brown algae extract as viscosity-enhancing admixtures for cement-based materials. *Constr Build Mater* 53:190–202. <https://doi.org/10.1016/j.conbuildmat.2013.11.068>
18. González-Sandoval DC, Luna-Sosa B, Martínez-Ávila GCG, Rodríguez-Fuentes H, Avendaño-Abarca VH, Rojas R (2019) Formulation and characterization of edible films based on organic mucilage from Mexican opuntia ficus-indica. *Coatings* 9(8):506. <https://doi.org/10.3390/coatings9080506>

# Reinforcement Methods for Timber Closed Lattice Vaults



Nadezhda Tsaritova , Anastasia Shtankevich , Oksana Osipova , Igor Kosogov , and Alexey Bulgakov 

**Abstract** The nodes of the reticulated vaults with metal connections provide a one-way connection of the jambs in the nodes and the transfer of forces only with compressive longitudinal forces in the jambs. With some regulatory loads, a nonholonomic state occurs, in which a certain zone in the grid is excluded from operation. Based on the research of the design solutions of the reticulated vaults, the basic principles of the shaping of these structures were derived and the task of studying the closed reticulated vaults with the reinforcement of jambs with prefabricated tapes was set.

**Keywords** Timber structures · Reticulated vaults · Nodal junctions · Prefabricated tapes

## 1 Introduction

The expressiveness of architectural forms can be achieved by combining elements, which gives design engineer an excellent opportunity to improve them from a constructive point of view. Currently, a large number of computational software

---

N. Tsaritova · A. Shtankevich · O. Osipova · I. Kosogov  
South-Russian State Polytechnic University, Prosveshcheniya St. 132, 346428 Novocherkassk,  
Russia

e-mail: [ncaritova@yandex.ru](mailto:ncaritova@yandex.ru)

A. Shtankevich

e-mail: [anastasiyashtankevich@mail.ru](mailto:anastasiyashtankevich@mail.ru)

O. Osipova

e-mail: [oksana.osipova9@mail.ru](mailto:oksana.osipova9@mail.ru)

I. Kosogov

e-mail: [kosogov.igar@gmail.com](mailto:kosogov.igar@gmail.com)

A. Bulgakov (✉)

Southwest State University, 50 Let Oktyabrya St. 94, 305040 Kursk, Russia

e-mail: [agi.bulgakov@mail.ru](mailto:agi.bulgakov@mail.ru)

systems have appeared, which has simplified the development of methods for their calculation. Spatial structures largely satisfy such needs as unification of elements, lightness, high load-bearing capacity, choice of structural material [1–5].

For the first time the company “Tsolbau” at the end of the XIX century introduced closed reticulated vaults (CMV), which are used to this day. The main advantage of such structures is the covering of large areas without supports inside. However, the study of the stress–strain state of the CS was not carried out in full, which makes practical work possible. The issues of CMV node compliance and constructive nonholonomy in CMV nodes remain unexplored [6].

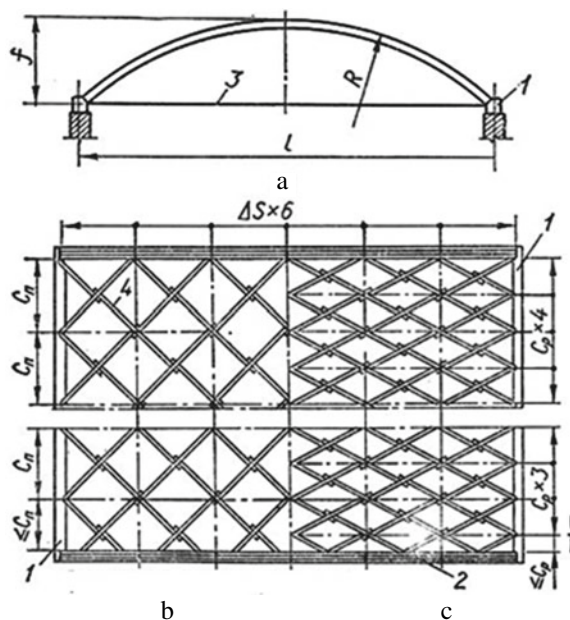
## 2 Methods and Materials

In accordance with the method of node coupling, the CMV is divided into:

1. A system Peselnik with a rectangular or rhombic grid of jambs (Fig. 1).
2. Metal (bolted) Tsolbau systems with a rhombic system of jambs (Fig. 2).

Nowadays, engineers continue to improve the designs of circle-mesh vaults of various systems. The most typical example of the use of a circle-mesh vault is the project of an indoor arena with an artificial football field, made for Tomsk (Fig. 3), where the constructive solution of an indoor training arena, rectangular in plan, with an artificial football field measuring  $55 \times 90$  m is of interest.

**Fig. 1** Reticular vaults a system Peselnik: a—general view; b—sweep of the vault with a rectangular grid; b–e same with the rhombic one; 1—wall beam; 2—pediment arch; 3—tighten; 4—main posts



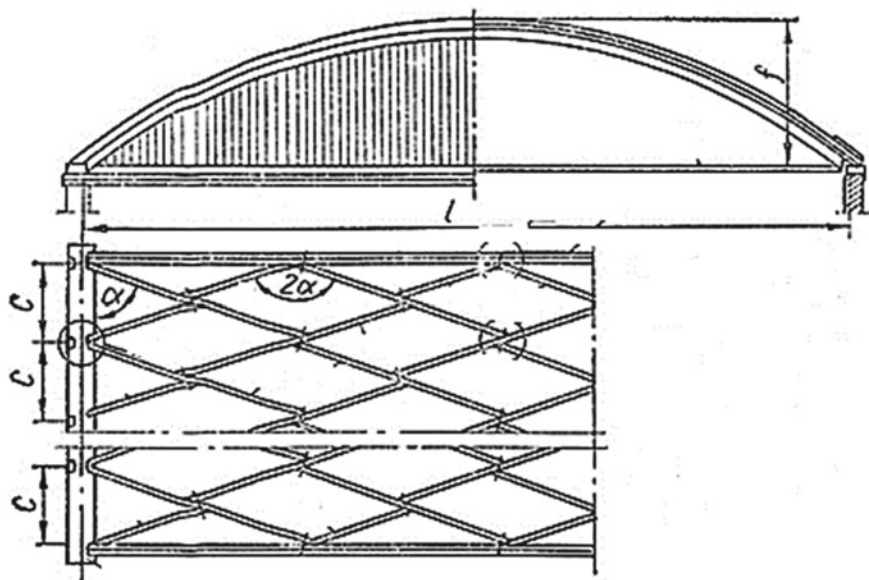


Fig. 2 Reticular vaults span of 14.7 m with knots on bolts



Fig. 3 Reticular vault in Tomsk

### 3 Results and Discussion

A solid flooring made of boards attached to the jambs from one side practically eliminates mobility in the metal joints of the nodes, thus extinguishing the structural nonholonomic [7], on the other hand it turns a closed circle-mesh vault into a room devoid of daylight (Fig. 4).

With the help of the PC Structure CAD software package [8, 9], knowing the coordinates of the points of intersection of the axes of the jambs with the axis of the arch edge, we will make a calculation scheme of a wooden closed CMV on a square plan (Fig. 5).

The authors carried out a numerical analysis of the forces arising in the jambs of a wooden closed CMV during loads from its own weight and temporary snow load. Figure 6 clearly shows the distribution of forces in the jambs of the CMV. The maximum value of negative forces that occurs in the jambs of the girth is 334 kN.

**Fig. 4** Timber closed CMV on a square plan with a solid flooring of boards: 1—girth; 2—footing; 3 и 4—left and right shoals; 5—solid flooring made of boards

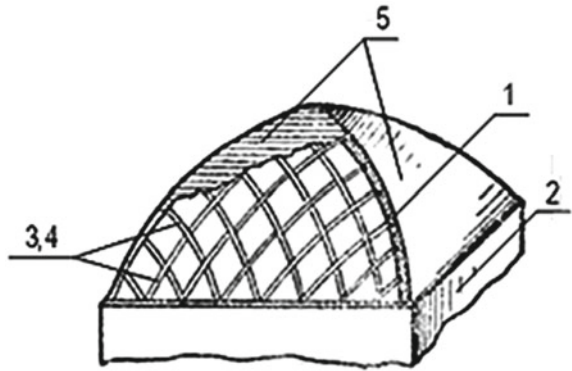


**Fig. 5** Design scheme of a timber closed CMV on a square plan

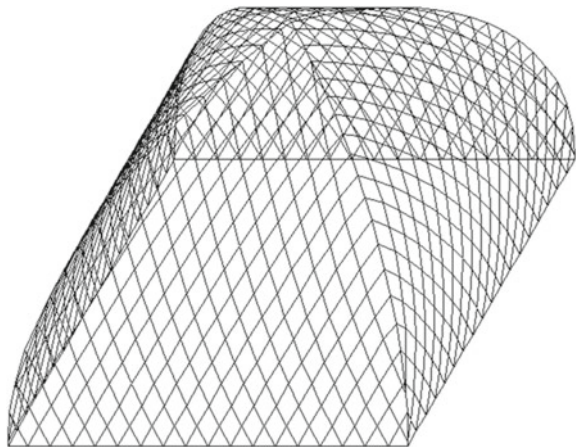
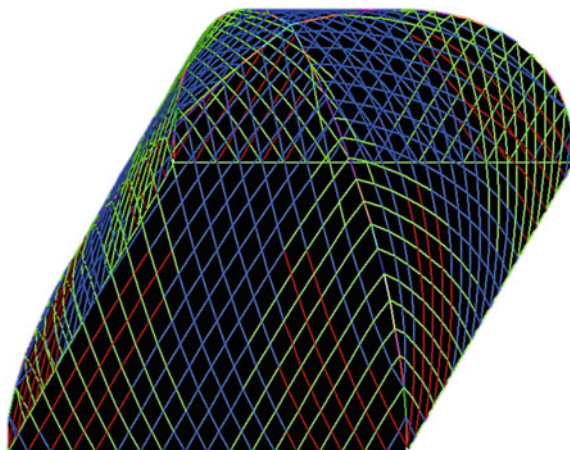




**Fig. 6** Diagram of forces occurring in CMV jambs when loaded by their own weight



Based on the data obtained, we will analyze the work of the CMV grid and draw conclusions that positive efforts arise in the area of herds in KSS shoals when loading from their own weight, with combined loading from their own weight and snow load, the number and values of positive efforts in CMV shoals increase.

The authors have developed a new constructive measure to extinguish constructive-nonholonomic effects without the use of solid flooring. The essence of this constructive event is as follows: the jambs of the grid of the wooden closed CMV are reinforced with prefabricated tapes connected to each other and with the jambs by steel capercaillie (Fig. 7).

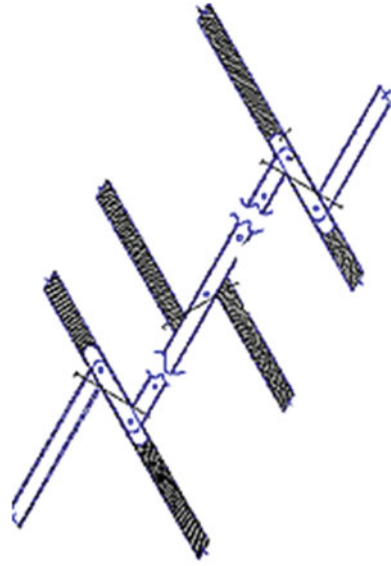
The width of the prefabricated steel belts is equal to 80% of the width of the reinforced jamb of the closed CMV (Fig. 8). This constructive measure extinguishes the constructive non-holonomy in the nodes of the wooden closed KSS on a square plan, which makes it possible to cover the arch from translucent polycarbonate panels

**Fig. 7** A fragment of a grid of a timber closed circle-mesh vault on a square plan





**Fig. 8** A fragment of a timber closed circular grid arch on a square plan with jambs reinforced with prefabricated bands



of zero Gaussian curvature. The panels are installed on the cells of the vault and secured with tapes of non-ferrous metal or stainless steel, pressed by galvanized grouse, through tape linings [10].

Thanks to such constructive measures to extinguish constructive-non-holonomic effects without the use of solid flooring, the authors have developed a model with a translucent coating of a wooden closed CMV on a square plan (Fig. 9).

## 4 Conclusions

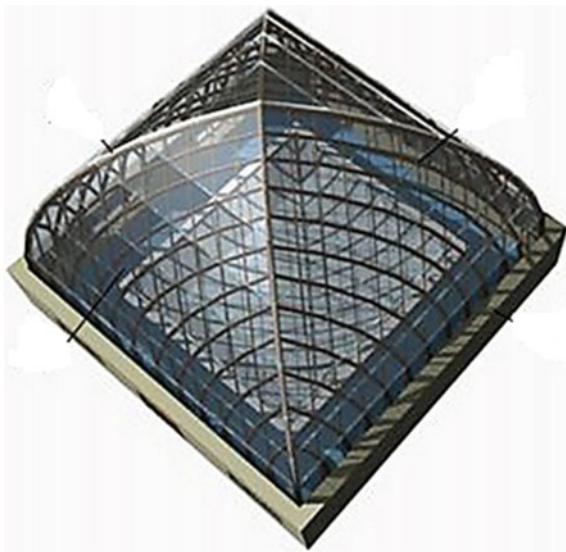
The geometric parameters of a timber closed circle-mesh vault on a square plan are determined.

The area of the appearance of positive forces arising from loads from their own weight and temporary snow load in the jambs of a timber closed CMV on a square plan is revealed.

A special constructive measure has been developed to reduce the amount of positive efforts arising from its own weight and snow load in the jambs of a timber closed CMV on a square plan.

A special constructive measure has been developed to offset the constructive-non-holonomic effects arising from its own weight and snow load in the jambs of a timber closed CMV on a square plan.

**Fig. 9** Timber closed CMV on a square plan



## References

1. Winter K, Rug W (1992) Innovations in timber construction. The Zollinger construction method. *Bautechnik* 4:193
2. Zhuravlyov AA (2003) Space wood constructions. Publishing House Rostov-na-Donu: "Malysh"
3. Beskopylny A, Zhuravlev A, Shilov A (2018) Buckling analysis of rod structure of the two-tier dome. In: *MATEC Web of Conferences*, p. 04024. Ho Chi Minh City: EDP Sciences. <https://doi.org/10.1051/mateconf/201819304024>
4. *Modern Space Frames* (1991) Shells in the form of a hyperbolic paraboloid. Guide, pp 441–443. Moscow
5. Błachut J (2016) Buckling of composite domes with localised imperfections and subjected to external pressure. *Compos Struct* 153:746–754. <https://doi.org/10.1016/j.compstruct.2016.07.007>
6. Klinshov IV (2012) Morphogenesis of rectangular reticulated double curvature vaults. Digest of works of graduate students, undergraduates and competitors. Technical sciences. Publishing House Nizhny Novgorod, NNGASU, pp 31–35
7. Shtankevich AV, Sadetov TS, Shurkhovets IA (2011) Features of the construction of a wooden closed circle-mesh vault on a square plan. *News of higher educational institutions. The North Caucasus region. Tech Sci* 3(161):74–76
8. Sadetov TS, Kruglaya NV (2006) Assessment of the malleability of the node of the circle-mesh arch according to the model of a transversally isotropic medium. *News of higher educational institutions. North Caucasian region. Technical sciences. Probl Const Archit* 12(1):30–33
9. Buzalo NA, Kruglaya NV (2008) Analysis of the malleability of the nodal joint of a wooden circle-mesh arch. *Bull MGSU* 4:205–208
10. Shurkhovets IA, Soldatov TS, Mironova AV. Utility model patent, No. 99034 U1 Russian Federation, IPC E04B 1/32. Closed circle-mesh vault: No. 2010120892/03: application 24.05.2010: publ. 2010/11/10. Applicant State Educational Institution of Higher Professional Education "South-Russian State Technical University (Novocherkassk Polytechnic Institute)"

# Study of the Concrete Resistance to the Action of Anti-Icing Agents



Alexey Bulgakov , Jens Otto , and Viacheslav Aseev 

**Abstract** The research is aimed at studying methods for determining the strength of concrete, taking into account the effect of anti-icing agents on it. The focus of the study considered in the article is aimed at determining the patterns and mechanisms of joint work of concrete and chloride reagents that prevent the formation of ice on the body of concrete structures at the time of strength gain. In the course of the study, formulas were considered that determine the strength development of the samples under study in the context of the joint work of the above materials. Next, the coefficient of influence of anti-icing chemical additives on concrete structures was determined. The scientific novelty of the work lies in the determination of the physical and chemical mechanism that explains the causes of the destruction of concrete and its components under the influence of anti-icing reagents, as well as the identification of the main classification features of chemical de-icing agents by the nature of the aggressive effect on concrete and its components. As a result of the study, experimental studies of nine concrete samples were carried out under the influence of various conditions that affect the strength characteristics and durability of the material, and a method for calculating concrete exposed to an aggressive chloride environment was developed.

**Keywords** Resistance of concrete · Anti-icing reagents · Chlorine substances · Coefficient of reagents influence

---

A. Bulgakov (✉) · V. Aseev  
Southwest State University, 50 Let Oktyabrya St. 94, 305040 Kursk, Russia  
e-mail: [agi.bulgakov@mail.ru](mailto:agi.bulgakov@mail.ru)

V. Aseev  
e-mail: [swsu\\_aseev@mail.ru](mailto:swsu_aseev@mail.ru)

J. Otto  
Technical University of Dresden, Mommsen St. 10, 01069 Dresden, Germany  
e-mail: [jens.otto@tu-dresden.de](mailto:jens.otto@tu-dresden.de)

## 1 Introduction

Concrete is a material widely used in both industrial and civil engineering. One of its most important characteristics, namely durability, depends on a number of different factors: the number and amplitude of the temperature difference, the strength of the acting loads, the impact of chemicals, the number of freeze–thaw cycles, and, of course, the use of anti-icing solutions.

A large number of works by scientists from different countries are devoted to the study of such characteristics as the durability of concrete, as well as the influence of aggressive chemicals and environments [1–3], but as the infrastructure for the production and maintenance of concrete products develops, other, newer ones began to appear. sources of influence, which also affect a number of characteristics of the material under consideration, including the service life [4–6]. Undoubtedly, the mechanism of action of new impurities and combinations of chemical compounds has not been fully studied even today, however, at the moment, studies show that the most relevant in the context of solving the problem of applying anti-icing coatings is the effect of chloride substances on the body of concrete [7–10].

To study this issue, it is necessary to determine the mechanism of destruction of concrete under the influence of the simultaneous influence of chlorine anti-icing chemical reagents and load [11–13], the dynamics of changes in the physical and mechanical parameters of the body of concrete and its components, to investigate changes in the physical and mechanical parameters of the properties of concrete in chemically aggressive environment, as well as to assess the physical and chemical changes occurring in the contact zone of concrete—anti-icing material.

## 2 Materials and Methods

In order to fulfill the task set, it is necessary to test concrete cubes of a solid section with dimensions of  $100 \times 100 \times 100$  mm for short-term loads, under the influence of which the samples will be destroyed (Fig. 1).

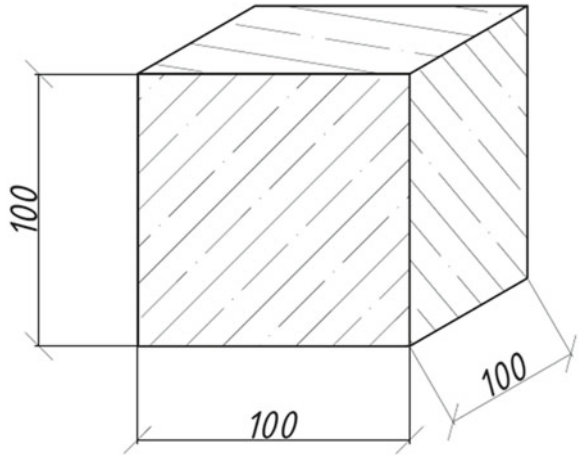
For the manufacture of a concrete cube, we use the following materials:

- Cement M500;
- River sand;
- Water.

These materials were mixed in a cement/sand ratio of 1:2. Water was added in a volume sufficient to obtain the desired consistency. The mass of water in the composition of the solution was 70–75% of the mass of cement. For the preparation of cubes of strength class B15, cement grade M500 was used. Some samples should have been placed in a 0.086% deicer solution.

To make a 0.086% deicer solution, 7 L of water are mixed with 660 g of a chloride deicer. The loading of the test cubes was carried out in accordance with

**Fig. 1** General view of the concrete sample



GOST 10,180–2012 and was carried out with an increasing load until the sample was destroyed. At the end of the destruction, readings were taken from the test facility.

The next step was to plot the dependence of the critical load on the curing time for samples that were not in a 0.086% solution of anti-icing agent, and then for samples that were in this solution. After that, the difference between the obtained materials was analyzed, on the basis of which formulas were derived that determine the laws of joint work of concrete and anti-icing chloride admixture.

A necessary step was also a comparison of the intended and actually obtained concrete grade, the definition formula of which is used from GOST 10,180–2012:

$$R = \alpha \frac{F}{A} k_w \tag{1}$$

To derive the most universal coefficients, the samples were tested on different days of curing. For this reason, the formula is also used:

$$R_{b,t} = R_{b28} \frac{(lg t)}{(lg 28)} \tag{2}$$

Based on the results of experimental and theoretical studies, a graph of the dependence of the critical load on the time of curing was constructed, according to which the level of the critical load of the samples treated with an anti-icing coating and being under its influence for different lengths of time was analyzed.

### 3 Experimental Section

For the purpose of the experiment, 9 samples of concrete cubes were made according to GOST 10,180–2012. M500 cement was taken as the components of the concrete samples. The next stage of this study was the manufacture of a 0.086% solution of anti-icing substance.

Several batches of samples were used for the experiment.

The first batch consisted of:

- A concrete cube that has gained strength in 7 days, not placed in a solution;
- A concrete cube that has gained strength in 7 days, placed in a solution for two days (located in a 0.086% solution of an anti-icing additive from 5 to 7 days);
- A concrete cube that has gained strength in 9 days, placed in a solution for four days (in a 0.086% solution of an anti-icing additive from days 5 to 9).

The second batch consisted of:

- A concrete cube that has gained strength in 14 days, not placed in a solution;
- A concrete cube that has gained strength in 14 days, placed in a solution for two days (being in a 0.086% solution of an anti-icing additive from 12 to 14 days).
- A concrete cube that has gained strength in 16 days, placed in a solution for four days (being in a 0.086% solution of an anti-icing additive from 12 to 16 days).

The third batch consisted of:

- A concrete cube that has gained strength in 21 days, not placed in a solution;
- A concrete cube that gained strength in 21 days, placed in a solution for two days (being in a 0.086% solution of an anti-icing additive from 19 to 21 days);
- A concrete cube that has gained strength in 23 days, placed in a solution for four days (being in a 0.086% solution of an anti-icing additive from 19 to 23 days).

The experiment was carried out according to the following algorithm:

1. Destruction of a concrete cube.
2. Taking readings.

During the experiment, the absolute values of the destruction of concrete samples under the action of short-term loads were obtained. The measurement results are shown in Fig. 2.

On the plot of the dependence of the critical load on the curing time (Fig. 2), we can observe that the level of the critical load perceived by concrete samples that were not in a 0.086% de-icing agent solution is higher than the level of other samples. Moreover, it can be noted that the critical load level for samples that have been in solution for two days is higher than the critical load level compared to samples that have been in solution for four days.

Based on the obtained values, the average  $R_{b28}$  for the samples not placed in the 0.086% solution was calculated, whose value corresponded to the expected strength class B15.

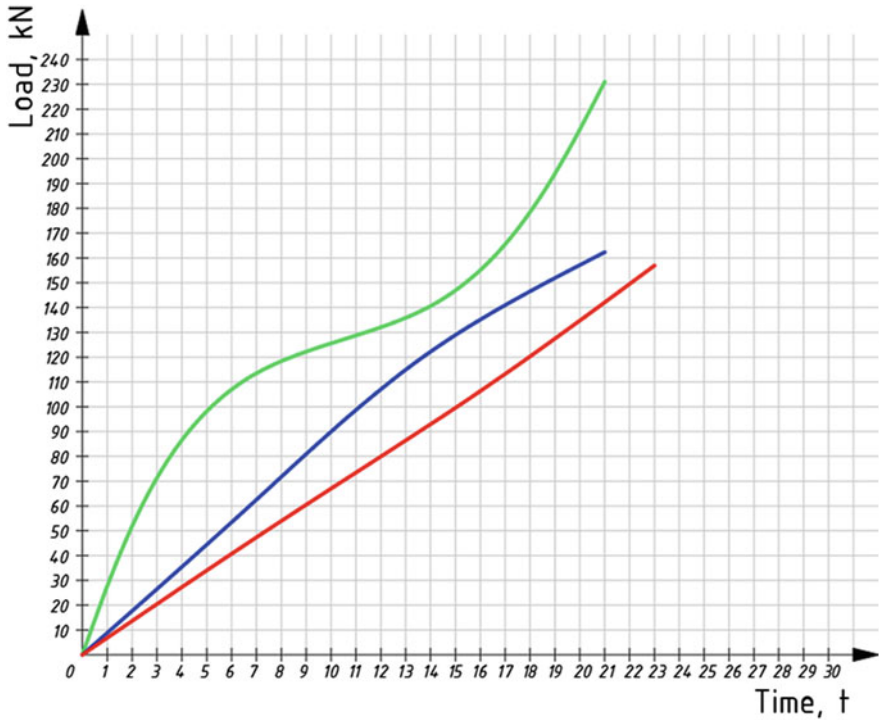


**Fig. 2** Comparison graph of the dependence of the critical load on the time of curing for all types of specimens considered

- Samples that were not in 0.086% anti-icing solution
- Samples that were in a 0.086% solution of anti-icing agent during the last two days of curing
- Samples that were in a 0.086% solution of anti-icing agent during the last four days of curing

Using (2), we introduce a formula that determines the strength of concrete in a chloride solution:

$$R_{b,t}^{cl} = R_{b28}^{cl} \frac{(tgt)}{(lg28)}, \tag{3}$$

where  $R_{b,t}^{cl}$ —the strength of concrete in an alkaline solution for t days.

$R_{b28}^{cl}$ —strength of concrete cured for 28 days and then placed in an alkaline 0.086% solution.

Based on the formulas described above, we introduce a coefficient that allows us to determine the effect of a chloride solution on the strength of concrete samples. Entered factor:

$$c_{t2} = \frac{R_{b,t}^{cl-2t}}{R_{b,t}}, \quad (4)$$

where  $c_{t2}$ —coefficient to determine the two-day effect of a chloride solution on the strength of concrete samples;  $R_{b,t}$ —strength of concrete cured in  $t$  days;  $R_{b,t}^{cl-2t}$ —strength of concrete that has gained strength in  $t-2$  days, and then gaining strength up to 28 days for two days in a 0.086% solution.

Hence, to determine the strength of a concrete sample that has gained 26-day strength, and then gaining full strength while in an alkaline 0.086% solution for 2 days, it will be determined by the formula:

$$R_{b28}^{cl-2t} = R_{b28} * \frac{R_{b,t}^{cl-2t}}{R_{b,t}} \quad (5)$$

or

$$R_{b28}^{cl-2t} = R_{b28} * c_{t2} \quad (6)$$

By the same principle, based on formulas (2) and (3), we introduce a coefficient that allows us to determine the effect of a chloride solution on the strength of concrete samples that have been in a chloride solution for the last 4 days of strength development. Entered coefficient:

$$c_{t4} = \frac{R_{b,t}^{cl-4t}}{R_{b,t}}, \quad (7)$$

where  $c_{t4}$ —coefficient to determine the four-day effect of a chloride solution on the strength of concrete samples;  $R_{b,t}$ —strength of concrete cured in  $t$  days;  $R_{b,t}^{cl-4t}$ —strength of concrete that has gained strength in  $t-4$  days, and then gaining strength to 28-day four days in a 0.086% solution.

Hence, to determine the strength of a concrete sample that has gained 24-day strength, and then gaining full strength while in an alkaline 0.086% solution for 4 days, it will be determined by the formula:

$$R_{b28}^{cl-4t} = R_{b28} * \frac{R_{b,t}^{cl-4t}}{R_{b,t}} \quad (8)$$

or

$$R_{b28}^{cl-4t} = R_{b28} * c_{t4} \quad (9)$$



### 4 Results and Discussion

As a result of the research, a graph was constructed for comparing the dependence of strength on time for all types of experimental samples considered, based on the introduced coefficients, as well as on the formulas used above (Fig. 3).

On the graph comparing the dependence of strength on time (Fig. 3), we can clearly observe that the level of strength shown by the samples that were not in the 0.086% solution is higher than the strength level of the remaining samples. In addition, it is natural that the strength for the type of samples that were in solution for two days is higher than the strength level compared to samples that were in solution for four days.

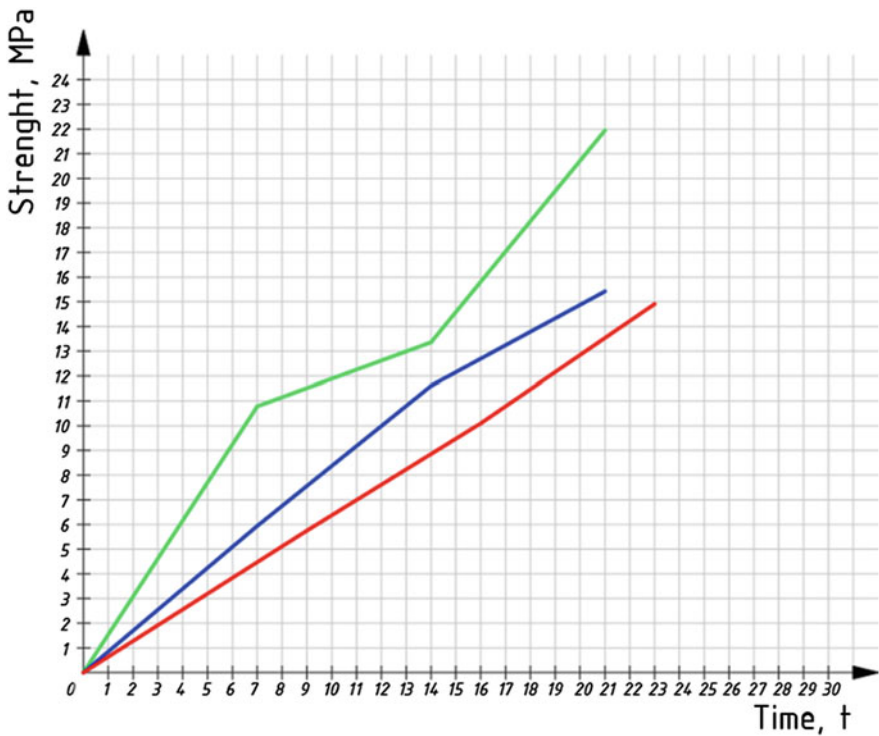


Fig. 3 Comparison dependence graph of the critical load on the curing time for all types of specimens considered, based on theoretical calculations

- Samples that were not in 0.086% anti-icing solution
- Samples that were in a 0.086% solution of anti-icing agent during the last two days of curing
- Samples that were in a 0.086% solution of anti-icing agent during the last four days of curing

## 5 Conclusion





Based on the data obtained and after analyzing the constructed dependency graphs, we conclude that the resulting calculation algorithm, together with the introduced coefficients, allows, with the accuracy necessary in the context of this study, to determine the effect of anti-icing coating on the strength of concrete at various stages of hardening.

## References

1. Assessment of Urban Air Quality (1988) Global environment monitoring system. UNEP, Nairobi and WHO, Monit Assess Res Cent. London
2. Biczysko SJ (1990) Asphalt performance at low temperatures. Highw Transp, London
3. Burl AR (1987) M4 Motorway, a composite pavement; surface cracking, highways and transportation. London
4. French WJ, Poole AB, Ravenscroft P, Khiabani M (1982) Results of preliminary experiments on the influence of fabrics on the migration of groundwater and Water—Soluble minerals in the capillary fringe. Q J Eng Geol
5. Netterberg F (1979) Salt damage to Roads—an interim guide to its diagnosis, prevention and repair. Insl Municipal Eng Southern Africa
6. Obika B, Freer-Hewish RJ (1988) Study of salt damage of bituminous surfaces for highway and airfield pavements H final contract report to overseas development administration. UK University, Birmingham
7. Obika B, Freer-Hewish RJ (1990) Soluble salt damage to thin bituminous surfacings of roads and runways H Australian road research
8. Ruth BE, Bloy LA, Avital AA (1982) Prediction of pavement cracking at low temperatures. Proc Assn Asphalt Paving Technol 51:53–90
9. Salter RJ (1989) Ambient temperature and thermal conditioning effects on an asphaltic mix incorporating EVA Co-Polymer. Highw Transp, London
10. Shahin MY, McGullough BF (1972) Prediction of flow temperature and thermal-fatigue cracking in flexible pavements. Tex Highw Department Res Rep 123–14 (1972).
11. Plotnikov VV (2015) Chemistry of binders and concretes. Publ House Assoc Constr Univ, Directory. Tutorial M
12. Bazhenov YM, Alimov LA, Voronin VV (2017) Nanomodified cement concretes. M.: Publishing house of the Association of construction universities
13. Usov BA (2016) Methods for selecting the composition of modified concrete. Tutorial.M.: Infra-M

# One of the Options for Using an Integrated Air Heater in Heat Supply Systems



Aleksey Burtsev , Dmitry Tyutyunov , Alexander Burtsev ,  
and Polina Akulshina 

**Abstract** This article presents a theoretical study of the functioning of an experimental installation of a complex air heater designed for waste gas heat recovery. The resulting heat is then partially used to maintain the required temperature of the incoming supply air. A variant of air flow control during ventilation of premises along with the use of the resulting excess heat according to the “smart home” scheme is considered. At the same time, the transients that inevitably arise during the operation of the studied structure are taken into account.

**Keywords** Recuperator · Utilization · Heat transfer · Experimental installation · Thermal balance · Cost management

## 1 Introduction

One of the main tasks of our time is the improvement of resource-saving technologies, as well as ensuring environmental safety. The solution of these problems involves the effective application of the latest scientific methods and approaches in the field of utilization of low-potential thermal energy of industrial waste gases and ventilation emissions [1, 2].

For this purpose, in this study, it is proposed to use a complex multilayer plate heat exchanger (CMPT), the principle of operation of which is to use a multilayer wall made of a material with a high coefficient of thermal conductivity, in which semiconductor Peltier elements are mounted for deep utilization of low-potential heat

---

A. Burtsev (✉) · D. Tyutyunov · A. Burtsev · P. Akulshina  
Southwest State University, 94, 50 Let Oktyabrya St, Kursk 305040, Russia  
e-mail: [ap\\_burtsev@mail.ru](mailto:ap_burtsev@mail.ru)

D. Tyutyunov  
e-mail: [dtyutyunov48@mail.ru](mailto:dtyutyunov48@mail.ru)

A. Burtsev  
e-mail: [burtsev-999@mail.ru](mailto:burtsev-999@mail.ru)

of waste gases and ventilation emissions with associated electrical energy generation to ensure autonomous operation of a ventilation installation or additional cooling/heating of the air [3].

During the experimental study in the CMPT, the function of the heat source was performed by the air heated in the heater, which played the role of hot exhaust gases. At the same time, air taken by a fan from the laboratory room was used as working heat in the ventilation system. It was considered as an incompressible gas, and the heat exchange between the heated and heating heat carriers was considered a stationary process. In this case, their turbulence is isotropic.

## 2 Materials and Methods

The heat  $Q$  obtained in the air heater is spent, respectively, on additional heating of the building (laboratory)  $Q_1 = b_1 \cdot Q$ , where  $b_1 = 0,85 \dots 0,88$  and obtaining thermal EMF  $Q_2 = b_2 \cdot Q$ , where  $b_2 = 0,12 \dots 0,15$  [3]. The considered component  $Q_1$  can be implemented according to the scheme, Fig. 1.

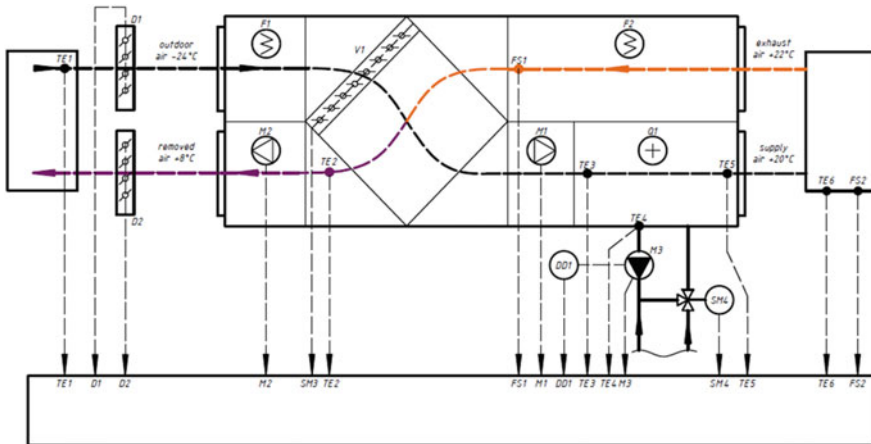


**Fig. 1** Control scheme of the supply and exhaust ventilation system with a recuperator:  $D1$ —Supply air damper;  $D2$ —Exhaust air damper;  $F1$ —Supply filter;  $F2$ —Exhaust filter;  $M1$ —Supply fan;  $M2$ —Exhaust fan;  $Q1$ —water heater;  $FS1$ —Channel humidity sensor;  $FS2$ —room humidity sensor;  $SM1$ ,  $SM2$ —Electric drive of the regulating damper;  $SM3$ —Electric bypass drive;  $SM4$ —Electric drive of the 3-way valve of the water heater;  $TE1$ —Outdoor air sensor;  $TE2$ —Air temperature sensor after the heat exchanger;  $TE3$ —Temperature sensor against freezing of the water heater;  $TE4$ —Temperature sensor of the reverse coolant;  $TE5$ —Channel temperature sensor;  $TE6$ —Room temperature sensor;  $DD1$  - Dry running protection relay;  $M3$ —water heater circulation pump; 1—plate heat exchanger; 2—room with control panel; 3—street; 4—controller

In this case, the ventilation system of the facility is designated by the thermal load  $R$ , which consumes part  $Q_1$  of the heat being disposed of  $Q$ . It includes the following equipment and materials:

$k$ —the heat transfer coefficient of the enclosure of the ventilated room,  $W/(m^2 \cdot ^\circ C)$ ;

$F$ —the area of the inner surface of the ventilated room,  $m^2$ ;

$Q_1, Q_2, Q_K, Q_N; Q_V; Q_F; Q_{1A}; Q_{2A}$ —respectively, heat flows carried in the supply and exhaust ducts, heated room, mixing circulation fan, in internal heat sources, in the devices of the supplied filtration, the mixing point of hot and cold flows  $A$ , supplied by fan  $M1$  and exhaust fan  $M2$ ,  $W$ .

### 3 Experimental Section

Consider the heat balance equation at point  $A$  [2, 4–6]:

$$Q_{inA} = Q_{entA} \tag{1}$$

where  $Q_{inA}$  and  $Q_{entA}$  are, respectively, the total heat flows at the inlet and outlet in the vicinity of point  $A$ ,  $W$ .

Obviously,  $Q_{entA}$  can be represented as:

$$Q_{inA} = Q_{1A} + Q_{2A} + Q_F + Q_V \tag{2}$$

It follows from the experiment:

$$Q_F = Q_V \approx 0 \tag{3}$$

When selecting between the exhaust and supply ventilation systems, the air consumption  $G_1, G_2$  and the mixing coefficient of hot and cold air masses  $U$  at point  $A$  should be taken into account in accordance with the requirements of [7–11]:

$$U = \frac{T_1 - T_A}{T_A - T_2} \tag{4}$$

It is important to note that the air flow in a stationary process has heat flows proportional to the corresponding flow rates  $Q_1 \sim G_1$  and  $Q_2 \sim G_2$ :

$$Q_1 = G_1 \cdot c_{1P} \cdot (T_1 - T_2) \tag{5}$$

$$Q_2 = G_2 \cdot c_{2P} \cdot (T_1 - T_2) \tag{6}$$

Temperatures  $T_1$  and  $T_2$  are taken in the range of 15...65 °C. The specific heat capacities at constant pressure  $c_{1P}$  and  $c_{2P}$  are equal to 1,005 kJ/kg · °C.

## 4 Results and Discussion

In this case, we consider the coordinated operation of the  $M1$  and  $M2$  actuators on their joint linearity sections with vertical boundaries 1–1 and 2–2, respectively, segment  $DE$  (curve I) and segment  $SL$  (curve II) (Figs. 2, 3).

Given (4, 5) and (6), it is easy to relate  $Q_1$  and  $Q_2$ :

$$Q_2 = \mu \cdot U \cdot Q_1 \quad (7)$$

$U = \text{const.}$ ,  $\mu$  determined from the experiment;  $Q_1$  and  $Q_2$  are nominal values corresponding to the stationary mode.

Obviously, due to this linearity, the heated air moves through the control valve  $V1$  with a fraction of the full opening of  $K_1$ . Then it is pumped through the heat load  $R$  by means of the fan  $M1$ , preheating at point  $A$  with a fraction of the full capacity of the pump  $K_2$ . In this case, we obtain the corresponding values  $Q_{1A}$ ,  $Q_{2A}$  at point  $A$ , taking into account (7):

$$Q_{1A} = K_1 \cdot Q_1 \quad (8)$$

$$Q_{2A} = K_2 \cdot Q_2 = \mu \cdot U \cdot Q_1 \cdot K_1 \cdot K_2 \quad (9)$$

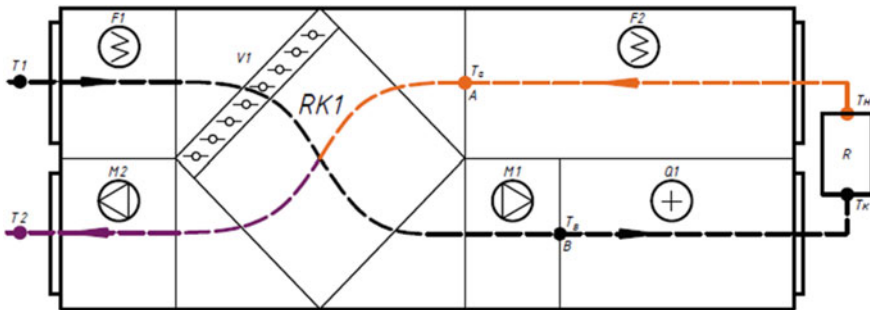
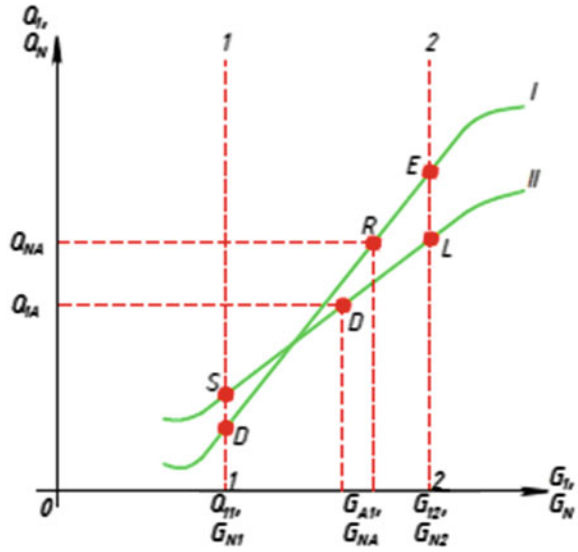


**Fig. 2** Design scheme of the installation:  $RK1$ —plate heat exchanger;  $F1$ —Supply filter;  $F2$ —exhaust filter;  $M1$ —Supply fan;  $M2$ —Exhaust fan;  $PI$ —control panel;  $Q1$ —water heater;  $T1$  and  $T2$ —supply and exhaust air temperatures;  $T_a$ —air temperature at point  $A$  at the bypass inlet;  $T_c$ —respectively, the air temperature in the heated room and at the outlet from it;  $K_1$ —the proportion of full opening of the bypass valve  $V1$  ( $0 \leq K_1 \leq 1$ );  $K_N$ —the proportion of full capacity of the supply fan  $M1$ ;  $M1$  ( $0 \leq K_N \leq 1$ );  $k$  is the heat transfer coefficient of the heat exchanger,  $W/m \text{ } ^\circ C$

**Fig. 3** Thermal characteristics of the actuators *M1, M2*



The heat flow from point A, entering the heat load R (heated room) creates in it a nominal temperature  $T_c = 20\text{ }^\circ\text{C}$  ( $T_c = 273\text{K}$ ). In stationary mode, the specified  $Q_k$  flow is transmitted through the fence wall, and:

$$Q_K = k \cdot F \cdot (T_k - T_H) \tag{10}$$

In this case,  $Q$ , taking into account (10), takes the form:

$$Q_{Bliz} = Q_k + Q_2 = k \cdot F \cdot (T_k - T_H) + Q_2 \tag{11}$$

$Q_2 = \text{const}$ ,  $Q_2 \geq 0$  is the heat entering the thermoelectric generator and considering (1–4), (7–11), we get:

$$Q_{1A} + Q_{2A} = Q_k + Q_2 \tag{12}$$

Substituting (8–10) into (12), we have:

$$Q_1 \cdot K_1 \cdot (1 + \mu \cdot U \cdot K_2) = k \cdot F \cdot (T_k - T_H) + Q_2 \tag{13}$$

The ratio (13) corresponds to the values of the nominal values of the parameters included in its left and right parts. Assuming that both of these parts are non-negative.

We investigate the dynamics of the thermal balance (13), assuming that the change in the temperature pressure of the  $\Delta T_{kn} = T_c - T_n$  occurs due to fluctuations in the outdoor air temperature  $T_n$  by a certain amount of  $\Delta T_n \geq 0$ .

In the case of a decrease in the temperature of  $T_n$  by the value of  $\Delta T_n$ , its new value  $T_{n1}$  can be represented in the form  $T_{n1} = T_n - \Delta T_n$ , in the case of an increase in the form  $T_{n2} = T_n + \Delta T_n$ .

Similarly, the temperature of the  $T_c$  of the thermal load  $R$  (ventilated room) changes in the form of  $T_{c1} = T_c - \Delta T_k$ —in the case of a decrease,  $T_{c2} = T_c + \Delta T_k$ —in the case of an increase. In this case, we assume  $\Delta T_c \geq 0$ .

Let's consider the main options:

- (1) Let's say the temperature of  $T_n$  has decreased by  $\Delta T_n$  degrees, which, with unchanged positions  $K_1$  and  $K_2$ , leads to a decrease in the temperature of  $T_c$  by the amount of  $\Delta T_k$  degrees. To restore the thermal balance, it is enough to reduce the proportion of  $K_1$  of the full opening of the valve  $VI$  by a certain amount of  $\Delta K_1$  and at the same time, respectively, increase the proportion of  $K_2$  of the full fan performance  $MI$  by a certain amount of  $\Delta K_2$ :

$$\begin{aligned} Q_1 \cdot (K_1 - \Delta K_1) \cdot (1 + \mu \cdot U \cdot (K_2 - \Delta K_2)) \\ = k \cdot F \cdot (T_k + \Delta T_k) - (T_H + \Delta T_H) \end{aligned} \quad (14)$$

Based on the actual conditions in the state of the weather, it can be assumed that the temperature difference between  $T_n$  and  $T_c$  is not abrupt.

In this case, it is permissible to put  $\Delta K_1 = 0$ ,  $\Delta K_N \geq 0$ . Given (13), we get:

$$\Delta K_2 = \frac{k \cdot F \cdot (\Delta T_H - \Delta T_k)}{Q_1 \cdot K_1 \cdot \mu \cdot U} \quad (15)$$

Given that  $\Delta K_2 \geq 0$ , we have:

$$\Delta T_k \geq \Delta T_H \quad (16)$$

- (2) Let's say the temperature of  $T_n$  has increased by  $\Delta T_n$  degrees, which, with unchanged positions  $K_1$  and  $K_2$ , leads to an increase in the temperature of  $T_c$  by the value of  $\Delta T_k$  degrees. And in this case, in order to preserve the thermal balance, we will reduce the proportion of  $K_2$  of the total capacity of the mixing pump by a certain amount of  $\Delta K_2$  and, accordingly, reduce the proportion of  $K_1$  of the full opening of the valve  $VI$  by a certain amount of  $\Delta K_1$ :

$$\begin{aligned} Q_1 \cdot (K_1 - \Delta K_1) \cdot (1 + \mu \cdot U \cdot (K_2 - \Delta K_2)) \\ = k \cdot F \cdot (T_k + \Delta T_k) - (T_H + \Delta T_H) \end{aligned} \quad (17)$$

By analogy with point (a), we assume  $\Delta K_N = 0$ ,  $\Delta K_1 \geq 0$ . Given (13), we get:

$$\Delta K_1 = \frac{k \cdot F \cdot (\Delta T_k - \Delta T_H)}{Q_1 \cdot (1 + \mu \cdot U \cdot K_2)} \quad (18)$$



Given that  $\Delta K_1 \geq 0$ , we get:

$$\Delta T_k \geq \Delta T_H \tag{19}$$

The ratio (13) allows you to work in the  $\Delta K_1 \cdot \Delta K_N \neq 0$  mode, but this approach complicates the control of the drives and increases the time of its implementation. In addition, in stationary conditions, the appearance of transients in the ventilation system and the corresponding heat supply is unlikely.

Using formulas (1–13), let’s imagine an air flow control scheme in a «smart house», Fig. 4.

It is important to understand that the constants and, respectively, included in expressions (15) and (18) are formed in advance and entered into multipliers in the scheme in the form of multipliers:

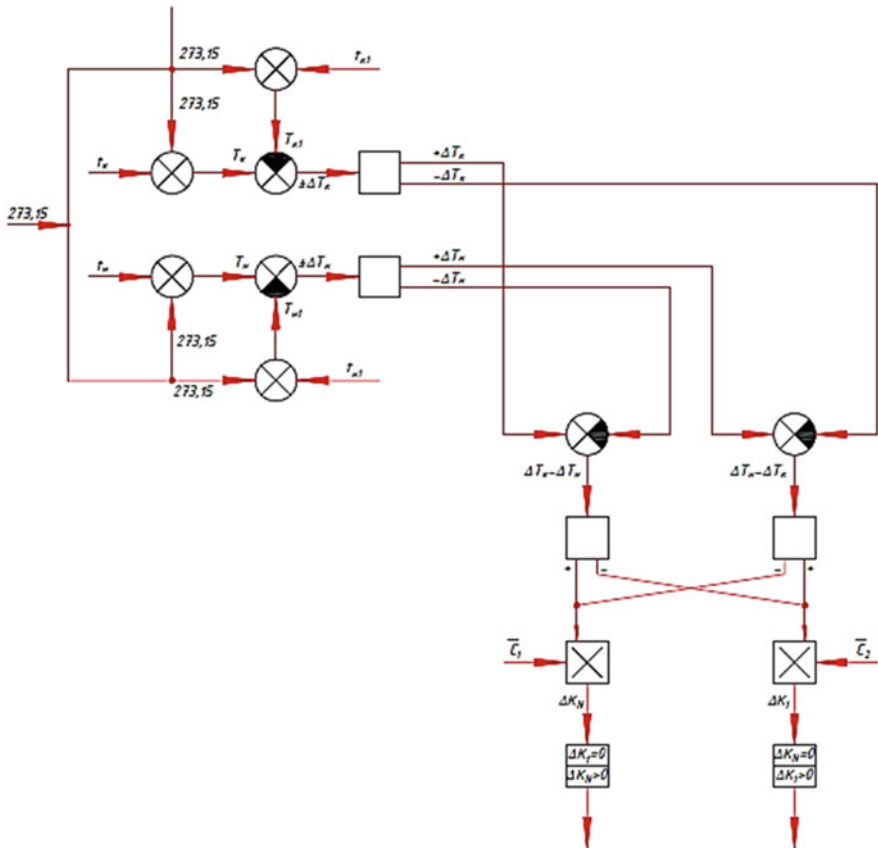


Fig. 4 Ventilation and heat supply control scheme of the facility

$$\bar{C}_1 = \frac{k \cdot F}{Q_1 \cdot K_1 \cdot \mu \cdot U} \quad (20)$$

$$\bar{C}_2 = \frac{k \cdot F}{Q_1 \cdot (1 + K_2 \cdot \mu \cdot U)} \quad (21)$$

$Q_1, K_1, K_2, \mu, U$  are the nominal values of the parameters.

At the inputs, if necessary, the temperatures  $t_k$  °C and  $t_n$  °C are translated into the scale of the  $SI, T_c, T_n$  system, which translates them into the positive region of the temperature scale.

It should be noted that the proportionality of the shares of  $K_1$  and  $K_2$  to the corresponding expenses of  $G_1$  and  $G_2$ ,  $K_1 \sim G_1$ ,  $K_2 \sim G_2$ , which allows for the appropriate calibration of flowmeters. In this case, the ratios  $\Delta K_1 \sim G_1$ ,  $\Delta K_2 \sim G_2$  are also valid for cost increments. This approach allows us to obtain the following working formulas:

$$\Delta G_2 = \frac{k \cdot F \cdot (\Delta T_H - \Delta T_k)}{Q_1 \cdot \mu \cdot U \cdot K_1} \quad (22)$$

If  $\Delta T_n \geq \Delta T_k$ ,  $\Delta G_1 = 0$ ,  $\Delta G_2 \geq 0$ .

$$\Delta G_1 = \frac{k \cdot F \cdot (\Delta T_k - \Delta T_H)}{Q_1 \cdot (1 + \mu \cdot U \cdot G_2)} \quad (23)$$

## 5 Conclusions

The design of a dependent heat supply has been developed, functioning with the help of an integrated air heater for waste gas heat recovery.

A mathematical model of heat flow control in the process of ventilation and associated heat supply is proposed and investigated.

A mobile scheme for controlling air heat flows based on the "smart home" principle has been created.

In order to increase the efficiency of the proposed heat exchanger, Peltier elements can be used in its design, which, with a temperature difference in the recuperator, will simultaneously generate electricity, additionally utilizing the heat of ventilation emissions.

## References

1. Sha H, Qi D (2020) Investigation of mechanical ventilation for cooling in high-rise buildings. *Energy Build* 228:110440. <https://doi.org/10.1016/J.ENBUILD.2020.110440>
2. Pekdogan T, Tokuç A, Ezan MA, Başaran T (2021) Experimental investigation of a decentralized heat recovery ventilation system. *J Build Eng* 35:102009. <https://doi.org/10.1016/J.JOBE.2020.102009>
3. Zhou W, Nie W, Liu X, Zhou C, Wei C, Liu C, Liu Q, Yin S (2020) Optimization of dust removal performance of ventilation system in tunnel constructed using shield tunneling machine. *Build Environ* 173(10):106745. <https://doi.org/10.1016/J.BUILDENV.2020.106745>
4. Shi Z, Lai D, Chen Q (2020) Performance evaluation and design guide for a coupled displacement-ventilation and passive-chilled-beam system. *Energy Build* 208(2):109654. <https://doi.org/10.1016/J.ENBUILD.2019.109654>
5. Gutiérrez González, V., Ramos Ruiz, G., Fernández Bandera, C.: Impact of actual weather datasets for calibrating white-box building energy models base on monitored data. *Energ*, 14(4) (2021). <https://doi.org/10.3390/EN14041187>
6. Wei G, Chen B, Lai D, Chen Q (2020) An improved displacement ventilation system for a machining plant. *Atmos Environ* 228:117419. <https://doi.org/10.1016/J.ATMOENV.2020.117419>
7. Shi Z, Chen Q (2021) Experimental and computational investigation of wall-mounted displacement induction ventilation system. *Energy Build* 241(5):110937. <https://doi.org/10.1016/J.ENBUILD.2021.110937>
8. Sha, H., Qi, D.: Investigation of mechanical ventilation for cooling in high-rise buildings. *Energy Build* 228 (2020). <https://doi.org/10.1016/J.ENBUILD.2020.110440>
9. Tyutyunov D, Pihtin A, Borodin A (2023) The temperature control methods for the heat supply system of buildings and structures. In: Vatin N, Pakhomova EG, Kukaras D (eds) *Modern problems in construction*. *Lect Notes Civ Eng*, 287, pp 165–176. Springer, Cham. [https://doi.org/10.1007/978-3-031-12703-8\\_17](https://doi.org/10.1007/978-3-031-12703-8_17)
10. Tyutyunov D, Burtsev A, Perepelitsa N, Burtsev A (2023) The mathematical model of automated control of heat flows in the supply and exhaust ventilation system. In: Vatin N, Pakhomova EG, Kukaras D (eds) *Mod Probl Construction Lect Notes Civ Eng*, 287, pp 177–187. Springer, Cham. [https://doi.org/10.1007/978-3-031-12703-8\\_18](https://doi.org/10.1007/978-3-031-12703-8_18)
11. Yezhov V, Semicheva N, Burtsev A, Perepelitsa N (2023) The mathematical model of a multi-layer wall of a plate heat exchanger. In: Vatin N, Pakhomova EG, Kukaras D (eds) *Modern problems in construction*. *Lect Notes Civ Eng*, 287, 1–11. Springer, Cham. [https://doi.org/10.1007/978-3-031-12703-8\\_1](https://doi.org/10.1007/978-3-031-12703-8_1)
12. Yezhov VS, Semicheva NE, Burtsev AP, Brezhnev AV, Perepelitsa NS (2022) Experimental research of main characteristics in a complex multi-layer plate heat exchanger. In: *IOP Conference Series: Materials Science and Engineering* 1242(1):012042. <https://doi.org/10.1088/1757-899X/1242/1/012042>
13. Ezhov V, Semicheva N, Tyutyunov D, Burtsev A, Perepelitsa N (2021) Version of a mathematical model of purge ventilation system with a complex recuperative heat exchanger. *J Appl Eng Sci* 19(1):246–251. <https://doi.org/10.5937/JAES0-30068>
14. Yezhov VS, Semicheva NE, Tyutyunov DN, Burtsev AP, Perepelitsa NS, Burtsev AP (2021) Mathematical model for automated heat flow control of an energy efficient ventilation system. In: *Proceedings of the Southwest State University* 25(1), 38–52. <https://doi.org/10.21869/2223-1560-2021-25-1-38-52>
15. Yezhov V, Semicheva N, Burtsev A, Perepelitsa N (2021) Experimental calculation of the main characteristics of thermoelectric EMF source for the cathodic protection station of heat supply system pipelines. In: Murgul V, Pukhkal V (eds). In: *International Scientific Conference Energy Management of Municipal Facilities and Sustainable Energy Technologies EMMFT 2019*. EMMFT 2019. *Advances in Intelligent Systems and Computing*, 1259. Springer, Cham. [https://doi.org/10.1007/978-3-030-57453-6\\_19](https://doi.org/10.1007/978-3-030-57453-6_19)

# Development of an Electromagnetic Monitoring System for Urbanized Areas Near Power Lines



Alexey Bulgakov , Jens Otto , and Pavel Maltsev 

**Abstract** The practical significance of the study is increasing every day, because human's life has changed a lot with the advent of electrical appliances and electrical equipment. Their functioning requires more and more energy, which, unfortunately, has negative properties that affect the human's body. Based on the analysis of the results of the International Project on Electromagnetic Fields, the World Health Organization (WHO) concluded that there was insufficient research on the results of the negative effects of prolonged low-level exposure to extremely low frequency electromagnetic fields and formulated recommendations, including the need to continue research to determine the negative impact on human health and ways to reduce the levels of exposure to electromagnetic fields during construction new structures. The relevance of the direction is determined by the need to develop monitoring and ways to improve the protection of the environment and people in urbanized areas near power lines of various voltage classes, which is important for ensuring the sustainable development of human settlements and protecting people from the negative effects of electromagnetic pollution of the urban environment.

**Keywords** Environmental monitoring · Urbanized territory · Power line · Electromagnetic field · Electric field strength · Magnetic field strength

---

A. Bulgakov (✉) · P. Maltsev  
Southwest State University, 50 Let Oktyabrya St. 94, 305040 Kursk, Russia  
e-mail: [agi.bulgakov@mail.ru](mailto:agi.bulgakov@mail.ru)

P. Maltsev  
e-mail: [maltsevpavel@mail.ru](mailto:maltsevpavel@mail.ru)

J. Otto  
Technical University of Dresden, Mommsen St. 10, 01069 Dresden, Germany  
e-mail: [jens.otto@tu-dresden.de](mailto:jens.otto@tu-dresden.de)

## 1 Introduction

Intensive use of electric energy in the modern information society has led to the fact that in recent decades another significant anthropogenic negative factor has emerged and formed—electromagnetic pollution of the environment. The facts show that the usual level of the low-frequency electromagnetic field of a large industrial city corresponds to the situation of a natural “magnetic storm” (abnormally high geomagnetic activity). Electromagnetic pollution in a number of cities already exceeds natural levels by a thousand or more times.

Electromagnetic safety of urbanized territories is the state of protection of urban territories from the potential danger of electromagnetic radiation. Such safety of populated areas is ensured by compliance with the established maximum permissible levels (MPD) of electric and magnetic field strength [1]. Engineering and environmental surveys for construction, which include the study of electromagnetic fields, are carried out to assess the current state and predict possible environmental changes under the influence of anthropogenic load in order to prevent, minimize or eliminate harmful and undesirable environmental and related social, economic and other consequences and maintain an optimal standard of living and living conditions of the population. During the construction, operation and liquidation of construction facilities, engineering and environmental studies and surveys should, if necessary, be continued [2] by organizing environmental monitoring of the state of natural and technical systems, the effectiveness of protective and environmental measures and the dynamics of the environmental situation. In order to ensure information management in the field of environmental protection, rational use of natural resources, ensuring environmentally safe sustainable development of the territory, maintaining a data fund on the state of the environment and ecosystems, natural resources, sources of anthropogenic impact, a unified environmental monitoring system has been created. Environmental monitoring includes monitoring of atmospheric air, lands, forests, water bodies, wildlife and the state of the subsoil.

Power transmission lines and construction facilities located next to them are a complex system characterized by long-term interaction and changing factors of the impact of its components on the environment and on each other, including electromagnetic factors. It should be noted that, although there is a developed electromagnetic monitoring system for high-frequency emitting equipment, supported by an appropriate regulatory and methodological framework, there is no such system for power equipment, and monitoring of the electromagnetic environment is currently carried out sporadically [3]. To assess the state of the natural environment by the factors of electromagnetic radiation of telecommunication equipment, an automated software package for the analysis of the electromagnetic environment has been created. There are practically no such software tools for power systems.

## 2 Methods

In this paper, the study of the electromagnetic field of power transmission lines was carried out using an analytical method and a field strength meter of industrial frequency PZ-50 [4].

PZ-50 is designed to measure the RMS value of the electric and magnetic field strength excited by high-voltage electrical installations of industrial frequency. The appearance of the PZ-50 is shown in Fig. 1.

Operating conditions of the device:

- Ambient temperature from + 5 to + 40° C;
- Relative humidity up to 90% at a temperature of + 25° C;
- Atmospheric pressure 70 - 106.7 kPa (537–800 mmHg).

The main elements of the meter are the reference device UO3-50 and directional reception antenna converters. The operation of the meter is based on excitation in the antenna converter under the influence of the measured field of alternating voltage proportional to the field strength. The alternating voltage is pre-amplified in the



**Fig. 1** Appearance of the industrial frequency field strength meter PZ-50

antenna converter and enters the input of the UO3-50, where it is filtered, further amplified, converted to a constant voltage and indicated.

PZ-50 is designed for measurements in the frequency range from 48 to 52 Hz. The measuring range of the electric field strength is from 0.01 to 100 kV / m, the measuring range of the magnetic field is from 0.1 to 1800 A / m [4].

The meter allows continuous operation under operating conditions (without replacing batteries) for at least 17 h when powered by a new set of batteries with a nominal capacity of at least 1 A/hour. The electrical power supply of the PZ-50 is carried out from the built-in battery of their 4 replaceable DC chemical elements with a rated voltage of 1.5 V. The power consumed from the battery does not exceed 0.1 watts.

To determine the RMS value of the electric (magnetic) field strength, measurements were carried out at a selected point in the projection space of the electric (magnetic) field intensity vector on three mutually orthogonal axes. After that, the modulus of the electric (magnetic) field intensity vector was determined [5].

The assessment of the levels of electromagnetic fields of power lines was carried out according to the analytical calculation according to the formulas that will be given in the next paragraph.

The electric and magnetic field strength was measured in the position of the measuring antenna at a height of 1.75 m above ground level.

However, these instructions do not consider the case of measuring the electric field when turning the power line route. In addition, there is currently no method for measuring the magnetic fields of power lines.

### 3 Results and Discussion

To study electromagnetic pollution from power lines in the city of Kurchatov (Russia, Kursk region), measurements of the electric and magnetic field strength of 115 kV power lines, 345 kV power lines, 495 kV power lines were carried out. Measurements were carried out at a height of 1.75 m from the earth's surface using a meter of electric and magnetic field intensity of industrial frequency PZ-50 along the flight route of the power line [6].

The initial ones for the analysis of nonstationary processes in a homogeneous isotropic medium are the nonstationary Maxwell equations in integral form [7]

Used to calculate the instantaneous value of the electric field vector, V/m:

$$\oint_l E dl = - \frac{d}{dt} \int_s B dS \quad (1)$$

This equation is used to determine the instantaneous value of the magnetic field vector, A/m:

$$\oint_l H dl = -\frac{d}{dt} \int_s D dS \quad (2)$$

Using this equality, we determine the instantaneous value of the electric induction vector, C/m<sup>2</sup>:

$$\oint_s D dS = 0 \quad (3)$$

The equation is used to determine the instantaneous value of the magnetic induction vector, Tl:

$$\oint_s B dS = 0 \quad (4)$$

All values are functions of the spatial coordinate  $r$  and time  $t$ . Equations (1 - 4) are equations of macroscopic electrodynamics [8].

The system (1–4) is not closed, since it is a system of 8 scalar equations for 16 scalar quantities [9], if we move from vector quantities to their components in any coordinate system. To close this system, the material equations are postulated:

$$D = \varepsilon_a E, \quad (5)$$

$$B = \mu_a H \quad (6)$$

where  $\varepsilon_a$  is the absolute permittivity of the medium, F/m [10];

$\mu_a$  is the absolute magnetic permeability of the medium, H/m [11].

Thus, when organizing field studies in the city of Kurchatov, which are supported by analytical calculations, the following data were obtained (Table 1) (Fig. 2).

This and the following graph shows the dependence of the voltage of the electric (magnetic) field on the point of the power line located between the two supports [12] (Fig. 3).

As a result of the experiment, based on both graphs presented, it is possible to draw a logical conclusion about the amplification of the electric and magnetic fields in the middle of the span ( $L/2$ ), since it is at this point that the transmission line has the greatest slack in relation to the two supports and is located at the closest distance to the antenna receiver of the electric field voltage measuring device, which is located at a distance of 1.75 m above ground level [13]. The reverse output follows at the points of the first ( $L = 0$ ) and the next supports ( $L$ ): the conductor is located at the maximum distance from the antenna, and therefore the sensor fixes the minimum value of the measured value. At the intermediate points, the values are approximately in the accepted ratio between the value calculated at the beginning of the support ( $L$



**Table 1** Electromagnetic field along the span of the route. A table with the measured magnetic field strength (H) and electric field strength (E), with the distance (L) between two supports of high-voltage power lines, obtained from the results of a full-scale survey of the line in the city of Kurchatov using the industrial frequency field strength meter PZ-50

The distance between the two poles of the power line	Power line 115 kV		Power line 345 kV		Power line 495 kV	
	E, kV/m	H, A/m	E, kV/m	H, A/m	E, kV/m	H, A/m
0	0,49	0,29	1,17	0,70	3,27	1,91
1/4L	1,14	0,66	2,80	1,63	5,31	3,11
1/2L	1,95	1,13	4,30	2,52	7,44	4,38
3/4L	1,15	0,66	2,81	1,63	5,28	3,10
L	0,50	0,29	1,18	0,69	3,24	1,90

Note L is the distance between the supports

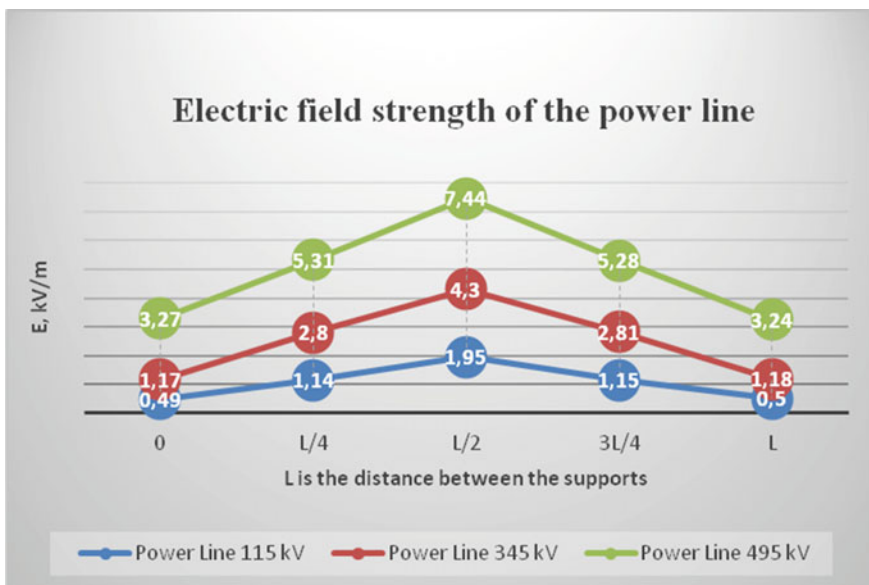


**Fig. 2** Electric field strength along a high-voltage power line

= 0) and the middle of the conductor between the two supports (L/2). Both graphs tend to adopt the function of a parabola [14].

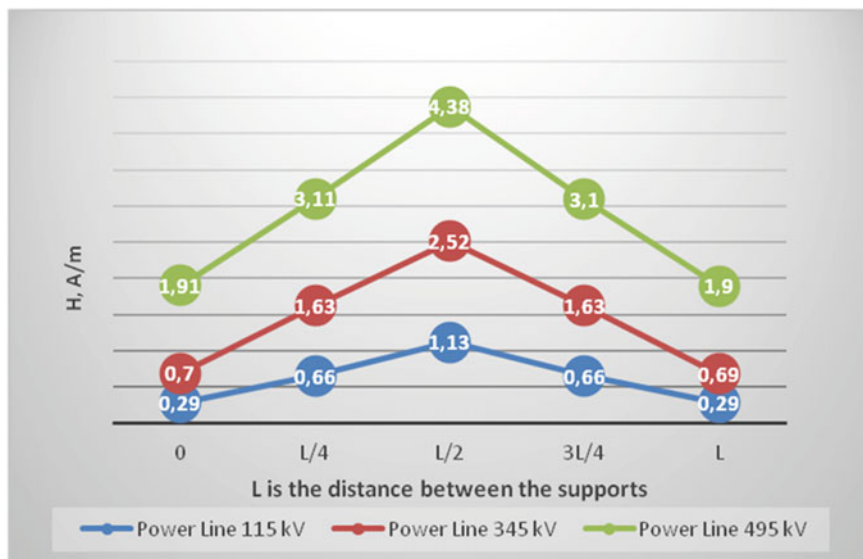


Fig. 3 Magnetic field strength along a high-voltage power transmission line

## 4 Conclusion

As a result of the conducted research, it was found that the level of electromagnetic radiation is a function of the nominal value of their voltage: with increasing voltage, the values of the electric and magnetic field intensity increase. It should be noted that with the linear route of the power line, the electric and magnetic components reach the highest values at the points of projection of the extreme wire to the ground, and the greatest amount of tension is observed at the point of maximum sagging of the wires, i.e. in the middle of the span [15].

The maximum permissible level of electric field intensity for the population is 0.5 kV/m, for residential areas—1 kV/m. According to the measurements carried out, it was revealed that at the border of the established sanitary protection zones of the city of Kurchatov [16], the level of electric field intensity does not exceed the maximum permissible value for a residential development zone.

Based on the conducted experiment, it was found that the existing method of measuring electromagnetic fields of power lines, according to which, in order to determine the rms value of the electric (magnetic) field strength, measurements must be carried out at a selected point in the projection space of the electric (magnetic) field intensity vector on three mutually orthogonal axes, can be simplified.

The lines of force of the electric field of the power line extend parallel to the wires of the power line, the lines of force of the magnetic field—perpendicular to the wires.

The values of the electric and magnetic field strength obtained by measurements differ from the corresponding values obtained by analytical techniques by no more than 1.4% [17].

**Acknowledgements** The work was carried out on the basis of South-West State University to participate in “Modern Problem in Construction: Setting Tasks and Ways to Solve Them” (MPC-2022) Topic of research work: Section 6. Environmental Engineering and sustainability.

## References

1. Sedykh VA, Savich VI, Balabko PN (2013) Soil-ecological monitoring. RGAU-MSHA im. K. A. Timiryazev. M.: RGAU-MSHA them. K. A. Timiryazeva. ISBN 978-5-9238-0164-4
2. Rodionov VG (2010) Problems of traditional energy. Energy: problems of the present and opportunities for the future. M.: ENAS. ISBN 978-5-4248-0002-3
3. Zoriy P, Dederichs H, Pillath J, Heuel-Fabianek B, Hill P, Lennartz R (2016) Long-Term measurements of the radiation exposure of the inhabitants of radioactively contaminated regions of Belarus—The Korma Report II (1998— 2015). Verlag Forschungszentrum Jülich, ISBN 978-3-95806-181-1
4. Arutyunyan RV, Bolshov LA, Borovoy AA, Velikhov EP (2018) System analysis of the causes and consequences of the accident at the Fukushima-1 nuclear power plant. Inst. M. : IBRAE RAN. ISBN 978-5-9907220-5-7
5. Bates RL (2019) Geology of non-metallic minerals. ISBN 978-5-458-48180-9
6. Sivukhin DC (2004) General course of physics. The textbook. benefit: For universities, 5t, T. III. Electrichestvo, 4th ed., stereot. M.: FIZMATLIT Publishing MIPT
7. Karipidis K, Mate R, Urban D et al. (2021) 5G mobile networks and health—a state-of-the-science review of the research into low-level RF fields above 6 GHz: J Expo Sci & Environ Epidemiol 31, 585–605 (2021). doi:<https://doi.org/10.1038/s41370-021-00297-6>.
8. Bakshi KA, Bakshi AV, Bakshi UA (2008) Electronic measurement systems, pp 4–14. US: Tech Publ. ISBN 978-81-8431-206-5
9. Olifer VG, Olifer NA (2010) Chapter 13. Switched Ethernet networks. Computer networks. Principles, technologies, protocols. 4th ed. St. Petersburg: Piter. ISBN 978-5-49807-389-7
10. McLaren, Peter G (1984) Elementary electric power and machines. Ellis Horwood, pp 182–183, ISBN 0-85312-269-5
11. Wood A, Mate R, Karipidis K (2021) Meta-analysis of in vitro and in vivo studies of the biological effects of low-level millimetre waves. J Expo Sci Environ Epidemiology 31:606–613. <https://doi.org/10.1038/s41370-021-00307-7>
12. Kudryashov YuB, Perov YuF, Rubin AB (2008) Biophysics: radiofrequency and microwave electromagnetic waves. Textbook for universities. M.: FIZMATLIT. ISBN 978-5-9221-0848-5
13. Cachada A, Rocha-Santos T, Duarte AC (2017) Chapter 1: Soil and pollution: an introduction to the main issues. soil pollution: from monitoring to remediation. academic press. pp 1–28. ISBN 9780128498729
14. Astafiev VN, Gogenko CA (2014) The levels of electromagnetic radiation produced by mobile phones and other portable transmitting devices. Aktual Probl Transp Med 1(35):46–57
15. Kharlov NN (2007) Electromagnetic compatibility in power generation: a training manual. Publishing house of TPU, Tomsk

16. Eremin NI (2007) Non-metallic minerals. 2nd. M.: MSU, Akademkniga. ISBN 978-5-211-05370-0
17. Yang D, Cai J, Hull V, Wang K, Tsang YP, Liu J (2016) New road for telecoupling global prosperity and ecological sustainability. *Ecosyst Health Sustain* 2(10):11879051. <https://doi.org/10.1002/ehs2.1242>

# Deflections and Free Vibrations of Circular Isotropic Plates of Thickness Varying in Accordance with a Parabola



Andrey Turkov , Kirill Marfin , Elena Finadeeva ,  
and Sergey Poleshko 

**Abstract** The paper considers the relationship between the dynamic and static parameters of circular isotropic plates under various boundary conditions. The studies of the plates were carried out under static and dynamic loading, taking into account the variability of the thickness. The authors established the relationship between the maximum deflection and the natural frequencies of the transverse vibrations of the plates, and assessed the matching of the coefficient  $K$  obtained by numerical studies with its analytical one. The curves for the frequencies of free vibrations and deflections under the static load and the change in the coefficient  $K$  depending on the thickness of the plate and boundary conditions were plotted. Studies showed that the coefficient  $K$  complies within 5% of the dependence of Professor V.I. Korobko only when the ratio of the thickness in the center to the thickness on the support  $t_2/t_1 = 60/50 < 1.2$  for both support schemes. This is due to the fact that formula (16) was derived for isotropic plates with constant thickness and the distribution of mass evenly over the entire area of the plate leads to a significant error already at the stage of a small difference between the thicknesses at the support and in the center. With a thickness ratio  $t_2/t_1 = 100/50 = 2$ , the difference between the  $K$  coefficient and the analytical one is about 16%.

**Keywords** Circular plate · Boundary conditions · Frequency of free transverse vibrations · Maximum deflection

---

A. Turkov (✉)  
The Southwest State University, 94, 50 Let Oktyabrya Ul., Kursk 305040, Russia  
e-mail: [aturkov@bk.ru](mailto:aturkov@bk.ru)

K. Marfin · E. Finadeeva · S. Poleshko  
Orel State University Named After I.S. Turgenev, 95, Komsomolskaya Ul., Orel 302026, Russia

## 1 Introduction

A large number of works are devoted to the calculation of solid and composite plates [1–9]. This article presents the study of the coefficient  $K$ , which express the relation between the frequencies of natural vibrations and the maximum deflections of the plates.

The determination of static and dynamic characteristics leads to determining the deflections [10–15] and frequencies of system vibrations [16–19] in solving the relevant differential equations. The functional relationship between the maximum deflection and the frequency of the fundamental mode of free transverse vibrations of elastic isotropic plates was proved by V. I. Korobko [5].

## 2 Materials and Methods

The differential equation of the plate transverse deflection has the form:

$$\frac{\partial^4 W}{\partial x^4} + 2 \frac{\partial^4 W}{\partial x^2 \partial y^2} + \frac{\partial^4 W}{\partial y^4} = \frac{q}{D} \quad (1)$$

With the use of biharmonic operators, the equation takes the form:

$$D \nabla^2 \nabla^2 W = \frac{q}{D}. \quad (2)$$

where  $W = W(x, y)$  is the deflection function of the plate at the transverse deflection;  $\nabla^2 \nabla^2 \nabla^2 \nabla^2$ —is a biharmonic operator;  $D = EH^3/(12(1 - \nu^2))$  is cylindrical stiffness of the plate;

$q(x, y)$  is the law of the lateral load change.

The differential equation of plate free vibrations:

$$D \left( \frac{\partial^4 W}{\partial x^4} + 2 \frac{\partial^4 W}{\partial x^2 \partial y^2} + \frac{\partial^4 W}{\partial y^4} \right) + m \frac{\partial^2 W}{\partial t^2} = 0 \quad (3)$$

$$D \nabla^2 \nabla^2 W + m \frac{\partial^2 W}{\partial t^2} = 0. \quad (4)$$

where  $W = W(x, y, t)$  is the deflection function of a freely oscillating plate;  $m$  is the mass per unit area of the plate;  $E, \nu$  are respectively the modulus of elasticity of the material and the Poisson's ratio.

If the vibrations are harmonic

$$W = W(x, y) \cdot \cos(\omega t), \quad (5)$$

then Eq. (1) can be transformed to the following form:

$$D\nabla^2\nabla^2W - m\omega^2W = 0$$

or

$$D\nabla^2\nabla^2W - \beta^2W = 0,$$

where  $\beta^2 = m\omega^2/D$  is the eigenvalue of the differential equation of vibrations of the plates.

Let us represent the deflection function as a product of the maximum deflection  $W_0$  by the unit function  $f(x, y)$  and substitute it in the differential equations of transverse deflection and free vibrations of the plates:

$$W(x, y) = W_0f(x, y) \tag{6}$$

$$\begin{cases} D\nabla^2\nabla^2f - m\omega^2f = 0 \\ DW_0\nabla^2\nabla^2f - q(x, y) = 0 \end{cases}$$

It should be noted that the precise solution of these differential equations is valid only in the frequent cases of plate forms and boundary conditions. Therefore, in practice, approximate methods of solution are mainly used.

If we assume that the plate is under a uniformly distributed load  $q$ , then having integrated Eq. (6) over the entire area of the region, and having performed the necessary transformations, we will get:

$$W_0 = \frac{q}{D} \frac{A}{\iint_A \nabla^2\nabla^2f dA}, \quad \omega^2 = \frac{D}{m} \frac{\iint_A \nabla^2\nabla^2f dA}{\iint_A f dA}. \tag{7}$$

The deflection function  $W(x, y)$  can approximately be put down in a one-parameter form in the polar coordinate system:

$$W(x, y) = W_0f(x, y) = W_0g\left[\frac{t}{r(\phi)}\right] = W_0g(\rho) \tag{8}$$

where  $r = r(\varphi)$  is the equation of the contour of the plate in the polar coordinate system,  $t$  and  $\varphi$  are polar coordinates,  $\rho = t/r(\varphi)$  is the dimensionless polar coordinate.

This function describes a surface which level lines are similar to the region contour and are similarly located. The representation of the function of deflections in this form is justified by the fact that through it we can write down the exact solution to the problem of transverse deflection of a rigidly pinched elliptical plate under the action of a uniformly distributed load. Since just in a single case it is possible to

represent the real deflection function in the form of a one-parameter function (8), further results are of an approximate nature.

We transform the integrals in (7), taking into account the deflection function in form (8).

$$\iint_A f dA = \int_0^{2\pi} \int_0^r g(\rho) t dt d\phi. \tag{9}$$

Multiplying and dividing the right-hand side by  $r^2$ , we get after the transformations:

$$\iint_A f dA = 2A \int_0^1 g(\rho) \rho d\rho. \tag{10}$$

Completing the transformation of the integral of the biharmonic operator according to, we finally write:

$$I = (K_f^2 \Phi_{g1} + K_f \Phi_{g2})/A = K_f (K_f \Phi_{g1} + \Phi_{g2})/A \tag{11}$$

where

$$\begin{aligned} \Phi_{g1} &= \frac{1}{2} \int_0^1 (g^{IV} \rho - 12g''' - 21g'' \rho^{-1} - 3g' \rho^{-2}) d\rho, \\ \Phi_{g2} &= \frac{\pi}{2} \int_0^1 (2g^{IV} \rho + 14g''' + 22g'' \rho^{-1} + 3g' \rho^{-2}) d\rho, \end{aligned} \tag{12}$$

The sign of the approximate equality in (11) appeared under the transformation of integrals by means of the Bunyakovsky inequality. We substitute integrals (9) and (11) into expressions (6). After the necessary transformations, we get:

$$\left\{ \begin{aligned} W_0 &\approx \frac{qA^2}{D} \frac{1}{K_f^2 \Phi_{g1} + K_f \Phi_{g2}}, \\ \omega^2 &\approx \frac{D}{2A^2 m} \frac{K_f^2 \Phi_{g1} + K_f \Phi_{g2}}{\int_0^1 g \rho d\rho} \end{aligned} \right. \tag{13}$$

Since all the values of the definite integrals occurring in the expressions (13) are constant numbers depending on the accuracy of the choice of function  $g(\rho)$ , they can be represented as the proportionality coefficients  $K_w, K_\omega$  and  $B$ . Then



$$W_0 = K_w \frac{q}{D} \frac{A^2}{K_f^2 + BK_f}, \quad \omega^2 = K_\omega \frac{D}{m} \frac{K_f^2 + BK_f}{A^2}. \quad (14)$$

where

$$K_w = 1/\Phi_{g1}; \quad K_\omega = \frac{1}{2}\Phi_{g1} \int_0^1 g\rho d\rho; \quad B = \Phi_{g2}/\Phi_{g1}. \quad (15)$$

Strictly speaking, the signs of approximate equalities should be put in expressions (14), in view of (12) and the approximation of function  $g(\rho)$ .

Let us multiply the expressions (14) to each other:

$$W_0\omega^2 = K_w K_\omega \frac{q}{m} = K \frac{q}{m}. \quad (16)$$

Taking into account that the coefficients  $K_w$  and  $K_\omega$  depend on the shape of the plate, the following regularity can be obtained from the expression (16): for elastic isotropic plates of identical shapes with homogeneous boundary conditions, the product of the maximum deflection  $W_0$  from the action of the uniformly distributed load  $q$  per square of their fundamental frequency of transverse vibrations in the unloaded state,  $\omega^2$  with accuracy up to the dimensional factor  $q/m$  is a constant. Thus, it is mathematically and rigorously proved that for the whole set of plates with homogeneous boundary conditions the product  $W_0 \cdot \omega^2$  will be represented by a single curve. An important feature of the formulated regularity is the fact that the product  $W_0 \cdot \omega^2$ , which is considered in it, does not depend on the flexural rigidity and dimensions of constructions.

The design structure is a circular isotropic plate, the thickness of which varies in accordance with a parabola (Fig. 1). The thickness of the plate on the support is 5 cm, the thickness in the span varies according to the parabola with maximum value at the middle:

$$t = 5 + k \cdot x^{\frac{1}{2}} (\text{cm}). \quad (17)$$

Numerical studies of the plates were carried out by the finite element method. The design schemes of composite plates are shown in Fig. 2. When calculating the plates, two support schemes were investigated: rigid pinching along the contour (Fig. 2a) and hinged support along the contour (Fig. 2b).

The plate with a diameter of 6 m is divided into 240 finite elements—24 elements in the annular direction and 10 finite elements in the radial direction (Fig. 1). The thickness of the plate on the support was taken constant 0.05 m; the thickness in the center was a variable parameter and varied from 0.05 m (plate of constant thickness) to 0.10 m with a step of 0.005 m. The plate was taken from steel of ordinary quality, volumetric weight  $78.5 \text{ kN} / \text{m}^3$ . The modulus of elasticity is taken as  $E = 2.06$

**Fig. 1** Circular plate with a linearly variable thickness (a—finite element scheme; b—plate thickness)

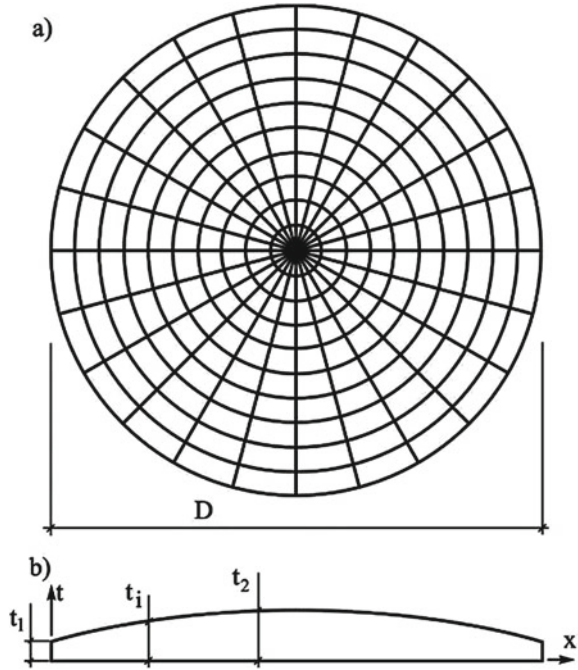
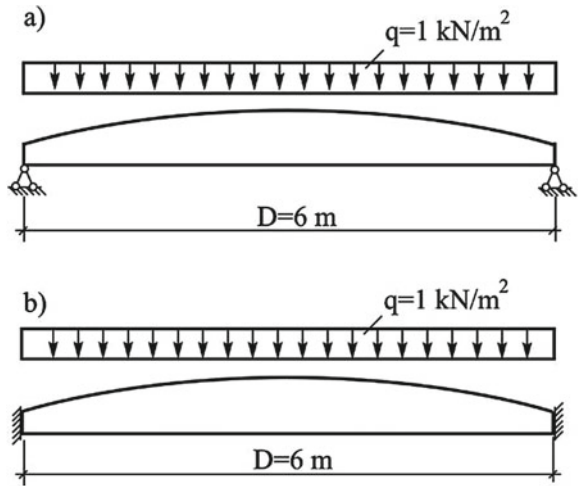


**Fig. 2** Design diagrams of plates (a—with hinged support along the contour; b—with pinching along the contour)



·10<sup>5</sup> MPa according to the Building Code of Russian Federation SP 16.13330.2017 “Steel structures”. All studies were carried out under the assumption of the elastic work of the material. Uniformly distributed load was assumed to be  $q = 1 \text{ kN/m}^2$  (Fig. 2). The support was carried out along the contour in the contour nodes of the plates. Two support schemes were provided—hinged support and fixing along the

contour. To determine the natural frequencies of the transverse vibrations of the plates, concentrated masses from the empty weight of the plate were applied to the structural nodes in accordance with the load area of the nodes.

### 3 Results and Discussion

Determination of vibration and deflection frequencies was carried out using the SCAD software package [20]. The results of numerical studies of the plate are shown in Tables 1 and 2.

According to the data of Tables 1 and 2, graphs of changes in the maximum deflections and vibration frequencies in the studied plates and the proportionality coefficient  $K$  are plotted. The deviation of the actual value of the coefficient  $K$  from the theoretical one was determined by the formula:

$$\Delta = \frac{K_{theor} - K}{K_{theor}} \cdot 100\% \tag{18}$$

Based on the results of the research, curves for the frequency of natural oscillations (Fig. 3), maximum deflections (Fig. 4) and the  $K$  coefficient (Fig. 5) are plotted.

**Table 1** Results of numerical studies of a circular plate, the thickness of which varies in accordance with a parabola,  $D = 6$  m with hinged support

$t_1$ (mm)	$t_2$ (mm)	Circular frequency of fundamental tone, $\omega$ (s <sup>-1</sup> )	Maximum deflection, $W_0$ (mm)	$K = W_0\omega^2 / (q/m)$	$K = W_0\omega^2 / (q/m)$ based on analytical $W_0$ and $\omega$	Deviation of $K$ from $K_{theor}$ . %
50	50	42.52237	21.8409	1.581	1.579	-0.11
50	55	45.19654	17.9303	1.542		2.35
50	60	47.88706	14.8697	1.507		4.58
50	65	50.56988	12.4814	1.477		6.45
50	70	53.25339	10.5797	1.451		8.10
50	75	55.93603	9.0470	1.428		9.55
50	80	58.61656	7.7981	1.408		10.84
50	85	61.29428	6.7700	1.390		12.00
50	90	63.96914	5.9159	1.373		13.04
50	95	66.64001	5.2006	1.358		13.99
50	100	69.30723	4.5969	1.345	14.84	

**Table 2** Results of numerical studies of a circular plate plate, the thickness of which varies in accordance with a parabola,  $d = 6$  m when pinched along the contour

$t_1$ (mm)	$t_2$ (mm)	Circular frequency of fundamental tone, $\omega$ ( $s^{-1}$ )	Maximum deflection, $W_0$ (mm)	$K = W_0\omega^2/(q/m)$	$K = W_0w^2/(q/m)$ based on analytical $W_0$ and $\omega$	Deviation of $K$ from $K_{theor.}$ %
50	50	89.80446	5.1396	1.658	1.629	-1.81
50	55	93.04019	4.4117	1.608		1.30
50	60	96.26179	3.8158	1.562		4.09
50	65	99.4389	3.3322	1.525		6.40
50	70	102.5884	2.9315	1.492		8.40
50	75	105.7178	2.5957	1.464		10.15
50	80	108.8287	2.3116	1.438		11.70
50	85	111.9266	2.0693	1.416		13.06
50	90	115.014	1.8609	1.396		14.29
50	95	118.0914	1.6806	1.378		15.39
50	100	121.1638	1.5235	1.362	16.39	

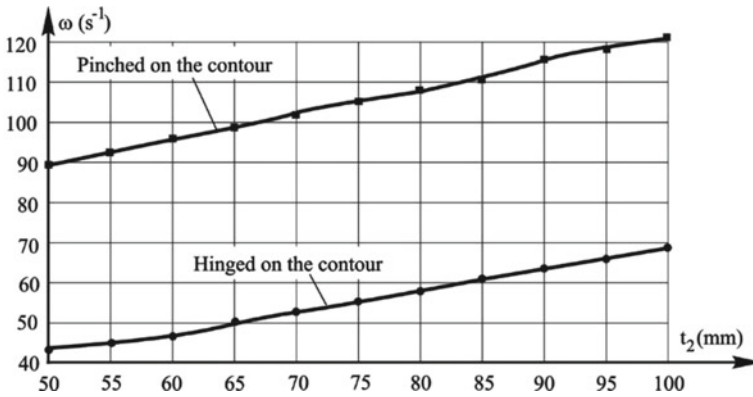


**Fig. 3** Change in free vibration frequencies depending on the thickness of the plate  $t_2$  in the center

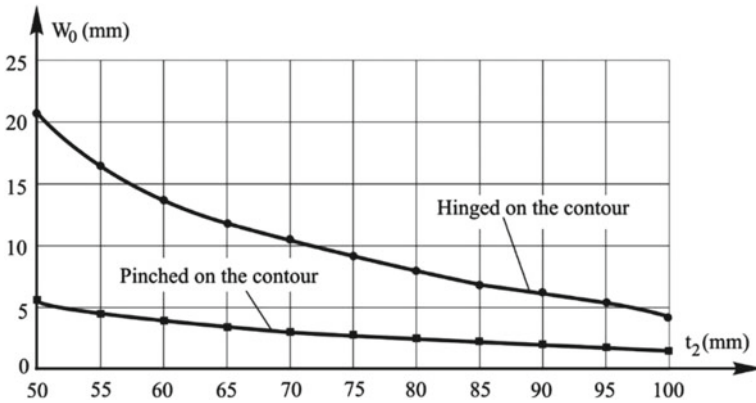


Fig. 4 Change in deflections by static load depending on the thickness of the plate  $t_2$  in the center

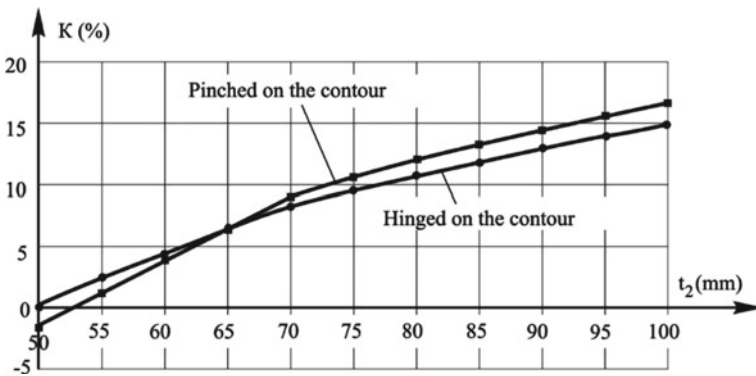


Fig. 5 Change in coefficient  $K$  depending on the thickness of the plate  $t_2$  in the center

### 4 Conclusion

As a result of numerical studies, the maximum deflections and free vibration frequencies were determined for circular isotropic plates with a thickness varying in accordance with parabola with a thickening in the center. Studies showed that the coefficient  $K$  matches within 5% of the dependence of Professor V.I. Korobko only for the ratio of the thickness in the center to the thickness on the support  $t_2 / t_1 = 60/50 < 1.2$  for both support schemes. This is due to the fact that formula (16) was derived for isotropic plates with constant thickness and the distribution of mass evenly over the entire area of the plate. This leads to a significant error already at the stage of a small difference between the thicknesses at the support and in the center. With a thickness ratio  $t_2 / t_1 = 100/50 = 2$ , the difference between the  $K$  coefficient and the analytical one is about 16%, and it should be expected that the difference will increase with increasing plate thickness in the center.

## References

1. Rzhnitsyn, Calculation of composite plates with absolutely tight cross couplings. Researches on the theory of constructions, issue XXII (Stroyizdat, Moscow, 1976)
2. Rzhnitsyn, Composite rods and plates (Stroyizdat, Moscow, 1986)
3. Kalmanok, Structural mechanics of plates (Mashstroyizdat, Moscow, 1950)
4. N. Shaposhnikov, Calculation of plates on a bend according to the finite-element method (Works of MITE, 1968)
5. Korobko V (1989) Journal construction and architecture 11:32–36
6. Korobko A, Chernyaev, Shlyakhov S (2016) Building and reconstruction 4, 19-29
7. Korobko A, Chernyaev, Shlyakhov S (2017) Building and reconstruction 1, 39-49
8. Korobko, Savin S (201) Building and reconstruction 5, 29–34
9. Korobko, Savin S (2013) Building and reconstruction 5, 13–18
10. Korobko V, Savin SY, Filatova SA (2016) Determination of stiffness and fundamental frequency of oscillations of fixed circuit plates, Izv Vyss Uchebnykh Zaved Seriya Teknol Tekst Promyshlennosti 3, 290–295
11. Korobko VI et al (2015) Determination of maximum deflection at cross bending parallelogram plates using conformal radius ratio interpolation technique. J Serbian Soc Comput Mech 9(1):36–45
12. Korobko VI et al (2016) Solving the transverse bending problem of thin elastic orthotropic plates with form factor interpolation method. J Serbian Soc Comput Mech 10(2):9–17
13. Hsueh H, Luttrell CR, Becher PF (2006) Modelling of bonded multilayered disks subjected to biaxial flexure tests, Int J Solids Struct 43, 20, 6014–6025 <https://doi.org/10.1016/j.ijsolstr.2005.07.020>
14. Wu K-C, Hsiao P-S (2015) An exact solution for an anisotropic plate with an elliptic hole under arbitrary remote uniform moments. Compos B Eng 75:281–287. <https://doi.org/10.1016/j.compositesb.2015.02.003>
15. Gohari S et al (2021) A new analytical solution for elastic flexure of thick multi-layered composite hybrid plates resting on Winkler elastic foundation in air and water. Ocean Eng 235:109372. <https://doi.org/10.1016/j.oceaneng.2021.109372>
16. Bharati RB, Mahato PK, Filippi M, Carrera E (2021) Flutter analysis of rotary laminated composite structures using higher-order kinematics. Composites Part C: Open Access 4:100100. <https://doi.org/10.1016/j.jcomc.2020.100100>
17. Perel VY, Palazotto AN (2003) Dynamic geometrically nonlinear analysis of transversely compressible sandwich plates, Int J Non-Linear Mech 38, 3, 337–356 [https://doi.org/10.1016/S0020-7462\(01\)00065-8](https://doi.org/10.1016/S0020-7462(01)00065-8)
18. Rao BN, Pillai SRR (1992) Large-amplitude free vibrations of laminated anisotropic thin plates based on harmonic balance method, J Sound Vib 154, 1, 173–177 [https://doi.org/10.1016/0022-460X\(92\)90411-P](https://doi.org/10.1016/0022-460X(92)90411-P)
19. Wang Z, Yu Xing (2021) An extended separation-of-variable method for free vibrations of orthotropic rectangular thin plate assemblies. Thin-Walled Structures 169, 108491 <https://doi.org/10.1016/j.tws.2021.108491>
20. Semenov, Gabitov F (2015) The SCAD project computer system in educational process (ASV publishing house, Moscow)

# The Use of GIS Systems as a Decision-Making Tool for the Placement of Urban Development Objects



Yana Zolotukhina , Ekaterina Prokshits , Olga Sotnikova ,  
and Vladislav Pozdnyakov 

**Abstract** One of the complex and difficult to formalize multi-criteria tasks when placing objects in an urban environment is making decisions about their placement, it is advisable to use scientific methods of system analysis and decision theory to solve it. Due to the large amount of open and accessible information for the analysis and active development of geoinformation systems, it became possible to use this information to solve various urban planning tasks when placing objects of any purpose, from residential to industrial facilities and organizing information support for decision-making when placing these objects. An urgent task for the authorities and self-government currently in the field of urban planning is the development of tools and methods that are based on information processing and that can be implemented as part of a decision support system.

**Keywords** Decision-making · Urban development objects · GIS systems · System analysis · Urban planning restrictions · Urban environment · Information processing

---

Y. Zolotukhina (✉) · E. Prokshits · O. Sotnikova  
Voronezh State Technical University, 20 Letiya Oktyabrya Ul., 84, 394006 Voronezh, Russia  
e-mail: [yana\\_zolotuhiny@mail.ru](mailto:yana_zolotuhiny@mail.ru)

E. Prokshits  
e-mail: [e.prokshits@mail.ru](mailto:e.prokshits@mail.ru)

O. Sotnikova  
e-mail: [hundred@vgasu.vrn.ru](mailto:hundred@vgasu.vrn.ru)

V. Pozdnyakov  
Southwest State University, 94, 50 Let Oktyabrya Ul., Kursk 305040, Russia  
e-mail: [blanderbot2003@mail.ru](mailto:blanderbot2003@mail.ru)

## 1 Introduction

Inefficiently used territories (degraded) or depressive appeared on the master plans of a large number of cities. Several zones in this category are highlighted on the interactive map of Voronezh:

- industrial zones defined for renovation;
- inefficiently used land plots;
- land plots in areas of dilapidated individual and low-rise buildings.

The sites of new housing construction are also singled out separately, large territories of the central part of the city that previously belonged to enterprises are transferred to the housing stock every year, which thereby creates a re-consolidation of the territory with an already poorly developed infrastructure. The degraded territories of the city of Voronezh are currently shown in Fig. 1.

It is possible to notice the trend of the decline of giant factories and the growth of the number of private new manufacturing firms in their place [1, 2]. New shopping malls and residential complexes are being built on the site of old industrial enterprises,

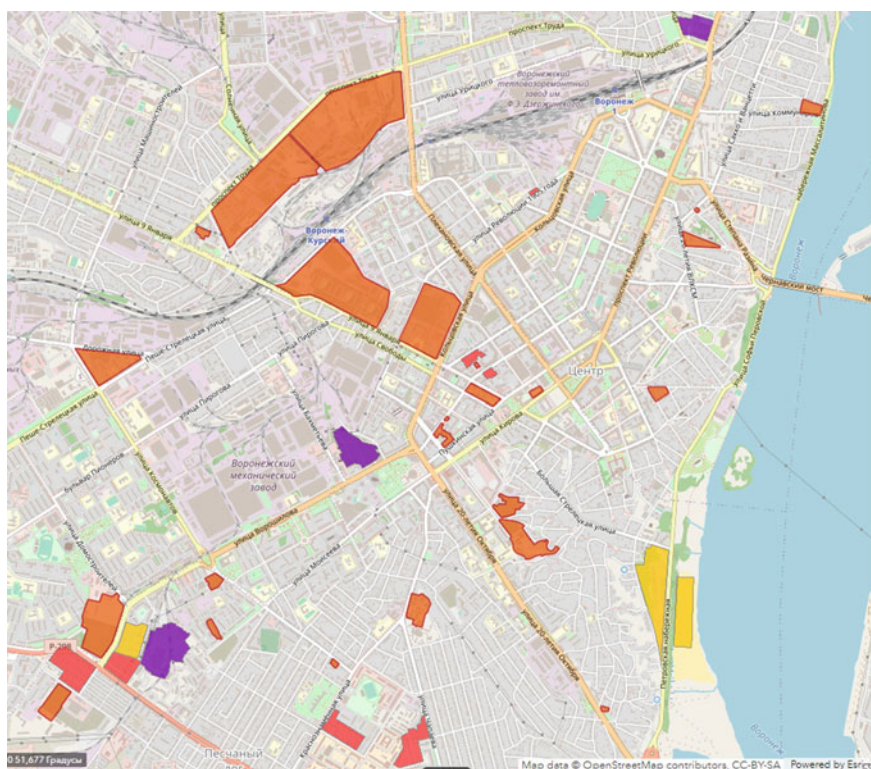


**Fig. 1** Degraded territories of the city of Voronezh (present)



which requires further systematic approach and development at the level of urban planning. Voronezh industrial facilities in the 2019 master plan are shown in Fig. 2.

Historical analysis shows that the growth of depressive territories is directly related and directly proportional to the past time due to the reasons of the economic downturn during the “perestroika”, the end of the service life of a large number of buildings within the city, the lack of a systematic approach in urban planning and design [3] (Table 1).

The need to manage land resources in the emerging socio-economic conditions requires a wide application of the principles of formation and organization of research and design work, as well as the creation of a unified information field in the land management industry [4].



Fig. 2 Voronezh industrial facilities on the 2019 master plan

**Table 1** Technical and economic indicators of Voronezh master plans of different periods

№ п/п	Indicators	Unit of measurement	Status on		Projected calculated indicators for
			2013	2020	2026
1	The total land area of the Voronezh city district	ha	59899.9	59948.93	59948.93
		%	100.0	100.0	100.0
2	Population size	thousands of people.	1003.6	1058.5	1327.6
3	Residential area	ha	12571.3	13374.03	13067.78
		%	21.0	22.4	21.9
4	Production area	ha	5235.9	4220.79	4209.05
		%	8.7	7.1	6.7
5	Area of green areas of common use	ha	706.6	703.77	703.48
		%	1.17	1.2	1.2

The use of a systematic approach and methods in scientific research, the development of mathematical cartography, computer technology and computing technologies, all this determines the development of modern land management and urban planning.

Tasks in the field of geoinformation are not limited only to cartographic research, but go far beyond its scope, thereby it becomes the basis for the integration of various fields and knowledge for the study of more complex systems. And the symbiosis of the acquired knowledge, information and data should be transformed into high-quality cartographic material [5, 6].

## 2 Materials and Methods

To select the most optimal option for the work, a comparative analysis of geoinformation systems was performed, 3 programs were considered: ArcGIS, MapInfo and InGEO. The most suitable for the purpose of the work was the ArcGIS program (Table 2).

The most optimal method for choosing a territory for placing objects in the city is the zoning method, since it assumes the presence of zones for various purposes that are built up by existing objects, this method is based on the division of the territory into polygonal plots, taking into account certain criteria and restrictions set for each case [7]. The task of constructing a zoning model with specified criteria and restrictions in geoinformation systems is the creation of layers of polygonal objects, each of which has a value or a range of values assigned depending on the specified criterion [8, 9].

**Table 2** Comparative analysis of geoinformation systems

Criteria	ArcGIS	MapInfo	InGEO
Ease of creating a custom coordinate system	–	+	–
Ability to project data	+	+	+
The function of converting the designation of the coordinates of the fields	+	+	+
Definition of projection	+	–	–
The ability to create a custom geographical transformation	+	–	+
Country of origin	USA	USA	Russia

To solve zoning problems in geoinformation systems, a large number of basic spatial analysis methods can be found, which in addition must be embedded in DSS in the form of complex procedures that are configured in a certain way to solve specific application problems using a specific data set. A description of such methods can be found in the ArcGIS program, which perfectly implements algorithms suitable for modeling development zones, these basic zoning methods include:

- dissolve–zoning using vector models of geographical objects by merging by attribute;
- create thiessen polygons -zoning by creating Thiessen polygons;
- point density–zoning using raster models of geographical objects based on point density analysis.

The factors influencing the placement of industrial facilities when making decisions by the zoning method are:

- natural;
- socio-demographic;
- economic and geographical;
- urban planning.

The initial data for constructing a zoning model for the placement of an object in an urban environment are many sets of geographical objects represented on the map. These objects are represented on the map as a set of layers  $S$ . Layer  $s_i \in S$  defines the type of spatial localization of objects and the attribute vector  $A^s = \langle a_1^s, \dots \rangle$ . Each object  $e_n$  in the layer has its own unique identifier  $n$ , a set of coordinates  $G = \{x_1, y_1, \dots, x_n, y_n\}$  defining its location and shape, and a vector of attribute values  $A_n = \langle a_1^s, \dots \rangle$

$$E = \langle e_1..e_n \rangle \quad (1)$$

The task of constructing a zoning model can be represented as an algorithmically defined function

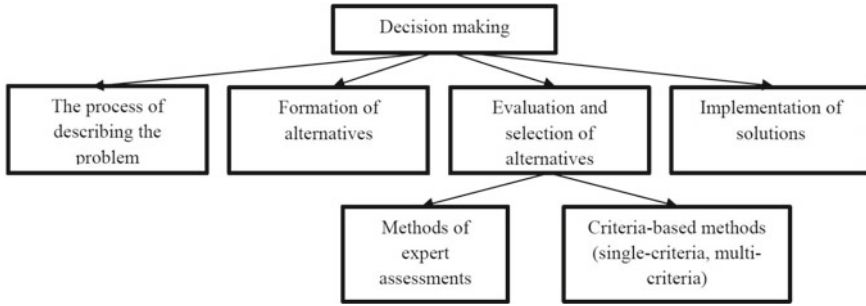


Fig. 3 Decision-making process

$$F(S') \rightarrow M, S' \in S. \quad (2)$$

The function  $F$  should implement two interrelated and non-trivial tasks:

1. Determination of the value of the  $a_i$  criterion for each polygon from  $M$  based on the  $S'$  data. This task is related to the summation of the indicators of the set of objects that are located in this zone under consideration, a common value is the integral over the area of the site for continuous quantities.
2. Defining the boundaries of all polygons in  $M$ .

Another indicator such as the remoteness of the zone from the source of the necessary resource is also not a simple and unambiguous task [10, 11]. In standard methods of analyzing the placement of an object, fixed points are usually specified, which are the centers of the areas of consumption of this energy resource, the method of determining the coordinates of these points is not specified, the Euclidean distances from the points to the source of the resource are indicated. Although in some cases in urban planning it is more logical to use a system of distances of city blocks, according to which the distance between two points is equal to the sum of the modules of the differences of their coordinates. Which shows the importance of an individual approach in choosing a method.

Based on everything described, a general decision support scheme based on zoning models was identified, shown in the Fig. 3.

The general scheme of decision support based on zoning models is shown in Fig. 4.

### 3 Results and Discussion

The method uses GIS spatial analysis tools to automatically evaluate all possible ways of connecting the land plots presented on the map to the electrical substations or power lines presented there. At the same time, the power declared for connection

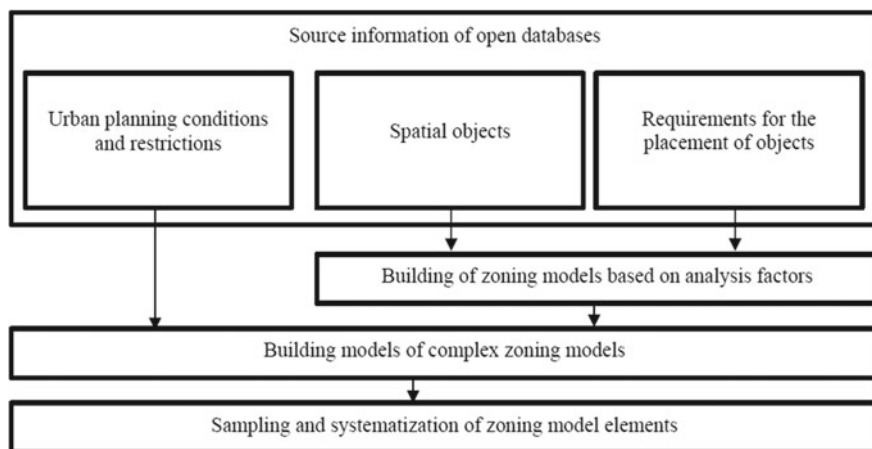


**Fig. 4** General scheme of decision support based on zoning models

and the values of the available power reserves at the facilities of the electric network are taken into account.

An example of the zoning method can be a map of the connection of objects to the electrical networks of the city of Voronezh. In this example, we consider the possibility of using these electrical substations with a voltage of 6–10 kV with an assessment of the possibilities of connecting to them. This method allows you to consider the possibility of connecting both via overhead power lines and by laying underground cables. Figure 5 shows a fragment of the map, which shows the green dots-electrical substations to which connection is possible, the red lines of the boundaries of the plots and the capital construction objects themselves. These objects are taken into account when predicting the length of the routes of cable power lines [12, 13].

Depending on the type of task, it is necessary to use a certain algorithm, for example, since the task of laying cable routes is an informal task, therefore, it cannot be solved automatically, but for a preliminary assessment of the amount of work, it is possible to use an algorithm for constructing shortest routes. To do this, routes are built on the raster model taking into account insurmountable obstacles, thereby allowing you to build routes taking into account existing buildings and structures. Objects are represented as a set of cells that are superimposed by a vector layer on the grid of the raster. In Fig. 6, yellow indicates objects with insurmountable obstacles around them (yellow and red cells) and green indicates a cable route.

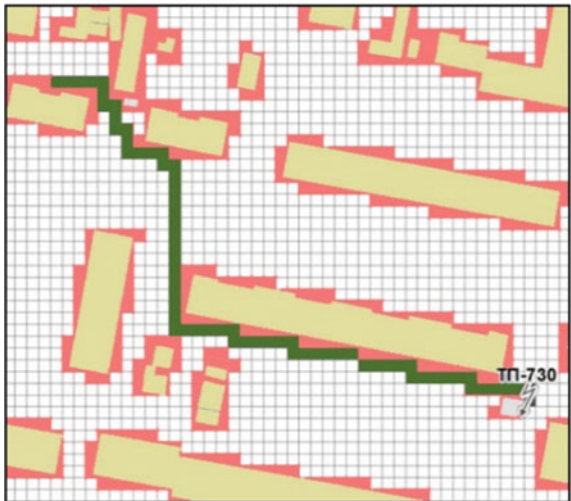
This method shows that the use of geoinformation systems justifies its use from a practical point of view and confirms its implementation option for further use of evaluation and decision-making on the placement of objects in urban infrastructure.

Trends in urban growth and expansion can be analyzed using GIS technologies and applied to the study of the suitability of urban spaces for the development of urban planning [14, 15]. To determine the areas suitable for urban growth, it is necessary to

**Fig. 5** Map of electrical substations and land plots



**Fig. 6** Example of a raster tracing algorithm



take into account some factors. Currently, GIS is a functional and accessible planning information system that increases the usability and functionality of the software. GIS finds its application in urban planning as an analytical and modeling tool. It can be applied to a wide range of tasks. GIS also helps to conduct a feasibility study of the object, for example, to determine whether the site is suitable for a specific functional building.

## 4 Conclusions

The versatility of this model will allow further analysis of various networks, the possibility of their connection, take into account the restrictions associated with the objects of site protection and many other criteria and restrictions, which in turn will provide information support for decision-making on the development of the infrastructure of the city as a whole. For example, it will be possible to determine the area of the city where there are difficulties with connecting to thermal or electrical networks, or there is no reserve of one of the key energy resources to support the city's vital activity, but there will be some other plus that will allow you to make an informed decision when placing objects.

Thus, this zoning technique is an element of the technology of spatial analysis of the territory and various systems located in these territories. The methodology will allow you to automatically obtain structural models of urban structures, which can then be used in the analysis of existing options for their further development. During the model-based analysis procedure, only information available in the public domain of urban planning documentation is used, which determines its use by various structural divisions of the city administration by persons involved in the development of urban development.

## References

1. Enin AE, Sheveljov VP, Stupak EV (2018) *Constr Reconstr* 4(78):64–75
2. Sepasian MN (2006) *IEEE Trans Power Syst* 21(2)
3. Sedghi M (2009) *Iran J Electr Electron Eng* 5(2)
4. Voropaj NI, Palamarchuk SI, Podkoval'nikov SV (2001) *Forecast Prob* 5:49–69
5. Lominogin AS (2006) *Manag Syst Inform Technol* 5:152–157
6. Denisov AR, Levin MG (2013) *Caspian J: Manag High Technol* 1(21):60–71
7. Kalinkina NA (2011) *Constr Reconstr* 2:53–56
8. Grosheva TI (2019) *Russ J Build Constr Architect* 4(44):103–120
9. Skryabin P, Sergeeva N (2020) *Architect Eng* 5(4):65–73
10. Lapshina KN, Bakaeva NV, Sotnikova OA (2017) *Int Sci Conf: Sustain Growth Small Open Econ* 1:143–146
11. Zavyalov AY, Maksimova SV, Mel'cova ES, Lorens PZ (2015) *Architecture and modern information technologies*, 2(31):2–5
12. Lacks R, Siepermann M (2009) *Comput Aided Chem Eng* 27:2115–2120
13. Dulesov AS, Prutovyh MA (2012) *Appl Comput Sci* 5(41):14–21
14. Szymański AI, Płaziak M (2014) *Procedia Soc Behav Sci* 110:381–389
15. Wang W, Zhao Q (2010) 2010 International conference on logistics systems and intelligent management (ICLSIM), vol 1, pp 212–215

# Substantiation of Criteria for Supported Decision-Making in Urban Zoning on the Basis of the Concept of Sustainable Development



Ekaterina Prokshits , Yana Zolotukhina , Olga Sotnikova ,  
and Olga Mischenko 

**Abstract** Currently, universities have a significant impact on the environment due to high energy consumption, intensive transport, large amounts of waste, high consumption of materials and intensive development of buildings and structures. The purpose of this study was to determine the key indicators for assessing the sustainable development of the university campus when choosing its spatial organization and functional planning. Sustainable development is the most important social problem. In recent years, many scientists have proposed to solve this problem on the basis of university communities, since they are leaders in the field of education, research and innovation. The different researches connected with questions of stability of territories of campus of that have been conducted as the universities can aim at creation of steady campuses. Options of interaction of the city with arrangement of functional zones of campus based on results of quantitative and quality expert standard have been revealed. Depending on the obtained data options of transformation of the university and its adjacent territory have been offered. The main advantages and shortcomings of each of options of the space organization are revealed. The road map on making decision for town-planning placement on the city of the innovation educational environment is created.

**Keywords** University campus · Sustainable campus · Sustainable development · The innovation educational environment · Functional zoning · Decision-making

---

E. Prokshits (✉) · Y. Zolotukhina · O. Sotnikova  
Voronezh State Technical University, 20 letiya Oktyabrya ul., 84, 394006 Voronezh, Russia  
e-mail: [e.prokshits@mail.ru](mailto:e.prokshits@mail.ru)

O. Mischenko  
Southwest State University, 94, 50 Let Oktyabrya ul., Kursk 305040, Russia



## 1 Introduction

In the conditions of global changes of the environment and climate interest in decrease in negative impact of anthropogenic load of the urban environment, including due to reduction of consumption of natural resources, ecologization, economy and rational territorial planning grows. Important role in achievement of goals of sustainable development is played by higher educational institutions. In recent years the role of the universities has sharply increased in achievement of goals of sustainable development and also the innovative development of the countries [1]. For decrease in negative environmental impact and optimization of environmental management at stage of planning of territories under campus it is necessary to distribute competently the areas according to required functionality and considering the purposes and problems of sustainable development.

Transformation of the system of Russian higher education is continued. In the next ten years in Russia it is going to construct not less than 30 world-class new university campuses [2].

The analysis of experiment of scientists and designers on creation of steady innovation campuses has allowed to allocate the main trajectories of development [3–7]. Creation of network of modern university campuses contributes to the development and improvement of certain territories of the city which is meant as increase in quantity of objects of service infrastructure and improvement of quality of the public spaces used by citizens daily [8].

Condition of infrastructure of the university—one of significant elements of its international competitiveness as making decision on the choice of the university by the Russian and foreign scientists, teachers and students depends including from it [9]. Further the last can find a job or create own business in the territory of Russia that can promote improvement of demographic and social and economic situation in the city and the region in general [3].

About growth of interest of the universities in questions of maintaining ecological, cultural and economic balance in the world shows creation of different associations of the universities, such as Association of advance of the ideas of sustainable development in the higher education (USA), Partnership of the higher education for sustainable development (Great Britain), etc. Now actively the initiative of the United Nations “Interaction with the academic circles” directed to cooperation increase in the field of observance and protection of human rights, access to education and sustainable development is implemented. In Russia in 2017 the Association of “green” higher education institutions has been created [5].

Territories of university complexes are important link of natural framework of the city in the modern urbanized environment [10].

Transformation of the universities represents global transition from the university as personnel agent for industrial production to the university as innovation corporation of creation and distribution of modern knowledge today, and it demands also absolutely new view on architectural and space decisions in creation of university campuses [11].

However it should be noted that criteria for support of decision-making process on the space organization of university territories and functional zoning of the innovation educational environment, based on mankind sustainable development concept are insufficiently in detail formulated. The offered criteria will be fundamental and will help to find answers to questions of need of transformation of the existing territory of the university and to its competent zoning as it is necessary to consider that set of functions integrate in one space.

## **2 Materials and Methods**

The research was conducted on the basis of a set of theoretical and empirical methods: contextual analysis of modern works on the management and planning of university territories; comparative analysis of the role of universities as institutions of sustainable development of regions, annual reports and reports of organizations on the implementation of sustainable development goals.

The object of the study was an innovative educational environment—campuses.

The work was based on the concept of sustainable development, which is a fundamental factor in the formulation of criteria for the functional composition and urban planning placement of campus territories in the structure of the city.

All the work was based on a systematic approach. The campus was considered as a complex integrated system. The principle of analyzing the interrelationships of environmental, economic and social factors of sustainable development was fundamental in determining the functional zones that make up the campus. In accordance with it, the criteria for evaluating the existing campus area and compliance with the required level were determined. The composition and ratios of functional zones were the main ones when choosing optimal solutions to improve the quality of the campus infrastructure and the urban environment as a whole.

## **3 Results and Discussion**

The world-class campus has to be provided with all necessary for comfortable life. Functional saturation and variety of environment of university campus in the city assumes that students and the staff of the universities use city infrastructure continuously, are closely connected with cultural institutions and services in it.

Students can combine study and elements of city life, and the space around the university can play important role for interaction and informal communication between students and teachers. The university itself also can create Wednesday for social and cultural life not only of students, but also locals: open lectures, concerts, university libraries can promote strengthening of local community.

For rational allocation of functional zones first of all key indicators of compliance of group of buildings and constructions of the university to the concept “steady

campus” (see Table 1) have been formulated. Indicators have been formulated on the basis of the world rating of the UI Greenmetric universities [12]; sustainable development concepts of campus of Alshuvaykhat and Abubakar [13], program of sustainable development of UKM [14], indicators of sustainable development of campus of the University of Nottingham [15] and indicators of sustainable development of campus of the University of Connecticut [16] and scientific research in the field [17, 18].

Taking into account the formulated key indicators of the effectiveness of assessing the sustainable development of the campus and the necessary from the point of view of management acts of general normative content in the territory of the innovative educational environment, the following functional zones should be identified: housing; education; healthcare; catering; recreation, recreation; sports; consumer services; trade; parking lots; territories for possible expansion of space.

It is possible to group the considered zones considering obligatory aspects of university processes. As a result we receive the following enlarged functions of territories of campus: educational and research, residential, retail trade and rest, entrepreneurial (commercial), infrastructure (Fig. 1).

Based on the formulated enlarged zones and the current set of rules for the design of buildings of educational institutions of higher education [19], groups of buildings and structures were identified, as well as territories necessary for the university to comply with the world-class innovative educational environment.

The data obtained were used to form the university compliance questionnaire, which is necessary for the quantitative assessment of the university facilities and territory (see Table 2). Thanks to the involvement of experts in this field, students and teachers, it is possible to obtain data on the basis of which it is possible to decide whether the university territory needs transformation or corresponds to the level of a “sustainable campus”.

Based on the results of this assessment, it is possible to determine in which functional areas there are no buildings and structures necessary for a comfortable life on the university campus.

For a qualitative assessment of the territory and facilities that make up the university, an assessment questionnaire was proposed, which provides questions for each functional zone that is part of the innovative educational environment (see Table 3).

On the basis of the obtained data it is possible to decide on further option of development of the innovation educational environment and to understand how considerable has to be transformation of the university.

Taking into account opportunities of the territory and the budget it is possible to allocate two ways of transformation: construction (forming) new (results of questioning—49% and below) or reconstruction (renovation) existing (see Fig. 2).

Each of the two options has its advantages and disadvantages. The first option assumes creation of campus from scratch, most often use of the territory on the periphery of the city or beyond its limits is characteristic of this option. This approach is justified if the city has no earth within the developed building or necessary functions in campus demand specific conditions and need the considerable territory.

**Table 1** Key performance indicators of assessment of sustainable development of campus

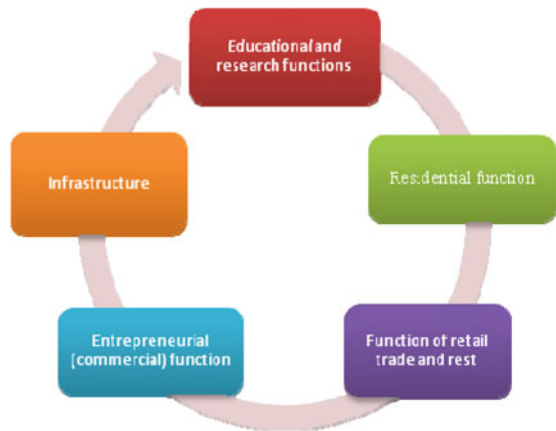
Sustainable development campus	Economic sphere	<b>1. Positive impact of infrastructure on achievement of goals of sustainable development and growth of national economy</b> <ul style="list-style-type: none"> <li>• Implementation of the project creates significant effect for region economy;</li> <li>• assistance to long-term and sustainable development of economy of the region</li> </ul>
		<b>2. Ensuring cost efficiency throughout all life cycle of implementation of the project</b> <ul style="list-style-type: none"> <li>• risk management mechanisms at all stages of life cycle;</li> <li>• use of the innovation technologies</li> </ul>
		<b>3. University as stakeholder organization</b> <ul style="list-style-type: none"> <li>• active interaction with society;</li> <li>• cooperation of bodies of the regional power, scientific and educational organizations, industrial enterprises and business communities;</li> <li>• cooperation of non-profit organizations in all spheres of social and economic and public life</li> </ul>
	Ecological sphere	<b>4. Integration of ecological aspects into the project</b> <ul style="list-style-type: none"> <li>• actions for minimization of negative impact on the environment;</li> <li>• actions for decrease in anthropogenic environmental impact;</li> <li>• actions for preservation of water resources;</li> <li>• recycling;</li> <li>• separate refuse collection;</li> <li>• Implementation of the program of energy saving;</li> <li>• Green construction;</li> <li>• Program of adaptation to climate change</li> </ul>
		<b>5. Resistance to natural disasters, emergencies and other risks</b> <ul style="list-style-type: none"> <li>• resistance to natural disasters and emergencies;</li> <li>• measures for protection against effects of natural disasters and emergency situations</li> </ul>
		<b>6. Transport and pedestrian road system</b> <ul style="list-style-type: none"> <li>• Organized pedestrian and walking network;</li> <li>• Bicycle infrastructure;</li> <li>• Use of the eco-friendly type of transport</li> </ul>

(continued)

**Table 1** (continued)

	Social sphere	<p><b>7. Integration of social aspects into the project</b></p> <ul style="list-style-type: none"> <li>• Ensuring open access about campus life for all residents;</li> <li>• Implementation of the concept “smart—the city” in the territory of campus (smart-campus)</li> </ul> <hr/> <p><b>8. Improvement of quality of administration by infrastructure</b></p> <ul style="list-style-type: none"> <li>• Courses on sustainable development;</li> <li>• Actions in the field of sustainable development;</li> <li>• Carrying out researches in the field of sustainable development;</li> <li>• Publications on scope of sustainable development</li> </ul>
--	---------------	---

**Fig. 1** Enlarged functional areas of the campus



Transformation of campus by reconstruction of the existing territory demands significantly smaller capital investments, than creation of campus “from scratch”. However specific norm of costs of one building (on the specified area) at reconstruction it is essential above, than at new construction [20].

Also it should be noted that at reconstruction the university not always has territories for implementation of new functional zones and also construction of new buildings. Besides, at reconstruction creators of campus are limited to design features of the existing buildings (bearing capacities of the bases, preservation of main walls, exterior of facades and other) [21].

In turn the option of reconstruction of the existing university and its territory has two ways:

- Consolidation and development of university built-up areas;
- Development of the campus on sites in the closest accessibility to universities.

**Table 2** Questionnaire of quantitative assessment of objects and territory of the university

Functional zones	Objects which are part of functional zones	Yes	No
Educational and research functions	The building or group of buildings with lecture audiences;	✓	
	The building or group of buildings with: audiences for work in small groups, etc.	✓	
	Laboratories	✓	
	Library with media library	✓	
	Co-working space	✓	
Residential function	Student residence	✓	
	The hostel for foreign students	✓	
	Housing for teachers	✓	
	Housing for support personnel	✓	
	Housing for short-term stay of students (entrants, students of other higher education institutions arriving within the competitions, conferences, etc.)	✓	
	Housing for short-term stay of teachers of other Higher education institutions	✓	
	Hotel complex	✓	
Function of retail trade and rest	Cafe	✓	
	Dining room	✓	
	Cultural center, museum	✓	
	Supermarket	✓	
	Building of consumer services	✓	
	Sports zones and respective buildings	✓	
Entrepreneurial (commercial) function	Business incubator	✓	
	Business center	✓	
	Bases the practician of the supervising employers	✓	
Infrastructure	Parking space	✓	
	Pedestrian road system	✓	
	Transport availability (stop of public transport close)	✓	

(continued)

**Table 2** (continued)

Functional zones	Objects which are part of functional zones	Yes	No
	The reserve territory for long-range planning of development of the educational organization of the higher education	✓	
Total		100%	

100%—the territory completely conform to standards of the innovation educational environment; 80–99%—the territory more conform to standards of the innovation educational environment, but need insignificant transformation;

50–79%—the territory partially conform to standards of the innovation educational environment, but need transformation;

49% and below—the territory do not conform to standards of the innovation educational environment and need considerable transformation

At option use the next territories it is necessary to allocate functional zones, being based not only on requirements of the university, but also considering requirements of city community.

In case of consolidation of space due to construction of additional university objects, sharing of public spaces or certain buildings (for example, libraries, the museums, sports facilities) together with normal citizens is possible that in turn will create attraction points in the urban environment.

Localization of university campus or option of the campus dispersed in the city depends on such factors as: historical features of development of the university in the city; opportunities and desire of the city and regional authorities or business to participate in this process; possibility of reconstruction of adjacent territories; redevelopment.

Despite the chosen option of space development of campus it is necessary to involve city communities in discussion of development plans for the university territory and to agree on development plans for the territory with the city authorities that updating of the university did not come to an end with expenditure for infrastructure, and gave effect for development of the city.

At the space organization of campus it is also necessary to consider that it should not be strongly removed from the existing centers of the industry. It is connected with need to provide contacts between teaching and specific productions that is especially relevant for the universities of technical orientation [22, 23]. The created campus becomes not only education and scientific center, it begins to create the environment, both in esthetic [24], and in the investment plan [25].

Thus, it is possible to formulate the main stages necessary at acceptance the solution on transformation and spatial arrangement of campus (See Fig. 3).

The modern campus is capable to be under construction with use of natural laws of development, to become part of ecosystem in general and to promote formation of balance between the nature and the person [2].

**Table 3** Questionnaire of quality standard of objects and territory of the university

Category of question according to functional zone	Question	That's good	So-so	Badly
Residential	1. Evaluate comfort and the present of dormitories of our Higher education institution today	✓		
	2. Evaluate comfort and the present of housing for teachers of our Higher education institution today	✓		
Education	3. Estimate condition of academic buildings of our higher education institution	✓		
	4. Evaluate scientific infrastructure, including laboratories, co-workings, the scientific-test centers of our university	✓		
Library complex	5. Estimate condition of library complex of our higher education institution	✓		
Health care	6. Evaluate the level and availability of objects of medical care in the territory of our higher education institution	✓		
Sport	7. Evaluate sports infrastructure of our higher education institution	✓		
Culture	8. Evaluate public and cultural spaces at our university	✓		
Leisure	9. Evaluate leisure infrastructure of our higher education institution	✓		
Trade	10. Estimate availability and level of trade enterprises near our university	✓		
Obshchestvennoyepitaniye	11. Evaluate the level of objects of power supply in the territory of our university	✓		
Social and household assignment	12. Estimate availability of all necessary social and household objects to student's life	✓		
Commercial (business activity)	13. Evaluate the level and the present of the objects relating to commercial and enterprise activity (including business incubators, business centers, bases the practician of the supervising employers) in the territory of our university	✓		

(continued)



**Table 3** (continued)

Category of question according to functional zone	Question	That's good	So-so	Badly
Parking of the motor transport	14. Evaluate the level of security with places for parking of the motor transport in the territory of our university	✓		
The reserve territory for long-range planning of development	15. Whether your Higher education institution the reserve territory for further long-range planning and development of the educational organization has?	✓		
Total		100%		

100%—the territory completely conform to standards of the innovation educational environment; 80–99%—the territory more conform to standards of the innovation educational environment, but need insignificant transformation; 50–79%—the territory partially conform to standards of the innovation educational environment, but need transformation; 49% and below—the territory do not conform to standards of the innovation educational environment and need considerable transformation

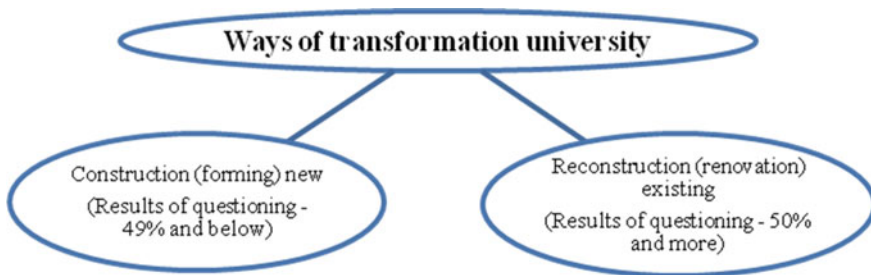
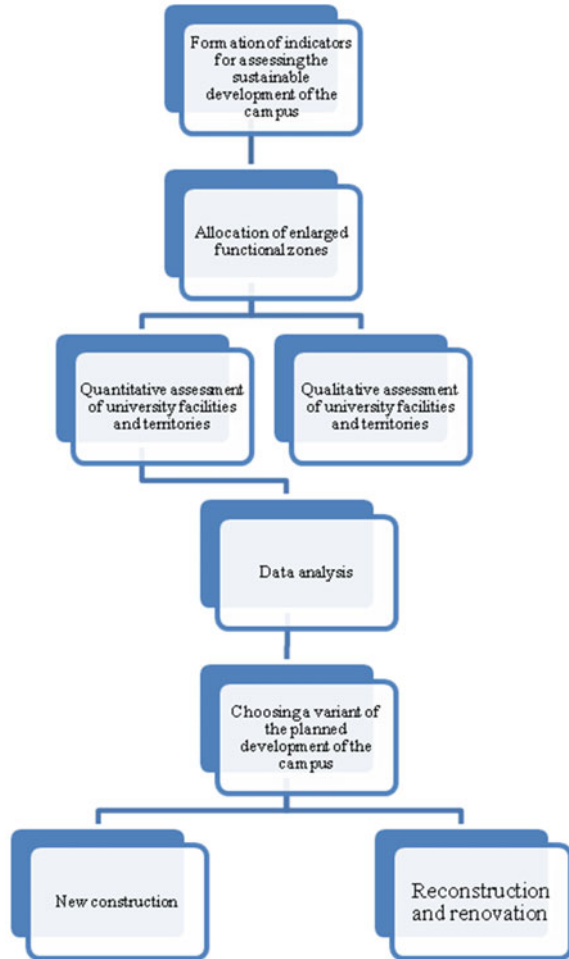


**Fig. 2** Ways of university transformation after expert evaluation

For modern universities, not only the academic function is important, but also the opportunity to cooperate with business. The platform for the formation of innovations in the city, the development of technological entrepreneurship is precisely this interaction between the university and business. With the help of such cooperation, an innovative business is being built. In addition, a well-designed campus can become a point of economic growth of the territory on which it is located.

All above shows obviously expressed need of rapprochement and combination of education and the city, disconnection of different cultural forms and institutions and forming of the open, rich educational space creating conditions for building of different educational trajectories.

**Fig. 3** The Roadmap of decision-making at town-planning placement of university campus



## 4 Conclusion

1. The conducted research made it possible to formulate criteria and indicators for evaluating university territories, taking into account the concept of sustainable development. The indicators correspond to three areas of campus activity: economic, ecological, and social.
2. Taking into account the mandatory aspects of university processes, the enlarged functional zones of the innovative educational environment are identified: educational and research, housing, retail trade and recreation, entrepreneurship, infrastructure.

3. Questionnaires have been formed for quantitative and qualitative assessment of university facilities and territories. With the help of the information received, it is possible to determine exactly what needs to be transformed and how large-scale it should be.
4. Various variants of the spatial organization of university campuses are analyzed and the pros and cons of each option are identified.
5. A roadmap is proposed for choosing a variant of the spatial organization of an innovative educational environment, which can be used by universities as a guide for the transformation of objects and territories into a sustainable campus.

## References

1. Dolotkazina NS, Prytkova YuP (2016) Principles of design of student's campuses. *Constr Messenger Prikaspiya* 1–2(15–16):9–15
2. University campuses and city: cooperation for the sake of competitiveness [Electronic resource]//the Website CSR.RU (2021)
3. Savvinov VM (2021) Sustainable development concept as basis of modern practices of management of education. *Prof Educ Russ Abroad* 1(41):136–146
4. Liu M (2023) The optimization of high-density campus transportation based on green transport. *Lect Notes Civ Eng* 211:248–254
5. Buckley AO, Strauss EJ (2023) Climate change and sustainable campus planning: a review of michigan universities' climate-related plans. *Lect Notes Civ Eng* 276:1123–1134
6. Liu Q, Wang Z (2022) Green BIM-based study on the green performance of university buildings in northern china. *Energy Sustain Soc* 12(1):1–17
7. Fan Z, Cao J, Jamal T, Fogwill C, Samende C, Robinson Z, Healey D (2022) The role of 'living laboratories' of in accelerating the energy system decarbonization. *Energy Rep* 8:11858–11864
8. Sima M, Grigorescu I, Bălțeanu D, Nikolova M (2022) A comparative analysis of campus greening practices at universities in Romania and Bulgaria: sharing the same challenges? *J Clean Prod* 373:13382
9. Guo W, Ding Y, Yang G, Liu X (2022) Research on the indicators of sustainable campus renewal and reconstruction in pursuit of continuous historical and regional context. *Buildings* 12(10):1508
10. Cumans INO (2014) Zoning of projectible university campus. *Eng Bull Don* 31(4–1):14–23
11. Prosekov AYU (2021) Concept of development of infrastructure of the southern campus of the network university of KUZBASS scientific education center. *Univ Manage: Pract Anal* 25(2):49–58
12. Nikolaev AN, Savvinov VM, Kugayevsky AA (2021) The university—the intellectual, innovation and spiritual platform of sustainable development of the macroregion. Yakutsk: Northeast federal university of M.K. Ammosov, 268
13. Alshuwaikhat HM, Abubakar I (2008) An integrated approach to achieving campus sustainability: assessment of the current campus environmental management practices. *J Clean Prod* 16:1777–1785
14. Universitas Indonesia (2014) Guidelines of UI Green Metric World University Ranking. <http://www.greenmetric.ui.ac.id>
15. Chan FTS, Chan HK, Lau HCW, Ip RWL (2006) An AHP approach in benchmarking logistics performance of the postal industry. *Benchmark Int J* 13:636–661
16. Fadzil ZF, Hashim HS, Che-Ani AI, Aziz S (2012) Developing a campus sustainability assessment framework for the National University of Malaysia. *Int J Environ Ecol Geol Min Eng* 6(6):44–48

17. University of Nottingham (2013) Sustainability report 2012–13. <http://www.nottingham.ac.uk/sustainability>
18. Amrina E, Imansuri F (2015) Key performance indicators for sustainable campus assessment: a case of Andalas University 349:11–18
19. Melo J, Coelho AL (2022) Sustainability from the perspective of a Brazilian university: discourse and relations with the sustainable development goals. *Revista Gestão Universitária na América Latina—GUAL* 15:244–262
20. Cumans INO (2014) Zoning of projectible university campus. *Eng Bull Don* 31(4–1):14–20
21. Isakova SA, Morgun NA (2011) Features of forming of functional and planning blocks for architectural modernization of the universities (on the example of Southern Federal University). *Bull Tomsk State Archit Constr Univ* 4:27–36
22. Chen Ya, Sonmez T (2002) Improving efficiency of on-campus housing: an experimental study. *Am Econ Rev* 92, 1669
23. Zakharevich VG, Obukhovets VA (2022) Problems of engineering support of the innovation transformations in the region. *Engineering bulletin of Don, Special issue “the II congress of engineers of Don. No 11, pp 17–27*
24. Kim SJ, Koo YM (2006) A strategic proposition for the improvement of campus town and an establishment of fine urban sight. *New ideas of new century: materials of the TOGA FAD international scientific conference T. 1, pp 342–345*
25. Puchkov MV (2011) Strategies of development for the urbanized territories: campus models as control facility regional development. *RAASN Acad Bull Uralniiprojekt* 1:25–29

# Truth May not Be Self-Evident but It is Demonstrable: The Case for the Construction of a Touristic Project at Ramla l-Hamra, Gozo



Lino Bianco 

**Abstract** This paper addresses the development applications which were granted planning consent for the construction of a tourist complex along the side of Ramla l-Hamra valley—the clay slope beneath the mythical Calypso Cave in which Homer’s Odysseus was allegedly held—a unique site of cultural and ecological significance. A third-party objector set up SaveRamla, an environmental, non-governmental committee, to challenge these applications. Once granted, this multi-million euro project was widely supported by the national planning and environment regulator and given significant coverage on state media, including a debate on a prime programme. Based on planning legislation, the third-party objector proved that the outline permit on which the full permit was grounded contained false, misleading or incorrect information which had material bearing on the issuance of same. Both permits were subsequently revoked, a decision confirmed at the appeal stage. The relevance of this case study to contemporary literature on development planning is outlined. It concludes by arguing that (i) development planning history is imperative to document the evolution of the planning process over time; (ii) incorrect declaration of ownership is sufficient for revocation of planning consent; and (iii) incomplete application leads to a decision that is informationally disabled.

**Keywords** Planning legislation · Planning fraud · Revocation of permit · Ramla l-Hamra · Ulysses Lodge · Malta

---

L. Bianco (✉)  
University of Malta, Msida MSD 2080, Malta, Bulgaria  
e-mail: [lino.bianco@um.edu.mt](mailto:lino.bianco@um.edu.mt)

University of Architecture, Civil Engineering and Geodesy, Sofia 1046, Bulgaria

© The Author(s), under exclusive license to Springer Nature Switzerland AG 2024  
N. Vatin et al. (eds.), *Modern Problems in Construction*,  
Lecture Notes in Civil Engineering 372,  
[https://doi.org/10.1007/978-3-031-36723-6\\_25](https://doi.org/10.1007/978-3-031-36723-6_25)

237

## 1 Introduction

When a Conservative MP from Witham, England, asked the Secretary of State for Communities and Local Government “what sanctions may be imposed on persons who have made false statements or provided false evidence in a planning application”, the response was: “The planning application process relies on people acting in good faith. There is an expectation that applicants and those representing them provide decision makers with true and accurate information upon which to base their decisions. However, under Sect. 65(6) of the Town and Country Planning Act 1990, it is an offence to issue a false ownership certificate knowingly or recklessly. If a local planning authority feels that an application does not accurately or fully describe the proposed development, or that it is in any way misleading, it is entitled to ask the applicant to amend it or rectify any omissions before it agrees to process the application. Planning applications are publicised during the determination period so that any interested parties have the opportunity to comment. If any party considers that the application includes deliberately misleading information, or lacks important information that would be material to the decision, they should report this to the relevant local authority who will decide what action is appropriate” [1].

Although Malta is the name of the main island of the Maltese archipelago—located in the central Mediterranean (Fig. 1a)—it also refers to its dependencies, which include Gozo, the second largest island (Fig. 1b). Having been a colony of Britain until 1964, this EU Member State’s public administration and governance are heavily grounded on Anglo-Saxon archetypes [2]. A first source of inspiration in drafting legislation in Malta is in fact often British. The Development Planning Act 1992 (DPA) [3] was modelled on the UK’s Town and Country Planning Act 1969 [4]; the Town and Country Planning Act 1990 (TCPA) [5] was a development of the 1969 Act.

A significant variation between the TCPA and the DPA is that in the former the legislative power is delegated to local and central government officials, whilst in the latter it is vested in the Planning Authority (PA), a centralised authority, renamed Malta Environment and Planning Authority (MEPA) in 2002 with the merger of the PA with the Environment Protection Department. It was demerged and replaced by the Planning Authority and the Environment and Resources Authority in 2016. This article addresses the case for the revocation of development planning permits PA5138/02 and PA7902/05 at Ramla l-Ħamra, Xagħra, Gozo (Fig. 1c). The consent was for the redevelopment of the area occupied by the Ulysses Lodge and the surrounding disturbed landscape (Fig. 1d and e) The author was requested by a third-party objector to put forward the case. The two main technical submissions—which became an issue in the 2008 electoral campaign, with the Harvard-educated opposition leader, Alfred Sant, pledging to block this development project within the limits of the law [6]—form the basis of this paper [7, 8]. These submissions initially first stopped MEPA from sending the PA7902/05 permit, and then “to revoke it in a cathartic public hearing” [9]. Following an outline of the development planning

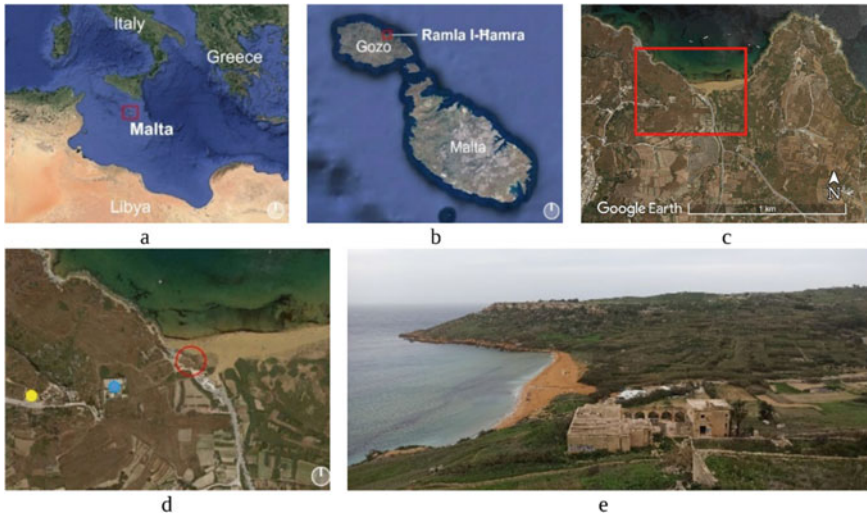


**Fig. 1** Site location: **a** the Mediterranean Sea showing the location of the Maltese archipelago, Greece, Italy and Libya; **b** the Maltese archipelago indicating the location of Ramla l-Hamra; **c** Ramla l-Hamra Bay, Xaghra (boxed in red); **d** Ramla l-Hamra Bay and the locations of the remains of the Roman Villa (circled in red), Calypso Cave (marked in yellow), and Ulysses Lodge (marked in blue); and **e** view of the Ramla l-Hamra Bay with Ulysses Lodge in the foreground

history at Ramla l-Hamra and pertinent instruments in local legislation, these applications were critically reviewed together with the process leading to the permits’ eventual revocation. The appraisal identified aspects of relevance to contemporary literature on planning practice.

## 2 Ramla l-Hamra

### 2.1 Background

Gozo has long been identified with Ogygia, the Island of Calypso, the mythical prison of love where Odysseus was entrapped in Homer’s epic poem, the *Odyssey*. Odysseus—Virgil’s Ulysses—washed up there, the sole survivor of a shipwreck. On reaching the shore he was detained for seven years by the queenly nymph Calypso—“the fair-tressed daughter of Atlas, ... a dread goddess”—who promised him immortality and eternal enjoyment of her sensual pleasures if he would be her husband [10]. Athena—Odysseus’ patron goddess—begged Zeus, the king of the gods, to order his release from sexual slavery so that he could return to his true wife, Penelope. Odysseus was freed on Zeus’s order.

Located on the north-east coast of the island, at the mouth of Wied tar-Ramla (Ramla Valley) between Marsalforn Bay and San Blas Bay, Ramla l-Hamra (Maltese for ‘red sand’) is Gozo’s largest sandy beach and the most popular in the Maltese Islands (Fig. 1d). It is one of the most picturesque and heritage-laden areas of the archipelago, notably due to the quasi-intact dune system and a Roman villa [11]. Although subjected to anthropogenic impacts, the coastal dunes at Ramla l-Hamra support flora and fauna typical to the area. A list of the vegetation cover characterising this sand dune habitat and other biotic communities is included in a number of studies [e.g., 11, 12]. These dunes likely protected the site of the Roman villa, first discovered in late 1910 by the director of the Museum of Archaeology and Rector of the University of Malta, Sir Themistocles Zammit [13, 14] (Fig. 1d). The perimeter of the villa was re-designed following studies undertaken over the period 2010 and 2017 [15]. The cave of the legendary nymph is situated to the west of the present site of Ulysses Lodge (Fig. 1d).

Ramla l-Hamra was scheduled in 1995 for its ecological and cultural significance under Article 46 of the DPA [3]; notification of this decision was published in The Malta Government Gazette [16]. It was designated an area of ecological importance as per Structure Plan Policy RCO 12 [17] and Clauses 15.34, 15:35, 15:38 and 15.39 of the plan’s Explanatory Memorandum [16, 18]. The list of scheduled cultural heritage assets at this site, including the relative classification, is given in Table 1. All are graded in terms of Structure Plan Policy UCO 7 [17] except for the remains of the Roman Villa which is in terms of Structure Plan Policy ARC 2 [17]. Given the conflict between conservation and the use of the beach for recreational purposes, the Gozo and Comino Local Plan Policy GZ-Xghr-3 made provision for the formulation of a visitor management plan to protect the vulnerable habitats to the levels requested by the scheduling, and maintain and upgrade the area in a manner compatible with national planning policies [19].

**Table 1** List of scheduled cultural heritage property at Ramla l-Hamra [16]

Scheduled property	Grading
Remains of Roman Villa	Class A
Part of blockhouse of Nadur Battery	Grade 1
Fougasse	Grade 1
Underwater obstacle (sea wall)	Grade 1
Salient of Ramla Redoubt	Grade 1
Remains of Belancourt Battery	Grade 1
Remains of Retrenchment	Grade 1
Pathway	Grade 1
Statue of Our Lady	Grade 1



## 2.2 Development Planning History

A historically informed approach to account for space-specific development planning is to trace the chronicle of applications and permits on site; this goes beyond a narrative-driven description [20]. Further to compiling historical documents, the practical role of planning history is for “a comprehensive understanding of the past in order to illustrate the complexity of the present and shape the future” [21: 1054]. In the case of Ramla l-Ħamra, the relative planning applications, their respective submission dates and final decisions are given in Table 2. Through archival research, a building notice bearing reference 95/62 was retrieved for the erection of a dwelling house in the road leading to Calypso Cave, Xagħra. The site profiles of applications and permits PAPB3291/1352/69, PAPB1240/73/1352/69 and PAPB2084/84 are shown in Fig. 2. Until 1992, development planning was regulated by the Planning Area Permits Board (PAPB). Thus, the file reference numbers bear the initials PAPB, or PA if issued by the Planning Authority.

PAPB3291/1352/69 was for the construction of tea rooms in unrendered local stone and included a proviso for clearance of material at Ramla Road, Xagħra, Gozo. PAPB1240/73/1352/69 was a renewal of PAPB3291/1352/69. Following issuance of the renewal, fresh drawings were submitted. In a correspondence dated 6 September 1974 copied to the Commissioner of Lands, the Minister of Development Albert V. Hyzler stated that “from an environmental point of view I strongly object to such buildings on the foreshore as they constitute a major threat of pollution of the sea and the foreshore”. At the time, planning was not regulated in Malta. Following a change in government in 1971, the Town and Country Planning Act 1969—drafted by Sir Desmond Heap, the author of similar legislation in the UK—though regularly enacted into law was not brought into force [4]. Applications PAPB2084/84 and PA2326/95 bore the same address of the site as previous applications.

The former, submitted on behalf of Gozo Hotels Ltd by John Portelli—one of the earliest entrepreneurs investing in tourism infrastructure in Gozo [28]—was for the extension of existing restaurant and conversion into a 144-bed hotel. It was refused on the basis that “a building permit cannot be issued because tourist accommodation is envisaged” [23: 12], a decision that was confirmed at the reconsideration stage on 15 October 1985 [23: 25]. A fresh application submitted on 26 December 1986,

**Table 2** Development planning applications [7]

Planning Application	Date submitted	Decision
PAPB3291/1352/69	22 March 1969	Granted (13 September 1969) [22: 11]
PAPB1240/73/1352/69	26 February 1973	Granted (12 April 1974) [22: 32]
PAPB2084/84	07 May 1984	Refused (31 July 1984) [23: 12]
PA2326/95	04 May 1995	Refused (20 December 1995) [24]
PA5138/02	12 September 2002	Granted (7 July 2005) [25]
PA7902/05	14 December 2005	Granted (6 June 2007) [26]

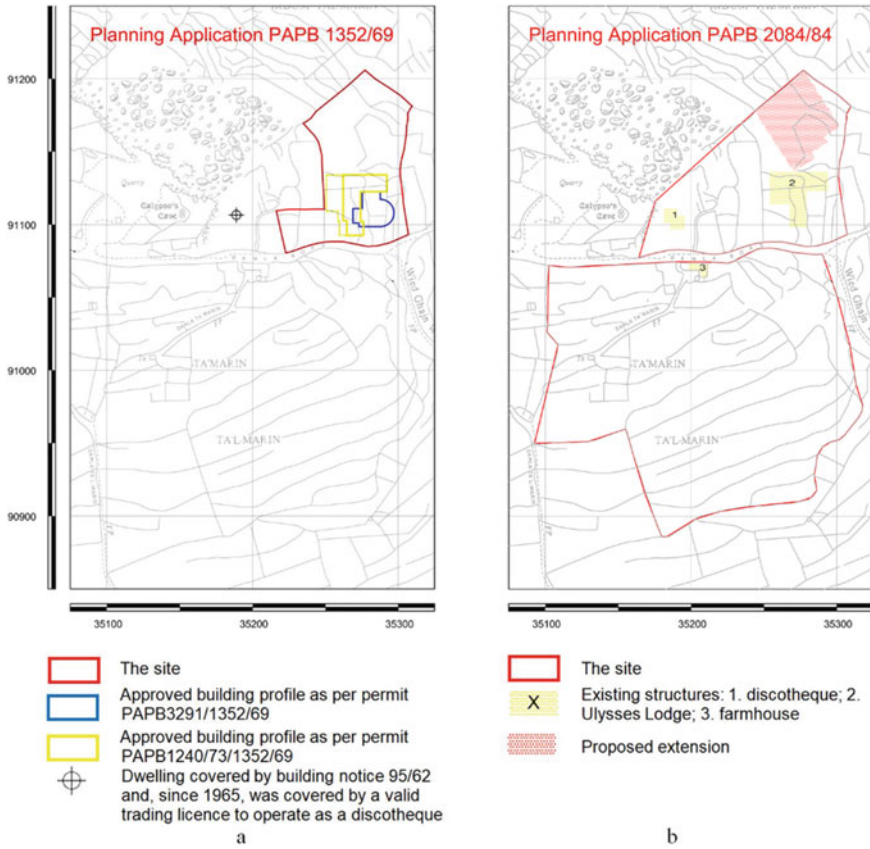


**Fig. 2** Planning applications (site profile outlined in red): **a** PAB1352/69; **b** PAB2084/84 (existing structures marked in yellow: 1. discotheque, 2. Ulysses Lodge, and 3. farmhouse; proposed, and eventually refused, extension is marked in red) [27]

which included new drawings, was refused on 17 February 1988 “on grounds of policy” [23: 41], and again on 17 February 1988 [23: 50]. Application PA2326/95, for the “conversion of an existing farmhouse building and extension—construction of swimming pool and terraces”, was refused as it ran counter to Structure Plan Policies SET 11, SET 12, BEN 5, RCO 4, RCO 21 and RCO 29 [17, 24], which prohibit developments outside urban development zones and in rural conservation areas which have adverse impacts on the scenic value of the site, are in areas prone to erosion, and on sides of valleys. It also ran counter to policy PLP 20, a blanket prohibition of any form of development outside areas designated for urban uses [29]. The decision was confirmed at reconsideration stage on 17 October 1996.

Both outline application PA5138/02 and full application PA7902/05, which were for the “re-development of an existing fully licenced commercial complex”, bore the same site address as previous applications, namely, Triq Ghajn Qamar, Xagħra. The

latter included the demolition of an existing commercial complex and the construction of dwelling units with pools, as per permit PA5138/02. Outline and full planning applications, encouraged through Structure Plan Policy BEN 8, were introduced through the DPA [3]. This policy states [17: 27]: “Intending applicants for permission to develop are advised to consider applications for outline permits which establish the principles and general characteristics of a development proposal before the applicant is faced with the expense of the more detailed application for a full permit to develop. Where this procedure is used, the application fee will be payable for the outline application only. Two types of development permit can be granted: 1. outline permit which gives approval in principle to the proposed development, but specifies reserved matters which need to be included in a full permit application or applications. A time is given within which full permit applications shall be submitted otherwise the outline permit becomes invalid. No development may commence without a full permit; and 2. full permit which is required before any development can commence whether or not an outline permit has been issued”. Thus, outline permission implies that the development is approved in principle but it does not give rise to any right/s to execute it. Permits PA5138/02 and PA7902/05 allowed construction to change an area that included a small farmhouse, a detached house covered by building notice 95/62, and a complex covered by permit PAPB1240/73/1352/69, into a hamlet of luxurious detached houses.

## ***2.3 Relevant Local Legislation***

### **2.3.1 Local Planning Legislation**

The DPA, as amended through Act XXI of 2001, introduced Article 39A, which addresses revocation and/or modification of development permission. Article 39A(1) [3] states that the MEPA may, “only in the cases of fraud or where public safety is concerned or where there is an error on the face of the record, by order revoke or modify any development permission granted under this Act”. Furthermore, Article 39A(2) [3] defines “fraud” as “the submission to the Authority of any information, declaration or plan on the basis of which the Authority has approved a development permission, where such information, declaration or plan is false, misleading or incorrect, irrespective of whether such deceit is the result of a wilful or negligible act”, whilst “error on the face of the record” is defined as “an error on the face of a record which offends against the law”. According to the same article, MEPA should not revoke or modify a development permission in cases of fraud when the information submitted has no material bearing on permission granted.

### 2.3.2 Laws of Malta

According to Articles 2143 and 2144(2) of the Civil Code of Malta, the prescriptive period for acquisition of title of immovable property is 30 years and 40 years for immovables belonging to thirty parties and to churches or other pious institutions, respectively [30]. Furthermore, under the terms of Article 2115(2), with exceptions, no prescription may be set up against any right or action of the Government of Malta [30]. On the contrary, under Sect. 85 of the Criminal Code, a pretended right carries a prison sentence and/or a fine [31]. Furthermore, in the case of property of the Government of Malta this may be disposed of only in terms of Article 31 of the Government Lands Act [32].

## 2.4 Third-Party Objectors

With respect to both planning applications, only PA7902/05 had registered objectors in terms of Article 32(5) of the DPA [3], namely, Gaia Foundation, Kunitat Reġjonali Alternattiva Demokratika Għawdex and two residents from Xagħra, one of them being Mary Carmen Bajada. At the time, Bajada was a councillor of Xagħra Local Council, a working mother of four with an unemployed husband. She subsequently set up the environmental non-governmental SaveRamla Committee.

The applicant had filed a judicial protest against Bajada which, although acknowledging her right to protest, requested her to (i) stop further actions, and (ii) withdraw the claim that fraud was present in the applications. Furthermore, the judicial protest stated that she was being held responsible for damages which might amount to hundreds of thousands of Maltese Liri [33: 2]: “l-esponenti ... tinterpellaha sabiex tiddesisti mill-aġir abbużiv u illegali u in mala fede da parti tagħha; u titira formalment l-allegazzjonijiet foloż kollha illi hija xerrdet kontra l-esponenti, u tinfirmaha illi hija qegħda minn issa iżżomm lill-intimata responsabbli għad-danni kollha illi l-esponenti qegħda u tista’ ‘l quddiem issofri per konsegwenza ta’ dan l-aġir abbużiv u illegali, u qegħda minn issa tirrizerva id-dritt illi tippoċedi kontra tagħha għar-rizarċiment ta’ dawn id-danni kollha illi hija sofriet u għad ‘il quddiem tista’ ssofri per konsegwenza” (the exponent ... requests her to desist from the abusive and illegal behaviour in bad faith on her part, and formally retract all the false allegations that she has spread against the exponent, and informs her that she is from now on being held responsible for all the damages that the exponent is and may in the future suffer as a consequence of this abusive and illegal behaviour, and the exponent is from now on reserving the right to proceed against her for the compensation of all these damages that the exponent has suffered and in the future may suffer as a consequence).

### 3 Applications PA5138/02 and PA7902/05

#### 3.1 General Considerations

Application PA5138/02 included three drawings: (i) the site plan, (ii) existing buildings, and (iii) proposed block plan. Section 23 of the application states that the internal road is to be redesigned, whilst Sect. 27, which refers to previous applications and/or permits on site, is filled in as ‘NA’, an acronym for ‘not available’ or ‘not applicable’ [25]. From consulting the relative planning file, notably the minutes included in same, it was noted that the files with respect to the following applications were not consulted by MEPA during its processing: PAPB1240/73/1352/69, PAPB2084/84 and PA2326/95.

In accordance with Article 36 of the DPA, the applicant is granted thirty days to put forth written submissions on the contents of the Development Permit Application Report (DPAR); submissions are attached to the same document when the application is referred to MEPA’s Board for a decision. In the case of PA5138/02, the DPAR, which recommended a grant, was cleared on 6 July 2005 [34, 35]. It was not sent to the applicant and the application was referred and approved by MEPA’s Board the day after. The agenda for 7 July 2005 was issued on 30 June 2006 and advertised in the local media on 2 July 2005 [36]. The eventual permit was subsequently assessed by MEPA’s auditor. His report raised the following two objections [37]:

1. The presence of a MEPA board member at a meeting between officials of the Planning Directorate and the developer; and
2. Failure of MEPA to publish the reasoned justification as to why it waived the environment impact assessment (EIA).

He argued that the former—not a part of the planning process—was tantamount to unethical behaviour, whilst the latter was a breach of legislation. His rejoinder stated that “MEPA did not publish a justification of its exemption from carrying out of an Environmental Impact Assessment. It just published a [public] notification [of a waiver] without adequate reasons being brought forward” [37]. The EIA was requested by the Environment Protection Directorate, but MEPA’s Planning Directorate “later waived it off due to a submission of a very detailed Project Description Statement, which included a geo-environmental impact assessment, an ecological assessment, a slope stability analysis, a geo-technical study of foundations and an archaeological heritage report” [35].

Section 14 of application PA7902/05 stated that neither new vehicular access nor altered access will be formed, whilst Sect. 18 listed the following application/s and permit/s on site: PAPB1240/73/1352/69, PA2326/95 and PA5138/02 [26]. This application stated that the expiry of the first and last cited permits were 12 April 1974 and 14 October 2010, respectively. Neither application PA5138/02 nor PA7902/05 referred to the refused application, PAPB2084/84. The site profile and existing and proposed structures covered by application PAPB2084/84 are shown in Fig. 2b. The DPAR, which recommended to grant the proposed development, was cleared on 24

May 2007 [39]. The report was not sent by post to the applicant and the file was placed on the MEPA Board agenda for 6 June 2007; the agenda was issued on 31 May 2007 and published on 2 June 2007 [40].

### 3.2 *Particular Considerations*

It is worth recalling the following:

1. During processing of application PA5138/02, the Planning Directorate did not consult any of the applications and permits on site, as the relevant Sect. 27 relating to this information was filled in as 'NA';
2. The legal developments covered by application PA5138/02 are: (a) dwelling unit, licensed to operate as discotheque, covered by building notice 95/62, and (b) Ulysses Lodge, covered by PAPB1240/73/1352/69 (Fig. 2a);
3. Application PA5138/02 states that the proposed development involves the redesign of the internal road. No applications were filed to redesign Ramla Road, nor was this road included as part of the proposed development, as Sect. 23 of the application stipulates. The road was still public land, as per the application of the Director of Estate Management Department, filed with the Lands Registry (Gozo Branch) in 2002 to register title of the same (Fig. 3). The profile of the road, which runs through the land of the applicant, as stated in application PAPB2084/84, is shown in Fig. 4b;
4. Permit PA5138/02 was to develop an existing complex which covers Zone C, "developed and disturbed land"; Zone A and Zone B corresponded to terraced fields and unspoilt land, respectively. Although it was claimed that it "will take up the committed and disturbed areas", this was not true to fact; half of its superficial area was never committed for development, as illustrated through official aerial imagery at the time (Fig. 4a). Also, the profile of Ramla Road was neither to be realigned nor included as part of the development of Ulysses Lodge. This is confirmed by the site plan attached to application PAPB2084/84. The road is government property and not owned by the applicant and thus the respective permits, which included the development of detached houses on the same, would have obliterated the road and trespassed on a public right of way;
5. Through permit PA5138/02 and, subsequently, permit PA7902/05, MEPA permitted the development of tenements on a public right of way, namely Ramla Road, a statement of fact which MEPA was not aware of when issuing both permits, as the applicant declared in the respective application that he is the sole owner of the site.

The information and declaration contained in application PA5138/02, the basis on which it was approved, qualify as "false, misleading or incorrect" as the undeclared contents of files PAPB3291/1352/69, PAPB1240/73/1352/69, PAPB2084/84

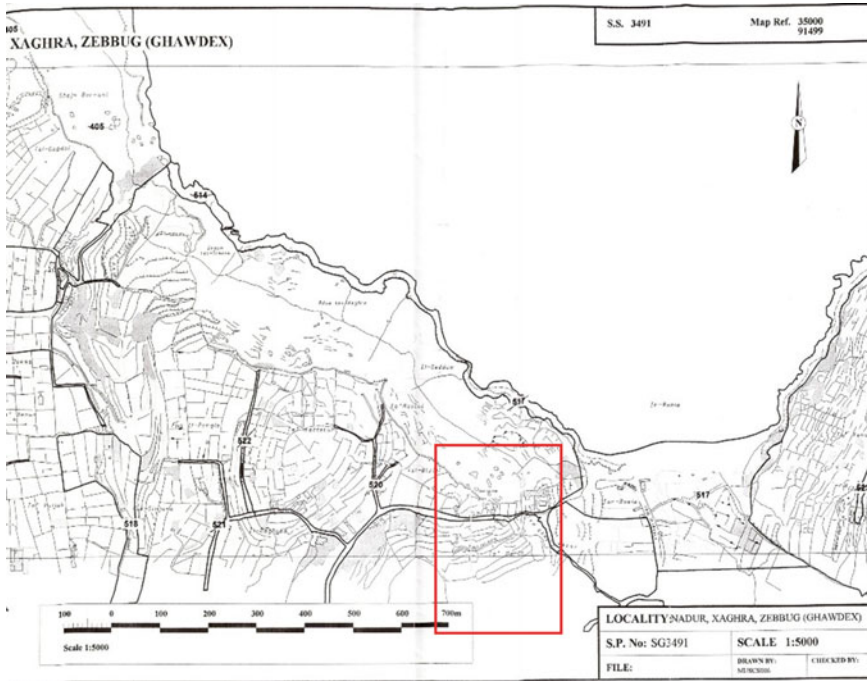


**Fig. 3** Government property at Ramla l-Hamra: site plan attached to the application of Director, Estate Management Department, to Land Registry: the perimeter of government property is marked with bold lines; the area outlined in red corresponds to Fig. 4b

and PA2326/95 have a material bearing on the issuance of said permit. Moreover, the declaration of ownership is not correct and, given that it is a public right of way, it is not just a matter of land ownership, but a planning control consideration with direct material bearing on the issuing of a permit.

### 3.3 Other Considerations

During the MEPA Board meeting when application PA7902/05 was granted, the description of the development proposal was changed from a residential to a touristic complex. This amounted to a significant material change from the original, and thus merited republication in the local media, as stipulated by Article 32 of the DPA [3]. Therefore, the permit was in breach of this article. In terms of Article 32(4) of this Act, MEPA was bound to (i) publish the amended proposal in the local press, (ii) advertise the said proposal by affixing a notice on site, and (iii) furnish Xagħra Local Council with a copy of the amended application.



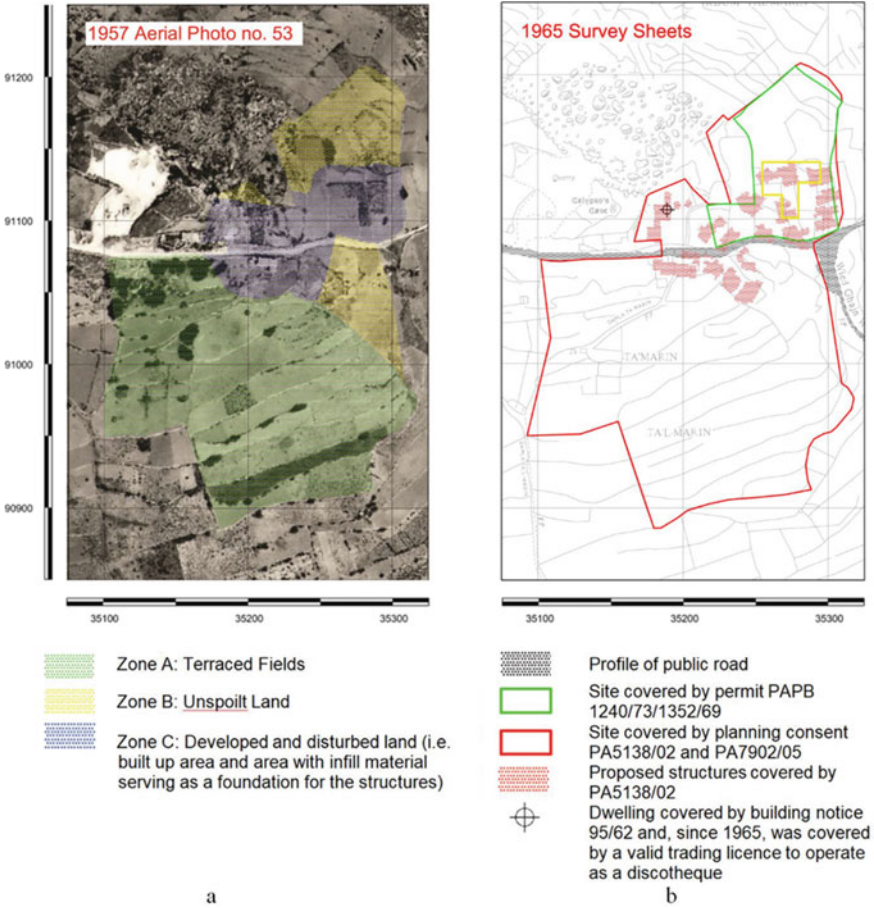


**Fig. 4** Planning applications PA5138/02 and PA7902/05: **a** site profile of zones A, B and C, hatched in green, yellow and blue, respectively plotted on an aerial photo; the profile of the public road shown in Fig. 3b can be read; **b** site covered by permits PA5138/02 and PA7902/05 is outlined in red, in contrast with the previous PAPB permit which is shown outlined in green; the profile of the public road shown in (a) is also plotted [7]

Furthermore, in terms of Article 32(5), MEPA denied people the opportunity to (i) review fresh plans submitted in the planning process and (ii) make representations regarding the amended development. Finally, in terms of Article 15(1)(d), MEPA denied any person the right to file a third-party appeal against the amended development, as said person would have failed to file their representation in terms of Article 32(5).



## 4 Revocation of Permits PA5138/02 and PA7902/05

### 4.1 *Advertising the Development*

To defend the permits issued, a campaign of systematic advertising commenced. Notable was the primetime investigative journalistic programme *Bondi Plus* broadcast on 25 June 2007 by the Maltese national television station [41], and an issue of *X-Plain* [42]. This publication—a full-colour four-page, nearly A3-sized pull-out distributed with the *Sunday Times of Malta* on 1 July 2007—covered the permit for the redevelopment of Ulysses Lodge. As noted in the Malta Environment and Planning Authority’s Annual Report, this was not a public relations campaign, but the time and effort put into it by the Public Relations Office of MEPA was nothing less than that that required for such an endeavour [43]. Although, according to Article 5(1) of the DPA, the functions of the MEPA include the promotion of proper planning and sustainable development, and controlling developments in accordance with plans and policies approved in terms of the Act [3], the content of this publication was not compatible with this mission, consisting as it did of advertising more fitting for a real-estate company involved in aggressively marketing speculative developments than a public authority entrusted with sustainable environmental planning [44].

### 4.2 *Request for Revocation*

Arguing for the development, the presenter of *Bondi Plus* exhibited file PAPB2084/84, a file that had not been made accessible to Bajada upon request some days earlier. After consulting it, the complete scenario of the development planning history could be comprehended. On 16 July 2007, the objector filed the following requests with MEPA [8]:

1. not to send by post the permit PA7902/05, otherwise MEPA would be held criminally responsible for granting consent to a pretended right by a private party to a stretch of Ramla Road, thus interfering with the enjoyment of a public right of way (the receipt of the physical copy of the permit would grant the right to the applicant to submit a commencement notice and start construction works); and
2. to revoke permit PA5138/02 under Article 39A of the DPA and, given that permit PA7902/05 was intrinsically dependent on it, to declare PA7902/05 null and void.

Furthermore, given that a significant part of Zone C was not covered by planning consent, and thus not legally committed, MEPA was requested to apply and enforce articles 51, 52 and 55A of the DPA and issue enforcement notice(s) with respect to infringements present on site [27].

### **4.3 *Deliberations Within MEPA***

The discussion at the MEPA Board meeting where revocation of the permits was debated was reviewed by several environmentalists and environmental non-governmental organisations. Among them was Edward Mallia—a retired Associate Professor of Astrophysics and Honorary Chairman of Friends of the Earth Malta, who was, and still is, at the forefront of the main environmental crusades in Malta. He noted that during this meeting most MEPA members objected to the notion of ‘disturbed land’, converging on the suggestion that one should make use of the term ‘disturbed ground’ instead, as it is “of no use to anybody except the developer” [45]. The defence of the permits “was shot down in flames” by the technical report submitted on behalf of the third-party objector, which “showed that the ‘disturbed land’, claimed to be part of the original development, was never covered by any permit. It was simply taken over” [45]. This tract of land begged the questions, “who ‘disturbed’ the ground in the first place, and under what dispensation?” [46].

Referring to points raised by the environmental non-governmental and non-profit voluntary organisations Din l-Art Helwa and the Gaia Foundation, the latter having managed the Ramla l-Hamra area since 2000, Mallia described this disturbed ground as “a surreptitious grab of public land, never covered by any permit” over an area circa twice the legal footprint of the existing development and thus with no legal basis under the present permit [46].

### **4.4 *Planning Appeals***

Following the revocation of the permits on 4 October 2007, the applicant submitted appeals, bearing reference numbers PAB312/07 and PAB320/07, with respect to PA5138/02 and PA7902/05, respectively. The Appeals Board dismissed the former appeal on 28 July 2011 on the basis that the applicant failed to submit the correct certificate of ownership, a fact which he admitted [47]. The applicant appealed this decision on a point of law to the Court of Appeal, which dismissed it on 30 October 2012 [48]. The appeal with respect to the latter was dismissed on 2 October 2009 on a preliminary issue: it was declared null and void on the basis that the applicant failed to make the additional payment for the appeal that was required by law, which amounted to a trivial figure, and thus the Appeals Board abstained from taking further cognisance of it. On 6 February 2009, the Board granted the appellant two months to make the payment of €5655.34; by 6 April a sum of €1025.32 was paid and a further €1170.78 on 13 May 2009 to tally with the revised amount issued by MEPA on 23 April 2009 as the original amount was erroneously computed by the same authority. Although the total amount tallied with the revised fee, the tribunal had requested the settlement of the original amount [49]. No appeal was filed against this decision with the Court of Appeal.

A third-party appeal against permit PA7902/05, bearing reference number PAB171/07, was filed by Din l-Art Helwa and the Gaia Foundation. On 1 November 2011, this appeal was deemed no longer necessary as the permit to which it related was revoked and the Appeals Board subsequently refrained from considering it further [50].

## **5 Relevance**

### ***5.1 The Role of a Planning Board***

The deliberations of the MEPA Board at the revocation stage—essentially focusing on a statement to rationalise a development—were illustrative of behaviour which went beyond the planning agenda. It played the role of a laboratory for conjuring legal jargon to bypass applications. Such board is neither there to defend a party (in this case, the MEPA's Planning Directorate vs the applicant/third party) nor is it a court of law (with respect to interpretation); it must rely on the facts and science on which legislation and policies are based. The board's role is to ensure that applications conform to policy, as drafted in the spirit of the law, and not to come up with suggestions which, for example, propose ways for applicants to circumvent the facts by using vague terminology. Its role is not to find reason/s to excuse a speculative development but to protect the environment for the common good; the responsibility is collective and the end does not justify the means.

### ***5.2 The Power of Third-Party Objectors***

Development and construction impact on the public domain and thus public opinion can make or break a proposal [51]. At law, third-party objectors may have a vested interest in a given development either directly or indirectly; they can be governmental agencies, local councils, environmental non-governmental organisations, or even individuals. In the case of Ramla l-Hamra, thanks to the perseverance of a private citizen, the permits were challenged and subsequently revoked. It is imperative that when third parties are given rights at law to object and/or provide feedback, these rights are made use of. This ensures not only public consultation but effective public participation in any process or decision which has an impact on the immediate area and/or the general public.

### 5.3 *Environmental Impact Assessments*

The significance of the environmental impact of a proposed construction on the site in 1974 provided the grounds for its refusal. Such environmental awareness followed the worldwide trend towards assessing the environmental impacts generated by development initiatives since the 1960s.

The objective of an environmental impact assessment (EIA)—“an assessment of the impact of a planned activity on the environment” [52: 1]—is to provide data for a less subjective decision-making process. It is undertaken “to identify and predict the impact on the environment and on man’s health and well-being of legislative proposals, policies, programmes, projects and operational procedures, and to interpret and communicate information about the impacts” [53: 8]. The International Association for Impact Assessment defines an EIA as “the process of identifying, predicting, evaluating and mitigating the biophysical, social and other relevant effects of development proposals prior to major decisions being taken and commitments made” [54: 1].

With respect to the outline planning stage, MEPA argued that “an EIA is a process whereby the Authority requests an applicant to predict, analyse and interpret significant environmental impacts of a proposed development. Since the proposed development could have qualified for an EIA the Authority, following the EIA procedures, requested the carrying out of certain studies during the Project Description Statement (PDS) stage” [42: 2]. An EIA was not requested, as “the applicant had submitted a sound and detailed PDS” which “was enough because the studies submitted to MEPA were sufficiently detailed to enable the Authority to waive the requirements for further studies” [42: 2]. This not only ran contrary to local planning legislation, but denied the authorities a rigorous assessment on which a decision could be reached on whether to commit the site for development. Third parties did challenge the fact that an EIA was not undertaken at the Auditor’s level, but did not question the PDS—its terms of reference and whether the studies undertaken were impartial and/or exhibited bias towards the proposed development. The PDS was submitted on 23 May 2005 [42], a fortnight prior to the MEPA sitting when the relative permit was issued. Furthermore, given that an EIA was not undertaken, no environmental monitoring and/or auditing of the project during and post-construction were thus included.

### 5.4 *Environmental Ethics*

The first chapter of Genesis, the first Biblical text, is an account of a number of stages of creation—God’s construction of the world—and includes an environmental audit undertaken at each phase [55]. In a joint declaration, dated 10 June 2002, Pope John Paul II and Patriarch Bartholomew stated that: “in our time we are witnessing a growth of an ecological awareness which needs to be encouraged, so that it will

lead to practical programmes and initiatives. ... In this perspective, ... all ... have a specific role to play in proclaiming moral values and in educating people in ecological awareness, which is none other than responsibility towards self, toward others, toward Creation” [56]. After the full permit was granted, publications and press releases issued by MEPA promulgated it as an upgrading of the site’s development. Projecting itself as the national compass for the protection of natural and cultural environs through planning policies and education campaigns, MEPA’s objective here was to ensure such a development took place, rather than to advance a speculative one.

### ***5.5 The End Does not Justify the Means***

Niccolò Machiavelli’s (1469–1527) dictum, “the end justifies the means”, is often read as a statement that any method suffices provided one’s objective is attained, even if said method goes beyond what is ethically correct. According to this interpretation, a goal may be morally important enough that any means of reaching it, any actions taken to support it, are justified. Actually, a closer reading of the work of this diplomat, author and philosopher suggests he was not putting forward an ethical code but a psychological argument: “if a leader does what it takes to win power and keep it, his methods will always be reckoned honourable and widely praised. The crowd is won over by appearances and final results. And the world is all crowd: the dissenting few find no space so long as the majority have any grounds at all for their opinions” [57: 71]. In either scenario, in contemporary environmental and development planning, such an approach may be unacceptable to the general public and, if tackled professionally, can be easily laid bare. This begs the question of whose actions are being justified. Are they the ones of the developer—which may win support from adjudicating bodies through lobbying or setting up and/or funding environmental NGOs to support the development proposal? The crux of the matter is individual versus collective responsibility. Patriarch Bartholomew called for the latter, as it champions the protection of the natural environment [58]. The common good is supreme. The two similar-sounding Maltese words, ‘is-sit’ and ‘is-sid’ (the site and the owner), are best used as a guidance: first is-sit, then is-sid. The integrity of the site comes before the desires of the owner.

### ***5.6 Construction Complements Creation***

Development planning complements creation; when it runs counter to nature, disasters are bound to happen. Development is imperative for progress; not the same cannot be said of speculation. Construction development involving excavation is irreversible in geological terms, yet the resultant development may compliment the site, even accentuate nature. A classical case study of a built project which complements nature on an ecologically sensitive slope is Kaufmann’s house. Erected partly

over a waterfall in the Laurel Highlands, Pennsylvania, this building was inscribed by UNESCO in 2019 as a World Heritage Site [59]. This iconic building, known as Fallingwater (1935–1938), was designed by Frank Lloyd Wright in 1935. It grows organically from the site; its integration with the natural landscape is impeccably dynamical; it was designed with nature.

The vocational call of architects and construction engineers is to design with nature, to complement creation. Phil Johnson (1906–2005) once claimed that “architects are pretty much high-class whores. We can turn down projects the way they can turn down some clients, but we’ve both got to say yes to someone if we want to stay in business”[60]. Architecture, as prostitution, is one of the oldest professions; indeed, it is the oldest vocation. Recalling the Homeric myth associated with Ramla l-Ĥamra and the pristine beauty of this unique picturesque and culturally laden site, one need not rape to make love. Although the action is identical, the intention is significantly different, and so are the consequences. Redeveloping the site at Ramla l-Ĥamra did not imply speculating on its beauty, metaphorically raping the site; one simply had to develop it—the unbuilt is as important as the built environs.

## 6 Conclusions

The development planning history of a given site not only outlines the chronology of planning applications; their respective files—including the site plan and drawings attached to an application—provide documentation of the processes and subsequent decisions in light of the legislation in force at the time. These files are therefore primary sources for the historical–legal circumstances of a given place, its immediate setting and the wider regional/national context. They document the evolution of the philosophy and practice of planning. The reason for including the location and previous applications and/or permits on site in any new request for development is not academic. It assists planning officials in tracing the relative files, reviewing them and assessing them in order to process the new request. Had the case officer been aware of all the files covering the development history of Ramla l-Ĥamra, s/he would have gained a holistic picture of the site, and been aware of the incongruency between the new and earlier requests for development.

The applicant’s failure to list previous applications and/or permits pertaining to the site meant not only that the application was filled incorrectly, but that the omission had a material bearing on the granted consent and thus qualified as fraud in terms of planning legislation. Furthermore, the applicant declared himself to be the sole owner of an area that included a third-party property—in this case a public road—and did not submit the correct certificate of ownership, on which basis the planning appeal for revocation of the outline permit was confirmed. This decision provides an interesting precedent. Although all planning permits are subject to third-party rights, and if a permit is issued on a site erroneously declared to belong to the applicant, the owner of the site may call on the court to issue a prohibitory injunction followed by a civil case, an incorrect certificate of ownership is a valid reason to revoke a permit.

When information submitted in applications is not complete, any resultant decisions will be informationally disabled. When factual elements of the case are excluded, the applicability or otherwise of policies will inevitably be misinformed. Including all information relevant to a given case helps determining the factual evidence necessary to assess it. Demonstrating the existence of such facts ensures comprehension of the holistic scenario of a given case; the facts establish the circumstances accurately. Truth may not be self-evident but it is demonstrable. In the case described here, despite MEPA's contestation of the objectors' factual claims, the planning regulator did concede the flawed decisions and revoke the permits unreservedly.

**Acknowledgements** The author is grateful to Professor Kevin Aquilina (former Dean, Faculty of Laws, University of Malta, Malta) for his comments and critical remarks on an earlier draft of this article and to Nadine Zammit for her help in preparing the figures. Photo/image credits: the base images of Fig. 1a to d are from Google Earth, and Fig. 4a from the Planning Authority (Malta), the owner of the survey sheet which was used in Fig. 2 and Fig. 4b.

**Declaration** The author was requested by Mary Carmen Bajada on her behalf and on behalf of SaveRamla Committee to put forward the case for the revocation of permits PA5138/02 and PA7902/05. Bajada—a resident and at the time a councillor at Xaghra Local Council—was a registered objector with respect to the latter permit under the terms of Article 32(5) of the DPA [3]. The author prepared a number of technical submissions with respect to this case; this article is primarily based on [7, 8, 27].

Bajada gave her consent to use the technical data, inclusive of the numerous technical reports prepared and submitted to the relevant public authorities in Malta. The professional fees and expenses relating to the case for the revocations were settled by Bajada.

**Conflicts of Interest** The author declares that he has no conflict of interest.

## References

1. House of Commons: Written Answers to Parliamentary Questions—Planning Permission: Fraud. HC Deb, 17 October 2011, c586W (2011). <https://publications.parliament.uk/pa/cm201011/cmhansrd/cm111017/text/111017w0001.htm#1110183000069>. Accessed 13 Nov 2022
2. Pirota G (1996) *The Maltese Public Service, 1800–1940: The administrative politics of a Micro-state*. Mireva Publications, Msida
3. Development Planning Act 1992. Chapter 356 of the Laws of Malta
4. Aquilina K (1999) *Development Planning Legislation: The Maltese Experience*. Mireva Publications, Msida
5. *Town and Country Planning Act 1990*. Central Government, United Kingdom (1990)
6. Anon (2007) Labour pledges to stop building of villas at Ramla l-Hamra. *Times of Malta* (5 Aug). <https://timesofmalta.com/articles/view/labour-pledges-to-stop-building-of-villas-at-ramla-l-hamra.9076>. Accessed 13 Nov 2022
7. Bianco L (2007) Revocation of outline planning permission PA5138/02. Letter to Chairman, Malta Environment and Planning Authority (16 July). [http://www.lino-bianco.com/otherprojects/images/6\\_revocation/25\\_07\\_6.pdf](http://www.lino-bianco.com/otherprojects/images/6_revocation/25_07_6.pdf). Accessed 12 Nov 2022
8. Bianco L (2007) Full development permit PA7902/05. Letter to Chairman, Malta Environment and Planning Authority and copies to the Director, Estate Management Department and the

- Commissioner of Police (16 July). [http://www.lino-bianco.com/otherprojects/images/6\\_revocation/25\\_07\\_7.pdf](http://www.lino-bianco.com/otherprojects/images/6_revocation/25_07_7.pdf). Accessed 12 Nov 2022
9. Mallia EA (2007) Ramla l-Hamra: Future danger? Times of Malta (13 Oct). <http://www.timesofmalta.com/articles/view/20071013/letters/ramla-l-hamra-futuredanger.2245>. Accessed 13 Nov 2022
  10. Homer: The Odyssey. William Heinemann, London (1919)
  11. Bianco L (ed) (2007) Socio-cultural initiatives for the locality of Xaghra, Gozo. Lino Bianco and Associates, Malta, 1. <https://www.um.edu.mt/library/oar/handle/123456789/45112>. Accessed 14 Nov 2022
  12. Vassallo J, Borg M, Cassar LF (2002) Case-study: Malta sites characterization. In: Scapini. Baseline research for the integrated sustainable management of Mediterranean sensitive coastal ecosystems: A manual for coastal managers, scientists and all those studying coastal processes and management in the Mediterranean, pp. 89–106. Istituto Agronomico per l’Oltremare, Florence (2002)
  13. Zammit T (1911) Annual report of the curator of the valletta museum in (1910–11). Government Printing Office, Malta
  14. Zammit T (1912) Archaeological discoveries in Malta and Gozo, during the year ending 31st March 1911. Archivium Melitense 1(1911–1912):189–194
  15. Mifsud C (2021) Revisiting Ramla l-Hamra Villa—New Discoveries and Observations on the Roman Villa Complex in Xaghra Gozo. Open Archaeol 7(1):84–97
  16. Department of Information: Government Notice No. 7. The Malta Government Gazette (6 January), 131–135 (1995)
  17. Planning Services Division: Structure Plan for the Maltese Islands: Draft final written statement with key diagram. Ministry for Development of Infrastructure, Beltissebħ, Malta (1990)
  18. Planning Services Division: Structure Plan for the Maltese Islands: Explanatory Memorandum. Ministry for Development of Infrastructure, Beltissebħ, Malta (1990)
  19. Malta Environment and Planning Authority: Gozo and Comino Local Plan. Malta Environment and Planning Authority, Floriana (2006)
  20. Hein C (2018) The What, Why and How of Planning History. In: Hein C (ed) The Routledge Handbook of Planning History. Routledge, New York and London, pp 1–10
  21. Zhao L, Kang C, Baihao L (2019) History, civilization and urban planning development in China—report from the 10th Academic Committee of Planning History & Theory Conference: 26–29 October 2018, Guilin, China. Planning perspectives 34(6):1051–1058
  22. Planning Authority Archive: Planning file PAPB1352/69. Floriana (1969)
  23. Planning Authority Archive: Planning file PAPB2084/84. Floriana (1984)
  24. <https://www.pa.org.mt/en/pacasedetails?CaseType=PA/02326/95>. Accessed 13 Nov 2022
  25. <https://www.pa.org.mt/en/pacasedetails?CaseType=PA/05138/02>. Accessed 13 Nov 2022
  26. <https://www.pa.org.mt/en/pacasedetails?CaseType=PA/07902/05>. Accessed 13 Nov 2022
  27. Bianco L (2007) Illegal development at site covered by planning applications PA5138/02 and PA7902/05. Letter to Chairman, Malta Environment and Planning Authority (05 October). [http://www.lino-bianco.com/otherprojects/images/6\\_revocation/25\\_07\\_25.pdf](http://www.lino-bianco.com/otherprojects/images/6_revocation/25_07_25.pdf). Accessed 12 Nov 2022
  28. Carbone G (2022) Former Parliamentary Assistant to MEP and later Deputy Prime Minister of Malta Louis Grech, Malta. Personal Communication
  29. Planning Authority: Development Control Guidance: Development outside built-up areas. Planning Authority, Marsa (1995)
  30. Civil Code of Malta. Chapter 16 of the Laws of Malta
  31. Criminal Code of Malta. Chapter 9 of the Laws of Malta
  32. Government Lands Act. Chapter 573 of the Laws of Malta
  33. Judicial protest 36/2007: Ulysses Lodge Company Limited vs Mary Carmen Bajada, Magistrates Court (Gozo) of General Superior Jurisdiction
  34. Planning Authority Archive: Planning file PA5138/02. Floriana (2002)
  35. Planning Directorate: Development Permit Application Report: PA5138/02. Malta Environment and Planning Authority, Floriana (2005)



36. Anon: MEPA: Notice of meeting to be held in public (07 July 2005). *The Malta Independent* (2 July), 4 (2005)
37. Malta Environment and Planning Authority: Report of the Auditor with respect to PA5138/02. Malta Environment and Planning Authority, Floriana (2005)
38. Planning Authority Archive: Planning file PA7902/05. Floriana (2005)
39. Planning Directorate: Development Permit Application Report: PA7902/05. Malta Environment and Planning Authority, Floriana (2007)
40. Anon: MEPA: Notice of meeting to be held in public (06 June 2007). *The Malta Independent* (2 June), 14 (2007)
41. Bondi L (2007) Bondi Plus (25 June). Public Broadcasting Services Archives, Gwardamangia
42. Malta Environment and Planning Authority: X-Plain 3, (2007)
43. Malta Environment and Planning Authority: Annual Report and Accounts 2007. Malta Environment and Planning Authority, Floriana, <https://era.org.mt/wp-content/uploads/2019/05/MEPA-Annual-Report-2007.pdf>. Accessed 18 Nov 2022
44. Bianco L (2007) Re Outline development permit PA5138/02, Full development permit PA7902/05. Letter to Chairman, Malta Environment and Planning Authority (02 July)
45. Mallia EA (2007) The mind readers. *Malta Today* (2 Sept). <http://archive.maltatoday.com.mt/2007/09/02/letters.html>. Accessed 13 Nov 2022
46. Mallia EA (2007) Disturbance at Ramla l-Hamra. *Times of Malta* (26 June). <https://timesofmalta.com/articles/view/disturbance-at-ramla-l-hamra.13278>. Accessed 13 Nov 2022
47. Emidio Azzopardi vs Malta Environment and Planning Authority, PAB 312/07 CF, 2 October 2009. <https://www.eprt.org.mt/en/search-details?cno=00312&cyr=07>. Accessed 13 Nov 2022
48. Emidio Azzopardi vs Malta Environment and Planning Authority, App. Civ. 39/2011 RCP, 30 October 2012
49. Emidio Azzopardi vs Malta Environment and Planning Authority, PAB 320/07 ISB, 28 July 2011. <http://www.eprt.org.mt/en/search-details?cno=00320&cyr=07>. Accessed 13 Nov 2022
50. Din l-Art Helwa and The Gaia Foundation vs Malta Environment and Planning Authority, PAB 00171/07 CF, 1 November 2011. <https://www.eprt.org.mt/en/search-details?cno=00171&cyr=07>. Accessed 13 Nov 2022
51. Bianco L (2018) Architecture, values and perception: Between rhetoric and reality. *Front Architect Res* 7:92–99
52. United Nations Economic Commission for Europe (1991) Policies and systems of environmental impact assessment. United Nations, New York
53. Munn RE (1979) Environmental impact assessment. Principles and procedures. Wiley, New York
54. Anon: What is impact assessment? International Association for Impact Assessment, Fargo (2009)
55. Bianco L (2021) The creation narrative in ‘Genesis’: A case of environmental monitoring and audit. *Eur J Sci Theol* 17(2):113–124
56. Pope John Paul II, Patriarch of Constantinople Bartholomew I: Common Declaration on Environmental Ethics. Venice (2002). [http://www.vatican.va/content/john-paul-ii/en/speeches/2002/june/documents/hf\\_jp-ii\\_spe\\_20020610\\_venice-declaration.html](http://www.vatican.va/content/john-paul-ii/en/speeches/2002/june/documents/hf_jp-ii_spe_20020610_venice-declaration.html). Accessed 14 Nov 2022
57. Machiavelli N (2014) *The Prince*. Penguin Classics, Great Britain
58. Chryssavgis J (2012) Call to vigilance and prayer. Patriarchal encyclicals for September 1<sup>st</sup>. In: *On earth as in heaven—ecological vision and initiatives of Ecumenical Patriarch Bartholomew*. Fordham University Press, New York, pp 23–64
59. UNESCO (2019) The 20th-Century Architecture of Frank Lloyd Wright. <https://whc.unesco.org/en/list/1496>. Accessed 16 Nov 2022
60. Glancey J (2008) Save us from this Tesco terroir. *Building Design* (Apr 25), 26

# Justification of the Heat Network Project Based on the Simulation of Hydraulic Models When Connecting Consumers



Dmitry Kitaev , Svetlana Tulskaia , and Tatiana Polivanova 

**Abstract** The object of the study is the water heating network of a residential area of the city. According to the development plan, it is planned to build 9 residential buildings, and the first stage of construction, consisting of 5 houses, has already been implemented. The remaining buildings will be commissioned one per year. The article discusses the issue of an expedient option for the construction of a water heating network, taking into account the development of its configuration when connecting new buildings. The problem is the fact that the heating network of the first stage of construction was designed without taking into account further development, i.e. it is intended to supply the estimated amount of heat for only five buildings. To solve the problem, water heating networks of promising development were designed. When connecting buildings of the second and subsequent stages of construction to the existing network, the flow rate will increase, and consequently, the hydraulic resistance, pressure losses and energy costs for fluid transportation will change. Based on the hydraulic modeling of the heating network, taking into account the input of all construction stages, the cost estimate for the costs of pumping the coolant and the project for the reconstruction of the existing network with an increase in throughput, an expedient option for building the network was determined.

**Keywords** City development · Heat network · Hydraulic regime · Head loss · Operating costs · Reconstruction · Estimated cost

---

D. Kitaev (✉) · S. Tulskaia  
Voronezh State Technical University, 84, 20-letiya Oktyabrya ul., Voronezh 394006, Russia  
e-mail: [dim.kit@rambler.ru](mailto:dim.kit@rambler.ru)

S. Tulskaia  
e-mail: [teplosnab\\_kaf@vgasu.vrn.ru](mailto:teplosnab_kaf@vgasu.vrn.ru)

T. Polivanova  
Southwest State University, 94, 50 let Oktyabrya ul., Kursk 305040, Russia  
e-mail: [viovr@yandex.ru](mailto:viovr@yandex.ru)

## 1 Introduction

The trend of today is the construction of new microdistricts of cities. In large cities, the central parts are densely built up and new construction is often carried out on the outskirts and territories adjacent to cities. A necessary condition for construction is to ensure the creation of communal infrastructure, in particular, a heat supply system. Existing master plans for urban development are long-term and consider a period of time of several decades. Territory planning projects take into account development in the short and medium term. The problem arises of synchronizing the development of the heat supply system with the construction of new buildings. The heat network is a complex and expensive construction project and it is difficult to attract investors for the implementation of long-term projects. A number of existing heat supply systems were built without considering the development perspective. A multivariant problem arises about the optimal development of the heat supply system. Similar tasks need to be solved within the framework of creating heat supply schemes for settlements. Not only the investment component of the initial project depends on the correctness of the decision, but also the operational component, which is borne by energy consumers in the form of a tariff for thermal energy.

The task of finding an expedient option for the development of a heat network is complicated by the need to consider several possible options, depending on the rate of commissioning of buildings. It is also necessary to resolve the issue of expediency indicators and their number. Modern researchers have proposed various criteria for the optimality of design solutions. Criteria such as the material characteristics of the network, construction and technological criteria, reliability criteria are used [1–3]. A number of researchers consider the criteria for hydraulic stability when connecting new consumers [4–6]. The solution of the problem of connecting the optimal number of heat network consumers is considered in [7]. Optimization of thermal–hydraulic regimes of a centralized heat supply network is considered in [8–11]. It should be noted that most works do not consider the prospect of operation during the design life of the network. According to a number of authors, a cost-effective solution without considering the time perspective is not optimal [11–13].

## 2 Materials and Methods

The paper considers the development area with residential buildings in the city of Tambov. The general plan of the construction area is shown in Fig. 1. According to the development plan of the area, in the first place of construction (I), residential buildings with the designation 2K1, 2K2, 2K3, 4K1, 4K2 fall into the second (II) 6K1, in the third (III) 6K2, in fourth (IV) 6K4, fifth (V) 6K3. The first stage of construction has already been implemented, and without taking into account the prospects for development. The remaining stages of construction are expected to be implemented one per year.

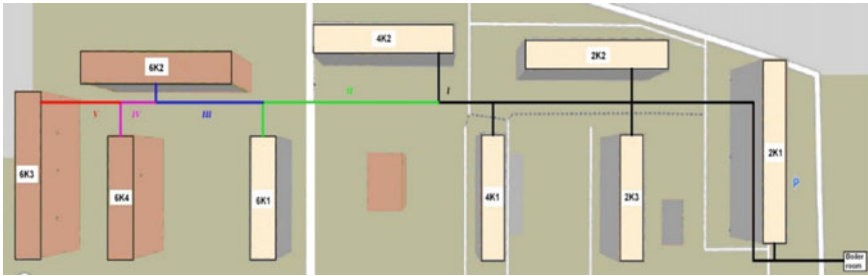


**Fig. 1** Scheme of the construction area with the queues for commissioning

Heating networks operate according to the temperature schedule 95/70 °C. The external pipelines are steel with polyurethane foam insulation, the laying of the heating network is underground in impassable channels. The heating network system is closed with independent connection of consumers.

For the buildings shown in Fig. 1, the calculated heat loads for each stage of construction were determined according to the aggregated indicators. The thermal power of the first stage of construction is 5.62 MW, and the total for the subsequent ones is 4.204 MW. Compared to the first stage, the load should increase by 74.8% over the entire construction period. Estimated water consumption for the heating network of the first stage of construction is 240.7 t/h. The total water consumption for subsequent stages of construction is 180.85 t/h, the consumption increases by 75.14%.

It is necessary to connect all subsequent stages of construction to the heating networks of the existing configuration of the first stage of construction. Water heating networks were designed for prospective development under the condition of fluid movement in the area of a developed turbulent regime, as is customary in direct hydraulic calculation. Obviously, when new consumers are connected to the existing network, the speed of water movement and pressure loss will change. The task is reduced to performing a reverse hydraulic calculation when the pipeline diameters and flow rates are known. Modeling of the hydraulic regime of the heating network of the first stage of construction was carried out when connecting new buildings 6K1, 6K2, 6K4, 6K3. Obviously, with an increase in flow rate and a constant diameter of the pipeline, the velocity of the liquid will increase. During the direct hydraulic calculation, the network was designed to operate in the region of a developed turbulent regime, therefore, the same regime will be maintained with an increase in flow. In this case, to calculate the coefficient of hydraulic friction  $\lambda$ , one can use the Prandel-Nikuradze formula

$$\lambda = \left( 1.14 + 2 \cdot \lg \frac{d}{k} \right)^{-2}, \tag{1}$$

d—is the pipe diameter, m; k—is the equivalent pipe roughness.

Figure 2 shows the results of calculations of the change in water velocity for sections of the design pipeline of the heating network of the first stage of construction with an increase in water consumption associated with the connection of new buildings.

From Fig. 2 it follows that when all consumers are connected, the speed of water movement in the first hydraulic section (in Fig. 2, the designation “1”) will increase from the initial value of 1.344–2.336 m/s, and in the fourth section it will increase by 4.24 times (from 0.9–3.82 m/s). An increase in speed will contribute to an increase in the values of specific pressure losses in the hydraulic sections of the network, shown in Fig. 3.

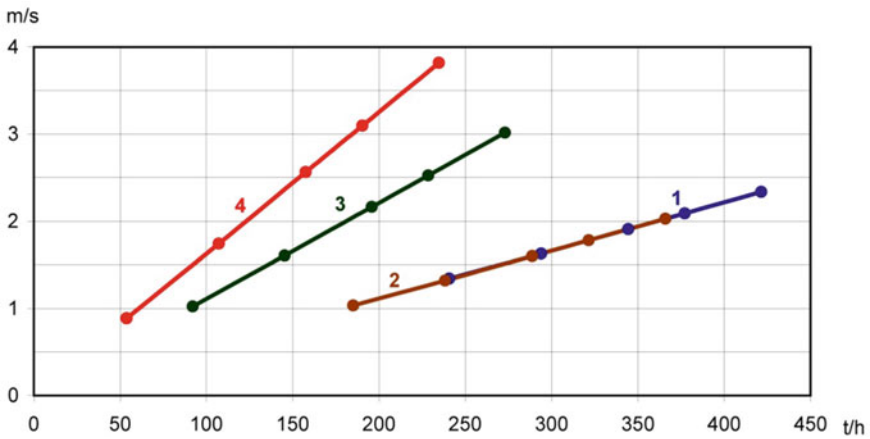


Fig. 2 Changes in speed by network sections

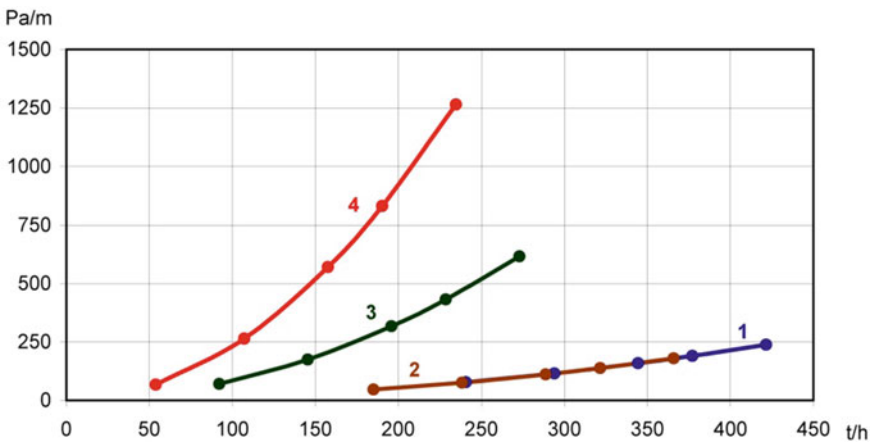


Fig. 3 Changes in specific head loss

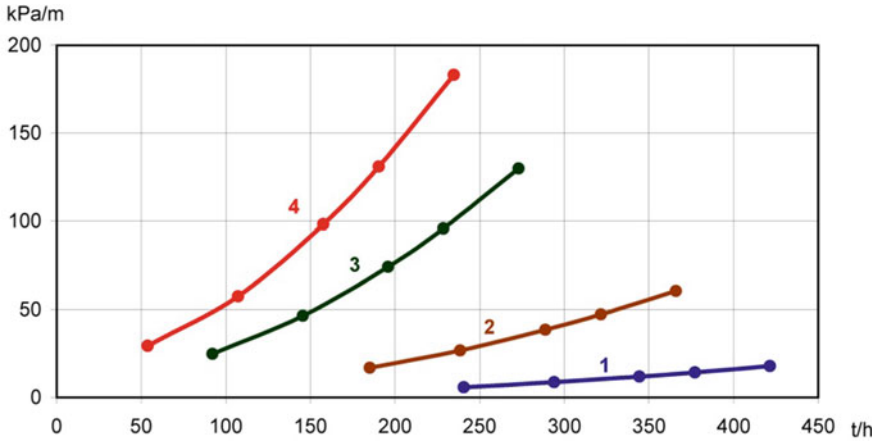


Fig. 4 Changes in head loss across network sections

According to Fig. 3, the most significant specific head loss will increase in Sect. 4 by 18.84 times (from 67.15 to 1265.15 Pa/m). The smallest increase will occur in Sect. 2 from 46.37 to 179.6 Pa/m (3.9 times). Obviously, in this case, the total pressure loss also increases (Fig. 4) to the greatest extent in Sect. 4 6.24 times (from 29.36 to 183.25 kPa).

To change the water flow in order to provide consumers with the calculated amount of heat at constant diameters, it is necessary to increase the pump drive power  $N$ , kW, which can be determined by the formula:

$$N = \frac{10^{-3} \cdot Q \cdot \rho \cdot g \cdot H}{3600 \cdot \eta \cdot \eta_m \cdot \eta_e}, \tag{2}$$

$Q$ —pump flow,  $m^3/h$ ;  $H$ —pump head,  $mH_2O$ ;  $\rho$ —is the density of water,  $kg/m^3$ ;  $g$ —is the acceleration of gravity,  $m/s^2$ ;  $\eta_m$ —mechanical transmission efficiency;  $\eta_e$ —electrical efficiency;  $\eta$ —is the efficiency of the pump.

The results of calculating the power expended for transporting the coolant while maintaining the diameters of the first stage of construction unchanged are shown in Fig. 5 (curve A).

It follows from Fig. 5 that power costs when connecting all consumers will increase by 20.4 times (from 2.2 to 44.8 kW). It should be noted that the standard service life of the pump unit specified by the manufacturer is 10 years. The recommended service life of the heating network in the calculations is assumed to be 30 years. The cost of electricity consumed for pumping the coolant at the current price level was determined. The total cost for 10 years, taking into account the cost of one pump, is 12,630,474.36 rubles, and for 30 years, taking into account the replacement of three pumps, 47,747,243.64 rubles.

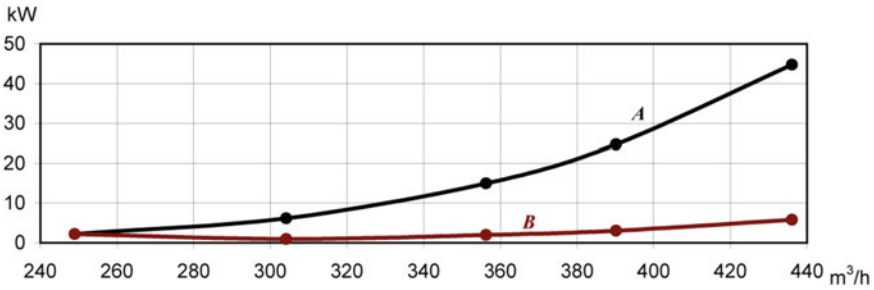


**Fig. 5** Changing the pump drive power: A—with constant diameters; B—taking into account the reconstruction of the network

The first option for the development of a heat network involves maintaining the existing network configuration and increasing the value of the pump power. Obviously, in this case, it will be necessary to replace not only the electric motor, but also the pump itself. With this option, the costs for the lifetime of the heating network will amount to 47.75 million rubles.

A variant of the network reconstruction with an increase in the diameters of the pipelines of the existing network was also considered in order to reduce subsequent operating costs for pumping the coolant. The hydraulic regime of the network was simulated when connecting from one to four buildings and the diameters were determined to provide the recommended water flow rates and losses. Commissioning of new buildings is carried out at the rate of one per year, and the network is planned to be reconstructed only once. In this case, the reconstructed network will operate for 4 years in the mode of reduced hydraulic resistance. As calculations have shown, during this period, in a number of sections of the network, fluid movement will be observed in the transition region of the turbulent regime. In this case, to find the coefficient of hydraulic friction, the Colebrook-White formula was used:

$$\lambda = \left[ -2 \cdot \lg \left( \frac{2,51}{\text{Re} \cdot \sqrt{\lambda}} + \frac{k}{3,7 \cdot d} \right) \right]^{-2}, \quad (3)$$

Re—Reynolds number.

Table 1 shows the sections of the network, indicating the values of the outer diameters  $D$  and wall thickness  $s$ , to be replaced and their length  $l$  in one-pipe terms.

Figure 5 (curve B) shows the results of calculating the power expended for transporting the coolant under the condition of reconstruction of the first stage heat network. The replacement of pipelines in the existing development with pipelines with large diameters will take place even before all four houses are put into operation, then the pressure in the network when connecting one, two and three houses will be less than at the design costs of the heating network when connecting four houses. This can explain the decrease in drive power in Fig. 5 (curve B) at flow rates of 304.139, 356.279 and 390.166 m<sup>3</sup>/h, because it directly depends on the pressure in the heating network.

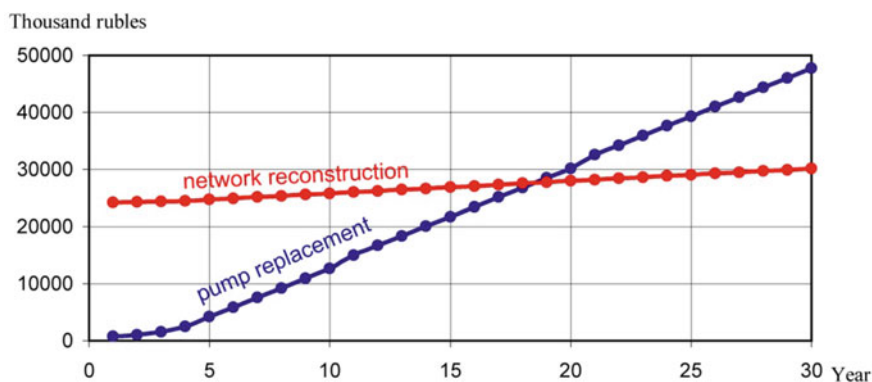
**Table 1** Pipeline sections to be replaced

Pipeline section number	Existing network diameter, D × s	Pipe diameter after reconstruction, D × s	pipe length l, m
1	273 × 8	377 × 9	46.01
2	273 × 8	325 × 8	177.56
3	194 × 6	325 × 8	91.96
4	159 × 4.5	273 × 8	35.97
10	159 × 4.5	273 × 8	116.47
11	152 × 4.5	219 × 6	70.77
13	152 × 4.5	194 × 6	23.5

### 3 Results and Discussion

To determine the economic feasibility of the considered approaches to the prospective development of the heating network, the cost of the options was determined. Taking into account the reconstruction of the heating network, the total cost of the option for 10 years will be 1,624,659.83 rubles for electricity, 425,761.48 rubles for the cost of one pump, 23,745,525.58 rubles for the cost of replacing pipelines, total 25 RUB 795,946.89 For 30 years of operation, the cost of electricity will be 5,999,888.66 rubles, the cost of three pumps will be 1,277,284.44 rubles, the cost of replacing pipelines will be 23,745,525.58 rubles, a total of 30,171,175.71 rubles.

Figure 6 shows the values of financial costs for the two considered options over time over a period of 30 years. It follows from Fig. 6 that the cost of increasing operating costs associated with pumping the coolant will become equal to the costs of network reconstruction with an increase in diameters in the 19th year of system operation (in 18.5 years). With the standard service life of the heating network of 30 years, it is economically feasible to reconstruct the heating network.

**Fig. 6** The cost of options for the development of a water heating network



The data obtained also indicate that, given the existing standard service life of thermal water networks, it is expedient to build, taking into account the prospective development of the region. It is also advisable to carry out the reconstruction of existing networks of small length with an increase in its capacity, because the costs of pumping coolant with large hydraulic losses after several years of operation begin to exceed the cost of reconstruction. The longer the standard service life of the equipment, the more effective the measures to increase the throughput of the heating network.

## 4 Conclusions

As a result of the work carried out, a feasibility study was proposed for an expedient option for the development of a water heating network. Based on the hydraulic modeling of the operating modes of the heating network when connecting new buildings according to the development plan of the area, changes in the speeds and pressure losses and costs for transporting the coolant were determined. Based on the reverse hydraulic calculation, sections of the existing network were identified that are subject to reconstruction in order to increase the throughput and reduce energy costs for pumping. Based on the calculation of the estimated cost of construction of heat networks for the options under consideration, taking into account the operating costs for pumping, an expedient development option was determined.

An approach is proposed to determine an expedient option for the development of heat networks based on hydraulic modeling of promising hydraulic regimes. It has been proved that with the recommended standard service life of heat networks, the option of reconstruction with an increase in throughput is the most appropriate.

## References

1. Melkumov VN, Sklyarov KA, Tulskeya SG, Chuikina AA (2018) Criteria of optimality and condition of the comparison of design solutions of systems of heat supply. *Russ J Build Constr Archit* 1(37):18–28. ISSN: 2542-0526
2. Melkumov VN, Chujkin SV, Papshickij AM, Sklyarov KA (2015) Modelling of structure of engineering networks in territorial planning of the city. *Russ J Build Constr Archit* 4(28):33–40. ISSN: 2075-0811
3. Semenov VN, Sazonov EV, Kitaev DN, Tertychny OV, Shchukina TV (2013) The influence of energy-saving on the development of the structure of thermal networks. *News of higher educational institutions. Construction* 8 (656):78–83. ISSN 0536-1052
4. Malakhov PI, Gushchin AS, Seminenko AS, Kireev VM (2019) Influence of connection of new consumers on hydraulic stability of thermal networks. *Bull Belgorod State Tech Univ; Shukhov VG* (2017) 8:82–87. [https://doi.org/10.12737/article\\_5968b450a65e68.85903478](https://doi.org/10.12737/article_5968b450a65e68.85903478)
5. Balaman SY, Selim H (2016) Sustainable design of renewable energy supply chains integrated with district heating systems: a fuzzy optimization approach. *J Clean Prod* 133:863–885. <https://doi.org/10.1016/j.jclepro.2016.06.001>

6. Minko VA, Seminenko AS, Alifanova AI, Elistratova JV, Tkach LV (2015) Assumptions and premises of heating systems hydraulic calculation methods: part 2. *Ecol Environ Conserv Pap* 21(2):1075–1080
7. Nemtinov VA, Terekhov SM, Nemtinova YU, Borisenko AB, Egorov SY (2017) Optimization model of heat supply consumers connection schedule to the heat supply system. In: 17TH international multidisciplinary scientific geoconferences, 29 June–5 July 2017, Albena, Bulgaria, pp 1013–1020. <https://doi.org/10.5593/sgem2017/21/S07.128>
8. Gumpert B, Wieland C, Spliethoff H (2019) Thermo-hydraulic simulation of district heating system. *Geothermics* 82:244–253. <https://doi.org/10.1016/j.geothermics.2019.07.001>
9. Wang H, Meng H, Zhu T (2018) New model for onsite heat loss state estimation of general district heating network with hourly measurements. *Energy Convers Manage* 157:71–85. <https://doi.org/10.1016/j.enconman.2017.11.062>
10. Chicherin S, Junussova L, Junussov T (2019) Minimizing the supply temperature at the district heating plant—dynamic optimization. In: E3S web of conferences, vol 118, p 02004. <https://doi.org/10.1051/e3sconf/201911802004>
11. Panferov SV, Panferov VI (2021) Optimum control of temperature and flow of the heating agent in heating networks with variable efficiency of pumps. *Bull S Ural State Univ Ser Constr Eng Archit* 21(2):52–59. <https://doi.org/10.14529/build210205>
12. Beloglazova TN, Romanova TN (2020) Directions of transformation of energy supply systems taking into account the prospective development of territories. *Constr Geotech* 12(4):68–82. <https://doi.org/10.15593/2224-9826/2021.4.05>
13. Chicherin SV (2020) Minimizing heat losses and enhancing reliability of a district heating network—analyzing project records and as-builts. *Bull Volgogr State Univ Archit Civ Eng. Ser: Constr Archit* 1(78):204–215

# Control of Structure Formation of Reaction Powder Concretes by Triboelectrization



Arsen Avakyan , Kirill Protsenko , Irina Erofeeva ,  
Elita Balathanova , Alexey Bulgakov , and Wen-der Yu 

**Abstract** Concretes containing dispersed fillers, reactive rock powders, microsilica and micro-hydrated kaolins are the object of research. The structural topology of such materials is predetermined by the activity of the dispersed filler. The unstable nature of the disperse systems, due to the high free surface energy, was used to increase the adhesion of cement to stone materials. Directional control of structure formation of reactive powder concretes is achieved by triboelectrification providing creation of transition layer on the surface of mineral material which interacts well with both cement and mineral substrate. An experimental research method based on a laboratory apparatus of a vortex layer is presented, which allows to form a triboelectric effect on the surface of fine-grained fillers. To break the aggregating effect of electromagnetic forces at the first stage of preparation of cement mortar for mixing cement with microfillers used energy-saturated high-speed mixers, and at the second stage for mixing cement composition with sand used traditional fillers.

**Keywords** Compressive strength · Microstructure · Silica · Concrete · Mechanical properties · Triboelectric effect

---

A. Avakyan · K. Protsenko  
South-Russian State Polytechnic University, 346428 Novocherkassk, Russia

I. Erofeeva · E. Balathanova  
National Research Mordovia State University, 430000 Saransk, Russia

A. Bulgakov (✉)  
Southwest State University, 305040 Kursk, Russia  
e-mail: [agi.bulgakov@mail.ru](mailto:agi.bulgakov@mail.ru)

W. Yu  
Chaoyang University of Technology, Jifeng East Road 168, 41349 Taichung, Taiwan  
e-mail: [wenderyu@cyut.edu.tw](mailto:wenderyu@cyut.edu.tw)

## 1 Introduction

Concretes based on composite binders have a complex structural topology. It is characterized by a special distribution of highly dispersed powder particles in them and is determined by the rate of flow, the mechanism of reaction interactions between the components and the degree of hydration of the binder, as well as the surface activity of the dispersed filler.

During rock crushing an instability of disperse systems occurs due to the high free surface energy, which can be used to increase the adhesion of cement to stone materials. As the bonds between the molecules are of electrical nature, it is possible to regulate the surface energy activity of contacting materials by means of electron-ion technology. One direction of this technology is triboelectrization. The triboelectric effect occurs when two materials with opposite electric charges intensive friction. Quartz sand forms a weak adhesion with cement stone. In order to achieve a strong bond between the mineral material and the cement it is necessary to create a transition layer on the surface of the mineral material which interacts well with both the cement and the mineral substrate. In order to create such a substrate, materials with a negative charge should be treated with a surface-active substance (surfactant) of the cationic type and surfactants of the anionic type with positive charges. A surfactant is a chemical compound which, when concentrated at the interface between thermodynamic phases, causes a reduction in surface tension. Triboelectric quartz sand particles with a negative charge are treated with a 2% lime suspension at a rate of 0.1% of the material weight and a 1% aqueous solution of cationic surfactants at a rate of 0.04%.

The formation of a permeable film of colloidal particles of hydrosilicates, hydroaluminates and hydroferrites, which themselves cannot diffuse, but does not stop the diffusion of ions through the layer of cement gel substance, creates the thinnest films of cement stone between the filler. It is known that micro-cracks occurring during hardening of the cement stone “eat away” up to 90% of the strength. Reducing the thickness of the cement film to the distance between the micro-cracks in the cement stone can significantly increase the strength of the cement stone and the material itself [1, 2].

The technology of production of concrete and other building materials with cement binders is based on surface phenomena at the boundaries of solid and liquid phases [1, 3–6]. In the process of hardening of binders during their interaction with water crystalline and gel-like products are formed which along with non-hydrated grains take part in the formation of the three-dimensional framework of the cement stone. Depending on the nature of the connection between the newly formed hardening structure is proposed to be divided into the following types: coagulation, crystallization, crystallization-condensation [7, 8].

Superplasticisers (SP) are used in concrete production. Cement mixed with water with SP adsorbs it primarily by hydrate formations, thus providing liquefaction of cement systems [9, 10]. In the process of clinker grinding with dry SP and following water mixing of resulting cement not only diluting ability of SP increases, but also

speed of cement stone strength gain radically changes. In order to obtain composite materials it is necessary to create strong and dense film at interphase boundaries of cement paste with aggregates [5, 11–14]. Increasing the chemical potential of the components [15] serves as a way of strengthening the adhesive contacts, which is achieved primarily by chemical action.

A number of works [16, 17] have experimentally determined the optimum strength values of concretes and other cement composites containing fine aggregates. It should be noted, however, that a large specific surface area causes adhesion of particles under electrostatic forces, which, in turn, leads to a loss of the interface. This fact is also confirmed by physico-chemical and other methods of investigation [7, 9, 16, 18–39].

By means of an electric charge of the required sign, energetically affecting the mineral component particles, it is possible to control the degree of molecular bonding of the cement matrix with the mineral filler and—simultaneously—the processes of structure formation. The electron–ion technology implies investigation of the processes of electric charges appearance on the surface of disperse materials [40–45]. Electric charges on the surface of particles under the influence of the environment are immediately neutralized, so it is necessary to ensure their fixation on the tribo-electrified surface with the help of surface-active substances, which is of practical importance [46–49].

Several stages can be distinguished in the mechanism of sand triboelectrification: mechanical action and “opening up” of the sand surface to reveal active nanostructures; pneumatic transport of sand grains through pipes to ensure dynamic contact with the pipe surface with the formation of an electrical double layer to charge the sand with charges equal in absolute value and opposite in sign; blocking of active nanostructures of the sand surface with an appropriate type of surfactant to prevent their neutralisation by the environment.

The aim of the study is to control the structure formation of reactive-powder concrete by triboelectrization in order to reduce cement consumption while achieving maximum homogeneity and strength.

## 2 Methods and Materials

Cement produced by Chechencement (Chiri Yurt village, Shali district, Chechen Republic, Russia) was used as binder. The chemical composition of this material contains the following elements (in %): CaO—64.67; SiO<sub>2</sub>—20.85; Al<sub>2</sub>O<sub>3</sub>—4.52; Fe<sub>2</sub>O<sub>3</sub>—4.02; SO<sub>3</sub>—1.81; MgO—13.9; K<sub>2</sub>O—0.7; Na<sub>2</sub>O—0.16; Cl—0.003; other calcination products—2.06.

The mineralogical composition of the binder includes (in %): 3CaO·SiO<sub>2</sub>—62.4; 2CaO·SiO<sub>2</sub>α—0; 2CaO·SiO<sub>2</sub>αβ—13.3; 3CaO·Al<sub>2</sub>O<sub>3</sub>(кyб)—4.1; 3CaO·Al<sub>2</sub>O<sub>3</sub>(opt)—4.1; 4CaO·Al<sub>2</sub>O<sub>3</sub>·Fe<sub>2</sub>O<sub>3</sub>—11.6; CaOSO<sub>4</sub>·2H<sub>2</sub>O—0; CaOSO<sub>4</sub>·0.5H<sub>2</sub>O—0; CaOSO<sub>4</sub>—0; K<sub>2</sub>SO<sub>4</sub>—0; Ca(OH)<sub>2</sub>—0; CaCO<sub>3</sub>—0; MgO—3.7; SiO<sub>2</sub>—0.

Chemical composition of dolomite and quartz powders used as fillers (in %). Quartz sand: SiO<sub>2</sub>—69.35; Al<sub>2</sub>O<sub>3</sub>—13.01; Fe<sub>2</sub>O<sub>3</sub>—3.42; CaO—3.88; MgO—2.41; SO<sub>3</sub>—0.06; K<sub>2</sub>O—2.05; Na<sub>2</sub>O—1.64; Cl—0.003; W—0.75; п.п.п.—4.55. Доломит: SiO<sub>2</sub>—0; Al<sub>2</sub>O<sub>3</sub>—0.02; Fe<sub>2</sub>O<sub>3</sub>—0.06; CaO—37.17; MgO—20.14; SO<sub>3</sub>—0.04; K<sub>2</sub>O—0; Na<sub>2</sub>O—0.18; Cl—0.049; W—0.40; other calcination products—46.83.

Mathematical experiment planning methods were used in the research. The implemented simplex-scheme plan Scheffe included ten experiments. Table 1 presents the third-order planning matrix for the three-component system.

The variation factors according to the experiment planning matrix were: X<sub>1</sub>—quartz powder with S<sub>sg</sub> = 3000–3100 cm<sup>2</sup>/g; X<sub>2</sub>—dolomite powder (CaO > 97%) with S<sub>sg</sub> = 6000–6200 cm<sup>2</sup>/g; X<sub>3</sub>—dolomite powder (CaO > 97%) with S<sub>sg</sub> = 9000–9200 cm<sup>2</sup>/g. The amount of each fraction was taken as control variable, the amount of other components was recorded and remained constant throughout the experiment. The composition-property diagram was studied with the vertices Z<sub>1</sub>(X<sub>1</sub> = 100%, X<sub>2</sub> = 0%); Z<sub>2</sub>(X<sub>2</sub> = 100%, X<sub>3</sub> = 0%); Z<sub>3</sub>(X<sub>3</sub> = 100%, X<sub>1</sub> = 0%). Flexural and compressive strength, dynamic modulus of elasticity and water demand were the optimised values for the suspension component.

Triboactivation can be carried out by blowing silica sand through a metal or dielectric tube [50]. The emergence of free radicals as a result of breaking chemical bonds, changing the structure of surface layers of mycelial particles formed in the process of dispersion, can be highlighted as key factors in this process. It should be noted that free radicals have extremely high activity, which allows them to easily interact chemically with ordinary molecules of other substances [51–53]. Triboelectricization of dry materials is promising in case of its application to all fractions of crushed stone, sand and mineral powder. This process is feasible if appropriate equipment is used [54].

For formation of triboelectric effect on the surface of fine-grained fillers a laboratory apparatus of vortex layer developed by Logvinenko D. D. was applied (Fig. 1) [55]. It is a pipeline with a diameter of 300 mm, which is located in the inductor of a rotating electromagnetic field. Several thousand (5 kg) cylindrical ferromagnetic elements (needles) with diameter of 1 mm and length of 20 mm are placed in the working area.

**Table 1** Third-order simplex lattice plan for a three-component mixture

N	X <sub>1</sub>	X <sub>2</sub>	X <sub>3</sub>	Y	N	X <sub>1</sub>	X <sub>2</sub>	X <sub>3</sub>	Y
1	1	0	0	Y <sub>1</sub>	6	0	2/3	1/3	Y <sub>223</sub>
2	0	1	0	Y <sub>2</sub>	7	0	1/3	2/3	Y <sub>233</sub>
3	0	0	1	Y <sub>3</sub>	8	2/3	0	1/3	Y <sub>113</sub>
4	2/3	1/3	0	Y <sub>112</sub>	9	1/3	0	2/3	Y <sub>133</sub>
5	1/3	2/3	0	Y <sub>122</sub>	10	1/3	1/3	1/3	Y <sub>123</sub>
1	1	0	0	Y <sub>1</sub>	6	0	2/3	1/3	Y <sub>223</sub>

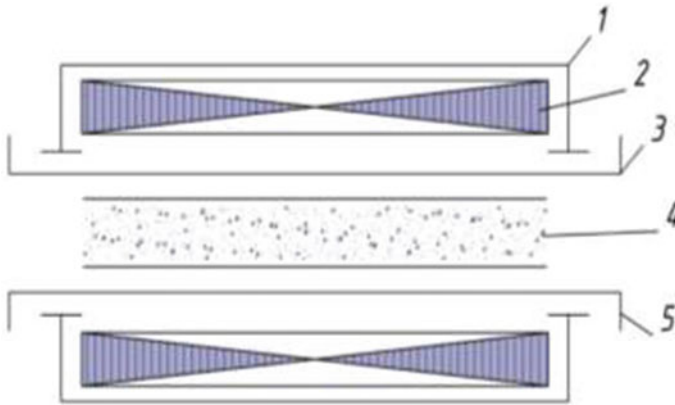


**Fig. 1** Vortex apparatus: 1—housing; 2—inductor; 3—working space; 4—ferromagnetic elements (needles); 5—exchangeable insert

A rotating electromagnetic field is created by an external source of electricity. The needles become a dipole as a result of the interaction of the primary field with the fields of the needles themselves, resulting in the appearance of chaotically rotating needles. Again, this chaos is only apparent, so the results are probabilistic. The rotation speed of the needles is in direct correlation with the rotation speed of the electromagnetic field. Filler and filler particles gain static electricity as a result of direct collisions of the needles with each other and with the material particles that are loaded into the work area. This process is accompanied by dispersion, “peeling off” of the surface layer of the particles and their homogenization. Note that the vortex layer apparatus increases the rate of chemical reactions by a factor of 1.5–2 times [56].

These processes are ensured primarily by fixing surfactant layers in the surface layer of low-active mineral particles, which interact well with both the mineral base and the binder, which is why they are intermediate chemical bonds. All this will bring the reaction centres of the juvenile mineral surface closer to the active functional groups of the cement to such distances, which are available for molecular action in order to activate their interaction.

### 3 Results and Discussion

Optimal conditions for agglomeration and particle cohesion in filled cement systems are achieved through the use of hydration-active microfillers and reduction of particle spacing through optimum particle size distribution and reduced water content. In this case the contact points between the cement or cement particles and the microfillers, brought close to minimum distances, may act as active crystallisation zones. The

**Table 2** Planning matrix and results of the experiment

Nr	Index	Z, m.p., %			Strength, MPa		D, E·10 <sup>3</sup> MPa	W, %
		Z <sub>1</sub>	Z <sub>2</sub>	Z <sub>3</sub>	FS	CS		
1	n <sub>1</sub>	100	0	0	16.6	43.7	48.7	48.7
2	n <sub>2</sub>	0	100	0	22.1	57.6	44.7	44.7
3	n <sub>3</sub>	0	0	100	19.8	58.1	24.16	46.7
4	n <sub>122</sub>	33	67	0	19.3	46.6	22.94	43.5
5	n <sub>133</sub>	33	0	67	9.9	29.8	17.96	46.7
6	n <sub>233</sub>	0	33	67	11.1	41.5	19.07	52.7
7	n <sub>112</sub>	67	33	0	21.4	62.8	26.62	42.0
8	n <sub>113</sub>	67	0	33	16.9	55.7	23.08	45.3
9	n <sub>233</sub>	0	67	33	26.0	63.8	29.03	40.7
10	n <sub>123</sub>	33.3	33.3	33.4	8.3	31.0	15.77	50.7

Where Z—mixture composition, mass of particle %, FS—flexural strength, CS—compressive strength, D—dynamic modulus of elasticity, E·10<sup>3</sup> MPa, W—water content, %

physical and mechanical properties of cement composites can be improved by using binary filler, which is a mixture of quartz and limestone powders [57, 58].

In the manufacture of the compositions, the cement content was assumed to be 100% and the amount of water was taken as an indicator of equal mobility. As for the other components, in particular the fillers of different fractions, their content was selected according to a planning matrix which contains the real values of the individual factors (Table 2). In addition to the planning matrix, Table 2 shows the values for the compositions of the cement composites determined by physical and mechanical tests and the experimental results.

Statistical methods were applied for the processing of experimental results. As a result, regression equations were obtained. Let's result equations of regression of indicators of composites on durability at a bending ( $R_b$ ), compression ( $R_c$ ), a modulus of elasticity (E) and water consumption (W):

$$\begin{aligned}
 R_b = & X_1 + 0.33X_2 + 1.19X_3 + 0.247X_1X_2 - 1.327X_1X_3 - 0.675X_2X_3 \\
 & + 1.552X_1X_2(X_1 - X_2) + 3.262X_1X_3(X_1 - X_3) \\
 & + 5.76X_2X_3(X_2 - X_3) - 12.915X_1X_2X_3
 \end{aligned} \quad (1)$$

$$\begin{aligned}
 R_c = & X_1 + 1.31X_2 + 1.32X_3 + 0.405X_1X_2 - 0.832X_1X_3 - 0.54X_2X_3 + \\
 & + 3.195X_1X_2(X_1 - X_2) + 4.702X_1X_3(X_1 - X_3) \\
 & + 3.465X_2X_3(X_2 - X_3) - 10.867X_1X_2X_3;
 \end{aligned} \quad (2)$$



$$\begin{aligned}
 E = & X_1 + 1.24X_2 + 1.2X_3 - 0.112X_1X_2 - 0.382X_1X_3 - 0.135X_2X_3 \\
 & - 0.067X_1X_2(X_1 - X_2) + +2.137X_1X_3(X_1 - X_3) \\
 & + 3.285X_2X_3(X_2 - X_3) - 8.01X_1X_2X_3;
 \end{aligned}
 \tag{3}$$

$$\begin{aligned}
 W = & X_1 + 0.91X_2 + 0.95X_3 - 0.36X_1X_2 - 0.157X_1X_3 - 0.112X_2X_3 \\
 & - 0.405X_1X_2(X_1 - X_2) - -0.247X_1X_3(X_1 - X_3) \\
 & - 1.597X_2X_3(X_2 - X_3) + 3.555X_1X_2X_3.
 \end{aligned}
 \tag{4}$$

Based on the regression equations obtained, the graphical relationships shown in Fig. 2 are constructed.

The graphs show that, from the point of view of improving the strength properties of cement composites, a filler in the form of particles of different particle size distribution is optimal. This option allows to increase the strength of cement composites by 10–15% in comparison with a single fraction. Optimisation of the composition of the filled binder makes it possible to reduce cement consumption and the cost of concrete.

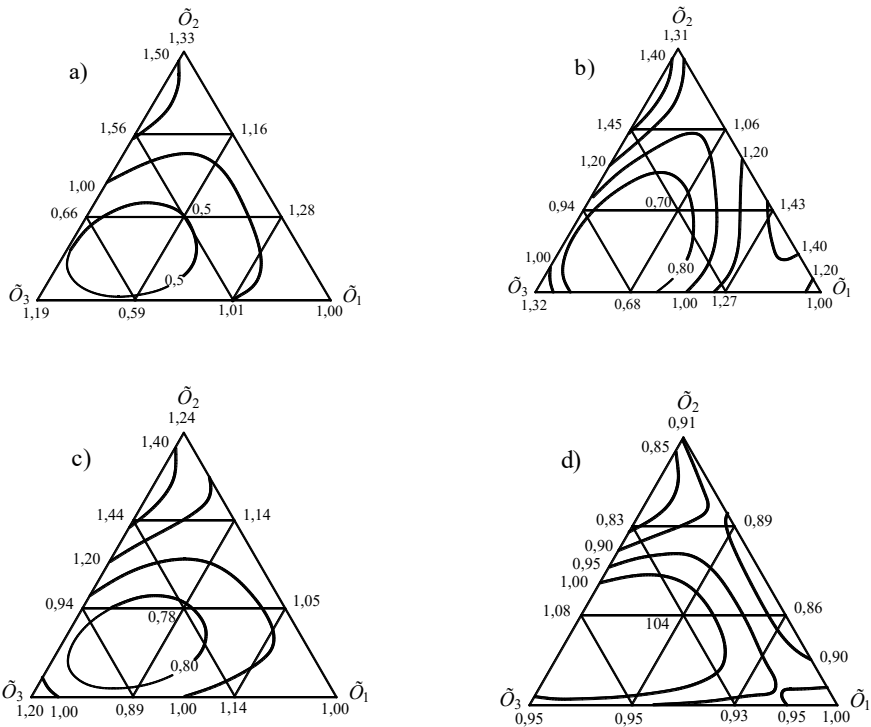


**Fig. 2** Changes in relative flexural strength (a), compressive strength (b), dynamic modulus of elasticity (c) and water demand (d) of cement composites

The application of surfactant and electrolyte additives creates additional conditions for purposeful formation of improved structure and improvement of physical and mechanical properties.

Triboelectrically activated sand served as the basis for the production of  $4 \times 4 \times 16$  cm samples. A cement-carbonate-quartz composition was used as a matrix. Information on the content of the components in the investigated compositions as well as the results of comparative tests of the samples made with inactivated and triboelectrified sand are presented in Table 3.

The analysis of the results of the study leads to the conclusion that triboactivation improves the strength properties of cement composites.

It should be emphasised that this technology of concrete preparation allows saving up to 70% of cement in comparison with conventional options and, what is equally important, to obtain high-strength concretes. It is implemented using a high-speed mixer by preparing a cement composition based on finely dispersed mineral materials and cement. The resulting mixture is then combined in a compulsory mixer with triboelectric fine aggregate.

Due to the destruction of the crystal lattice of the activated materials, surface energy is accumulated and further increased due to the triboelectricity effect. At the stage of composite material formation, the process of defect formation must be inhibited by the same defects (pores, microcracks, dislocations) that were the sources of the acts of destruction at the stage of activation, as well as by increasing the dispersibility of the stone structure, i.e. increasing the number of dislocation movement obstacles. This requires minimum W/C at the most efficient compaction methods and optimal grain sizes of the composition. The combination of amorphous structures in the process of activation, combined with crystalline structures in the form of sand in the architecture of the cement stone are the best in terms of synthesis of its strength. This requires an optimum grain size and ratio of cement slurry components with a developed surface area and a minimum W/C at the most efficient compaction methods [59–62].

**Table 3** Test results

Nr	Mixture composition, mass of particle						Type of aggregate	Strength, MPa	
	PC	DP1	DP2	QP	W/C	KII		FS	CS
1	100	33.3	33.3	33.4	0.4	200	Non-activated	9.6	35
2	100	33.3	33.3	33.4	0.4	200	Activated	11.5	45

Where PC—Portland cement; DP1—dolomite powder with  $S_{sg} = 6000\text{--}6200$  cm<sup>2</sup>/g; DP2—dolomite powder with  $S_{sg} = 9000\text{--}9200$  cm<sup>2</sup>/g; QS—quartz powder with  $S_{sg} = 3000\text{--}3100$  cm<sup>2</sup>/g; W/C—water/cement; FS—flexural strength, CS—compressive strength

## 4 Conclusions

1. Fine-grained mineral powders are primarily subject to electrostatic forces in contrast to coarse-grained components which are subject to gravitational forces. In this regard, two steps are necessary in the preparation of the cement mortar. In order to break the aggregating action of electromagnetic forces in the first stage of mixing cement with the micro filler it is necessary to use energy-saturated high-speed mixers. At the second stage of mixing cement composition with sand traditional mixers can be used.
2. The effectiveness of the combined use of acidic quartz and alkaline lime microfillers in the cement composition has been determined.
3. The optimum specific surface area of microfillers is determined: dolomite powder  $S_{sg} = 6000\text{--}6200 \text{ cm}^2/\text{g}$ , quartz powder  $S_{sg} = 3000\text{--}3100 \text{ cm}^2/\text{g}$ ; quartz sand fractions 0.315–0.63.
4. By methods of mathematical planning of experiment the quantitative relation between cement and microfillers has been determined: Portland cement: dolomite powder  $S_{sg} = 6000\text{--}6200 \text{ cm}^2/\text{g}$ ; dolomite powder  $S_{sg} = 9000\text{--}9200 \text{ cm}^2/\text{g}$ ; quartz powder with  $S_{sg} = 3000\text{--}3100 \text{ cm}^2/\text{g}$ ; quartz sand fractions 0.315–0.63.
5. It was found that the compressive strength of the activated mixture is 1.3 times higher than the strength of the non-activated mixture, and the flexural strength is 1.2.

## References

1. Kalashnikov V, Erofeev V, Tarakanov O (2016) Suspension-filled concrete mixtures for new generation powder-activated concretes. In: Proceedings of higher education institutions. Construction 10–11(694–695):120
2. Erofeev V, Bobryshev A, Shafigullin I, Khalilov I, Sibgatullin K, Igtisamov R, Lakhno A (2016) Theoretical evaluation of rheological state of sand cement composite systems with polyoxyethylene additive using topological dynamics concept. Solid State Phenom 871:96–103
3. Maximova I, Makridin N, Polubarova Y, Erofeev V (2018) Comprehensive assessment of the kinetic parameters of structural strength of cement stone in the time range from 28 days to 4.5 years after steaming. Reg Arch Constr 3(36):23–30
4. Maximova I, Erofeev V, Makridin N (2018) Kinetic parameters of hydration structure formation and hardening of cement stone at age up to 9.5 years after steaming. In: Proceedings of higher educational institutions. Construction 3(711):24–33
5. Erofeev V, Makridin N, Maximova I (2019) Kinetic parameters and defining equations of structure formation and hardening of cement stone of different structure in the time interval up to 18 years after steaming. In: Proceedings of higher education institutions. Construction 3(723):5–19
6. Mehta P, Monteiro PJM (2006) Concrete: microstructure, properties, and materials, 3rd edn. McGraw-Hill, New York, NY, USA, 659 p
7. Taylor HFW (1996) The chemistry of cement. M.: Mir, 560 p
8. Aïtcin P-C, Flatt RJ (2015) Science and technology of concrete admixtures, 1st edn. Elsevier Science & Technology, Cambridge, UK

9. Batrakov V (1998) Modified concretes. Theory and practice. M. Technoproject, 768 p
10. Lea FM, Hewlett PC (1998) Lea's chemistry of cement and concrete, 4th edn; Arnold; Copublished in North, Central, and South America; Wiley, London, UK; New York, NY, USA, 1053p
11. Erofeev V, Emelyanov D, Tretiakov I, Kalashnikov V, Balathanova E, Erofeeva I, Smirnova O, Matvievskiy A (2016) Biological resistance of cement composites filled with limestone powders. *Solid State Phenom B* 871:22–27
12. Erofeev V (2016) Frame construction composites for buildings and structures in aggressive environments. *Procedia Eng* 1444–1447
13. Erofeev V, Emelyanov D, Tretiakov I, Kalashnikov V, Balathanova E, Erofeeva I, Smirnov V, Matvievskiy A (2016) Biological resistance of cement composites filled with dolomite powders. *Solid State Phenom B* 871:33–39.
14. Bohac M, Stanek T, Zezulova A, Rybova A, Kubatova D, Novotny R (2019) Early hydration of activated belite-rich cement. *Adv Mater Res* 1151:23–27. [CrossRef]
15. Prokhorov A (1998) The Encyclopaedia of physics. Moscow: The Big Russian Encyclopaedia. T.5: Stroboscopic devices—brightness, 760 p
16. Bobrishev A, Shafigullin L, Sotnikov M, Vyacheslav A, Erofeev V, Treshchev A (2016) Study of effects of redispersable latex powders on hardening kinetics of cement-sand composites. *Res J Pharmaceut Biol Chem Sci B* 7(4):795–802
17. Maksimova I, Erofeev V, Makridin N, Polubarova Y (2016) Analysis of superplasticizer effect on phase composition and fracture structural mechanics parameters of cement stone of different age. *Izvestia vysshee uchebnykh obrazovatel'nykh uchebnykh obrazov.* Construction 5(689):29–38
18. Ramachandran V (1988) Additives in concrete: a reference manual—M. Stroyizdat, 286 p
19. Kalashnikov V, Tarakanov O (2017) On the use of complex additives in new generation concrete. *Build Mater* 1–2:62–67
20. Afanas'ev N, Tseluyko M (1989) Additives in concretes and mortars. Kiev, Budivelnik, 128 p
21. Kapriyelov S, Schoenfeld A (2002) MB series modifiers and high performance concretes. Technical bulletin of the research institute of reinforced concrete
22. Blanco R, Lam M (2005) Non-conventional aggregates and mineral admixtures in high-performance concrete. In: Proceedings of the seventh international symposium on the utilization of high strength/high-performance concrete, Washington, WA, USA, pp 123–143
23. Schneider M (2019) The cement industry on the way to a low-carbon future. *Cem Concr Res* 124:105792. [CrossRef]
24. Bulgakov A, Erofeev V, Bogatov A, Smirnov V, Schach R (2016) Innovative production technology of binding and building composite materials on the basis of glass wastes. In: Zingoni A (ed) Insights and innovations in structural engineering, mechanics and computation. Taylor & Francis Group, London, pp 1583–1586. ISBN 978-1-138-02927-9. Proceedings of the sixth international conference on structural engineering, mechanics and computation (SEMC 2016), 5–7 September 2016, Cape Town, South Africa
25. Ludwig U, Pohlmann R (1985) Production of low-lime portland cements. *Zem.-Kalk-Gips* 1985 38:595–598
26. Kalashnikov V, Erofeev V, Tarakanov O (2016) Technical and economic efficiency of implementation of architectural and decorative powder-activated carbonate sand concretes. *Izvestiya vysokikh uchebnykh obrazovatel'nykh obrazov.* Construction № 6 (690), pp 39–46
27. Kovalev Ya (2002) Activation technologies of road composite materials. Minsk, BelEn, 336 p
28. Stark J, Moser B, Eckart A (2001) New approaches to cement hydration. Part 1. *ZKG International*, № 54, pp 52–60
29. Morsli K, De la Torre A, Stober S, Cuberos AJM, Zahir M, Aranda MAG (2007) Quantitative phase analysis of laboratory-active belite clinkers by synchrotron powder diffraction. *J Am Ceram Soc* 90:3205–3212. [CrossRef]
30. Odler I (2000) Special inorganic cements; E & FN Spon, New York, NY, USA, 395 p
31. Luo Z, Li W, Wang K, Shah SP (2018) Research progress in advanced nanomechanical characterization of cement based materials. *Cem Concr Compos* 94:277–295. [CrossRef]

32. Plank J, Hirsch C (2007) Impact of zeta potential of early cement hydration phases on superplasticizer adsorption. *Cem Concr Res* 37:537–542. [CrossRef]
33. Plank J, Sachsenhauser B (2006) Impact of molecular structure on zeta potential and adsorbed conformation of .ALPHA.Alyl.OMEGA. Methoxypolyethylene Glycol-Maleic Anhydride Superplasticizers. *J Adv Concr Technol* 4:233–239. [CrossRef]
34. Marushchak U, Sanytsky M, Mazurak T, Olevych Y (2016) Research of nanomodified portland cement compositions with high early age strength. *East-Eur J Enterp Technol* 6:50–57. [CrossRef]
35. Sanytsky MA, Maruschak UD, Mazurak TA (2016) Nanomodified Portland cement compositions with high early strength. *Constr Mater Sanit Equip* 57:147–154
36. Wille K, Boisvert-Cotulio C (2015) Material efficiency in the design of ultra-high performance concrete. *Constr Build Mater* 86. [CrossRef]
37. Skibsted J, Snellings R (2019) Reactivity of supplementary cementitious materials (SCMs) in cement blends. *Cem Concr Res* 124:105799. [CrossRef]
38. Ashraf W (2018) Microstructure of chemically activated gamma-dicalcium silicate paste. *Constr Build Mater* 185:617–627. [CrossRef]
39. Mucsi G, Papné N, Ulsen C, Oliveira P, Kristály F (2021) Mechanical activation of construction and demolition waste in order to improve its pozzolanic reactivity. *ACS Sustain Chem Eng* 9:3416–3427. [CrossRef]
40. Arora A, Yao Y, Mobasher B, Neithalath N (2019) Fundamental insights into the compressive and flexural response of binder- and aggregate-optimized ultra-high performance concrete (UHPC). *Cem Concr Compos.* [CrossRef]
41. Harper WR (1967) Contact and frictional electrification. Clarendon Press, Gloucestershire, UK
42. Chang J, Kelly A, Crowley JM (1995) Handbook of electrostatic processes. Taylor & Francis, Abingdon, UK
43. Cross J (1987) Electrostatics: principles, problems and applications. Adam Hilger, Bristol, UK
44. Matsusaka S, Maruyama H, Matsuyama T, Ghadiri M (2010) Triboelectric charging of powders: a review. *Chem Eng Sci* 65:5781–5807
45. Duff N, Lacks DJ (2008) Particle dynamics simulations of triboelectric charging in granular insulator systems. *J Electrostat* 66:51–57
46. Jeziorska R, Szadkowska A, Studzinski M, Zubrowska M (2021) The use of modified silica to control the morphology of polyamide 11 and poly(phenylene oxide) blends. *Polimery* 66:399–410. [CrossRef]
47. Zhou H, Rong M, Zhang M, Friedrich K (2006) Effects of reactive compatibilization on the performance of nano-silica filled polypropylene composites. *J Mater Sci* 41:5767–5770. [CrossRef]
48. Elias L, Fenouillot F, Majeste JC, Cassagnau P (2007) Morphology and rheology of immiscible polymer blends filled with silica nanoparticles. *Polymer* 48:6029–6040. [CrossRef]
49. Lee SH, Kontopoulou M, Park CB (2010) Effect of nanosilica on the co-continuous morphology of polypropylene/polyolefin elastomer blends. *Polymer* 51:1147–1155. [CrossRef]
50. Kravchenko S (1987) Preparation and application of triboactivated sands in road asphalt concrete. PhD candidate of technical sciences, Minsk, 143 p
51. Gallo C, Lama W (1976) Some charge exchange phenomena explained by a classical model of the work function. *J Electrostat* 2:145–150
52. Šupuk E, Seiler C, Ghadiri M (2009) Analysis of a simple test device for tribo-electric charging of bulk powders. *Part Part Syst Charact* 26:7–16
53. Budnichenko S, Kovalev J, Goig E, Mikhalenok D (2010) Activation of mineral materials in the production of asphalt mixtures. *Automob Roads Bridg* 2:31–38
54. Prokopets V (2005) Increasing the efficiency of road-building materials by mechanical-activation modification of the initial raw materials. Doctoral thesis, Omsk, 342 p
55. Vershinin I, Vershinin N (2007) Apparatuses with rotating electromagnetic field. *Salsk* 368 p
56. Mishchenko M, Bokov M, Grishaev M (2015) Activation of material processing processes in apparatuses with rotating electromagnetic field. *Fundam Res* 2(16):3508–3512

57. Shi C, Qu B, Provis JL (2019) Recent progress in low-carbon binders. *Cem Concr Res* 122:227–250. [CrossRef]
58. Feng Y, Kero J, Yang Q, Chen Q, Engström F, Samuelsson C, Qi C (2019) Mechanical activation of granulated copper slag and its influence on hydration heat and compressive strength of blended cement. *Materials* 12:772. [CrossRef]
59. Uzal B, Turanlı L (2012) Blended cements containing high volume of natural zeolites: properties, hydration and paste microstructure. *Cem Concr Compos* 34:101–109. [CrossRef]
60. Hu C, Li Z (2015) A review on the mechanical properties of cement-based materials measured by nanoindentation. *Constr Build Mater* 90:80–90. [CrossRef]
61. Lee H, Vimonsatit V, Chindaprasirt P (2016) Mechanical and micromechanical properties of alkali activated fly-ash cement based on nano-indentation. *Constr Build Mater* 107:95–102. [CrossRef]
62. He Z, Qian C, Zhang Y, Zhao F, Hu Y (2013) Nanoindentation characteristics of cement with different mineral admixtures. *Sci China Technol Sci* 56:1119–1123. [CrossRef]

# Rational Design of Composite Strengthening of Reinforced Concrete Elements for Experimental Research



Vladimir Rimshin  and Pavel Amelin 

**Abstract** In recent years, due to the increase in design loads in operated buildings, there is a need to strengthen their load-bearing structures. The use of high-modulus composite materials contributed to the further development of reinforcement methods. The analysis of the works related to the composite reinforcement of reinforced concrete bendable structures showed the need for experiments with a variation in the ratio of the length of the composite reinforcement to the calculated length of the element. This paper presents a preliminary calculation and selection of options for strengthening reinforced concrete bendable elements, including their inclined sections, for further field experimental studies using normative methods. Reinforced concrete beams made of concrete of strength class B15 were selected as the studied samples. The reinforcement is made in the form of a flat frame using rods of classes B500 and A400. Composite reinforcement is made using SikaWrap carbon tapes. The location of the breakage of the composite reinforcement in the stretched zone of the element is determined when plotting the load-bearing capacity of the non-reinforced element and the bending moments from the maximum possible load of the reinforced elements. An increase in the bearing capacity may lead to a change in the pattern of destruction of the sample, which requires additional calculation and design of composite reinforcement of inclined sections of the element.

**Keywords** Bearing capacity · Bendable elements · Reinforcement · Composite reinforcement · Experiment

---

V. Rimshin (✉)

National Research Moscow State University of Civil Engineering, Yaroslavskoe Shosse, 26,  
Moscow 129337, Russia  
e-mail: [v.rimshin@niisf.ru](mailto:v.rimshin@niisf.ru)

P. Amelin

Belgorod State Technological University Named After V.G. Shukhov, 46, Kostyukov St.,  
Belgorod 308012, Russia

## 1 Introduction

Buildings and structures in the process of long-term operation require repair and restoration work. The process of reconstruction of buildings with a reinforced concrete frame is often associated with an increase in the design loads on their load-bearing elements [1–4]. In this regard, there is a need to strengthen reinforced concrete structures. The use of polymer composite materials in construction contributed to the further development of reinforcement methods. These materials have high strength and deformation characteristics, while they can be operated in aggressive environments [5–7].

At the moment, experimental and scientific experience of research on the operation of reinforced concrete structures has been accumulated. The development and application of composite reinforcement methods became possible thanks to the theoretical and experimental work of Rimshin I., Mailyan D. R., Morozov I., Bokarev S. A., Polsky P. P., Georgiev V., Granovsky V., Kostenko A. N., Plevkov V., Kudyakov A. V., Krishan A. L., Truntova P. S., Khozina V. G., Ketsko E. S., Travush V. I., Al-Ruzan R., R. K., Gonzalez-Libreros I. N., Isfahani M. R., H. Rahimi, Jariwala V. H., Richie P. A., Saadatmanesh H., Ehsani M. R., Triantafillou T. S., Shahawy M. A., Hutchinson A., Lee H., Deng J., Xie Yu., Wang E. Yu., Chen Y. and others [1–16].

The analysis of the scientists' work showed that a multiple increase in the bearing capacity of the normal section of the element during bending can be achieved by using high-modulus composite materials, increasing the area of composite reinforcement by sticking several layers of canvases and lamellas in a stretched face, using U-shaped composite clamps of various angles of inclination to the longitudinal axis and clips in the support zone as an anchoring device.

However, to date, there have been no tests of reinforced concrete bendable elements having different ratios of the length of the composite reinforcement along the stretched face to its value of its estimated length. It is necessary to conduct comprehensive experimental studies on this topic.

## 2 Methods and Materials

To solve this problem, it is necessary to design and calculate the composite reinforcement of bent reinforced concrete structures. Reinforced concrete beams made of heavy concrete of class B15 were selected as control samples. The dimensions of the prototypes are  $120 \times 220$  (h)  $\times 1290$  mm. The estimated span was 1100 mm. The geometric dimensions of the cross sections of the prototypes, the classes of concrete and reinforcement, the configuration and diameters of the reinforcement rods were adopted on the basis of preliminary calculations, taking into account the prevention of destruction along inclined sections or due to loss of overall stability. The prototypes of the beams are reinforced with a flat welded frame made of A400  $\varnothing 12$  mm reinforcing steel in the stretched zone and A400  $\varnothing 6$  mm in the compressed



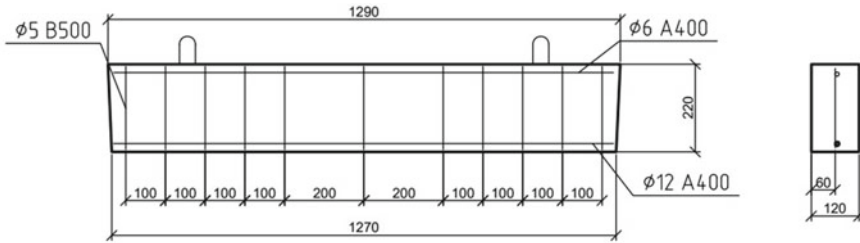


Fig. 1 Scheme of formation of the studied structure

zone. Rods made of reinforcing steel B500 Ø5 mm are accepted as transverse reinforcement. The pitch of the transverse reinforcement along the length of the beam is variable: in the extreme quarters—100 mm, in the middle—200 mm. The value of the protective layer of concrete is 20 mm. The reinforcement scheme of the samples is shown in Fig. 1.

The characteristics of materials required for calculations for the first group of limit states are shown in Table 1.

The bearing capacity of the cross section of the beam  $M_{ult}$  is determined according to SP 63.13330.2018 by the Eq. (1):

$$M_{ult} = R_b b x (h_0 - 0.5x) + R_{sc} A'_s (h_0 - a') \tag{1}$$

where:

- $R_b$  resistance of concrete to compression;
- $R_{sc}$  resistance of the rebar Ø6 A400 to compression;
- $b$  section width;
- $x$  the height of the compressed concrete zone, determined by the Eq. (2):

$$x = \frac{R_s A_s - R_{sc} A'_s}{R_b b} \tag{2}$$

Table 1 Design characteristics of concrete and reinforcement

Concrete characteristics				Rebar characteristics				
Strength class	$R_b$ , MPa	$R_{bt}$ , MPa	$E_b$ , MPa	Diameter and class	$A_s$ , cm <sup>2</sup>	$R_s$ , MPa	$R_{sc}$ , MPa	$E_s$ , MPa
B15	8.5	0.75	24,000	Ø12 A400	1.131	350		210,000
				Ø5 B500	0.196		300	210,000
				Ø6 A400	0.283		350	210,000

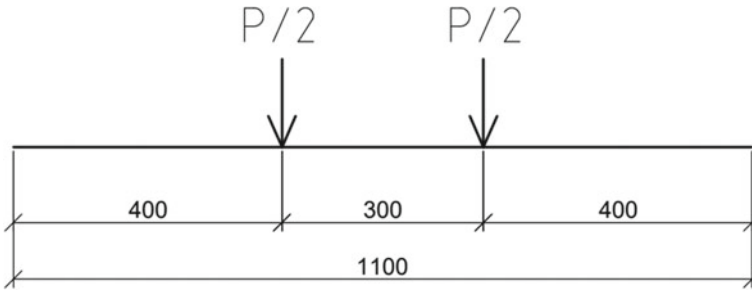


**Fig. 2** Diagram of the load application on the beam

$h_0$  the working height of the section, defined as the difference between the height of the section  $h$  and the thickness of the protective layer of concrete  $a$  and  $a'$ ;  
 $R_s$  resistance of the reinforcement  $\text{Ø}12$  A400 to stretching.

To determine the transverse force perceived by the beam, we will take a calculated scheme of loading the beam in the form of a four-point bend, with a projection of a long projection of an inclined section  $C$  equal to 400 mm (Fig. 2).

The transverse force perceived by the beam  $Q$  calculating by the Eq. (3):

$$Q = Q_b + Q_{sw} = \frac{\varphi_{b2} \cdot R_{bt} \cdot b \cdot h_0^2}{C} + \frac{\varphi_{sw} \cdot R_{sw} \cdot A_{sw} \cdot C}{s_w} \quad (3)$$

where

- $\varphi_{b2}$  coefficient for concrete, accepted 1.5;
- $\varphi_{sw}$  coefficient for reinforcement, accepted 0.75;
- $A_{sw}$  cross-sectional area of the transverse reinforcement  $\text{Ø}5$  B500;
- $R_{sw}$  resistance of transverse reinforcement  $\text{Ø}5$  B500 to compression;
- $s_w$  the pitch of the transverse reinforcement rods  $\text{Ø}5$  B500 in the cut span.

A unidirectional woven strip of carbon fiber SikaWrap—530 C is used as reinforcement, which is glued in a stretched zone 120 mm wide in one layer.

The SikaWrap—530 C tape has the following physical and mechanical characteristics:

- strength  $R_{f,n} = 3200$  MPa;
- modulus of Yong  $E_f = 225,000$  MPa;
- estimated tape thickness  $t_f = 0.29$  mm;
- the cross-sectional area of the tape  $A_f = 34.8$  mm<sup>2</sup>.

According to the recommendations of SP 164.13330.2014, the calculated tensile resistance of a composite material  $R_f$  calculating by Eq. (4):

$$R_f = \frac{\gamma_{f1} \cdot \gamma_{f2} \cdot R_{fn}}{\gamma_f} \quad (4)$$

where

- $\gamma_f$  the reliability coefficient of the composite material, depending on the type of material and the group of limiting states, which is equal to 1.2;
- $\gamma_{f1}$  the coefficient of the working conditions of the composite material, depending on the type of material and operating conditions, for structures located inside the building is equal to 0.9;
- $\gamma_{f2}$  the coefficient of the working condition of the composite material, taking into account its adhesion to the structure, and determined by Eq. (5):

$$\gamma_{f2} = \min \left[ \left[ \frac{0.9}{\frac{1}{2.5 \cdot \varepsilon_{f,ult}} \sqrt{\frac{R_b}{n \cdot E_f \cdot t_f}}} \right] \right] \tag{5}$$

where:

- $n$  estimated number of layers of composite material;
- $t_f$  thickness of one layer of composite material, mm;
- $\varepsilon_{f,ult}$  limiting relative deformations that are found for the resistance of a composite material  $R_f$  with a coefficient  $\gamma_{f2} = 1$ , and calculating by Eq. (6):

$$\varepsilon_{f,ult} = \frac{R_f}{E_f} \tag{6}$$

Next, the condition is checked  $\xi \leq \xi_{rf}$ , where  $\xi = \frac{x_f}{h}$ —relative height of the compressed zone,  $x_f$ —the height of the compressed zone, determined from the Eq. (7):

$$x_f = \frac{R_s A_s - R_{sc} A'_s + R_f A_f}{R_b b} \tag{7}$$

The value of the maximum relative height of the compressed zone  $\xi_{rf}$  calculating by the Eq. (8):

$$\xi_{rf} = \frac{\omega}{1 + \frac{R_f}{\varepsilon_{bu1} E_f} \left(1 - \frac{\omega}{1.1}\right)} \tag{8}$$

- $\varepsilon_{bu1} = 0.002$  maximum relative deformation of concrete during compression;
- $\omega = 0.85 - 0.008 \cdot R_b$  the relative height of the compressed concrete zone at which the actual zero line passes through the reinforcement.

Based on the obtained values of the height of the compressed zone of reinforced concrete, as well as the calculated resistance of the composite material to stretching, the actual value of the load-bearing capacity of the reinforced beam section is determined by the Eq. (9):

$$M_{f,ult} = R_b b x_f (h_0 - 0.5x_f) + R_{sc} A'_s (h_0 - a') + R_f A_f a \quad (9)$$

The increase in the bearing capacity of the cross section of the element is achieved mainly by increasing the height of the compressed zone of the element from the use of composite reinforcement.

### 3 Results and Discussion

The results of calculations based on the Eqs. (1–9) for control and enhanced experimental samples are shown in Table 2.

Based on the data on the bearing capacity of the reinforced element  $M_{f,ult}$ , and the known two-point loading scheme shown in Fig. 2, it is possible to calculate the limit value of the load  $F$  on the element from each traverse by the Eq. (10):

$$\frac{P}{2} = F = \frac{M_{f,ult}}{c} \quad (10)$$

where

$c$  distance from the support to the point of application of the load  $F$ .

To determine the rational length of the composite gain along the longitudinal axis of the stretched face, we construct a plot (Fig. 3) of the moment from the application of a two-point load with an equivalent maximum value of  $M_{f,ult}$  and the moment perceived by the cross section to the gain of  $M_{ult}$  along the length of the element (Fig. 3).

As can be seen, at a distance of 230 mm from the support, the cross section perceives the load from the traverse only with working steel reinforcement, which leads to the irrational use of carbon fiber.

The magnitude of the transverse forces  $Q'$ , the effect on the reinforced element is numerically determined by the magnitude of the load from the traverse  $F$  which for this element is 31.21 kN, which is greater than the magnitude of the transverse force  $Q = 31.14$  kN. Strengthening of the normal cross-section can lead to the destruction of the element along the inclined section, therefore it is necessary to ensure minimal reinforcement of the inclined sections with composite materials.

Based on the results obtained on the basis of preliminary calculations on the reinforcement of reinforced concrete bendable elements, as well as in order to rationalize the use of composite reinforcement, the author has developed an experimental

**Table 2** Calculated values of the carrying capacity of the experimental sample

$M_{ult}$ , kNm	$Q$ , kN	$R_f$ , MPa	$x_f$ , mm	$M_{f,ult}$ , kNm
7.287	31.14	854.4	57.9	12.485

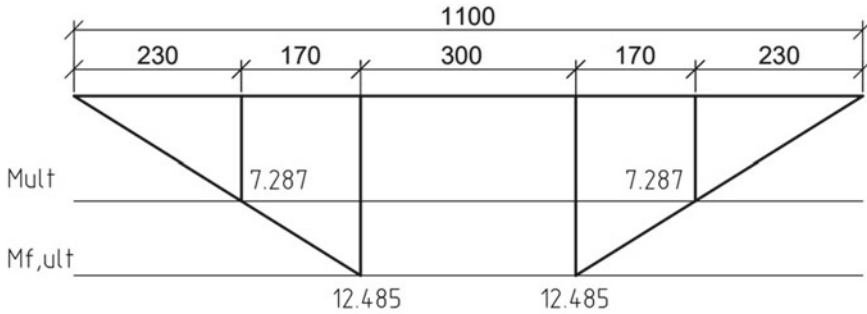


**Fig. 3** Plot of moments perceived by the cross section before amplification and from the application of a two-point load

program, in accordance with which the destruction of 4 series of bendable elements and auxiliary samples to them is envisaged (Fig. 4):

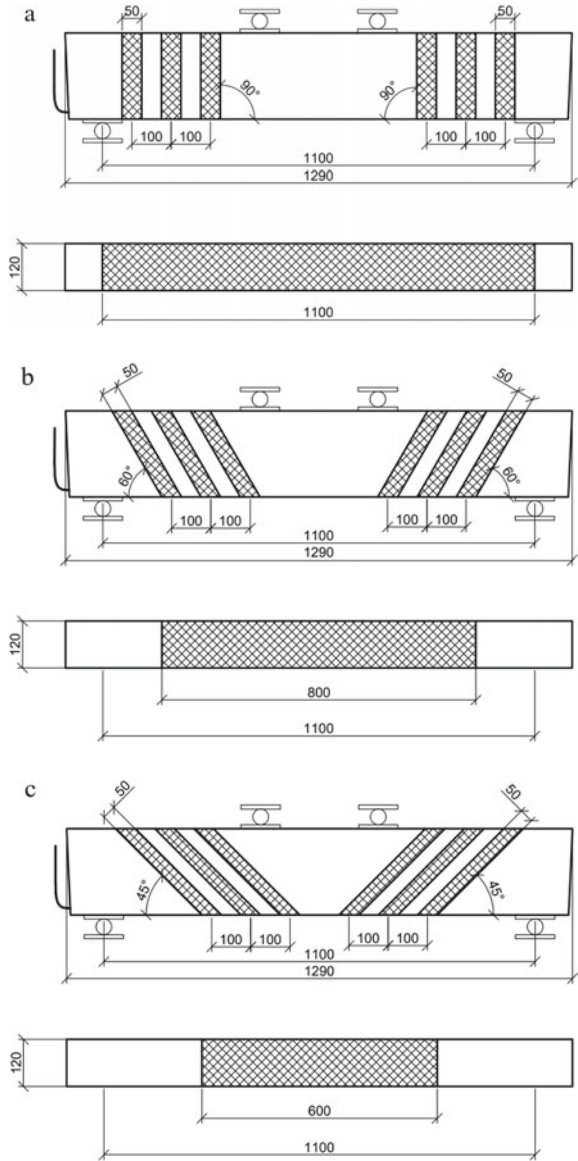
- testing of auxiliary concrete samples of the design class for compressive strength B15 in the form of cubes with a size of  $10 \times 10 \times 10$  cm and prisms with a size of  $10 \times 10 \times 40$  cm for compression, bending, determination of the initial modulus of elasticity in the amount of 6 pcs. per series;
- testing of auxiliary samples in the form of reinforcing bars B500, A240 and A500 and unidirectional woven strips of carbon fiber SikaWrap—230 C for longitudinal stretching;
- testing of control samples of reinforced concrete elements with a short-term static bending load (series 1);
- static bending test of reinforced concrete elements previously damaged under the influence of an aggressive environment, unloaded and reinforced with carbon fiber canvases (series 2, 3, 4).

The ratio of the length of the reinforced section  $L_{yc}$  to the calculated length of the element  $L_{yc}$  was chosen as the variable parameters during the test L (1/1, 0.8/1.1, 0.6/1.1), as well as the angle of inclination of the transverse composite reinforcement  $\alpha$  (90, 60, 45%). The transverse composite reinforcement in the elements, while strengthening the inclined section of the element, has the function of anchoring carbon tapes in the stretched zone to concrete.

The transverse reinforcement is designed from carbon fiber SikaWrap 230C tapes with a width of 50 mm and a pitch of 100 mm, having the following physical and mechanical characteristics:

- strength  $R_{f,n} = 3200$  MPa;
- modulus of Yong  $E_f = 225,000$  MPa;
- estimated tape thickness  $t_f = 0.129$  mm;
- the cross-sectional area of the tape  $A_f = 14.48$  mm<sup>2</sup>.

**Fig. 4** Design schemes of experimental reinforced samples: a—series 1 ( $L_{yc}/L = 1; \alpha = 90^\circ$ ), b—series 2 ( $L_{yc}/L = 0,8/1,1; \alpha = 60^\circ$ ), c—series 3 ( $L_{yc}/L = 0,6/1,1; \alpha = 45^\circ$ )



## 4 Conclusion

The calculation made by the authors was carried out with the aim of rational use of composite material when performing experimental studies on strengthening reinforced concrete bendable elements.

The values of the destructive moments allowed us to plot the effective operation of the composite material along the length of the element. Variation of the angle of inclination of the transverse composite reinforcement to the longitudinal axis of the element will allow to obtain extensive data on the work of reinforced concrete elements on bending.

**Acknowledgements** This work was realized in the framework of the Program of flagship university development on the base of the Belgorod State Technological University named after V. G. Shukhov, using equipment of High Technology Center at BSTU named after V. G. Shukhov.

## References

1. Rimshin VI, Varlamov AA (2018) Three-dimensional model of elastic behavior of the composite *Izvestiya Vysshikh Uchebnykh Zavedenii. Seriya Tekhnologiya Tekstil'noi Promyshlennosti* 375(3):63–68
2. Varlamov A, Rimshin V, Tverskoi S (2019) A method for assessing the stress-strain state of reinforced concrete structures. In: *E3S web of conferences*, vol 91, pp 20–46
3. Krishan AL, Rimshin VI, Astafeva MA (2018) Deformability of a volume-compressed concrete. In: *IOP conference series: materials science and engineering*, vol 463, issue 2, pp 22–63
4. Sergeev M, Rimshin V, Lukin M, Zdravovic N (2020) Multi-span composite beam. In: *IOP conference series: materials science and engineering*, vol 896, issue 1, pp 152–158
5. Kuzina E, Rimshin V (2019) Strengthening of concrete beams with the use of carbon fiber. *Adv Intell Syst Comput* 983:911–919
6. Neverov AN, Truntov PS, Ketsko ES, Rimshin VI (2022) Calculating the strengthening of construction structures before the reconstruction of the building. *Lecture notes in civil engineering*, vol 182, pp 173–179
7. Polskoy PP, Mailyan DR, Dedukh DA, Georgiev SV (2016) Design of reinforced concrete beams in a case of a change of cross section of composite strengthening reinforcement. *Glob J Pure Appl Math* 12(2):1767–1786
8. Podnebesov PG, Teryanik VV (2016) Compressed column strengthening by holder constructions with the use of a self-consolidating fiber concrete. In: *2nd International conference on industrial engineering (ICIE-2016)*. *Procedia Eng* 150:1733–1740
9. Granovskiy A, Kostenko A (2007) Use of carbon fibers for strengthening masonry and reinforced concrete structures. In: *The eighth international symposium on fiberreinforced polymer reinforcement for concrete structures (FRPRCS-8)*. University of Patras, Department of Civil Engineering, Patras, Greece, pp 682–683
10. Travush VI, Konin DV, Krylov AS (2018) Strength of reinforced concrete beams of high-performance concrete and fiber reinforced concrete. *Mag Civ Eng* 77(1):90–100. <https://doi.org/10.18720/MCE.77.8>
11. Plevkov V, Baldin I, Kudyakov KL, Nevskii AV (2017) Mechanical properties of composite rebar under static and short-term dynamic loading. In: *V.S. AIP conference proceedings*, vol 1800, pp 040018-1–040018-5. <https://doi.org/10.1063/1.4973059>
12. Gizdatullin GA, Khusainov RR, Khozin VG, Krasnikova NM (2016) Strength and deformability of concrete structures reinforced with fibre-reinforced polymer bars. *Mag Civ Eng* 62(2):32–41. <https://doi.org/10.5862/MCE.62.4>
13. Gonzalez-Libreros JH, Sneed LH, D'Antino T, Pellegrino C (2017) Behavior of RC beams strengthened in shear with FRP and FRCM composites. *Eng Struct* 150(1):830–842

14. Al-Rousan R, Abo-Msamh I (2020) Impact of anchored CFRP on the torsional and bending behaviour of RC beams. *Mag Civ Eng* 4(96):79–93
15. Jariwala VH, Patel PV, Purohit SP (2013) Strengthening of RC beams subjected to combined torsion and bending with GFRP composites. *Procedia Eng* 51(1):282–289
16. Rashid K, Li X, Deng J, Xie Y, Wang Y, Chen S (2019) Experimental and analytical study on the flexural performance of CFRP strengthened RC beams at various pre-stressing levels. *Compos Struct* 227:1–12



# Modeling of Reinforced Concrete in the “LIRA” Intelligence for the Problem of Crack Opening



Vladimir Kolchunov 

**Abstract** In most of the world-famous computing complexes, when designing reinforced concrete structures, is not taken into account the current development of a finite element model, where it is necessary to adequately take into account the nature of the development and opening of cracks in them. The criterion for the disclosure of cracks in reinforced concrete structures is carried out using the achievement of completely different criteria. Completely different criteria should be used when analyzing the appearance and development of discrete cracks for modeling discrete cracks, taking into account the effect of violation of the discontinuity of concrete and the reaction of reinforcement from the mechanics of destruction of two elements and the development of cracks in reinforced concrete. The physical essence of which is the additional deformation effect of the reaction of reinforcement and concrete in the form of an ellipsoid for an alternative kinematic crack, from a universal two-console element in reinforced concrete. At the same time, in the stretched area of concrete for the distance between cracks and the width of the opening has in these local zones adjacent to the crack adhesion and importantly compressed concrete tensions. A classification of the basic spatial cracks in spatial reinforced concrete composite structures is constructed for discrete levels,—cracks that develop to zones of concentration of geometric, force, deformation loading or the inter-environment region, where the full picture of various types of cracks. Based on the basic cracks, a complete scheme of spatial cracks is applied by finding adjacent cracks with the involvement of the deformation criterion of their formation and the method of finding the extremum of the function of many variables using Lagrange multipliers. Nevertheless, the method of modeling discrete cracks, including using most of the world’s well-known, has not been developed by the intelligence of computing complexes. The development of spatial cracks is carried out on special bilinear surfaces. Then approximating spatial finite elements are inserted into them, which are “expanded”,

---

V. Kolchunov (✉)

Moscow State University of Civil Engineering, 26, Yaroslavskoye Shosse, Moscow 129337, Russia

e-mail: [vlik52@mail.ru](mailto:vlik52@mail.ru)

Southwest State University, 94, 50 Let Oktyabrya, Kursk 305040, Russia

modeling a spatial crack, the disclosure of which is set in the form of a deformation effect, taking into account the effect of reinforced concrete continuity violation. When solving the inverse problem of determining the width of crack opening, the deformation effect is not set, and with the help of “stitching”, only the presence of a gap of the minimum possible width is modeled, its opening under appropriate loading and determines the width of crack opening as the divergence of the banks of this gap. The article considers the pairs of finite elements adjacent to such a crack from opposite sides—a special calculated two-element console model. These pairs are considered in two states: before their “stitching” and after their “stitching”, taking into account the deformation effect and the effect of breaking the continuity of concrete. To find the level distance between cracks and the width of their opening from a reinforced concrete structure, which allows determine the desired parameters, tools or modules of the LIRA program.

**Keywords** Discontinuity effect · Reinforced concrete · Opening width · Methodology · Modeling of discrete cracks · Bilinear surface · Classification · Function of variables · Two-element console · Analytical coupling · Stitching finite elements · Modules—tools

## 1 Introduction

In connection with the recommendations, in recent decades, the construction practice has been increasingly introduced, which necessitates the use of their spatial design scheme, the complex resistance of reinforced concrete buildings, structures and structures, plane-stressed finite elements (panel buildings, pylons, etc.) are used or performed with the help of volumetric finite elements, taking into account their complex resistance of spatial cracks (building cores, hydraulic structures, arched reinforced concrete dam, nuclear power plants, etc.) [1–14, 22–24].

Schemes of discrete cracks—this classification is based on the geometric, force (deformation) and inter-medium concentration of the stress–strain state with the corresponding concentrator sources proposed in the works [22–24]. The criterion for crack disclosure in reinforced concrete structures is performed using the achievement of completely different criteria should be used when analyzing the appearance and development of discrete cracks for modeling discrete cracks, taking into account the effect of violation of the discontinuity of concrete and the reaction of reinforcement from the mechanics of destruction of two elements and the development of cracks in reinforced concrete [1–14].

Considering that to date, the development of a finite element model, where it is necessary to adequately take into account the nature of the development and opening of cracks in them. Nevertheless, the intelligence of computing complexes (direct and inverse problems of discrete cracks) has not been developed before the methods of modeling discrete cracks, including using the most well-known in the world [22–24], Relevance more and more attention is paid to the development of models of

deformation of reinforced concrete with the use and development of tools and basic provisions of fracture mechanics [24, etc.].

## 2 Materials and Methods

The method of modeling discrete cracks and calculating the rigidity of spatial reinforced concrete constructions, buildings and structures with their complex resistance will be based on the following design positions:

1. The author has developed the effect of reinforced concrete (discovered in reinforced concrete by Professor Vladimir Kolchunov) [1–9, 16, 23, etc.], the physical essence of which is the additional deformation effect of the reaction of fittings and concrete in the form of an ellipsoid crack (at a distance of two diameters of the working reinforcement from the axis of its rod or its alternative kinematic crack), related with a violation of the continuity of concrete for its tools from a two-console element (TCE) in reinforced concrete based on the mechanics of destruction.

The main aspects of fracture mechanics focus on the features of the stress–strain state in areas with broken continuity, including cracks. The mechanism of crack straining (during its development) is laid in the zone of pre-collapse, with localized deformation  $w$  in this zone and with the formation of new specific crack surfaces. Determination of the energy release rate is performed on the basis of the functional of fracture mechanics:

$$\zeta_{bu} = \lim_{\delta A \rightarrow 0} \left( \frac{\delta W - \delta V}{\delta A} \right) = \frac{dW}{dA} - \frac{dV}{dA} + \frac{1}{3} \sum_{i=1}^n \left( \frac{P_i^2 \cdot \delta C_i}{\delta A} - C_i P_i \frac{\delta P_i}{\delta A} \right). \quad (1)$$

Here— $\delta W$  is a decrease in the potential energy of the body when the crack moves by a small increment;— $\delta V$  is additional work performed on the body when the crack moves by a small increment  $\delta a$ .

To implement the obtained dependence, we use Fig. 1, where, in relation to a selected two-console element under the influence of a number of forces,  $(\Delta T, P_1, P_2, M_{con})$  and movements in any sections of interest  $(\Delta_1 \dots \Delta_i)$  are determined by methods of structural mechanics.

Two-element (TCE) universal spatial cracks in its surface were obtained to implement the dependencies of fracture mechanics in reinforced concrete. Linger on the main provisions and features of cutting out a two-console element (TCE), including a crack for constructing a calculation apparatus of reinforced concrete. For a solid body, the stress–strain state is analyzed by the methods of the theory of elasticity and plasticity, an elementary cube is allocated describing the dependence between tension and deformations at a point. Then, when moving to the cross section, the established connection is integrated throughout the cross section. As a result, the problem is reduced to differential equations, the exact solution of which, as a rule, is very difficult. In the resistance of materials, the hypothesis of plane deformations

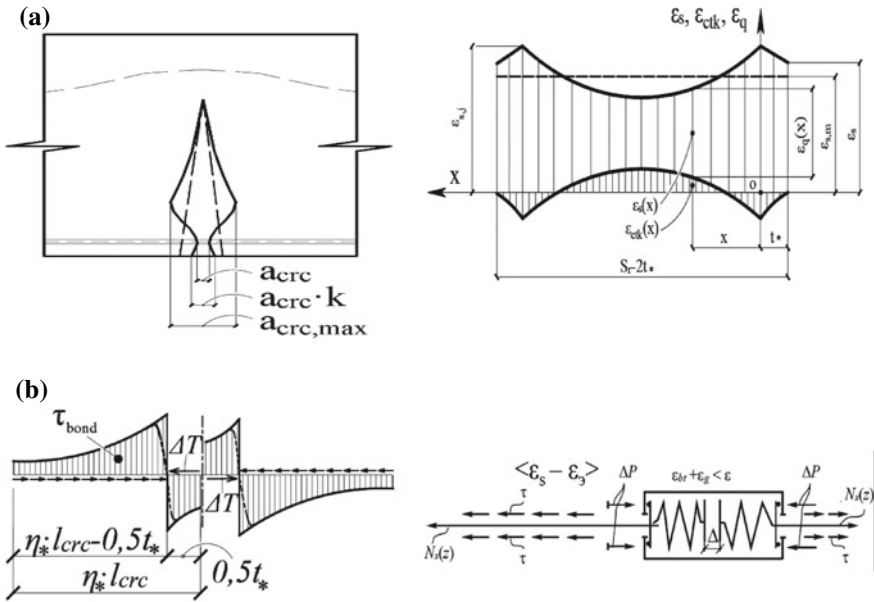


**Fig. 1** Reinforced concrete effect: crack shape,—from triangle to ellipsoid (a); reaction from discontinuous concrete to solid reinforcement (b); c—mechanical model for its physical essence (process)); relative deformations of reinforcement and stretched concrete along the x axis

for the entire cross section is adopted, which greatly simplifies the solution of the problem. For a discontinuous body with a crack (where the continuity of the body is broken), when establishing a connection between tension and displacements, the methods developed in the theory of elasticity, plasticity and resistance of materials are not applicable. Nevertheless, the use of the fundamental method of cross sections in relation to the material with cracks brings its positive results. This also applies to the approximate method of determining the tension intensity coefficient, it can also be used in the allocation of a special TCE, which has found application in fracture mechanics.

The allocation of such TCE, including a crack, in relation to a core reinforced concrete element has its own specifics.

Firstly, if DCE is allocated for a long two-console element (fully including the entire crack), for the entire length of the crack, and not for some of its elementary section, then the crack length is generally determined from the condition of the following condition of fracture mechanics:

$$\frac{d\zeta_{bu}}{dh_{crc}} = 0. \tag{2}$$

At the same time, it should be noted that the difficulties arising here are the main reason (along with the need to use complex numbers) for which the detailed tools of

fracture mechanics are developed (allowing to study the features of the stress–strain state in the vicinity of the crack), these tools have not yet found proper application in the theory of reinforced concrete.

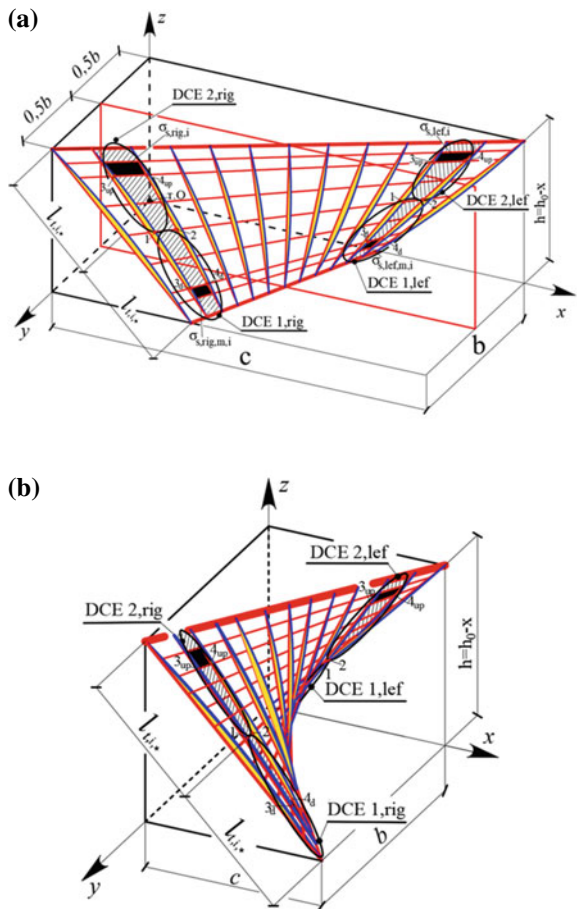
Formula (2) is due to the Saint–Venant principle, applied to the near-armature zones of working reinforcing rods adjacent to the spatial crack and is confirmed by a number of experimental studies [1–9, 16, etc.].

Let’s consider a short TCE, the length of which is known for design reasons (it is allocated at half the length of the zone adjacent to the crack located between the working reinforcing rods, for example, clamps or tiered longitudinal reinforcement), Fig. 2.

Secondly, the forces in the cross sections passing at a distance and (for a universal two-console element) from the crack must be associated with the desired parameters of the stress–strain state of the reinforced concrete element.

Thirdly, we should not forget about the virtual movements of the dedicated TKE consoles when the neutral axis of the reinforced concrete element is rotated and the

**Fig. 2** A two-console element with torsion bending (a) and (b) in model A and model B, respectively,—the nodes of the spatial crack in its surface for a separate polyline (middle) strip of TCE 1,rig; TCE 1,lef—the first (lower) for the right and left elements; TCE 2,rig; TCE 2,lef—the second (upper) for the right and left elements



rotation angles of the working reinforcing rod caused by the pressure forces, i.e. the pinching of the consoles on both sides DKE, in some cases, may not be absolutely rigid.

Thus, the allocation of TCE for reinforced concrete (which is transformational between the dependencies of fracture mechanics and the theory of reinforced concrete) is a very important and difficult problem. It should be linked not only with the task of determining the stress–strain state of the cross-section of a reinforced concrete element, but also with the problem of the distribution of adhesion between reinforcement and concrete, since the appearance of a crack in a solid body can be considered as some deformation effect, affecting the features of the coupling of reinforcement and concrete in the areas adjacent to the crack.

With the help of TCE, the connection of its stress–strain state with the value  $\zeta_{bu}$  in the pre-collapse zone seems to be the most successful (in contrast to the use of the Gurs function with complex numbers). At the same time, the malleability of the crack banks, through which the value of  $\zeta_{bu}$  can be expressed, is determined using the functional of fracture mechanics.

Thus, the TCE is used as a link between the dependencies of the mechanics of a solid deformable body and the mechanics of fracture.

The above considerations were used in the development of universal two-channel elements, suitable, among other things, for solving the problem of resistance of reinforced concrete structures during torsion with bending (Fig. 2).

As a result, the effect of reinforced concrete for the disclosure of spatial cracks and the rigidity of reinforced concrete structures during bending with torsion has been developed [1–9, 16, 23, 24, etc.]. At the same time, from a small separate strip (medium width and length) for a two-console element (TCE) (Fig. 2). In the calculated models A and B of strips  $\Delta b_i$  for the left and right elements up to half the width of the structure from the neutral axis to the lower and upper elements (length  $l_{t,*}$ , —Fig. 2a and b), respectively.

Then a universal TCE was obtained to implement the dependencies of the fracture mechanics in reinforced concrete of spatial cracks in its surface for a separate polyline (middle) strip: characteristic stress plots in stretched concrete and the cutting of a special TCE in the vicinity of a spatial crack adjacent to the working armature of the axes  $X_s Y_s Z_s$  through the  $i$ -th axes  $X_i Y_i Z_i$  for displacement types,—separation (for displacement  $\pm 0,5a_*$ ); transverse shear (for displacement  $\pm 0,5b_*$ ); longitudinal shear (for displacement  $\pm 0,5c_*$ ); node for the features of the stress–strain state at the tip of the crack (Figs. 1 and 2). In this case, we perform a sequential displacement and rotation of the axes along  $x, y, z$  (Fig. 2), we have:  $x_i = x_c \pm 0.5a_{*,i}$ ;  $y_i = y_c \pm 0.5b_{*,i}$ ;  $z_i = z_c \pm 0.5c_{*,i}$ , as well as rotation angles,— $\alpha_i$  (for cosine  $l$ ),  $\beta_i$  (for cosine  $m$ ),  $\theta_i$  (for cosine  $n$ ),— $x_i = x_c \cdot (\pm l_i)$ ;  $y_i = y_c \cdot (\pm m_i)$ ;  $z_i = z_c \cdot (\pm n_i)$ .

Then after the joint displacement and rotation of the axes, we get (see Fig. 2):

$$\begin{cases} x_i = (x_c \pm 0.5a_{*,i}) \cdot (\pm l_i); \\ y_i = (y_c \pm 0.5b_{*,i}) \cdot (\pm m_i); \\ z_i = (z_c \pm 0.5c_{*,i}) \cdot (\pm n_i). \end{cases} \quad (3)$$

Here, the parameter, in accordance with the Saint–Venant principle and studies of the near-armature zone performed using semi-analytical and numerical methods, is in the first approximation equal to one and a half of the diameter of the reinforcement. The tensile tensions in the selected sections are distributed according to the square parabola law from the neutral axis to the point where the sign of these tensions changes. At the same time, their maximum value is limited by the value  $R_{br}$  therefore, in a significant area, the actual distribution of tensile tensions is close to the rectangle, regardless of the law of their distribution in the elastic stage. Compressive stresses in the same sections in the areas adjacent to the armature are distributed along a triangle.  $\Delta b$  is taken in the area adjacent to the reinforcement equal to the value of the protective layer plus half the diameter and this value is doubled (since the strip is allocated from both sides of the reinforcement rod), Fig. 2.

During bending (tension–compression), the expression (4) is not used, because the geometry of the crack in thickness  $b$  does not change. The spatial crack is twisted, i.e. its profile changes in thickness.

Finally, and no more than  $4d$  diameters of working fittings are accepted.

$$\Delta b = 2(a_s - 0.5d), \quad (4)$$

Here  $a_s$  and  $d$  are the distance from the center of the working armature to the lower face of the cross section and the diameter of the working armature, respectively.

For the selected TCE at the thickness  $\Delta b$  determined by the formula (4), it is logical to simplify this surface by taking its slope constant within  $\Delta b$  (angle  $\Theta$ —the angle of inclination of the spatial crack in the plane, cross-section). In turn, the angle of inclination of the spatial crack in the vertical longitudinal plane perpendicular to the cross section—the angle  $\alpha_{crc}$  is also assumed to be constant within the distance between the clamps. Up to half the thickness  $b$  of a rectangular reinforced concrete structure, it is assumed to be equal  $\alpha_{1,crc}$ , and for the second half,—  $\alpha_{2,crc}$ :

$$\alpha_{2,crc} = \alpha_{1,crc} \pm 90^\circ. \quad (5)$$

The sign “plus” or “minus” is taken depending on which side of the side surface (right or left) the angle starts counting.

The accepted simplifications make it possible to significantly simplify the resolving equations, without closing the complex equation of the spatial crack surface on them into a single system (at each iteration step), but using it discretely for the selected strip, thickness  $\Delta b$ .

The iterative process is organized when using a transitional (transformational) TCE as a tool. The two- console element is a connecting link and serves as a transformational element between the dependencies of fracture mechanics and the equations of the theory of reinforced concrete.

**3. Equation of the linear spatial surface of the crack.** The formation of the subsequent level of spatial cracks is carried out after the stretched concrete fibers reach their

**maximum deformations**  $\epsilon_{bt,u}$  along the axes of the working reinforcement (longitudinal or transverse). There may be several levels of cracking. The development of spatial cracks is carried out on special bilinear surfaces. To do this, knowing the equation of a bilinear surface in parametric form [18–24], the value of the angular points of the cross-section of a reinforced concrete structure (points  $A, B, C, D$ ) is entered into it—the **equation of a bilinear surface** is concretized in relation to a given cross-section.

$$[x_k; y_k; z_k] = [x_A; y_A; z_A] \cdot (1 - u_k) \cdot (1 - w_k) + [x_B; y_B; z_B] \cdot (1 - u_k) \cdot w_k + [x_C; y_C; z_C] \cdot u_k \cdot (1 - w_k) + [x_D; y_D; z_D] \cdot u_k \cdot w_k \quad (6)$$

From the equation of the bundle of planes, where is written in the following form:

$$(y_N - y_M) \cdot x - (x_N - x_M) \cdot y - x_M(y_N - y_M) + y_M(x_N - x_M) + \lambda \cdot [(z_N - z_M) \cdot x - (x_N - x_M) \cdot z - x_M(z_N - z_M) + z_M(x_N - x_M)] = 0. \quad (7)$$

**4. On the extremum of the function of many variables for reinforced concrete using Lagrange multipliers.** Projections of different cracks on the horizontal (vertical) are found on the basis of a block model with calculated cross-sections passing through the beginning and end of the crack (refined during iterations; one of these sections, as a rule, is attached to the greatest force—the reference reaction  $R_{sup}$  or goes to one of the faces of the construction) with the involvement of analytical dependencies, which are based on the extremum of the function of many variables using Lagrange multipliers  $F_{1,2} = f(q_{sw}, x_B, \sigma_s, x, \sigma_b, \sigma_{s,I}, \sigma_{b,1}, C_2, \lambda_1, \lambda_2, \lambda_3, \lambda_4, \lambda_5, \lambda_6, \lambda_7)$  and  $F_3 = f(q_{sw}, x_{B,2}, \sigma_{s,3}, c_2, \lambda_1, \lambda_2, \lambda_3)$ , respectively, and the resulting conditions of equality of partial derivatives to zero [1–9, 16, etc.]:

$$\left. \begin{aligned} \frac{\partial f}{\partial x_1} + \lambda_1 \frac{\partial \phi_1}{\partial x_1} + \lambda_2 \frac{\partial \phi_2}{\partial x_1} + \dots + \lambda_m \frac{\partial \phi_m}{\partial x_1} &= 0 \\ \frac{\partial f}{\partial x_2} + \lambda_1 \frac{\partial \phi_1}{\partial x_2} + \lambda_2 \frac{\partial \phi_2}{\partial x_2} + \dots + \lambda_m \frac{\partial \phi_m}{\partial x_2} &= 0 \\ \dots &\dots \\ \frac{\partial f}{\partial x_n} + \lambda_1 \frac{\partial \phi_1}{\partial x_n} + \lambda_2 \frac{\partial \phi_2}{\partial x_n} + \dots + \lambda_m \frac{\partial \phi_m}{\partial x_n} &= 0 \end{aligned} \right\} \quad (8)$$

the projection of a spatial crack is found  $C$ .

The parameters depend on the geometric characteristics of reinforced concrete composite structures, geometric and mechanical characteristics of concrete and reinforcement, coupling parameters, parameters of the stress–strain state of the design sections I–I and II–II, which pass through the beginning and end of the spatial (or inclined) crack, respectively— $S, B', B'_{a,1}, B'_{a,2}, A_{sw}, E_{sw}, q_{sw}, q_{sw,hor}, Q'_{s,3}, h_0, \tau_b, x, x_{B,2}, \sigma_b, \sigma_s, \sigma_{s,1}, \tau_{xy,2}, a, b, R_{sup}, A_{S,i}, \alpha, \psi_S, v_b$ .

**5. Analytical model of reinforcement coupling with concrete and their compliance.**

The proposed analytical model, along with modeling the reinforcement process with



concrete, can be used to determine the secant stiffness of reinforcement joints crossing a crack—a necessary parameter for calculating structures using a discrete crack model. The longitudinal (transverse for clamps) compliance  $\lambda_{sm}$  (rigidity of the  $C_{sm}$  connection) is determined by the ratio of the  $U_{sm}$  movement to the reaction of the  $N_{sm}$  connection in it:

$$\lambda_{sm} = \frac{1}{C_{sm}} = \frac{U_{sm}}{N_{sm}}. \tag{9}$$

This reaction (also known as the force at the end of the rod) depends on the boundary conditions that we vary during the study.

The model considers a reinforced concrete element (representative volume) with a single central reinforcement. The case of central reinforcement with one rod when pulling it out of a concrete matrix most fully reveals the pattern manifested when pulling a reinforcing rod out of a concrete block (a representative volume in the form of a prism with a reinforcing rod), which is one of the most important tasks of the structural mechanics of reinforced concrete in the presence of discrete cracks [6, etc.]. All types of reinforcement of reinforced concrete structures by a system of reinforcing rods are precisely or approximately reduced to this case [1–9, etc.].

The left end of the element is rigidly fixed from any movement, the right end is free. A tensile force  $N_s$  is applied to the reinforcing rod, causing the rod and the end face of the element  $U_s$  and  $U_b$  to move, respectively, along the entire length of the reinforced concrete rod (Fig. 3).

The coupling forces acting on the contact of the reinforcement with concrete are characterized by linear tangential forces  $\tau_{bond}(x)$ , in concrete—in the direction of the acting load, and in the reinforcement—oppositely directed [1–9, etc.].

The law of adhesion between concrete and reinforcement in the studied model is elastic–plastic, described using a bilinear diagram  $\tau_{bond} - \varepsilon_q(x)$  that takes into account the experimental data of Golyshev, Kolner, Kholmyansky, Babich [1–9, 16, 24, etc.].

$$\tau_{bond} = k \cdot \varepsilon_q(x) = 0,4 \cdot E_{cm} \cdot [\varepsilon_s(x) - \varepsilon_c(x)], \tag{10}$$

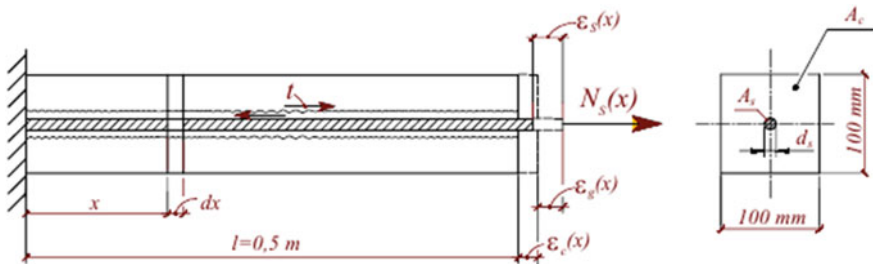


Fig. 3 Calculation element of the model

$$\text{of } \varepsilon_q(x) = [\varepsilon_s(x) - \varepsilon_c(x)] \leq \varepsilon_q^*(x) = 4,95 \cdot \frac{f_{ctm}}{E_{cm}};$$

$$\tau_{bond} = 0,0232 \cdot E_{cm} \cdot [\varepsilon_s(x) - \varepsilon_c(x)] + 1,866 \cdot f_{ctm}, \tag{11}$$

$$\text{of } \varepsilon_q(x) = [\varepsilon_s(x) - \varepsilon_c(x)] > \varepsilon_q^*(x) = 4,95 \cdot \frac{f_{ctm}}{E_{cm}}.$$

Where  $\varepsilon_q(x)$  is the relative mutual displacement of concrete and reinforcement, in cross section  $x$  (Fig. 4); accumulation of relative mutual displacements of concrete and reinforcement in the area between cracks and constitutes the value of the crack opening width  $a_{cr,c}$ ;  $\varepsilon_g^*(x)$ —boundary relative mutual displacement of concrete and reinforcement corresponding to the endpoint of the first section of the coupling diagram (Fig. 4).

The work of concrete in this model is also described using a bilinear diagram  $\sigma_c - \varepsilon_c$ , shown in Fig. 4.

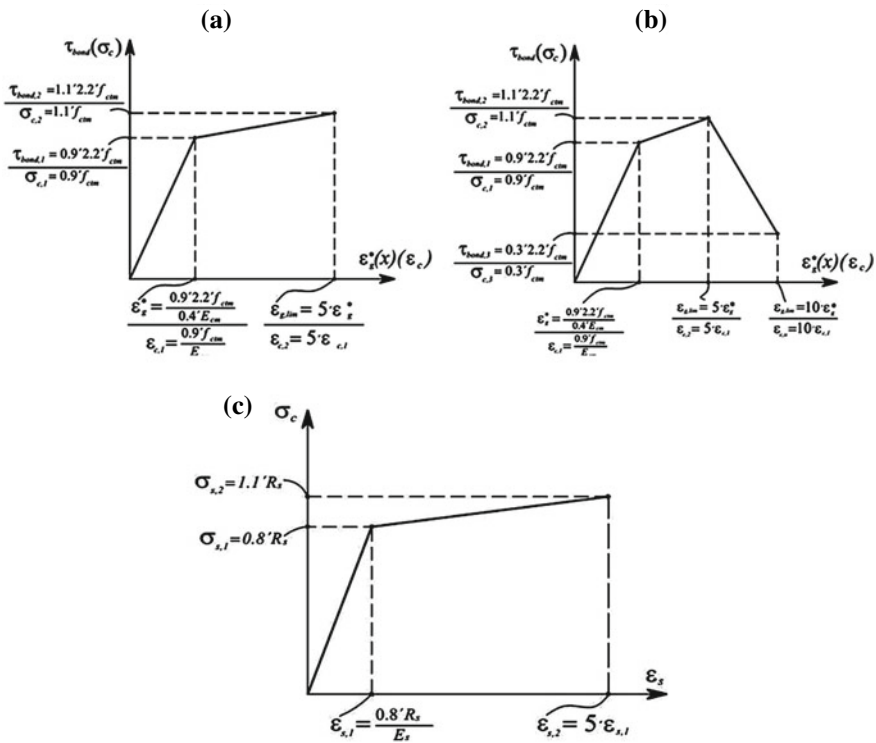


**Fig. 4** Coupling dependencies and deformation diagrams implemented in the analytical model: **a**—bilinear coupling dependence and concrete deformation diagram, linear reinforcement steel deformation diagram; **b**—bilinear coupling dependence and concrete and reinforcement steel deformation diagrams; **c**—trilinear coupling dependence and concrete deformation diagram, bilinear reinforcement operation

For concrete, we use the following dependence modeling elastic–plastic work (Fig. 4):

$$\varepsilon_c(x) = \begin{cases} \frac{N_c(x)}{E_{cm} \cdot A_c}, & e\sigma\pi u \quad \frac{N_c(x)}{A_c} \leq 0,9 \cdot f_{ctm}, \\ \frac{18 \cdot N_c(x)}{E_{cm} \cdot A_c} - 15,3 \cdot \frac{f_{ctm}}{E_{cm}}, & e\sigma\pi u \quad \frac{N_c(x)}{A_c} > f_{ctm}; \end{cases} \quad (12)$$

Also in this model, the following variants of diagrams of reinforcement deformation, concrete and reinforcement coupling with concrete are implemented (Fig. 4) by changing the expressions of the system of equations:

- a variant of the model with nonlinear concrete, coupling dependence and linear reinforcement operation (Fig. 4a);
- a variant of the model with nonlinear concrete, reinforcement and coupling dependence (Fig. 4b);
- a variant of the model with trilinear concrete, coupling dependence and a bilinear diagram of reinforcement deformation (Fig. 4c).

The fittings in this model are described using a line diagram.

Using the equilibrium conditions of concrete and reinforcement rods, we obtain the following two differential equations connecting the forces in the rods and the tangential coupling stresses (Fig. 5):

- for fittings:

$$-N_s + N_s + dN_s - t \cdot dx = 0; \quad (13)$$

- for concrete:

$$-N_c + N_c + dN_c + t \cdot dx = 0. \quad (14)$$

After the corresponding algebraic transformations, we will have:

- for fittings:

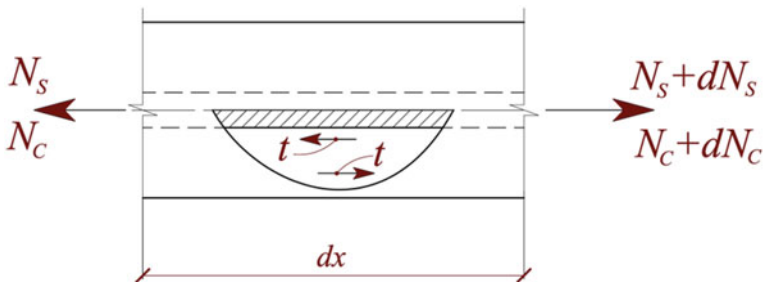


Fig. 5 Reinforcement work in concrete

$$\frac{dN_s}{dx} = \tau_{bond} \cdot \pi d_s; \quad (15)$$

– for concrete:

$$\frac{dN_c}{dx} = -\tau_{bond} \cdot \pi d_s. \quad (16)$$

Hooke's law is valid for fittings:

$$\sigma_s = E_s \cdot \varepsilon_s; \Rightarrow \varepsilon_s = \frac{\sigma_s}{E_s} = \frac{N_s(x)}{E_s \cdot A_s}. \quad (17)$$

From here, we get:

$$\varepsilon_s(x) = \frac{1}{E_s A_s} \cdot N_s(x). \quad (18)$$

Thus, a nonlinear boundary value problem consisting of four equations, two of which are differential of the first order, has the following form:

$$\left\{ \begin{array}{l} \varepsilon_s(x) = \frac{1}{E_s \cdot A_s} \cdot N_s(x); \\ \varepsilon_c(x) = \begin{cases} \frac{N_c(x)}{E_{cm} \cdot A_c}, & \text{если } \frac{N_c(x)}{A_c} \leq 0,9 \cdot f_{ctm}, \\ \frac{18 \cdot N_c(x)}{E_{cm} \cdot A_c} - 15,3 \cdot \frac{f_{ctm}}{E_{cm}}, & \text{если } \frac{N_c(x)}{A_c} > f_{ctm}; \end{cases} \\ \frac{dN_s(x)}{dx} = \begin{cases} \pi \cdot d_s \cdot 0,4 \cdot E_{cm} \cdot [\varepsilon_s(x) - \varepsilon_c(x)], & \text{если} \\ \varepsilon_q(x) \leq \varepsilon_q^*(x) = 4,95 \cdot \frac{f_{ctm}}{E_{cm}} \\ \pi \cdot d_s \cdot \{0,0232 \cdot E_{cm} \cdot [\varepsilon_s(x) - \varepsilon_c(x)] + 1,866 \cdot f_{ctm}\}, & \text{если} \\ \varepsilon_q(x) > \varepsilon_q^*(x) = 4,95 \cdot \frac{f_{ctm}}{E_{cm}} \end{cases} \\ \frac{dN_c(x)}{dx} = \begin{cases} -\pi \cdot d_s \cdot 0,4 \cdot E_{cm} \cdot [\varepsilon_s(x) - \varepsilon_c(x)], & \text{если} \\ \varepsilon_q(x) \leq \varepsilon_q^*(x) = 4,95 \cdot \frac{f_{ctm}}{E_{cm}} \\ -\{0,0232 \cdot E_{cm} \cdot [\varepsilon_s(x) - \varepsilon_c(x)] + 1,866 \cdot f_{ctm}\}, & \text{если} \\ \varepsilon_q(x) > \varepsilon_q^*(x) = 4,95 \cdot \frac{f_{ctm}}{E_{cm}} \end{cases} \end{array} \right. \quad (19)$$

The boundary conditions of the problem are written as follows:

$$N_c(x = 1) = 0, \quad N_s(x = 1) = C. \quad (20)$$

**6. Modeled with the help of “stitching” with finite elements.** Then the spatial cracks—surfaces are approximated by parallelepipeds inscribed into them after modeling a reinforced concrete structure with the same spatial finite elements (Fig. 6c).

A classification of **discrete basic spatial cracks** is introduced. In spatial reinforced concrete composite structures [15–21, etc.], the following basic cracks may occur: (1) cracks that develop to or from zones of geometric concentration of stress–strain, etc.); states (in places where the cross-sections change in size, in the incoming corners, in the zones of non-circular holes and states (in places where the cross-sections change in size, in the incoming corners, in the zones of non-circular holes and (2) cracks that develop to or from the zones of concentration of force and deformation loading (locations of support reactions and concentrated, places where the intensity of loading changes along the contour of the structure, places of deformation loading from subsidence; of particular importance is the type of loading—bending, shifting, compression—stretching); (3) longitudinal cracks that develop in the zones of compression—stretching); inter-medium concentration of deformations (in the

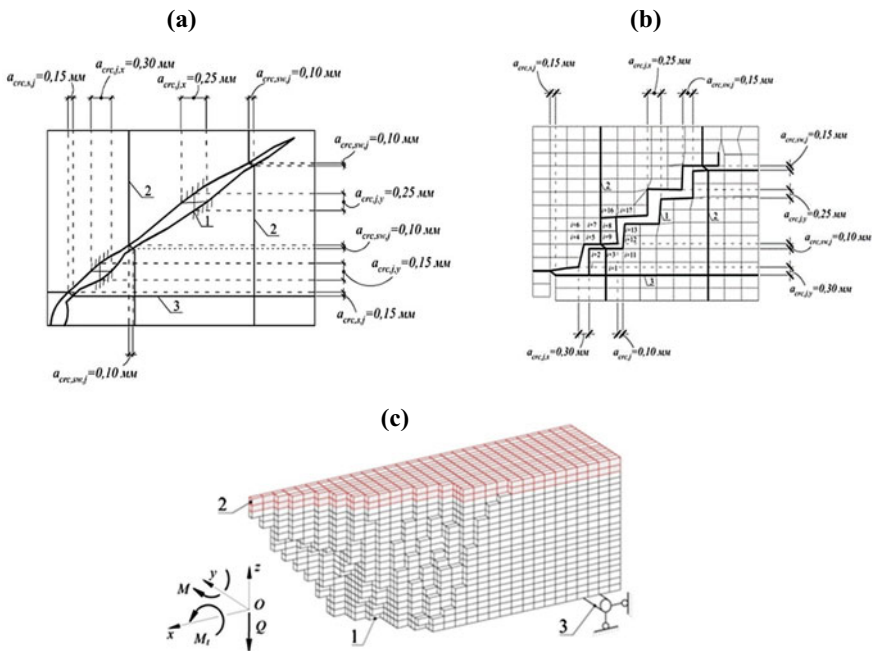


**Fig. 6** The proposed crack model: **a**—a real crack; **b**—modeled with the help of “expansion” of plane–stressed finite elements (CE) and deformation effects; **c**—modeled with the help of “expansion”, spatial finite elements (CE) and deformation effects in a block computational model with a spatial and normal cross-section passing through the end of a spiral crack; 1—crack; 2—transverse reinforcement and its modeling with 201 CE, 3—longitudinal reinforcement and its modeling with 201 CE; 4—possible crack closure and its modeling with 255 CE

joints between concretes in flat-stressed reinforced concrete composite structures; along the longitudinal reinforcement in anchoring zones, etc.).

In the practice of construction (for example, in complex engineering and geological conditions), the most common schemes of force and deformation loading, which, as a rule, cause the imposition of various cracks [15–21, 24, etc.].

With complex resistance, as already noted above, the building (Fig. 1a) can be modeled using both planar and spatial finite elements.

The essence of the proposed crack model [15–21, 24] is that a real crack (Fig. 2a for flat reinforced concrete structures and described by formula (2) for spatial reinforced concrete structures) is replaced by a model in the form of a polyline corresponding to the inscribed finite elements (Fig. 2b for flat and Fig. 2c for spatial, is considered on the example of the Lira-CAD VC), which are “embroidered” by modeling a crack, and its disclosure is given in the form of *a deformation effect*  $\Delta = a_{cr,c,j}$  directed perpendicular to the surface of the spatial crack [1–9], described by the dependence (1). Consideration of the effect of discontinuity violation [15–21, 24, etc.], is performed with the help of the introduction of a variable crack opening width depending on its distance from the axis of the working (longitudinal or transverse) reinforcement.

When solving the inverse problem [15–21, 24, etc.],—determining the width of crack opening, the deformation effect is not set, and with the help of stitching, only the presence of a gap of the minimum possible width is modeled, and its opening under appropriate loading determines the width of crack opening, as the divergence of the banks of this gap.

7. Special calculated two-element console model (TCM) for finite elements. Another variant of modeling discrete cracks is also possible [15–21, 24, etc.]. It is used in the case when the renumbering of the nodes of the design scheme of a reinforced concrete structure (building or structure), associated with the need for “stitching”, considered in the first variant, is undesirable.

In this variant, the final elements are not “stitched” along the entire crack, and at the first stage of modeling discrete cracks, only imaginary discrete cracks are used, the development of which is predicted by the introduced crack classification in relation to a specific calculation.

At the second stage of crack modeling, pairs of finite elements adjacent to such a crack from opposite sides are distinguished along the trajectory of an imaginary crack. These pairs are considered in two states: before their “stitching” and after their “stitching”. To do this, a special *two-element console model* is involved in the calculation (in the first case, it is flat in accordance with Fig. 4a, b. In the second case, it is a spatial one in accordance with Fig. 4c–e), with the help of which a sequential iterative analysis of the stress–strain state of spatial cantilever elements adjacent to the simulated spatial crack from opposite sides is performed and implemented with the help of “stitching” and deformation effects, which also takes into account the effect of continuity violation concrete. In this case, the distributed reinforcement is replaced by two (for a flat model) and four (for a spatial model) stubble end elements in each mutually perpendicular direction, respectively.

The movements of the nodes are determined from the calculation of a two-element calculation model with loads specified in the nodes (nodal finite element forces). At the same time, the support anchorages of two nodes in a flat model and four nodes in a spatial model (alternating pivotally fixed and pivotally movable supports), for averaging purposes, must be set from left to right, front to back, bottom to top. It is also important that, along with nodal loads, the deformation effects associated with the crack opening width are also set in the two-element model, which, in turn, is associated with the effect of continuity violation [24, etc.].

The deformation action is set in each node (except for the reference ones) according to three etchings in accordance with Fig. 3, *e*, where *l*, *m* and *n* are the guiding cosines of the main vector of crack opening at one or another of its points to the *x*, *y* and *z* axes, respectively.

Then, with the applied efforts and movements in the console nodes, the values of the works in two states are compared: “before the stitching” and “after the stitching” of the two-element model. From the condition of equality of these works, the thickness of the finite elements in the state “before stitching” decreases. This procedure is performed for all pairs of finite elements adjacent to the crack from different sides (along horizontal, vertical or their lateral surfaces). As a result, the thickness of the finite elements decreases along the imaginary crack, which provokes the formation and development of cracks according to the criterion of regular dispersed cracks, without resorting to the expansion of the finite elements.

The averaged forces in the nodes in different directions for a two-element console model are determined from a physically nonlinear calculation of the entire structure. For this purpose, nodal forces are used in the corresponding end elements of concrete and reinforcement.

As a result, the new thickness of the finite elements adjacent to the crack is found by the formula:

$$b = \frac{W_1}{W_2} \cdot b_1 \quad (21)$$

where  $W_1$  and  $W_2$  are the works of the two-element model “before stitching” and “after stitching”, respectively.

The proposed algorithm provides for an iterative process regulated by the achieved accuracy of the thickness of the marked finite elements that are adjacent to imaginary cracks, and the dynamic characteristics of a reinforced concrete structure (building or structure).

It is appropriate to note here that the rigidity of core reinforced concrete structures in areas with inclined cracks, including intersecting ones (characteristic of seismic impacts for supporting sections and junctions), is replaced by equivalent rigidity:

$$B(\lambda) = \frac{M^2 \cdot \Delta x}{2 \cdot W_3} \quad (22)$$

where  $W_3$  is the sum of the forces of the selected area.

Here the iterative process ends after reaching the specified error in determining  $B_1(\lambda)$ .

In areas with normal cracks, the rigidity of core reinforced concrete structures is determined using the values of the bending moment  $M$  and the radius of curvature and  $\rho$  according to the standard methodology for the corresponding stretched zone (the area with normal cracks is recommended to be divided into 4–6 zones):

$$B_i(\lambda) = M_i \cdot \rho_i \quad (23)$$

*The algorithm* in the intelligence “LIRA” for modeling reinforced concrete and the problem of cracking and creating the effect of reinforced concrete in the form of concrete discontinuity and reinforcement reaction based on the mechanics of destruction and additions to modules 1–7 and tools:

1. Effect—module 1—tools. The author has developed *the effect of reinforced concrete* (discovered in reinforced concrete by Professor Vladimir Kolchunov) [1–9, 16, 23, etc.], the physical essence of which is the additional deformation effect of the reaction of reinforcement and concrete in the form of an ellipsoid crack
2. TCE = Module 2—tools. Tools from a spatial *crack of a two-console element (TCE)* in reinforced concrete based on the mechanics of destruction associated with a violation of the continuity of concrete.
3. Surface—module 3—tools. To do this, it is written from the equation of the beam of *a bilinear surface*, where it is concretized with respect to a given cross-section.
4. Lagrange module 4—tools. *At the extremum of the function of many variables for reinforced concrete* and the maximum crack width, a multi-level development process involving inequalities and the deformation criterion of their formation and the method of finding using Lagrange multipliers allows finding projections and distances of adjacent cracks.
5. *Analytical model of reinforcement coupling with concrete and their compliance*—module 5—tools.
6. “*Stitching*” of finite elements—module 6—for the instrument program “LIRA”. and along the seam between the layers of concrete;
7. *TCM console*—module 7—tools. For the nonlinear calculation of the entire reinforced concrete structure for the specified force and deformation effects, *pairs of finite elements* adjacent to such a crack are allocated and a special *two-element console model (TCM)* of reinforced concrete resistance is involved. These pairs are considered in two states: before their “expansion” and after their “expansion”. The deformation action is performed in each node (except for the support ones) according to three alignments in accordance with Fig. 7, д, where  $l$ ,  $m$  and  $n$  are the guiding cosines of the main crack opening vector at one or another of its points to the  $x$ ,  $y$  and  $z$  axes, respectively.



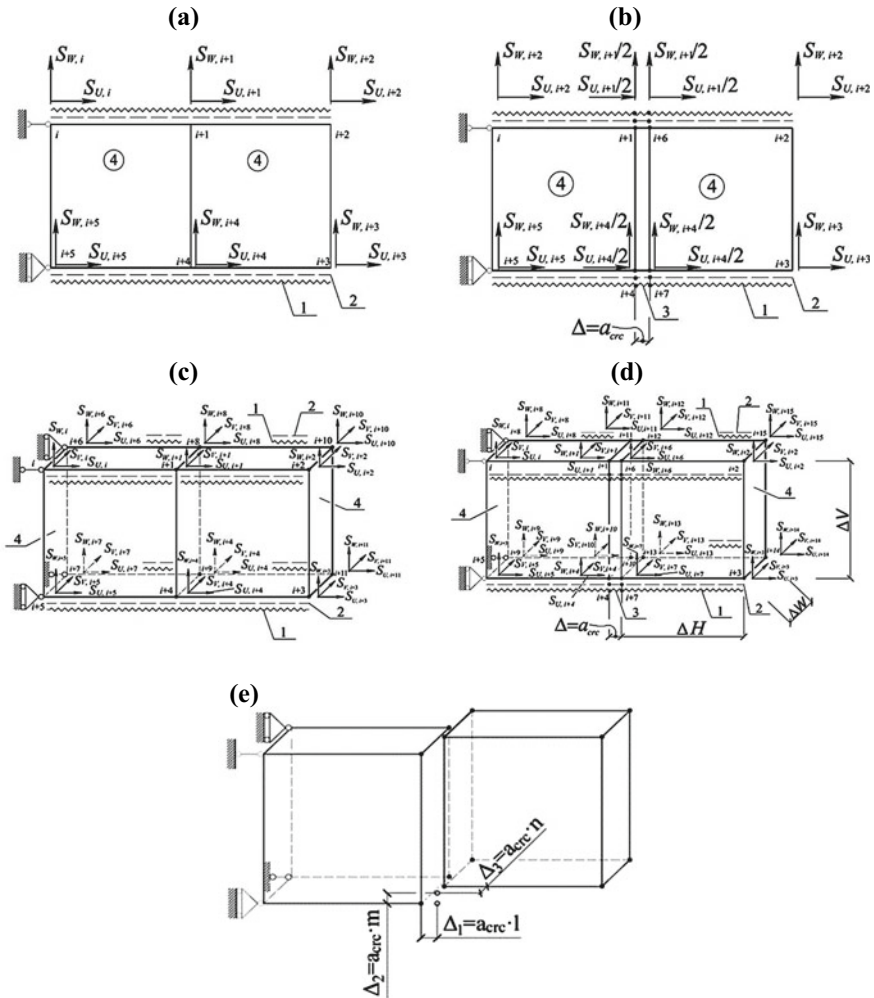


**Fig. 7** Construction of two-element flat and spatial models: **a**—flat, without “stitching”; **b**—the same, after “stitching”; **c**—spatial, before “stitching”; **d**—also, after “stitching”; **e**—deformation effects: 1—255 CE before “stitching”; 2—201 CE; 3—255 CE after “stitching”; 4—233 CE

With the help of which a sequential iterative analysis of the stress-strain state of spatial cantilever elements adjacent from opposite sides to the simulated spatial crack is performed.

8. **“Closing the crack”** after “stitching” is a tool for the final element. 255CE program “LIRA” and implemented with the help of “stitching” and deformation effects, which also takes into account *the effect of breaking the continuity of*

**concrete** for incompatibility of deformations of concrete and reinforcement—reinforcement rods are modeled with additional 201 CE, and possible crack closure—concrete with 255 CE.

9. The proposed **method of opening the width** or along the seam between layers of concrete; stiffness and determination of the distance between cracks of flat-stressed and spatial reinforced concrete composite structures with the involvement of the software package PC “Lira-CAD” is considered in two versions [1–9, 16, 23, 24, etc.]. According to the first variant, the stiffness is determined using a special technique for modeling the explicit **reverse** method of minimal **cracks** of their movements of its banks for opening and closing (Fig. 7). For the second **direct** method, the construction of **formulas for the disclosure of the width** of reinforced concrete (deformation effect  $\Delta = a_{crc}$ ).
10. It is also possible to model cracks along the trajectory of an implicit (imaginary) crack and stiffness, adjacent **pairs of finite elements** are allocated to reduce their thickness. Then the work of  $W_1$  and  $W_2$ , respectively, of each pair of CE is calculated twice using a two-element cantilever model (Fig. 7): before the “plugging” of the CE and after the “plugging” of the CE with the applied nodal forces and deformation effects from the opening of cracks and taking into account the effect of breaking continuity. In this case, the distributed reinforcement is replaced by two (for a flat model) and four (for a spatial model) core fiber end elements.

### 3 Results and Discussion

As a result, the new thickness of the finite elements adjacent to the crack is found according to formula (21), as well as the stiffness of the core reinforced concrete structures in areas, including normal or intersecting cracks, is replaced by equivalent stiffness according to formulas (22) or (23), respectively.

The averaged forces in the nodes in different directions for a two-element cantilever model are determined from a physically nonlinear calculation of the entire structure. For this purpose, nodal forces are used in the corresponding end elements of concrete and reinforcement. In the places of transitions of horizontal sections of simulated cracks to vertical and lateral, the work of angular finite elements is determined by averaging them. As a result, the thickness of the finite elements decreases along the imaginary crack, which provokes the formation and development of cracks according to the criterion of discrete cracks, without resorting to the expansion of the finite elements.

The iterative process ends after reaching the specified deviation in determining  $B_1(\lambda)$ .

11. The procedure is first performed by the constructor of enough pairs of finite elements adjacent to the crack near the working armature, for a rod of lateral and lower faces, where their concentrations are included along perpendicular straight lines. Further loading in **the intelligence of “LIRA” automatically** includes corridors

along the directions of stretching (their criteria) of their finite elements through the already stepped *spatial surface*.

Such a comprehensive comparative analysis of the values of opening width and stiffness will certainly contribute to an in-depth study of these values [1–9, 16, 23, 24, etc.].

## 4 Conclusion

1. Until today, there have already been a large number of well-known computing complexes in the world that use finite element models. Nevertheless, there remains a need to find an adequate type of development and crack opening. For the design of reinforced concrete structures, a block calculation model with spatial (or flat) working sections is also involved. The calculation of the disclosure of discrete cracks is performed using completely different analysis criteria, taking into account the effect of reinforced concrete. The physical essence of the effect lies in the additional deformation effect of disruption of the continuity of the reaction of reinforcement and concrete in the form of an ellipsoid for an alternative kinematic crack using a universal two-console element from fracture mechanics. At the same time, in the stretched area of concrete, in order to determine the distance between cracks and the opening width in these local areas adjacent to the crack, it is important to take into account the adhesion and tensions of compressed concrete.
2. In reinforced concrete conventional and composite structures for discrete levels, a classification of basic spatial cracks is constructed from a picture of various types that develop to zones of concentration of geometric, force, deformation loading or the inter-environment region. The complete scheme is applied to the base and adjacent cracks, as well as by finding projections and distances. This makes it possible to obtain a multilevel development process involving the deformation criterion of their formation and the method of finding the extremum of a function of many variables using Lagrange multipliers.
3. The technique of modeling discrete cracks, including for intelligence, has not yet been developed for most of the known computing complexes in the world. The development of spatial cracks is carried out by special bilinear surfaces. Loadings in the “LIRA” intelligence are automatically included in the corridors along the directions of stretching (criteria) of their finite elements through an already stepped spatial surface. Then approximating spatial finite elements are inserted into them, which “embroider” the spatial crack. For the direct method, the opening is set in the form of a deformation effect and a formula for the width of the crack opening, taking into account the effect of breaking the continuity of reinforced concrete. When solving the inverse problem of determining the width of crack opening, the deformation effect is not set, but only the presence of a “gap” (the minimum possible width) is modeled, where in the corresponding loading it determines the width of crack opening, as the divergence of the banks.

4. The article considers pairs of finite elements adjacent to the crack from opposite sides—a special calculated two-element console model (TCM). These pairs are considered in two states: before their “stitching” and after their “stitching”, taking into account the deformation effect and the effect of breaking the continuity of concrete. Tools or modules of the “LIRA” program are used to find the level distance between cracks and the width of their opening in a reinforced concrete structure, which allows determining additional desired parameters.
5. Based on the analysis and generalization of experimental and theoretical studies, a methodology and algorithm have been developed that allow modeling discrete cracks and rigidity of reinforced concrete structures with complex resistance. In the “LIRA” intelligence, a crack opening simulation was performed and the effect of reinforced concrete was obtained in the form of concrete discontinuity, reinforcement reaction based on fracture mechanics and additions to modules 1–7. The following tools were also used: a two- console element (TCE) based on a spatial crack; from the bilinear surface beam equation; finding projections of adjacent spatial cracks: at the extremum of functions of many variables for reinforced concrete and the maximum crack width using Lagrange multipliers; an analytical model of reinforcement coupling with concrete and their compliance; the proposed classification of basic spatial cracks; “expansion” for the instrument, the program “LIRA”; a special calculated two-element console model (TCM); “closing the crack” after “stitching” is a tool for the final element of the 255CE program “LIRA”. The proposed methodology for determining the width of the opening, stiffness, distance between cracks for the direct method of constructing formulas for the width of the crack or the reverse method of minimal cracks, the movements of their banks during opening and closing. It is also possible, when modeling an implicit (imaginary) crack, to replace the stiffness with an equivalent stiffness to reduce the thickness of the finite elements, which provokes the formation and development of cracks according to the criterion of discrete cracks, without resorting to the expansion of the finite elements. The procedure is first performed by the constructor, and then the loadings in the “LIRA” intelligence automatically include corridors in the direction of stretching (their criteria) of their finite elements through an already stepped spatial surface.

## References

1. Karpenko NI (1996) General models of reinforced concrete mechanics. Stroyizdat, Moscow. ISBN: 5-274-01682-0
2. Golyshev AB, Kolchunov VI (2009) Reinforced concrete resistance. Osnova, Kiev
3. Bondarenko VM, Kolchunov VI (2004) Design models of the power resistance of reinforced concrete. Publishing House ABC, Moscow. ISBN: 5-93093-279-4
4. Bashirov KhZ, Kolchunov VI, Fedorov VS, Yakovenko IA (2017) Reinforced concrete composite structures of buildings and structures. Publishing House ABC, Moscow
5. Veruzhsky YV, Kolchunov VI (2005) Methods of reinforced concrete mechanics. NAU, Kiev

6. Veryuzhsky YV, Golyshev AB, Kolchunov VI, Klyueva NV, Lisitsin BM, Mashkov IL, Yakovenko IA (2014) A reference guide to structural mechanics, vol II. Publishing House ABC, Moscow. ISBN: 978-5-4323-0007-2
7. Kolchunov VI, Fedorov VS (2020) Conceptual hierarchy of models in the theory of resistance of building structures. *Promyshlennoe i grazhdanskoe Stroitelstvo (Ind Civ Eng)* 8:16–23. <https://doi.org/10.33622/0869-7019.2020.08.16-23>
8. Golyshev AB, Kolchunov VI (2015) Resistance of reinforced concrete structures, buildings and structures erected in difficult engineering and geological conditions. Kiev
9. Fedorov VS, Kolchunov VI, Pokusaev AA, Naumov NV (2020) Calculation models of deformation of reinforced concrete constructions with spatial cracks. *Russ J Build Constr Arch* 6–26. <https://doi.org/10.36622/VSTU.2020.47.3.001>
10. Karpenko NI, Kolchunov VI, Travush VI (2021) Calculation model of a complex stress reinforced concrete element of a boxed section during torsion with bending. *Russ J Build Constr Arch* 7–26. <https://doi.org/10.36622/VSTU.2021.51.3.001>
11. Kim C, Kim S, Kim K-H, Shin D, Haroon M, Lee J-Y (2019) Torsional behavior of reinforced concrete beams with high-strength steel bars. *ACI Struct J* 116:251–233. <https://doi.org/10.14359/51718014>
12. Bernardo L (2019) Modeling the full behavior of reinforced concrete flanged beams under torsion. *Appl Sci* 9:2730. <https://doi.org/10.3390/app9132730>
13. Lin W (2021) Experimental investigation on composite beams under combined negative bending and torsional moments. *Adv Struct Eng* 24:1456–1465. <https://doi.org/10.1177/1369433220981660>
14. Travush VI, Karpenko NI, Kolchunov VI, Kapriylov SS, Dem'yanov AI, Konorev AV (2018) The results of experimental studies of structures square and box sections in torsion with bending. *Build Reconstr* 6:32–43
15. Kolchunov V, Smirnov B, Naumov N (2020) Physical essence of the “Nagel effect” for main reinforcement in an inclined crack of reinforced concrete structures. *IOP Conf Ser Mater Sci Eng* 896:012055. <https://doi.org/10.1088/1757-899X/896/1/012055>
16. Kolchunov V, Dem'yanov A, Naumov N (2020) Analysis of the “Nagel effect” in reinforced concrete structures under torsion with bending. *IOP Conf Ser Mater Sci Eng* 953:012052. <https://doi.org/10.1088/1757-899X/953/1/012052>
17. Kolchunov VI, Dem'yanov AI, Naumov NV, Mikhaylov MM (2019) Calculation of the stiffness of reinforced concrete structures under the action of torsion and bending. *J Phys Conf Ser* 1425. <https://doi.org/10.1088/1742-6596/1425/1/012077>
18. Kolchunov VI, Dem'yanov AI, Naumov NV (2020) The second stage of the stress-strain state of reinforced concrete constructions under the action of torsion with bending (theory). *IOP Conf Ser Mater Sci Eng* 753:032056. <https://doi.org/10.1088/1757-899X/753/3/032056>
19. Kolchunov VI, Dem'yanov AI (2019) The modeling method of discrete cracks and rigidity in reinforced concrete. *Mag Civ Eng* 4(88):60–69. <https://doi.org/10.18720/MCE.88.6>
20. Demyanov A, Kolchunov VI (2017) The dynamic loading in longitudinal and transverse reinforcement at instant emergence of the spatial crack in reinforced concrete element under the action of a torsion with bending. *Istraz i Proj za privredu* 15:377–382. <https://doi.org/10.5937/jaes15-14663>
21. Kolchunov VI, Dem'yanov AI (2018) The modeling method of discrete cracks in reinforced concrete under the torsion with bending. *Mag Civ Eng* 5(81):160–173. <https://doi.org/10.18720/MCE.81.16>
22. Kolchunov VI, Dem'yanov AI, Mikhaylov MM (2020) Static-dynamic deformation of compressed concrete in an indeterminate reinforced concrete frame during bending with torsion. *News of higher educational institutions. Construction* 4:5–21
23. Kolchunov VI, Fedorova, NV (2018) Deformation Models of Reinforced Concrete under Special Impacts. *Promyshlennoe i grazhdanskoe Stroitelstvo (Ind Civ Eng)* 8:54–60
24. Kolchunov VI, Yakovenko IA, Tugay TV (2014) Method for calculating the stiffness of plane-stressed reinforced concrete structures using the Lira-Pro software package. *Sbornik nauchnyh trudov (seriya otraslevoe mashinostroenie, stroitel'stvo) (Collect Sci Pap (Ser Ind Eng, Constr))* 3(42):55–66

# Experimental Investigation of RC Frame with Sway Columns Under Corner Column Removal Scenario



Sergey Savin , Natalia Fedorova , and Pavel Korenkov 

**Abstract** Although the progressive collapse has a small probability in economically developed countries, it can lead to catastrophic consequences. Therefore, this paper is aimed to experimental and numerical investigation of impact parameters on the reinforced concrete frames under scenario of sudden column removal. As well as it provides the analysis of the failure mechanisms of the frame under consideration, and substantiation of the criteria for assessing these failure mechanisms. For the purposes of the study, a two-story reinforced concrete scaled frame was designed, manufactured and tested. A nonlinear dynamic and quasi-static analysis of reinforced concrete frame have been performed using finite element bar models both of the structure and leverage loading system. Numerical and physical modeling of an accidental impact such as sudden removal of the corner column of the shows that the exhaustion of the load capacity of eccentrically compressed column of a structural system can be caused by the stability failure.

**Keywords** Reinforced concrete · Sway column · Frame · Accidental impact · Stability failure

## 1 Introduction

The problem of resistance of structural systems of buildings and structures after a failure of one of the structural member or ties have a great interest to engineers and the scientific community. In recent years, a large number of experimental and numerical studies has been carried out in this field [1–10]. Authors of such researches investigated the features of deformation and fracture of buildings and structures, proposed various design solutions in order to prevent disproportionate failure and increase

---

S. Savin (✉) · N. Fedorova · P. Korenkov

Moscow State University of Civil Engineering, 26 Yaroslavskoe Shosse, 129337 Moscow, Russia  
e-mail: [savinsyu@mgsu.ru](mailto:savinsyu@mgsu.ru)

Research Institute of Building Physics of Russian Academy of Architecture and Construction Sciences, 21 Street Lokomotivny Proezd, 127238 Moscow, Russia

© The Author(s), under exclusive license to Springer Nature Switzerland AG 2024

313

N. Vatin et al. (eds.), *Modern Problems in Construction*,

Lecture Notes in Civil Engineering 372,

[https://doi.org/10.1007/978-3-031-36723-6\\_30](https://doi.org/10.1007/978-3-031-36723-6_30)

the resistance structural members and its joints [11–14] under impacts which are not provided for by the normal operation conditions. Reinforced concrete structures have widely application in modern construction. Therefore, a wide layer of publications on progressive collapse problem provides the research results on the resistance to disproportionate failure of such structures. However, research in this area is mostly focused on assessing and improving the resistance of joints and structures of beams, slabs and roofs of civil buildings under a removal of load bearing member, usually such as column [1–3, 15]. The issues of resistance of vertical load-bearing structures of reinforced concrete frames have a less coverage the scientific literature. This is due to the fact that reinforced concrete columns have significant bending stiffness and a significant margin of load capacity under loading only with dead and reduced live loads, which should be accounted in analysis for progressive collapse in accordance with design codes [16–18]. However, it is not uncommon when in civil buildings, which allow massive presence of people, columns with great slenderness ratio are used [19–21]. For some building frames, such columns allow the displacement of the upper and lower end sections relative to each other (sway columns), or the effective slenderness ratio of the columns increases due to environmental impacts on structures [22–24]. The deformation of such columns is associated with the manifestation of inelastic second-order effects, leading to a decrease in the load capacity compared to short columns. Therefore, this paper is aimed to experimental and numerical investigation of impact parameters on the reinforced concrete frames under scenario of sudden column removal. As well as it provides the analysis of the failure mechanisms of the frame under consideration, and substantiation of the criteria for assessing these failure mechanisms.

## 2 Method

For the purposes of the study, a two-story reinforced concrete frame with slender sway columns of the second floor was designed and manufactured. The test frame was designed in accordance with a preliminary performed numerical simulation. The composition of the concrete mixture for the test frame was selected in order to obtain concrete of compressive class B25, i.e., characteristic strength of the cube specimens was not less than 25 MPa. A spatial steel reinforcement carriage with a symmetrical arrangement of longitudinal bars was adopted as Fig. 1 shows.

Tests of the physical model of the reinforced concrete frame consisted of two stages. At the first stage, a gravitational load was applied stepwise in 10 steps to the upper nodes of the test frame using a leverage loading system. At the second stage, a special device that simulate corner column sudden removal had been transformed to instantaneously changeable mechanism. The Fig. 2 presents loading scheme of the test frame both at normal operation mode and accidental impact caused by corner column removal.

To estimate the reaction redistribution time of the suddenly removed support simulating corner column, numerical simulation was performed using a rod model,

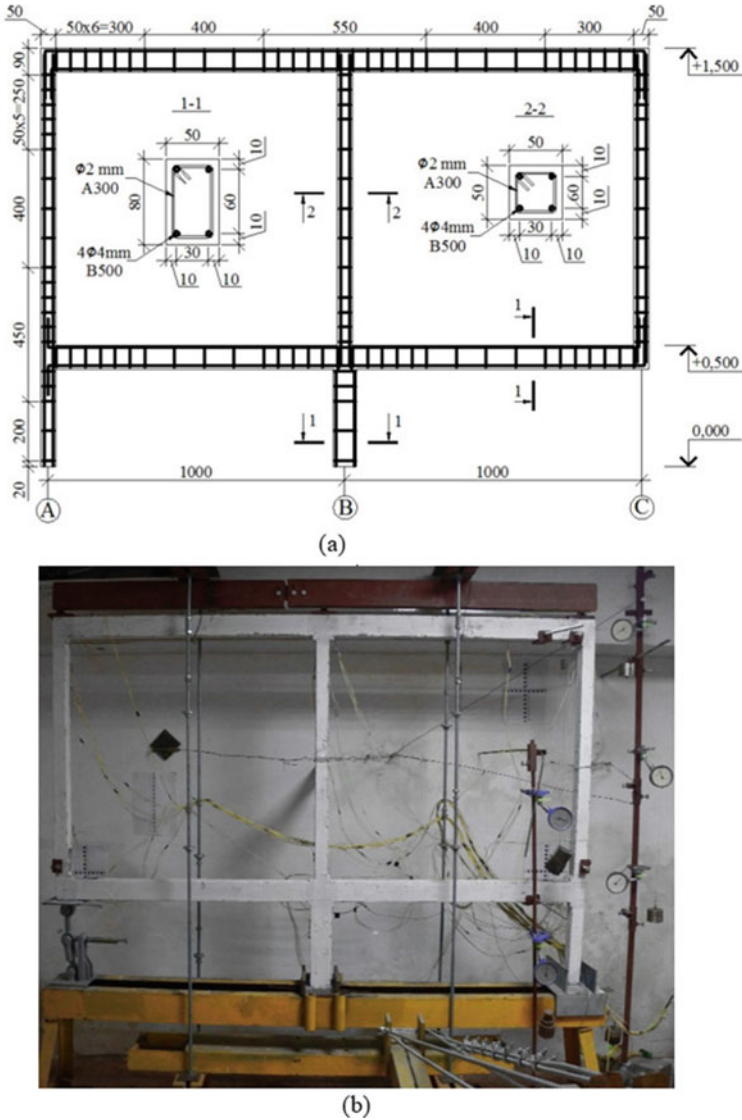


**Fig. 1** The design of the experimental reinforced concrete frame: reinforcement scheme (a), general view of the stand with the frame installed (b)

including the design of an experimental frame and a lever load system. Lira CAD software had been applied to perform finite element analysis of the test frame under accidental impact [25]. Finite elements of universal physically nonlinear bar FE 210 simulated structural members of the test frame and leverage loading system. The time for redistribution of the removed support reaction was adopted in regard with



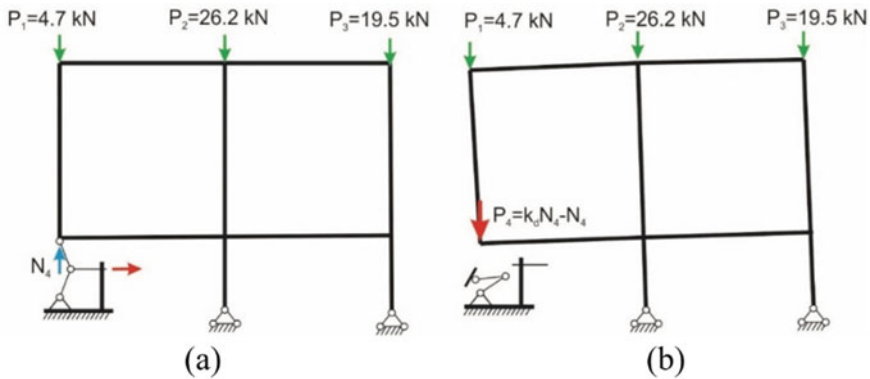


**Fig. 2** Design scheme of the test frame for normal operation mode (a), and the same one for sudden removal of corner column (b)

comparison of test and preliminary simulation results. It was 0.1 s that almost corresponds to 1/10 of the period of free vibration of the frame for a lowest mode. A strain had been accepted as a criteria of a special limiting state (failure criteria) for frame member's cross section. Ultimate strain for compressed concrete was 0.0035, and ultimate strain for steel reinforcement in tension was 0.033, which is in accordance with Building Code requirements [18].

### 3 Results and Discussion

The mechanical contact between the frame joint and support simulating column removal was abruptly in the range from 0.1 to 0.133 s after support removal. After, for the time range from 0.133 to 0.167 s, a change in the direction of the frame joint movement had been observed. Beginning from the time 0.83 s, there was an intensive increase in the displacement of the considered frame joint had been fixed. This increasing was accompanied with stability failure of second floor middle column of the test frame at 1.167 s as Fig. 3a presents.

Numerical simulation showed a pattern of dynamic displacements similar to experimentally obtained one for the following parameters of impact and bending stiffness:

- the factors 0.6 and 0.3 were accepted for initial deformation modulus of concrete of columns and girders respectively that accounts the nonlinear behavior of these structural members;
- the time of the reaction redistribution for the collapsed structural member was accepted as 0.1 s, which is about 1/10 of the period of free vibrations of the frame ( $T = 0.9 \text{ s}$ ) without corner column for a lowest mode associated with static deformed state of the frame after accidental impact.

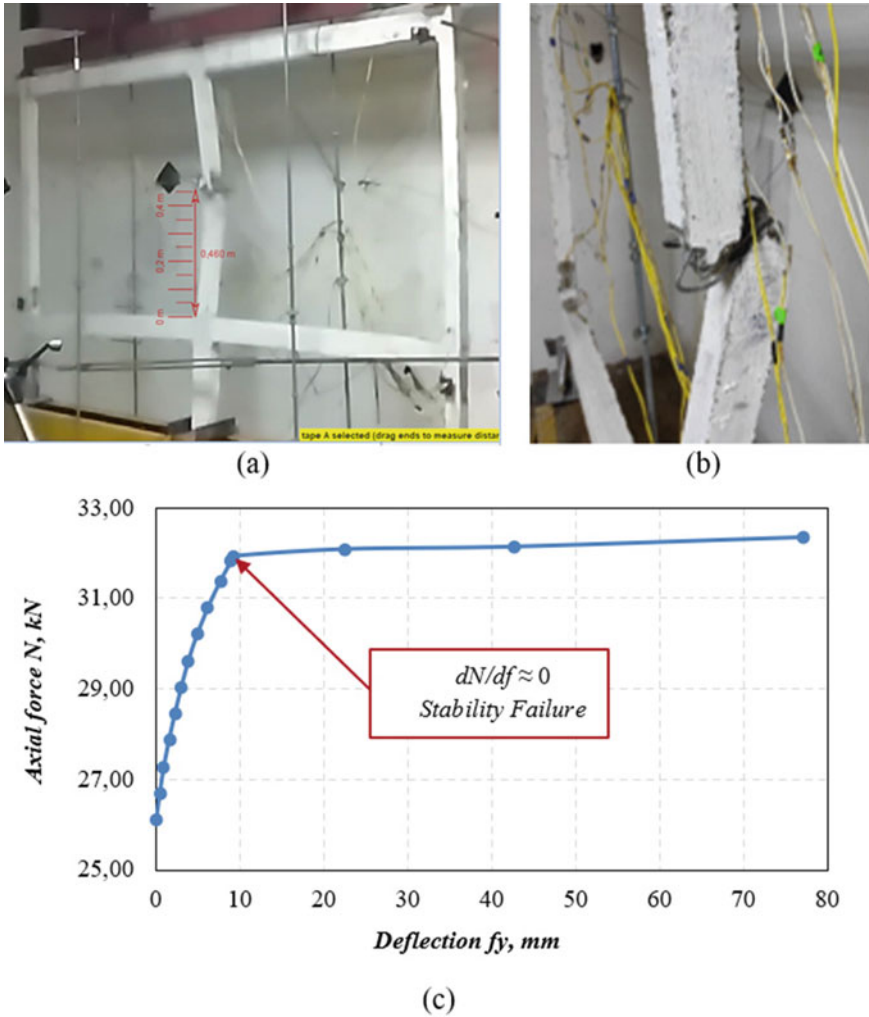


**Fig. 3** The frame stability failure: general view at 1.200 s after sudden corner column removal (a); view of the failure of the middle column on the second floor of the test frame after accidental impact (b); N–f curve based on the results of a nonlinear finite element analysis (c)

The non-linear dynamic and quasi-static deterministic finite element analysis showed failure propagation similar to experimental one when kinematic impact in the form of the FEM node displacement in the middle of the column height was of 0.184 cross-sectional depth was applied. The achievement of null incremental stiffness or  $dP/df = 0$  was adopted as a criterion for evaluating the special limiting state of the structure under initial local failure (corner column removal).

## 4 Conclusions

The present article provides an experimental and numerical study of the parameters of impacts on reinforced concrete frames subjected to sudden corner column removal, as well as an analysis of the failure mechanisms for the frame with sway slender columns.

Numerical analysis and physical simulation of an accidental impact caused by sudden removal of load bearing structural member or ties allowed us to establish that such an impact on frame with sway column causes it stability failure.

The paper showed that achieving of null increment bending stiffness can be considered as an integral criterion for evaluating the special limiting state of the sway slender columns of the frame subjected to column removal scenario.

## References

1. Wang H, Zhang A, Li Y, Yan W (2014) A review on progressive collapse of building structures. *Open Civ Eng J* 8(1):183–192. <https://doi.org/10.2174/1874149501408010183Hh>
2. Abdelwahed B (2019) A review on building progressive collapse, survey and discussion. *Case Stud Constr Mater* 11:e00264. <https://doi.org/10.1016/j.cscm.2019.e00264>
3. Fedorova NV, Savin SYu (2021) Progressive collapse resistance of facilities experienced to localized structural damage—an analytical review. *Build Reconstr* 95(3):76–108. <https://doi.org/10.33979/2073-7416-2021-95-3-76-108>
4. Kiakojouri F, De Biagi V, Chiaia B, Sheidaii MR (2019) Progressive collapse of framed building structures: current knowledge and future prospects. *Eng Struct* 206:110061. <https://doi.org/10.1016/j.engstruct.2019.110061>
5. Adam JM, Parisi F, Sagaseta J, Lu X (2018) Research and practice on progressive collapse and robustness of building structures in the 21st century. *Eng Struct* 173:122–149. <https://doi.org/10.1016/j.engstruct.2018.06.082>
6. Fedorova NV, Phan DQ, Egorov EA, Grigoriev MI (2022) Analysis of methods of experimental studies of the survivability of reinforced concrete structures. *Byulleten' stroitel'noy tekhniki* 1054(6):19–26. <http://bstmag.ru/article?id=2316>
7. Travush VI, Fedorova NV (2017) Survivability parameter calculation for framed structural systems. *Russ J Build Constr Arch* 33(1):6–14. <https://vestnikvgasu.wmsite.ru/ftpgetfile.php?id=564>
8. Fialko SY, Kabantsev OV, Perelmuter AV (2021) Elasto-plastic progressive collapse analysis based on the integration of the equations of motion. *Mag Civ Eng* 102:10214. <https://doi.org/10.34910/MCE.102.14>
9. Alekseytsev AV (2021) Mechanical safety of reinforced concrete frames under complex emergency actions. *Mag Civ Eng* 103(3). <https://doi.org/10.34910/MCE.103.6>
10. Alekseytsev AV (2020) Optimal design of steel frame structures subject to level of mechanical safety. *Build Reconstr* 89(3):51–62. <https://doi.org/10.33979/2073-7416-2020-89-3-51-62>
11. Fedorova NV, Iliushchenko TA (2019) Influence of pre-stressing over parameters of diagram of static-dynamic deformation of RC elements. *IOP Conf Ser Mater Sci Eng* 687(3):033033. <https://doi.org/10.1088/1757-899X/687/3/033033>
12. Kolchunov VI, Fedorova NV, Savin SYu, Kovalev VV, Iliushchenko TA (2019) Failure simulation of a RC multi-storey building frame with prestressed girders. *Mag Civ Eng* 92(8):155–162. <https://doi.org/10.18720/MCE.92.13>

13. Fedorova N, Kolchunov V, Vu NT, Phan DQ, Medyankin M (2020) The dynamic effect in a structural adjustment of reinforced concrete structural system. IOP Conf Ser Mater Sci Eng. 869:052078. <https://doi.org/10.1088/1757-899X/869/5/052078>
14. Kodysh EN (2018) Designing the protection of buildings and structures against progressive collapse in view of the emergence of a special limiting state. Ind Civ Eng 10:95–101. <http://www.pgs1923.ru/ru/index.php?m=4&y=2018&v=10&p=12>
15. Kabantsev O, Mitrovic B (2018) Deformation and power characteristics monolithic reinforced concrete bearing systems in the mode of progressive collapse. In: MATEC web of conferences 251:02047. <https://doi.org/10.1051/mateconf/201825102047>
16. UFC 4-023-03 Design of buildings to resist progressive collapse. <https://www.wbdg.org/ffc/dod/unified-facilities-criteria-ufc/ufc-4-023-03>. Last accessed 2022/09/01
17. GSA (2016) Alternate path analysis and design guidelines for progressive collapse resistance. <https://www.gsa.gov/real-estate/design-excellence-program/engineering-and-architecture/security-engineering/2016-alternate-path-analysis-design-guidelines-for-progressive-collapse-resistance>. Last accessed 2022/09/01
18. Building Code of RF SP 385.132580.2018 Protection of buildings and structures against progressive collapse. Design code. Basic statements. <https://docs.cntd.ru/document/551394640>. Last accessed 2022/09/01
19. Hales TA, Pantelides CP, Reaveley LD (2017) Analytical buckling model for slender FRP-reinforced concrete columns. Compos Struct 176:33–42. <https://doi.org/10.1016/j.compstruct.2017.05.034>
20. Bazant ZP, Kwon YW (1994) Failure of slender and stocky reinforced concrete columns: tests of size effect. Mater Struct 27:79–90. <https://doi.org/10.1007/BF02472825>
21. Abdelazim W, Mohamed HM, Benmokrane B (2020) Inelastic second-order analysis for slender GFRP-reinforced concrete columns: experimental investigations and theoretical study. J Compos Constr Am Soc Civ Eng (ASCE) 24(3). [https://doi.org/10.1061/\(asce\)cc.1943-5614.0001019](https://doi.org/10.1061/(asce)cc.1943-5614.0001019)
22. Tamrazyan AG, Popov DS (2019) Stress-strain state of corrosion-damaged reinforced concrete elements under dynamic loading. Ind Civ Eng 2:19–26. <https://doi.org/10.33622/0869-7019.2019.02.19-26>
23. Selyaev VP, Selyaev PV, Alimov MF, Sorokin EV (2017) Estimation of residual resources of reinforced concrete bending elements subjected to the action of chloride corrosion. Build Reconstr 74(6):49–58. <https://construction.elpub.ru/jour/article/view/83>
24. Xiao J, Long X, Qu W, Li L, Jiang H, Zhong Z (2022) Influence of sulfuric acid corrosion on concrete stress–strain relationship under uniaxial compression. Meas J Int Meas Confed 187. <https://doi.org/10.1016/j.measurement.2021.110318>
25. Barabash MS, Romashkina MA (2018) Lira-Sapr program for generating design models of reconstructed buildings. Int J Comput Civ Struct Eng 14(4):70–80. <https://doi.org/10.22337/2587-9618-2018-14-4-70-80>

# Energy Consumption Analysis During the Life Cycle of Buildings in Palestine



Elena Gorbaneva , Elena Vinogradova , Mahmoud A. M. Hamdan ,  
and Munther M. H. Abuasad 

**Abstract** Buildings are responsible for about 40% of all energy consumed in Palestine; therefore, buildings are responsible for most greenhouse gas emissions. It's necessary as the first step to developing the building sector in Palestine to be an energy-saving is to quantify the amount of embodied energy and the corresponding greenhouse gas emissions releases (CO<sub>2</sub> equivalent) associated with each stage of the building life cycle; therefore, the result can be used to determine the stages and activities that need improvement. In this study, we've done the life cycle analysis of embodied energy and greenhouse gas emissions (CO<sub>2</sub> equivalent), as well as the estimated cost of emissions for the typical building in Palestine. It's found that 73% of energy consumption and 82% of greenhouse gas emissions happen during the operation phase. The construction phase takes 45% of the life-cycle cost. The embodied energy is about 40 GJ/m<sup>2</sup>, and greenhouse gas emissions equal 3.9 t/m<sup>2</sup>.

**Keywords** Life cycle analysis embodied · Embodied energy · Greenhouse gas emission · Energy · Palestine · CO<sub>2</sub> equivalent

## 1 Introduction

Palestine depends on imported energy resources and electricity from neighboring countries. The buildings increasing of (from 2007 to 2017) 30.6% [1, 2] makes this sector consume 59% of total amount of electricity in 2019 with 175% of increment from 2010 [1], furthermore 17% of oil products with 10.5% decrement from

---

E. Gorbaneva (✉) · M. A. M. Hamdan · M. M. H. Abuasad  
Voronezh State Technical University, 84, 20th-Letie Oktyabrya St., 394006 Voronezh, Russia  
e-mail: [egorbaneva@vgasu.vrn.ru](mailto:egorbaneva@vgasu.vrn.ru)

E. Gorbaneva  
Research Institute of Building Physics RAASN, Novy Arbat Street, 19, 127025 Moscow, Russia

E. Vinogradova  
Don State Technical University, 162, Socialistheskaya Str., 344003 Voronezh, Russia

(2010–2019) [1, 2]. Analyzing energy consumption and greenhouse gas emissions throughout the life cycle gives the potential to develop the building to be more energy efficient.

This study aims to determine the quantity of energy consumed and greenhouse gas emission (CO<sub>2</sub> equivalent) for each m<sup>2</sup> in Palestinian residential buildings.

The building life cycle consists of 4 phases: construction, operation, maintenance and demolition [3].

The quantity of embodied energy (EE) and greenhouse gas emission (GHG) throw out the building life cycle can be calculated by Eqs. (1) and (2), respectively.

$$EE = EE_{\text{construction}} + EE_{\text{operation}} + EE_{\text{maintenance}} + EE_{\text{demolition}} \quad (1)$$

$$\text{CO}_2 \text{ eq} = \text{CO}_{2\text{construction}} + \text{CO}_{2\text{operation}} + \text{CO}_{2\text{maintenance}} + \text{CO}_{2\text{demolition}} \quad (2)$$

## 2 Methods

### 2.1 Construction Phase

The construction phase can be divided into three steps: extraction of raw material; fabrication of primary construction material; building construction activities. The authors used a (BSRIA guide ICE 10/2011) [4] to determine the (EE) and (CO<sub>2</sub> eq) for materials due to lack of information in Palestine.

The main building material and their corresponding (EE) and (CO<sub>2</sub> eq) are shown in Table 1. These values are the sum of the three steps of the construction phase [4–6].

**Table 1** Embodied energy (EE) and greenhouse gas emission (GHG) for main building material

Materials	EE (MJ/unit)	CO <sub>2</sub> (kg CO <sub>2</sub> /unit)
Bitumen	51	0.43
Reinforced concrete	2.34	0.214
Paint	70	2.42
Lime stone	1.5	0.087
Cement	1.33	0.208
Concrete	0.78	0.106
Paint	70	2.42
Sand	0.081	0.0048
Block	0.83	0.1

## 2.2 Operation Phase

It considers all the energy used to maintain comfort life, such as lighting, heating, cooling, etc. The operation phase is one of the most complicated phases because it depends on many factors that interact with each other, such as economic situation, price change, availability of energy resources, consumer behavior, etc.

In this study, all the data of energy consumed is given from the Palestinian Central Bureau of Statistics (Household Energy Survey: (January 2015)). Calculating the total cost of energy throughout a life cycle can be done by using Eq. (3).

$$FC = PV(1 + r)^t \quad (3)$$

where:

- FC future cost
- PV Present value
- r inflation rate
- t number of years.

## 2.3 Maintenance Phase

Major maintenance is assumed to occur every 30 years. The main activity is removing and installing plaster, paint, asphalt (water insulation), ceramic and tiles (if needed), and cleaning external wall envelope limestone.

The consumed energy is calculated using (BSRIA guide ICE 10/2011) data.

## 2.4 Demolition Phase

In this section, the volume of the primary building material must be calculated to estimate the quantity of (EE) and (CO<sub>2</sub> eq) for trucks and excavators. The cost of demolition in Palestine is 63.6 \$/m<sup>2</sup>.

## 2.5 General Information

The analysis was made for a typical building in Bethlehem city. The weather is hot in summer and cold in winter, temperature range from (−1 °C) to (+41 °C).

**Table 2** Specifications of building

Building area	160 m <sup>2</sup>
The life span	100 year
Number of floors	1
Internal floor height	2.75 m
External wall thickness	27 cm
Internal wall thickness	14 cm
Ground floor thickness	15cm
Top floor thickness	27 cm
Thermal insulation	No

## 2.6 Building Description

The building is a low-rise building (one floor) concrete structure. The total height of the building is 3.5 m. There is no thermal insulation on walls or on the floor. The ground floor is a reinforced concrete solid slab (10 cm thickness); on the other hand, the top floor is a reinforced concrete ribbed slab (27 cm) covered with asphalt (water insulation). External walls consist of limestone blocks, concrete and concrete blocks. All internal layers are covered with plaster and paint. summarize the building information (Table 2).

## 2.7 Construction Phase

Table 3 shows the construction elements, embodied energy, and greenhouse gas emissions.

The result of the construction phase shows that the ground floor has the largest EE and GHG Figs. 1 and 2, respectively.

## 2.8 Operation Phase

Buildings in Palestine generally use natural gas, wood, and electricity for heating. They mainly use natural gas for cooking.

This section also calculates the amount of energy used to deliver water to the building. Table 4 shows the average energy consumed by each family, the delivered amount of water, and their corresponding EE and GHG [4]. Formula (3) used to calculate the all-over energy cost through the life cycle Table 5. Figures 3, 4 and 5 shows the results.



**Table 3** Construction elements, embodied energy, and greenhouse gas emissions

Member	Materials	Quantity	Unit	EE (MJ/unit)	GHG (kg CO <sub>2</sub> eq / unit)	Total EE (MJ)	Total (kg CO <sub>2</sub> eq)	Total (kg CO <sub>2</sub> eq) element	Total EE (MJ) element
Foundation	Bitumen	42	kg	51	0.55	2142	23.1	12,347.48	94,279.50
	Reinforced concrete	39,375	kg	2.34	0.313	92,137.5	12,324.375		
Columns	Reinforced concrete	10,800	kg	2.34	0.313	25,272	3380.4	3820.04	33,305.76
	Plaster	1915.2	kg	1.8	0.13	3447.36	248.976		
	Paint	65.52	kg	70	2.91	4586.4	190.6632		
	Lime stone	31,250	kg	1.5	0.09	46,875	2812.5		
	Cement	11,604.6	kg	1.33	0.182	15,434.118	2112.0372		
Walls	Concrete	65,000	kg	0.78	0.113	50,700	7345	18,609.03	182,295.13
	Block	48,628.8	kg	0.67	0.078	32,581.296	3793.0464		
	Plaster	18,498.4	kg	1.8	0.13	33,297.12	2404.792		
	Paint	48.68	kg	70	2.91	3407.6	141.6588		
	Reinforced concrete	92,000	kg	2.34	0.313	215,280	28,796		
	Cement	13,440	kg	1.33	0.182	17,875.2	2446.08		
	Sand	28,800	kg	0.081	0.0051	2332.8	146.88		
Floor	Block	25,600	kg	0.83	0.107	21,248	2739.2	46,448.16	432,736.00
	Tiles and ceramic	17,600	kg	10	0.7	176,000	12,320		

(continued)

Table 3 (continued)

Member	Materials	Quantity	Unit	EE (MJ/unit)	GHG (kg CO <sub>2</sub> eq / unit)	Total EE (MJ)	Total (kg CO <sub>2</sub> eq)	Total (kg CO <sub>2</sub> eq) element	Total EE (MJ) element
Roof	Bitumen + Asphalt	1760	kg	51	0.55	89,760	968	19,983.20	232,688.00
	Block	25,600	kg	0.83	0.107	21,248	2739.2		
	Reinforced concrete	52,000	kg	2.34	0.313	121,680	16,276		
Others	Windows (aluminum)	60	unit	5470	0	328,200	0	37.00	473,856.00
	Doors (aluminum)	20	kg	7179	0	143,580	0		
	Doors (wood)	50	kg	11	0.74	550	37		
	Doors (steel)	70	kg	21.8	0	1526	0		
Total								101,244.91	1,449,160.39

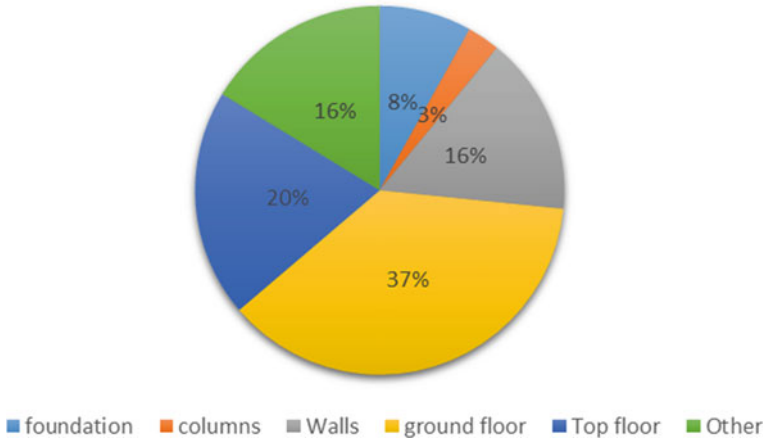


Fig. 1 Life-cycle embodied energy percentages

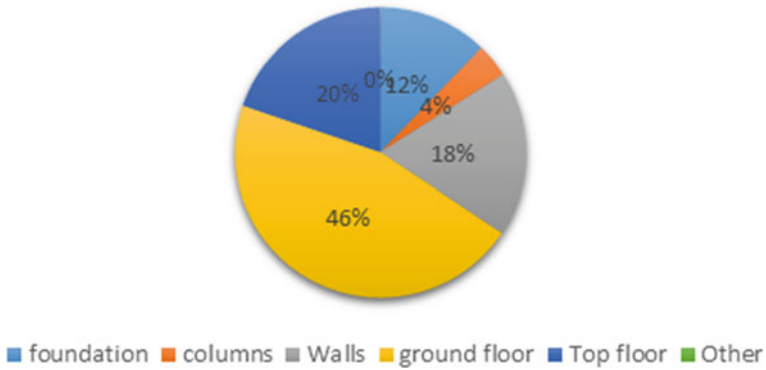


Fig. 2 Life-cycle greenhouse gas emissions percentages

Table 4 Average energy consumed and delivered amount of water

	Quantity	Unit	Energy eq (MJ)	GHG (kg CO <sub>2</sub> eq)
Natural gas (L)	264	L	2956.8	53.592
Electricity (kw/h)	6000	kw/h	21,600	2856
Wood	550	kg	8800	1045
Water	420,000	kg	4200	420
Kerosene (L)	252	L	9649.189	745.92
Total	47,205.989		5120.512	

**Table 5** Future cost over a life span

PV	9015.68
Inflation RATE	0.02867
Life span	100
FC	152,267.045

**Table 6** Shows the results of the maintenance phases

	First maintenance	Second maintenance
Energy until maintenance MJ	2,865,340.064	4,281,519.734
CO <sub>2</sub> eq until maintenance kg	254,860.2686	408,475.6286
Energy maintenance MJ	171,920.4038	171,920.4038
CO <sub>2</sub> eq maintenance kg	5097.205372	5097.205372
Total energy MJ	3,037,260.468	4,453,440.138
Total CO <sub>2</sub> eq kg	259,957.474	413,572.834

## 2.9 Maintenance Phase

Maintenance activities are assumed to occur every 30 years over the building life cycle (Table 6).

## 2.10 Demolition Phase

It's important to calculate the total volume of waste and machinery specification used for activities in the demolition phase. The total waste was 220 m<sup>3</sup> in this section. The truck's volume 20 m<sup>3</sup>, and the fuel consumption is 15 l of diesel per 100 km. The excavator consumes 26 l of diesel per hour (Table 7).

**Table 7** Shows the results of the demolition phases

Cost \$/m <sup>2</sup>	63.6
Total area of building	160
Total cost	10,182
Energy until demolition	6,341,680
CO <sub>2</sub> e until demolition	618,393
Energy demolition	12,683
Total energy	6,354,363
CO <sub>2</sub> e demolition	1677
Total CO <sub>2</sub> e	620,070

### 3 Results

Floors have the largest embodied energy and greenhouse gas emissions in the construction phase.

The operating phase is responsible for 73% of energy consumption and 82% of greenhouse gas emissions happen over the buildings' 100-year lifetime.

Electricity is the primary source of energy used in Palestinian buildings. Furthermore, it's the latest producer of GHG.

The embodied energy and GHG for each m<sup>2</sup> are considered high valued in contrast to energy-efficient buildings.

The total cost of the building is 131,523 \$.

The embodied energy is about 40 GJ/m<sup>2</sup>, and greenhouse gas emissions equal 3.9 t/m<sup>2</sup>. over the life-cycle.

The construction and operating phases are responsible for 84% of the total cost (Figs. 3, 4, and 5; Table 8).

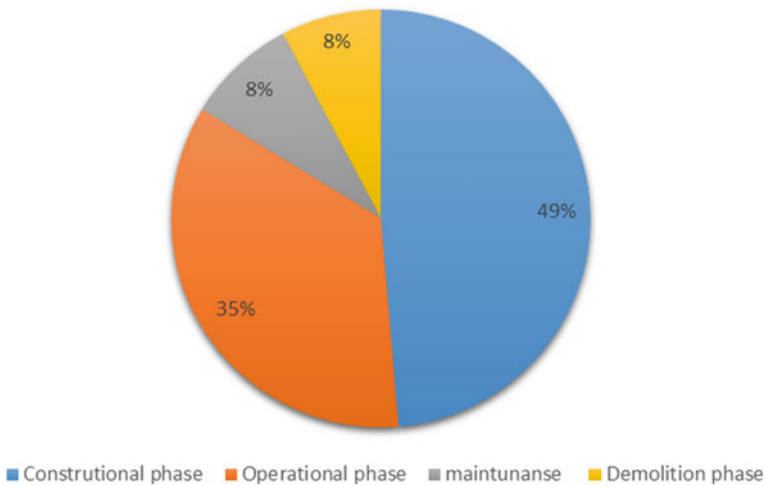


**Fig. 3** Cost percentage of each phase

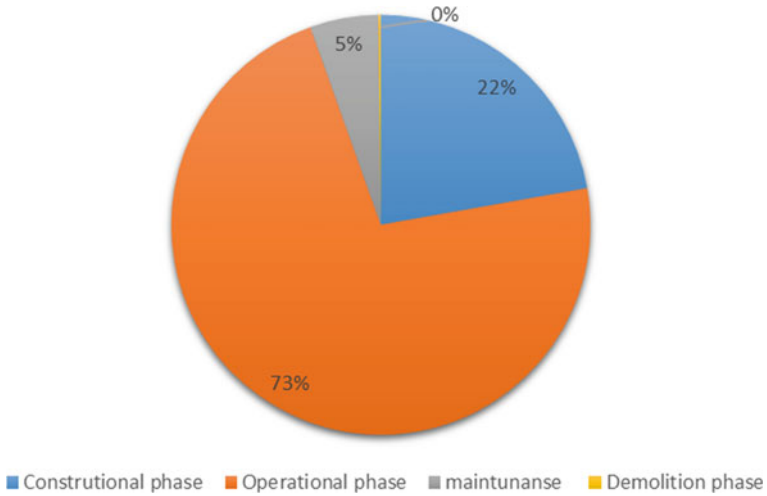


Fig. 4 EE percentage of each phase

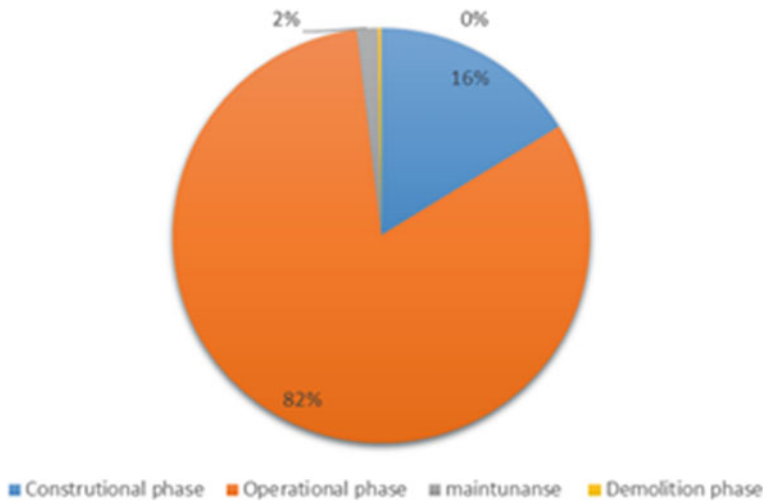


Fig. 5 GHG percentage of each phase

Table 8 Shows the final results

	EE (MJ)	CO <sub>2</sub> (kg)	Cost \$
Constructional phase	1,449,160.394	101,244.9086	64,000
Operational phase	4,720,598.9	512,051.2	46,142
Maintenance	343,840.8077	10,194.41074	11,200
Demolition phase	12,683.3594	1677.021965	10,182
Total	6,526,283.461	625,167.5413	131,523
For each m <sup>2</sup>	40,789.27163	3907.297133	822

## 4 Conclusion

The main reason for high energy consumption and the Greenhouse gas in buildings is the low thermal resistance value of the building envelope (due to lack of thermal insulation materials). Improving it provides a high potential for energy-saving and reduces air pollution. In addition, it is necessary to reduce dependence on electrical energy generated by burning fossil fuels and find alternative solutions to generate electricity using renewable energy.

**Acknowledgments** This research was supported by Project # 3.1.7.1 within the 2021–2023 Plan of Fundamental Research of the Russian Academy of Architecture and Civil Engineering and Ministry of Civil Engineering and Public Utilities of the Russian Federation. The experimental studies have been carried out using the facilities of the Collective Research Center named after Professor Yu. M. Borisov, Voronezh State Technical University, which is partly supported by the Ministry of Science and Education of the Russian Federation, Project No. 075-15-2021-662.

## References

1. Palestinian Central Bureau of Statistics (2015) Household energy survey: main results. Ramallah—Palestine
2. Palestinian Central Bureau of Statistics. <https://www.pcbs.gov.ps/>
3. Citherlet S, Defaux T (2007) Energy and environmental comparison of three variants of a family house during its whole life span. *Build Environ* 42(2):591–598. <https://doi.org/10.1016/j.buildenv.2005.09.025>
4. Prof Hammond G, Jones C (2011) In: Lowrie F, Tse P (eds) Embodied carbon—the inventory of carbon and energy (ICE) (BG 10/2011). University of Bath with BSRIA, iCAT. ISBN-13: 9780860227038
5. Treloar GJ, Fay R, Ilozor B, Love P (2001) Building materials selection: greenhouse strategies for built facilities. *Facilities* 19(3/4):139–150. <https://doi.org/10.1108/02632770110381694>
6. Huberman N, Pearl MD (2008) A life cycle energy analysis of building materials in the Negev desert. *Energy Build* 40(5):837–8. <https://doi.org/10.1016/j.enbuild.2007.06.002>
7. Bromilow FJ, Pawsey MR (2003) Life cycle cost of university buildings. *Constr Manag Econ* 5(4):3–22. <https://doi.org/10.1080/01446193.1987.10462089>
8. Peuportier BLP (2001) Life cycle assessment applied to the comparative evaluation of single family houses in the French context. *Energy Build* 33(5):443–450. [https://doi.org/10.1016/S0378-7788\(00\)00101-8](https://doi.org/10.1016/S0378-7788(00)00101-8)
9. Stephan A, Stephan L (2014) Reducing the total life cycle energy demand of recent residential buildings in Lebanon. *Energy* 74:618–637. <https://doi.org/10.1016/j.energy.2014.07.028>
10. Stephan A, Crawford RH, Myttenaere K (2012) Towards a comprehensive life cycle energy analysis framework for residential buildings. *Energy Build* 55:592–600. <https://doi.org/10.1016/j.enbuild.2012.09.008>

# Failure Mechanism of Reinforced Concrete Frames Under Accidental Impacts



Pavel Korenkov  and Sergey Fedorov 

**Abstract** The collapse of building objects during design, construction and operation is present throughout modern civilization. This article studied in detail the features of the exhaustion of the bearing capacity and the nature of the destruction of four series of experimental studies of monolithic reinforced concrete frame structural systems, which differ in the nature of the destruction of the sections (brittle or plastic), as well as the use of such methods of protection against progressive collapse, such as prestressed elements and indirect reinforcement. As the initial prerequisites for the calculation analysis, a diagrammatic calculation method was used, using the actual static-dynamic parameters of the “strain stress” diagrams for reinforcement and concrete, adopted in the current standards for the design of reinforced concrete structures. When assessing the nature of the destruction of the supporting sections (localization of cracks and the depth of their development), a satisfactory convergence with the accepted model of static-dynamic deformation of structural materials adopted for the calculation analysis was established. The considered and experimentally tested technical solutions make it possible to implement such stiffness characteristics of the design scheme, in which energy dissipation occurs without disturbing the geometric variability of the building’s supporting system.

**Keywords** Progressive collapse · Nonlinear deformation model diagram method · Reinforced concrete accidental impact special limiting state

## 1 Introduction

In recent years, natural, man-made and even terrorist impacts have become more frequent all over the world. Until recently, such special impacts on buildings and structures were not taken into account by design standards, however, these impacts

---

P. Korenkov (✉) · S. Fedorov

Moscow State University of Civil Engineering, (National Research University), 26, Yaroslavskoe Shosse, Moscow 129337, Russian Federation

e-mail: [korenkovpa@mgsu.ru](mailto:korenkovpa@mgsu.ru)

© The Author(s), under exclusive license to Springer Nature Switzerland AG 2024

333

N. Vatin et al. (eds.), *Modern Problems in Construction*,

Lecture Notes in Civil Engineering 372,

[https://doi.org/10.1007/978-3-031-36723-6\\_32](https://doi.org/10.1007/978-3-031-36723-6_32)



often led to damage to load-bearing structures, sometimes caused the collapse of individual parts, and in some cases the entire structure [1–4].

In many countries of the world [5, 6], including Russia [7], in order to improve the mechanical safety of buildings and structures, preserve the life and health of the people in them, new generation regulatory documents for the protection of buildings have been developed and introduced into design practice and structures from progressive collapse under such impacts.

In scientific publications, separate problems related to this problem have been considered and solved, a number of new features of the stress–strain state of structures of buildings and structures under such influences, which cause a special limit state in structures, have been studied [8–13].

Considering the most common methods of experimental studies of the resistance of structural systems to progressive collapse, in the form of quasi-static tests on individual substructures, separated by the decomposition method from the building frame, described in the works of Yu and Tan [14], Kang et al. [15], Forquin and Chen [16], Han et al. [17], we can note the use of hydraulic jacks that transfer force to the structure at a controlled speed of movement of the moving part of the loader. device, it can be noted that this method contradicts the dynamic nature of the processes under study. The method of modeling loads on experimental structures by means of a mechanical lever system, described in [18], more strictly corresponds to the actual nature of the work when the elements of the carrier system are locally switched off from work.

The purpose of this work is a comprehensive analysis of the mechanisms of destruction and exhaustion of the bearing capacity according to specially planned and conducted physical experiments of reinforced concrete frame-rod frames of buildings with different types of destruction (plastic and brittle), as well as design features, in the form of prestressed elements and indirect reinforcement of nodal compounds under the specified special effects.

## 2 Materials and Methods

For a more detailed study of the features of the exhaustion of the bearing capacity and the nature of the destruction of buildings with a monolithic reinforced concrete frame, we will consider four series of experimental studies conducted jointly by scientists from the Southwestern State University, the National Research Moscow State Civil Engineering University on the basis of the V.I. Vernadsky Crimean Federal University.

The key feature of the experimental studies performed is the completely identical simulation of the operation of the carrier system in the event of an emergency impact due to the shutdown of the first floor column. All work on transferring the load to the prototype is performed by a mechanical lever system of the gravitational type, without reducing the load parameters, allowing you to fully evaluate the resulting

dynamic impact in a time frame similar to real objects [18, 19]. A general view of the test setup is shown in Fig. 1.

As examples, consider several types of monolithic reinforced concrete frame-rod structural systems:

- a system in which the destruction of elements occurs along the reinforcement, i.e.  $\xi < \xi_R$ , concrete class B15, reinforcement class A400C [20], Fig. 2a
- a system in which the destruction of elements occurs along the concrete, i.e.  $\xi > \xi_R$ , concrete class B15, reinforcement class A400C [20–22], Fig. 2a
- bearing system, using indirect reinforcement in the supporting sections of the crossbars, class B15 concrete, class A240C reinforcement, indirect reinforcement with meshes B500 [23], Fig. 2c
- load-bearing system, using a prestressed crossbar at the second floor level, class B40 concrete, class A600C reinforcement, structural reinforcement B500C [24], Fig. 2d

All large-scale prototypes of two-span three-story frames are made of monolithic reinforced concrete of different classes from B15 to B40, with different reinforcement classes A240, A400, A500, A600. The reinforcement parameters of the crossbar section for each of the series of experimental structures are shown in Fig. 2.

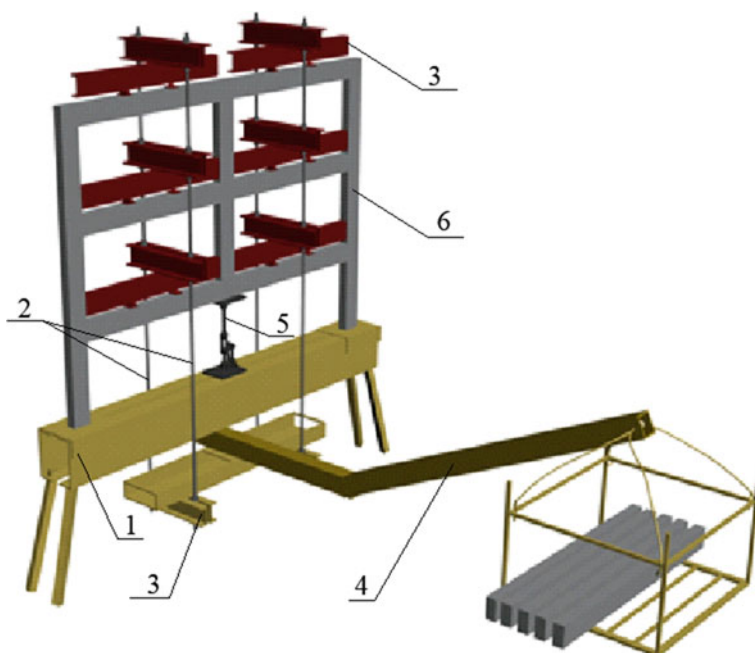


**Fig. 1** General view of the installation during experimental studies: 1—power frame; 2—strands; 3—distributive beam; 4—lever; 5—switching off connection device, 6—experimental design of reinforced concrete frame

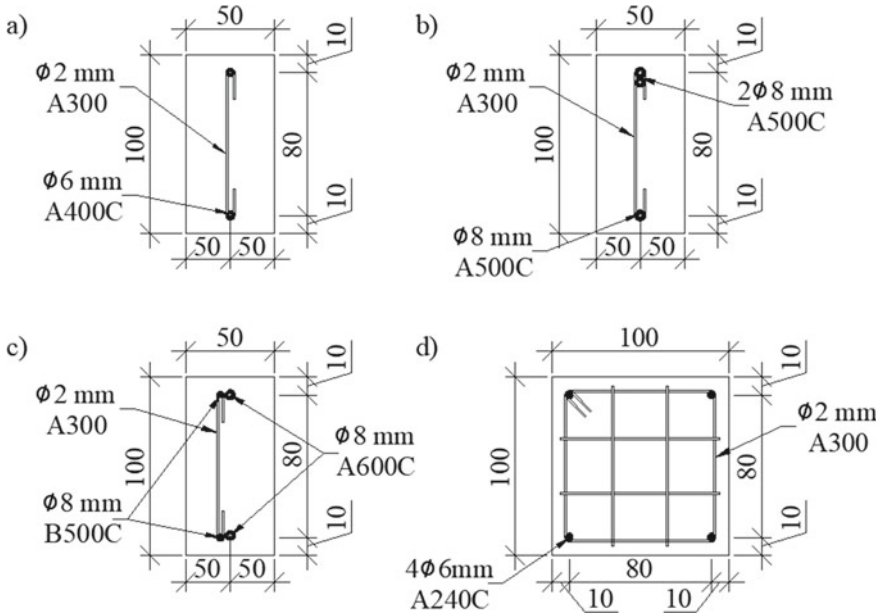


**Fig. 2** Reinforcement of sections of crossbars for the first (a), second (b), third (c) and fourth (d) series of experimental structures

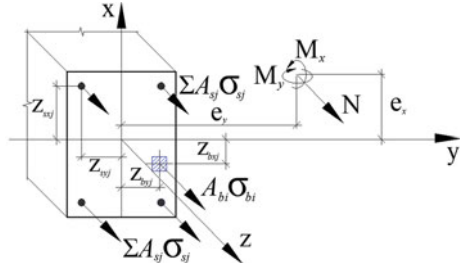
To estimate the parameters of the stress state of the considered sections of reinforced concrete elements, we use the diagram method of calculation. The transition from the diagram of stresses in concrete to generalized internal forces is determined using the procedure of numerical integration of stresses over a normal section. To do this, the normal section is conditionally divided into small sections: with oblique eccentric compression (tension) and oblique bending—along the height and width of the section; in case of eccentric compression (tension) and bending in the plane of the axis of symmetry of the cross section of the element—only along the height of the section. Stresses within small sections are assumed to be uniformly distributed (averaged).

When calculating the elements using the deformation model, we will accept:

- values of the compressive longitudinal force, as well as compressive stresses and deformations of shortening of concrete and reinforcement with a “minus” sign;
- values of the tensile longitudinal force, as well as tensile stresses and deformations of elongation of concrete and reinforcement with a plus sign.

The signs of the coordinates of the centers of gravity of the reinforcing bars and the selected sections of concrete, as well as the points of application of the longitudinal force are taken in accordance with the assigned XOY coordinate system. In the general case, the origin of this system is located at an arbitrary location within the cross section of the element (Fig. 3).

**Fig. 3** Calculation scheme of the normal section of a reinforced concrete element



When calculating normal sections for strength, in the general case, use:

- equations of balance of external forces and internal forces in the normal section of the element:

$$M_x = \sum_i \sigma_{bi} \cdot A_{bi} \cdot Z_{bxi} + \sum_j \sigma_{sj} \cdot A_{sj} \cdot Z_{sxj} \tag{1}$$

$$M_y = \sum_i \sigma_{bi} \cdot A_{bi} \cdot Z_{byi} + \sum_j \sigma_{sj} \cdot A_{sj} \cdot Z_{syj} \tag{2}$$

$$N = \sum_i \sigma_{bi} \cdot A_{bi} + \sum_j \sigma_{sj} \cdot A_{sj} \tag{3}$$

- equations that determine the distribution of deformations over the section of the element:

$$\epsilon_{bi} = \epsilon_0 + \frac{1}{r_x} \cdot Z_{bxi} + \frac{1}{r_y} \cdot Z_{byi} \tag{4}$$

$$\epsilon_{bi} = \epsilon_0 + \frac{1}{r_x} \cdot Z_{bxj} + \frac{1}{r_y} \cdot Z_{byj} \tag{5}$$

- dependencies linking stresses and relative deformations of concrete and reinforcement:

$$\sigma_{bi} = E_b \cdot \nu_{bi} \cdot \epsilon_{bi} \tag{6}$$

$$\sigma_{sj} = E_{sj} \cdot \nu_{sj} \cdot \epsilon_{sj} \tag{7}$$

where  $M_x, M_y$ —bending moments from an external load relative to the coordinate axes selected and located within the cross section of the element (respectively acting in the XOZ and YOZ planes or parallel to them), determined by the formulas:

$$M_x = M_{xd} + N \cdot e_x \quad (8)$$

$$M_y = M_{yd} + N \cdot e_y \quad (9)$$

here  $M_{xd}$ ,  $M_{yd}$ —bending moments in the respective planes from an external load, determined from the static analysis of the structure;

$N$ —longitudinal force from external load;

$e_x$ ,  $e_y$ —distances from the point of application of the longitudinal force to the respective selected axes;

$A_{bi}$ ,  $Z_{bxi}$ ,  $Z_{byi}$ ,  $\sigma_{bi}$ —area, coordinates of the center of gravity of the  $i$ -th section of concrete and stress at the level of its center of gravity;

$A_{sj}$ ,  $Z_{sxj}$ ,  $Z_{syj}$ ,  $\sigma_{sj}$ —area, coordinates of the center of gravity of the  $j$ -th rebar and stress in it;

$\varepsilon_0$ —relative deformation of the fiber located at the intersection of the selected axes;

$\frac{1}{r_x}$ ,  $\frac{1}{r_y}$ —curvature of the longitudinal axis in the considered cross section of the element in the planes of action of bending moments  $M_x$  и  $M_y$ ;

$E_b$ —initial elastic modulus of concrete;

$E_{sj}$ —elastic modulus of the  $j$ -th rebar;

$\nu_{bi}$ —coefficient of elasticity of concrete of the  $i$ -th section;

$\nu_{sj}$ —coefficient of elasticity of the  $j$ -th rebar.

Coefficient values  $\nu_{bi}$  и  $\nu_{sj}$  are taken according to the corresponding diagrams of the state of concrete and reinforcement.

Coefficient values  $\nu_{bi}$  и  $\nu_{sj}$  is defined as the ratio of stress and strain values for the considered points of the corresponding state diagrams of concrete and reinforcement, taken in the calculation, divided by the modulus of elasticity of concrete and reinforcement.

$$\nu_{bi} = \frac{\sigma_{bi}}{E_b \cdot \varepsilon_{bi}} \quad (10)$$

$$\nu_{sj} = \frac{\sigma_{sj}}{E_{sj} \cdot \varepsilon_{sj}} \quad (11)$$

To assess the parameters of the force resistance, static-dynamic diagrams of the deformation of structural materials were used, taking into account the time of dynamic additional loading and the level of the stress state at the time of the emergency impact [25].

### 3 Results and Discussion

In the first series of prototypes, we will consider the most loaded section of the crossbar of the first floor. The first stage of the stress–strain state of a reinforced concrete element ends at the level of stresses in the reinforcement equal to 6%; in concrete, the stresses do not reach 20% of the compressive strength of concrete.

The next transition point is the formation of the first crack at  $M_{crc} = 0.3M_{ult}$ . When comparing the obtained results with the experiment, one can see a similar pattern of destruction. (Fig. 4). In this case, the depth of the crack reaches 60 mm. A special limit state occurs when the reinforcement reaches the yield strength and the stress level in concrete is about 60% of the compressive strength of concrete. The depth of the original crack is increased by 30%.

In the second series of prototypes, the opening of the first crack, 10 mm high, occurs at  $M_{crc} = 0.13M_{ult}$ . The bearing capacity is exhausted when concrete reaches its compressive strength.

In the study of frames with indirect reinforcement of the supporting sections of the crossbars, the cracking threshold occurs at  $M_{crc} = 0.45M_{ult}$ , which is explained by the increased tensile strength of concrete when creating a three-dimensional stress state with meshes of indirect reinforcement. After the formation of the first crack, by analogy with the first series of prototypes, with the only difference that the stress level in the reinforcement is at the level of 8% (10% in the first series) of the yield strength, and the stress in the compressed reinforcement is 8% of the yield strength. In the first series, this parameter did not exceed 5%. The destruction occurred along the reinforcement, at a stress level in concrete of 45% of the compressive strength of concrete.

When considering the stress state of the sections of frames with a prestressed lower crossbar, an increased crack resistance was established. The cracking moment is  $M_{crc} = 0.55M_{ult}$ . The destruction occurred due to the achievement of the yield strength by the reinforcement at a stress level in concrete not exceeding 70% of the compressive strength.

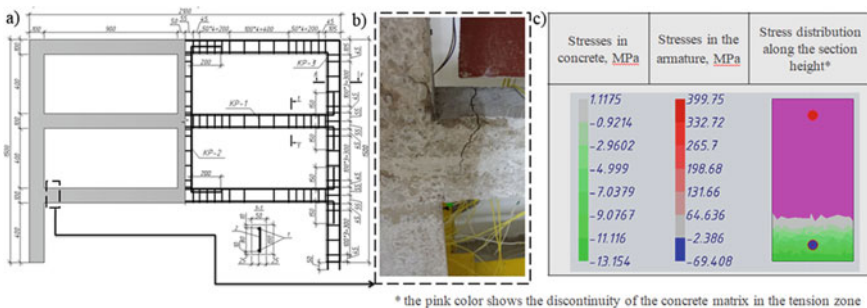
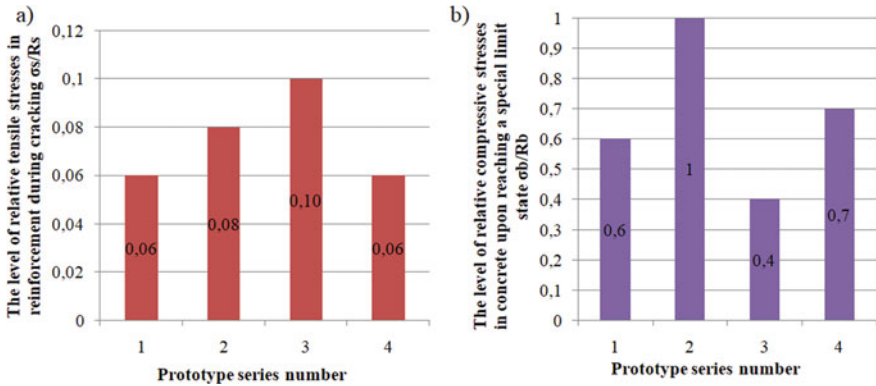


Fig. 4 Structural scheme 1 of a series of prototypes (a), the nature of the destruction (b) and the stress state before the destruction of the supporting section of the crossbar



**Fig. 5** Level of stress state in reinforcement at the time of cracking (a) and concrete upon reaching a special limit state (b)

Based on the calculations performed, in comparison with experimental studies, it was established that the level of cracking is of a different nature due to the design features of each series of prototypes and ranges from 13 to 55%. The stress level in the reinforcement does not exceed 10%. In all prototypes, except for series 2, the plastic nature of destruction was realized, and a non-critical (from 60 to 70%) stress level in concrete was revealed. A comparative analysis of the stress state level in reinforcement and concrete is shown in Fig. 5.

Assessing the pattern of destruction of the sections of the elements, we can conclude that the stresses in them have reached the conditional yield strength, but significant deflections are not observed in the case. The pre-stress played the role of a damper, acting as a vibration damper, and all the energy was absorbed by the opening of cracks and their subsequent closure due to a decrease in the effect of dynamic additional loads after an emergency impact.

## 4 Conclusion

Analyzing the nature of the destruction of the support sections (localization of cracks and the depth of their development), one can see a satisfactory convergence with the accepted model of static-dynamic deformation of structural materials adopted for the calculation analysis.

The impact of design features that minimize damage and sometimes prevent progressive collapse is very significant. The solutions considered and tested experimentally make it possible to implement such stiffness characteristics of the design scheme, in which energy dissipation occurs without violation of geometric variability and by relatively simple means, without resorting to significant labor and material

costs to ensure the required level of structural safety and survivability of buildings and structures made of monolithic reinforced concrete.

**Acknowledgements** The research was carried out with the financial support of a grant from the President of the Russian Federation for state support of young Russian scientists—candidates of science (Contract No. 075-15-2021-312/2)

## References

1. Shakib H, Zakersalehi M, Jahangiri V, Zamanian R (2020) Evaluation of Plasco Building fire-induced progressive collapse. *Structures* 28:205–224. <https://doi.org/10.1016/j.istruc.2020.08.058>
2. Elsanadedy H, Sezen H, Abbas H, Almusallam T, Al-Salloum Y (2022) Progressive collapse risk of steel framed building considering column buckling. *Eng Sci Technol Int J* 35:101193. <https://doi.org/10.1016/j.jestch.2022.101193>
3. Lu JX, Wu H, Fang Q (2022) Progressive collapse of Murrah federal building: revisited. *J Build Eng* 57:104939. <https://doi.org/10.1016/j.jobe.2022.104939>
4. Hua Y, Chun Q (2022) Influence of Puzuo on progressive collapse behavior of ancient southern Chinese timber buildings built in the Song and Yuan dynasties: experimental research. *Eng Fail Anal* 137:106405. <https://doi.org/10.1016/j.engfailanal.2022.106405>
5. UFC 4-023-03. Design of buildings to resist progressive collapse. <https://www.wbdg.org/ffc/dod/unified-facilities-criteria-ufc/ufc-4-023-03>. Last accessed 2022/09/01
6. GSA (2016) Alternate path analysis and design guidelines for progressive collapse resistance. <https://www.gsa.gov/real-estate/design-excellence-program/engineering-and-architecture/security-engineering/2016-alternate-path-analysis-design-guidelines-for-progressive-collapse-resistance>. Last accessed 2022/09/01
7. Building Code of RF SP 385.132580.2018 Protection of buildings and structures against progressive collapse. Design code. Basic statements. <https://docs.cntd.ru/document/551394640>. Last accessed 2022/09/01
8. Wang H, Zhang A, Li Y, Yan W (2014) A review on progressive collapse of building structures. *Open Civ Eng J* 8(1):183–192. <https://doi.org/10.2174/1874149501408010183Hh>
9. Adam JM, Parisi F, Sagaseta J, Lu X (2018) Research and practice on progressive collapse and robustness of building structures in the 21st century. *Eng Struct* 173:122–149. <https://doi.org/10.1016/j.engstruct.2018.06.082>
10. Abdelwahed B (2019) A review on building progressive collapse, survey and discussion. *Case Studies in Construction Materials* 11:e00264. <https://doi.org/10.1016/j.cscm.2019.e00264>
11. Kiakojouri F, De Biagi V, Chiaia B, Sheidaii MR (2019) Progressive collapse of framed building structures: current knowledge and future prospects. *Eng Struct* 206:110061. <https://doi.org/10.1016/j.engstruct.2019.110061>
12. Savin SYu, Kolchunov VI (2021) Dynamic behavior of reinforced concrete column under accidental impact. *Int J Comput Civ Struct Eng* 17(3):120–131. <https://doi.org/10.22337/2587-9618-2021-17-3-120-131>
13. Savin S (2022) Criteria for special limiting state of eccentrically compressed members of RC frames. In: *Lecture notes in civil engineering*, vol 197, pp 135–146. [https://doi.org/10.1007/978-981-16-6593-6\\_15](https://doi.org/10.1007/978-981-16-6593-6_15)
14. Yu J, Tan KH (2013) Structural behavior of RC Beam-column subassemblages under a middle column removal scenario. *J Struct Eng* 139(2):233–250. [https://doi.org/10.1061/\(ASCE\)ST.1943-541X.0000658](https://doi.org/10.1061/(ASCE)ST.1943-541X.0000658)
15. Kang SB, Tan KH, Yang EH (2015) Progressive collapse resistance of precast beam-column sub-assemblages with engineered cementitious composites. *Eng Struct* 98:186–200. <https://doi.org/10.1016/j.engstruct.2015.04.034>



16. Forquin P, Chen W (2017) An experimental investigation of the progressive collapse resistance of beam-column RC sub-assemblages. *Constr Build Mater* 152:1068–1084. <https://doi.org/10.1016/j.conbuildmat.2017.05.179>
17. Han Q, Li X, Liu M, Spencer BF (2019) Experimental investigation of beam-column joints with cast steel stiffeners for progressive collapse prevention. *J Struct Eng* 145(5):04019020. [https://doi.org/10.1061/\(ASCE\)ST.1943-541X.0002301](https://doi.org/10.1061/(ASCE)ST.1943-541X.0002301)
18. Korenkov P, Chemodurov V, Korenkova O, Manaenkov I (2020) Determination of the scale factor in the physical modeling of reinforced concrete structures exposed to emergency loads. In: IOP conference series: materials science and engineering, vol 23, Construction—the formation of living environment, Hanoi, p 052053. <https://doi.org/10.1088/1757-899X/869/5/052053>
19. Chemodurov VT, Korenkov PA, Leonenko YS, Korenkova OO (2020) Physical modeling of reinforced concrete structures exposed to emergency loads. *J Phys Conf Ser* 2019, Institute of Physics Publishing, Moscow 012061. <https://doi.org/10.1088/1742-6596/1425/1/012061>
20. Fedorova NV, Korenkov PA (2021) Static and dynamic deformation of monolithic reinforced concrete frame building in ultimate limit and beyond limits states. *Build Reconstr* 6(68):90–100. <https://doi.org/10.33979/2073-7416-2021-95-3-76-108>
21. Fedorova NV, Ngoc VT (2020) Deformation and failure of monolithic reinforced concrete frames under special actions. *J Phys Conference Ser*, Institute of Physics Publishing, Moscow 012033. <https://doi.org/10.1088/1742-6596/1425/1/012033>
22. Kolcunov VI, Tuyen VN, Korenkov PA (2020) Deformation and failure of a monolithic reinforced concrete frame under accidental actions. In: IOP conference series: materials science and engineering, p 032037. <https://doi.org/10.1088/1757-899X/753/3/032037>
23. Kolchunov VI, Korenkov PA, Quoc PD (2021) A special limit state of reinforced concrete frames with laterally reinforced nodes in the case of emergency impacts. *Vestnik MGSU* 16(11):1462–1472. <https://doi.org/10.22227/19970935.2021.11.1462-1472>
24. Kolchunov V, Iliushchenko T, Savin S (2022) Deformation and failure of prestressed reinforced concrete frames in ultimate states. In: *Lecture notes in civil engineering*, vol 182, pp 41–53. [https://doi.org/10.1007/978-3-030-85236-8\\_4](https://doi.org/10.1007/978-3-030-85236-8_4)
25. Fedorova N, Medyankin M, Fedorov S, Savin S (2022) Experimental and theoretical studies of the concrete static-dynamic stress–strain curves. In: *Lecture notes in civil engineering*, vol 170, pp 151–161. [https://doi.org/10.1007/978-3-030-79983-0\\_14](https://doi.org/10.1007/978-3-030-79983-0_14)

# Experimental Study of the Survivability of Monolithic Reinforced Concrete Frames



Vitaly Kolchunov  and Olesya Bushova 

**Abstract** To increase the protection of monolithic reinforced concrete frames during destruction along inclined sections, the article offers a variant of a technical solution for cross-reinforcement of crossbars in such structures. The results of tests of monolithic reinforced concrete frames with a special impact in the form of a sudden hypothetical removal from the work of the extreme column are presented and experimental parameters of deformation, cracking and destruction of such structures in extreme conditions are given. The results obtained have shown the effectiveness of using the proposed variant of cross reinforcement of crossbars of monolithic frames to increase their survivability.

**Keywords** Reinforced concrete frame · Survivability · Progressive collapse · Reinforcement · Inclined rods

## 1 Introduction

With the ever-increasing volume of natural, man-made and terrorist impacts on buildings and structures, their local and even progressive collapses are possible. Thus, on the basis of new theoretical and experimental studies in domestic [1–9] and foreign [10–15] scientific publications, various methods of protecting reinforced concrete frames of buildings from progressive collapse under special influences are proposed. For example, it is proposed to increase the cross-sections of structural elements of load-bearing frames of buildings [1, 16], to install continuous double upper and lower working reinforcement in the crossbars [1, 16], to install indirect reinforcement [4],

---

V. Kolchunov · O. Bushova (✉)  
National Research Moscow State University of Civil Engineering, 26, Yaroslavskoe shosse,  
129337 Moscow, Russia  
e-mail: [bushova96@mail.ru](mailto:bushova96@mail.ru)

V. Kolchunov  
Southwest State University, 50 let Oktyabrya street, 94, Kursk 305040, Russia

to install prestressed reinforcement [5, 17], to ensure reliable anchoring of the reinforcement at the junctions of the crossbars with columns [18] and other constructive solutions [19]. However, the issues related to ensuring the protection of reinforced concrete frames of buildings from progressive collapse along inclined sections for the considered structural systems remain practically unexplored. At the same time, a number of recent studies have shown that, in relation to reinforced concrete frames of multi-storey buildings, such destruction along inclined cross-sections of crossbars can be fragile and, accordingly, become more dangerous [20]. According to the results of the analysis of the stress–strain state of traditionally reinforced crossbar structures, it is shown that their reinforcement in cases of special emergency impacts is ineffective, and such solutions can lead to disproportionate failures of buildings and structures. It follows from this that the study of force deformation and the development of ways to strengthen the load-bearing structures of reinforced concrete frames of multi-storey buildings to increase their survivability is an urgent task.

Therefore, the aim of the work was an experimental study of the survivability of the support zones of the crossbars of reinforced concrete frames of multi-storey buildings. In accordance with this goal, the following tasks were formulated and solved:

- The scheme of reinforcement of the supporting zones of the crossbars of the reinforced concrete frame is proposed, which increases their force resistance in case of sudden changes in force flows;
- An algorithm has been developed and experimental studies of experimental structures of reinforced concrete frames with accepted reinforcement schemes have been carried out under special influence in the form of sudden removal of the extreme supporting column of the first floor;
- An analysis of experimental studies has been carried out.

## 2 Materials and Methods

The picture of the stress–strain state, as well as the picture of the destruction of the structural system as a whole, is affected by sudden changes in the structure of the structure under beyond-design influences [17, 21]. That is, when the connection is turned off in the constructive system, the degree of static indeterminability changes and, accordingly, the force flows between the structural elements are redistributed. At the same time, it is possible to change the sign of the forces, in this case, for example, if the support area of the bolt is reinforced with inclined rods of one direction, then when the sign of the transverse force changes, this reinforcement does not work. Consequently, the traditional scheme of reinforcing the crossbars of reinforced concrete frames with inclined rods of the same direction under special influences does not provide criteria for limiting states.

The paper proposes an alternative scheme of reinforcement of the support zones of the crossbars of reinforced concrete frames of multi-storey buildings, which allows, when changing the force flows caused by a structural change in the system, to ensure

their protection from progressive collapse. To do this, it is proposed to perform transverse reinforcement with inclined rods in two mutually orthogonal directions.

As part of experimental studies, two samples were manufactured and tested: one with the traditional option of reinforcing crossbars, and the second with the proposed option.

The prototypes were made in the form of monolithic two-span three-storey reinforced concrete frames made of concrete B30 with a cross section of  $50 \times 100$  mm. The reinforcement is calculated according to [22] and is assumed to be symmetrical, the working reinforcement is made of  $\phi 8A500C$ , the transverse reinforcement and inclined rods of the crossbars are  $\phi 2B500$ . Cross rods with a pitch of 35 mm were installed in the supporting sections. Such a technical solution made it possible to ensure the perception of force flows changing in the frame with a special impact caused by the sudden removal of one of the supporting columns, and as a result, to increase the resistance of the frame to progressive collapse.

The prototypes were alternately tested for out-of-design effects. The experimental study of the samples took place in two stages:

1. At the first stage, the specified operational load was applied (primary calculation scheme);
2. At the second stage, the column-stand was suddenly removed (the forbidden effect was realized).

Prior to the design load, the frame was loaded using a lever-suspension system (Fig. 1) with concentrated forces located symmetrically at a distance of 150 mm from the supports. The out-of-design impact was realized by the sudden removal of the extreme column of the first floor. For this purpose, a special collapsible mechanism was used, which made it possible to instantly turn off the rack installed instead of the missing column.

The deformations and displacements were evaluated using the IC10 hour-type indicators with a division price of 0.01 mm, 6-PAO deflectors (Fig. 2) and strain gauges (strain gauges with a base of 10 mm were glued to the reinforcement rods, and on the side surfaces of the concrete frame sample—with a base of 50 mm).

### 3 Results and Discussion

According to the results of experimental studies, characteristic patterns of cracking were obtained and graphs of the dependences of the deflection change on the load before and after the frame rack was turned off were constructed.

From the analysis of these data, it can be seen that before the load-bearing column is turned off, the deformations and deflections of the frames are almost the same and are less than 1 mm (fragments C and D Figs. 3 and 4). At the same time, the maximum crack opening width was 0.25 mm in the area of the crossbar interface with the column. A crack opened at the XIV stage of loading, before the implementation of the project impact.



**Fig. 1** Test installation: 1—Prototype, 2—lever-suspension system, 3—design load, 4—distribution beams and strands, 5—strain gauge station, 6—collapsible mechanism

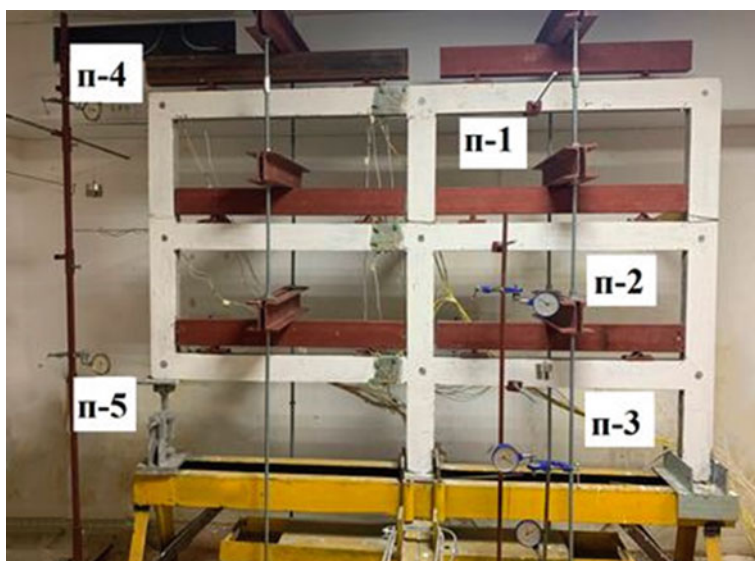


**Fig. 2** The layout of the deflection meters

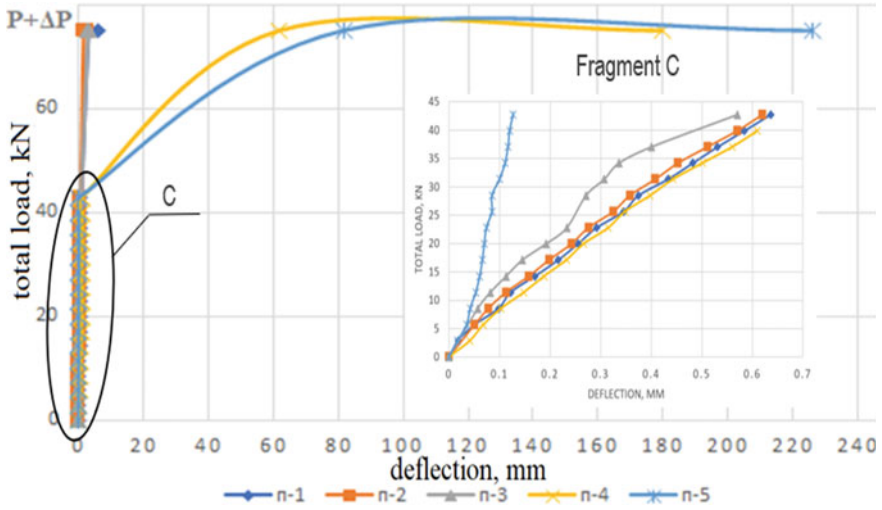


Fig. 3 Dependence load-deflection of the frame reinforced with rods of the same direction

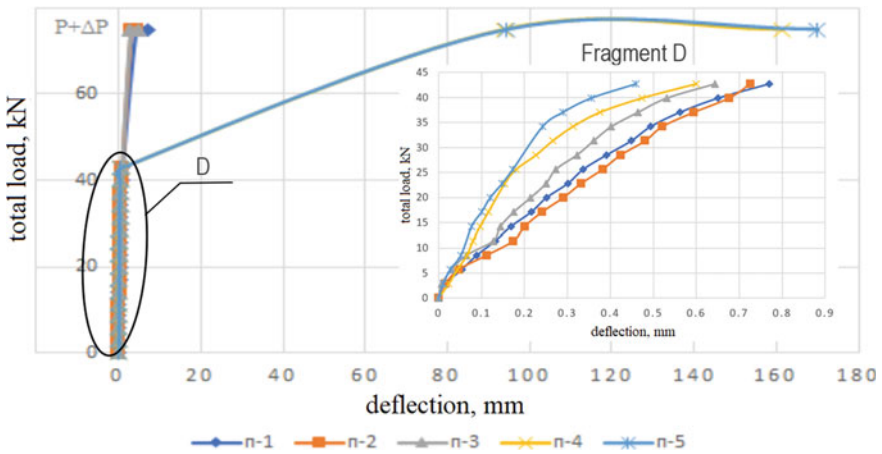


Fig. 4 Dependence load-deflection of the frame reinforced with double-sided inclined rods

After the application of a sudden emergency impact, the deflections of frames reinforced with inclined rods installed in two mutually orthogonal directions are 30% lower than those of frames reinforced in the traditional way (Figs. 3 and 4). They are 240 mm (relative deflection was 1/4) with traditional reinforcement and 180 mm (relative deflection is 1/6) with the proposed version.





The proposed reinforcement of the crossbars of monolithic frames can be considered as one of the ways to protect reinforced concrete frames of buildings from progressive collapse.

## References

1. Almazov VO, Khoi KZ (2013) Dynamics of progressive destruction of monolithic multi-storey frames. DIA, Moscow, p 128
2. Yu S, Fialkoa OV, Kabantsevb AV (2021) Perelmuter Elasto-plastic progressive collapse analysis based on the integration of the equations of motion. *Mag Civ Eng* 102(2). (Article no. 10214)
3. Kodysh EN (2016) Protection of multi-storey buildings from progressive collapse/Kodysh EN, Trekin NN, Chesnokov DA. *Ind Civ Constr* (6):8–13
4. Fedorova NV, Fan DG, Nguyen TC (2020) Experimental studies of the survivability of reinforced concrete frames with crossbars reinforced with indirect reinforcement. *Constr Reconstr* (1):92–100
5. Ilyushchenko TA, Kolchunov VI, Fedorov SS (2021) Crack resistance of prestressed reinforced concrete frame-rod structures under special influences. *Constr Reconstr* 1:74–84
6. Fedorova N (2018) In., Koren'kov PA, Wu NT Methods of experimental studies of the deformation of monolithic reinforced concrete frame of a building during emergency effects. *Constr Reconstr* 2018 4(78):42–52
7. Kodish EN (2018) The protection design of buildings and structures against progressive collapse, given the emergence of limit state. *Ind Civ Constr* 10:95–101
8. Kolcunov VI, Tuyen NV, Korenkov P (2020) A deformation and failure of a monolithic reinforced concrete frame under accidental actions, vol T. 753. In: IOP conference series: materials science and engineering, p S. 032037
9. Fedorova NV, Ngoc TV (2019) Deformation and failure of monolithic reinforced concrete frames under special actions, vol T. 1425. In: Journal of physics: conference series, p 012033
10. Adam JM, Parisi F, Sagaseta J, Lu X (2018) Research and practice on progressive collapse and robustness of building structures in the 21st century. *Eng Struct* 173:S. 122–149
11. Yu J, Tan KH (2013) Experimental and numerical investigation on progressive collapse resistance of reinforced concrete beam column sub-assemblages. *Eng Struct* T. 55:90–106
12. Deng X-F, Liang S-L, Fu F, Qian K (2020) Effects of high-strength concrete on progressive collapse resistance of reinforced concrete frame. *J Struct Eng* 146(6):04020078. [https://doi.org/10.1061/\(asce\)st.1943-541x.0002628](https://doi.org/10.1061/(asce)st.1943-541x.0002628)
13. Xuan W, Wang L, Liu C, Xing G, Zhang L, Chen H (2019) Experimental and theoretical investigations on progressive collapse resistance of the concrete-filled square steel tubular column and steel beam frame under the middle column failure scenario. *Shock Vib* 2019:1–12. <https://doi.org/10.1155/2019/2354931>
14. Alogla K, Weekes L, Augusthus-Nelson L (2017) Theoretical assessment of progressive collapse capacity of reinforced concrete structures. *Mag Concr Res* 69(3):145–162
15. Shan S et al (2016) Experimental study on the progressive collapse performance of RC frames with infill walls. *Eng Struct* 111:80–92
16. Tuen WN (2020) Study of the survivability of a structurally nonlinear reinforced concrete frame-rod system of a multi-storey building frame in a dynamic formulation. *Constr Reconstr* 90(4):73–84
17. Fedorova NV, Khalina TA (2017) Investigation of dynamic reloading in reinforced concrete structural systems during sudden structural rearrangements. *Ind Civ Constr* (8):32–36
18. Bondarenko VM, Kolchunov VI (2004) Computational models of the force resistance of reinforced concrete. M.: DIA, p 472



19. SP 385.1325800.2018 Protection of buildings and structures from progressive collapse
20. Bondarenko VM, Klyueva NV (2008) On the calculation of structures that change the design scheme as a result of corrosion changes. *Izvestiya Vuzov* (1):4–12
21. Geniev GA (1992) On the evaluation of dynamic effects in rod systems made of brittle materials. *Concr Reinf Concr* 9:25–27
22. SP 63.13330.2018 (2019) Concrete and reinforced concrete structures. The main provisions. SNiP 52-01-2003 (with change N 1). Official publication, Standartinform, Moscow

# Analysis of Heat and Moisture Damage of Enclosing Structures Based on Contactless Diagnostics



Margarita Tselyaritskaya , Yulia Pashchenko , Olga Sotnikova ,  
and Vladislav Pakhomov 

**Abstract** Thermal imaging surveys of residential premises in monolithic houses built in 2018 and 2019 of the cities of Russia are analyzed. Based on the regulatory requirements of the federal law “on energy saving”, the question arises about the existing shortcomings in the structural units of the monolithic overlap.

**Keywords** Monolithic housing construction · “Cold bridge” · Thermal insulation liner · Thermal imaging examination

## 1 Introduction

Monolithic housing construction for a number of reasons prevails against the background of panel and brick buildings. The advantages of this method of building construction become especially relevant with the adoption “On Energy Conservation and Energy Efficiency Improvement” [1]. The wide possibilities of monolithic housing construction technology allow us to solve current problems in the perspective of sustainable development of the construction industry. Ecological construction, which includes the solution of a complex of tasks, such as architectural, construction, environmental, urban planning, economic and social, has the definition of “sustainable construction”.

To solve the environmental problem of sustainable development, it is necessary to minimize the impact of heat and moisture defects of building structures on the operation of the house. Damages that cannot be determined visually are subjected

---

M. Tselyaritskaya (✉) · Y. Pashchenko · O. Sotnikova  
Voronezh State Technical University, 84, 20-Letiya Oktyabrya Street, Voronezh 394006, Russia  
e-mail: [marchenko@vgasu.vrn.ru](mailto:marchenko@vgasu.vrn.ru)

O. Sotnikova  
e-mail: [ksenija.sotnikova@yandex.ru](mailto:ksenija.sotnikova@yandex.ru)

V. Pakhomov  
Southwest State University, 94, 50 Let Oktyabrya Street, Kursk 305040, Russia  
e-mail: [vlad-pakhomov-03@mail.ru](mailto:vlad-pakhomov-03@mail.ru)

to thermal imaging diagnostics. Thermal imaging surveys reveal the so-called “cold bridges”.

“Cold bridges” are one of the most common damages to building structures. There are various types of “cold bridges”: due to design features, properties of the material of structures, location (geometry) [2]. Thus, geometric “cold bridges” are a joint of homogeneous materials with similar density, but diametrically opposite in terms of the coefficient of thermal conductivity. Low temperature indicators on damaged surfaces, increased transmission losses, and the occurrence of “dew points” serve as an indicator of “cold bridges”.

The physical properties of structural materials contribute to capillary movement in their thickness, as well as increased humidity create favorable conditions for heat and moisture damage. Moreover, the lack of systematic ventilation of the room leads to an oversaturation of the air with water vapor. Excess moisture in the air at a certain temperature can no longer be retained and is released in the form of water droplets. The temperature at which this phenomenon is observed is called the “dew point” temperature. In this case, the relative humidity of the air is 100%.

There are such layers of air in the room that have direct contact with the colder surfaces of building elements. These layers are cooled more significantly than others—to the surface temperature [3]. If in the area of the “cold bridge” the minimum temperature of the surface is lower than the temperature of the “dew point”, therefore, the air temperature in this zone is also lower than the temperature of the “dew point”. As a result, the moisture contained in this layer of air is released as condensate on a cold surface [4].

Spontaneous heat losses are possible in vulnerable places, such as room corners, wall joints, door and window openings, balconies and protruding slabs.

A number of measures to improve thermal protection properties, accounting for thermal heterogeneity, quality control of construction and installation work—this is what allows you to avoid the formation of “cold bridges”.

## 2 Materials and Methods for Solving Problems

Avoiding the formation of “cold bridges” at the stage of the construction of a monolithic house is a difficult task, as a rule, the solution to the problem of “heat leakage” is dealt with after the commissioning of the object, when the outdoor temperature reaches negative values [5]. Tele-visor is a modern device for diagnosing building structures. Thermal imaging examination is the acquisition of images of objects with the power of thermal (infrared) radiation emanating from them [6].

The method of thermal imaging examination is focused on the remote measurement of temperature fields of the surfaces of enclosing structures. The result is a snapshot in an infrared image. The thermal imager perceives electromagnetic radiation of a building structure: the higher its temperature, the brighter it is. The calculation of heat transfer resistances and temperatures of the inner surfaces of enclosing structures is based on fixing the temperature difference between the inner and outer surfaces of the fence.

Contactless diagnostics using thermal imaging technology also makes it possible to identify errors in the design and installation at the early stages of their formation, which reduces the need for expensive measures to strengthen structures [7].

### 3 Results and Discussion

One of the main tasks of heat conservation and the formation of a comfortable microclimate during the operation of a residential building is the creation of effective thermal insulation of external enclosing structures. The level of thermal protection and microclimate parameters in residential premises are regulated, according to regulatory documents in force on the territory of the Russian Federation. Indoor microclimate parameters”.

At the design stage of a monolithic residential building, the floor-by-floor support of the exterior walls on the cantilever outlets of the floor slabs is provided. This method implies the clearest separation of structural elements into load-bearing and enclosing structures according to their functional purpose. Of course, the presence of “cold bridges” is possible in places where the outer enclosing structure rests on the cover.

At the stage of installation work, they provide for the location of the walls along the perimeter with an offset from the edge by 100 mm.

For interfaces with the floor slab, the minimum temperatures on the inner surface of the wall depend on the thickness of the wall and the presence of ventilation [10]. In the nodes of this type, freezing is practically not observed. An example of the application of this solution is shown in Fig. 1.

Subject to the conditions of energy saving, ensuring sanitary and hygienic conditions, we will model the temperature isofield in the LIRA LAND software (see Fig. 2). The indoor air temperature is taken to be  $t_{\text{inside}} = +20$  °C, the temperature of the coldest five-day period with a security of 0.92  $t_{\text{outside}} = -24$  °C.

The minimum temperature at the location of the heat-conducting inclusions does not exceed the normalized temperature drop equal to  $\Delta t^n = +4$  °C, therefore, the sanitary and hygienic condition [8] is fulfilled. We come to the conclusion that there are no “cold bridges”.

Experimental studies were carried out in residential buildings in Voronezh, during which the TESTO 865 thermal imager (serial number 62280818) was used.

The survey of the above-mentioned residential buildings, which have been in operation since 2019 and 2018, was carried out in a contactless way.

The main technical characteristics of the TESTO 865 thermal imager are presented in Table 1.

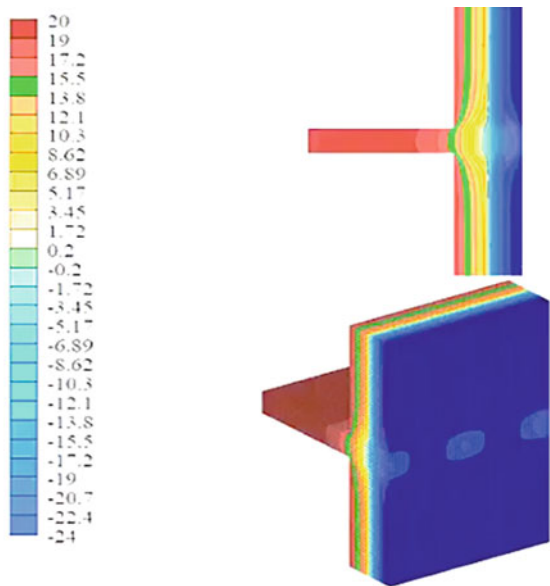
Survey thermography of the internal surfaces of enclosing structures was performed in residential premises having the characteristics given in Table 2.

Detailed measurements were made in a perpendicular direction to the wall or with a deviation not exceeding 30°. Thermography was performed sequentially, with frame-by-frame recording of thermograms and one-time measurement, and fixing the



Fig. 1 Thermal pads in a monolithic overlap

Fig. 2 Thermographic visualization of perforation of monolithic overlap disk releases



temperatures of reference sites. In Figs. 3, 4, 5 and 6, the dark color zone indicates the area of the maximally lowered temperature values on the inner surface of the fence. The results of thermal imaging surveys are presented in the Tables 3, 4, 5 and 6.

**Table 1** Technical characteristics of TESTO 865

N	Name	Name
1	Detector size, pixels	160 × 120
2	Temperature measurement range, °C	From -20 to +280
3	Temperature sensitivity (NETD), mK, no more	120
4	Operating temperature, °C	From -15 to +50
4	Measurement accuracy, °C, no more	2

**Table 2** Technical characteristics of TESTO 865

Location	Type of building	Commissioning, year	Number of floors	The temperature of the air on the gun, °C	Temperature in the living room, °C
The first object	Monolithic	2019	25	-15.0	+22.5
The second object	Brick-monolithic	2018	17	-14.0	+21.0

**Fig. 3** Thermographic visualization of the upper zone of the outer wall of the residential building of the first object

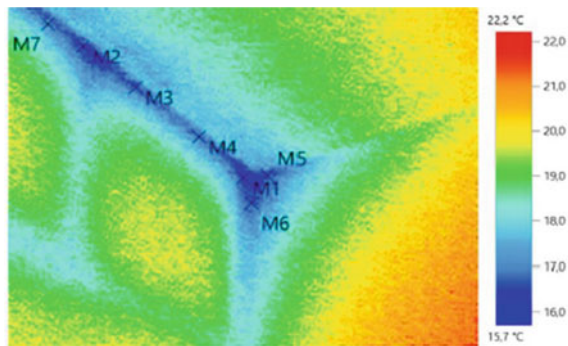


**Fig. 4** Thermographic visualization of thermal imaging examination of the lower zone of the outer wall of a residential building of the first object

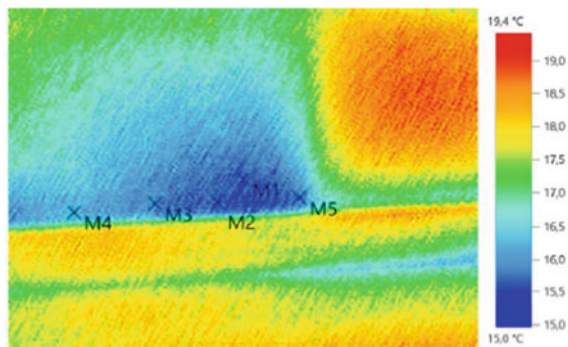


**Fig. 5** Thermographic visualization of a thermal imaging survey of the lower zone of the outer wall of a residential building of the second object

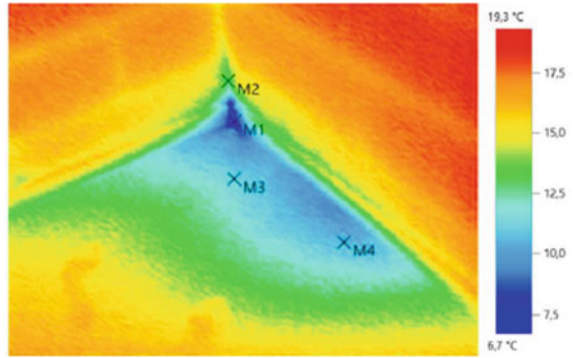


**Fig. 6** Results of thermal imaging examination of the upper zone of the outer wall of a residential building of the second object

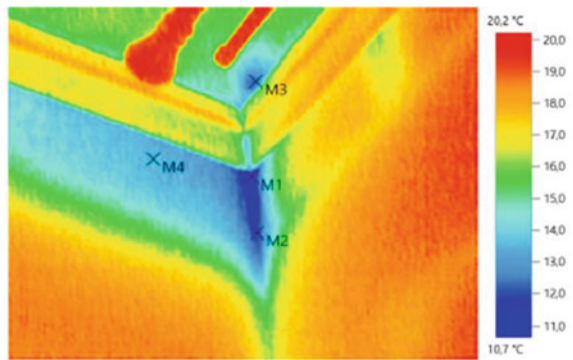


**Table 3** Results of thermal imaging examination of the upper zone of the outer wall of the residential building of the first object

Measured objects	Temperature, °C	Internal air temperature, °C	Temperature difference, °C
Measuring point 1	16.3	22.5	6.2
Measuring point 2	16.3	22.5	6.2
Measuring point 3	16.8	22.5	5.7
Measuring point 4	16.7	22.5	5.8
Measuring point 5	16.6	22.5	5.9
Measuring point 6	16.6	22.5	5.9
Measuring point 7	16.8	22.5	5.7

**Table 4** Results of thermal imaging examination of the lower zone of the outer wall of a residential building of the first object

Measured objects	Temperature, °C	Internal air temperature, °C	Temperature difference, °C
Measuring point 1	15.5	22.5	5.0
Measuring point 2	15.4	22.5	7.1
Measuring point 3	15.9	22.5	6.6
Measuring point 4	16.1	22.5	6.4
Measuring point 5	15.7	22.5	6.8

**Table 5** Results of a thermal imaging survey of the lower zone of the outer wall of a residential building of the second object

Measured objects	Temperature, °C	Internal air temperature, °C	Temperature difference, °C
Measuring point 1	7.0	21.0	14.0
Measuring point 2	12.8	21.0	8.2
Measuring point 3	11.2	21.0	9.8
Measuring point 4	10.4	21.0	10.6

**Table 6** Results of thermal imaging examination of the upper zone of the outer wall of a residential building of the second object

Measured objects	Temperature, °C	Internal air temperature, °C	Temperature difference, °C
Measuring point 1	10.7	21.0	10.3
Measuring point 2	11.7	21.0	9.3
Measuring point 3	12.3	21.0	8.7
Measuring point 4	13.7	21.0	7.3

## 4 Conclusion

The analysis of thermograms is based on the identification of the causes of thermal insulation violations of external enclosing structures or a decrease in its qualities. The main criterion for comparing different sections of the surface of enclosing structures is the temperature difference at the selected point on the compared surface area.

The temperature difference between the indoor temperature and the surface temperature of the wall of a residential building of the first object exceeds  $+6.0\text{ }^{\circ}\text{C}$  with a normalized value of  $\Delta t^n = +4.0\text{ }^{\circ}\text{C}$ . The temperature difference between the indoor temperature and the temperature on the top of the wall of a residential building of the second object exceeds  $+11.0\text{ }^{\circ}\text{C}$  with a normalized value of  $\Delta t^n = +4.0\text{ }^{\circ}\text{C}$ .

The above results of the thermal imaging survey allow us to conclude that thermal pads were either not installed along the perimeter of the cantilever disks of the ceilings, or were mounted with gross errors.







Uncontrolled loss of heat through fixed “cold bridges” leads to a significant increase in heat consumption for heating the building. This is contrary to the law “On Energy Conservation and Energy Efficiency Improvement”. It is quite labor-intensive to exclude existing bridges in operated apartments. It is advisable to prevent their formation at the design stage and during installation work [3] by means of perforation of a monolithic floor slab. The use of thermal pads leads to a decrease in specific heat loss by an average of 1.5 times and practically eliminates freezing under standard conditions.

## References

1. On energy saving and energy efficiency improvement and on amendments to certain Legislative Acts of the Russian Federation: Federal Law No. 261-FZ of 23.11.2009. Assembly of Legislation of the Russian Federation. No. 261-FZ. – St. 93 (2009).
2. Sheina SG, Minenko AN (2012) Analysis and calculation of “cold bridges” in order to increase the energy efficiency of residential buildings. *Eng Bull Don* 4–1(22):131
3. Aloyan RM, Fedosov SV, Oparina LA (2016) Energy-efficient buildings—state, problems and solutions. PresSto, Ivanovo
4. Egorova TS, Cherkas VS (2011) Improving the energy efficiency of buildings by eliminating critical cold bridges and continuous insulation of exposed building structures. *Vestnik MGSU* 3–1:421–428
5. Shilova EA, Shilov SO, Hakimova VA. Experimental determination of vulnerable places for the formation of “cold bridges”. *Stud*
6. Nikitina OS, Maksimtsev DS, Kharebin II, Kuznetsova YuV (2017) Bridges of cold: a modern solution to the problem. *Mod Trends Dev Sci Technol* 2:134–136
7. Golitsyn AA (2014) With the eye of a thermal imager. *Sci First Hand* 3(4):198–203
8. Chang JR, Yang SR (2013) Innovation and sustainable technology in road and airfield pavement. *Trans Tech Publications Ltd., Germany*, pp 82–83
9. LLC (2017) “PENOPLEX SPb” Thermal pads PENOPLEX®—an innovative product for use in monolithic housing construction. “PENOPLEX SPb” LLC. *Sci Tech Prod J* 8:12–13
10. Rudenko NN, Fursova IN (2013) Influence of non-stationary thermal conditions on the determination of thermal resistance of the fence. *Eng Bull Don* 4(27):225

# Investigation of Methods and Algorithms for Predicting Sound Insulation Characteristics of Prefabricated Enclosing Structures



Yulia Pashchenko , Margarita Tselyaritskaya , Semyon Podvalny ,  
and Daniil Fedyanin 

**Abstract** The traditional method of determining the isolation of air noise of a massive structure is considered, in accordance with SP 23-103-2003 “Design of sound insulation of enclosing structures of residential and public buildings”, in order to substantiate the composition and list of expert and design work to ensure sufficient sound insulation properties of enclosing structures. The relevance of the study is justified by the increase in noise comfort in residential buildings. Enclosing structures made of ceramic porous and aerated concrete blocks plastered with solutions, different in composition and density, were selected as the studied ones. Experimental design work has been carried out: the sound insulation index has been calculated, variable calculations have been performed, and variants of wall structures recommended for further experimental research have been substantiated. Analytical methods were applied, as well as the analysis of the results of theoretical research. The results obtained can be used in the design of residential apartment buildings.

**Keywords** Sound insulation · Wall blocks · Aerated concrete · Porous block

---

Y. Pashchenko (✉) · M. Tselyaritskaya · S. Podvalny  
Voronezh State Technical University, 84, 20-Letiya Oktyabrya Street, Voronezh 394006, Russia  
e-mail: [julia\\_pashchenko@mail.ru](mailto:julia_pashchenko@mail.ru)

S. Podvalny  
The Russian Presidential Academy of National Economy and Public Administration, Moscow,  
Russia

D. Fedyanin  
Southwest State University, 94, 50 Let Oktyabrya Street, Kursk 305040, Russia

## 1 Introduction

In recent years, the volume of housing construction has increased significantly, in particular, multi-storey. The growth rate continues to grow. In our country, the greatest preference is given to the method of monolithic construction of houses. With this design scheme, the load-bearing elements are carried out directly during installation. Inter-apartment partitions are erected at the last stages of construction. Hence, there are problematic situations of the technological process associated with the timing of the construction and commissioning of the building. The standard design of the partition is brickwork, but the installation is quite laborious, which leads to an increase in the construction time, as well as the cost of future apartments. Therefore, one of the solutions is the implementation of walls made of large-sized blocks, which often do not meet acoustic requirements [1].

In addition, apartments with the so-called “free layout” have now become popular, when the owner or tenant independently determines the boundaries of the rooms inside the room. In the future, an independent finishing of the walls is carried out. All these factors lead to a decrease in the acoustic comfort of the surrounding apartments.

## 2 Materials and Methods

The main method for calculating sound insulation is the graphoanalytic method. As the studied materials for the execution of inter-apartment partitions, the following were selected:

- (1) ceramic porous blocks with dimensions  $380 \times 250 \times 219$  mm, density 800, 900, 1000 kg/m<sup>3</sup>;
- (2) aerated concrete blocks with dimensions of  $625 \times 250 \times 250$  mm, density of 800, 600, 500 kg/m<sup>3</sup>.

According to SP 275.1325800.2016 “Structures enclosing residential and public buildings. Rules for the design of sound insulation” [2], the graphoanalytic method is based on the construction of the frequency response of the isolation of air noise, which is represented as a polyline constructed at points A, B, C, D (Fig. 1).

The beginning of the construction begins with finding the coordinates of point B, depending on the density and thickness of the enclosing structure, in accordance with the graphs and tables of this set of rules [2].

The value of air noise isolation  $R_B$ , dB, at point B is determined by the formula

$$R_B = 20\log(m_\vartheta) - 12, \quad (1)$$

$m_\vartheta$ —the equivalent surface density, kg/m<sup>2</sup>, is determined by the formula

$$m_\vartheta = K \cdot m, \quad (2)$$

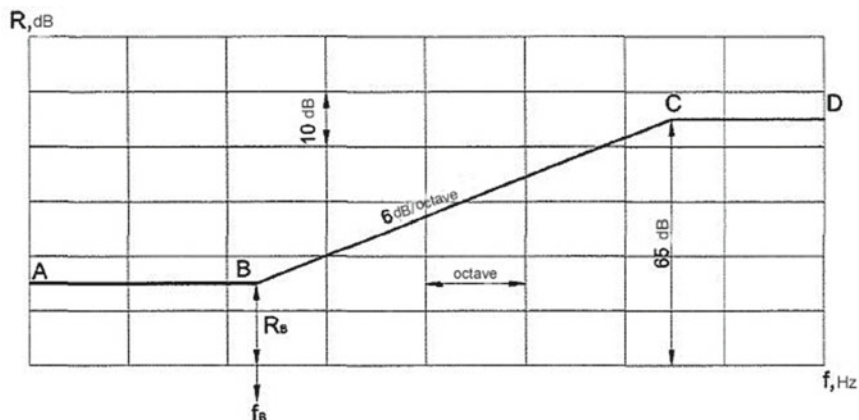


**Fig. 1** Frequency response of air noise isolation by a single-layer flat fence

where  $K$  is a coefficient that takes into account the relative increase in the bending stiffness of the fence made of concrete on light aggregates, porous concrete, etc. in relation to structures made of heavy concrete with the same surface density.

$m$  is the surface density of the enclosing structure,  $\text{kg/m}^2$ .

During the calculation using this method, it became difficult to construct the frequency response of air noise insulation, since the coordinates of point B and the value of the coefficient  $K$  can be determined for a limited number of materials, namely:

- expanded clay concrete;
- perlite concrete;
- sinter concrete;
- cinder-block concrete;
- aerated concrete, foam concrete;
- brick;
- gypsum concrete, gypsum.

There are no  $K$  values for masonry made of ceramic porous blocks with a density range of  $800\text{--}1000 \text{ kg/m}^3$ , as well as for aerated concrete blocks of the lowest density, such as  $500$  and  $400 \text{ kg/m}^3$ .

In addition to the listed types of large-block wall structures, many new types of building materials have appeared in our country, such as granular materials, shotcrete, polystyrene concrete and others that are promising. However, it is not possible to calculate their sound-insulating properties according to the method [2].

Another significant disadvantage of this calculation method according to [2] is rounding the value of the critical frequency  $B$  to the geometric mean frequency of the third octave band, within which is  $f_B$  [3].

Since, due to the above problems, it is not possible to choose exact data, and there is currently no other method for calculating the sound insulation of massive structures, the calculations carried out are not accurate.

After drawing on the graph, in order to construct the calculated frequency response, point B to the left, the AB section is postponed to the mean geometric frequency of 100 Hz. To construct a segment of a polyline BC, it is necessary to form its slope of 6 dB per octave, while taking into account that the point C always has an ordinate  $R_c = 65$  dB. After determining the frequencies  $f_{CD}$ , Hz, a complete design characteristic is obtained. Next, the values of the air noise isolation indices are set according to the calculated characteristic for the corresponding frequencies [4].

The next step is to determine the presence of unfavorable deviations, the values of which are entered into the table based on the values obtained as a result of constructing the calculated frequency response. The condition must be met

$$R_{OC,i} > R_{calc,i}. \quad (3)$$

where  $R_{OC,i}$ , dB—the values of the air noise isolation indices according to the estimated curve for the corresponding frequencies;

$R_{calc,i}$ , dB—the values of the air noise isolation indices according to the calculated curve for the corresponding frequencies.

The values of unfavorable deviations of the calculated frequency response from the estimated curve are calculated  $NO_i$  dB, according to the frequencies of the third octave bands:

$$NO_i = R_{OC,i} - R_{calc,i}. \quad (4)$$

Next, the amount of unfavorable deviations is determined on the basis of which the analysis of the obtained numerical values is carried out. It is important that the total value does not exceed 32 dB [2].

### 3 Results and Discussion

In the calculation, various variants of blocks plastered with solutions of different composition and density, in one or two layers, were considered. Below, in Table 1, the variants of enclosing structures are presented, which were calculated by the graphoanalytic method according to [2].

The results of numerical calculations are presented in Tables 2, 3, 4, 5, 6 and 7.

A graphic illustration of the dependence of  $R_i$ , dB, air noise isolation index on the frequency range  $f_i$ , Hz, is shown in the figure. The calculated frequency characteristics of various variants of wall structures are based on the results of calculations given in Tables 2, 3, 4, 5, 6 and 7 (Fig. 2).

**Table 1** Calculated index of air noise insulation of wall structures

Nº	The composition of the wall structure	Air noise isolation index, calculated $R_c$ (dB)
1	2 × 10 mm—plaster, 800 kg/m <sup>3</sup> 250 mm—ceramic porous block, 800 kg/m <sup>3</sup> 2 × 10 mm—plaster, 800 kg/m <sup>3</sup>	51
2	2 × 10 mm—lime plaster, 1600 kg/m <sup>3</sup> 250 mm—ceramic porous block, 900 kg/m <sup>3</sup> 2 × 10 mm—lime plaster, 1600 kg/m <sup>3</sup>	55
3	10 mm—cement-sand plaster, 1800 kg/m <sup>3</sup> 250 mm—ceramic porous block, 1000 kg/m <sup>3</sup> 10 mm—cement-sand plaster, 1800 kg/m <sup>3</sup>	53
4	10 mm—cement-sand plaster, 1800 kg/m <sup>3</sup> 250 mm—aerated concrete block, 800 kg/m <sup>3</sup> 10 mm—cement-sand plaster, 1800 kg/m <sup>3</sup>	54
5	2 × 10 mm—plaster, 800 kg/m <sup>3</sup> 250 mm—aerated concrete block, 600 kg/m <sup>3</sup> 2 × 10 mm—plaster, 800 kg/m <sup>3</sup>	51
6	2 × 10 mm—lime plaster, 1600 kg/m <sup>3</sup> 250 mm—aerated concrete block, 500 kg/m <sup>3</sup> 2 × 10 mm—lime plaster, 1600 kg/m <sup>3</sup>	52

## 4 Conclusion

1. According to the normative values of air noise insulation indices by internal enclosing structures  $R_w^{req}$  for residential and public buildings, walls and partitions between apartments, between apartment rooms and offices; between apartment rooms and stairwells, halls, corridors, lobbies should take 52 dB [5].
2. The wall is made of ceramic porous blocks, with dimensions of 380 × 250 × 219 mm, density of 900 kg/m<sup>3</sup>, plastered with lime plaster in two layers of 10 mm on each side, density of 1600 kg/m<sup>3</sup>, as well as of ceramic aerated concrete blocks, with dimensions of 625 × 250 × 250 mm, density of 800 kg/m<sup>3</sup>, plastered with cement-sand plaster in one layer of 10 mm with a density of 1800 kg/m<sup>3</sup> is calculated to meet the requirements.
3. The wall is made of ceramic porous blocks, with dimensions of 380 × 250 × 219 mm, density of 1000 kg/m<sup>3</sup>, plastered with cement-sand plaster in one layer of 10 mm, density of 1800 kg/m<sup>3</sup>, as well as of ceramic aerated concrete blocks, with dimensions of 625 × 250 × 250 mm, density of 500 kg/m<sup>3</sup>, plastered with lime plaster in two layers of 10 mm on each side, with a density of 1600 kg/m<sup>3</sup>, according to calculations, meet the requirements.
4. The wall is made of ceramic porous blocks, with dimensions of 380 × 250 × 219 mm, density of 800 kg/m<sup>3</sup>, plastered with gypsum plaster in two layers of 10 mm on each side, density of 800 kg/m<sup>3</sup>, as well as of ceramic aerated concrete blocks, with dimensions of 625 × 250 × 250 mm, density of 600 kg/m<sup>3</sup>, plastered with















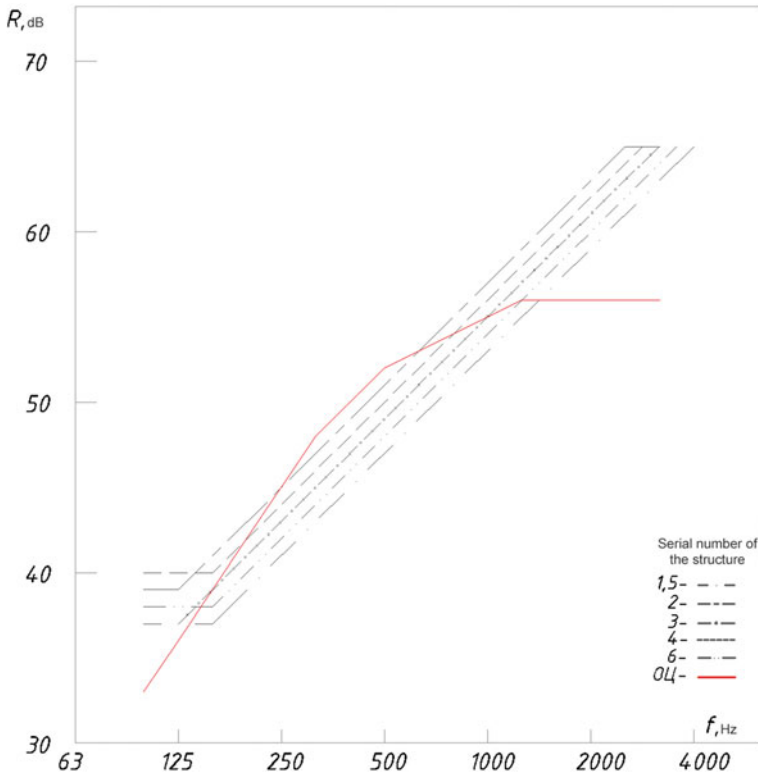


**Fig. 2** Calculated frequency characteristics of various variants of wall structures: 1—ceramic porous block, 800 kg/m<sup>3</sup>; 2—ceramic porous block 900 kg/m<sup>3</sup>; 3—ceramic porous block 1000 kg/m<sup>3</sup>; 4—aerated concrete block 800 kg/m<sup>3</sup>; 5—aerated concrete block 600 kg/m<sup>3</sup>; 6—aerated concrete block 500 kg/m<sup>3</sup>; OC—evaluation curve

gypsum plaster in two layers 10 mm on each side, with a density of 800 kg/m<sup>3</sup>, according to calculations do not meet the requirements.

5. It is necessary to conduct experimental studies for further evaluation and comparison with calculations made by the graphoanalytic method of the Set of Rules.





## References

1. Angelov VL (2009) Problems of ensuring sound insulation of fences of monolithic residential and public buildings. *Acad Archit Constr* 5:193–195
2. SP 275.1325800.2016. Structures enclosing residential and public buildings. Rules of sound insulation design. The Ministry of Construction of Russia dated 17.06.2017. Techexpert: [website]. <https://docs.cntd.ru/document/456050583>

3. Shchelokov YuA (2015) Calculation of air noise insulation (sound insulation) of single-layer plates. *Noise Theory Pract* 1(1):70–76
4. Ananyin MYu, Kremleva DV (2014) Calculations of sound insulation by enclosing structures of buildings: textbook manual. Ural University, Yekaterinburg. ISBN 978-5-7996-1336-5
5. A set of rules. SP 51.13330.2011. Noise protection. Updated version of SNiP 23-03-2003. Gosstroy of Russia dated 30.06.2003 No. 136. Techexpert: [website]. <http://docs.cntd.ru/document/1200035251>

# Design and Calculation of Multifunctional Canopies in the Form of Shallow Shells



Alexander Kolesnykov , Tatyana Tsurik , Sofya Kurakina , and Ksenia Litvinova 

**Abstract** Multifunctional canopies with a covering using a shape of shallow shells having a skylight for higher insolation are investigated. A derivation of equation is presented in view of the geometric nonlinearity of the thin-walled structure performance. A technique for solving systems of equations using the Bubnov-Galyorkin method is given. The concept of a universal shell canopy is proposed. Structures with various ways of fixing is simulated. The skylight is set on an arbitrary section of the structure with changing parameters. The influence of the shape and location of the skylight on the value of the critical load is investigated. The results of the investigations are given in a dimensionless form and are illustrated by graphs, which makes it convenient to use them in engineering calculations. Recommendations are given for correcting the shape and thickness of covering structures in the form of shallow shells with a skylight to maintain their bearing capacity.

**Keywords** Shallow shell · Stress–strain state · Spatial structure · Canopy · Critical load

## 1 Introduction

Large-span canopies can be used as structures for various purposes. They have great imaginative potential and were originally designed as exhibition spaces to showcase achievements in the field of art, science and technology. The world practice of construction has accumulated extensive experience in the use of large-span structures by the most famous architects. The ancestor of this phenomenon can be considered world trade exhibitions. For instance, in London in 1851, there was an exhibition located in the huge Crystal Palace, designed by Joseph Paxton, who used standard

---

A. Kolesnykov (✉) · T. Tsurik · S. Kurakina · K. Litvinova  
Southwest State University, 94, 50 Let Oktyabrya Street, Kursk 305040, Russia  
e-mail: [ag-kolesnikov@mail.ru](mailto:ag-kolesnikov@mail.ru)

© The Author(s), under exclusive license to Springer Nature Switzerland AG 2024  
N. Vatin et al. (eds.), *Modern Problems in Construction*,  
Lecture Notes in Civil Engineering 372,  
[https://doi.org/10.1007/978-3-031-36723-6\\_36](https://doi.org/10.1007/978-3-031-36723-6_36)

373

elements in the form of a factory cast-iron grate filled with sheet glass, which eventually formed a greenhouse of enormous size. Paxton's Crystal Palace was characterized by the maximum use of the materials which became available. The structure, 563 m long and 124 m wide, clearly demonstrated the metal architectural possibilities. Metal trusses with a cross lattice were used for the floors.

Further development of large-span constructions demonstrated their new capabilities: lightness, quick assembly, versatility and expressiveness. The use of new materials, as well as the idea of openness inherent in modern architecture, has led to the fact that large-span buildings have become widespread, including exhibition centers, fair spaces, sports facilities, railway stations, and trade facilities.

Examples of the use of long-span shells are extremely diverse. At the same time, according to volumetric and spatial characteristics, three types of them can be distinguished: shell as roofing; shell as a covering of a part of a building; shell as a building [1]. From our point of view, buildings of the third type are of the greatest interest, since they are devoid of the problem of establishing the scale of structures for a person. The specificity of large buildings with a shell, as with a late formative view, is that the form itself is a facade embodiment, giving the building additional attractiveness. We have provided the concept of a multifunctional canopy, which can be located in residential security and serve as a point of attraction, depending on the purpose. This conceptual design has a great potential, has different aesthetic and economic characteristics and can be integrated into any environment (Fig. 1).

The most difficult structure for design and calculation in the considered multifunctional canopy is a cover in the form of a shallow shell with a skylight. The explore of structures in the form of shallow shells is currently receiving considerable attention all over the world. Stability [2, 3], strength [4, 5], and oscillations of thin shells [5] are explored, including those in a nonlinear formulation [6, 7] and various forms of the middle surface [8, 9]. Works that analyze the behavior of layered [10–12] and orthotropic shallow shells [13], explores of the long-term strength of coating shells and its reduction due to various factors [14, 15], are of particular interest, as the results of them can be used to model reinforced concrete and reinforced cement structures.

Currently, most of these structures are calculated using software based on the finite element method [16, 17]. However, in the case of non-linear problems, it is possible to obtain results whose accuracy is difficult to estimate, since the solution strongly depends on the type and number of finite elements. At the same time, designers often face the task of not only calculation of structures, but also exploring them, so the development of methods for their analysis is an important task.

## 2 Materials and Methods

The task of calculating the roofing of buildings and structures in the form of shallow shells with a skylight in an arbitrary section (Fig. 2) with any aspect ratio in the plan and type of support, as well as loaded with a vertical uniformly distributed load,





**Fig.1** General view of the multifunctional canopy

can be represented by a system of equations (1). At the same time, the thickness of the structure is relatively small compared to the dimensions in the plan, and the deflections are commensurate with the thickness, therefore, it is necessary to take into account the geometric nonlinearity of the structure [18, 19]:

$$\begin{cases} \frac{1}{h} \nabla^2 \nabla^2 \frac{1}{E(x,y)} \varphi + k_y \frac{\partial^2 w}{\partial x^2} + k_x \frac{\partial^2 w}{\partial y^2} - 2k_{xy} \frac{\partial^2 w}{\partial x \partial y} + \frac{\partial^2 w}{\partial x^2} \frac{\partial^2 w}{\partial y^2} - \frac{\partial^2 w}{\partial x \partial y} = 0, \\ \frac{h}{12} \nabla^2 \nabla^2 \frac{E(x,y)}{(1-\nu(x,y)^2)} w - \frac{\partial^2 \varphi}{\partial y^2} \left( k_x + \frac{\partial^2 w}{\partial x^2} \right) - \frac{\partial^2 \varphi}{\partial x^2} \left( k_y + \frac{\partial^2 w}{\partial y^2} \right) + 2 \frac{\partial^2 \varphi}{\partial x \partial y} \left( k_{xy} + \frac{\partial^2 w}{\partial x \partial y} \right) - Z = 0. \end{cases} \quad (1)$$

where  $\varphi$  is the stress function,  $w$  is the deflection function,  $F = F(x, y)$  is the median surface function,  $Z$  is the load function.

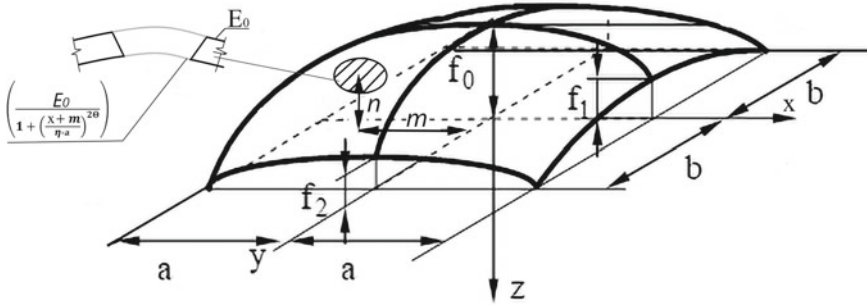


Fig. 2 Covering a multifunctional canopy in the form of a shallow shell with a skylight

$$F(x, y) = f \left[ \alpha \left( \frac{x}{a} \right)^{2\xi} + \beta \left( \frac{y}{b} \right)^{2\xi} + 1 \right]. \tag{2}$$

where

- $f$  is the arch camber in the center of the shell,
- $\alpha = -\frac{f_1}{f}, \beta = -\frac{f_2}{f}$ —parameters characterizing the shape of the shell,
- $f_1, f_2$ —support arch lifting booms of the shell,
- $a, b$ —plan dimensions.

The skylight is modeled as a change in the modulus of elasticity on an arbitrary area of the structure in the following way:

$$E(x, y) = E_0 - \left( \frac{E_0}{1 + \left( \frac{x+m}{\eta \times a} \right)^{2\theta}} \right) \left( \frac{E_0}{1 + \left( \frac{y+n}{\gamma \times b} \right)^{2\vartheta}} \right). \tag{3}$$

where

- $E_0$ —stands for initial modulus of elasticity (Fig. 3);
- $\eta, \gamma$ —coefficients characterizing the skylight size  $[0; a)$ ;
- $m$ —coefficient characterizing the displacement of the center of the skylight along the  $x$  axis  $[-a; a]$ ,
- $n$ —coefficient characterizing the displacement of the center of the skylight along the  $y$  axis  $[-b; b]$ ,

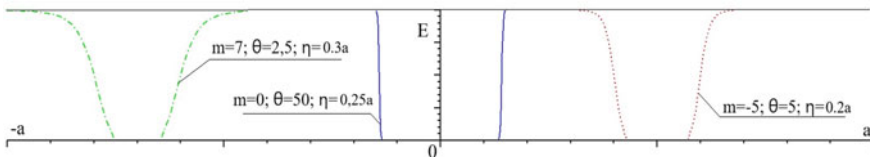


Fig. 3 The shape and location of the skylight depending on the variation of parameters  $m, \eta, \theta$

$\theta, \vartheta$ —coefficients characterizing the shape of the skylight faces along the  $x$  and  $y$  axes, respectively ( $0, 5; \infty$ ).

Variation of the coefficients  $m, \eta, \theta$  gives the opportunity to set a large number of options for possible cuts (their location, size and shape of the faces).

Stresses at any point of the shell can be determined using the Bubnov-Galerkin method [20]:

$$\bar{\sigma} = \sqrt{\frac{1}{2}[(\bar{\sigma}_1 - \bar{\sigma}_2)^2 + (\bar{\sigma}_3 - \bar{\sigma}_2)^2 + (\bar{\sigma}_2 - \bar{\sigma}_1)^2]}. \quad (4)$$

where

$$\begin{aligned} \bar{\sigma}_1 = & \left| \frac{6}{\bar{t}} \overline{DB} \left( \frac{\partial^2}{\partial x^2} Z_x Z_y + \nu \frac{\partial^2}{\partial y^2} Z_y Z_x \right) \right| + \left| \overline{A} \frac{\partial^2}{\partial y^2} Z_y Z_x \bar{t} \right| \\ & + \left| \frac{g}{\bar{t}^2} \overline{DB} \left( \frac{\partial^3}{\partial x^3} Z_x Z_y + \frac{\partial}{\partial x} Z_x \frac{\partial^2}{\partial y^2} Z_y \right) \right|, \end{aligned} \quad (5)$$

$$\begin{aligned} \bar{\sigma}_2 = & \left| \frac{6}{\bar{t}} \overline{DB} \left( \nu \frac{\partial^2}{\partial x^2} Z_x Z_y + \frac{\partial^2}{\partial y^2} Z_y Z_x \right) \right| + \left| \overline{A} \frac{\partial^2}{\partial x^2} Z_x Z_y \bar{t} \right| \\ & + \left| \frac{g}{\bar{t}^2} \overline{DB} \left( \frac{\partial^3}{\partial y^3} Z_y Z_x + \frac{\partial}{\partial y} Z_y \frac{\partial^2}{\partial x^2} Z_x \right) \right|, \end{aligned} \quad (6)$$

$$\bar{\sigma}_3 = \left| \frac{6}{\bar{t}} (1 - \nu) \overline{DB} \frac{\partial}{\partial x} Z_x \frac{\partial}{\partial y} Z_y \right| + \left| \overline{A} \frac{\partial}{\partial x} Z_x \frac{\partial}{\partial H} Z_y \bar{t} \right| \quad (7)$$

$$\overline{D} = \frac{D}{E_0 h^3}, \quad D = \frac{E_0 h^3}{12(1 - \nu^2)}, \quad (8)$$

$$\overline{A} = \frac{A \cdot a^2}{E f_0^5}, \quad \overline{B} = \frac{B \cdot a^2}{f_0^2} \quad (9)$$

$$g = \frac{f_0}{a}, \quad \bar{t} = \frac{h}{f_0}, \quad (10)$$

$$A = -\frac{1}{J_1} (B J_2 + B^2 J_3), \quad (11)$$

$$\begin{aligned} B = & \frac{1}{6C_1} \left( 36C_3 C_2 C_1 + 108q C_1^2 - 8C_2^3 + 12\sqrt{3}(4C_3^3 C_1 - C_3^2 C_2^2) \right. \\ & + 18C_3 C_2 C_1 q + 12\sqrt{3}(4C_3^3 C_1 - C_3^2 C_2^2 + 18C_3 C_2 C_1 q \\ & + 27q^2 C_1^2 - 4q C_2^3)^{1/2} C_1 \left. \right)^{1/3} \\ & - \frac{2}{3} (3C_3 C_1 - C_2^2) / (C_1 (36C_3 C_2 C_1 + 108q C_1^2 - 8C_2^3) \end{aligned}$$

$$\begin{aligned}
 & + 12\sqrt{3} (4C_3^3 C_1 - C_3^2 C_2^2 + 18C_3 C_2 C_1 q + 27q^2 C_1^2 - 4q C_2^3)^{1/2} C_1 \Big)^{1/3} \\
 & - \frac{1}{3} \frac{C_2}{C_3} \Big). \tag{12}
 \end{aligned}$$

$$C_1 = 2E_0 h \frac{J_3^2}{J_1 J_4}, \quad C_2 = 3E_0 \frac{J_3 J_2}{J_1 J_4}, \quad C_3 = D \frac{J_1^2}{J_1 J_4} + E_0 h \frac{J_2^2}{J_1 J_5}. \tag{13}$$

$$\begin{aligned}
 J_1 = \int_{-a}^a \int_{-b}^b & \left( - \frac{2 \left( \frac{\partial}{\partial y} E(x, y) \right) \left( \frac{\partial^3}{\partial y^3} \bar{w}(x, y) \right)}{h E(x, y)^2} + \frac{2 \left( \frac{\partial}{\partial y} E(x, y) \right)^2 \left( \frac{\partial^2}{\partial y^2} \bar{w}(x, y) \right)}{h E(x, y)^3} \right. \\
 & + \frac{\left( \frac{\partial^2}{\partial y^2} E(x, y) \right) \left( \frac{\partial^2}{\partial y^2} \bar{w}(x, y) \right)}{h E(x, y)^2} + \frac{\frac{\partial^4}{\partial x^4} \bar{w}(x, y)}{h E(x, y)} - \frac{2 \left( \frac{\partial}{\partial y} E(x, y) \right)^2 \nu \left( \frac{\partial^2}{\partial x^2} \bar{w}(x, y) \right)}{h E(x, y)^3} \\
 & + \frac{\left( \frac{\partial^2}{\partial y^2} E(x, y) \right) \nu \left( \frac{\partial^2}{\partial x^2} \bar{w}(x, y) \right)}{h E(x, y)^2} - \frac{2 \left( \frac{\partial}{\partial x} E(x, y) \right) \left( \frac{\partial^3}{\partial x^3} \bar{w}(x, y) \right)}{h E(x, y)^2} \\
 & + \frac{2 \left( \frac{\partial}{\partial x} E(x, y) \right) \left( \frac{\partial^2}{\partial x^2} \bar{w}(x, y) \right)}{h E(x, y)^3} - \frac{\left( \frac{\partial^2}{\partial x^2} E(x, y) \right) \left( \frac{\partial^2}{\partial x^2} \bar{w}(x, y) \right)}{h E(x, y)^2} \\
 & - \frac{2 \left( \frac{\partial}{\partial x} E(x, y) \right) \left( \frac{\partial^2}{\partial x^2} \bar{w}(x, y) \right)}{h E(x, y)^3} - \frac{\left( \frac{\partial^2}{\partial x^2} E(x, y) \right) \left( \frac{\partial^2}{\partial x^2} \bar{w}(x, y) \right)}{h E(x, y)^2} \\
 & - \frac{2 \left( \frac{\partial}{\partial x} E(x, y) \right)^2 \nu \left( \frac{\partial^2}{\partial y^2} \bar{w}(x, y) \right)}{h E(x, y)^3} + \frac{\left( \frac{\partial^2}{\partial x^2} E(x, y) \right) \nu \left( \frac{\partial^2}{\partial y^2} \bar{w}(x, y) \right)}{h E(x, y)^2} \\
 & - \frac{2 \left( \frac{\partial^3}{\partial x^2 \partial y} E(x, y) \right) \left( \frac{\partial}{\partial y} \bar{w}(x, y) \right)}{h E(x, y)^2} - \frac{2 \left( \frac{\partial^3}{\partial y^2 \partial x} E(x, y) \right) \left( \frac{\partial}{\partial x} \bar{w}(x, y) \right)}{h E(x, y)^2} \\
 & - \frac{2 \left( \frac{\partial^2}{\partial y \partial x} E(x, y) \right) \left( \frac{\partial^2}{\partial x \partial y} \bar{w}(x, y) \right)}{h E(x, y)^2} + \frac{4 \left( \frac{\partial}{\partial x} E(x, y) \right) \left( \frac{\partial}{\partial y} E(x, y) \right) \left( \frac{\partial^2}{\partial x \partial y} \bar{w}(x, y) \right) \nu}{h E(x, y)^3} \\
 & \left. - \frac{\frac{\partial^4}{\partial y^4} \bar{w}(x, y)}{h E(x, y)} - \frac{2 \left( \frac{\partial^2}{\partial y \partial x} E(x, y) \right) \left( \frac{\partial^2}{\partial x \partial y} \bar{w}(x, y) \right) \nu}{h E(x, y)^2} \right) \bar{w}(x, y) dx dy, \tag{14}
 \end{aligned}$$

$$J_2 = \int_{-a}^a \int_{-b}^b \left( \frac{\partial^2 F}{\partial y^2} \frac{\partial^2 \bar{w}}{\partial x^2} + \frac{\partial^2 F}{\partial x^2} \frac{\partial^2 \bar{w}}{\partial y^2} - 2 \frac{\partial^2 F}{\partial x \partial y} \frac{\partial^2 \bar{w}}{\partial x \partial y} \right) \bar{w} dx dy, \tag{15}$$

$$J_3 = \int_{-a}^a \int_{-b}^b (\Delta \bar{w}) \bar{w} dx dy, \tag{16}$$

$$J_4 = \int_{-a}^a \int_{-b}^b Z \bar{w} dx dy, \tag{17}$$

$$\begin{aligned}
 J_5 = & \int_{-a}^a \int_{-b}^b \left( \left( \frac{\partial^2}{\partial x^2} D(x,y) \right) \left( \frac{\partial^2}{\partial x^2} \bar{w}(x,y) \right) + 2 \left( \frac{\partial}{\partial x} D(x,y) \right) \left( \frac{\partial^3}{\partial x^3} \bar{w}(x,y) \right) \right. \\
 & + \left( \frac{\partial^2}{\partial x^2} D(x,y) \right) \nu \left( \frac{\partial^2}{\partial y^2} \bar{w}(x,y) \right) + D(x,y) \left( \frac{\partial^4}{\partial x^4} \bar{w}(x,y) \right) \\
 & + 2 \left( \frac{\partial^2}{\partial x \partial y} D(x,y) \right) \left( \frac{\partial^2}{\partial x \partial y} \bar{w}(x,y) \right) + 2 \left( \frac{\partial^2}{\partial y} D(x,y) \right) \\
 & + \left( \frac{\partial^3}{\partial x^2 \partial y} \bar{w}(x,y) \right) + D(x,y) \left( \frac{\partial^4}{\partial y^4} \bar{w}(x,y) \right) - 2 \left( \frac{\partial^2}{\partial x \partial y} D(x,y) \right) \\
 & \times \left( \frac{\partial^2}{\partial x \partial y} \bar{w}(x,y) \right) \nu + 2 \left( \frac{\partial}{\partial x} D(x,y) \right) \left( \frac{\partial^3}{\partial x \partial y^2} \bar{w}(x,y) \right) \\
 & + 2D(x,y) \left( \frac{\partial^4}{\partial x^2 \partial y^2} \bar{w}(x,y) \right) + 2 \left( \frac{\partial^2}{\partial y^2} D(x,y) \right) \left( \frac{\partial^2}{\partial y^2} \bar{w}(x,y) \right) \\
 & + 2 \left( \frac{\partial}{\partial y} D(x,y) \right) \left( \frac{\partial^3}{\partial y^3} \bar{w}(x,y) \right) \\
 & \left. + \left( \frac{\partial^2}{\partial y^2} D(x,y) \right) \nu \left( \frac{\partial^2}{\partial x^2} \bar{w}(x,y) \right) \right) \bar{w}(x,y) dx dy. \tag{18}
 \end{aligned}$$

Here  $h$  stands for thickness of the coating structure in the form of a shallow shell,  $\nu$  is the Poisson's ratio,

$A, B$ —indeterminants of the Bubnov-Galerkin method,

$Z_x, Z_y$  are the V.Z. Vlasov beam functions.

Since the structures under consideration can be attributed to thin shallow shells (the thickness is much less than the plan dimensions), in most cases it becomes necessary to check the structure for stability. The critical load factor for shallow shells on an elastic foundation can be represented by the equation:

$$p_{cr} = \frac{2}{27} \frac{1}{C_1^2} \left[ (C_1^2 - 3C_1 C_3)^{3/2} + C_2 \left( C_2^2 - \frac{9}{2} C_1 C_3 \right) \right]. \tag{19}$$

The values obtained using the presented method were compared with the results of other authors. The results of the solution showed good convergence with the values of the authors using other numerical methods [19]. When calculating by the finite element method, the result strongly depended on the number of finite elements used in the model.

### 3 Results and Discussion

The presented method for determining the stresses and critical load in coatings in the form of shallow shells with skylights makes it possible to study the influence of various factors on the stress–strain state of structures, which is not always possible using methods based on the finite element method.

For example, we considered the construction of a coating in the form of a shell on a square plan with a ratio of thickness to size in plan  $h/a = 1/10$ . Figure 4 shows a decrease in the value of the critical load of a thin-walled coating structure, determined by formula (19), with an increase in the parameter  $m$ , i.e. displacement of the hole from the center to the edge of the structure.

The figure clearly illustrates the decrease in the strength characteristics of shells as the skylight approaches the support zone and the possibility of using the above equations to determine the stress–strain state in them.

Figure 5 shows the change in critical load depending on the size of the skylight located in the center  $\eta$ .

The graphs show the possibility of using the presented numerical technique for determining the stress–strain state of structures in the form of shallow shells to analyze the influence of various cutout parameters (location, size, shape of the hole edges) and structure dimensions (thickness, structure shape, lifting boom) on the studied characteristics.

The technique for determining the stress–strain state of structures in the form of shallow shells with cutouts makes it possible to conduct research and evaluate the bearing capacity of a structure based on design conditions.

The representation of Eq. (19) in a dimensionless form is convenient for obtaining dependencies and analyzing the changes introduced without reference to specific dimensions.

**Fig.4** Influence of the location of the skylight on the value of the critical load

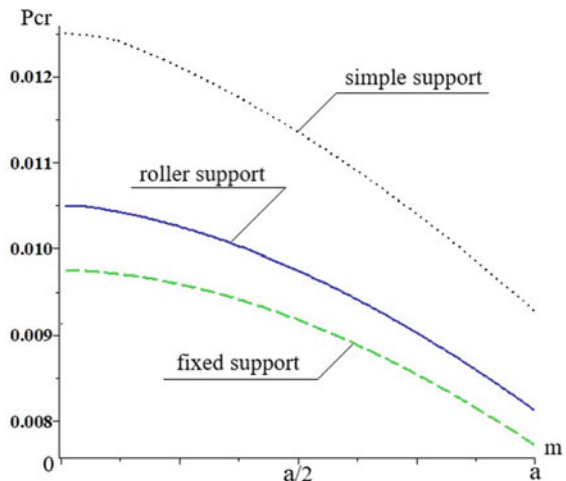
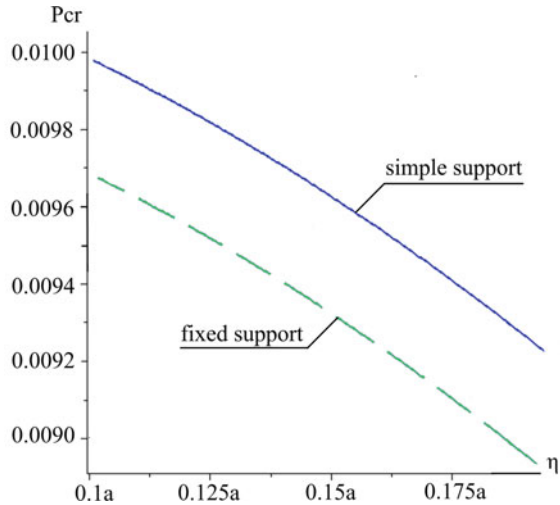


**Fig. 5** Dependence of the critical load on the size of the skylight in the center of the shell



Setting the function of the middle surface  $F$ , which is included in the system (1) in the form of a transfer surface [23], made it possible to study the effect of a skylight on structures of various shapes with the same dimensions in plan and lifting boom. For structures in the form of shallow shells with a generatrix in the form located between the spherical and chain functions, the influence of defects on the value of the critical load is manifested to a lesser extent.

The use of a changing shape and location of the cutout (Fig. 3) allows us to model a skylight that is as close as possible to the design requirements.

Graph 4 shows the effect of notch placement on the critical load value, as the most important defect parameter after its value, the influence of which is obvious (Fig. 5). It allows us to evaluate the degree of reduction in the bearing capacity, depending on the approach of the cutout to the support zone. The analysis of these parameters, along with the characteristics of the structure shape and thickness distribution along the generatrix, makes it possible to achieve the best values of the critical load for given design parameters. It is possible to reduce the value of the influence of the cutout by giving a shape close to optimal at the design stage of the structure or by setting a rational change in the thickness of the structure along its generatrix [20, 21].

## 4 Conclusion

The proposed design of canopies makes it possible to erect structures with a changing functional purpose. The presented technique can be used to determine and study the stress-strain state of structures in the form of shallow shells, taking into account the geometric nonlinearity of work in the presence of cutouts in them. The constructed graphs of the dependence of the critical load on various parameters made it possible

to evaluate the operation of structures, taking into account changes in various factors of skylights. The use of varying characteristics of cuts allows you to get results that are close to real conditions.

## References

1. Dushkevich H (2017) The role of the high-span shell forms in architecture of public buildings. *Archit Mod Inf Technol* 4(41):163–178
2. Ivanov VN, Krivoshapko SN. Analytical methods for analysis of shells of non-canonical form. RUDN University, 540 pp
3. Coman CD (2022) Self-weight buckling of thin elastic shells: the case of a spherical equatorial segment. *Z Angew Math Phys* 73:228. <https://doi.org/10.1007/s00033-022-01858-x>
4. Pavlysh VN, Storozhev SV, Nombre SB (2020) Study of fuzzy models of stability and resonant vibrations, closed spherical and ellipsoidal shells. *J Theor Appl Mech* 3:32–42
5. Marchuk AV, Shevchuk LO (2022) Free and forced vibrations of functionally graded shallow shells based on the 3D elasticity theory. *Acta Mech* 233(11): 4729–4746. <https://doi.org/10.1007/s00707-022-03346-9>
6. Sofiyev AH, Turan F (2021) On the nonlinear vibration of heterogenous orthotropic shallow shells in the framework of the shear deformation shell theory. *Thin-Walled Struct* 161:107181. <https://doi.org/10.1016/j.tws.2020.107181>
7. Krivoshapko SN, Mathieu G-O (2013) Geometry & strength of a shell of velaroidal type on annulus plan with two families of sinusoids. *Int J. Soft Comput Eng* 3(3):71–73
8. Aleshina OO, Ivanov VN, Cajamarca-Zuniga D (2021) Stress state analysis of an equal slope shell under uniformly distributed tangential load by different methods. *Struct Mech Eng Constr Build* 17(1):51–62. <https://doi.org/10.22363/1815-5235-2021-17-1-51-62>
9. Quan TQ, Cuon NH, Duc ND (2019) Nonlinear buckling and post-buckling of eccentrically oblique stiffened sandwich functionally graded double curved shallow shells. *Aerosp Sci Technol* 90:169–180. <https://doi.org/10.1016/j.ast.2019.04.037>
10. Huang S, Qiao P (2020) A new semi-analytical method for nonlinear stability analysis of stiffened laminated composite doubly-curved shallow shells. *Compos Struct* 251:112526. <https://doi.org/10.1016/j.compstruct.2020.112526>
11. Trushin S, Zhavoronok S (2002) Nonlinear analysis of multilayered composite shells using finite difference energy method. In: *Space structures 5 proceedings of the fifth international conference on space structures, held at the University of Surrey*, pp 1527–1533
12. Qin Z, Shengnan Z, Xuejia P, Safaei B, Chua F (2019) A unified solution for vibration analysis of laminated functionally graded shallow shells reinforced by graphene with general boundary conditions. *Int J Mech Sci* 170:105341. <https://doi.org/10.1016/j.ijmecsci.2019.105341>
13. Wang J, Li ZL, Wei Yu (2019) Structural similitude for the geometric nonlinear buckling of stiffened orthotropic shallow spherical shells by energy approach. *Thin-Walled Struct* 138:430–457. <https://doi.org/10.1016/j.tws.2018.02.006>
14. Bondarenko VM, Kolchunov VI, Klyueva NV (2007) Once again about constructive safety and survivability of buildings. *RAACS. Anniversary issue for the 15th anniversary of RAACS. Bull Dep Build Sci* 11:81–86
15. Geniev GA, Pyatikrestovsky KP (2000) *Issues of long-term dynamic strength of anisotropic structural materials*. V.A. Kucherenko Central Research Institute of Building Structures, Moscow, p 38
16. Mathieu G-O, Farhan IT (2016) Using FGM for cyclic shell structures. *Struct Mech Eng Constr Build* 4:14–20
17. Andreev V, Barmenkova E, Potekhin I (2016) Way of optimization of stress state of elements of concrete structures. *Procedia Eng* 153–169:37–44. <https://doi.org/10.1016/j.proeng.2016.08.077>



18. Stupishin LY, Kolesnikov AG, Nikitin KE (2017) Variable form forming investigation for flexible shallow shells on circular base. *Asian J Civ Eng* 18(2):163–171
19. Straughan W (1980) Analysis of plates on elastic foundations. Texas Tech University, Texas, p 125
20. Stupishin L, Kolesnikov A, Tolmacheva T (2017) Analysis of flexible layered shallow shells on elastic foundation. *IOP Conf Ser: Mater Sci Eng* 201(1):012018. <https://doi.org/10.1088/1757-899X/201/1/012018>
21. Serpik IN, Tarasova NV (2020) Optimization of steel trusses with a choice of multi-stage prestressing conditions. *Mag Civ Eng* 5(97):9705. <https://doi.org/10.18720/MCE.97.5>

# The Influence of Operational Factors on the Thermal Conductivity of Polystyrene Foam Boards



Pavel Monastyrev , Oleg Evdokimtsev , and Mikhail Loktionov 

**Abstract** The influence of operational factors on the thermal conductivity coefficient of polystyrene foam boards is investigated. In the study the initial density, humidity, the number of cycles of alternating freezing-thawing of polystyrene foam boards and the amplitude of the transition temperature through zero were taken as operational factors. To describe the response surface a four-factor laboratory experiment was conducted according to the second-order plan:

$$Y = (X_1, X_2, X_3, X_4) \quad (1)$$

At the same time a composite three-level symmetrical plan was used as it has a sufficiently high efficiency according to the main statistical criteria and includes 24 experiments. Based on the results of the laboratory experiment a regression model was constructed for further in-depth analysis which resulted in the conclusion about the influence of the investigated operational factors on thermal conductivity of polystyrene foam boards.

**Keywords** Polystyrene foam boards · Operational impacts · Coefficient of thermal conductivity

---

P. Monastyrev · O. Evdokimtsev  
Tambov State Technical University, Sovetskaya street. 106/5, 392000 Tambov, Russia  
e-mail: [monastyrev68@mail.ru](mailto:monastyrev68@mail.ru)

O. Evdokimtsev  
e-mail: [evdokimcev.ov@mail.tstu.ru](mailto:evdokimcev.ov@mail.tstu.ru)

M. Loktionov (✉)  
Southwest State University, 50 let Oktyabrya street. 94, 305040 Kursk, Russia  
e-mail: [mt-50@yandex.ru](mailto:mt-50@yandex.ru)

## 1 Introduction

Multi-year experience in the use of exterior walls made from homogeneous materials allowed us to evaluate their service life and evaluate the rate of frequency between major and ongoing repairs. However, the implementation of energy-saving policy in the field of construction has caused the emergence of new structural and technological solutions for exterior walls which have turned from single-layer structures into multi-layer ones consisting of materials with different strength, density, thermal conductivity, vapor permeability, etc. [1, 2]. The use of materials with various thermophysical properties in enclosing structures has an impact on the temperature and humidity regime of external walls, which in its turn affects the service life of the enclosure and its operational qualities [3–6].

From the point of view of operational reliability the construction of a multilayer wall can be represented as a complex system that from the point of view of the functional relationship of its elements, can be represented as a system comprised by the load-bearing part of the wall—thermal insulation layer—protective and decorative layer.

This system should ensure the temperature and humidity conditions and comfort in the premises, the performance of the wall within the specified regulatory limits, its decorative and protective functions.

A multilayer wall consists of elements connected in series, the failure of which is determined by the failure of the weakest link [5, 6]. The load-bearing part of the wall is designed to be nonrecoverable in almost all cases. The probability of trouble-free operation during a given service life can be taken as the safety in failure indicator. In such situation the thermal insulation material and protective decorative layer can be considered the elements that determine the reliability of the system as a whole. In this article we will focus on the thermal insulation layer that is typically made of mineral wool or expanded polystyrene boards.

The main operational indicator of thermal insulation boards in the walls is their ability to provide heat-protective qualities for a certain time period. Therefore it is possible to take the time constancy of their thermal conductivity coefficient as the main criterion for the operational resistance of thermal insulation boards. In the works [5, 6] the influence of operational factors on thermal and physical-mechanical properties of mineral wool slabs was studied, however, there were no comprehensive studies of the influence of operational factors on the thermal conductivity coefficient of expanded polystyrene boards. In this regard, the article presents a study of the change in the thermal conductivity coefficient of polystyrene boards depending on the initial density, humidity, the number of polystyrene board alternating freezing-thawing cycles and the amplitude of the transition temperature through zero.

## 2 Materials and Methods

An experimental study of the change in the thermal conductivity coefficient  $\lambda$ , W/(m·°C) (function  $Y_\lambda$ ) of polystyrene foam board samples was carried out considering the following factors:

- initial density of polystyrene foam boards  $\gamma$  ( $X_1$ ) kg/m<sup>3</sup>;
- humidity of polystyrene foam boards  $\omega$  ( $X_2$ ) %;
- the number of alternating freezing-thawing cycles of polystyrene foam boards  $n$  ( $X_3$ ), cycles;
- amplitudes of the transition temperature through zero °C,  $A_0$  ( $X_4$ ).

Polystyrene foam plates of the “NOVOPLAST” company were used as the object of the study.

All factors in the study varied on three levels.

The variation limits of the first factor ( $X_1$ )—initial density were taken considering the product line of the manufacturer of expanded polystyrene boards, “NOVOPLAST” company, as well as their technical specifications and recommendations for the use in enclosing structures. Polystyrene foam boards with a declared density of 25, 35 и 50 kg/m<sup>3</sup> were selected for the study. Actual density of the samples was as follows: 15, 30, 40 kg/m<sup>3</sup>. In this regard the variation levels of factor  $X_1$  were as follows:

- 1—minimum value (15 kg/m<sup>3</sup>);
- 0—average value (30 kg/m<sup>3</sup>);
- +1—maximum value (40 kg/m<sup>3</sup>).

For the lower limit of variation (–1) of the second factor, the humidity value is taken as equal to 0%.

As an intermediate (0) limit of variation, the value of the sorption humidity of the polystyrene foam board is used, which was determined experimentally according to GOST 17177-94 [7] and was 20%.

The upper limit of variation (+1) of the second factor ( $X_2$ ), the moisture content of the samples, was taken based on the maximum value of water absorption of polystyrene foam boards. This value was determined experimentally according to GOST 17177-94 [7].

For the lower limit of variation (–1) of the third factor ( $X_3$ )—the number of freezing and thawing cycles of the experimental study, a value equal to 10 cycles was taken. As an intermediate (0) limit of variation, a value equal to 55 cycles was used. Accordingly, the upper limit (+1) of the variation of the fourth factor is 100 cycles.

As a fourth variation factor ( $X_4$ )—the doubled average value of the amplitude of outdoor temperature transition through 0 °C during the day was taken into consideration. In the experiment this value varied from 4 °C (lower level of variation) to 40 °C (upper level of variation) (Table 1). The lower level of variation was taken based on the possible assignment of the smallest amplitude and the upper one based on SP 131.13330.2012 [8].

**Table 1** The area of variation of factors and their coded values

Factor		-1	0	+1
1	Initial density of polystyrene foam boards $\gamma$ ( $X_1$ ) kg/m <sup>3</sup>	15	30	40
2	Humidity of polystyrene foam boards $\omega$ ( $X_2$ ), %	0	20	40
3	Number of cycles of alternating freezing-thawing of polystyrene foam boards $n$ ( $X_3$ ), cycles	10	55	100
4	Amplitude of the transition temperature through 0 °C in the layer of thermal insulation material $A_0$ ( $X_4$ ), °C	4	22	40

The areas of variation of factors and their coded values are shown in Table 1.

Response values were supposed to be obtained on the basis of a laboratory experiment. To do this an experiment was carried out according to a special plan.

To describe the response surface a four-factor laboratory experiment was conducted according to a second-order plan:

$$Y = (X_1, X_2, X_3, X_4) \quad (2)$$

At the same time we used a composite three-level symmetrical plan that has a sufficiently high efficiency according to the main statistical criteria and includes 24 trials. The experimental plan is shown in Table 2.

To describe the required dependencies, the following model was built:

$$\begin{aligned} \hat{Y} = & b_0 + b_1X_1 + b_2X_2 + b_3X_3 + b_4X_4 + b_5X_1X_2 + b_6X_1X_3 + \\ & + b_7X_1X_4 + b_8X_2X_3 + b_9X_2X_4 + b_{10}X_3X_4 + b_{11}X_1^2 + b_{12}X_2^2 + \\ & + b_{13}X_3^2 + b_{14}X_4^2 \end{aligned} \quad (3)$$

When implementing the experimental plan, the variants of varying factors were randomized. To do this, the sequence of tests was determined by using the table of uniformly distributed random variables.

We tested the “NOVOPLAST” polystyrene foam board samples.

To run the tests for the changes in the thermal conductivity coefficient, the samples of polystyrene foam boards were cut out with a size of (a)100 × (b)100 × (h)25 mm. The sample sizes were selected based on the possibility of measuring the thermal conductivity coefficient and the dimensions of the testing equipment.

Samples of polystyrene foam boards with a minimum humidity value were dried to a constant weight according to GOST 17177-94 [26]. The sample was considered prepared when it reached its constant weight, i.e. the mass loss after repeated drying for 0.5 h should not exceed 0.1%.

**Table 2** Planning matrix and results of the experiment to determine the coefficient of thermal conductivity

N <sup>o</sup> exp	$\gamma (X_1)$ kg/m <sup>3</sup>	$\omega (X_2)$ , %	$n (X_3)$ , cycles	$A_0 (X_4)$ , °C	$Y_1$	$Y_2$	$Y_3$	$\bar{Y}_\lambda$	$S_i^2$
1	15(-1)	0(-1)	10(-1)	4(-1)	0.038	0.039	0.037	0.038	0.0000015
2	40(+1)	0(-1)	10(-1)	4(-1)	0.032	0.031	0.033	0.032	0.0000015
3	15(-1)	40(+1)	10(-1)	4(-1)	0.042	0.041	0.043	0.042	0.0000015
4	40(+1)	40(+1)	10(-1)	4(-1)	0.035	0.036	0.037	0.036	0.0000001
5	15(-1)	0(-1)	100(+1)	4(-1)	0.04	0.039	0.041	0.040	0.0000015
6	40(+1)	0(-1)	100(+1)	4(-1)	0.041	0.042	0.04	0.041	0.0000015
7	15(-1)	40(+1)	100(+1)	4(-1)	0.043	0.044	0.045	0.044	0.0000001
8	40(+1)	40(+1)	100(+1)	4(-1)	0.046	0.041	0.043	0.043	0.0000145
9	15(-1)	0(-1)	10(-1)	40(+1)	0.04	0.041	0.042	0.041	0.0000001
10	40(+1)	0(-1)	10(-1)	40(+1)	0.042	0.041	0.043	0.042	0.0000015
11	15(-1)	40(+1)	10(-1)	40(+1)	0.044	0.04	0.041	0.042	0.0000105
12	40(+1)	40(+1)	10(-1)	40(+1)	0.045	0.043	0.044	0.044	0.0000025
13	15(-1)	0(-1)	100(+1)	40(+1)	0.043	0.044	0.045	0.044	0.0000001
14	40(+1)	0(-1)	100(+1)	40(+1)	0.039	0.04	0.041	0.040	0.0000001
15	15(-1)	40(+1)	100(+1)	40(+1)	0.046	0.044	0.045	0.045	0.0000025
16	40(+1)	40(+1)	100(+1)	40(+1)	0.045	0.045	0.043	0.043	0.0000002
17	15(-1)	20(0)	55(0)	22(0)	0.041	0.04	0.042	0.041	0.0000015
18	40(+1)	20(0)	55(0)	22(0)	0.041	0.039	0.043	0.041	0.0000006
19	30(0)	0(-1)	55(0)	22(0)	0.039	0.037	0.038	0.038	0.0000025
20	30(0)	40(+1)	55(0)	22(0)	0.038	0.039	0.037	0.037	0.0000025
21	30(0)	20(0)	10(-1)	22(0)	0.041	0.04	0.042	0.041	0.0000015
22	30(0)	20(0)	100(+1)	22(0)	0.042	0.04	0.044	0.042	0.0000006
23	30(0)	20(0)	55(0)	4(-1)	0.037	0.038	0.036	0.037	0.0000015
24	30(0)	20(0)	55(0)	40(+1)	0.038	0.037	0.039	0.038	0.0000015

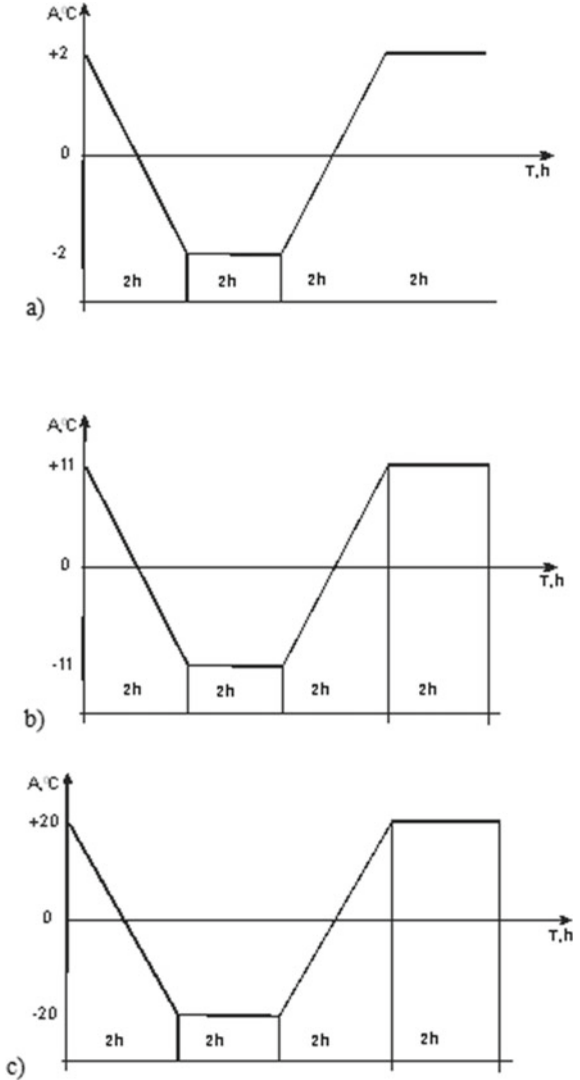
The samples with average and maximum humidity values were prepared according to GOST 17177-94 [7].

The samples of polystyrene foam boards were subjected to cyclic temperature exposure in the climatic chamber THV-80.

Freezing and thawing of samples was carried out according to the algorithm proposed in the work of Alexandrovsky [9]. The temperature–time change pattern is shown in Fig. 1.

The coefficient of thermal conductivity was measured according to GOST 7076-99 [10] by means of ETP MG4 (100) device.

**Fig. 1** The course of temperature change from time to amplitude: **a** 4 °C; **b** 22 °C; **c** 40 °C



### 3 Results and Discussions

The planning matrix and the results of the experiment made to determine the thermal conductivity coefficient are shown in Table 2.

Based on the results of the experiment (Table 2), a regression model is constructed:

$$\hat{Y}_\lambda = 0,0389 - 0,0006X_1 + 0,0014X_2 + 0,0010X_3 + 0,0012X_4 + 0,0009X_1X_4 + 0,0014X_3X_4 + 0,0026X_1^2 - 0,0014X_2^2 + 0,0026X_3^2 - 0,0014X_4^2. \quad (4)$$

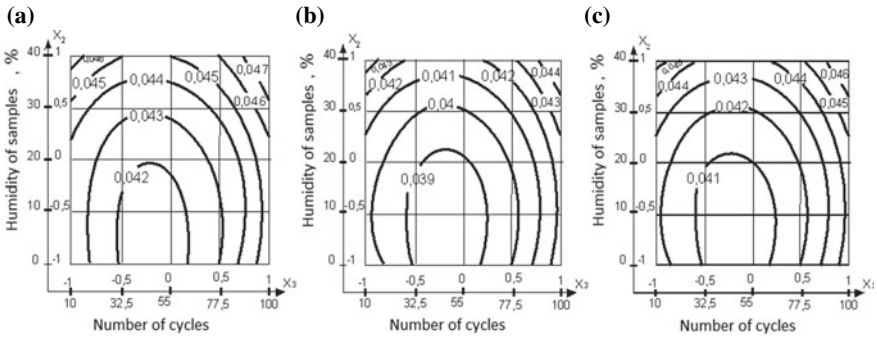
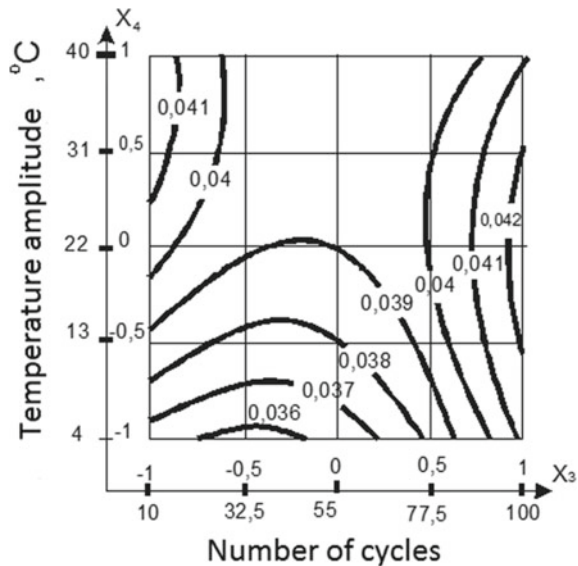


**Fig. 2** Change in the coefficient of thermal conductivity  $\lambda$ , W/(m °C) depending on the humidity of polystyrene foam boards  $\omega$ , % (factor  $X_2$ ) and the number of cycles of alternating freezing-thawing  $n$ , cycles (factor  $X_3$ ) with the density of polystyrene foam boards: **a**  $-1$  (15 kg/m<sup>3</sup>); **b**  $0$  (30 kg/m<sup>3</sup>); **c**  $+1$  (40 kg/m<sup>3</sup>) and the amplitude of the temperature 22 °C

**Fig. 3** Change in the thermal conductivity coefficient of expanded  $\lambda$ , W/ (m·°C) polystyrene boards depending on the number of cycles of alternating freezing-thawing of expanded polystyrene boards  $n$ , cycles (factor  $X_3$ ) and the amplitudes of the transition temperature through zero  $A_0$ , °C (factor  $X_4$ ) at the density of polystyrene foam boards 30 kg/m<sup>3</sup> and humidity 20%



A graphical interpretation of the experimental results is shown in Figs. 2 and 3.

### 4 Conclusions

The interpretation of the results of the study is based on the analysis of the regression equation. First of all, we revealed the influence of individual factors.



The strongest influence on the thermal conductivity coefficient of expanded polystyrene boards is exerted by the factor  $X_2$ —the humidity of the thermal insulation material. Positive linear and negative quadratic effects of this factor have been revealed, which indicates an increase in the thermal conductivity coefficient of expanded polystyrene boards with a change in their humidity from 0 to 40%. A slight increase of  $\hat{Y}_\lambda$ , up to 8.3% from 0.036 to 0.039 W/m·°C is observed when humidity changes from 0 to 20%. In the range from 20 to 40%, the thermal conductivity coefficient of polystyrene foam boards remains at the same level (0.039 W/m·°C).

The factor  $X_4$ —the amplitude of the transition temperature through 0 °C in a layer of thermal insulation material - took the second place in terms of the influence on the thermal conductivity coefficient of polystyrene foam boards. Positive linear and negative quadratic effects of this factor have been revealed, which indicates an increase in the thermal conductivity coefficient of expanded polystyrene boards with a change in amplitude from 4 to 40 °C. An increase of  $\hat{Y}_\lambda$ , up to 8.3% (from 0,036 to 0,039 W/m·°C) is observed when the amplitude changes from 4 to 22 °C. In the range from 22 to 40°C the thermal conductivity coefficient of polystyrene foam boards remains at the same level (0,039 W/m·°C). The nature and strength of the influence of factor  $X_4$  is slightly influenced by its interaction with factors  $X_1$  (the initial density of expanded polystyrene boards),  $X_3$  (the number of cycles of alternating freezing-thawing of expanded polystyrene boards).

Factor  $X_3$  (the number of cycles of alternating freezing-thawing of expanded polystyrene boards) was in third place in terms of the strength of influence. Positive linear and quadratic effects of this factor have been revealed, which indicates an increase in thermal conductivity with an increase in freeze-thaw cycles from 10 to 100 cycles. However the change  $\hat{Y}_\lambda$  depending on this factor is uneven. With a change in  $X_3$  from 10 to 55 cycles  $\hat{Y}_\lambda$  it decreases by 4.8% (from 0.041 to 0.039 W/m·°C), at the same time in the interval from 55 to 100 cycle is observed an increase  $\hat{Y}_\lambda$ , of 10,2% (from 0.039 to 0.043 W/m·°C). The nature and strength of the influence of factor  $X_3$  is slightly influenced by its interaction with factor  $X_4$  (the amplitude of the transition temperature through 0 °C in a layer of thermal insulation material).

In the last place in terms of the strength of the influence on the thermal conductivity coefficient of expanded polystyrene boards was the factor  $X_1$ —the density of the thermal insulation material. Negative linear and positive quadratic effects of this factor have been revealed, which indicates a decrease in the thermal conductivity coefficient of expanded polystyrene boards with a change in their density from 15 to 40 kg/m<sup>3</sup>. However, the change  $\hat{Y}_\lambda$  depending on this factor is uneven. A decrease of  $\hat{Y}_\lambda$ , up to 7,1% (from 0.042 to 0,039 W/(m·°C)) is observed when the density of the thermal insulation material changes from 15 to 30 kg/m<sup>3</sup>. In the range from 30 to 40 kg/m<sup>3</sup> here is an increase in the thermal conductivity coefficient of expanded polystyrene boards (from 0.039 to 0,041 W/(m·°C)) by 5,1%. The nature and strength of the influence of factor  $X_1$  is slightly influenced by its interaction with factor  $X_4$  (the amplitude of the transition temperature through 0 °C in a layer of thermal insulation material).

A graphical interpretation of the experimental results is shown in Figs. 2 and 3. From them it can be seen that when the number of cycles of alternating freezing-thawing of expanded polystyrene plates changes, the thermal conductivity coefficient decreases at the first stage, and increases at the second. The turning point of the dynamics of the change in the coefficient of thermal conductivity, regardless of the density of the samples under study, is 50 freeze-thaw cycles. It was found that the samples of expanded polystyrene boards with a density of  $30 \text{ kg/m}^3$  have lower thermal conductivity compared to expanded polystyrene with a density of 15 and  $40 \text{ kg/m}^3$ .

The influence of humidity of polystyrene foam boards has the same effect on the coefficient of thermal conductivity of thermal insulation material of different densities. Namely, in samples of any density when their humidity changes from 0 to 40%, the thermal conductivity coefficient changes by approximately  $0.002 \text{ W/(m}\cdot\text{°C)}$ .

The conducted research has shown that operational factors can have a significant impact on the change in the thermal conductivity coefficient of expanded polystyrene boards, which must necessarily be taken into account when designing, building and operating external enclosing structures.

## References

1. Akimov PA, Chernyshov EM, Monastyrev PV (2017) Research and development of the Russian Academy of Architecture and Construction Sciences: state, directions and prospects of development. In: 4th International scientific and practical conference "sustainable development of the region: architecture, construction, transport". Tambov, TSTU, Publishing house Pershina R.V., pp 12–28
2. Dubrakova KO, Monastyrev PV, Klychnikov RY, Yezersky VA (2019) Optimization of thermal modernization of a group of buildings using simulation modeling. *J Appl Eng Sci* 17(2):192–197
3. Erofeev AV, Yartsev VP, Monastyrev PV (2017) Decorative and protective plates for facade decoration of buildings. *Izvestiya Vysshikh Uchebnykh Zavedenii, Seriya Tekhnologiya Tekstil'noi Promyshlennosti* 1:101–104
4. Mamontov SA, Yartsev VP, Monastyrev PV (2017) An artificial and natural aging of wood-fiber composite. *Izvestiya Vysshikh Uchebnykh Zavedenii, Seriya Tekhnologiya Tekstil'noi Promyshlennosti* 1:95–100
5. Gusev BV, Yezersky VA, Monastyrev PV (2005) Heat-conductivity of mineral wool slabs when subjected to operation effects. *Promyshlennoe i Grazhdanskoe Stroitel'stvo* 1:48–49
6. Gusev BV, Ezerskiy VA, Monastyrev PV (2004) Change in the linear dimensions of mineral wool slabs subjected to operation effects. *Promyshlennoe i Grazhdanskoe Stroitel'stvo* 8:32–24
7. GOST 17177-94 (20001) Materials and products of thermal insulation construction. Test methods. M: IPK Publishing House of Standards
8. SP 131.13330.2012 (2012) Construction climatology
9. Alexandrovsky SV (2003) Durability of external enclosing structures. M NIISF RAASN 9
10. GOST 7076-99 (2000) Construction materials and products. A method for determining thermal conductivity and thermal resistance in a stationary thermal regime

# Comparative Analysis of Enclosing Facade Structures in Terms of Energy Efficiency



Anastasiia Grokhovskaia  and Daria Nemova 

**Abstract** The purpose of the study is to evaluate the energy efficiency of the structure depending on the various options of the facade enclosing system. The variability of the facade system consists in considering several types of thermal insulation material. The following materials are selected for comparison: mineral wool, glass wool, and XPS insulation. The comparative analysis is based on the consideration of the total heat loss of the building, if the remaining parameters of the object remain unchanged, as well as on the basis of separate data on carbon emissions for each material under consideration. Based on the results obtained, conclusions are drawn about a more energy-efficient design with minimal impact on the environment.

**Keywords** Energy efficiency · Carbon footprint · Life cycle assessment · Thermal insulation material · Thermal resistance · Thermal conductivity · Transmission losses

## 1 Introduction

Nowadays the issue of ecology is one of the most discussed and demanded in all spheres of human activity. Any activity of the Earth's population has a negative impact on natural conditions. The consequence of which is global climate change [1, 2], depletion of natural resources. Of course, there is a natural-time factor in changing the climatic parameters of the environment, but the human aspect accelerates and worsens the situation [3]. Another important problem of our time is the greenhouse effect [4, 5], which is more related to the activity of people [6–8].

The construction industry is no exception. According to recent studies, the construction sector occupies one of the primary places in terms of energy consumption, namely, the share of consumption is approximately 40%, which also corresponds

---

A. Grokhovskaia (✉) · D. Nemova  
Institute of Civil Engineering, Peter the Great St. Petersburg Polytechnic University,  
Polytechnicheskaya, 29, 195251 Saint Petersburg, Russia  
e-mail: [grohovskaya.anastasia@yandex.ru](mailto:grohovskaya.anastasia@yandex.ru)

to the share of CO<sub>2</sub> gas emissions [9, 10]. Of the exact 39% of emissions, 28% is accounted for by energy consumption during the life cycle of the facility and 11% of emissions are produced by construction materials [11]. It is also worth noting that according to the forecasts made by experts, energy consumption is expected to increase by up to 71% in the period up to 2030 [12].

Thus, the greatest popularity and demand in modern construction is the concept of energy-efficient construction [13–17] of energy-efficient structures and such science as construction ecology, the main tasks of which more closely echo the goals set to minimize the impact of construction activities on the environment. Therefore, the following aspects can be distinguished [18–20]:

1. Rational consumption of natural resources
2. Increasing the volume of secondary use;
3. Forecasting the negative impact at the design stages and taking measures to reduce it at the beginning of the process.

The main rule that distinguishes an energy-efficient building from other structures is the ability to produce more energy compared to the volume consumed, as well as the amount of energy spent during its construction [21, 22].

However, as mentioned earlier, the energy efficiency assessment of a building is a complex process that should take into account all stages of the life cycle of a structure.

The life cycle of a construction object is a period of time from the moment of production of materials for the construction of a particular structure to the moment of its deconstruction and disposal of the remaining materials [23–29]. With the use of information technology systems that greatly simplify the monitoring of all systems, this approach allows you to track data about the construction object throughout the entire process of its existence [30, 31], which also significantly affects the economic aspect of construction activity [32, 33].

In accordance with the European standard EN 15978 (2011), the following stages of the life cycle of an object are distinguished, during which greenhouse gases are released:

Stage A:

Stage “Product” (A1–A3).

Describes the complete production process of materials used for construction.

Stage “Construction” (A4–A5).

This stage includes the process of transporting manufactured materials between the manufacturer and the construction site. In addition, this stage takes into account the installation carried out on the construction site.

**Stage B (B1–B7):**

Describes the stage of the project life cycle during which its operation is performed. Thus, this stage describes direct greenhouse gas emissions due to the electricity consumed by the facility.

**Stage C “End of Life” (C1–C4):**

Stage C describes the end of the facility’s operating time. This stage includes indicators related to the transportation of recycled raw materials, the process of recycling, recycling and reuse.

**Stage D:**

This stage, similar to stages A and C, characterizes indirect greenhouse gas emissions. The final stage of the construction life cycle assessment takes into account aspects related to the estimated potential for reuse of materials.

In accordance with the long-term experience of using these stages of the object’s life cycle, statistics show that the most significant stage is the “Product” stage, that is, Stage A. Despite the fact that greenhouse emissions are indirect at the pre-operational stage, their share is significant. In addition, the change of construction solutions in the direction of reducing the greenhouse effect, at this stage is the easiest compared to the subsequent stages. This fact is the basis for an active study of the stages A1–A5 of the project life cycle.

## **2 Materials and Methods**

This work presents a comparative analysis of various variants of the enclosing structure of the facade system of the building was carried out from the point of view of the energy efficiency of the object. Insulation materials were also evaluated at stages A1–A3 of the facility’s life cycle.

For a more comprehensive assessment, the building of a high-rise business center was modeled. Based on immutable designed data, the influence of variability of thermal insulation materials on the energy efficiency of the structure was analyzed.

Autodesk Revit 2021 software was chosen as the main software package for modeling the structure. In this program, an architectural model is developed, structural parameters are set and an analytical energy model of a structure based on a BIM model is created.

Figure 1 shows a 3D view of the design object. The basic information on the object, as well as the summary characteristics of the proposed construction site are presented in Tables 1 and 2, respectively.

**Fig. 1** 3D-view of the object**Table 1** The main characteristic of the design object

Characteristic	Value
Functional purpose	Office building
Height	45 m
Heated area	13991,7 m <sup>2</sup>
Heated volume	53168,46 m <sup>3</sup>
Address	Russia, Saint Petersburg
Estimated number of the stuff	1400

**Table 2** Climatic characteristics of the construction area

Characteristic	Value
Estimated outdoor air temperature for thermal protection design	-24 °C
Average outdoor temperature during the heating period	-1,3 °C
Duration of the heating period	213 day/year
Degree-day of the heating period	4110,9 °C * day/year
Estimated internal air temperature for thermal protection design	18 °C
Estimated temperature of the technical field	8 °C

The following options were selected as the considered options for the enclosing structures of the facade system—Table 3.

The main characteristic affecting the energy consumption of a building is the thermal resistance of the structure. The reduced value is calculated by the following formula (1):

$$R_o^r = r * \left( \frac{1}{\alpha_{int}} + \sum \frac{\delta_{\Pi}}{\alpha_{\Pi}} + \frac{1}{\alpha_{ext}} \right) \tag{1}$$

$r$ —the coefficient of thermal uniformity of the enclosing structure, taking into account the influence of joints, slopes of openings, framing ribs, flexible connections and other heat-conducting inclusions,  $r = 0,65$

$\alpha_{int}$ —the coefficient of heat transfer of the inner surface of the enclosing structures for cold period conditions,  $\alpha_{int} = 8,7W/(m^2 * ^\circ C)$ .

**Table 3** Variants of enclosing structures

Nº	Description of the variant (composition of the structure)	Figures	Resistivity
1	Fiber cement slabs—20 mm Mineral wool—70 mm Aerated concrete on cement binder (400 kg/m³)—300 mm	Figure 2	2,54 m² * °C/W
2	Fiber cement slabs—20 mm XPS isolation—70 mm Aerated concrete on cement binder (400 kg/m³)—300 mm	Figure 3	2,99 m² * °C/W
3	Fiber cement slabs—20 mm Glass wool—70 mm Aerated concrete on cement binder (400 kg/m³)—300 mm	Figure 4	2,95 m² * °C/W

**Fig. 2** Option №1:

- 1—Aerated concrete on cement binder (400 kg/m³);
- 2—Carrier subsystem;
- 3—Mineral wool;
- 4—Insulation dowel with steel/plastic nail;
- 5—Fiber cement slabs;
- 6—Professional all-season mounting foam

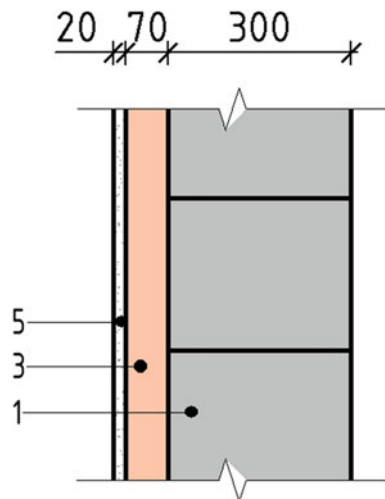


**Fig. 3** Option №2:  
 1—Aerated concrete on cement binder (400 kg/m<sup>3</sup>);  
 2—Carrier subsystem;  
 3—XPS insulation;  
 4—Insulation dowel with steel/plastic nail; 5—Fiber cement slabs;  
 6—Professional all-season mounting foam

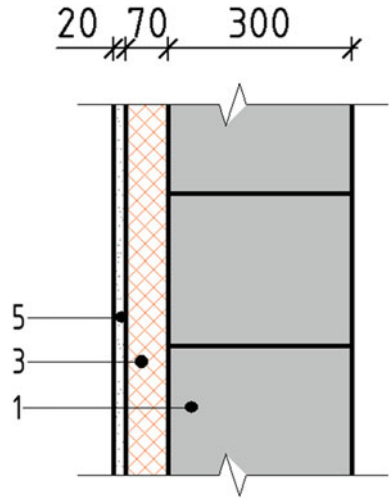
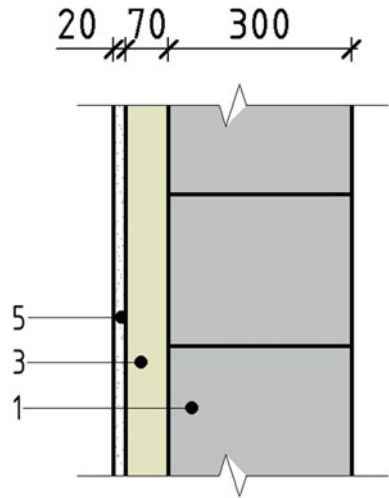


**Fig. 4** Option №3:  
 1—Aerated concrete on cement binder (400 kg/m<sup>3</sup>);  
 2—Carrier subsystem;  
 3—Glass wool;  
 4—Insulation dowel with steel/plastic nail; 5—Fiber cement slabs;  
 6—Professional all-season mounting foam



$\alpha_{ext}$ —the heat transfer coefficient of the outer surface, enclosing structures for cold period conditions,  $\alpha_{ext} = 12W/(m^2 * ^\circ C)$ .

$\delta$ —layer thickness, mm.

$\alpha_{\Pi}$ —thermal conductivity of the layer material,  $W/(m * ^\circ C)$ , the thermal conductivity of the materials under consideration is shown in Table 4.



**Table 4** Thermal conductivity of building materials

Nº	Material	The value of thermal conductivity, W/(m * °C)
1	Aerated concrete on cement binder (400 kg/m³)	0,15
2	XPS insulation	0,029
3	Mineral wool	0,041
4	Glass wool	0,030

Based on the resistivity of the enclosing structure, the transmission coefficient of heat transfer of the building is calculated (2). This characteristic has a direct effect on the class of energy characteristics of the structure.

$$K_m^{tr} = \frac{\left( \frac{A_{wall}}{R_{wall}^r} + \frac{A_{window}}{R_{window}^r} + \frac{A_{door}}{R_{door}^r} + n * \frac{A_{fl}}{R_{fl}^r} + \frac{A_{roof}}{R_{roof}^r} \right)}{A_e^{sum}} \tag{2}$$

$A_X$ —square of the X construction;

$R_X^r$ —calculated values of the heat transfer resistances of the structure X;

$n$ —the coefficient taken depending on the position of the outer surface of the enclosing structure X in relation to the outside air.

### 3 Results and Discussion

In the course of the conducted studies for the same building, taking into account the various enclosing structures of the facade system, the transmission coefficients of the heat transfer of the building were determined, the data are presented in Table 5.

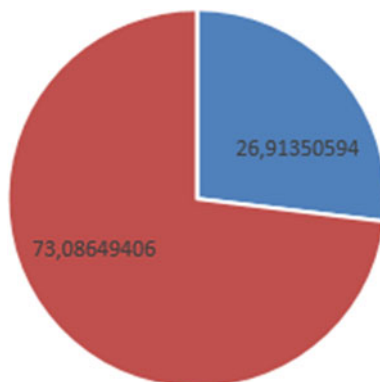
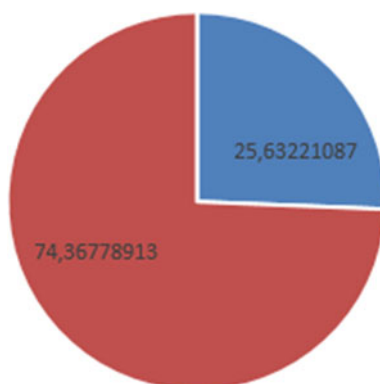
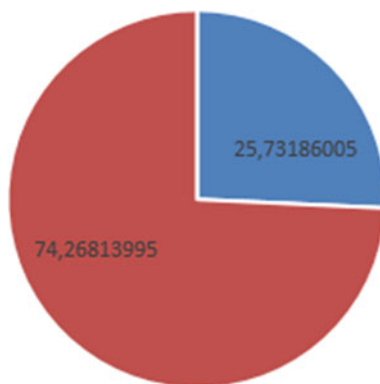
Figures 5, 6 and 7 show the distribution of transmission and ventilation losses for each variant of the enclosing structure, respectively.

The red area in the diagrams indicates transmission losses, while the blue area indicates ventilation losses.

Thermal energy losses were also determined for each structure. The percentage of data is presented in Table 6.

**Table 5** Transmission coefficients of building options

Option	Type of insulation	$K_m^{tr}$ , W/(m² * °C)
1	Mineral wool	0,418
2	XPS insulation	0,391
3	Glass wool	0,394

**Fig. 5** Option №1**Fig. 6** Option №2**Fig. 7** Option №3

**Table 6** Percentage of heat loss for design options

Option	Type of insulation	Percentage of heat loss (%)
1	Mineral wool	26,9
2	XPS insulation	25,6
3	Glass wool	25,7

**Table 7** The amount of CO<sub>2</sub>e according to the thermal insulation materials

Option	Type of insulation	Kg CO <sub>2</sub> e (A1–A3)
1	Mineral wool	12,23
2	XPS insulation	29,71
3	Glass wool	4,82

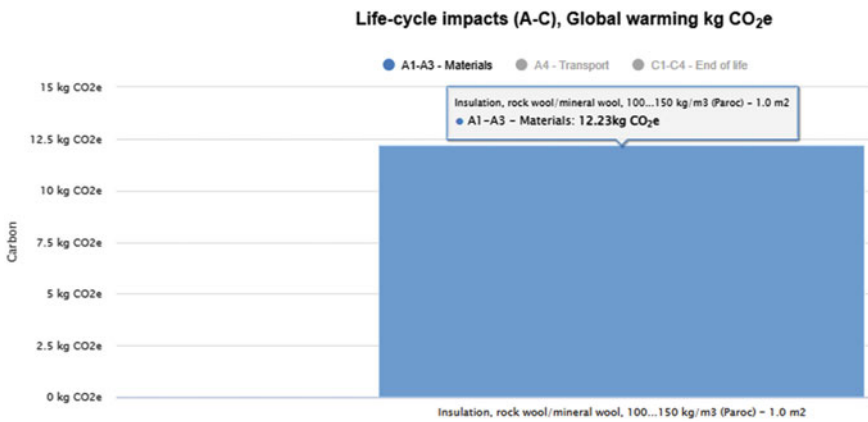


**Fig. 8** Mineral wool

The main difference between the facade structures under consideration is the type of material of the thermal insulation layer. That is why, with the help of the One Click LCA program, a comparative characteristic of these materials was carried out. Stages A1-A3 were taken as the main stages of the object’s life cycle for comparison. The data were obtained using the One Click LCA software package and are presented in Table 7 and Figs. 8, 9 and 10.

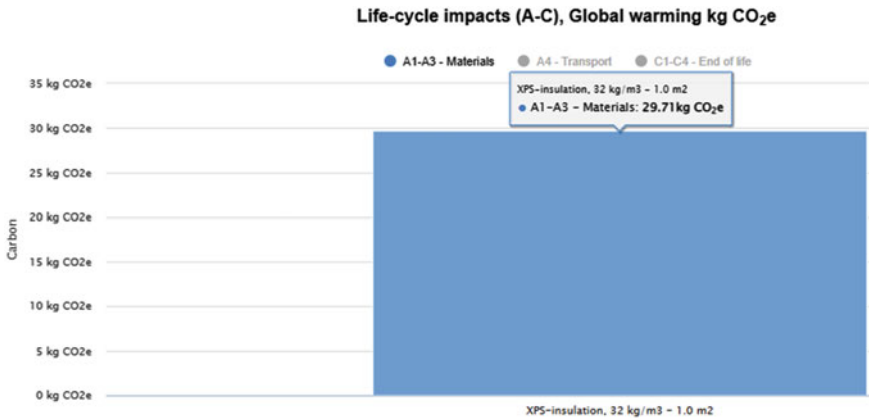


Fig. 9 XPS insulation

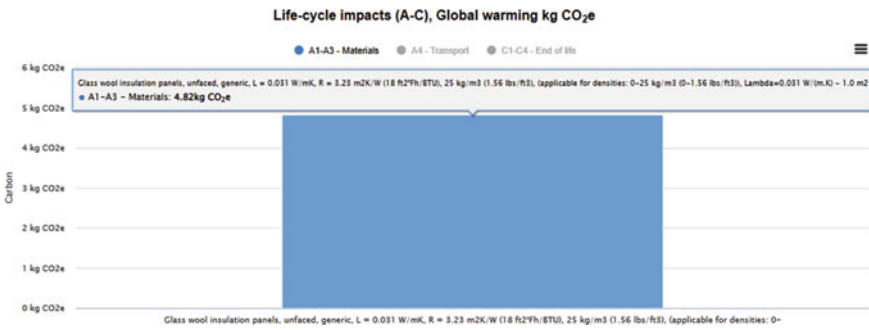


Fig. 10 Glass wool

## 4 Conclusion

After analyzing the results obtained, it can be concluded that:

1. The smallest percentage of transmission losses of the whole building, depending on the change in the insulation of the enclosing structure of the facade, has a building using XPS insulation.
2. At the stages of the life cycle of the A1–A3 XPS facility, insulation has the highest amount of emissions.
3. The smallest amount has a glass wool material, which assumes approximately the same amount of heat loss in the whole building.

The generalized data is presented in the diagram format in Fig. 11.

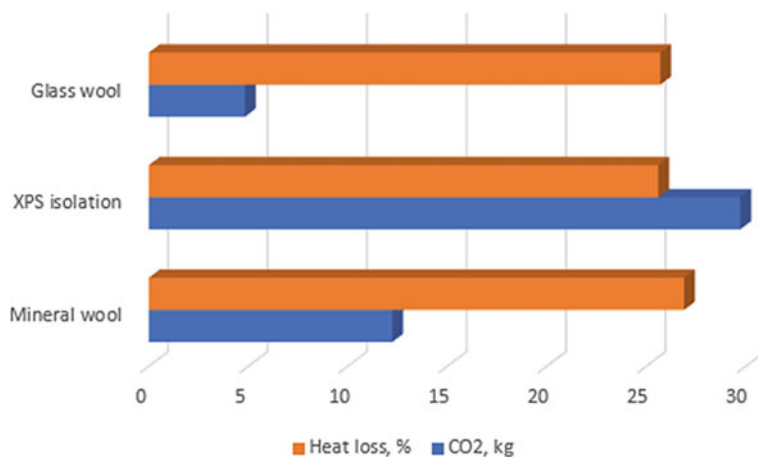


**Fig. 11** Generalized comparative data

**Acknowledgements** This work is supported by the Russian Science Foundation under grant 21-79-10283, date 29 July 2021, <https://rscf.ru/project/21-79-10283/>.

## References

1. Daurbekov AM, Daurbekov KM, Katsiev ZV (2017) The impact of new technologies in construction on the environment. In: Relevant lines of scientific research: development prospects, pp 226–228. Cheboksary, SCC “Interaktiv Plus”, LLC. <https://doi.org/10.21661/a-418>
2. Ruban DA, Serpova KI, Yashalova NN, Vasiltsov VS, Yakovleva EN (2018) Global climate changes as a risk factor for Russian economy: metodological issues. *Vestnik NSUEM* 3:10–25
3. Gruza GV, Rankova EY (2004) Detection of changes in climate state, climate variability, and climate extremity. *Russ Meteorol Hydrol* 4:50–66
4. Arutyunov VS (2001) Greenhouse effect: the problem of choosing a strategy. *Russ Chem J* 45(1):55–63
5. Romanov EV, Leletsky A, Labutin KA (2019) Greenhouse effect: causes, consequences, optimization methods. *Achiev Sci Educ* 8–1(49):27–28
6. Hinzman LD, Bettez ND, Bolton WR, Chapin FS, Dyurgerov MB, Fastie CL, Griffith B, Hollister RD, Hope A, Huntington HP, Jensen AM, Jia GJ, Jorgenson T, Kane DL, Klein DR, Kofinas G, Lynch AH, Lloyd AH, McGuire AD, Nelson FE, Oechel WC, Osterkamp TE, Racine CH, Romanovsky VE, Stone RS, Stow DA, Sturm M, Tweedie CE, Vourlitis GL, Walker MD, Walker D, Webber PJ, Welker JM, Winker KS, Yoshikawa K (2005) Evidence and implications of recent climate change in Northern Alaska and other Arctic regions. *Clim Change* 72(3):251–298. <https://doi.org/10.1007/S10584-005-5352-2>
7. Babkov-Esterkin AS (2011) International experience in reducing greenhouse gas emissions and their impurities in the Russian Federation. *Min Inf Anal Bull (Sci Tech J)* 10:131–135
8. Kudusov II (2019) Global warming and climate change: realities and impact on mankind. *Izvestiya Chechenskogo Gosudarstvennogo Universitetaechenskogo Gosudarstvennogo Universiteta* 3(15):74–81

9. Levada AV, Nemova DV (2021) Life cycle assessment of buildings based on BIM-models for green building. In: ISI science week: proceedings of the all-Russian conference in 3 parts. Part 1. St. Petersburg, pp 374–376
10. Suhendro B (2014) Toward green concrete for better sustainable environment. *Procedia Eng* 95:305–320
11. Bykau AA, Rodnyansky DV, Khaustovich NA, Shutsilin VY (2019) “Embodied energy” economic analysis: methodology and applications. *Belarusian Econ J* 4(89):71–85
12. Menoufi KAI (2012) Life cycle analysis and life cycle impact assessment methodologies: a state of the art, p 84
13. Tsitsin KG (2013) Energy-efficient technologies-the future of housing construction. *Strat Decis Risk Manag* 2:77
14. Grabovy PG, Starovoitov AS (2012) Innovative construction-energy efficiency and environmental friendliness. *R Estate Econ Manag* 2:68–71
15. Kornienko S, Popova ED (2017) “Green” construction in Russia and abroad. *Constr Unique Build Struct* 4(55):67–93. <https://doi.org/10.18720/CUBS.55.516>
16. Robati M, Daly D, Kokogiannakis G (2019) A method of uncertainty analysis for whole-life embodied carbon emissions (CO<sub>2</sub>-e) of building materials of a net-zero energy building in Australia. *J Clean Prod* 225:541–553
17. Michalak J, Michałowski B (2022) Understanding sustainability of construction products: answers from investors, contractors, and sellers of building materials. *Sustainability* 14:3042
18. Tetior AN (2015) Architectural building ecology as a new science. *Arch Constr Mosc* 2:30–39
19. Koshkina SY, Korchagina OA, Voronkova ES (2013) The factor of improving the quality of the environment and human health. *Issues Mod Sci Pract* 1:150–158
20. Rissman J, Bataille C, Masanet E, Aden N, Morrow WR, Zhou N, Elliott N, Dell R, Heeren N, Huckestein B et al (2020) Technologies and policies to decarbonize global industry: review and assessment of mitigation drivers through 2070. *Appl Energy* 266:114848
21. Bekov AM (2016) Energy efficient buildings. Thermal modernisation of building facades. Intellectual building composites for green building: international scientific and practical conference. Part 1. Belgorod, pp 90–94
22. Hurtado PL, Rouilly A, Vandenbossche V, Raynaud C (2016) A review on the properties of cellulose fibre insulation. *Build Environ* 96:170–177
23. Belyaev AV, Antipov SS (2019) Life cycle of construction objects at information simulation of buildings and structures. *Ind Civ Constr* 1:1–8
24. Brezhneva OV (2018) Life cycle of construction objects. *IOP Conf Ser: Manag. Econ Anal. Finance* (1):12–16
25. Losev KY (2019) Buildings life cycle methodology aspects. *Eurasian Sci J* 6(11)
26. Gusakova EA (2018) Information modeling of the life cycle of high-rise construction projects. *Bull MGSU* 13(1):14–22. <https://doi.org/10.22227/1997-0935.2018.1.14-22>
27. Häfliger I-F, John V, Passer A, Lasvaux S, Hoxha E, Saade MRM, Habert G (2017) Buildings environmental impacts’ sensitivity related to LCA modelling choices of construction materials. *J Clean Prod* 156:805–816
28. Carabaño R, De Madrid UP, Hernando SM, Ruiz D, Bedoya C (2017) Life cycle assessment (LCA) of building materials for the evaluation of building sustainability: the case of thermal insulation materials. *Rev Constr* 16:22–32
29. Ben Alon L, Loftness V, Harries K, Di Pietro G, Hameen EC (2019) Cradle to site life cycle assessment (LCA) of natural versus conventional building materials: a case study on cob earthen material. *Build Environ* 160:106150
30. Marchuk VY, Dzwigol H (2020) Integrated logistics support for the life cycle of building objects. *Electron Sci J Intellect Logist Supply Chain Manag* #1 1(1):17–25. <https://doi.org/10.46783/smart-scm/2020-1-2>.
31. Oparina LA (2011) Development of technologies for modeling the life cycle of buildings. *Hous Constr* 12:45–46
32. Kuzina ON (2019) Information modeling of the cost of a construction object at each stage of the life cycle. *Sci Tech Bull Volga Reg* 1:107–111

33. Kutsenko OI, Naumova NV (2018) Construction of energy-efficient houses as a way of saving in construction. In: Resource conservation and ecology of building materials, products and structures: collection of scientific papers of the international scientific and practical conference, Kursk, November 16, 2018, pp 243–246. <https://www.elibrary.ru/item.asp?id=36758288>. Last Accessed 16 Dec 2021

# Changes in the Heating Period Parameters for the Belgorod Region in the Context of Global Warming



E. O. Sheremet and A. S. Seminenko

**Abstract** Currently, we can observe an increasing trend toward the global warming of our planet. Multiple studies are aimed at assessing the impact of climate change on the construction industry and the infrastructure sector in general. At the same time, relatively few studies are dedicated to the climate change impact on the buildings' need of energy for heating. The goal of this paper is to consider the change in the main parameters of the heating period in the Belgorod Region, which are required to calculate the heat protection of buildings. We have analyzed the duration of heating periods; the minimum temperatures during heating periods; the temperatures during the five coldest days in each heating period; the average temperatures during heating periods; and the number of heating degree days from 1936 to 2021. We have identified trends towards increasing minimum temperatures during heating periods; increasing temperatures of the five coldest days in each heating period; increasing average temperatures during heating periods, and a decreasing number of heating degree days. We have drawn a conclusion on the correlation between the global warming and the climate warming in the Belgorod Region. We have found that warming in the Belgorod Region occurs faster than it is estimated based on data in several studies in the early twenty-first century. We have given some recommendations for designing heating systems taking into account the trend towards increasing the number of heating degree days per heating period.

**Keywords** Climate change · Heating · Energy saving · Heating system

---

E. O. Sheremet (✉) · A. S. Seminenko  
Belgorod State University of Technology Named After V.G. Shukhov, 46, Kostyukova Street,  
Belgorod, Russia  
e-mail: [sheremet.eo@bstu.ru](mailto:sheremet.eo@bstu.ru)

A. S. Seminenko  
e-mail: [seminenko.as@bstu.ru](mailto:seminenko.as@bstu.ru)

© The Author(s), under exclusive license to Springer Nature Switzerland AG 2024  
N. Vatin et al. (eds.), *Modern Problems in Construction*,  
Lecture Notes in Civil Engineering 372,  
[https://doi.org/10.1007/978-3-031-36723-6\\_39](https://doi.org/10.1007/978-3-031-36723-6_39)

409



## 1 Introduction

The current energy policy in the Russian Federation [1–3] includes some activities for increasing the energy efficiency and energy saving throughout the energy sector of our country. These activities also involve reducing the energy intensity and energy consumption, increasing the functionality and flexibility of heating system operation [4–8]. These issues cannot be solved in the context of the Russian Federation without taking into account the global warming in general and each region in particular.

Many studies are dedicated to the research of climate change in various regions of our planet and in the territory of the Russian Federation. However, relatively few studies are aimed at researching the main parameters of a heating period, which can affect the design of future buildings and the assessment for reducing the thermal need of existing structures. Mostly, these are large-scale studies are focused on the general assessment of the global warming impact on various fields of infrastructure [9]. There are some foreign studies [10–14] of the global warming impact on the energy saving of buildings.

The most detailed study of changes in the heating period parameters in the European part of Russia as a result of global warming is presented in paper [15] published in 2002. Based on the data from 90 meteorological stations located in the central part of Russia, calculations were carried out for the duration of heating periods, the average temperature, and the shortage of heat during heating periods within the time range from 1881 to 1995. As stated in this study, its data was also subjected to smoothing by a 10-year moving average. In order to research the dynamics of regional climatic parameters, the authors of the above study used a regression analytical model of climate [16], the algorithm of which is described in [17, 18]. Following this analysis, they obtained the maps of the central part of Russia with isograms of the heating period duration, the average temperature during heating periods, and the shortage of heat during heating periods at the moment of their study with a forecast for 2050. For Belgorod, the heating period durations were about 190 days at the moment of the study and 180 days by 2050.

## 2 Objective of the Study

The purpose of this study is analyzing the dynamics of the main parameters of heating periods in the Belgorod Region and comparing them with the existing data.

### 3 Materials and Research Methods

In order to study the main parameters of heating periods in the Belgorod Region, we needed the region's climatic data for the most extended time interval. Initially, we planned to analyze the data from the meteorological station of the International Airport named after V.G. Shukhov, that is available in the public domain [19]. However, the depth of the data from this meteorological station is limited by the year of 2005, which we considered as an insufficient time interval for our study. After some search for the nearest meteorological station with a sufficient depth of meteorological data, we have chosen the Gotnya meteorological station located in the Village of Proletarsky, Rakitnoye District, Belgorod Region. This meteorological station is located at a distance of 73 km from Belgorod and possess data of average daily temperature in this area starting from 1936. When processing this data, years with uncomplete annual data were not taken into account. The sampling does not include data from 1941 to 1944 inclusively, as well as the data for 1976.

At the first stage, we decided the issue of how much the meteorological data of the International Airport named after V.G. Shukhov differs from the data of the Gotnya meteorological station. For this purpose, we decided to compare the average monthly temperature for the time interval from 2006 to 2021. At the second stage, we processed the data from the Gotnya meteorological station.

For processing this information, we used Pandas—a software library in the Python language for data processing and analysis; Matplotlib—a library in the Python programming language for data visualization; Seaborn—a library in the Python programming language based on Matplotlib. To improve the visual presentation of information, to smooth short-term fluctuations, and to highlight the clearest key trends for building up graphs, we used the moving average with a period of 10 (hereinafter referred to as the MA (10)).

### 4 Results of the Study

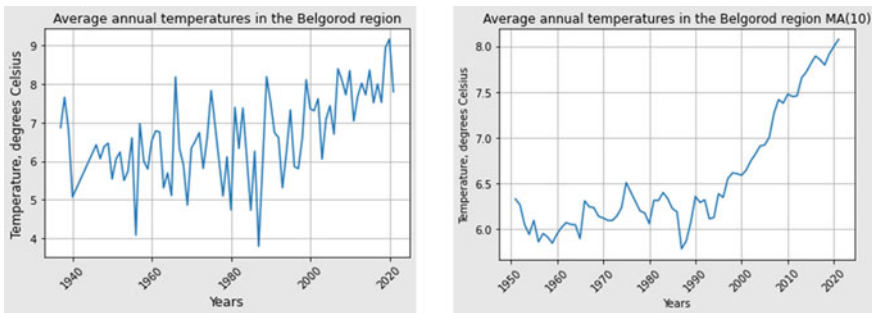
In order to assess the similarity of meteorological data from the meteorological stations under consideration, we have calculated the difference between the average monthly temperatures at the meteorological stations in Belgorod and Gotnya. We have compared the average monthly temperatures from 2006 to 2021 in the number of 192 months. Based on the calculation results, we have found out that a difference between the average monthly temperatures over 1 °C was recorded only during 10 of 192 months. The difference between the average monthly temperatures from 0.5 to 1 °C was recorded when comparing data for 71 months. In the other 111 cases, we observed a difference between the average monthly temperatures less than 0.5 °C. At the same time, there were 135 positive deviations of the average monthly temperatures and 57 negative deviations. Based on the data obtained, we concluded on an insignificant difference between the climatic conditions in Belgorod and in

Gotnya; however, Belgorod, being located further south-east than Gotnya, turned to be some warmer.

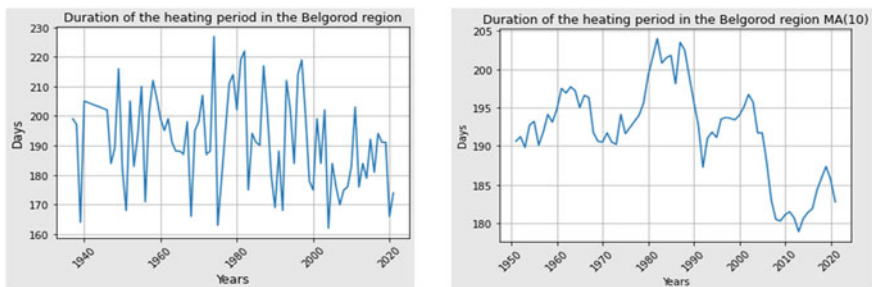
Figure 1 shows the graphs of changes in the average annual temperatures in the Belgorod Region according to the data from the meteorological station in Gotnya. As we can see from this graph, the average annual temperature in the period from 1950 to 1990 varied within a range of 6–6.5 °C. Since the late 1990s, there has been a trend to a drastic increase in the temperature which has reached 8 °C and more by 2020.

Figure 2 shows the graphs of changes in the heating period duration in the Belgorod Region. The heating period duration has a wave-shaped graph. Since 1980, there has been a trend towards decreasing minima and maxima. Since the early 2000s until 2010, we can observe a sharp decrease in the average values of the heating period duration from 195 to 180 days with a slight rebound of about 185 days which we can observe in the recent years.

Figure 3 shows the graphs of temperature changes during the coldest days of heating periods in the Belgorod Region. The temperatures during the coldest days have wave-shaped graphs with increasing maxima and minima, which can be seen



**Fig. 1** Dynamics of the average annual temperatures in the Belgorod Region: according to the meteorological station’s data (on the left) and MA (10) (on the right)



**Fig. 2** Duration of heating periods in the Belgorod Region: according to the meteorological station’s data (on the left) and MA (10) (on the right)

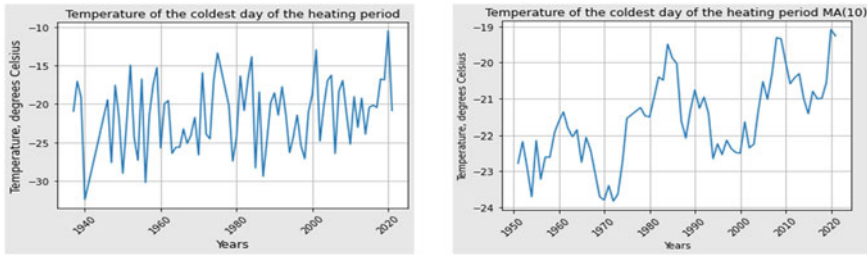


**Fig. 3** Dynamics of the coldest day temperatures in the Belgorod Region: according to the meteorological station’s data (on the left) and MA (10) (on the right)

most clearly in the time interval from 1970 to 2021. Whereas from the 1950s till the late 1970s, the temperature of the coldest day was within a range of  $-24$  to  $-21$  °C, the average temperatures from the 1990s to 2005 varied within a range of  $-22.5$  to  $-19.5$  °C, and from 2005 to 2022, within a range of  $-21.5$  to  $-19$  °C, if we consider rounded value. If we consider peak values, the average temperature of the coldest day did not fall below  $-10.5$  °C for the first time in the history of observations.

A similar pattern can be found also when analyzing the temperature change graphs during the five coldest days (Fig. 4). In this case, averaged temperatures from the 1980s did not fall below  $-18$  °C, whereas the maximum temperature limits during the five coldest days approached the average values of about  $-15$  °C. We can also see that, during the abnormally warm heating period of 2019–2020, the temperature during the five coldest days was about  $-8$  °C.

A rather good indicator of the climate warming in the region is the averaged change in the average temperature during the heating period (Fig. 5 (on the right)). We can observe a rather smooth increase in the average temperature during heating periods within the entire range of studies. The temperature change to the present day, as compared with the 1950–1960s, is about  $2.5$  °C. The highest average temperature during the heating period was recorded in 2019–2020 (Fig. 5 (on the left)), being equal to  $2.73$  °C.

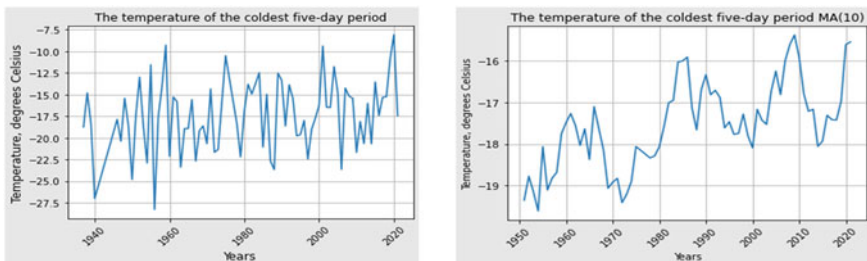


**Fig. 4** Temperatures during the five coldest days in the Belgorod Region: according to the meteorological station’s data (on the left) and MA (10) (on the right)

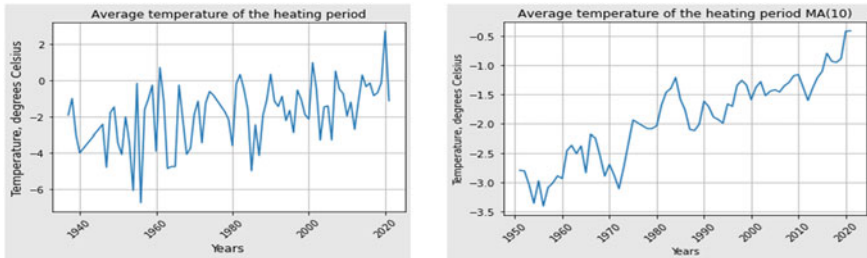


**Fig. 5** Dynamics of the average temperatures during heating period in the Belgorod Region: according to the meteorological station’s data (on the left) and MA (10) (on the right)

### 5 Discussions

Based on the comparison with the date obtained in this study, we can say that the heating period duration in 1995–2000 is consistent with the existing data [15]. However, the actual decrease in the heating period duration down to 180 days according the results of this study occurred by 2012–2013; currently, it is about 183 days.

The average temperature values during heating periods in [15] at the moment of the study and the forecast for 2050 have changed insignificantly, being about  $-1.5\text{ }^{\circ}\text{C}$ . In this study, we can see that, in the 2000–2010s, the average temperature during heating periods was really about  $-1.5\text{ }^{\circ}\text{C}$ . However, in the recent decade, there was a significant jump: by the 2020–2021, the average values reached  $-0.5\text{ }^{\circ}\text{C}$ .

When examining the graph of changes in the number of heating degree days per heating period, taking into account the indoor air temperature equal to  $18\text{ }^{\circ}\text{C}$  (Fig. 6), we can draw a conclusion on a smooth decrease in the number of heating degree days per heating period over time. If in the 1950–1960s, the averaged value of heating degree days was within a range of 4,000 to 4,100, in the 2010–2020s, this value fell below 3,500. The minimum number of heating degree days per heating period was recorded in the heating period of 2019–2020, being equal to 2,535.

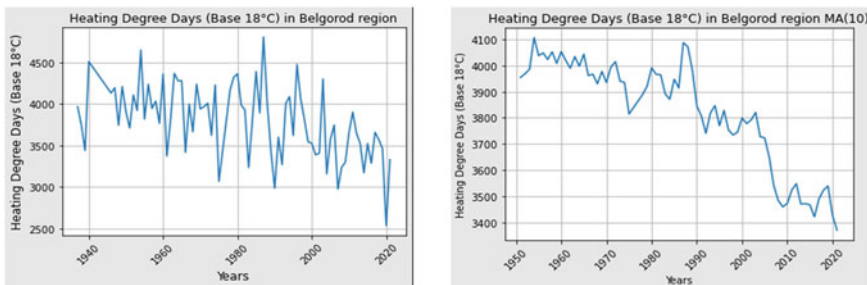


**Fig. 6** Heating degree days per heating period in the Belgorod Region: according to the meteorological station’s data (on the left) and MA (10) (on the right)

If we compare heating degree days per heating period, the change from 2000 to 2050 according to the author's data [15] was about 3,900 in 2000 and 3,300–3,400 in 2050. However, the actual decrease in the number of heating degree days per heating period according to the results of this study fell below 3,400 by 2021.

Therefore, we can conclude that, in general, the warming in the Belgorod Region occurs faster as compared to the indicator forecast in studies [15]. The forecast values of the heating period duration, the average temperatures during heating period, and the number of heating degree days per heating period by 2050 can be observed already in 2021, and they often exceed the value forecast by 2050.

## 6 Conclusion

When analyzing the main parameters of heating periods in the Belgorod Region, such as the heating period duration, the average temperatures during heating period, and the number of heating degree days per heating period, we have found that the Belgorod Region shows the general trend towards the global climate warming, whereas the warming develops more than twice as intensively as scientists predicted in the early 2000s.

Undoubtedly, for a more global assessment, this study should be scaled up to the level of Federal Districts and, possibly, to the entire territory of the European part of Russia. However, we need to talk already now about a possible change in the methods for calculating the heating period parameters, such as heating degree days per heating period calculated using averaged data over the last 50 years of observations, which poorly reflects the latest climate change trends.

A rational change in the number of heating degree days towards decreasing the same will allow to reasonably reduce the required thermal resistance in the construction of enclosing structures of new buildings, which will affect the insulation thickness and the design of external walls in general. This solution will save the construction costs depending on the scale of its application, which will undoubtedly allow to reduce the carbon footprint on the atmosphere in the future.

For existing buildings, the warming trend observed during the heating period will increase the thermal efficiency and create conditions for reducing energy consumption in the winter season.

This work was realized in the framework of the Program “Priority 2030” on the base of the Belgorod State Technological University named after V.G. Shukhov. The work was realized using equipment of High Technology Center at BSTU named V.G. Shukhov.

## References

1. Federal Law of the Russian Federation (2009) "On energy saving and on improving energy efficiency and on amendments to certain legislative acts of the Russian Federation" dated November 23, 2009, no. 261-FZ
2. Ukaz Prezidenta RF of 09.05.2017 № 203 "O Strategii razvitiya informacionnogo obshhestva v Rossijskoj Federacii na 2017–2030 gody" (Presidential Decree of 09.05.2017 No. 203 "On the Strategy for the development of the information society in the Russian Federation for 2017–2030"). <http://www.garant.ru/products/ipo/prime/doc/71570570/>
3. Rasporyazhenie Pravitel'stva RF №1632-r ot 28.07.2017. Ob utverzhdenii programmy "Cifrovaya ekonomika Rossijskoj Federacii" (Order of the Government of the Russian Federation No. 1632-p dated July 28, 2017. On approval of the program "Digital Economy of the Russian Federation"). <http://base.garant.ru/71734878/>
4. Lupey AG (2004) On diagnostics of the state of heating systems of consumers of thermal energy (Electronic resource). JUICE, no. 8. <https://www.c-o-k.ru/articles/o-diagnostike-sostoyaniya-sistem-otopleniya-potrebitel'ev-teplovoy-energii>
5. Safiullin RN, Afanasyev AS, Reznichenko VV (2019) The concept of development of monitoring systems and management of intelligent technical complexes. *J Min Inst* 237:322–330. <https://doi.org/10.31897/pmi.2019.3.22>. (In Russ)
6. Paramonova E, Elistratova YV, Seminenko AS (2013) The problem of overflows and underdots in the heating period. *Mod High-Tech Technol* 8–1:48–50
7. Trukhniy AD, Zroychikov NA, Lomakin BV, Sedov IV (1998) Information and diagnostic control system for mains water heaters of the turbine unit T-250/300-240. *Heat Power Eng* 1:30–34
8. Tol H, Desmedt J, Salenbien R (2020) A novel demand-responsive control strategy for district heating systems, featuring return temperature reduction. *Energy Built Environ* 2:105–125. <https://doi.org/10.1016/j.enbenv.2020.05.001>
9. Khlebnikova EI, Sall' IA, Shkol'nik IM (2012) Regional climate as the factors if impact on the objects of construction and infrastructure. *Russ Meteorol Hydrol* 37(11/12):735–745
10. Li Y, Wang W, Wang Y, Xin Y, He T, Zhao G (2021) A Review of studies involving the effects of climate change on the energy consumption for building heating and cooling. *Int J Environ Res Public Health* 18:40. <https://doi.org/10.3390/ijerph18010040>
11. Shi Y, Wang G, Gao X et al (2018) Effects of climate and potential policy changes on heating degree days in current heating areas of China. *Sci Rep* 8:10211. <https://doi.org/10.1038/s41598-018-28411-z>
12. Andrade C, Mourato S, Ramos J (2021) Heating and cooling degree-days climate change projections for Portugal. *Atmosphere* 12(6):715. <https://doi.org/10.3390/atmos12060715>
13. Chidiac SE, Yao L, Liu P (2022) Climate change effects on heating and cooling demands of buildings in Canada. *CivilEng* 3:277–295. <https://doi.org/10.3390/civileng3020017>
14. Janković A, Podračanin Z, Djurdjević V (2019) Future climate change impacts on residential heating and cooling degree days in Serbia. *IDŐJÁRÁS Q J HUNG METEOROL SERV* 123(3):351–370. ISSN 0324-6329
15. Klimenko VV, Klimenko AV, Tereshin AG et al (2002) Changes of the parameters of the heating period on the European Territory of Russia as a result of global warming. *Izv Ross Akad Nauk, Energetika* 2:10–17
16. Klimenko VV, Klimenko AV, Andreichenko TN et al (1997) *Energy, nature and climate*. M.: MPEI Publishing House
17. Klimenko VV, Mikushina OV, Larin DA (2001) Temperature trends in the Taimyr region under global climate change. *Geocology* 3:195–203
18. Klimenko VV, Dovgalyuk VV, Mikushina OV (2001) Forecast of climate change in the Moscow region under the influence of anthropogenic and natural factors. *Vestnik MEI* 2:36–45
19. Raspisanie pogody homepage, <https://rp5.ru/>. Last Accessed 16 Sept 2022



# Structural Construction Optimization of Fire Protection Systems



Oleg Kochnov , Svetlana Sazonova , Alexey Kochegarov , Pavel Korkunov , and Roman Yemelyanov 

**Abstract** This paper analyzes basic structural constructions of fire protection systems and demonstrates reliability and evaluation methods of such constructions. Even in the best year, 9565 people got injured by fire, with the risk being 65 times more than acceptable. Today, the main approach is a so-called “risk-oriented approach”, aimed at minimizing the value of individual fire risk, or, maximizing the safety of people in residential and public buildings and structures. It would be more correct to consider this model as dynamic, as in need of constant improvement. Various methods and formulas were used to draw dependencies and assess risk of fire. The results show that the most significant system is Fire Alarm System (which is evident on the fact that this system is responsible for fire detection). The most usefulness is provided by Smoke Control System; however, it has the lowest reliability. Emergency Notification System, having the lowest usefulness, has a high reliability. Emergency Notification System reliability (effectiveness) can affect (control) the Fire Protection System effectiveness, but within certain limits. It was determined that one of the most important ways to minimize the risk is to use higher type Emergency Notification System. Paper also shows significance of the Fire Protection Systems in two aspects—reliability and structural reliability. System performance is fully disclosed in such parameter as—technical or functional efficiency, that depends on reliability and other parameters, for instance, human error, connectivity coefficient, topology efficiency etc.

---

S. Sazonova · A. Kochegarov (✉) · P. Korkunov  
Voronezh State Technical University, 84, 20 Letiya Oktyabrya St, Voronezh 394006, Russia  
e-mail: [kochiegharov77@mail.ru](mailto:kochiegharov77@mail.ru)

P. Korkunov  
e-mail: [pelelano786@gmail.com](mailto:pelelano786@gmail.com)

O. Kochnov  
ESCORT GROUP” LLC, Suite 907, 23a K.2, Avtozavodskaya St, Moscow 115280, Russia

R. Yemelyanov  
FGBU VNIPO EMERCOM of Russia, VNIPO, 12Moscow Oblast, Mikrorayon  
Balashiha 143903, Russia



**Keywords** Fire protection system · Effectiveness · Reliability · Risk. smoke control system · Factor · Emergency control system · Fire alarm system

## 1 Introduction

In the methodology for determining the magnitude of an individual fire risk [1], there is a coefficient that takes into account the compliance of the fire protection system (FPS), aimed at ensuring the safe evacuation of people in case of fire, with the requirements of regulatory documents (RD) on fire safety (FS). Initially, this unconditional coefficient had a different (more adequate) interpretation in the form of an (unconditional) probability of the effective operation of the FPS, aimed at ensuring the safe evacuation of people in case of fire. The coefficient in its right interpretation is currently present in active and up-to-date standard [2]. Conformity factor is, in turn, determined by other such factors (basic values are:  $R_{FAS} = 90\%$ ,  $R_{ENS} = 80\%$ ,  $R_{SCS} = 80\%$ ), which would be more correct to interpret and apply as conditional probabilities. By substituting these factors into a base formula, the FPS conformity factor takes a value of 92%, which is not entirely accurate for two reasons: firstly, it was said that these factors (coefficients) should be replaced with conditional probabilities of efficiency; secondly, they must be calculated in each individual case. Furthermore, in reality, the Fire Alarm System, which activates Emergency Notification System (ENS) and Smoke Control System (SCS), cannot have the reliability rate which exceeds itself (90%), if not doubled. Practically, with parallel-daisy chaining, and, usually, without doubling and even a backup, the reliability rate of the whole system takes a value of 86% and not 92%. This serious discrepancy cannot be unaccounted for. The alternate result shown in this paper is confirmed by statistical data [3], which was analyzed in this paper.

Ensuring fire safety of buildings and structures is one of the urgent problems being solved today. In the process of ensuring said safety, a wide spectrum of specialists is involved—engineers, designers, installers, operators, risk management personnel, etc. The main issue is the responsibility for making a final decision on the structure and content (manufacturer) of technical means. It is easy to say that every specialist, responsible for the safety of buildings and structures, is interested in this publication.

## 2 Materials and Methods

It should be recognized, that some of the methods, stated in [1], are not perfect, and there is a reason to believe that the situation may worsen even more, as hinted at by the first edition of the upcoming new risk calculation methodology, in which the accounting for the effectiveness of fire protection systems used at the facilities will become even more formal.

The Conformity factor of technical solution, used in methodology for calculating the value of an individual fire risk [1], even in the form of “probability of effective operation of the technical solution”, have not received proper justification from the competent authorities, as of today. This paper makes another attempt [4] to understand the reliability meaning and the correct interpretation of this parameter.

Efficiency is generally understood as the ratio of the economic (technical) effect to the cost of producing it. To put it another way, by applying the system it is expected to have some effect, or gain. To achieve this effect, many technical and organizational decisions are made to improve the output. The feasibility of implementing such solutions should be tested by both technical and economic factors [5]. To accurately evaluate the specific solution’s effectiveness, it is necessary to choose evaluation methods and compile a list of expected effects, as well as expected losses. Making the appropriate decisions while performing these operations is supported by knowledge of certain technical solution’s features. Applying this approach to FPS, by “technical efficiency” we will understand gain as in the form of minimizing risk, which would be achieved by applying the system in comparison to its absence. An example of such gain can be seen in the standard [2] and methodology [1], designed for hard fire-preventing objects and accounting for safe evacuation under all possible fire scenarios and options.

Let’s turn to the method [6], in which, the conditional probability of a person getting injured when he is in the  $i$  room during the implementation of the  $j$  scenario of fire:

$$Q_{dij} = (1 - P_{\ni ij}) \cdot (1 - D_{ij}), \quad (1)$$

$P_{\ni ij}$ —probability of people evacuating, located in the  $i$  area of the building during the implementation of the  $j$  scenario of fire;

$D_{ij}$ —probability of effective work of the technical means of ensuring safety of people in  $i$  area of building during the implementation of the  $j$  scenario of fire.

Formula (1) shows, that if technical means are available (for one area) with a probability of effective operation  $D_{ij} = 0,8$  (80%), the probability of injury (risk value) will be reduced by 5 times compared to their absence.

The probability of effective operation of Fire Protection Systems (FPS), generally [2], is determined by effectiveness of each technical solution:

$$P_{FP} = 1 - \prod_{i=1}^n (1 - R_i), \quad (2)$$

$n$ —a number of technical fire preventive solutions in the building;

$R_i$ —probability of effective operation of  $i$  technical solution.

In the means of reliability, the formula (2) reflects the parallel connection of technical solutions. In practice, however, the way in which technical solutions (FPSs) are constructed and tailored can vary significantly.

Remark: In the calculation example [2], probabilities of effective operation of Emergency Notification Systems and Smoke Control Systems are taken as equal:  $R_{ENS} = R_{SCS} = 0.95$ . And even with such elevated values, and theoretically assumed doubling, individual risk could not be ensured [7].

Let's write down the coefficient for determining the FPS conformity factor, in the form of probabilities of effective operation of FPS [1, 2]:

$$P_{FPi} = 1 - (1 - R_{FASi} \cdot R_{ENSi}) \cdot (1 - R_{FASi} \cdot R_{SPSi}) \quad (3)$$

$R_{FASi}$ —probability of effective fire alarm system operation. The  $R_{FASi}$  parameter value is defined by technical reliability of the elements of Fire Alarm System (FAS) provided in technical documentation;  $R_{ENSi}$ —conditional probability of effective operation of ENS in case of effective operation of FAS;  $R_{SPSi}$ —conditional probability of effective operation of SCS in case of effective operation of FAS.

Remark: According to [1], If there is no information on technical reliability parameters, we can accept that:  $R_{FASi} = R_{ENSi} = R_{SPSi} = 0,8$ . The question of means to define given parameters has been raised a number of times, for instance, on the forum “0–1 RU”, addressed in VNIPO, but was not given any resolution.

Addressing the Emergency Notification System: as stated in regulatory documents, the  $R_{ENSi}$  reliability parameter is taken as 0,8, if at least one of the following conditions is met: the building is equipped with ENS, that meets the requirements of RD on Fire Safety; the equipment of building with ENS is not required in accordance with the requirements of RD on Fire Safety.

Therefore, if ENS is present on the object of protection and has certification, it is safe to assume that it is sufficient for the  $R_{ENSi}$  reliability parameter to be taken as 0,8. In other cases the  $R_{ENSi}$  is taken as 0. It is clear that there is a stretch, since even 80% reliability rate is still needed to be provided, not to mention the effectiveness, the system may simply not be turned on. To clarify what has been said, it is time to turn to statistics.

## 2.1 Statistical Data on ENS Performance

FGBU VNIPO EMERCOM of Russia annually issues a statistical compendium—“Fire and fire hazard” [3]. Analyzing the data from 2012 to 2020, we can draw several important conclusions:

1. From the analysis of the overall fire dynamics, it can be seen that the maximum number of fires (471) reached in 2019, which is a negative fact. On the report of the official data, the number of public buildings in Russia is 213000. In the worst-case scenario, the frequency of occurrence of a fire in a building or a structure is:  $Q_{2019} = \frac{471}{213000} = 0.0022$ , which is lower than the average ( $Q_F = 0,028$ ) value for buildings and structures, as stated in the method [9], meaning the value is in the (conditional) norm.

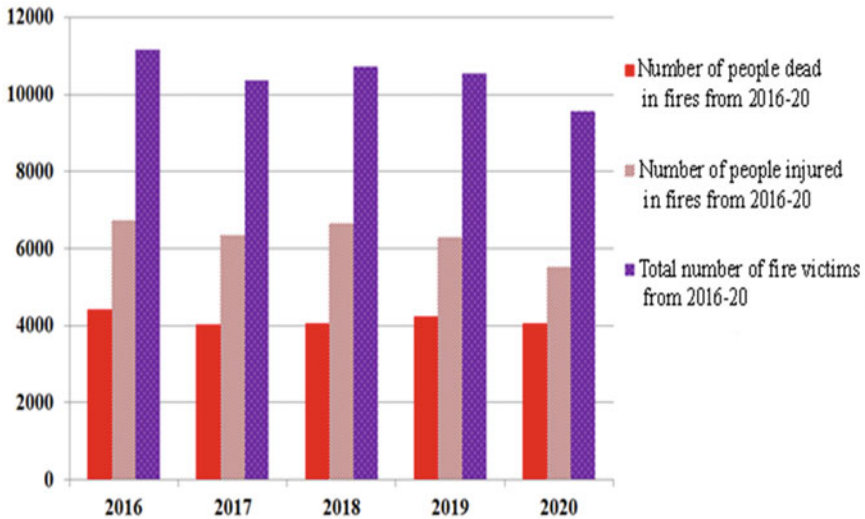


Fig. 1 Number of injured people from 2016 to 2020

2. The case is much worse with a number of injured people: not only is it not decreasing, but in the relative case—increasing.

Figure1 provides statistical data on injured from 2016 to 2020.

Using statistics let’s calculate the risk for the best year—2020: Russia’s population in 2020—146 000 000 people. Number of injured people by fire (2020) —9565 people. Risk equals:  $Q_{2020} = \frac{9565}{146000000} = 6,55137E - 05$ .

We can draw the conclusion that the risk is 65 times higher than acceptable.

Let’s consider the statistics for automated fire systems (AFS). Average data from 2012 to 20 is provided in Table 1.

Let’s note the following indicators:

1. Based on the provided data, ratio of failure (not activating and therefore not performing) to total number of system activations, the statistical reliability of the systems can be assessed.
2. The table shows that even with a functioning system there are a large number of victims.

This gives us the reason to introduce new parameters:

$K_u$ —Coefficient of usefulness, which should be understood as a ratio of a number of victims with systems not working to a total number of victims.

Let’s turn to formula (3), that defines the FPS structure (Fig. 3a), and allows to calculate such parameters, as reliability  $B_R$  and structural  $B_S$  significance of the system [8].

The structural significance of the system can be defined as the result of differentiation:

**Table 1** Average automated fire systems performance data from 2012 to 20

	EVENT	SWS	SWF	SDW	SOFF	SUM	USEFULNS	STRSIG
F	Fires number	1021.8	0	157.63	54.5	1233.88		
A	Dead	228	0	96	25	349.00		
S	Injured	679	0	167	24	870.00		
	Reliability		1.00	0.87	0.96	<b>0.83</b>	0.26	1.15
S	Fires number	126.13	4.5	40.125	9.625	180.38		
C	Dead	76	0	27	6	109.00		
S	Injured	190	9	61	3	263.00		
	Reliability		0.98	0.78	0.95	<b>0.70</b>	0.28	0.24
E	Fires number	185.38	3.25	20	7.75	216.38		
N	Dead	70	4	6	2	82.00		
S	Injured	117	19	8	1	145.00		
	Reliability		0.98	0.91	0.96	<b>0.86</b>	0.18	0.35

FAS—Fire Alarm System; SCS—Smoke Control System; SWS—System worked and Successfully completed its task; SWF—System worked but failed its task; SDW—System did not work (failed its task); SOFF—System was disabled; USEFULNS—usefulness; STRSIG—Structural significance.

$$B_S \left( \frac{i}{P} \right) = \frac{\partial P_{FP}}{\partial R_i} \tag{4}$$

$P_{FP}$ —probability of failure-free operation of FPS, which depends on reliability of  $i$  system (SCS, ENS).

By opening the brackets and differentiating (3), for example, relative to  $R_{ENS}$  we can define the ENS structural significance in the FPS structure:

$$B_{ENS} \left( \frac{i}{P} \right) = \frac{\partial P_{FP}}{\partial R_{ENS}} = R_{FAS} - R_{FAS}^2 \cdot R_{SPS} \tag{5}$$

Substituting statistical data from Table 1, we get:  $B_{ENS} = 0,35$ . Calculated results is provided in the STRSIG column of Table 1.

The results show that the most significant system is Fire Alarm System (which is evident on the fact that this system is responsible for fire detection). The most usefulness is provided by SCS; however, it has the lowest reliability. ENS, on the other hand, having the lowest usefulness, has a high reliability. The product of coefficients of usefulness and reliability, in this evaluation, can be interpreted as a (functional) effectiveness of the system.

Remark: Analyzing a number of injured people with a not working ENS is a hard task, compared to a not working Smoke Control System. The important question is why people were affected by Dangerous Fire Factor (DFF) and were not able to

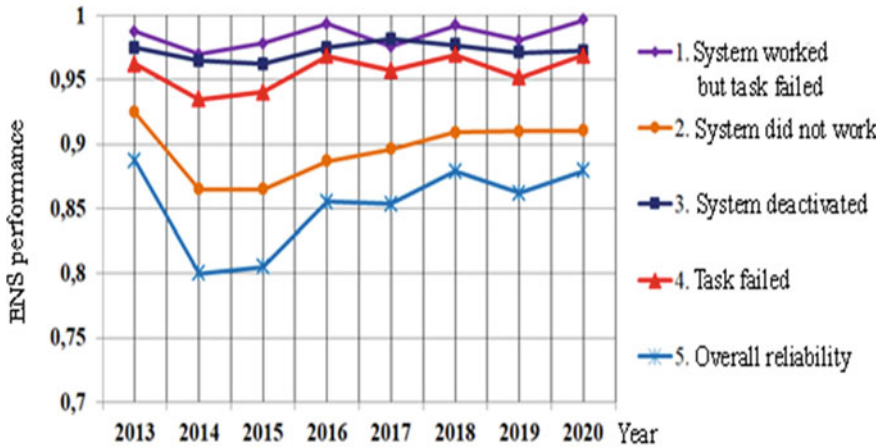


Fig. 2 Statistics of effective operation of ENS from 2013–20

evacuate before DFF reached critical values. Consequently, we have to appeal to the importance of ENS, as a combination of organizational events and technical means; as a system, that minimizes delay of the start of evacuation and has the highest importance at the initial stages of evacuation.

When calculating reliability, making technical specifications, we can rely on statistics of effective operation of ENS from 2013–20 (Fig. 2).

When constructing a dependency “Task was failed” (Fig. 2), as a summary of (1) and (3), following considerations were made. Deactivated system can mean the following: it was out of order, or, if it was working, it had some kind of a defect or malfunction. The graph shows that the ENS reliability varies from 80 to 88 percent, in which, from 8 to 14%—because of malfunction, and from 3 to 7%—because of not working. Additional reasons (not yet defined) could affect the reliability too.

Let’s address the definition of Fire Protection System (FPS) reliability.

## 2.2 Evaluation of the Reliability of Fire Protection Systems

The resulting likelihood of an effective FPS operation (which has been shown to either provide or not provide risk) is determined by the structural design.

Figure 3 shows the structural scheme of Fire Protection System, in accordance to formula (3):

We can highlight the following:

1. In the reliability means, (formula (1) of methodology [1]) automatic fire extinguishing systems (AFES) and Fire Protection System (FPS) are connected in parallel (they double each other), though, in practice other connection methods are present.

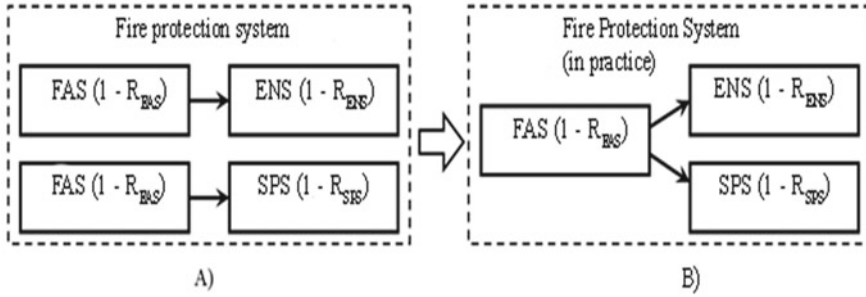


**Fig. 3** Structural scheme of FPS; (A) According to method №382; (B) According to practice

2. Structure shown on Fig. 3A (doubled FAS), in practice does not occur. In accordance with this scheme, and also formula (3), when  $R_{FAS} = R_{ENS} = R_{SPS} = 80\%$ , overall FPS reliability would be  $P_{FPS} = 87\%$ , which is possible only with reservation (doubling).
3. The FPS reliability shown on Fig. 3B (serial-parallel connection) is:

$$P_{FP} = R_{FAS} \cdot [1 - (1 - R_{ENS}) \cdot (1 - R_{SPS})]. \tag{6}$$

### 3 Results and Discussion

Let's draw the dependencies of FPS from probability of ENS operation with these constant parameters:  $R_{FAS} = R_{SPS} = 80\%$ , Fig. 4:

Figure 4 shows:

1. Probability of FPS activation, calculated with formula (3) and with constant  $R_{FAS} = R_{SPS} = 80\%$  and with raised  $R_{ENS}$  from 80 to 100%,  $P_{FP}$  increased from 87 to 93%. At the same time the real effectiveness with the same parameters increases only from 77 to 80%.
2. If SCS is not present,  $R = 0$ , FPS effectiveness is defined by ENS and FAS effectiveness (increasing from 64 to 80%).

With the same technique we can calculate structural significance  $B_S$  of ENS, opening the brackets and differentiating (6) relative to  $R_{ENS}$ , we get:

$$B_S \left( \frac{i}{P} \right) = \frac{\partial P_{FP}}{\partial R_{ENS}} = R_{FAS} \cdot R_{SPS} \tag{7}$$

With  $R_{FAS} = 0,83$ ,  $R_{SPS} = 0,75$ ,  $B_{ENS} = 0,25$ .

The calculation shows that the real value differs from the theoretical one  $B_{ENS} = 0.35$ .

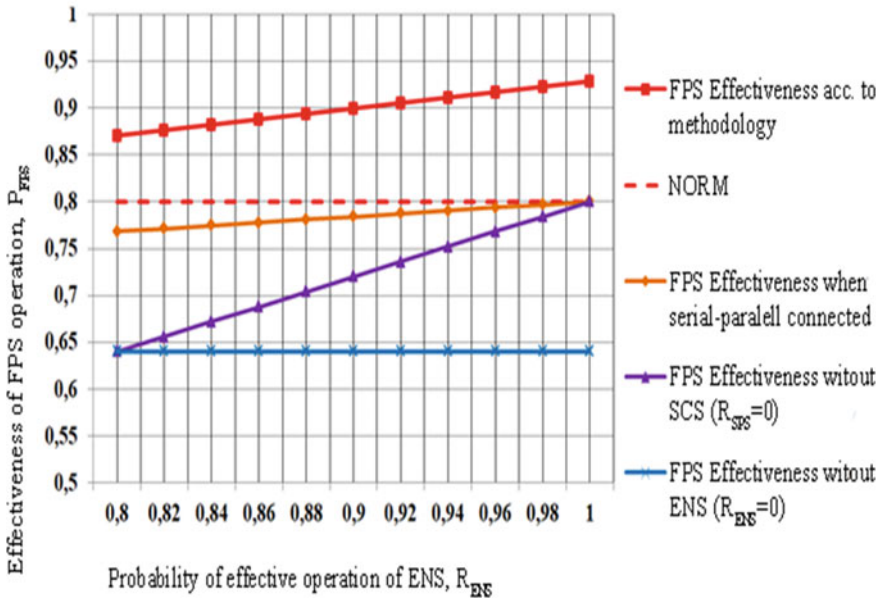


Fig. 4 Dependency of FPS effectiveness from probability of ENS operation with  $R_{FAS} = R_{SPS} = 80\%$

Let's calculate and compare probabilities of FPS effective operation, using statistics from Table 1.

Based on theoretical (calculated with the help of methodology) formula (3):

$$P_{FP} = 1 - (1 - 0.83 * 0.7) * (1 - 0.83 * 0.86) = 0.88(88\%)$$

Based on practical (calculated with the help of the alternative) formula (6):

$$P_{FP} = 0.83 * (1 - (1 - 0.86) * (1 - 0.7)) = 0.795.$$

Comparing these results, we see an elevated value from formula (3), compared to the practical value calculated with formula (6).

Now we can draw and compare probabilities of FPS effective operation based on statistics (Fig. 5).

Using obtained result, we can draw a dependency (Fig. 6) of individual risk (formula (1) from methodology [1]) from a probability of FPS effective operation with the following constant parameters:

- Probability of fire occurrence (for supermarkets),  $Q_F = 0,0293$ ;
- Probability of evacuation (assuming the maximum value),  $P_e = 0,999$ ;
- Probability of people present (taking a high number),  $P_{pr} = 18/24 = 0,75$
- Probability of AFES effective operation,  $R_{AFES} = 0,9$ :



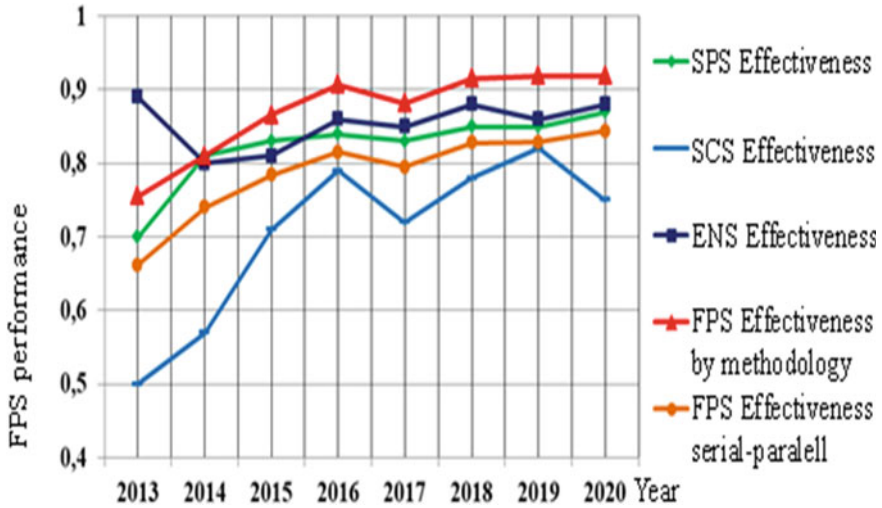


Fig. 5 Probabilities of FPS effective operation based on statistics from 2013–20

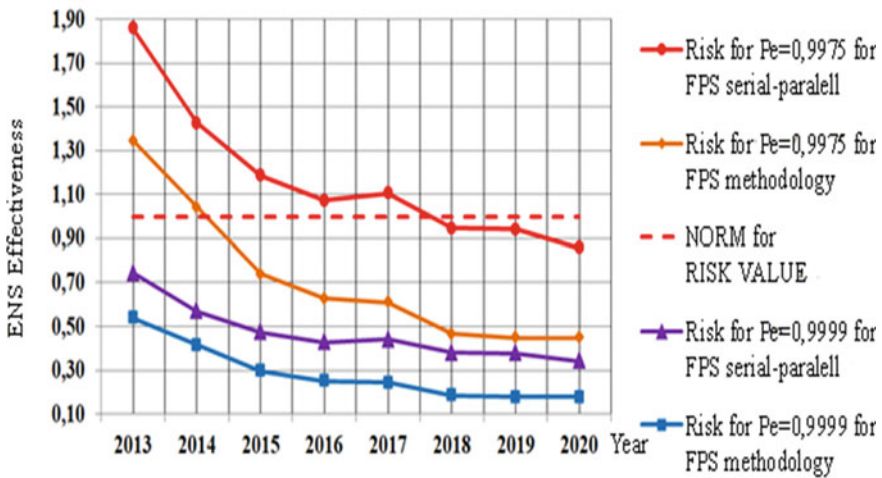


Fig. 6 Risk when located in a supermarket depending on effectiveness of FPS (based on statistics from 2013–20)

Let’s make the task a little harder and calculate the risk with the evacuation probability  $P_e < 0,999$ .

For that, using formula (3) from methodology [1], let’s calculate evacuation probability relative to the data ( $t_e = 12$  min,  $t_{bl} = 20$  min) and delay time  $t_d = 0,26$  min. For the starting evacuation delay time,  $t_{se1} = 3,75$  min,  $P_{e1} = 0,9975$ , where  $t_{se1}$ —average delay time for ENS type I-II (Fig. 6).

The graph shows that with some delay ( $t_d = 0,26$  min is assumed accurate), the probability of evacuation takes a value of  $P_e = 0,9975$ ; risk increases fast. According to the graph, for 2013–14, risk was not achieved even for the base formula (3). Critical (located at the top) curves were drawn taking into account the starting evacuation delay time, typical for ENSs type I–II.

A note: this example uses parameters that were selected deliberately. This was done to graphically demonstrate a dynamic. Although, those parameters are possible.

We are ready to draw the first and important conclusion: switching ENSs type I–II to ENSs of higher type (III and IV), risk goes back to normal. Therefore, one of the most important ways to minimize the risk is to use higher type ENSs.

Depending on the problem being solved, reliability and effectiveness of FPSs can be controlled. FPS reliability depending on risk can be evaluated (calculated) based on required value of individual fire risk using formula (8):

$$P_{FP} \geq 1 - (Q_H / (Q_F \cdot P_{pr} \cdot (1 - P_e) \cdot (1 - R_{AFES}))) \quad (8)$$

ENS reliability according to theoretical formula (3):

$$R_{ENS1} = [1 - \frac{1 - P_{FPS}}{(1 - R_{FAS} \cdot R_{SPS})}] / R_{FAS} \quad (9)$$

ENS reliability according to practical formula (6):

$$R_{ENS} = 1 - \frac{(1 - P_{FP} / R_{FAS})}{(1 - R_{SPS})} \quad (10)$$

## 4 Conclusion

Locking the parameters and using formulas (8), (9), (10), dependencies can be drawn. Nonetheless, there is no point, since we already have shown the main results. ENS reliability (effectiveness) can affect (control) the FPS effectiveness, but within certain limits (Fig. 4). According to (3) and (6), while changing  $R_{ENS}$  ranging from 0 to 1, the FPS reliability changes within limits:  $(R_{FAS} \cdot R_{SPS}) \leq P_{FP} \leq R_{SPS}$ .

Several important conclusions were made:

1. When considering the system reliability, we need to point out 2 of its aspects ([9])—reliability of elements, defined in the production stage, and structural reliability, defined in the designing stage.
2. From statistics (Table 1) we can see, that the system could be functional, but not working (not effective). By injured people and by presence or lack of presence of the system we can evaluate its usefulness. Parameters, such as usefulness, reliability, and structural significance can be very useful when evaluating a structural solution.

3. Paper shows significance of the FPS in two aspects—reliability and structural reliability. Individual fire risk value can be minimized by several parameters, including FPS reliability, that depends, firstly, on effectiveness of structural construction, and only secondly, on reliability of its subsystems. Reliability of a subsystem (ENS for example) is not self-sufficient on its own.
4. System performance is fully disclosed in such parameter as—technical or functional efficiency, that depends on reliability and other parameters, for instance, human error, connectivity coefficient, topology efficiency etc.
5. Although reliability of ENS  $R_{ENS}$  affects the FPS reliability,  $P_{FP}$  is present within certain limits, which is enough to improve the situation by minimizing individual fire risk value.

**Acknowledgements** The work was done at the Voronezh State Technical University, with the support of the Department of Technosphere and Fire Safety, from where the idea of this paper was born. We want to thank all teachers at VSTU who helped to carry this project from an idea to the full paper.

## References

1. Order No. 382. “On approval of the methodology for determining the calculated values of fire risk in buildings, structures and structures of various classes of functional fire hazard.”
2. GOST 12.1.004–91 “Occupational safety standards system. Fire safety. General requirements”
3. “Fire and Fire Hazards in 2020”. Statistical Collection. Ministry of the Russian Federation for Civil Defense and Emergency Situations and Disaster Management of the Russian Emergencies Ministry
4. Mironenko Y (2014) «Probability of efficient operation of technical means of fire safety. Algorithm of Safety magazine No. 6
5. Ershova I (2016) Technical Cost Efficiency
6. EMERCOM of Russia Order No. 404. (10.07.2009). Methods of determination of calculated values of fire risk at production facilities
7. Kochnov O (2021) Features of ENS design. Role and significance of fire alarm system in risk assessment. Part 2, All-Russian specialized magazine “Security”
8. Andreev A, Yakovlev V, Korotkaya T (2018) Theoretical bases of reliability of technical systems
9. Baburov V, Baburin V, Fomin V, Smirnov V (2007) Production and fire automation, part 2. Automatic fire extinguishing installations
10. Sharovar F (2013) Fire prevention automation
11. Bubir N, Baburov V, Potapov V (1986) Industrial and fire automatics

# Application of the White Noise Generator to Evaluate the System for Modeling the Impact of Soil on the Working Body of the Bulldozer



Alexey Bulgakov , Georgii Tokmakov , and Wen-der Yu 

**Abstract** Improvement of quality, decrease of terms and cost of construction are inseparably linked with problems of effective use of bulldozer equipment. The most important problem of control tractions modes of the bulldozer is the fullest use of traction opportunities of the machine at the expense of management of work tool. Automatic maintenance of the maximum traction power or resistance preset value on work tool is complicated by a large number of the random factors operating on the bulldozer. In this regard the system of automatic control has to possess possibility of self-adjustment. In this paper with applying of analytical simulation method and neural network technologies, been decomposed model bulldozers workflow as mechatronic system realized. Models of the sub-processes are included into the general structure of bulldozer's workflow simulation model. They are intended to be used to study bulldozer's separate units applying analytic dependences of between their workflow parameters and to simulate bulldozer's workflow in general. Technique of identification and modeling of bulldozer's workflow based on neural networking technologies is described.

**Keywords** Robotics and mechatronics · Automation and control · Bulldozer

---

A. Bulgakov (✉)

Southwest State University, 50 let Oktyabrya St. 94, 305040 Kursk, Russia

e-mail: [agi.bulgakov@mail.ru](mailto:agi.bulgakov@mail.ru)

G. Tokmakov

South-Russian State Polytechnic University, Prosveshcheniya St. 132, 346428 Novocherkassk, Russia

e-mail: [tokmakov\\_ge@npi-tu.ru](mailto:tokmakov_ge@npi-tu.ru)

W. Yu

Chaoyang University of Technology, Jifeng East Road 168, 41349 Taichung, Taiwan

© The Author(s), under exclusive license to Springer Nature Switzerland AG 2024

N. Vatin et al. (eds.), *Modern Problems in Construction*,

Lecture Notes in Civil Engineering 372,

[https://doi.org/10.1007/978-3-031-36723-6\\_41](https://doi.org/10.1007/978-3-031-36723-6_41)

## 1 Introduction

On the basis of bulldozer's workflow dynamics modeling and analyses described in a variety of works, we have concluded that the models to describe kinematics and dynamics of its working equipment, hydraulic and transmission features tend to be analytical formulas derived from well-known laws of physics and from information on bulldozer's structure and mechanisms. If some parameters of the workflow are unknown or constantly changing, the models are either statistical tables or empiric dependences summarizing experimental data. The models depict interaction of end-effectors, engines and environment as well as statistic features of bulldozer's complex units.

Application of regulators based on classical control theory is difficult due to the frequent changes in workflow conditions. Thus, it is necessary to develop adapted control systems to eliminate the difficulties described. The system includes both the bulldozer's dynamics modeling and bulldozer's workflow control method to take into consideration the complex non-linear dependencies between workflow parameters and incomplete information on its working conditions changes [1, 2].

## 2 Materials and Methods

### 2.1 Structure of Bulldozer Working Process Model

The main goals for analytic simulation modeling of bulldozer workflow are:

- Bulldozer simulation as a controlled object to realize bulldozer's workflow parameters for using them at workflow neural network identification;
- Efficient traction modes parameters definition to be supported by the control system;

Simulation tasks:

- To single out the main sub-systems in bulldozer's structure and interrelations between the sub-systems;
- To develop analytic and simulation models for workflow elements and to include them into the general structure of the model.

General structure of the workflow model for automated bulldozers is developed (Fig. 1). The structure meets the goals of workflow control. When moving soil by the bulldozer, it is necessary to utilize bulldozer's traction capacity in full keeping the nominal traction value  $N$ ; when surfacing, the altitudes of the right and left side of the blade  $y = (y_n; y_l)$  are to correspond the design marks. The key element at the scheme (Fig. 1) shows the choice for the first or the second operational mode.

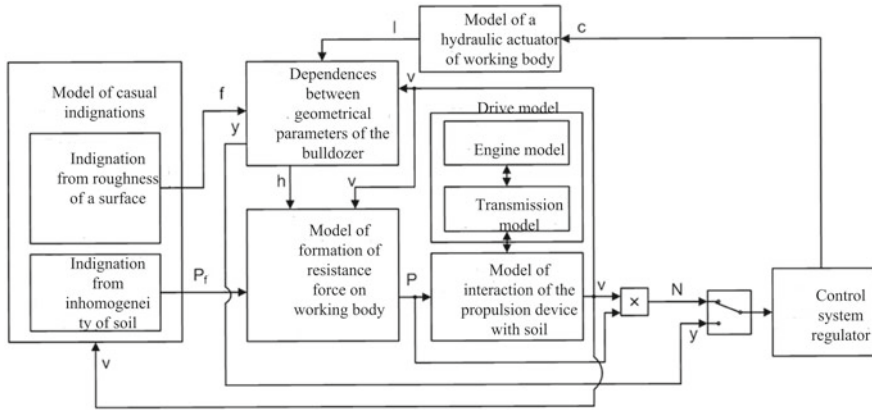


Fig. 1 Structure of bulldozer working model

### 2.2 Formation of casual resistance force on working blade

At developing the models, we use mathematical apparatus of the random processes theory, transfer functions, table interpolation, numerical solution of algebraic equations and ordinary differential equations in the Cauchy form. Random changes in the coordinates of untreated soil surface  $f$ , as well as normalized fluctuations in the resistance forces on the working organ  $P_f$ , caused by the heterogeneity of the soil are highlighted among the disturbing effects on the working organ of the bulldozer from soil conditions. Disturbance  $f$  cause unwanted vertical movement of the working organ that affects both the  $y$  coordinates and the change in the digging depth  $h$ . Dependence of the blade position and dig depth from disturbances  $f$  reflects the intricate relationship between the geometric parameters of the bulldozer in space. Loading conditions on the working organ are due to random variation in the dig depth and heterogeneity of soil properties. Soil digging process with bulldozer working organ is studied on the base of the finite element model of the soil mass, a mathematical model of random forces of resistance on the working organ  $P$  being developed. The actual bulldozer velocity  $v$  depends on the strength  $P$  and the properties of the mover, transmission and the power unit. In its turn, disturbance parameters, movement of the working organ and the formation of stress depend on the velocity  $v$ . Bulldozer drive model and mover interaction with the soil include engine model, mechanical and hydro mechanical transmission, as well as slipping. Control system regulator depending on the objectives, control algorithm and the incoming data from the bulldozer as a control object produces electrical signals  $c$  to the electro-hydraulic distributors being part of the working organ hydro drive. Lifting or burying the blade is done to control either the pulling power  $N$ , or the blade coordinates  $y$ . The following describes the models of the bulldozer workflow elements. A formation model of the random forces of resistance on the working organ being developed as follows:

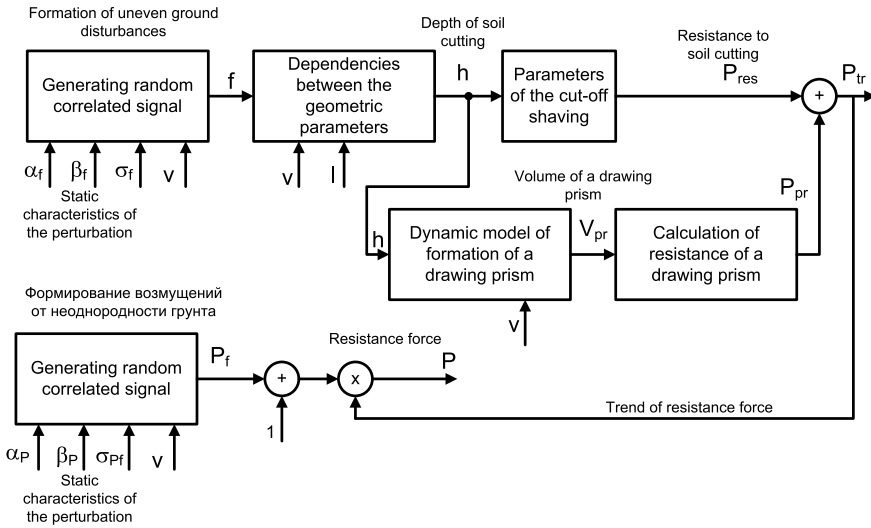


Fig. 2 Formation of casual resistance force on working blade

$$P = P_{tr}(1 + P_f); \tag{1}$$

where  $P_{tr}$ —is the trend of resistance forces depending on the dig depth  $h$ ;  $P_f$ —are the normalized random fluctuations caused by the heterogeneity of the soil (Fig. 2).

### 2.3 Simulation model impact of soil on the working body of the bulldozer

The developed models for bulldozer workflow elements are to be used for separate bulldozer units study with the help of analytical dependences between workflow parameters as well as for bulldozer general workflow simulation [3].

Elements models of bulldozer workflows being developed are intended both for the research of individual bulldozer units using analytical relationships between the parameters of the workflows and simulation of bulldozer workflows in general [4, 5].

When constructing a discrete simulation model, the following assumptions are taken:

- the linear motion of the machine is investigated;
- the design is considered to be rigid;
- backlash and friction between the elements of the working equipment are not considered;
- the elastic- damping properties of movers are not considered;
- the dynamic characteristics of a diesel engine with fuel regulator and hydro mechanical transmission torque converter are replaced with static;

- coordinates of the treated soil surface are completely determined by the coordinates of the cutting edge of working organ;
- engine power selection to the drive of the working organ and auxiliaries are neglected;
- rate of motion of hydraulic cylinders rods for lifting and burial of the working organ is identical and does not depend on the applied load;
- mover rolling resistance is constant.

A simulation model is implemented in MATLAB/Simulink [6, 7].

Experimental data loaded simulation model. Simulation tasks:

To single out the main sub-systems in bulldozer's structure and interrelations between the sub-systems;

To develop analytic and simulation models for workflow elements and to include them into the general structure of the model.

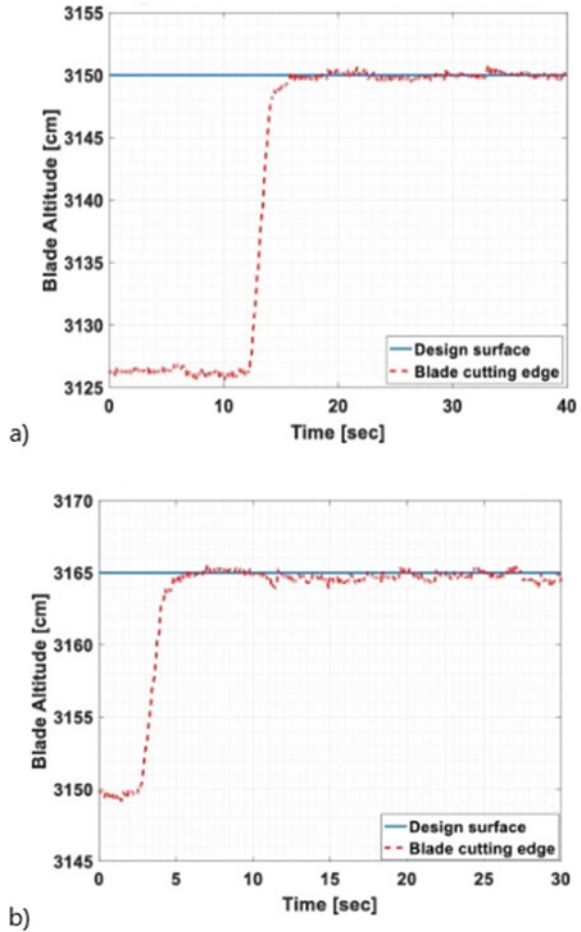
The structure meets the goals of workflow control. When moving soil by the bulldozer, it is necessary to utilize bulldozer's traction capacity in full keeping the nominal traction value; when surfacing, the altitudes of the right and left side of the blade are to correspond the design marks. The key element at the scheme (Fig. 3) shows the choice for the first or the second operational mode.

At developing the models, we use mathematical apparatus of the random processes theory, transfer functions, table interpolation, numerical solution of algebraic equations and ordinary differential equations in the Cauchy form. Random changes in the coordinates of untreated soil surface, as well as normalized fluctuations in the resistance forces on the working organ, caused by the heterogeneity of the soil are highlighted among the disturbing effects on the working organ of the bulldozer from soil conditions. Disturbance cause unwanted vertical movement of the working organ that affects both the coordinates and the change in the digging depth. Dependence of the blade position and dig depth from disturbances reflects the intricate relationship between the geometric parameters of the bulldozer in space. Loading conditions on the working organ are due to random variation in the dig depth and heterogeneity of soil properties. Soil digging process with bulldozer working organ is studied on the base of the finite element model of the soil mass, a mathematical model of random forces of resistance on the working organ being developed. The actual bulldozer velocity depends on the strength and the properties of the mover, transmission and the power unit. In its turn, disturbance parameters, movement of the working organ and the formation of stress depend on the velocity. Bulldozer drive model and mover interaction with the soil include engine model, mechanical and hydro mechanical transmission, as well as slipping. Control system regulator depending on the objectives, control algorithm and the incoming data from the bulldozer as a control object produces electrical signals to the electro- hydraulic distributors being part of the working organ hydro drive. Lifting or burying the blade is done to control either the pulling power, or the blade coordinates.

After training the model, load the data into the on-board complex of the bulldozer to check the adequacy of the model. To evaluate the proposed system, two experiments were carried out:



**Fig. 3** Verification system modeling surface



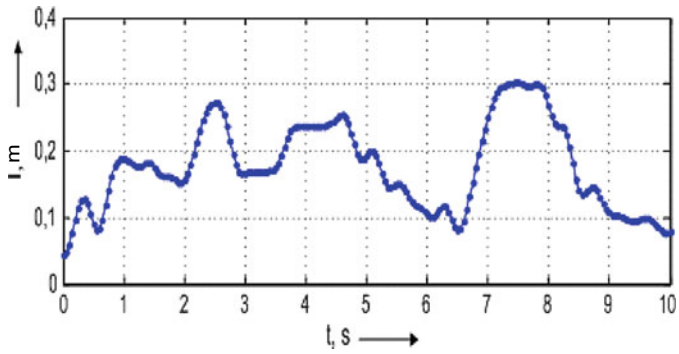
Operator controlled without using an automatic system (Fig. 3a);  
When controlling the operator using the developed system (Fig. 3b);

After that, the results were compared.

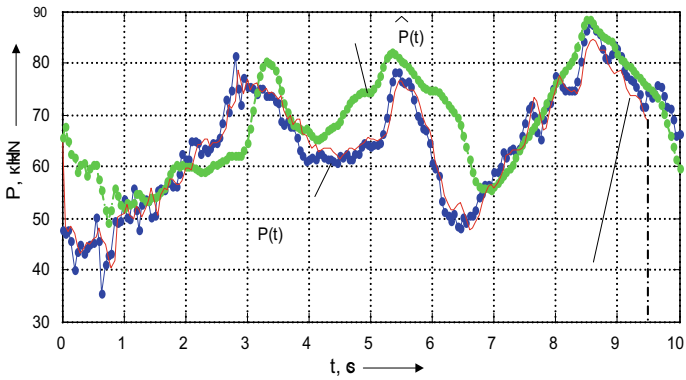
Thus, it can be noted that the system allows you to simulate a bulldozer digging surface with a deviation not exceeding 2 cm.

### 3 Conclusions

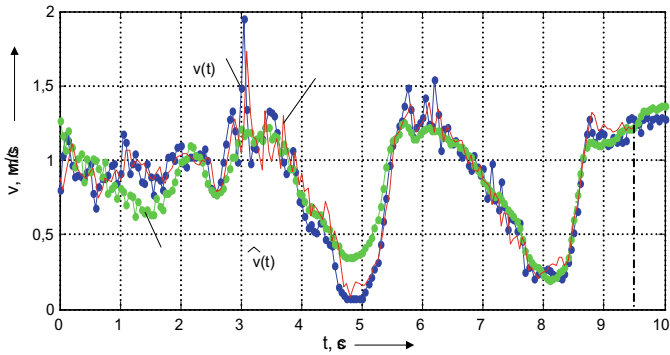
Input model signal, used for training, simulation and verification is presented in Fig. 4a. Adaptive learning for the model is stopped at time  $t=9,5$  s. Receiving at this moment a neural network model parameter values, modeled digging resistance force



a) Deepening Dozer Blade



b) Digging Resistance Force



c) Bulldozer Current Velocity

**Fig. 4** Comparison of Bulldozer operational parameters obtained with the Model and actual operational parameters

and speed of the machine (Fig. 4b, d) are accomplished, as well as the forecast for another 0.5 seconds is developed.

This is due to a change in unmeasurable chip thickness, as well as the rapidly changing conditions of the mover clutch with the ground. Therefore, the parameters of the adaptive neural network model must be adjusted in real time. The accuracy of prediction of pulling power  $N(t)$  has been estimated; the average relative error being 14.7 % on an interval from 7 to 10 s. Identification Technique of bulldozer workflows and models obtained on its basis, are designed for use in the development of adaptive systems of automatic workflow management of bulldozer.

Thus, after a comparative analysis of the results, the following conclusions can be drawn:

- (1) the digging resistance force simulation system allows you to calculate the working process of the bulldozer;
- (2) training methods applied to the control system allow integrating control principles into the earth-moving machines operation system to increase work efficiency.

## References

1. ROBO Industries Autonomous Machine Control System On-line <http://www.aee.us.com/page-video.html>, Accessed 4th Jul 2019
2. Yin G, He F, Li Z, Ling J (2020) Workspace description and simulation of a backhoe device for hydraulic excavators, 103325 Automation in Construction Volume 119, November 2020
3. Lee, Y-S., Kim, S-H., Seo, J., Han, J., Han, C-S.: Blade control in Cartesian space for leveling work by bulldozer, Automation in Construction Volume 118, October 2020.
4. Komatsu Corporation. Intelligent Machine Control. On-line <https://www.komatsu.eu/en/Komatsu-Intelligent-Machine-Control>, Accessed 4th Jul 2019
5. Trimble Corporation. Civil Engineering and Construction, Grade Control for Dozers. On-line <https://construction.trimble.com/products-and-solutions/grade-control-dozers>, Accessed 4th Jul 2019.
6. Georgy ME, Chang LM, Zhang L (2005) Prediction of engineering performance: a neurofuzzy approach. J Constr Eng Manag 131(5):548–557
7. Bulgakov A, Bock T, Tokmakov G (2015) Adaptive control of bulldozer's workflows. In: 5th International Construction Specialty Conference, Vancouver, June 7–10, pp. 434–442

# The Study of the Suction Activated by the End Supply Jet from Plasma Cutting Area



Oleg Zaitsev , Natalia Semicheva , Andrey Ishutin , Yuri Sivachenko ,  
and Sergey Egorov 

**Abstract** The study of a local suction activated by perpendicular straight-flow jet from plasma cutting areas in the outlet space of the heterogeneous jet has been carried out. The results of the numerical simulation of various options for suction torch activation and experimental studies of the proposed suction apparatus design are presented. Axial velocity values at different air flow rates with the optimal flow rate ratio  $\beta$  are determined for the patented design of the local suction. It is revealed that the absence of negative factors of jets interaction during supply air jet formation in the form of radial air jet is achieved for the activating and removing jets ratio  $\beta = 0.8\text{--}1$ . It is also determined that schemes when the values of the flow ratios are  $\beta > 1$  lead to an increase in the suction range, and the opening angle of the cutting radial air jet is close to  $90^\circ$ . Experimental data obtained by modelling the effects of suction and radially directed limiting flow has been obtained and substantiated. The geometrical parameters of the device at which an improvement in the conditions of the suction flow performance is observed have been obtained.

**Keywords** Removal · Local suction · Plasma cutting · Suction torch

## 1 Introduction

In the Russian Federation, in 2013–2022, the production of metal-cutting machines increased from 2,928 to more than 5,500 pieces, among which the number of plasma cutting machines is about 1.8–2 thousand pieces [1]. A wide range of various low-efficient exhaust devices, which remove significant volumes of air, is used to localize

---

O. Zaitsev (✉) · Y. Sivachenko · S. Egorov  
Crimean Federal University Named After V.I. Vernadsky, 181, Street, Kyiv, Simferopol 295943,  
Republic of Crimea  
e-mail: [zon071941@mail.ru](mailto:zon071941@mail.ru)

N. Semicheva · A. Ishutin  
Southwest State University, 94, 50 Let Oktyabrya Street, Kursk 305040, Russia

© The Author(s), under exclusive license to Springer Nature Switzerland AG 2024  
N. Vatin et al. (eds.), *Modern Problems in Construction*,  
Lecture Notes in Civil Engineering 372,  
[https://doi.org/10.1007/978-3-031-36723-6\\_42](https://doi.org/10.1007/978-3-031-36723-6_42)

437

and remove harmful emissions from plasma cutting. For such systems, the average volume of air removed varies from 5000 to 7000 m<sup>3</sup>/h.

However, despite the variety of exhaust systems, they require significant volumes of exhaust air and are characterized by low efficiency due to the rapid attenuation of the suction flow rates. Therefore, localization and removal of harmful emissions, which make up the bulk of plasma cutting, from the area below the metal plane using a local suction activated by a radial air jet, seems to be the most promising hypothesis.

Thus, there is a significant potential for upgrading the means of local exhaust ventilation used for plasma metal processing in order to improve the quality of working conditions and reduce energy costs [1–5].

**The purpose of the work** is to reduce emissions of harmful substances into the environment and maintain the required parameters of the microclimate by improving the means for localizing, removing air from non-stationary places of plasma metal cutting.

**The objectives of the study** are as follows:

- To investigate the interaction of a heat heterogeneous jet emerging at the cutting points with the gas flow and the suction with the help of numerical simulation, and to develop a highly effective technique of localizing and removing harmful emissions based on the results obtained;
- to develop a coaxial air distribution device with an end flow distribution for ventilation systems which allows localizing the released harmful emissions in the places where a plasma arc passes through metal;
- to investigate experimentally the design of the suction applying the proposed technique for removing harmful emissions [6].

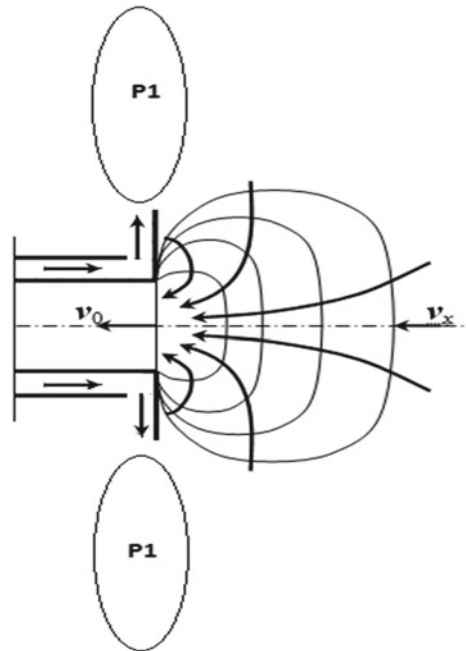
## 2 Materials and Methods

The objectives set were solved by mathematical methods of physical modelling and numerical simulation [7–11]. Physical modelling was applied to obtain dependencies that formulate methods for calculating aerodynamic and ecology and energy parameters of the resulting flow during the interaction of the plasma flow with the suction spectrum and the radial activated jet. Numerical simulation was used to obtain a spatial representation of flow lines, temperature, velocity, and pressure fields. The reliability of the obtained scientific considerations, conclusions and recommendations is based on contemporary views on aerodynamics and heat transfer and is confirmed by the fact that the results obtained do not contradict the conclusions of the known provisions. Aerodynamic studies of the process of removing harmful emissions from the places of plasma metal cutting were carried out on an experimental setup which is based on the installation of the proposed local suction activated by a radial supply jet.

### 2.1 A Digital Model of the Coaxial Suction with End Distribution of Limiting Flow

The model consists of two pipes installed coaxially, and the air ducts are arranged in such a way that they form an inter-tube space. The suction jet moves through the internal air duct. In the inter-tubular space, the feeding jet moves in the opposite direction. After flowing out of the hole, the feeding jet forms a limiting zone, that is, it is reflected from the limiting diffuser and propagates coaxially into space. The following data were accepted as the initial conditions for modelling: atmospheric pressure— $P_a = 101,325 \text{ Pa}$ , air temperature— $t_H = 20 \text{ }^\circ\text{C}$ , air flow rate passing in the inter-tubular space and in the inner pipe— $Q_{By} = 1000 \text{ m}^3/\text{h}$ , inner pipe section length— $l_{By} = 500 \text{ mm}$ , external pipe section length  $l_{BH} = 490 \text{ mm}$ . In the first approximation, the diameter of the limiting diffuser was  $D_{\pi} = 100 \text{ mm}$ , then it was increased by 100 mm with a final value of 200 mm. The diameters of the inner  $D_B$  and outer  $D_H$  air ducts were 100 mm and 115 mm, respectively. The angle of the limiting diffuser relative to the axis of the ducts was  $90^\circ$ . The computational diagram of the model is shown in (Fig. 1). In this task, the motion of the flowing media, i.e. the gases being removed and the supply jet, is modelled applying the Navier–Stokes equations, which in a non-stationary formulation describe the laws of conservation of mass, momentum and energy of these media, the numerical implementation of which is performed in the SolidWorks software package.

**Fig. 1** Computational diagram of the numerical model



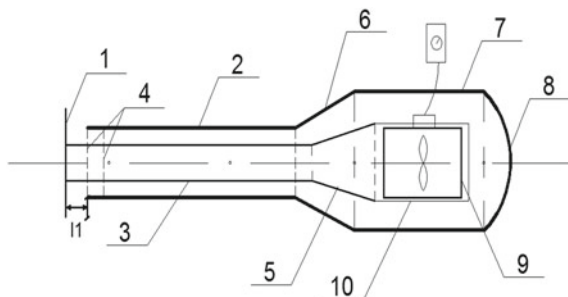
## 2.2 Experimental Studies. Research Conditions

The operation of the experimental setup (Fig. 2) is as follows: the air flow is sucked through an inner pipe (3) on which a round limiting diffuser (1) is fixed; an inner air duct of a smaller diameter is inserted into the outer duct of a larger diameter and the outer duct is installed at some distance from the diffuser, which is fixed on the air duct of a smaller diameter forming an air distribution device. The second flow passes through the inter-tubular space formed by the inner tube (3) and the outer tube (2). The pipes are fixed together by centering guides to adjust the distance between the pipes, and, as a result, the volume of air passing between them from one side of the inter-tubular space, and also to adjust the direction of air distribution from the inter-tubular space, and, respectively to change the volume of the inter-tubular space. The flow passing through the inter-tubular space moves to the outlet formed by the outer pipe (2) and the limiting diffuser (1) flows around the limiting diffuser and then is distributed into the space around the device, thereby forming an area of increased pressure. The distribution is controlled by a nozzle-regulator (5) fixed to the outer pipe (2).

To determine the main characteristic features of the suction flow, a set of experimental studies was carried out, consisting in determining the zone of the suction flow action, the distribution of velocities at different distances from the suction hole as well as determining the axial flow velocity.

At the first stage, the zone of action of the suction flow was determined. To do this, at a distance of 800 mm from the suction inlet, a tripod with an ATE 1034 Aktakom anemometer was installed. An axial marking was applied to the limiting diffuser to determine the center of the hole. The tripod was adjusted relative to the axis of the suction hole by the laser level, installing the level, the diffuser and then the tripod with an anemometer coaxially. During the experiment, the tripod was placed on a stencil of  $1000 \times 1000$  mm marked in increments of 50 mm; in this case one of the sides of the stencil was placed in the center relative to the axis of the diffuser so that the axis of the diffuser coincided with the central axis of the stencil. Focusing on the values of the distances obtained from the results of the simulation when carrying out measurements, the tripod moved from the suction hole in the opposite direction shifting to the previously defined boundary of the suction flow area at the control

**Fig. 2** Scheme of the experimental installation



points at a fixed distance of 50 mm until the readings were fixed on the anemometer scoreboard; a set of experiments was carried out with averaging the final readings. A set of at least five measurements was carried out at control points with a difference between the results by more than  $\pm 5\%$ ; in the opposite case, the sets of measurements were repeated.

Thus, the range of the suction flow and the deviation from the values obtained from the simulation results were determined.

### 3 Results and Discussion

#### 3.1 Results of Numerical Modelling

As a result of the conducted modelling of the air flow formed during the operation of the suction device with a given flow rate of  $1000 \text{ m}^3/\text{h}$ , it was obtained that the leakage of air flows occurs from the entire sphere to the suction inlet, which corresponds to the statements set out in [5–7, 12–16] and is shown in (Fig. 3). The axial velocity was 0.8–1.2 m/s at a distance of 10–15 cm from the suction inlet; it was 0.4–0.6 m/s at a distance of 30 cm; the air velocity was 0.1 m/s at a distance of 45 cm. At a given distance  $l_1 = 15 \text{ mm}$  (Fig. 4), a flow pattern in which a limitation of the leakage of flows from the backward hemisphere was achieved was obtained; at the same time, in the frontal zone the stability of flows relative to each other was not achieved. The modelling results show that for the values of the flow ratio (Figs. 5 and 6)  $\beta = 0.8\text{--}1$ , the absence of negative factors of jet interaction during the formation of the supply air flow in the form of a radial air jet was achieved.

#### 3.2 Experimental Study Results

Based on the data obtained, a dependence of axial velocities on the distance from the axis of the suction hole at different values of  $Q$  and the value of  $\beta = 1$  was built. A summary graph of the dependence of axial velocities on the distance from the axis of the suction hole at specified flow rates  $Q_1\text{--}Q_4$  and the value  $\beta = 1$  is shown in (Fig. 7).

As a result of numerical modelling of the activated suction operation, schemes in which the values of the flow ratios at  $\beta > 1$  lead to a slightly greater stabilization of the flow, the opening angle of the cutting-off radial flow approaches  $90^\circ$  have been identified; however, for the layout design of the installations for local exhaust ventilation, it is not advisable to adjust the value of  $\beta$  upwards, for example, for devices with one agitator for the distributing and suction flow. Thus, the range of variation of the ratios of air flow rates for the formation of the limiting jet is determined (Fig. 6), the flow rate of the removed air is equal to  $0.8 \leq \beta \leq 1$ .



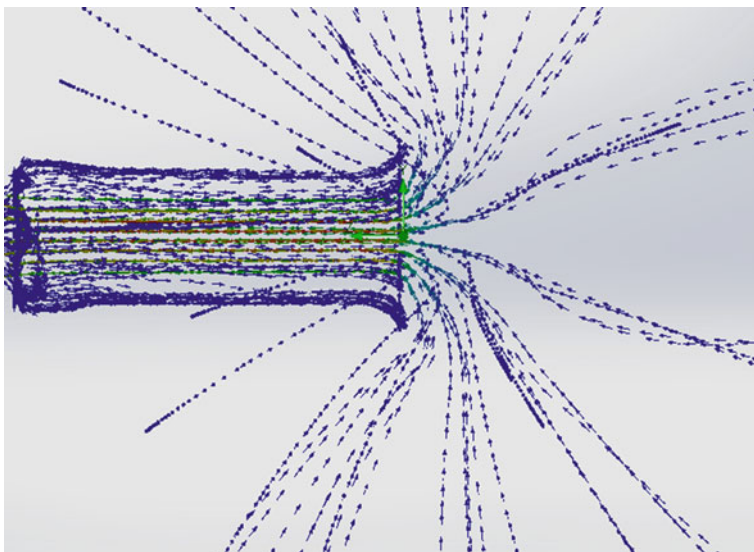


**Fig. 3** Visualization of flow lines during the operation of the non-activated suction

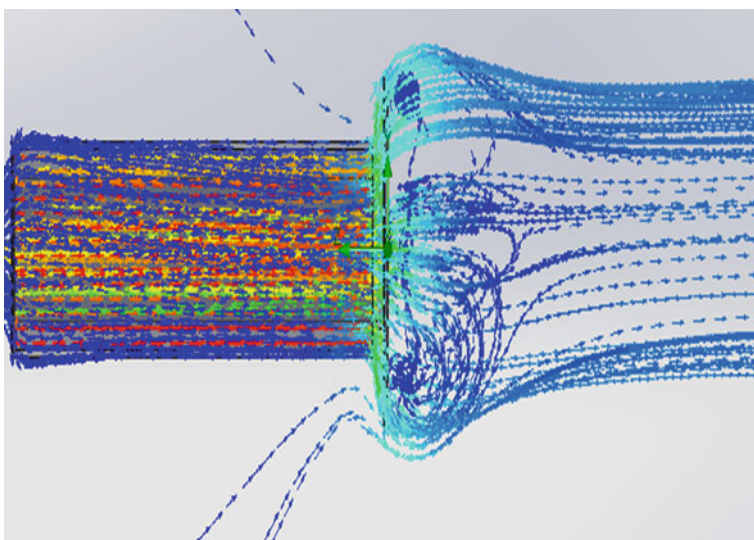


**Fig. 4** Visualization of the flow lines at a distance from the external duct to the limiting diffuser  $l_1 = 15$  mm

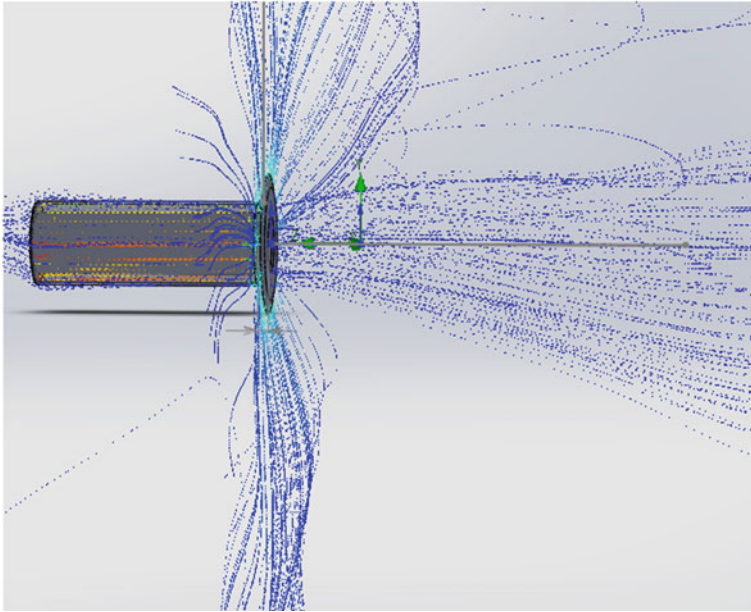
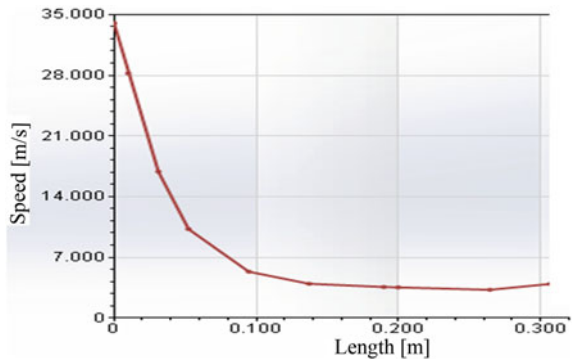


**Fig. 5** Visualization of flows at  $\beta = 7.2$ ,  $Q_{b2} = 3,600 \text{ m}^3/\text{h}$ ,  $Q_{b1} = 500 \text{ m}^3/\text{h}$

**Fig. 6** Diagram of the dependence of the velocity on the distance to the axis of the suction hole at  $Q_{By} = 1000 \text{ m}^3/\text{h}$



As a result of the performed experiment, the data of numerical modelling of the impact of the suction and radially directed limiting flow were substantiated. The geometrical parameters of the device at which an improvement in the conditions of the suction flow is achieved are also obtained. Some structural design solutions of the exhaust device for local ventilation systems to remove harmful emissions during plasma treatment of metals which allows to improve working conditions were proposed [6].

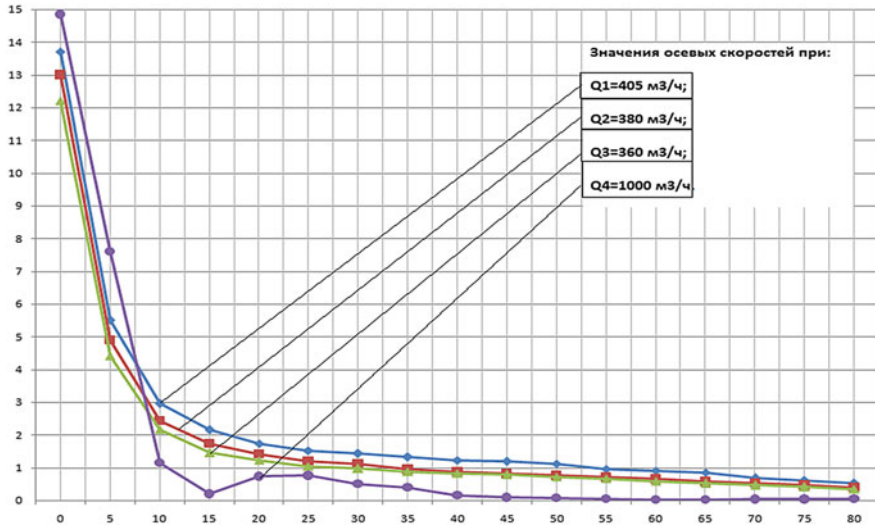


**Fig. 7** A summary graph of the dependence of velocities on the distance from the axis of the suction hole at specified flow rates  $Q_1$ - $Q_4$  and the value  $\beta = 1$

## 4 Conclusion

1. Based on the experimental and theoretical studies of the suction torches of a coaxial exhaust device limited by a radially directed distributing flow the values of axial velocities at various air flow rates with the optimal flow ratio  $\beta$  for the patented local suction design were determined for the first time.
2. As a result of numerical modelling, it was revealed that for the values of the flow ratio  $\beta = 0.8$ – $1$ , the absence of negative factors of jet interaction during the formation of the supply air flow in the form of a radial air jet is achieved. It was also determined that the schemes in which the values of the flow ratios at  $\beta > 1$  lead to a slightly greater stabilization of the flow, the opening angle of the cutting-off radial flow approaches  $90^\circ$ .
3. It was revealed that for the layout solutions of installations for local exhaust ventilation, it is not advisable to adjust the value of  $\beta$  upwards the value of  $\beta$  is not advisable to adjust upwards for devices with one agitator for the supply and suction flow. At the same time, the range of variation of the ratios of air flow rates for the formation of a limiting jet equal to  $0.8 \leq \beta \leq 1$  was determined.

## References

1. Burokova AV, Rakhmanov YuA (2014) On the issue of heat recovery of gases from heat treatment furnaces of metal products. *Sci J NRU ITMO Ser Econ Environ Manag* 1:17–27
2. Dorokhova NA (2017) Utilization of the heat of the flue gases of a boiler unit using a heat pump. In: *Materials of the XVII international scientific and technical conference students, graduate students and young scientists*. GSTU named after P.O. Sukhoi, Gomel
3. Imal M (2016) A new system design for energy management in HVAC control systems for textile plants. *Acta Phys Polonica A* 130(1):245–248. <https://doi.org/10.12693/APHYSPOLA.130.245>
4. Zaitsev ON, Logachev KI, Goltsov AB (2021) Calculation of axial air velocity near vortex suction. In: *Heat and mass transfer and hydrodynamics in swirling flows (October 18–21, 2021): proceedings of the VIII international conference*. MEI, Moscow
5. Schlichting G (1974) *The theory of the boundary layer*. Trans. from German. Nauka, Moscow
6. Zaitsev ON, Savchenko YuA. Coaxial suction with end flow distribution for exhaust ventilation systems. Utility model patent F24F 9/00 No. 207611 dated 2021/11/03
7. Kryzhanovsky YuV, Kryzhanovsky VN (2012) *Structure and calculation of a gas torch*. Monograph K.: the enlightenment of Ukraine
8. Shtym AN, Shtym KA, Dorogov EY (2012) *Boiler installations with cyclone pretopstacks: monograph*. Far Eastern Federal University
9. Boyaghchi FA, Molaie H (2015) Investigating the effect of duct burner fuel mass flow rate on exergy destruction of a real combined cycle power plant components based on advanced exergy analysis. *Energy Convers Manag* 103:827–835. <https://doi.org/10.1016/j.enconman.2015.07.008>
10. Klymchuk O, Denysova A, Shramenko A, Borysenko K, Ivanova L (2019) Theoretical and experimental investigation of the efficiency of the use of heat-accumulating material for heat supply systems. *EUREKA Phys Eng* 3:32–40. <http://eu-jr.eu/engineering/article/view/901/892>
11. Klymchuk AA, Lozhechnikov VF, Mykhailenko VS, Lozhechnikova NV (2019) Improved mathematical model of fluid level dynamics in a drum-type steam generator as a controlled object. *J Autom Inf Sci* 51(5):65–74. <http://jais.org.ua/zhurnal-3-22.html#more-1310>
12. Bystrov YA, Isaev SA, Kudryavtsev NA, Leontiev AI (2005) *Numerical simulation of vortex intensification of heat exchange in stacks of pipes*. Shipbuilding, St. Petersburg
13. Grimitlin AM, Datsyuk TA, Denisikhina DM (2013) *Mathematical modeling in the design of ventilation and air conditioning systems: monograph*. ABOK North-West, St. Petersburg
14. Logachev IN, Logachev KI (2014) *Industrial air quality and ventilation: controlling dust emissions*. CRC Press, Boca Raton
15. Averkova OA, Logachev IN, Logachev KI, Zaytsev ON (2017) Ejecting properties of a bucket elevator. In: *5th International conference on particle-based methods—fundamentals and applications, PARTICLES 2017*, pp 45–56. Conference paper
16. Zaytsev ON, Lapina EA (2017) Increasing the efficiency of the condensing boiler. *J Phys: Conf Ser* 891(1):012158. Conference paper

# A Technique for Determining a Polymer Product Temperature Time Dependence Under Process Air Cooling



Evgeny Umerenkov , Elina Umerenkova , Ekaterina Savelyeva ,  
and Victor Budnikov 

**Abstract** The issue of heat removal in various processes is topical and often determines the efficiency of the achieved result. The authors of the article consider the issue of heat removal in the process of manufacturing rectangular and cylindrical polymer products under specified process conditions. The authors propose an approach for determining the operating and design parameters of a cooling chamber based on the technique for determining the time dependence of the temperature of air-cooled workpieces in a turbulent flow regime. To estimate the time dependence of the temperature of the cooled rectangular workpieces, it is assumed that each of them is in approximately the same conditions. Therefore, to perform such an evaluation, the cooling of an individual product is considered. A similar approach is used for products in the form of thick-walled hollow cylinders. The complexity of formalization due to the random loading of workpieces into the container, is resolved by considering the so-called triangular packaging, closest to the natural laying of products. Thus, a method of engineering evaluation of air cooling of polymer products of various shapes required within the manufacturing process has been developed. The proposed approach makes it possible to evaluate the time dependence of the temperature of workpieces of various shapes and to select the optimal input parameters of the cooling method, i.e. it can be adapted to other materials of products.

**Keywords** Air cooling · Flow regime · Heat transfer · Thermal conditions · Operating parameters · Design parameters

## 1 Introduction

The problem of heat removal in various technological processes is important and often determines the efficiency of the process. A wide range of works presents both classical methods for solving heat transfer issues [1–6] and applied ones [7–9]. Individual

---

E. Umerenkov · E. Umerenkova (✉) · E. Savelyeva · V. Budnikov  
Southwest State University, 50 Let Oktyabrya Street., 94, Kursk 305040, Russia  
e-mail: [elinaelya@gmail.com](mailto:elinaelya@gmail.com)

© The Author(s), under exclusive license to Springer Nature Switzerland AG 2024  
N. Vatin et al. (eds.), *Modern Problems in Construction*,  
Lecture Notes in Civil Engineering 372,  
[https://doi.org/10.1007/978-3-031-36723-6\\_43](https://doi.org/10.1007/978-3-031-36723-6_43)

447

technological techniques for cooling production processes have been developed for each industry. Depending on the specifics of the equipment and the amount of thermal energy removed, cooling can be performed with water, air or oil. To implement the cooling process a tool is needed to determine the operating and design parameters of the cooling chamber under specified process conditions.

The authors of this article propose a method for determining the temperature time dependence for air-cooled workpieces in a turbulent flow regime.

## 2 Methods and Materials

The issue is considered in relation to the cooling process of rectangular and cylindrical polymer products.

To estimate the time dependence of the temperature of rectangular workpieces, we assume that each of them is in approximately the same conditions. Therefore, to perform such an assessment, let us consider the cooling of an individual product. The diagram of the problem is provided in Fig. 1.

The thermal state of a workpiece with  $L_z$  (length - height)  $\times \delta_z$  (thickness)  $\times h_z$  (width) can be described by the following balance expression

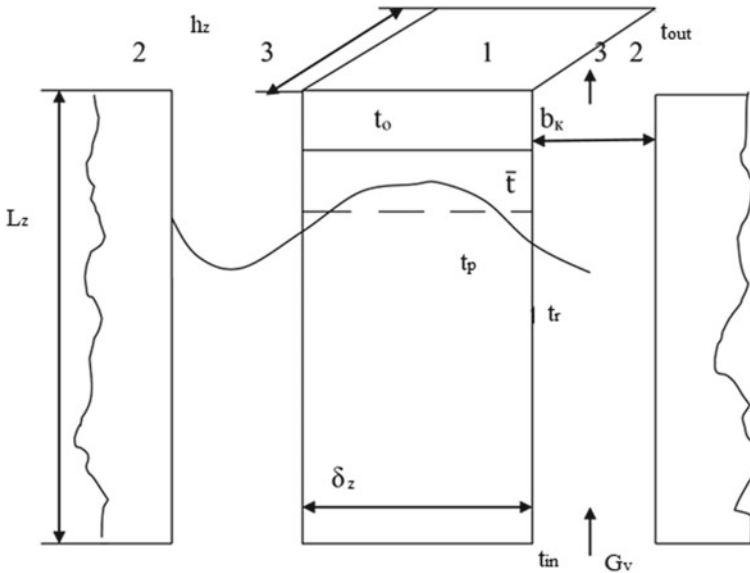


**Fig. 1** The diagram of the problem of air cooling a rectangular workpiece: 1—design workpiece; 2—adjacent, symmetrically arranged workpieces; 3—channels (clearance) for the movement of cooling air

$$M \times C_p \times \frac{d\bar{t}}{d\tau} = -q, \quad (1)$$

where  $M$  is the weight of the workpiece, kg;  $C_p$  is the specific heat of the product material (polymer),  $\frac{J}{kg \cdot ^\circ C}$ ;

$\bar{t}$  is the volumetric average temperature of the workpiece,  $^\circ C$ ;

$\tau$  is the time, *sec*;

$q$  is the heat flow from the workpiece to the cooling air,  $W$ .

It is obvious that,

$$M + L_z + \delta_z + h_z + \rho_p,$$

where  $\rho_p$  is the material density,  $kg/m^3$ .

According to the information from the customer,  $L_z = 650$  mm,  $\delta_z = 133$  mm,  $h_z = 154$  mm.

The thermophysical properties of the polymer [10] are  $C_p = 1130$  J/kg  $\times$   $^\circ C$ .;  $\rho_p = 1140$  kg/m<sup>3</sup>; conductivity  $\lambda_r = 0,19$  W/m  $^\circ C$ .

For the heat flow  $q$  the following is true

$$q = F \times \alpha \times (t_p - t_r), \quad (2)$$

where  $F$  is the lateral surface of the workpiece (heat exchange surface), m<sup>2</sup>. In this case,

$$F = 2 \times L_z(\delta_z + h_z); \quad (3)$$

$\alpha$  is the coefficient of the heat transfer (exchange) from the workpiece surface to the cooling air, W/m<sup>2</sup>  $^\circ C$ .;  $t_p$  is the average surface temperature;  $t_r$  is the design temperature of the air in the clearance between the workpieces, as a rule, taken equal to the arithmetic average input and output air temperatures in the channel, i. e.

$$t_r = 0,5 \times (t_{in} - t_{out}). \quad (4)$$

On the other hand, expression for  $q$  can be written in the following form

$$q = G \times c_v \times (t_{out} - t_{in}), \quad (5)$$

where  $G$  is the air mass flow (per workpiece) in the channel, kg/sec;  $c_v$  is the air heat capacity at the design temperature  $t_r$ . Taking into account the slight impact of the temperature on the air thermophysical properties we will consider them to be constant and determined at the design temperature

$$t_{ro} = 0,5 \times (t_{in} + t_o),$$

where  $t_o$ —is the initial workpiece temperature.

To calculate using  $t_{ro}$  let us use interpolation equations [11]

$$c_v = (1,0005 + 1,1904 \times 10^{-4} \times t_{ro}) \times 10^3;$$

Air density (at the normal atmospheric pressure) is

$$\rho_v = \frac{101325}{287,4(t_{ro} + 273)}$$

$$\lambda_v = 2,44 \times 10^{-2} \times \left(\frac{t_{ro} + 273}{273}\right)^{0,82};$$

dynamic viscosity is

$$\mu_v = 1,717 \times 10^{-5} \times \left(\frac{t_{ro} + 273}{273}\right)^{0,683}.$$

Making  $q$  equal according to (2) and (5) taking into account (4), on rearrangement we obtain

$$t_{out} = \frac{2}{W+1} \times t_p + \frac{W-1}{W+1} \times t_{in}, \quad (6)$$

which plugging in (5) gives

$$q = \frac{W}{W+1} \times F \times \alpha \times (t_{vn} - t_{in}). \quad (7)$$

Here, the equivalent of the flowrate according to E.Ya. Sokolov [12]) is

$$W = \frac{G \times c_v}{F\alpha \times 0,5}. \quad (8)$$

If we bear in mind that body condition changes quite quickly into the regular thermal condition [13], then

$$\frac{d\bar{t}}{d\tau} = \frac{dt_p}{d\tau}$$

And taking into account (1) and (7) we obtain

$$M \times C_p \times \frac{dt_p}{d\tau} = -\frac{W}{W+1} \times F \times \alpha \times (t_p - t_{in}), \quad (9)$$

Which is the ordinary differential equation of the 1<sup>st</sup> degree for function  $t_p(\tau)$ . The solution (9) by means of the separation of variables gives



$$t_p = t_{in} + (t_o - t_{in}) \times e^{-rt}, \tag{10}$$

where  $r = \frac{W}{W+1} \times \frac{F \times \alpha}{M \times C}$  has a dimension inverse to time.

In the provided expressions, heat transfer coefficient  $\alpha$  is used. To determine it let us calculate the Reynolds number, in this case for close clearance of width  $b_k/2$  (flowrate  $G$  refers to one product). Then,

$$Re = G/(2b_k\mu_v) \tag{11}$$

Supposing that in significant from the practical point of view cases air flow in the channel is turbulent, the Nusselt number for the air is determined as [13]

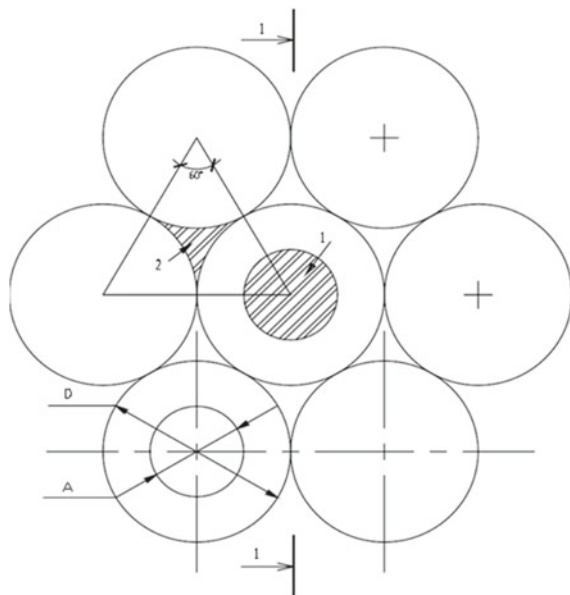
$$Nu = 0,018Re^{0.8} \tag{12}$$

And the heat transfer coefficient is.

$$\alpha = Nu\lambda_v/2/b_k. \tag{13}$$

A similar approach is used to estimate the time dependence of the temperature of workpieces in the form of thick-walled hollow cylinders. The complexity of formalization is due to the random loading of workpieces into the container. In our opinion, the closest to the natural packaging of products is their packaging when each cylinder is surrounded by six adjacent ones, the so-called triangular packaging (Fig. 2).

**Fig. 2** Triangular packaging of workpieces: 1—internal cooling channel; 2—external cooling channel (one of 6)



In addition to the internal cooling channel, each cylinder has 6 external channels formed by the arcs of the circles corresponding to the central angles  $60^\circ$ .

The cooling air flowrate per workpiece  $G$  is distributed to the inner  $G_{vn}$  and outer  $G_n$  parts in proportion to the corresponding cross-sections, although, strictly speaking, this is a more complex hydrodynamic problem that requires taking into account the hydraulic resistances of the channels.

The cross-sectional area of the inner channel (see Fig. 2) is

$$S_{vn} = \pi d^2/4 \tag{14}$$

and the area of the curvilinear triangle (2 in Fig. 2) as the area of an equiangular triangle with side  $D$  minus three circular sectors is  $S_v = D^2(2\sqrt{3} - \pi)/8$ .

Since the air passing through such a channel provides heat exchange with three adjacent, symmetrically arranged cylinders, we will define the share of the channel area related to one workpiece as one third of  $S_v$ , and taking into account the presence of six such cavities for the total cross-sectional area of the outer channel (per workpiece) we will get.

$$S_n = D^2(23 - \pi)/4. \tag{15}$$

According to the customer,  $d = 30$  mm,  $D = 110$  mm, product length  $L = 1,450$  mm.

Then according to (14) and (15)  $S_{vn} = 706.8$  mm<sup>2</sup>,  $S_n = 975.6$  mm<sup>2</sup>. The total area  $S = 1682.4$  mm<sup>2</sup>, and the proportions of the inner and outer parts are 0.42 and 0.58, respectively. In the same proportion, the total consumption  $G$  (per workpiece) is divided into internal and external parts, i.e.  $G_{vn} = 0.42G$  and  $G_n = 0.58G$ . Note that the difference between  $G_{vn}$  and  $G_n$  is small, which serves as a justification for further simplification.

The design diagram of the thermal problem is provided in Fig. 3 (in Sect. 1 of Fig. 2).

$$q = \frac{W_{vn}}{W_{vn} + 1} F_{vn} \alpha_{vn} (t_{p,vn} - t_{in}) + \frac{W_n}{W_n + 1} F_n \alpha_n (t_{p,n} - t_{in}), \tag{16}$$

where:

$$W_{vn} = G_{vn} c_v / (F_{vn} \alpha_{vn} \theta, 5); W_n = G_n c_v / (F_n \alpha_n \theta, 5)$$

$$F_{vn} = \pi dL; F_n = \pi DL.$$

However, the direct use of  $q$  together with (1) is not possible, since (16) contains two independent variables  $t_{p,vn}$  and  $t_{p,n}$ . In this regard, we assume that these temperatures are equal:  $t_{p,vn} = t_{p,n} = t_p$ . Consequently, the difference in heat flows from the

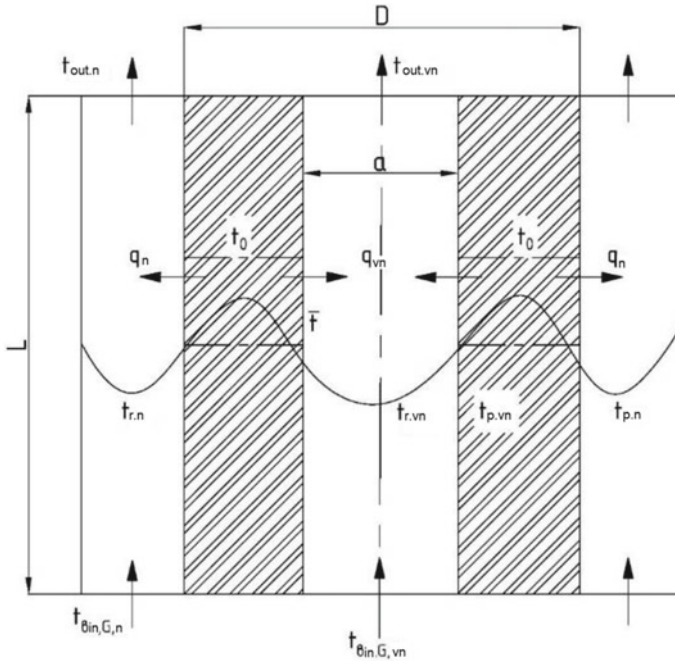


**Fig. 3** The diagram of the cooling problem for a workpiece in the form of a hollow cylinder

outer and inner surfaces of the hollow workpiece will be determined by the difference in the surfaces themselves  $F_{vn}$  and  $F_n$ , air flowrates  $G_{vn}$  and  $G_n$  and heat transfer coefficients  $\alpha_{vn}$  and  $\alpha_n$ , i.e., ultimately,  $G_{vn}$  and  $G_n$ .

Thus, the temperature change  $t_p$  on the cylinder surface is calculated by (10), where the exponential factor is equal to

$$r = (F_{vn}\alpha_{vn} + F_n\alpha_n) \tag{17}$$

The workpiece weight in this case is  $M = \pi(D^2 - d^2)L\rho_p/4$ .

We will also focus on the specific features of calculating the heat transfer coefficients of  $\alpha_{vn}$  and  $\alpha_n$ .

For the inner surface of the tube.

$$Re_{vn} = 4G_{vn}/(\pi d\mu_v). \tag{18}$$

The Nusselt number  $Nu_{vn}$  for the developed turbulent conditions is calculated according to (12) and.

$$\alpha_{vn} = Nu_{vn}\lambda_v/d. \tag{19}$$

As for  $\alpha_n$ , in this case, the calculation is reduced to determining the heat transfer coefficient during the flow of the air in a triangular channel with curvilinear walls—each side of the triangle is an arc equal to 1/6 of the circumference. The coolant flow rate in such a channel is equal to the tripled (the channel is surrounded by three cylinders) value of one sixth of the flow rate  $G_n$ , i.e.  $G_n/2$ , and the hydraulic diameter of the channel is.

$$d_{ekv} = D(-1). \quad (20)$$

Taking into account the design flow rate in the channel and (20) Reynolds criterium is

$$Re_{vn} = 4G_n/(\pi D\mu_v), \quad (21)$$

And heat transfer coefficient is

$$\alpha_n = Nu_n\lambda_v/d_{ekv}. \quad (22)$$

### 3 Results and Discussion

The results of the determination of the time dependence of the temperature of rectangular workpieces cooled by air under the turbulent flow regime  $t_p$  ( $\tau$ ) according to (10) taking into account (9, 11–13) at different flow rates  $G$  are provided in Fig. 4.

As the initial temperature of the workpiece in the calculations  $t_0 = 80$  °C is taken, the air temperature at the inlet of the channels (clearance between workpieces with a width of 1 cm) is  $t_{in} = 25$  °C.

The results of the calculation of the time dependence of the temperature of air-cooled workpieces in the form of thick-walled hollow cylinders  $t_p(\tau)$  for various air flow rates  $G$  (per workpiece) according to (10), taking into account (17–22) are provided in Fig. 5.

As can be seen from Figs. 4 and 5, the cooling of workpieces is significantly accelerated with an increase in the cooling air flowrate  $G$ . The relative position of the parts (the dimensions of the channels for air passage) has a certain value for the intensity of heat exchange.

### 4 Conclusion

Thus, the proposed technique for estimating the time dependence of the temperature of workpieces of various geometric shapes allows us to choose the optimal input parameters for the cooling method and can be adapted to other materials. Special

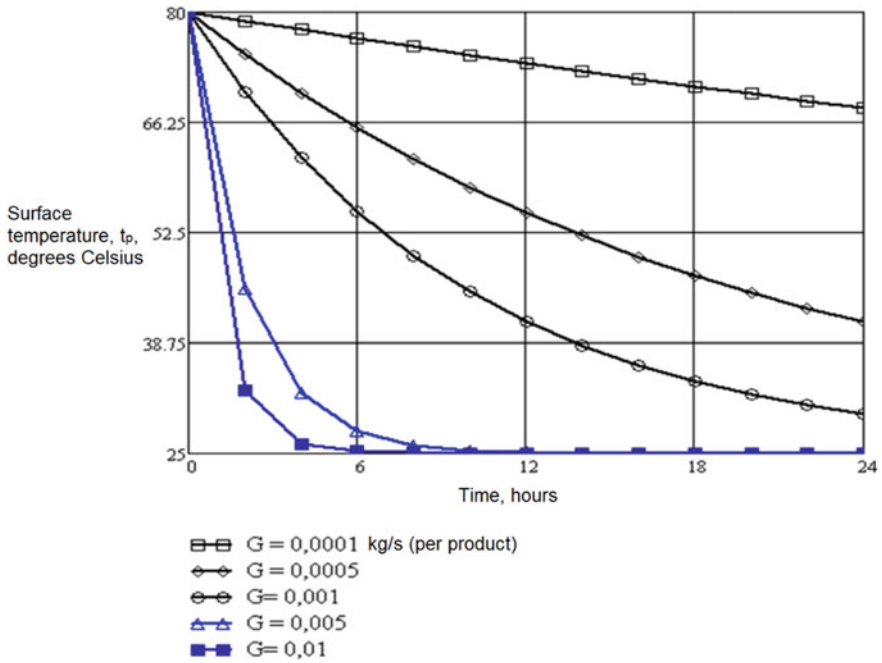


Fig. 4 Surface temperatures of flat workpieces

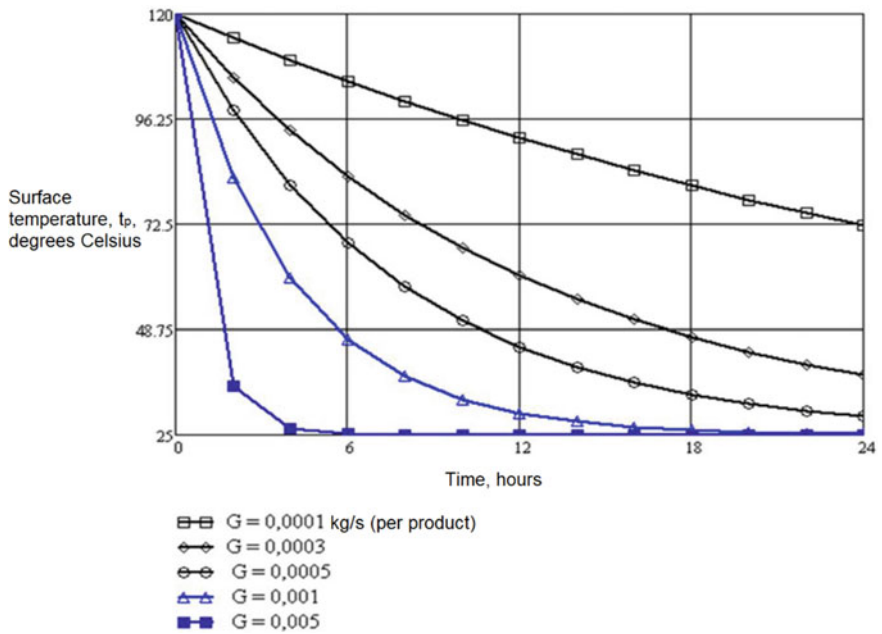


Fig. 5 Temperatures of cylindrical workpieces surfaces

optimization of the above-mentioned parameters in terms of the given schemes of loading workpieces into containers is a separate task that requires consideration.

## References

1. Lykov AV (1967) Theory of thermal conductivity. Publishing house "Higher School"
2. Mikheev MA, Mikheeva IM (1977) Fundamentals of heat transfer. M.: Energiya
3. Dymnich AH, Troyansky AA (2004) Thermal conductivity. Nord-Press, Donetsk
4. Egorov VI (2006) Exact methods for solving problems of thermal conductivity. St. Petersburg: ITMO
5. Kuznetsov GV, Sheremet MA (2008) Difference methods for solving thermal conductivity problems. Tomsk: TPU
6. Kalitaev AN (2004) Identification of heat transfer coefficients of a continuously cast ingot in the zone of secondary cooling of a continuous casting machine by optimal control methods. Nauka. Technologies. Innovations: tez. dokl. All-Russian conf.: in 2 v. Novosibirsk: NSTU, Vol. 1. pp. 91–92
7. Ilyinsky IV, Prokhach EE, Pershin VP (1974) Unsteady convective heat transfer during natural cooling of vertical plates. Eng Phys J 27(3):524
8. Petrazhitsky GB, Polezhaev VI (1962) Engineering method for calculating non-stationary thermal conductivity processes in thin multilayer walls. Thermal Power Eng 2:73—76
9. Novichenok LN, Shulman ZP (1971) Thermophysical properties of polymers, ed. by A. G. Shashkov. Minsk, Science and Technology
10. Vargaftik NB (1972) Reference book of thermophysical properties of gases and liquids. N.B. Vargaftik. - M.: Nauka
11. Sokolov EYa (2001) Heating and heating networks. Publishing house of MEI. Moscow. ISBN 5-7046-0703-9
12. Yurenev VN, Lebedev PD (1976) Heat engineering Handbook. Vol.2. Ed. 2, revised ed., M., "Energy"

# Some Aspects of Heat Accumulators Application in Thermal Power Engineering



Evgeny Umerenkov , Elina Umerenkova , Ekaterina Savelyeva ,  
and Rostislav Markov 

**Abstract** The given paper poses some problems and possible ways of their solution concerning the applicability of heat accumulators in thermal power engineering. The need to install heat accumulators in the systems with different modes of heat supply and consumption is evident. It is suggested that the efficiency of such devices, in particular with respect to the physical data of the device, be increased through accumulation using the latent heat of the melting-solidification phase transition. By objective selection criteria, such as melting point, heat of phase transition, accessibility and non-toxicity, technical paraffin is of particular interest for the accumulation of thermal energy. In addition, the authors have justified the conditions for the implementation of ecological effectuality of heat accumulators application, including phase-shifting heat accumulators (FSHA), in traditional decentralized heat consumption systems, namely, reducing greenhouse gas emissions, primarily CO<sub>2</sub>. It has been established that if, with the growth in the heat load, and consequently the boiler capacity, the product of the square of CO<sub>2</sub> volume concentration in the exhaust gases per their mass flow increases non-linearly, and this dependence is convex, switching off the heat source for the time of accumulated heat use gives a positive environmental effect, i.e., contributes to reduction in greenhouse gas emissions.

**Keywords** Heat-retaining material · Phase transition · Heat accumulator · Ecology · Greenhouse gases

## 1 Introduction

At present, the introduction of new technologies in the field of heat consumption and modern energy-saving equipment solves not only the problems of reducing the consumption of traditional energy sources in the thermal power industry, but also, no less important environmental problems. Atmospheric pollution by harmful

---

E. Umerenkov · E. Umerenkova (✉) · E. Savelyeva · R. Markov  
Southwest State University, 50 Let Oktyabrya Str., 94, Kursk 305040, Russia  
e-mail: [elinaelya@gmail.com](mailto:elinaelya@gmail.com)

© The Author(s), under exclusive license to Springer Nature Switzerland AG 2024  
N. Vatin et al. (eds.), *Modern Problems in Construction*,  
Lecture Notes in Civil Engineering 372,  
[https://doi.org/10.1007/978-3-031-36723-6\\_44](https://doi.org/10.1007/978-3-031-36723-6_44)

substances, such as carbon monoxide, sulfur dioxide, nitrogen oxides, hydrocarbons, dust emissions, thermal pollution of the environment is caused by energy consumption as such.

Despite a fairly high level of energy saving technology development and the use of renewable energy sources, there is a certain range of problems that require additional research.

In particular, almost all solar and heat pump heat supply systems (heat sensor—soil, reservoirs, outdoor air) contain heat accumulators.

Typical examples of such systems are solar heat supply systems, heat pump systems using soil, water of natural or artificial reservoirs, outdoor air, and systems using secondary energy resources as a heat sensor [1, 2].

As a rule, a heat accumulator is a container with water or solid elements of natural or artificial origin (stones, pebble, etc.). Thus, of all possible options for storing heat, the simplest method is used—accumulation in heat-intensive masses (at least in products brought up to the consumer level).

At the same time, it is well known that accumulation using the latent heat of the melting-solidification phase transition is significantly more effective, in particular with respect to the mass and dimensional characteristics of the device [3]. However, its application in engineering practice is hindered by a number of concomitant negative factors, the overcoming of which is the subject of quite intensive studies. They are conducted both in research centers and in the laboratories of corporations in different countries [3–13].

The expediency of installing heat accumulators, including those with heat-retaining material undergoing melting-solidification phase transitions, in systems with different modes of heat supply and consumption is obvious. These can be both solar installations and systems for recycling secondary energy resources, in which periods of heat supply with capacities exceeding the required one alternate with time intervals when the heat efficiency of the source is less than the calculated thermal load. At the ordinary level, however, there is an idea of the possibility of saving energy resources (and related costs) when installing an additional element—a heat accumulator in conventional systems (a boiler—a heat consumer in the form of a heating system or hot water supply). To a large extent, this approach reflects the authors' misconception, because it does not stand the elementary verification by energy conservation law—the heat consumption system will receive from the accumulator (within 24 h or a longer period) the same amount of heat (minus additional losses from the heat accumulator) as if it (the accumulator) received from the source during the charging period. Since the duration of charging and discharging a heat accumulator is generally different (it is desirable for the consumer to have a short charge, but a long discharge), then the heat flows (power) at which heat is pumped into the accumulator and its consumption are different. Direct savings (in monetary terms) can be said only in terms of reducing labor costs for servicing a heat source, if it is not automated and requires regular supervision during operation (solid fuel boilers) and the consumer or none at all (equal to zero).



It is possible to assume that the application of heat accumulators, including phase-shifting heat accumulators (FSHA) is ecologically effective in conventional decentralized heat consumption systems; this refers to reducing greenhouse gas emissions, primarily CO<sub>2</sub>.

## 2 Materials and Methods

By now, a large number of substances and compounds have been tested as heat-retaining materials (HRM) for various temperature levels, although the search for a HRM that meets the entire set of requirements continues. Analyzing the studies by domestic and foreign authors on the thermophysical properties of a number of organic and inorganic substances [14, 15] shows that four groups of substances can be used as HRMs: paraffins, fatty acids, salt hydrates and a number of metal compounds. Their main parameters are given in Table 1.

In low-potential systems (solar hot water and heating systems), crystalline hydrates with a low melting point are widely used.

Another equally significant, along with the search for materials, is the problem of heat transfer between the heat medium and the working fluid.

In order to minimize thermal resistance, methods of active heat exchange are used, where the attachment of the solid phase to the heat exchange surface is forcibly prevented. Currently, several variants of an active heat exchange method have been proposed, these are:

- (1) scraping of the solid phase from the inner surface of the heat transfer tube;
- (2) scraping of the solid phase from the outer surface of the heat transfer tube;
- (3) shell-and-tube heat exchanger with heat-retaining material circulation (coated heat transfer tubes are used);
- (4) spraying a jet of heat-retaining material;
- (5) direct contact of HRM and heat medium;
- (6) using abrasive formed during the polishing of the drum.

**Table 1** Main parameters of phase transition HRMs

Heat-retaining materials	Melting temperature range (°C)	Volume density of accumulated energy (MJ/m <sup>3</sup> )
Salt hydrates and their mixtures	30–50	200–400
Organic compounds	30–60	150–200
Salts	140–1000	300–1900
Metals and their alloys	270–1000	540–3000
Alkalis	300–500	1280

Active heat exchange that assumes the direct contact of the heat medium and the working fluid. It would be more efficient. However, the implementation of such exchange is technically much more complicated and more expensive.

At present, shell-and-tube devices (passive heat exchange) have become the most widespread ones. In the passive method, heat exchange is carried out through the heat exchange surface. The main type of devices implementing this method are:

- shell-and-tube storage units in which the heat medium moves through the tubes, and the heat-retaining material is located in the inter-tube space;
- capsule-type devices in which the accumulating material in the form of capsules (cylindrical rods, granules, hollow cylinders) is placed in the storage housing, in which the circulation of the heat medium is provided.

The design of heat accumulators (HA) with the required technical specifications is impossible without appropriate algorithms and calculation techniques. In its turn, the development of such algorithms and techniques presupposes the existence of an adequate model of the thermal state of HRM—the heat medium. At the same time, as shown in a number of studies [7, 10], the accumulator discharge mode (heating of the heat-exchanging medium) plays a decisive role, due to the specifics of heat and mass transfer during this period of the process. We are talking about the formation of a layer of solidifying HRM on the heat exchange surface (on the surface of heat exchange tubes), which has a significant thermal resistance, and which leads to the “locking” of the heat flow carried away by the heat medium. Therefore, the parameters of HA defined for the discharge conditions are directly related to its consumer properties.

The proposed environmental effectuality of using a heat accumulator, including a phase-shifting one, in conventional heat consumption systems is based on reducing greenhouse gas emissions, primarily CO<sub>2</sub>. However, the conditions for the implementation of this assumption require an appropriate justification.

We shall compare carbon dioxide emissions for two variants of the traditional heat consumption system that differ in the presence (variant 2) of a heat accumulator.

So, in the basic variant (No. 1), the heat source works T<sub>1</sub> hours a day with a capacity of Q<sub>1</sub>, in the second variant, respectively, T<sub>2</sub> (for charging the accumulator) and Q<sub>2</sub>. We assume that both in the first and in the second variants the same boiler is used, the power modulation range of which includes both Q<sub>1</sub> and Q<sub>2</sub>.

Based on the daily balance of heat consumption and neglecting the heat loss of the accumulator itself, one can write

$$T_1 \cdot Q_1 = T_2 \cdot Q_2. \quad (1)$$

If, in the basic variant, the heat source works around the clock, T<sub>1</sub> = 24 h. A longer period can also be considered as a balance period (up to a year, if we are talking about seasonal accumulation).

Now we shall calculate the daily CO<sub>2</sub> emissions, kg for both variants as

$$M_1 = (\rho_{co}/\rho_g)_1 \cdot G_{g1} \cdot (CO_2)_1 \cdot T_1 \cdot 3600 \text{ and}$$

$$M_2 = (\rho_{co}/\rho_g)_2 \cdot G_{g2} \cdot (CO_2)_2 \cdot T_2 \cdot 3600, \quad (2)$$

where  $\rho_{co}$  and  $\rho_g$ —densities of  $CO_2$  and exhaust gases, respectively;  $G_g$ —their mass flow, kg/s;  $CO_2$ —volume content of carbon dioxide in dry waste gases, %. Subscripts “1” and “2”, as said above, mean the 1st and 2nd (with accumulator) comparison variants. Then the reduction of  $CO_2$  emissions per day (as percentage) will be

$$\delta M = \frac{M_1 - M_2}{M_1} \cdot 100 = \left[ 1 - \frac{\left(\frac{\rho_{co}}{\rho_g}\right)_2}{\left(\frac{\rho_{co}}{\rho_g}\right)_1} \right] \cdot \frac{G_2}{G_1} \cdot \frac{(CO_2)_2}{(CO_2)_1} \cdot \frac{T_2}{T_1} \cdot 100. \quad (3)$$

When assessing the density ratio, we will proceed from the fact that flue gases are a mixture of ideal gases, one of the components of which is carbon dioxide. Using the Mendeleev-Clapeyron equation for  $CO_2$  and the mixture as a whole and bearing in mind that the temperatures of all its components are the same, we obtain

$$(\rho_{co}/\rho_g)_2/(\rho_{co}/\rho_g)_1 = (P_{co}/P_g)_2/(P_{co}/P_g)_1,$$

where  $P_{co}$ —partial pressure of carbon dioxide, a  $P_g$ —the pressure of exhaust gases (we mean the static pressure at the point of the chimney flue, where the flow rate  $G$  and the concentration of  $CO_2$  are measured). For  $P_g$ , as for the pressure of the mixture, Dalton’s law is valid, and, consequently, the ratio of partial and total pressures represent volumetric (molar) concentrations of carbon dioxide.

Thus, in the designations we have adopted and (3) takes the form

$$\delta M = \left[ 1 - \frac{G_2}{G_1} \cdot \frac{(CO_2)_2^2}{(CO_2)_1^2} \cdot \frac{T_2}{T_1} \right] \cdot 100$$

or with having (1) in mind

$$\delta M = (1 - \alpha) \cdot 100, \quad (4)$$

where

$$\alpha = \frac{G_2}{G_1} \cdot \frac{(CO_2)_2^2}{(CO_2)_1^2} \cdot \frac{Q_2}{Q_1}. \quad (5)$$

### 3 Results and Discussion

Some materials have been proposed thus far. They provide almost any temperature value in the considered range.

According to some objective selection criteria, such as melting point, heat of phase transition, accessibility and non-toxicity, technical paraffin is of particular interest for the accumulation of thermal energy.

The choice of petroleum paraffin as a heat-retaining material (HRM) for a phase-shifting heat accumulator is effectual for the following advantages:

- it is available;
- it does not have an aggressive effect on the materials of the structure;
- it is non-toxic;
- it facilitates simple implementation of heat exchange due to a suitable level of phase transition temperature for low-temperature modes of heat supply systems.

The design of heating accumulators (HA) with the required technical specifications is impossible without appropriate algorithms and calculation techniques. In its turn, the development of such algorithms and techniques presupposes the existence of an adequate model of the thermal state of HRM. At the same time, as was shown in a number of studies [7, 10], the accumulator discharge mode (heating of the heat-exchanging medium) plays a decisive role, due to the specifics of heat and mass transfer during this period of the process. We are talking about the formation of a layer of solidifying HRM on the heat exchange surface (on the surface of heat exchange tubes), which has a significant thermal resistance, which leads to the “blockage” of the heat flow being drawn off by the heat medium. Therefore, the parameters of HA defined for the discharge conditions are directly related to its consumer properties.

The comparative calculation performed above allows us to conclude that the emissions reduction is provided if  $\alpha$  being calculated from the results of heat sources tests is less than 1.

To illustrate the above circumstance, we will analyze the possibility of obtaining  $\delta M > 0$  when using modern water heating devices manufactured by the German company BUDERUS and designed for heating individual residential buildings. Resorting to this type of heat sources is due not only to their high consumer qualities and a significant share in the heating equipment market, but also to the availability of sufficiently detailed information necessary to determine the required parameters. Examples of BUDERUS boilers [16] that reduce carbon dioxide emissions when using heat accumulators are shown in Table 2.

As can be seen from Table 2, the values of  $\delta M$  are small (with rare exceptions). Nevertheless, given the prevalence of heat sources, the operation of which is accompanied by the release of greenhouse gases, the reduction of CO<sub>2</sub> emissions in absolute terms when using heat storage can amount to millions of tons of carbon dioxide, which will certainly contribute to the improvement of the environment and will postpone for a significant period (if not completely eliminate) the threat of global warming. We emphasize once again that in this case it is necessary to use sources with the parameter  $\alpha$  at (5) less than 1.

**Table 2** Examples of BUDERUS boilers that reduce carbon dioxide emissions when using heat accumulators

Boiler serial number	Dimension type	Q (kW)		CO <sub>2</sub>		G <sub>g</sub> (kg/s)		ΔM (%) at (3)
		1	2	1	2	1	2	
GB132T	19	7.8	18.8	8.7	9.2	0.0044	0.0084	11.4
GB112	11	5.2	10.9	8.5	9.2	0.0024	0.0043	7.5
GB122	11	4.3	10.0	8.7	9.2	0.0026	0.0049	9.4
GB434	169	78.2	156.3	5.9	6.9	0.0655	0.0862	9.9
G215	40	35.0	40.0	10.0	10.0	0.0160	0.0180	1.6
SB315	70	27.8	63.5	10.0	10.0	0.0089	0.0198	2.6
SB815	1500	805.0	1631	10.5	10.5	0.3244	0.6408	2.5

## 4 Conclusion

In accordance with the above said, it is necessary to conduct further research in the areas under consideration and develop reliable mathematical models of thermal modes of phase transition heat accumulators, which, in their turn, will serve as the basis of calculation techniques. The urgency of this problem is dictated by the need for alternative heat supply systems in highly efficient heat accumulators, the most promising of which, at present, are phase transition accumulators.

Whereas, it was found that with an increase in the heat load, and therefore the boiler capacity, the product of the square of the volume concentration of CO<sub>2</sub> in the exhaust gases per their mass flow increases non-linearly, and this dependence is convex. Turning off the heat source for the time of using the accumulated heat gives a positive environmental effect, i.e. provides a reduction in greenhouse gas emissions.

## References

1. Popel' OS, Proshkina IA (2005) Solar Russia. In the world of science, vol 1, pp 14–18
2. Golitsyn MV, Golitsyn AM, Pronina NV (2004) Alternative energy carriers. Russian Academy of Sciences. Institute of Atmospheric Physics, Moscow State University, Nauka, Moscow
3. Levenberg VA, Tkach MP, Gol'strem VA (1991) Heat accumulation. Tekhnika, Kyiv
4. Umerenkov EV (2013) Development of phase transition heat accumulators for heat supply systems. Author's abstract of ... Cand. Sc. Engineering. Southwest State University, Kursk
5. Tsybalyuk YuV (2006) Research of processes with phase transitions of materials with plate inclusions in thermal accumulators: author's abstract of ... Cand. Sc. Engineering: 01.04.14. Astrakhan
6. Kamimoto, Abe E, Kanari K (1980) Heat exchangers in latent heat energy storage units. Solar Energy 24:581–622
7. Umerenkov EV, Kotenko EV (2011) Modeling of the discharge process of a phase-transition shell-and-tube heat accumulator. Russ J Build Constr Archit 1(21):34–39
8. Kobelev NS, Kotenko EV, Umerenkov EV (2011) About the problem of calculating the characteristics of a phase transition shell-and-tube heat accumulator. Proc Southwest State Univ 5–2(38):331–334

9. Umerenkov EV (2011) Modelling of the phase transition heat battery charging mode. In: Umerenkov EV, Kotenko EV (eds). Proc Southwest State Univ 5-2(38):348–350
10. Umerenkov EV, Kotenko EV (2012) Modelling of the solidification process of heat-retaining material. Russ J Build Constr Archit 1(25):41–49
11. Krygina AM, Kotenko EV, Umerenkov EV (2012) Method of thermal calculation of shell-and-tube phase-transition heat accumulator. Resid Constr 8:38–41
12. Umerenkov EV, Kotenko EV (2012) Thermal calculation of a phase transition shell-and-tube heat accumulator based on a quasi-stationary approximation. Proc Southwest State Univ 4(43):211–216
13. Umerenkov EV, Kotenko EV (2012) Partitioning of a phase transition shell-and-tube heat accumulator as a way to increase its efficiency. Proc Southwest State Univ Eng Technol Part 2 2:39–43
14. Bystrov VP, Livchak AV (1984) Heat accumulators based on phase transition. Issues of saving heat and energy resources in ventilation and heat supply systems: collection of scientific works. TSNIIEPIO, Moscow, pp 75–90
15. Shabalina SG, Borovskaya LV (2010) Heat-accumulating properties of natural and synthetic waxes. Mod High Technol 4:98–99
16. Buderus HEIZTECHNIK Design documentation on specifications of heating boilers for determining the geometry and dimensions of the flue gas removal system (2003)

# Device for Extracting Water from Atmospheric Air



Adylbek Akmatov  and Olga Volichenko 

**Abstract** A person faces the problem of finding water sources when he due to certain circumstances finds himself in waterless, arid regions. Prolonged dehydration is detrimental to humans. It is well known that the loss of even one percent of the total amount of water in the body leads to painful disorders. In arid and desert regions, fresh water is found mainly in the atmosphere. Condensation (dew) appears at night. The problem is that people who find themselves in adverse conditions often do not have the skill to get water from it. The solution to this problem is the development of autonomous compact plants that provide the possibility of obtaining water under any conditions and in any natural situation. The article analyzes various methods for collecting water from the air and discusses the advantages and disadvantages of the proposed devices. The result of the work is the implementation of the author's device for obtaining water from atmospheric air, which differs from previously presented analogs with compactness and mobility.

**Keywords** Autonomous compact unit · Fresh water · Solar thermal concentrator · Refrigerant · Heat exchange · Electric heater · Accumulator · Wind turbines

## 1 Introduction

Lack and shortage of water is a real disaster for many regions of the planet, primarily for areas of steppes and deserts with a hot, arid climate. At the same time, the Earth's atmosphere has huge resources of fresh water (almost 13,000 billion tons), which

---

A. Akmatov

Kyrgyz—Russian Slavic University Named After B.N. Yeltsin, 44, Kiyevskaya St,  
Bishkek 720000, Kyrgyzstan

O. Volichenko (✉)

Federal State Budget Educational Institution of Higher Education «Moscow State University of  
Civil Engineering (National Research University)», 26, Yaroslavskoye shosse, Moscow 129337,  
Russia

e-mail: [wolitschenko@mail.ru](mailto:wolitschenko@mail.ru)

also can quickly replenish due to the evaporation of moisture from the surface of water bodies and land. Every year it is about 600 thousand cubic meters of water [1] returns to the earth in the form of precipitation. The concentration of fresh water in the atmosphere is so high that most of it—almost more than half—is never used. Therefore, the methods and possibilities of obtaining water from air space are becoming one of the urgent problems of the current time.

There is always some moisture in the atmosphere, even in hot desert climates. In arid areas with sharp air cooling at night, water vapor forms condensate—the transition of excess vapor into a wet state and the formation of tiny droplets of water—dew or fog.

Since ancient times, people have been developing tools and devices for collecting moisture from the air and converting it into drinking water, for example, fog collection has long been practiced in a hot and humid climate [1–4]. Currently, a lot of research is being carried out in this direction and a number of methods for obtaining water from the air are proposed.

*The method of cooling* has been used since ancient times. It provides for the development of a cold surface, from which the protruding moisture is collected—condensate formed from contact with the surface of rapidly cooling water vapor in the air [5, 6].

At the end of the 20th century, an installation was proposed, consisting of a cold accumulator, an air duct, a water collector, a solar collector connected to an air heater, and heat pipes [7]. The cold accumulator made in of solid material is placed on the water collector, together they form a volume with a large internal condensation surface and good airflow permeability. The air duct in the form of an extractor pipe with an air heater is located above the cold accumulator. In the lower part of the cold accumulator, there are air channels and heat pipes. The obvious disadvantages of this device include the low efficiency of the accumulator and heat pipes.

*The method of simultaneous air heating and cooling* for extracting water from the atmosphere is implemented with the help of refrigeration compressors. The device consists of heating and cooling elements, a vertical air duct, and a water collector [8]. The cooling element in the form of a cylinder is located in the center of the air duct channel, and the cone-shaped heating element is located on the outer skin of the device. Between them distributing cup made of heat-insulating material is installed, facing the open side down. It is surrounded by two expanding cavities—the first is located between the cooling element and the glass, and the second is between the glass and the heating element.

With all the advantages of the device, its negative side is the limitation of its operation in bad weather and at night, since the heating element depends on solar energy. Significant disadvantages are also:

- (1) large heat losses when the air temperature drops to the required level;
- (2) cost increase when using efficient but expensive heat exchangers;
- (3) the freons in refrigeration compressors are harmful to the environment.

*The sorption method* consists in using of a sorbent that is capable to absorb water vapor from the air intensively (adsorption stage). The water vapor saturated sorbent is



heated (desorption stages) using various heat sources, after that the desorbed water vapor is removed from the sorbent by condensing moisture in the water collector [9–11]. By utilizing an efficient sorbent (that is capable to absorb a large amount of water from the air even under conditions of low humidity and releasing moisture at very low temperatures) and solar energy for thermal processes, several completely autonomous devices for extracting water from the air layers of the atmosphere have been developed [12–14]. Photothermal materials can increase the device's efficiency in the absence or weakening of sunlight [15, 16].

The disadvantage of such water generators from atmospheric air is, first of all, the complex design of the device and its stationarity. The negative aspects of the device include the heating process, which can be carried out in several ways:

- (1) by passing an alternating or direct current through a heating element placed in a sorbent layer;
- (2) an electric current is passed through a layer of conductive sorbent;
- (3) a catalyst is placed in the sorbent layer in which the hydrocarbon oxidation reaction takes place.

Other types of devices require deepening into the ground, thereby becoming dependent on the type and quality of the soil [17]. The use of wind turbines instead of expensive solar panels also makes the operation of the device dependent on weather conditions and the availability of air flows sufficient for its operation.

The analyses of all considered devices from open sources show that they are mainly intended for stationary use. We tried to develop a mobile device that, in our opinion, can be operated under any weather conditions.

## 2 Materials and Methods

The main materials for engineering the device for extracting water from the atmosphere are the thermal processes of water condensation, through the use of solar or (in the absence) wind energy. In the absence of both, a pre-charged battery from the wind turbine can be used, with the battery connected to the resistance electric heater through a switch, turning off the wind turbine. In the absence of all energy carriers, it is possible to use the heat of the earth, since a refrigerant is used that evaporates at relatively low temperatures, for example, freon—11 (R11), whose boiling point is 23.7 °C.

The condensate released during cooling is collected in the air collector.

The method of experimental modeling was used for engineering the device. The proposed experimental plant for obtaining water from atmospheric air consists of the following main structural blocks: a heating element—a concentrator, a pipeline, a cooling element designed as an evaporative-condensation system, and a water collector.

### 3 Results and Discussion

The proposed economical device for extracting drinking water from water vapor contained in the ambient air, using renewable energy sources, can be used in extreme conditions, as well as in arid regions of steppes, semi-deserts, and deserts.

The main tasks that were set during the development of this device were: firstly, the expansion of its operational capabilities, the solution to the mobility problem; secondly, ensuring the autonomy of the device.

As we noted above, the disadvantages of many proposed devices were dependence on any one type of energy—electric, solar, wind, etc. The device proposed for consideration for obtaining water from air, in addition to the solar power plant, is equipped with a wind power plant. At the same time, the design of the device also provides for the presence of battery that is charged from a wind power plant and can be used in the absence of wind (calm) and sunlight. Another alternative energy source that the device can operate on is the earth heat—the low-grade heat of the upper layers of the soil, heated by the sun, is transferred to the refrigerant. Uninterrupted operation of the device is attributable to its complete autonomy and ensured in any weather conditions being located in the most remote, hard-to-reach areas of the earth, far from sources of electricity.

The structural arrangement of fresh water generator. The generator consists of a water collector, heating and cooling elements of a refrigeration machine, and a solar- and wind-power plant.

The heating element of the refrigeration machine uses three types of heat sources:

- (1) A solar thermal concentrator operating in the presence of solar radiation;
- (2) A resistive electric heater connected to an electric generator of a wind power plant. It operates in the absence of solar radiation and the presence of wind energy;
- (3) An electric battery connected to a wind power plant starts to work in the absence of solar radiation and wind energy.

The cooling element is made in the form of a circulating evaporative-condensing cooling system, consisting of a heat exchanger located in the solar-powered thermal concentrate, with which the evaporator and condenser are connected in series by pipelines. The pipelines that connect the evaporator and condenser are made in the form of cylindrical collectors located concentrically around the collector, and the resistive electric heater is located on the outer side of the bottom of the evaporator. The expansion of the operational capabilities of the proposed device for extracting water from the air predetermines the versatility of its application for the specified purpose.

Next, we consider in detail the construction of the device for extracting water from atmospheric air. First of all, the most inexpensive devices in extreme conditions are one that uses renewable energy sources.

The proposed device for obtaining water from atmospheric air has universal applicability in various extreme situations of the need for drinking water and has no analogs

in the technical research that are available to the authors, which, in their opinion, ensures that it meets the criteria of the invention. The invention is illustrated by drawings (Figs. 1 and 2).

A general view of the device for extracting water from atmospheric air and a vertical section of the installation is shown (Fig. 1a and b). Placement of the evaporator of the evaporation–condensation system in the ground (Fig. 2).

A device for extracting water from atmospheric air operates as follows.

The ambient atmospheric air enters through the inlet air duct 16 into chamber 15, where condenser 8 condenses. In the presence of solar radiation, the heat carrier (oil or water) located in heat exchanger 2 is heated by the solar thermal concentrator 1 and is fed through pipeline 3 to jacket 5 of the evaporator 6, as a result, it heats up. The refrigerant in the evaporator 6 (for example, freon-11) evaporates, and its vapors through the steam pipeline (collector) 7 enter the condenser 8, where they condense and cool the walls 21. At the same time, the water vapor contained in the atmospheric air begins to condense on the cooling surfaces of the chamber condensation 15. The

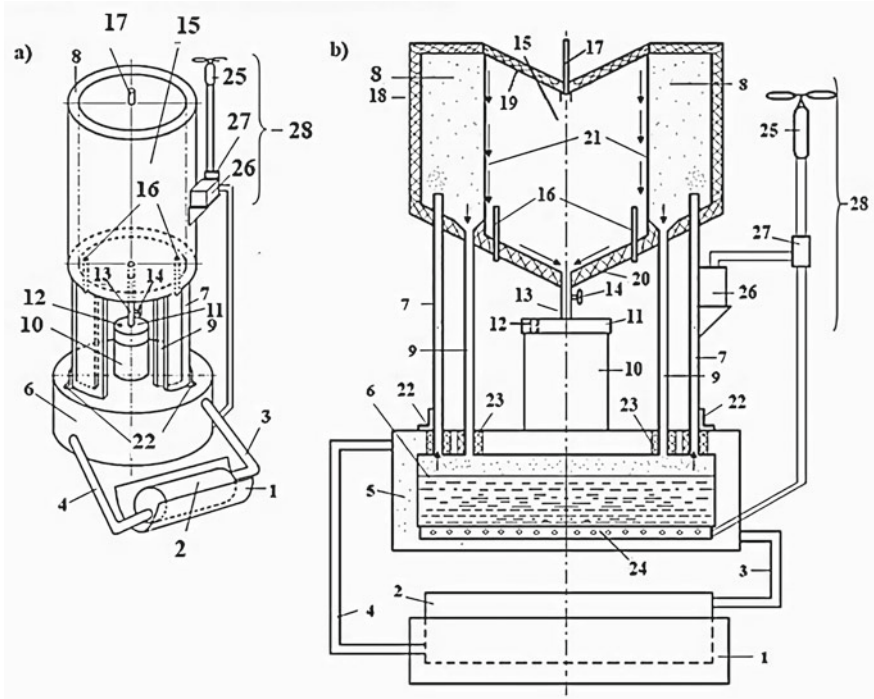


**Fig. 1** Device for obtaining water from atmospheric air: **a** General view, **b** Vertical section. 1-concentrator, 2-heat exchanger, 3-pipeline, 4-pipeline, 5-jacket, 6-evaporator, 7-pipeline, 8-condenser, 9-pipeline, 10-water collector, 11-cover, 12-hole, 13-branch pipe, 14-valve, 15-chamber, 16-inlet air ducts, 17-outlet air ducts, 18-walls, 19-cover, 20-bottom, 21-wall, 22-interlocks, 23-rubber gaskets, 24-resistive electric heater, 25-electric generator, 26-electric battery, 27-switch, 28-wind turbine

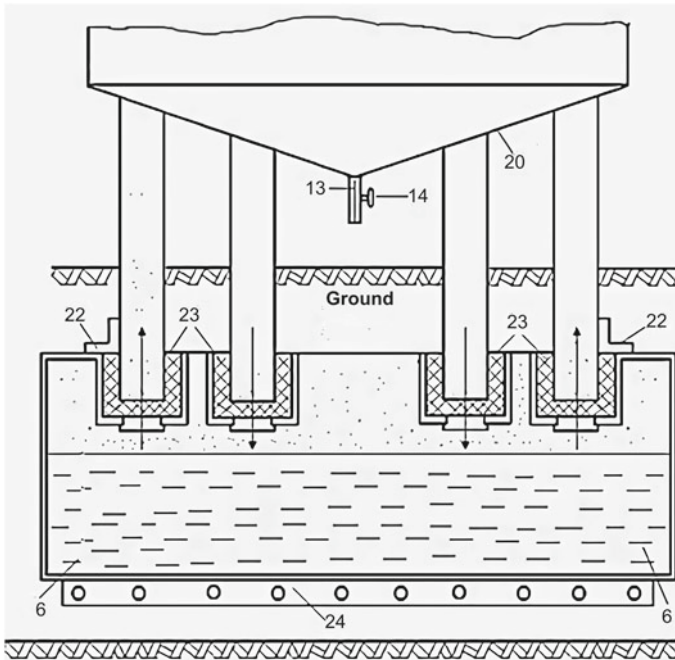


**Fig. 2** Evaporative-condensing system. 6-evaporator, 13-branch pipe, 14-valve, 20-bottom, 22-locking connections, 23-rubber gaskets, 24-resistive electric heater

condensed water flows along the walls 21 and the tropospheric bottom 20 through pipe 13 with valve 14 open into vessel 10 (water collector) located inside the cavity limited by collector 9.

Excess air from vessel 10 is discharged into the atmosphere through opening 12. The spent ammonia condensate (refrigerant) flows from condenser 8 through the pipeline (collector) 9 to evaporator 6, and the coolant that has given off heat is returned by the drain pipeline 4 from the jacket 5 of the evaporator 6 to the heat exchanger 2, and the described process of cooling by the circulating evaporative-condensing system is repeated.

In the absence of solar radiation and the presence of wind energy, a resistive electric heater 24 is used as a heating element, connected to an electric generator 25, which is part of the wind power plant 28. In the absence of solar radiation and wind energy, a resistive electric heater 24 is connected to an electric battery 26, through a switch 27 also included in the wind turbine 28, while the wind turbine is turned off.

The design of the device for extracting water from atmospheric air allows use in circumstances of the absence of solar and wind power and when the electric battery is discharged. In this case, the natural environment below the atmospheric level is used as the heat exchanger 2, i.e., priming. Then, in place of the evaporator 6 with the jacket 5, the evaporator without the jacket is installed with the help of locking

joints 22 and is buried in the ground, the heat from which ensures the process of cooling the atmospheric air as described above.

## 4 Conclusion

In sunny weather, solar radiation is used to operate the condenser; in the absence of sunny weather, a resistive electric heater powered by a wind turbine can be used. In the absence of solar radiation and wind energy, the resistive electric heater is heated through an electric accumulator, powered in advance through the wind turbine generator. In the absence of both solar radiation and wind energy and the electric battery being discharged, the design of the device allows the use of the heat of the soil heated during the day to operate the condenser evaporator.

The design concept of the device assumes its mobility, which is ensured by small dimensions (height 0.5 m) and manufacturing materials (steel structural elements, insulation and plastic case), as well as a water tank with a capacity of 3–5 L. The total weight of the device is expected to be up to 10 kg.

**Acknowledgements** The concept was developed on the basis of the Kyrgyz-Slavonic University. B.N. Yeltsin (Bishkek) and Southwestern State University (Kursk) on the initiative of the authors.

## References

1. Renyuan L, Shi Y, Alsaedi M, Mengchun W, Shi L, Wang P (2018) Hybrid hydrogel with high water vapor harvesting capacity for deployable solar-driven atmospheric water generator. *Environ Sci Technol* 52(19):11367–11377. <https://doi.org/10.1021/acs.est.8b02852>
2. Estrela MJ, Valiente JA, Corell D, Millan MM (2008) Fog collection in the Western Mediterranean Basin (Valencia region, Spain). *Atmos Res* 87(3):324–337. <https://doi.org/10.1016/j.atmosres.2007.11.013>
3. Olivier J, de Rautenbach CJ (2002) The Implementation of fog water collection systems in South Africa. *Atmos Res* 64(1):227–238. [https://doi.org/10.1016/S0169-8095\(02\)00094-7](https://doi.org/10.1016/S0169-8095(02)00094-7)
4. McHugh TA, Morrissey EM, Reed SC, Hungate BA, Schwartz E (2015) Water from air: An overlooked source of moisture in Arid and Semiarid Regions. *Sci Rep* 5:13767. <https://doi.org/10.1038/srep13767>
5. Wikramanayake ED, Ozkan O, Bahadur V (2017) Landfill gas-powered atmospheric water harvesting for oilfield operations in the United States. *Energy* 138:647–658. <https://doi.org/10.1016/j.energy.2017.07.062>
6. Wahlgren RV (2001) Atmospheric water vapour processor designs for potable water production: A review. *Water Res* 35(1):1–22. [https://doi.org/10.1016/S0043-1354\(00\)00247-5](https://doi.org/10.1016/S0043-1354(00)00247-5)
7. Alekseev VV, Rustamov Nariman Ahmed oglu, Chekarev KV (1999) Installation for receiving fresh water from atmospheric air. Patent RU No. 2131000 IPC B01D 5/00, IPC E03B 3/00. The publication date of the patent is May 27, 1999
8. Sharov VV, Dzegilenok VN (1996) A device for extracting water from air. Patent RU No. 2064036, IPC E 03 B 3/28. Publication date 20.07.1996

9. Wang JY, Liu JY, Wang RZ, Wang LW (2017) Experimental investigation on two solar-driven sorption based devices to extract fresh water from atmosphere. *Appl Therm Eng* 127:1608–1616. <https://doi.org/10.1016/j.applthermaleng.2017.09.063>
10. Ji JG, Wang RZ, Li LX (2007) New composite adsorbent for solar-driven fresh water production from the atmosphere. *Desalination* 212(1):176–182. <https://doi.org/10.1016/j.desal.2006.10.008>
11. Aristov YI, Okunev AG, Parmon VN (2006) A method of obtaining water from air. Patent RU 2 272 877, E03B 3/28, B01D 53/04, F25 D 17/06. Patentee Institute of Catalysis. G.K. Boreskov of the Siberian Branch of the Russian Academy of Sciences; 200412271010/03, published 03/27/2006
12. Kim H, Rao SR, Kapustin EA, Zhao L, Yang S, Yaghi OM, Wang EN (2018) Adsorption-based atmospheric water harvesting device for Arid climates. *Nat Commun* 9(1):1191. <https://doi.org/10.1038/s41467-018-03162-7>
13. Kim H, Yang S, Rao SR, Narayanan S, Kapustin EA, Furukawa H, Umans AS, Yaghi OM, Wang EN (2017) Water harvesting from air with metal-organic frameworks powered by natural sunlight. *Science* 356:430. <https://doi.org/10.1126/science.aam8743>
14. Li R, Shi Y, Shi L, Alsaedi M, Wang P (2018) Harvesting water from air: Using anhydrous salt with sunlight. *Environ Sci Technol* 52(9):5398–5406. <https://doi.org/10.1021/acs.est.7b06373>
15. Furukawa H, Gandara F, Zhang Y-B, Jiang J, Queen WL, Hudson MR, Yaghi OM (2014) Water adsorption in porous metal-organic frameworks and related materials. *J Am Chem Soc* 136(11):4369–4381. <https://doi.org/10.1021/ja500330a>
16. Canivet J, Fateeva A, Guo Y, Coasne B, Farrusseng D (2014) Water adsorption in MOFs: Fundamentals and applications. *Chem Soc Rev* 43(16):5594–5617. <https://doi.org/10.1039/C4CS00078A>
17. Antufiev IA (2014) A device for obtaining water in the desert. Patent RU No. 2526 628, IPC E 03 B 3/28. Patent holders State scientific institution All-Russian Research Institute of Electrification of Agriculture of the Russian Academy of Agricultural Sciences (VIESSH of the Russian Agricultural Academy), published on 27.08.2014. Bull. No. 9

# Optimization of the Technological Process of Polymer Concrete Processing with a Change in the Magnetic Field



Andrey Matrosov , Viktor Afonin , Ekaterina Matrosova ,  
and Ekaterina Pakhomova 

**Abstract** As a result of experimental studies, a positive effect of a magnetic field on the properties of epoxy composites has been established. The article investigated the influence of an electromagnetic field created by using a constant electric current of various strengths passed through a rectangular metal plate, which was the base of the molds in the manufacture of samples from epoxy compositions. Epoxy compositions were made on the basis of epoxy-diane resin. The composites were cured with polyethylene polyamine. Pyrite cinders served as a filler in the filled compositions. In the course of the study, the following were experimentally determined: compressive strength, tensile strength in bending, dynamic modulus of elasticity, fracture energy and microhardness. The results obtained show an improvement in the physical and mechanical properties of polymer composites processed using a magnetic field.

**Keywords** Materials · Polymer concrete · Production technology · Activation · Magnetic field

## 1 Introduction

The continuously increasing requirements for the physical and technical properties of building materials necessitate the creation of new samples with a set of improved indicators. Composite materials, which have found wide application in construction, mechanical engineering, aircraft building and rocket science, the chemical industry, etc., have recently attracted the greatest attention all over the world.

---

A. Matrosov · V. Afonin · E. Matrosova (✉)  
National Research Ogarev Mordovia State University, 68, Bolshevistskaya ul., Saransk 430005,  
Republic of Mordovia, Russia  
e-mail: [k\\_matr@bk.ru](mailto:k_matr@bk.ru)

E. Pakhomova  
South West State University, 50 Let Oktyabrya Street, 94, Kursk 305040, Russia

© The Author(s), under exclusive license to Springer Nature Switzerland AG 2024  
N. Vatin et al. (eds.), *Modern Problems in Construction*,  
Lecture Notes in Civil Engineering 372,  
[https://doi.org/10.1007/978-3-031-36723-6\\_46](https://doi.org/10.1007/978-3-031-36723-6_46)

Scientists and specialists in various fields of materials science are working on the development of the theory of calculation, design, manufacturing technology, optimization of compositions and the study of the properties of composite materials [1–14].

Despite the ever-increasing rate of polymer-based concretes use in construction, some problems of their structure formation and manufacturing technology remain poorly understood. In particular, the technological processes for the manufacture of polymer concretes have not been studied in the production of which activation by a magnetic field is used.

## 2 Materials and Methods

The influence of an electromagnetic field created with the help of a constant electric current of various strengths, passed through a metal rectangular plate, which was the base of the molds in the manufacture of samples from epoxy compositions, has been studied. The influence of the electromagnetic field on the properties and structure of epoxy compositions has been studied on compositions filled with pyrite cinders and without filler (Table 1).

In general, the regression model according to the planning matrix is presented as follows:  $Y = b_0 + b_1 \times 1 + b_2 \times 2 + b_{12} \times 1 \times 2 + b_{11} \times 1^2 + b_{22} \times 2^2$ .

In the course of the study, the following were experimentally determined: compressive strength, tensile strength in bending, dynamic modulus of elasticity and fracture energy.

**Table 1** Planning matrix and working matrix

№	Planning matrix		Working matrix	
	$x_1$	$x_2$	Current strength (A)	Time (h)
<b>1</b>	<b>0</b>	<b>0</b>	<b>6</b>	<b>6</b>
2	1	1	9	9
3	–1	1	3	9
4	–1	–1	3	3
5	1	–1	9	3
<b>6</b>	<b>1</b>	<b>0</b>	<b>9</b>	<b>6</b>
7	0	1	6	9
<b>8</b>	<b>–1</b>	<b>0</b>	<b>3</b>	<b>6</b>
9	0	–1	6	3



### 3 Results and Discussion

The implementation of the experiment planning matrix made it possible to obtain polynomial models. Dependences of the properties of unfilled epoxy compositions on the strength and duration of the electromagnetic field are as follows:

$$R_c = 116.54 - 3.71x_1 - 0.55x_2 - x_1x_2 - 5.11x_1^2 + 1.18x_2^2.$$

$$R_u = 58.8 - 4x_1 + 6.48x_2 + 0.05x_1x_2 + 0.36x_1^2 - 5.98x_2^2.$$

$$E_d = 3251.08 + 14.16x_1 + 694.44x_2 - 17.75x_1x_2 + 1292.38x_1^2 - 748.4x_2^2.$$

$$U = 67.76 - 3.38x_1 + 8.67x_2 - 1.15x_1x_2 - 5.75x_1^2 + 3.1x_2^2.$$

According to the above equations, graphs with current or time parameters are constructed (Figs. 1, 2, 3, 4, 5, 6, 7 and 8).

An analysis of the graphs shows that the extreme points on them can be determined by unconditional optimization methods for one variable [15, 16].

The results of optimizing the dependencies shown in Figs. 1, 2, 3, 4, 5, 6, 7 and 8:

Strength minimization results  $R_c$  (compressive)

Tok: 3, Time = -0.190678, rel. units;  $R_{c\min} = 115.097097$ .

Tok: 6, Time = 0.233051, rel. units;  $R_{c\min} = 116.475911$ .

Tok: 9, Time = 0.656780, rel. units;  $R_{c\min} = 107.210996$ .

Strength maximization results  $R_c$

Tok: 3, Time = 1.000000, rel. units;  $R_{c\max} = 116.770001$ .

Tok: 6, Time = -1.000000, rel. units;  $R_{c\max} = 118.270001$ .

Tok: 9, Time = -1.000000, rel. units;  $R_{c\max} = 110.450001$ .

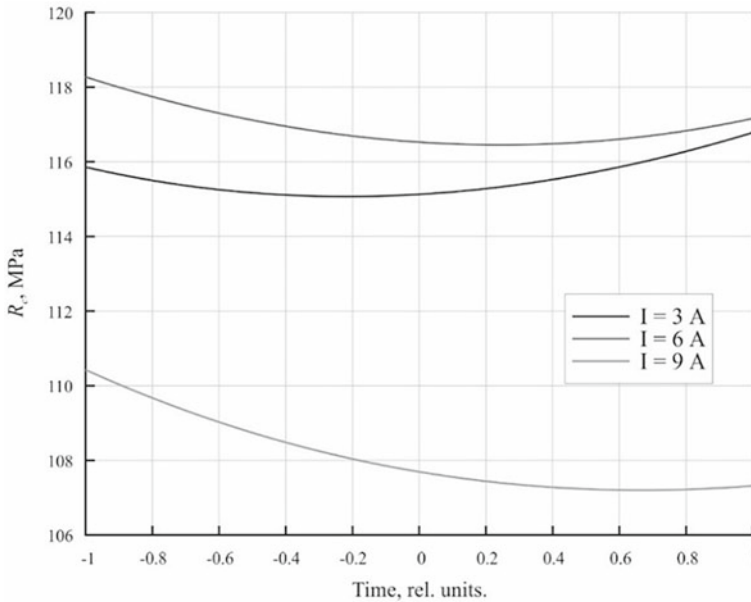
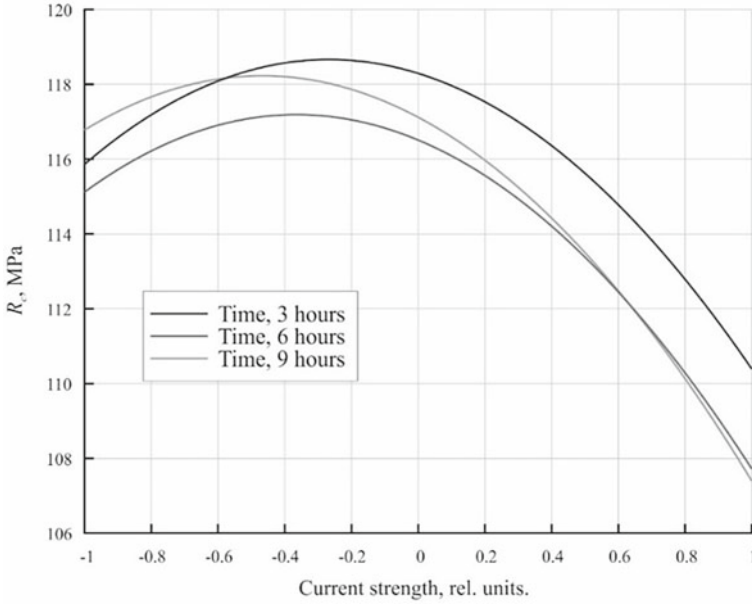
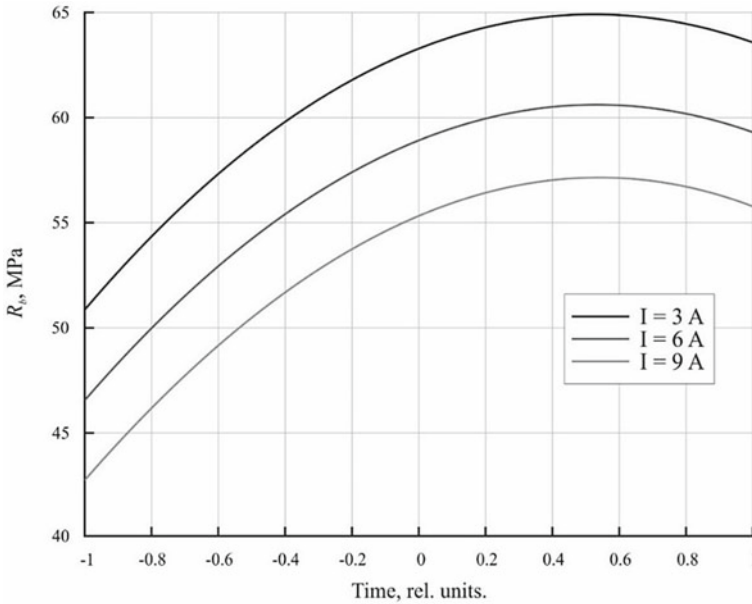


Fig. 1 Change in compressive strength as a function of time in rel. units



**Fig. 2** Change in compressive strength depending on the effect of electric current in rel. units  $R_c = 116.54 - 3.71x_1 - 0.55x_2 - x_1x_2 - 5.11x_1^2 + 1.18x_2^2$



**Fig. 3** Change in bending strength as a function of time in rel. units  $R_u = 58.8 - 4x_1 + 6.48x_2 + 0.05x_1x_2 + 0.36x_1^2 - 5.98x_2^2$

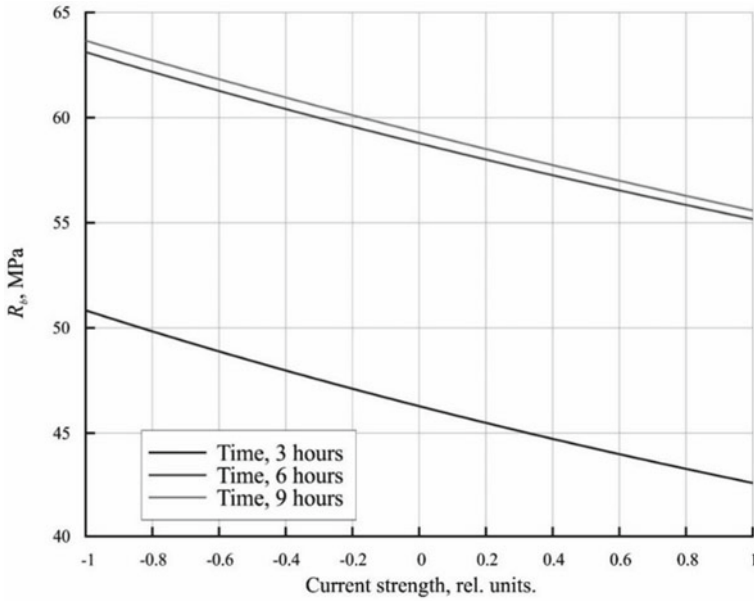


**Fig. 4** Change in bending strength from the impact of electric current in rel. units  $R_u = 58.8 - 4x_1 + 6.48x_2 + 0.05x_1x_2 + 0.36x_1^2 - 5.98x_2^2$

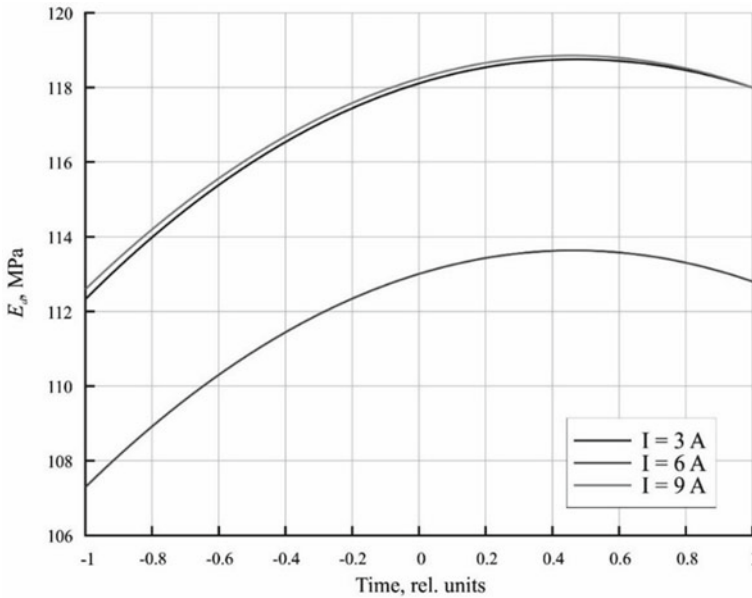


**Fig. 5** Change in the dynamic modulus of elasticity for compression depending on time in rel. units  $E_d = 3251.08 + 14.16x_1 + 694.44x_2 - 17.75x_1x_2 + 1292.38x_1^2 - 748.4x_2^2$

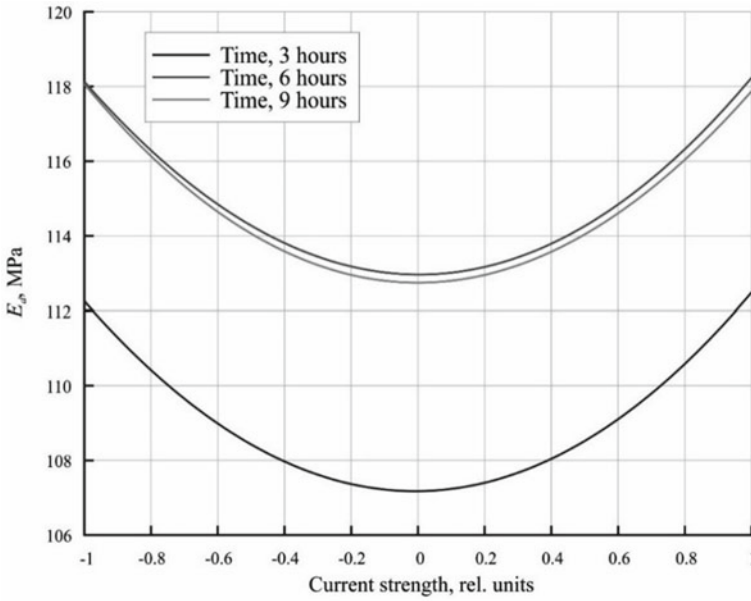


**Fig. 6** Change in the dynamic modulus of elasticity depending on the impact of electric current in rel. units  $E_d = 3251.08 + 14.16x_1 + 694.44x_2 - 17.75x_1x_2 + 1292.38x_1^2 - 748.4x_2^2$

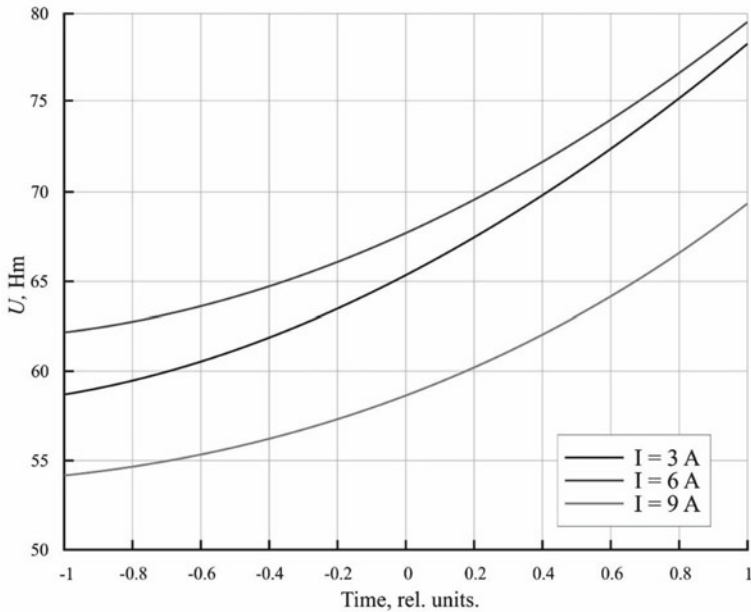


**Fig. 7** The dependence of the fracture energy as a function of time in rel. units  $U = 67.76 - 3.38x_1 + 8.67x_2 - 1.15x_1x_2 - 5.75x_1^2 + 3.1x_2^2$

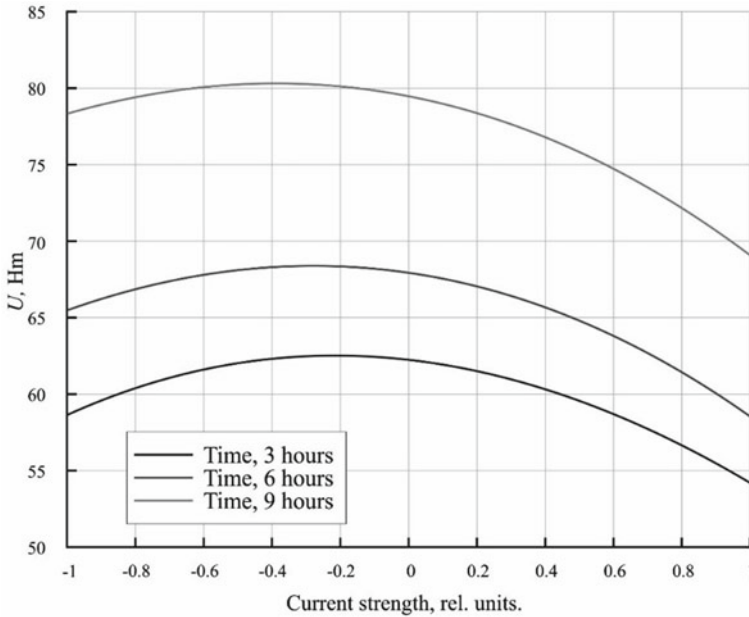


**Fig. 8** Dependence of the fracture energy depending on the impact of electric current in rel. units  
 $U = 67.76 - 3.38x_1 + 8.67x_2 - 1.15x_1x_2 - 5.75x_1^2 + 3.1x_2^2$

**Strength minimization results  $R_c$**

Time: 3, Tok = 1.000000, rel. units;  $R_{c,min} = 110.449998$ .

Time: 6, Tok = 1.000000, rel. units;  $R_{c,min} = 107.719997$ .

Time: 9, Tok = 1.000000, rel. units;  $R_{c,min} = 107.349997$ .

**Strength maximization results  $R_c$**

Time: 3, Tok = -0.265166, rel. units;  $R_{c,max} = 118.629300$ .

Time: 6, Tok = -0.363014, rel. units;  $R_{c,max} = 117.213390$ .

Time: 9, Tok = -0.460861, rel. units;  $R_{c,max} = 118.255328$ .

**Strength minimization results  $R_i$  (in bending)**

Tok: 3, Time = -1.000000, rel. units;  $R_{i,min} = 50.749997$ .

Tok: 6, Time = -1.000000, rel. units;  $R_{i,min} = 46.339997$ .

Tok: 9, Time = -1.000000, rel. units;  $R_{i,min} = 42.649997$ .

**Strength maximization results  $R_i$**

Tok: 3, Time = 0.537625, rel. units;  $R_{i,max} = 64.888466$ .

Tok: 6, Time = 0.541806, rel. units;  $R_{i,max} = 60.555452$ .

Tok: 9, Time = 0.545987, rel. units;  $R_{i,max} = 56.942646$ .

Elapsed time is 0.541018 s.

**Strength minimization results  $R_i$**

Time: 3, Tok = 1.000000, rel. units;  $R_{i,min} = 42.649999$ .

Time: 6, Tok = 1.000000, rel. units;  $R_{i,min} = 55.159999$ .

Time: 9, Tok = 1.000000, rel. units;  $R_{i,min} = 55.709999$ .

Strength maximization results  $R_i$

Time: 3, Tok = -1.000000, rel. units;  $R_{i\max} = 50.750001$ .

Time: 6, Tok = -1.000000, rel. units;  $R_{i\max} = 63.160001$ .

Time: 9, Tok = -1.000000, rel. units;  $R_{i\max} = 63.610001$ .

Elapsed time is 0.748482 s.

Strength minimization results  $E_d$  (dynamic modulus of elasticity)

Tok: 3, Time = -1.000000, rel. units;  $R_{c\min} = 3068.709585$ .

Tok: 6, Time = -1.000000, rel. units;  $R_{c\min} = 1808.239588$ .

Tok: 9, Time = -1.000000, rel. units;  $R_{c\min} = 3132.529592$ .

Strength maximization results  $E_d$

Tok: 3, Time = 0.475808, rel. units;  $R_{c\max} = 4698.732989$ .

Tok: 6, Time = 0.463950, rel. units;  $R_{c\max} = 3412.172635$ .

Tok: 9, Time = 0.452091, rel. units;  $R_{c\max} = 4710.582773$ .

Strength minimization results  $E_d$

Time: 3, Tok = -0.012345, rel. units;  $R_{c\min} = 1808.043029$ .

Time: 6, Tok = -0.005478, rel. units;  $R_{c\min} = 3251.041214$ .

Time: 9, Tok = 0.001389, rel. units;  $R_{c\min} = 3197.117507$ .

Strength maximization results  $E_d$

Time: 3, Tok = 1.000000, rel. units;  $R_{c\max} = 3132.530492$ .

Time: 6, Tok = 1.000000, rel. units;  $R_{c\max} = 4557.620488$ .

Time: 9, Tok = -1.000000, rel. units;  $R_{c\max} = 4493.090486$ .

Fracture energy minimization results  $U$

Tok: 3, Time = -1.000000, rel. units;  $U_{\min} = 58.669999$ .

Tok: 6, Time = -1.000000, rel. units;  $U_{\min} = 62.190000$ .

Tok: 9, Time = -1.000000, rel. units;  $U_{\min} = 54.210000$ .

Fracture energy maximization results  $U$

Tok: 3, Time = 1.000000, rel. units;  $U_{\max} = 78.310003$ .

Tok: 6, Time = 1.000000, rel. units;  $U_{\max} = 79.530003$ .

Tok: 9, Time = 1.000000, rel. units;  $U_{\max} = 69.250003$ .

Fracture energy minimization results  $U$

Time: 3, Tok = 1.000000, rel. units;  $U_{\min} = 54.209997$ .

Time: 6, Tok = 1.000000, rel. units;  $U_{\min} = 58.629997$ .

Time: 9, Tok = 1.000000, rel. units;  $U_{\min} = 69.249997$ .

Fracture energy maximization results  $U$

Time: 3, Tok = -0.193913, rel. units;  $U_{\max} = 62.406213$ .

Time: 6, Tok = -0.293913, rel. units;  $U_{\max} = 68.256713$ .

Time: 9, Tok = -0.393913, rel. units;  $U_{\max} = 80.422213$ .

For filled compositions, the dependences of changes in the properties of epoxy composites on the factors under consideration are described by other equations:

$$R_c = 116.47 - 1.76x_1 - 2.5x_2 - 0.17x_1 x_2 + 1.03x_1^2 - 2.76x_2^2.$$

$$R_u = 37.68 + 1.16x_1 + 1.43x_2 + 2.85x_1 x_2 + 1.56x_1^2 - 3.03x_2^2.$$

$$E_d = 5370.55 - 85.66x_1 + 56.83x_2 + 11.25x_1 x_2 + 123.66x_1^2 - 35.83x_2^2.$$

$$U = 69.41 - 2.18x_1 - 3.53x_2 + 0.05x_1 x_2 + 2.08x_1^2 - 3.66x_2^2.$$

According to the given equations, graphs with current or time parameters were constructed (Figs. 9, 10, 11, 12, 13, 14, 15 and 16).

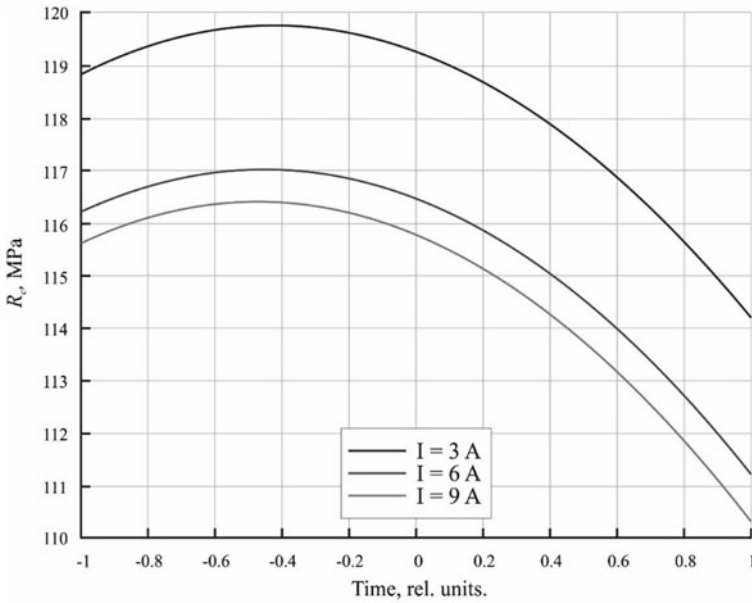


**Fig. 9** Change in compressive strength as a function of time in rel. units  $R_c = 116.47 - 1.76x_1 - 2.5x_2 - 0.17x_1x_2 + 1.03x_1^2 - 2.76x_2^2$

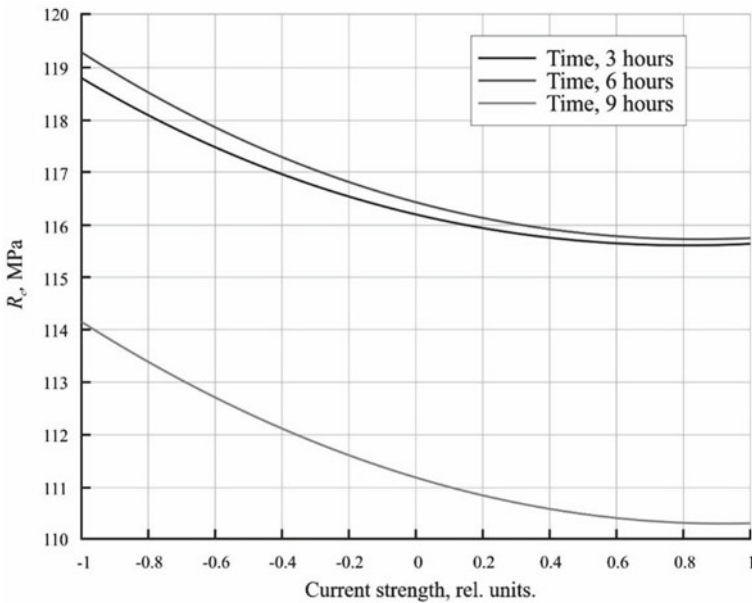


**Fig. 10** Change in compressive strength depending on the effect of electric current in rel. units  $R_c = 116.47 - 1.76x_1 - 2.5x_2 - 0.17x_1x_2 + 1.03x_1^2 - 2.76x_2^2$

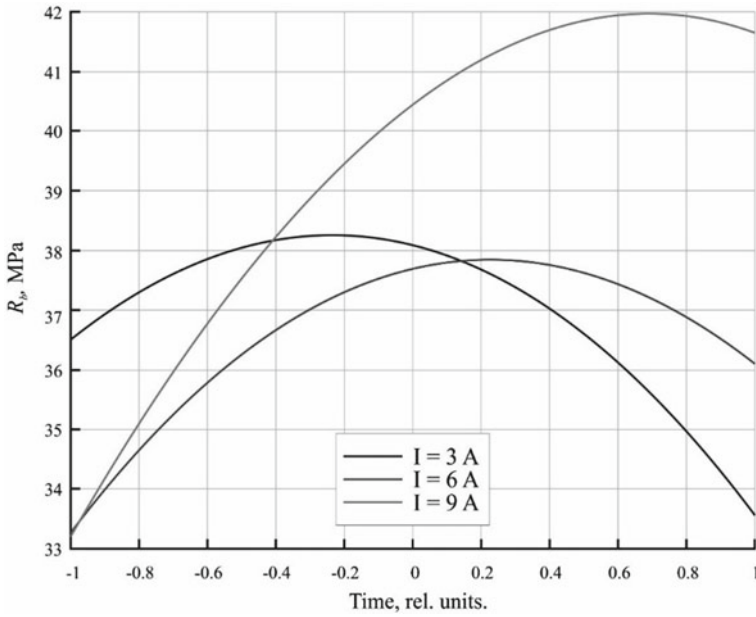


**Fig. 11** Change in bending strength depending on time in rel. units  $R_u = 37.68 + 1.16x_1 + 1.43x_2 + 2.85x_1x_2 + 1.56x_1^2 - 3.03x_2^2$

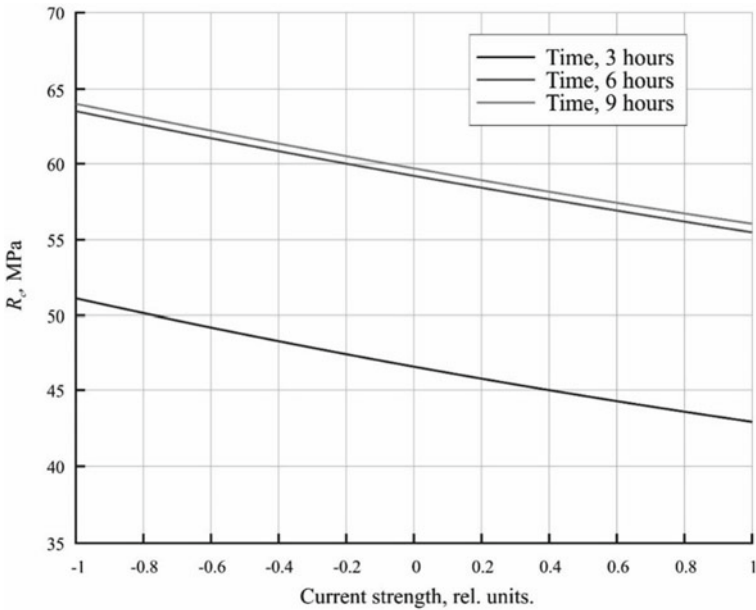


**Fig. 12** Change in bending strength depending on the impact of electric current in rel. units  $R_u = 37.68 + 1.16x_1 + 1.43x_2 + 2.85x_1x_2 + 1.56x_1^2 - 3.03x_2^2$



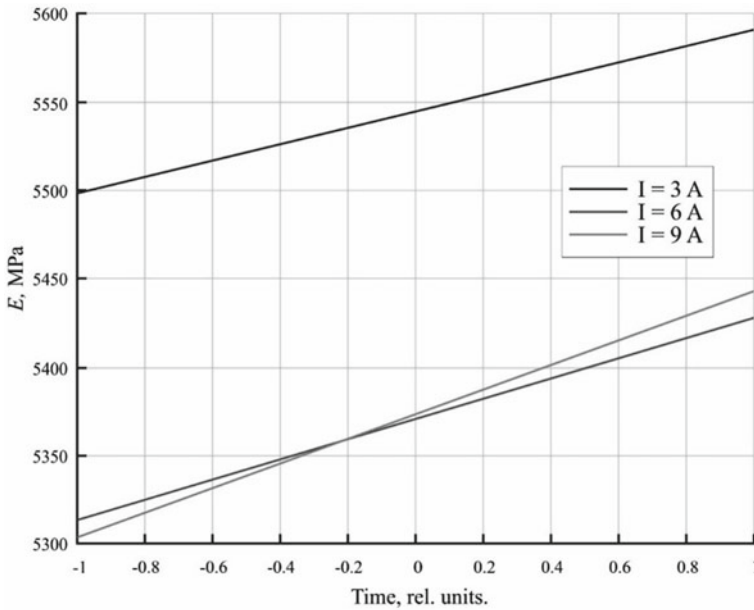


**Fig. 13** Change in the dynamic modulus of elasticity depending on time in rel. units  $E_d = 5370.55 - 85.66x_1 + 56.83x_2 + 11.25x_1x_2 + 123.66x_1^2 - 35.83x_2^2$

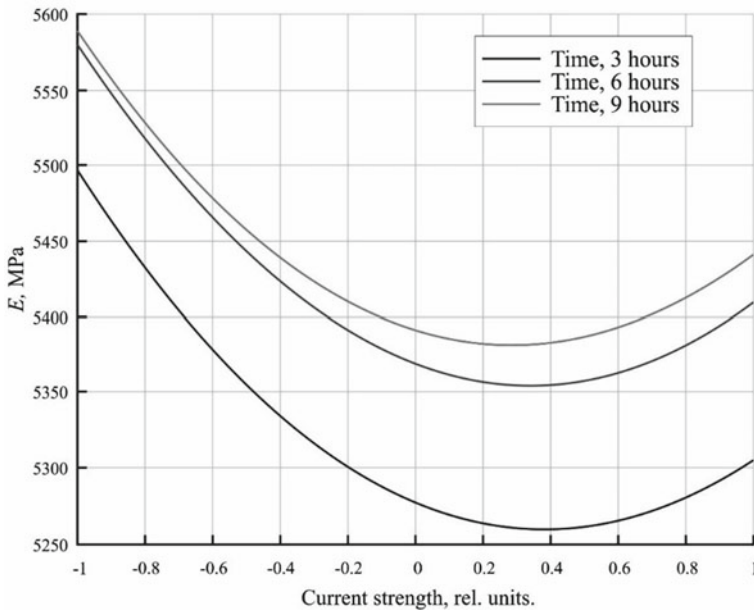


**Fig. 14** Change in the dynamic modulus of elasticity under the influence of electric current in rel. units  $E_d = 5370.55 - 85.66x_1 + 56.83x_2 + 11.25x_1x_2 + 123.66x_1^2 - 35.83x_2^2$

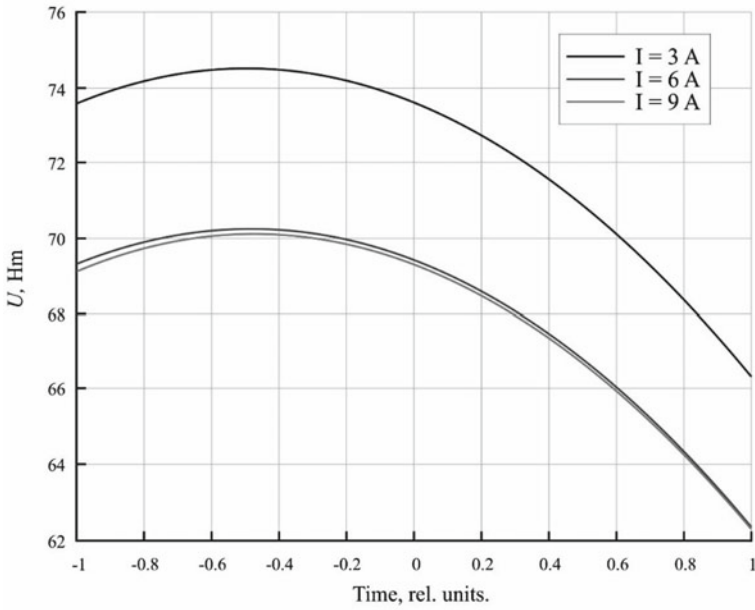


**Fig. 15** Dependence of the fracture energy as a function of time in rel. units  $U = 69.41 - 2.18x_1 - 3.53x_2 + 0.05x_1x_2 + 2.08x_1^2 - 3.66x_2^2$

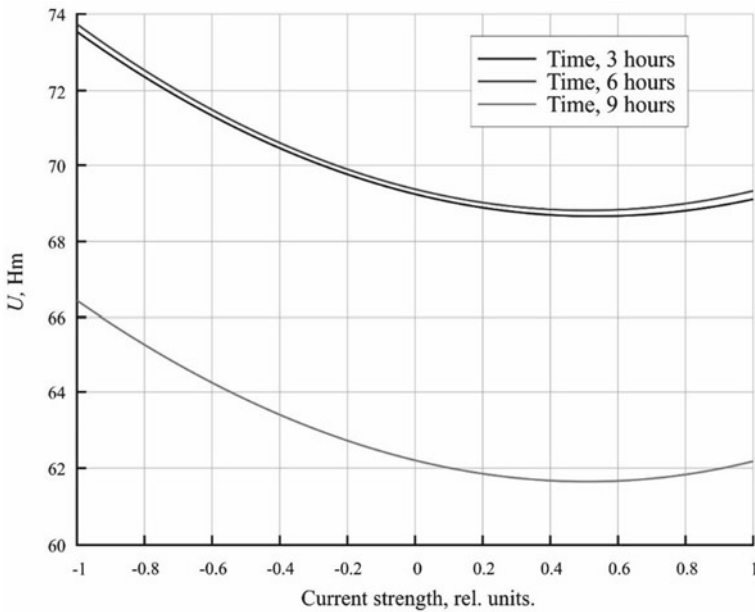


**Fig. 16** Dependence of fracture energy depending on the impact of electric current in rel. units  $U = 69.41 - 2.18x_1 - 3.53x_2 + 0.05x_1x_2 + 2.08x_1^2 - 3.66x_2^2$

Analysis of the graphs shows that the extreme points on them can be determined by unconditional optimization methods for one variable [15, 16].

The results of optimizing the dependencies are shown in Figs. 9, 10, 11, 12, 13, 14, 15 and 16:

Strength minimization results  $R_c$  (compression)

Tok ( $x_1$ ): 3, Time ( $x_2$ ) = 1.000000, rel. units;  $R_c$ .min = 114.169999.

Tok ( $x_1$ ): 6, Time ( $x_2$ ) = 1.000000, rel. units;  $R_c$ .min = 111.209998.

Tok ( $x_1$ ): 9, Time ( $x_2$ ) = 1.000000, rel. units;  $R_c$ .min = 110.309998.

Strength maximization results  $R_c$  (compression)

Tok ( $x_1$ ): 3, Time ( $x_2$ ) = -0.422101, rel. units;  $R_c$ .max = 119.751748.

Tok ( $x_1$ ): 6, Time ( $x_2$ ) = -0.452899, rel. units;  $R_c$ .max = 117.036123.

Tok ( $x_1$ ): 9, Time ( $x_2$ ) = -0.483696, rel. units;  $R_c$ .max = 116.385734.

Strength minimization results  $R_c$  (compression)

Time ( $x_2$ ): 3, Tok ( $x_1$ ) = 0.771845, rel. units;  $R_c$ .min = 115.596383.

Time ( $x_2$ ): 6, Tok ( $x_1$ ) = 0.854369, rel. units;  $R_c$ .min = 115.718155.

Time ( $x_2$ ): 9, Tok ( $x_1$ ) = 0.936893, rel. units;  $R_c$ .min = 110.305898.

Strength maximization results  $R_c$  (compression)

Time ( $x_2$ ): 3, Tok ( $x_1$ ) = -1.000000, rel. units;  $R_c$ .max = 118.830001.

Time ( $x_2$ ): 6, Tok ( $x_1$ ) = -1.000000, rel. units;  $R_c$ .max = 119.260001.

Time ( $x_2$ ): 9, Tok ( $x_1$ ) = -1.000000, rel. units;  $R_c$ .max = 114.170001.

Strength minimization results  $R_i$

Tok ( $x_1$ ): 3, Time ( $x_2$ ) = 1.000000, rel. units;  $R_i$ .min = 33.629999.

Tok ( $x_1$ ): 6, Time ( $x_2$ ) = -1.000000, rel. units;  $R_i$ .min = 33.219999.

Tok ( $x_1$ ): 9, Time ( $x_2$ ) = -1.000000, rel. units;  $R_i$ .min = 33.089998.

Strength maximization results  $R_i$

Tok ( $x_1$ ): 3, Time ( $x_2$ ) = -0.234323, rel. units;  $R_i$ .max = 38.246370.

Tok ( $x_1$ ): 6, Time ( $x_2$ ) = 0.235974, rel. units;  $R_i$ .max = 37.848721.

Tok ( $x_1$ ): 9, Time ( $x_2$ ) = 0.706271, rel. units;  $R_i$ .max = 41.911419.

Strength minimization results  $R_i$  (bending)

Time ( $x_2$ ): 3, Tok ( $x_1$ ) = 0.541667, rel. units;  $R_i$ .min = 32.762292.

Time ( $x_2$ ): 6, Tok ( $x_1$ ) = -0.371795, rel. units;  $R_i$ .min = 37.464359.

Time ( $x_2$ ): 9, Tok ( $x_1$ ) = -1.000000, rel. units;  $R_i$ .min = 33.630000.

Strength maximization results  $R_i$  (bending)

Time ( $x_2$ ): 3, Tok ( $x_1$ ) = -1.000000, rel. units;  $R_i$ .max = 36.470001.

Time ( $x_2$ ): 6, Tok ( $x_1$ ) = 1.000000, rel. units;  $R_i$ .max = 40.400001.

Time ( $x_2$ ): 9, Tok ( $x_1$ ) = 1.000000, rel. units;  $R_i$ .max = 41.650001.

Strength minimization results  $E_d$  (dynamic modulus of elasticity)

Tok ( $x_1$ ): 3, Time ( $x_2$ ) = -1.000000, rel. units;  $R_c$ .min = 5498.459991.

Tok ( $x_1$ ): 6, Time ( $x_2$ ) = -1.000000, rel. units;  $R_c$ .min = 5313.719989.

Tok ( $x_1$ ): 9, Time ( $x_2$ ) = -1.000000, rel. units;  $R_c$ .min = 5304.639987.

Strength maximization results  $E_d$

Tok ( $x_1$ ): 3, Time ( $x_2$ ) = 1.000000, rel. units;  $R_c$ .max = 5589.620009.

Tok ( $x_1$ ): 6, Time ( $x_2$ ) = 1.000000, rel. units;  $R_c$ .max = 5427.380011.

Tok ( $x_1$ ): 9, Time ( $x_2$ ) = 1.000000, rel. units;  $R_c$ .max = 5440.800013.

Strength minimization results  $E_d$

Time ( $x_2$ ): 3, Tok ( $x_1$ ) = 0.391841, rel. units;  $R_i$ min = 5258.903367.

Time ( $x_2$ ): 6, Tok ( $x_1$ ) = 0.346353, rel. units;  $R_i$ min = 5355.715705.

Time ( $x_2$ ): 9, Tok ( $x_1$ ) = 0.300865, rel. units;  $R_i$ min = 5380.356307.

Strength maximization results  $E_d$

Time ( $x_2$ ): 3, Tok ( $x_1$ ) = -1.000000, rel. units;  $R_i$ max = 5498.460065.

Time ( $x_2$ ): 6, Tok ( $x_1$ ) = -1.000000, rel. units;  $R_i$ max = 5579.870063.

Time ( $x_2$ ): 9, Tok ( $x_1$ ) = -1.000000, rel. units;  $R_i$ max = 5589.620060.

Fracture energy minimization results  $U$

Tok ( $x_1$ ): 3, Time ( $x_2$ ) = 1.000000, rel. units;  $R_c$ min = 66.429998.

Tok ( $x_1$ ): 6, Time ( $x_2$ ) = 1.000000, rel. units;  $R_c$ min = 62.219998.

Tok ( $x_1$ ): 9, Time ( $x_2$ ) = 1.000000, rel. units;  $R_c$ min = 62.169998.

Fracture energy maximization results  $U$

Tok ( $x_1$ ): 3, Time ( $x_2$ ) = -0.489071, rel. units;  $R_c$ max = 74.545437.

Tok ( $x_1$ ): 6, Time ( $x_2$ ) = -0.482240, rel. units;  $R_c$ max = 70.261154.

Tok ( $x_1$ ): 9, Time ( $x_2$ ) = -0.475410, rel. units;  $R_c$ max = 70.137213.

Fracture energy minimization results  $U$

Time ( $x_2$ ): 3, Tok ( $x_1$ ) = 0.536058, rel. units;  $R_i$ min = 68.682296.

Time ( $x_2$ ): 6, Tok ( $x_1$ ) = 0.524038, rel. units;  $R_i$ min = 68.838798.

Time ( $x_2$ ): 9, Tok ( $x_1$ ) = 0.512019, rel. units;  $R_i$ min = 61.674700.

Fracture energy maximization results  $U$

Time ( $x_2$ ): 3, Tok ( $x_1$ ) = -1.000000, rel. units;  $R_i$ max = 73.590001.

Time ( $x_2$ ): 6, Tok ( $x_1$ ) = -1.000000, rel. units;  $R_i$ max = 73.670001.

Time ( $x_2$ ): 9, Tok ( $x_1$ ) = -1.000000, rel. units;  $R_i$ max = 66.430001.

Changes in the tensile strength during bending, compression, dynamic modulus of elasticity, fracture energy, for epoxy compositions without filler, depending on the duration of magnetic treatment are shown in Figs. 1, 2, 3 and 4. From the graph (Fig. 3) it can be seen that the increase in the tensile strength during bending occurs with an increase in the duration actions of the electromagnetic field. The composition treated for 9 h at a current of 3 A has the highest strength characteristics. The lowest value of tensile strength in bending shows the composition processed in an electromagnetic field at a current strength of 9 A.

The compressive strength (Fig. 1), for compositions hardening at a current strength of 3 and 6 A, decreases by 6 h when the samples are in an electromagnetic field, after which, by 9 h, it rises to its original value, and for the composition processed at a current strength of 3 A by this time it is the highest. Epoxy compositions cured in an electromagnetic field at a current strength of 3 A and a curing time of 9 h have the greatest strength characteristics, the smallest—at a current strength of 9 A, and with increasing processing time, the strength decreases.

The different nature of the change in the compressive and tensile strengths can obviously be explained by the fact that the electromagnetic field affects the change in the structure in the volume of the composite adjacent to the substrate through which the electric current is passed. Therefore, the ultimate tensile strength in bending is a characteristic more sensitive to these changes than the compressive strength. The latter characteristic depends on the change in the structure in the bulk of the sample.

A change in the sample structure only in the layers adjacent to one face can adversely affect the compressive strength of the composite.

The dynamic modulus of elasticity (Fig. 5) increases with the curing time. The highest elastic properties show compositions that harden in an electromagnetic field at a current of 3 and 9 A. Samples cured at 6 A current have the lowest value of the dynamic modulus of elasticity, although it also increases with increasing processing time.

The highest value of fracture energy (Fig. 7) was recorded at 3 and 9 h of hardening, when treated with an electromagnetic field. Of the other samples, the highest value of the above indicator is those that were exposed to an electromagnetic field at a current strength of 3 A. The smallest—at a current strength of 6 A.

Next, consider the graphical dependences of the physical and mechanical characteristics of epoxy composites without filler depending on the current strength (Figs. 5, 6, 7 and 8).

It can be seen in Fig. 4 that for composites of all compositions, with increasing current strength, the values of ultimate tensile strength in bending decrease. The greatest tensile strength in bending has a composition cured in an electromagnetic field for the greatest amount of time (9 h).

The compressive strength of epoxy composites (Fig. 2) with an increase in current strength above 4–5 A up to 9 A also decreases. Compositions that are under the influence of an electromagnetic field for 3 and 9 h have the highest strength characteristics.

The dynamic modulus of elasticity (Fig. 6) of epoxy composites has the highest values at a current strength of 3 A, after which, with an increase in current strength up to 6 A, it drops and returns to its original value, with an increase in current strength up to 9 A. Again, the greatest elastic properties show epoxy compositions hardening for the maximum amount of time (9 h).

The energy of destruction, the highest in the compositions that have hardened for 3 and 9 h, at a current strength closer to 3 A, after which it decreases with increasing current strength (Fig. 8).

Figures 9, 10, 11, 12, 13, 14, 15 and 16 show the results of tests of filled composites. The change in tensile strength in bending (Fig. 11) with an increase in time up to 9 h increases for samples processed in an electromagnetic field at a current strength of 6 and 9 A. For compositions treated at a current of 3 A, the value of tensile strength in bending increases by 6 o'clock and then drops and is the lowest value. Epoxy compositions hardening in an electromagnetic field for 9 h at a current strength of 9 A have the highest indicator.

The compressive strength limit (Fig. 9) reaches its maximum value for the composition treated with an electromagnetic field at a current strength of 3 A for a period of 3–6 h. Other compositions have similar dependencies, with less strength.

The dynamic modulus of elasticity (Fig. 13) increases markedly with increasing activation time. As in the previous case, the composition that hardens at a current strength of 3 A has the greatest elastic properties.

The fracture energy (Fig. 15), on the contrary, decreases with increasing time, although epoxy compositions treated with an electromagnetic field at a current strength of 3 A still have the best indicators.

Considering the dependences of the strength characteristics of filled epoxy compositions depending on the current strength, it can be seen that the flexural strength (Fig. 12) for samples cured for 6 and 9 h increases with increasing current strength. This is most noticeable in the composition, which was under the influence of an electromagnetic field for 9 h at a current strength of 9 A.

The compressive strength (Fig. 10) gradually decreases with increasing current strength. The composition that hardens in an electromagnetic field for 6 h has the greatest strength.

The highest values of the dynamic modulus of elasticity (Fig. 14) show compositions cured at a minimum current strength (3 A), after which, with an increase in it, their elastic properties decrease. For compounds treated for 6 and 9 h, from 6 to 9 A again there is a slight rise after the fall, but still remains much lower than the initial value. The fracture energy (Fig. 16) decreases with increasing current for all epoxy compositions with filler. Compositions processed in an electromagnetic field for 3 and 6 h have the highest fracture energy.

## 4 Conclusion

Studies have been carried out to establish the influence of an electromagnetic field on the properties of polymer epoxy composites. The studies are carried out using mathematical methods of planning experiments, according to which the variation factors are the current strength and the duration of processing of the samples, and the optimized properties are the ultimate strength in bending and compression, the modulus of elasticity, and the fracture energy.

For epoxy composites unfilled and filled with pyrite cinders, regression equations are obtained and graphic dependences of changes in properties on technological parameters of activation by a magnetic field are plotted.

Optimal activation modes of epoxy composites have been obtained. For unfilled compositions, improved physical and technical properties are achieved when treated with a current of 3 A, with a duration of 9 h. For filled compositions, the highest performance is achieved when activated with a current of 3 A with a duration of 9 h.

Epoxy composites have been obtained with compressive strength of MPa and bending strength of 42–62 MPa, exceeding by 10% compared to non-activated materials.

## References

1. Solomatov VI, Bobrushev AN, Proshin AP (1982) On the influence of dimensional factors of dispersed filler on the strength of epoxy composites. *Mech Compos Mater* 6:1008–1013
2. Solomatov VI, Vyrovoy VN. Cluster formation of composite building materials. In: *Technological mechanics of concretes*. RPI, Riga, 5–21
3. Bobryshev AN, Erofeev VT, Kozomazov VN (2012) Physics and synergetic of dispersed disordered condensed composite systems. *Nauka*
4. Erofeev VT, Rodin AI, Bochkin VS, Yakunin VV, Ermakov AA (2020) Lightweight geopolymers made of mineral wool production waste. *Mag Civ Eng* 93(1):3–12. <https://doi.org/10.18720/MCE.93.1>
5. Erofeev V, Smirnov V, Myshkin A (2019) The study of polyester-acrylate composite's stability in the humid maritime operating conditions. *Mat Today: Proc* 19:2255–2257. <https://doi.org/10.1016/j.matpr.2019.07.547>
6. Startsev VO, Molokov MV, Blaznov AN, Zhurkovskii ME, Erofeev VT, Smirnov IV (2017) Determination of the heat resistance of polymer construction materials by the dynamic mechanical method. *Polym Sci Ser D* 10(4):313–317. <https://doi.org/10.1134/S1995421217040141>
7. Yusupova AA, Akhmetova RT, Treshchev AA, Erofeev VT, Bobrishev AA, Shafigullin LN, Lakhno AA (2016) Production and investigation of properties of sulfide composite materials based on technogenic sulfur waste with titanium chloride as an activator. *Res J Pharm Biol Chem Sci* 7(6):1614–1619
8. Erofeev V, Rodin A, Rodina N, Kalashnikov V, Irina E (2016) Biocidal binders for the concretes of underground constructions. *Procedia Eng* 165:1448–1454. <https://doi.org/10.1016/j.proeng.2016.11.878>
9. Erofeev V, Korotaev S, Bulgakov A, Tretiakov I, Rodin A (2016) Getting fired material with vitreous binder using frame technology. *Procedia Eng* 165:166–171. <https://doi.org/10.1016/j.proeng.2016.11.606>
10. Shafigullin LN, Bobrishev AA, Erofeev VT, Treshchev AA, Erofeev VT, Shafigullina AN (2015) Development of the recommendations on selection of glass-fiber reinforced polyurethanes for vehicle parts. *Int J Appl Eng Res* 10(23):43758–43762
11. Akutin MS, Yegorova LN, Andriyanov BV, Rekus GG, Govor AI (1974) Strength of cross-linked polymers during curing in a magnetic field. *Plast Mass* 12:49–50
12. Rodin YuP (1980) Influence of homogeneous and inhomogeneous magnetic fields on structure and properties of polymeric materials. Dissertation for the degree of Candidate of Technical Sciences. Riga
13. Molchanov YuM, Martynenko OP, Rodin YUP (1978) Effect of a magnetic field on the structure of an epoxy compound. *Polym Mech* 3:537–592
14. Matrosov AV (1999) Influence of electromagnetic fields on technological and operational properties of building composite materials. Author's abstract of thesis for the degree of Candidate of Technical Sciences. Mordovian University, Saransk
15. Afonin VV, Nikulin VV (2017) Modelling and optimization methods with examples in C/C++ and MATLAB: textbook in 2 parts. Part 2. Methods of unconditional optimization. Afanasiev B. S., Saransk
16. Lesin VV, Lisovets YuP (2016) Fundamentals of optimization methods: textbook, 4th edn. Lan